On the Archean geologic history of eastern Hall Peninsula, Baffin Island, Nunavut, Canada

by

Richard Eric From

A Thesis submitted to the Faculty of Graduate Studies of

The University of Manitoba

in partial fulfillment of the requirements of the degree of

DOCTOR OF PHILOSOPHY

Department of Geological Sciences
University of Manitoba
Winnipeg

Copyright © 2017 by Richard Eric From

ABSTRACT

Eastern Hall Peninsula on southeastern Baffin Island, lies at the junction of a complex Paleoproterozoic collision between the Rae craton, Meta Incognita microcontinent and the North Atlantic craton from ca. 1.88 to 1.80 Ga. The original configuration of these cratons is not well understood because eastern Hall Peninsula, which lies at the triple junction between these plates, lacks detailed geoscience mapping and geochemical data. Consequently, detailed mapping was conducted in eastern Hall Peninsula and zircons separated from selected samples were analyzed for U-Pb and Lu-Hf isotopes.

Magmatic zircons yielded U-Pb crystallization ages between ca. 2976 to 2720 Ma and metamorphic zircons record tectonothermal disturbances between ca. 2740 to 2700 Ma, a period coinciding with metamorphism documented in adjacent crustal blocks. Magmatic rocks older than ca. 2740 Ma yielded positive **ε**Hf(t) and consistent model ages of ca. 3.1 to 3.0 Ga, indicating the time that protolith melt was extracted from the mantle. The oldest, granodioritic crust crystallized at ca. 2976 Ma and was then reworked periodically at ca. 2.93, 2.84-2.81 and 2.77-2.69 Ma, forming other rock units. Two rock units younger than ca. 2740 Ma yielded negative **ε**Hf(t) model ages of ca. 3.4 and 3.3 Ga respectively, indicating derivation from an older crustal source yet to be identified in outcrop on Hall Peninsula.

Zircons from a suite of relatively undeformed magnetite-bearing granites yielded U-Pb magmatic ages between ca. 2750 to 2612 Ma. Sm-Nd data from these granites outline a spatial trend across eastern Hall Peninsula with negative $\varepsilon Nd_{(t)}$ in the west becoming more positive $\varepsilon Nd_{(t)}$ to the east. This trend outlines an increase of crustal reworking and

recycling in the west compared with more mantle-derived, juvenile crust towards the east, delineating a boundary between Paleoproterozoic rocks of Meta Incognita microcontinent and Archean rocks of eastern Hall Peninsula.

Synthesizing all data we propose a new regional correlation model that incorporates previous models and other recent studies. This new model groups eastern Hall Peninsula, southern Cumberland Peninsula and southern Aasiaat domain into a "core zone" that shared a geologic history prior to 1.90 Ga and potentially prior to 2.75 Ga.

Word Count: 347 (Max:350)

ACKNOWLEDGMENTS

There are many people, institutions and places throughout Canada that have been integral to the completion of this project and deserve thanks for their contributions. The following is a brief list of those who require special mention and thanks for their mentorship, patience and contributions

Firstly, I must thank my thesis advisor, Alfredo Camacho for the opportunity to pursue this dynamic project studying rocks on Hall Peninsula, Baffin Island, Nunavut in the Sub-Arctic of Canada. Alfredo's guidance, advice and countless hours spent reviewing my work has been a vital part of this project and it would not have been possible without him.

Big thanks also go out to the staff and collaborators at the Canada-Nunavut Geoscience Office (CNGO) for their hard work making the Hall Peninsula Integrated Geoscience Project (HPIGP) not only possible but also an amazing success. I would like to acknowledge David Mate, Gabriel Machado, Mike Young and Holly Steenkamp for

spearheading this huge project and Celine Gilbert, Serge Basso, Tommy Tremblay and Mannasie Qillaq RIP (1996-2013) for their important contributories to the HPIGP. Thanks to the CNGO and Natural Resources Canada (NRCAN) for a Research Associate Bursary funding received during the majority of this project

Thank you to the HPIGP collaborators at the Geological Survey of Canada (GSC), Marc-St-Onge and Nicole Rayner for their leadership in the field and support during subsequent investigation of geological problems.

Grateful thanks goes to my to my advisory committee including Alfredo Camacho, Norman Halden, Christian Bohm and Jens Ehn for their guiding questions, queries and feedback during this process. The Ph.D. Candidacy exam was a particularly lofty hurdle to navigate so their time and patience was enormously appreciated.

The amazing researchers and support staff at analytical laboratories in beautiful cities across Canada were very important to the success of this project and the assistance in data acquisition and interpretation was greatly appreciated. A special thanks goes to Nicole Rayner and the support staff at the Sensitive High Resolution Ion MicroProbe Laboratory at the GSC building in Ottawa, Ontario, Canada as well as Graham Pearson, Yan Luo, Qioa Shu and Chiranjeeb Sarkar at the Arctic Resources Laboratory at the University of Alberta in Edmonton, Alberta, Canada.

The City of Iqaluit and the entirety of Hall Peninsula, Baffin Island, Nunavut, Canada along with the locals and wildlife are thanked for their hospitality, accommodation and various contributions including the rock samples collected for this thesis.

Thanks and well wishes goes out to all of my fellow graduates students for their support as fellow travelers along this graduate school journey, especially Kevin Jones, Rachel ten Bruggencate, Camille Partin, Russell Hiebert, Halya Petzold, Joe McLeod, Jemma Harrison, Lauren Eggie, Max Day, Greg Ashcroft, Maliheh Rabie, Aminul Haque and Samuel Banash.

Lastly, but certainly not least, thanks to family and friends for their belief and support on this Ph.D. voyage, especially my partner Kana for providing encouragement and unyielding motivation to pursue success no matter what the obstacle.

TABLE OF CONTENTS

ABSTRACT ..... **ii**

ACKNOWLEDGEMENTS ..... **iii**

TABLE OF CONTENTS ..... **vi**

LIST OF FIGURES ..... **viii**

LIST OF TABLES ..... **xiv**

COPYWRITED MATIERAL FOR WHICH PERMISSION WAS OBTAINED ..... **xiv**

1. Chapter 1. Introduction **1**
1.1. General Introduction **1**
1.1.1. Northern Labrador – Baffin Island – West Greenland Segment of the THO 4
1.1.2. What is Hall Peninsula's role ? 9
1.2. Objectives and Significance of Research **13**
1.3. Structure of the thesis **15**
1.4. References **18**
1.5. Data Appendices **22**

2. Chapter 2. Preliminary characterization of the Archean orthogneiss complex of Hall Peninsula, Baffin Island, Nunavut: Insights from the "snow bowl" study area. **25**
2.1. Abstract **25**
2.2. Introduction **26**
2.3. Geological background and previous work **29**
2.4. Geology of the "snow bowl" study area **32**
2.4.1. Description of Lithological units 32
2.4.2. Structural and metamorphic character of the study area 38
2.5. Conclusions **40**
2.6. Future work **41**
2.7. Acknowledgements **41**
2.8. References **42**

3. Chapter 3. Archean magmatism and metamorphism of eastern Hall Peninsula, southern Baffin Island, Nunavut **45**
3.1. Abstract **45**
3.2. Introduction **46**
3.3. Previous age determinations **47**
3.4. Hypothesis for further investigation **50**
3.5. Analytical methods **52**
3.6. U-Pb results **54**
3.6.1. 12MBC-S116A – monzogranite gneiss 54

3.6.2. 13SUB-F151A – megacrystic granodiorite gneiss 56
3.6.3. 13SUB-F155B – grey tonalite gneiss 58
3.6.4. 13SUB-F155C – mafic lenses 60
3.6.5. 13SUB-F155A – porphyroclastic monzogranite gneiss 62
3.6.6. 13SUB-F152A – magnetite-bearing monzogranite gneiss 63
3.6.7. 13SUB-F150A – porphyroclastic monzogranite gneiss 66
3.7. Discussion 67
3.7.1. Magmatic versus metamorphic zircon ages 67
3.7.2. Revised age relations between units 70
3.8. Conclusions 73
3.9. Future work 74
3.10. Economic considerations 74
3.11. Acknowledgments 75
3.12. References 75
3.13. Data appendices 79

4. Chapter 4. U-Pb and Lu-Hf isotopes of the Archean orthogneiss complex on eastern Hall Peninsula, southern Baffin Island, Nunavut 104
4.1. Abstract 105
4.2. Introduction 106
4.3. Geological setting 110
4.4. Geology of the snow ball area 115
4.5. Analytical Techniques 117
4.5.1. Sample Collection 117
4.5.2. U-Pb SHRIMP 117
4.5.3. U-Pb and Lu-Hf LASS-ICPMS 118
4.6. Results 120
4.6.1. snow bowl area 122
4.6.2. Regional samples (LASS for U-Pb and Lu-Hf) 128
4.7. Discussion 132
4.7.1. SHRIMP versus LASS-ICPMS U-Pb results 133
4.7.2. Archean magmatism and metamorphism on eastern Hall Peninsula 135
4.7.3. εHf(t), magmatic provenance and model ages 138
4.7.4. Paleoproterozoic metamorphism 143
4.7.5. Regional tectonic synthesis 145
4.8. Conclusions 149
4.9. Acknowledgements 150
4.10. References Cited 151
4.11. Data appendices 161

5. Chapter 5. Sm-Nd isotopes of magnetite-bearing granites on eastern Hall Peninsula, Baffin Island 219
5.1. Abstract 220
5.2. Introduction 221
5.3. Previous work and Geological setting 227
5.4. Magnetite-bearing granites 229
5.5. Analytical Methods 230
5.5.1. Sample Collection 230

5.5.2. Zircon seperation and imaging 230
5.5.3. U-Pb and Lu-Hf Laser Ablation Split-Stream (LASS) 231
5.5.4. Sm-Nd analyses 233
5.6. Results 234
5.6.1. Southern transect 237
5.6.2. Northern transect 243
5.7. Discussion 247
5.7.1. Archean magmatic suites on eastern Hall Peninsula 248
5.7.2. Late-stage syenogranite magmatism 248
5.7.3. Paleoproterozoic zircon crystallization 249
5.7.4. Sm-Nd data trends from west to east 250
5.7.5. Lu-Hf in zircon 251
5.7.6. Zircon Lu-Hf data versus whole rock Sm-Nd analyses 255
5.7.7. A geologic terrane boundary on west-central Hall Peninsula? 258
5.7.8. Regional tectonic implications 259
5.8. Conclusions 263
5.9. Acknowledgements 264
5.10. References Cited 265
5.11. Data appendices 275

6. Chapter 6. Summary, significance and future work 319
6.1. Summary and significance of the thesis 319
6.2. Going Further: a revised regional tectonic model 322
6.2. Future Work 333
6.3. References 336

LIST OF FIGURES

Figure 1.1: Regional geologic compilation map showing the extent of the Trans-Hudson orogen (green portion) throughout North America and Greenland. The lower plate Superior province has promontory points in present day Manitoba (M) and Quebec (Q). Crustal sutures bounding the Archean cratons are shown with black lines with triangles indicating direction of underthrusting (St-Onge et al., 2009).

Figure 1.2: Regional map of the Baffin Island-Northern Labrador-West Greenland segment of the Trans-Hudson orogen with ages of crustal amalgamation and proposed suture locations. Abbreviations: BaS, Baffin suture; BeS, Bergeron suture; DBS Disko Bugt suture; NIS, Nordre Isortoq steep belt; SRS, Soper River suture; TgS, Tasiuyak gneiss structure. Modified from St-Onge et al. (2009).

Figure 1.3: Cartoon map illustrating the geological evolution of the THO during the time interval 1.83–1.80 Ga. The location of the Sugluk Block is within the current day Hudson Bay, just prior to it's accretion to Meta Incognita microcontinent. Crustal sutures are shown with thin black lines: BeS, Bergeron suture; BS, Baffin suture; BiS, Big Island suture; Sugluk suture. Abbreviations; GFtz, Great Falls tectonic zone; GLsz, Granville Lake structural zone, LTsz, Lac Tudor shear zone; MHB, Medicine Hat block; PT, Pelican thrust. Modified from Corrigan et al. (2009).

Figure 1.4: Regional geological maps of northeast Laurentia and southeast Asia showing a similar size, shape and extent of crustal constituents and intervening sutures (St-Onge et al., 2009).

Figure 1.5: Total-field magnetic susceptibility of southern Hall Peninsula in NTS areas 025O, P, I and J (Dumont and Dostaler, 2010a–q), highlighting strongly linear features (in purple) trending approximately north-south down central Hall Peninsula.

Figure 2.1: Compilation map of Hall Peninsula from mapping during the 2012 and 2013 field seasons showing the distribution of principal tectonostratigraphic units. The snow bowl area is shown with a red star.

Figure 2.2: Compilation map of Baffin Island, which predates the initiation of the CNGO Hall Peninsula project, showing the alternative hypotheses for suture locations on Baffin Island with specific convergence on Hall Peninsula. Abbreviations: B, Borden basin; F, Franklinian basin; FH, Fury and Hecla basin; HP, Hall Peninsula. Map modified from St-Onge et al., 2009).

Figure 2.3: Preliminary geological map of the snow bowl area; regional location shown in Figure 2.1. The legend lists units from oldest (1) to youngest (7). The numbered locations refer to locations of outcrops shown in Figures 2.4 and 2.5.

Figure 2.4: Field photographs from the study area. Unit numbers and color codes correspond to those of Figure 2.3 and are shown in the bottom right of each photograph. a) Unit 1 fine grained pyroxene diorite that occurs as a 5-10m wide panel within Unit 7; b) Unit 2 medium grained grey tonalite gneiss with thin trondhjemitic segregations. c) Unit 2 medium grained grey tonalite gneiss intruded by monzogranitic veining mm to 10's of cm in width. d) Unit 3 medium grained leopard gneiss with plagioclase phenocrysts. e) Unit 3 leopard gneiss characterized by fine-grained enclaves of hornblende + biotite + epidote quartz diorite. f) Mafic monzogranite of Unit 4

containing abundant clinopyroxene and orthopyroxene-bearing mafic enclaves and discontinuous layering.

Figure 2.5: Field photographs from the study area. Unit numbers and color codes correspond to those of Figure 2.3 and are shown in the bottom right of each photograph. a) Typical field aspects of the Unit 5 Ribbon granite gneiss with alternating bands of differential mineral composition giving a "ribbon" textured appearance; b) Unit 5 ribbon granite gneiss crosscutting the foliation and layering in the Unit 4 mafic monzogranite gneiss; c) Unit 6 magnetite-bearing monzogranite characterized by syn-tectonic melt segregations and depletion halos enriched in mafic minerals.; d) Unit 7 fine grained porphyroclastic monzogranite characterized by K-feldspar porphyroclasts (disaggregated syenogranite veins); e) Clots of biotite + hornblende with light-coloured depletion halos within Unit 7 biotite + epidote + hornblende monzogranite; f) Weakly defomed syenogranite vein of Unit 8 crosscutting foliation (parallel to the direction of the hammer) in Unit 2 grey tonalite gneiss.

Figure 3.1: Geology of southern Hall Peninsula, Nunavut from data collected during the 2012 and 2013 field seasons, showing the distribution of the principal units and the locations of previous U-Pb age determinations (modified from Machado et al., 2013). Location of the study area (snow bowl area) is shown with a red star. Abbreviations: grt, garnet; bt, biotite; mag, magnetite; opx, orthopyroxene; cpx, clinopyroxene.

Figure 3.2: Detailed geology of the snow bowl area on east-central Hall Peninsula, Nunavut, with inset schematic map showing the general geology of the surrounding area. The geological unit legend of the study area lists units from oldest to youngest (from top to bottom), as interpreted in From et al. (2014), with black dots and sample numbers indicating the positions of samples analyzed for U-Pb geochronology.

Figure 3.3: Representative zircon images and concordia diagrams for a-c) sample 13SUB-S166A; d-f) sample 13SUB-F151A; dark grey ellipses correspond to ages used to calculate the crystallization age; light grey ellipses are ages excluded from the crystallization-age calculation; unfilled ellipses denote ages used to calculate the weighted-mean age of metamorphism (see text for discussion). Back scattered electron (BSE) images show spot analyses (correspond to analyses in APPENDIX 3B; errors given at 1σ); white scale bars all 50 μm; mean ages reported at the 2σ confidence level.

Figure 3.4: Representative zircon images and concordia diagrams for a-e) sample 13SUB-F155B; f-h) sample 13SUB-F155C; i-k) sample 13SUB-F155A; dark grey ellipses correspond to ages used to calculate the crystallization age; light grey ellipses are ages excluded from the crystallization-age calculation; unfilled ellipses denote ages used to calculate the weighted-mean age of metamorphism (see text for discussion). Back scattered electron (BSE) images show spot analyses (correspond to analyses in APPENDIX 3B; errors given at 1σ); white scale bars all 50 μm; mean ages reported at the 2σ confidence level.

Figure 3.5: Representative zircon images and concordia diagrams for a-c) sample 13SUB-F152A; d-f) sample 13SUB-F150A; dark grey ellipses correspond to ages used to calculate the crystallization age; light grey ellipses are ages excluded from the crystallization-age calculation; unfilled ellipses denote ages used to calculate the weighted-mean age of metamorphism (see text for discussion). Back scattered electron (BSE) images show spot analyses (correspond to analyses in APPENDIX 3B; errors given at 1σ); white scale bars all 50 μm; mean ages reported at the 2σ confidence level.

Figure 3.6: Summary of zircon U-Pb ^{207}Pb / ^{206}Pb age data for each sample analyzed from the snow bowl area and two samples (12MBC-F105A, 12MBC-F096A) from the eastern Hall Peninsula orthogneiss complex dated by Rayner (2014). General zonation characteristics associated with age clusters are shown in the legend. Zircon zonation is based purely on characterization from BSE images independent of U-Pb isotopic age interpretation.

Figure 4.1: Regional map of the Baffin Island-northern Labrador-west Greenland segment of the Trans-Hudson orogen with ages of crustal amalgamation and proposed suture locations. Abbreviations: BaS, Baffin suture; BeS, Bergeron suture; DBS Disko Bugt suture; NIS, Nordre Isortoq steep belt; SRS, Soper River suture; TgS, Tasiuyak gneiss structure. Map modified from St-Onge et al. (2009).

Figure 4.2: Geology of southern Hall Peninsula, Baffin Island, Nunavut showing the distribution of the principal geologic units and the locations of previous U-Pb age determinations. The location of the snow bowl area is shown with black box. The locations of regional scale orthogneisses sampled in the larger scale study area are shown by red stars with their ages of crystallization in green. Abbreviations: grt, garnet; bt, biotite; mag, magnetite; opx, orthopyroxene; cpx, clinopyroxene. Map modified from Machado et al. (2013).

Figure 4.3: Geology of the snow bowl area on east-central Hall Peninsula, Nunavut. Units are presented from oldest (1) to youngest (7), as interpreted in From et al. (2014). The majority of rocks are pervasively deformed and gneissic; the prefix 'meta' is omitted from rock units for brevity. Samples locations analyzed with SHRIMP U-Pb geochronology are shown with a black dot and their ages of crystallization in green.

Figure 4.4: Representative zircon grains from orthogneiss units outlining the characteristics of inherited, magmatic and metamorphic zircons as defined in the text; A) inherited cores with a well-defined discontinuity between the core and overgrowth material; B) magmatic zircon with well-defined, oscillatory growth zonation, typically at a fine scale; C) metamorphic zircon as unzoned overgrowths on domain 1 zircon; D) metamorphic zircon as ovoid, single weakly sector zoned grains. $^{207}Pb/^{206}Pb$ ages shown in red are interpreted as metamorphic.

Figure 4.5: Summary of 207Pb/206Pb dates from all analyzed zircon from the snow bowl area (SHRIMP) and regional samples (LASS-ICPMS) across the northern portion of the eastern Hall Peninsula orthogneiss complex. Dates used to calculate the weighted mean crystallization age are shown in blue. Zircon zonation is based purely on characterization from BSE images independent of U-Pb date.

Figure 4.6: εHf(t) vs. $^{207}Pb/^{206}Pb$ ages A) for samples from the snow bowl area; B) for regional samples across the northern portion of the eastern Hall Peninsula orthogneiss complex.

Figure 5.1: Regional map of the Quebec-Baffin segment of the Trans-Hudson orogen with ages of crustal amalgamation and proposed suture locations. Hall Peninsula is outlined with a blue polygon. Map modified from Kolb, (2014).

Figure 5.2: Total-field magnetic susceptibility of southern Hall Peninsula in NTS areas 025O, P, I and J (Dumont and Dostaler, 2010a–l), highlighting defined domains and trends reflected in the bedrock geology. Locations of Sm-Nd samples from the southern transect are shown with white circles.

Figure 5.3: Geology of southern Hall Peninsula, Baffin Island, Nunavut showing the distribution of the principal geologic units and the locations of U-Pb age determinations and Sm-Nd isotopic data. The locations of southern and northern transect samples are shown by black circles with their ages of crystallization in green and Nd data in orange and black. Abbreviations: grt, garnet;

bt, biotite; mag, magnetite; opx, orthopyroxene; cpx, clinopyroxene. Map modified from Machado et al. (2013).

Figure 5.4: Back-Scatter Electron images showing representative zircons from the three types recognized consistently throughout the zircon populations: inherited, magmatic and metamorphic.

Figure 5.5: U-Pb Concordia diagrams with examples of zircon morphology and zonation for **a-e)** southern transect samples and **f-j)** northern transect samples. Light grey ellipses represent $^{207}Pb/^{206}Pb$ ages derived from inherited zircon, medium grey ellipses with black rims represent $^{207}Pb/^{206}Pb$ ages derived from magmatic zircon and dark greyish black ellipses represent $^{207}Pb/^{206}Pb$ ages derived from metamorphic zircon. Data point error ellipses are 2σ.

Figure 5.6: A) **ε**Nd(t) vs. $^{207}Pb/^{206}Pb$ age diagram for samples from the southern and the northern transects. B) $^{143}Nd/^{144}Nd$ vs. $^{147}Sm/^{144}Nd$ diagram for samples from the southern and the northern transects.

Figure 5.7: **ε**Hf(t) vs. $^{207}Pb/^{206}Pb$ age diagram for samples from A) the southern transect and B) the northern transect.

Figure 6.1: Summary of existing Archean U-Pb age data from eastern Hall Peninsula and the surrounding Archean blocks. Crustal affinity is shown on the left side with dashed lines indicating an interpreted suture seperating crust with similar Archean geologic histories.

Figure 6.2: Regional crustal correlation model highlighting cratonic affinity and locations of interpreted crustal sutures (shown in red). Dates are in Ga and indicate timing of terrane accretion. CP, Cumberland Peninsula; CZ, Core zone; HP, Hall Peninsula; NAC, North Atlantic craton; MI, Meta Incognita microcontinent; RC, Rae craton. Modified after the full-fit plate reconstruction model of North America - Greenland margins (120 Ma) by Hosseinpour et al., (2013).

Figure 6.3: Simplified regional geologic maps of a) southeast Asia showing a similar size, shape and extent of crustal constituents and intervening sutures to b) northeast Laurentia with revised crustal suture locations presented in this thesis and c) northeast Laurentia from St-Onge et al. (2009). HP, Hall Peninsula; CP, Cumberland Peninsula.

LIST OF TABLES

Table 3.1: Summary of the field relationships presented in Chapter 2 compared to the zircon U-Pb age data for six samples from the snow bowl area.

Table 4.1: Summary of previous U-Pb geochronology work on eastern Hall Peninsula, Nunavut.

Table 4.2: Summary of zircon characteristics, U-Pb geochronology and Lu-Hf isotopic data results from eastern Hall Peninsula.

Table 5.1: Summary of U-Pb geochronology, Lu-Hf and Sm-Nd isotopic data results from southern and northern transects across eastern Hall Peninsula.

Table 6.1: Data summary of Archean terranes with their lithological, structural, metamorphic and isotopic characteristics

COPYWRITED MATIERAL FOR WHICH PERMISSION WAS OBTAINED

Entirety of Chapter 2 and Chapter 3 are reproduced herein (although modified to promote consistency throughout this thesis) with the express permission of the CNGO and NRCAN.

1. Chapter 1. Introduction

1.1. General Introduction

During assembly of supercontinent Columbia, Paleoproterozoic orogenic belts represent convergent boundaries between different Archean provinces (Hoffman, 1988). Seven main Archean crustal blocks were initially recognized as having been amalgamated into Laurentia, a component of supercontinent Columba: Superior, Wyoming, Slave, North Atlantic, Hearne, Rae, and Burwell (Hoffman, 1989). Advances in micro-analytical techniques, which have improved precision and sensitivity, then allowed the recognition of further subdivisions within each of these cratons leading to more refined models of their crustal architecture and inferred geologic processes (e.g., Bethune et al., 2009; Wodicka et al., 2014). These models for how Paleoproterozoic tectonic processes operated can then be compared with tectonic models for Archean accretionary tectonism (e.g., Card, 1990; White et al., 2003) and Cenozoic accretionary tectonism (Yin and Harrison, 1999) drawing inferences on how plate tectonics processes may have evolved throughout geologic time (e.g., St-Onge et al., 2006; Condie and Kröner, 2013).

The Trans-Hudson orogen (THO) of Laurentia, which was originally thought to have welded the Wyoming and Hearne provinces to the Superior province (Hoffman, 1989), is now interpreted to be much more laterally continuous from south central United States to west Greenland (Figure 1.1; St-Onge et al., 2009). The THO represents the convergent margin between the lower plate Archean Superior province and upper plate Churchill province, a collage of Archean crustal blocks including the Wyoming, Slave, Rae, Hearne and North Atlantic cratons (St-Onge et al., 2009). Collision and accretion within the THO

initiated at ca. 1920 Ma and ended with collision between the Superior province and the Churchill province at ca. 1820 to 1795 Ma (Lewry and Collerson, 1990; Corrigan et al., 2009). The Archean components of the THO are typically intensely deformed and metamorphosed having been subjected to multiple episodes of tectonic amalgamation and breakup. Moreover, the level of erosion and exhumation of these Archean blocks or crustal fragments usually exposes their ancient crustal roots. With only a small proportion of preserved Archean rocks and restricted cross-sectional exposure throughout most regions of the THO it is difficult to exactly relate the tectonic processes that must have operated at mid-crustal levels during the Archean to those inferred to have operated during Paleoproterozoic continental collisions or continuing in modern times (Garde and Hollis, 2010).

This thesis aims to provide a characterization of the Archean geology of Hall Peninsula, therefore, a brief examination of the architecture and geologic history of the Paleoproterozoic THO may aid characterization of the Archean rocks as these have been incorporated into and affected by the THO. With the effects of Paleoproterozoic deformation and metamorphism distinguished, these can then be stripped away to examine any older preserved geologic history.

Figure 1.1. Regional geologic compilation map showing the extent of the Trans-Hudson orogen (green portion) throughout North America and Greenland. The lower plate Superior province has promontory points in present day Manitoba (M) and Quebec (Q). Crustal sutures bounding the Archean cratons are shown with black lines with triangles indicating direction of underthrusting (St-Onge et al., 2009).

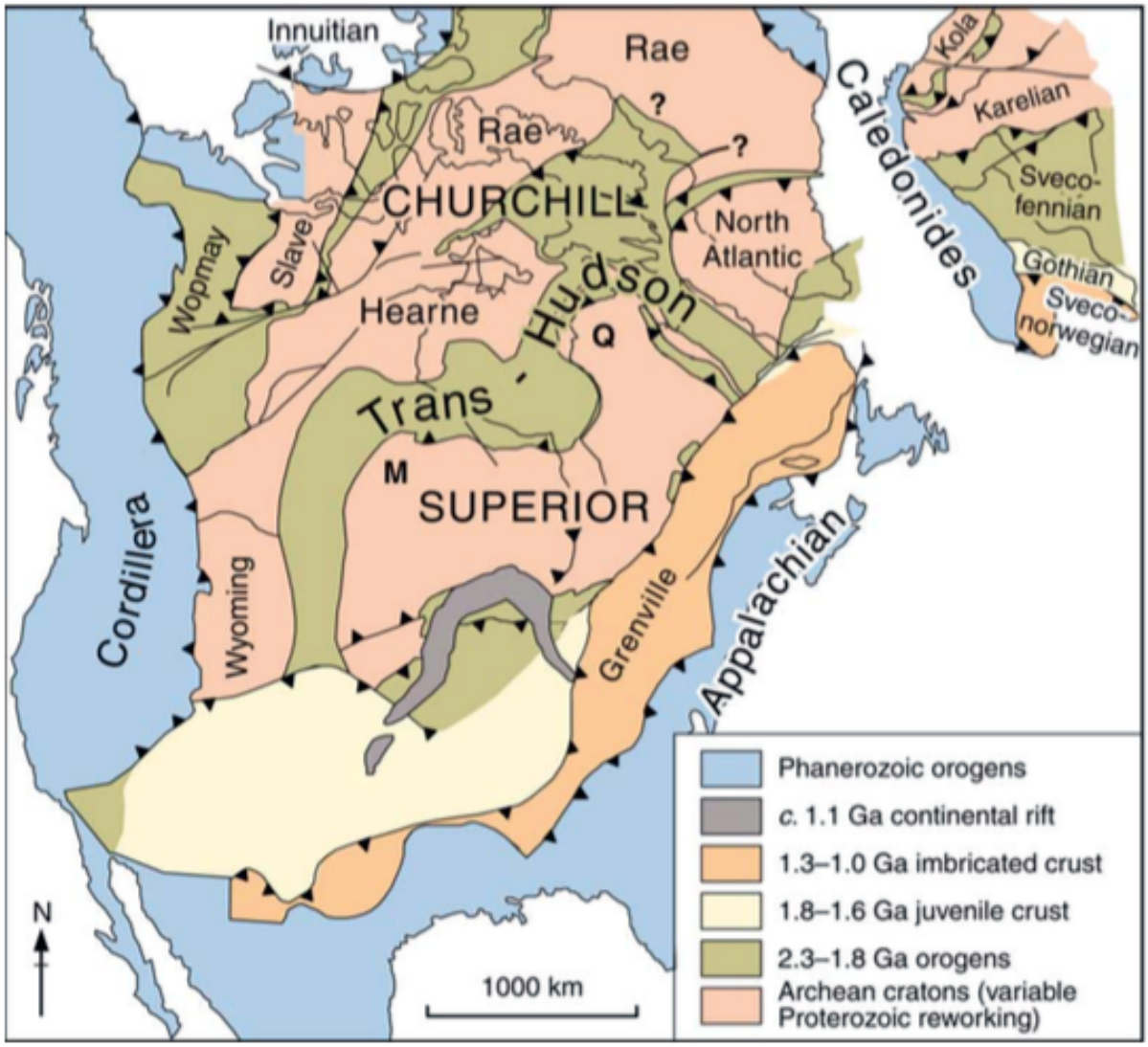

1.1.1. Northern Labrador – Baffin Island – west Greenland segment of the THO

Rocks of the THO, have been documented on northern Labrador, southern Baffin Island and west Greenland on the basis of rocks of similar lithologic, metamorphic and isotopic characteristics (e.g., Scott, 1999; Connelly et al., 2006). In regional compilation studies, this sub-arctic region of the THO has been termed the "Quebec-Baffin" segment and the tectonometamorphic history has largely been determined through previous field mapping, geochemistry and U-Pb geochronology (e.g., St-Onge et al., 2009; Corrigan et al., 2009; Figure 1.2). As a brief summary, on southern Baffin Island, Archean basement and Paleoproterozoic supracrustal rocks interpreted to be part of Meta Incognita microcontinent, accreted to the Rae craton between ca. 1880 and 1870 Ma, likely with a northward dipping subduction polarity (St-Onge et al., 2007). On the southern coast of Baffin Island, a different cratonic block termed the Sugluk block has been delineated based on unique lithological characteristics of rocks, structural orientations and U-Pb isotopic data that indicates underthrusting and accetion to Meta Incognita microcontinent between ca. 1950 to 1850 Ma (St-Onge et al., 2007; Wodicka et al., 2010). This geologic interpretation is consistent with geophysical interpretations that identified a seismic discontinuity and anisotropy indicating the presence subducted crust (Snyder, 2010) in this region. The Archean Sugluk basement exposed on southern Baffin Island is limited to a small area but has been correlated with rocks to the southwest towards continental Canada on the shore of Hudson Bay (Figure 1.2; Corrigan et al., 2009).

Regional metamorphism and crustal shortening of Meta Incognita microcontinent is related to north-dipping subduction and accretion of the Sugluk block by ca. 1850 Ma or

an intervening intra-oceanic arc terrane that may have accreted at ca. 1840 Ma (Figure 1.3; St-Onge et al., 2007; Berman et al., 2013). The Cumberland Batholith (ca. 1865 to 1848 Ma), which straddles Meta Incognita microcontinent and the Rae craton, resulted from continued subduction in this region, and has been variably interpreted as an Andean-type continental arc batholith (St-Onge et al., 2006, 2009) or as a post-accretion batholith resulting from lithospheric mantle delamination and upwelling of asthenospheric mantle following the accretion of Meta Incognita microcontinent to the Rae craton (Whalen et al., 2010). Lastly, the Superior province (lower-plate) accreted to the Churchill province (upper-plate) between ca. 1820 and 1795 Ma marking the end of continental collision in the THO (Wodicka and Scott, 1997; St-Onge et al., 2007).

Understanding the evolution of this segment of the THO is important since it has been compared in numerous aspects to the upper plate Asian continent prior to its early Eocene collision with the lower plate Indian subcontinent (e.g., St-Onge et al., 2006; Figure 1.4). Similarities between these continent-continent orogens in the sequence of plate convergence, subduction, crustal accretion and continental margin arc magmatism along with structural and metamorphic characteristics substantiates the notion of tectonic uniformitarianism for the past 2000 Ma of Earth history. This pattern of continental growth is also an integral part of the global amalgamation process that eventually leads to the formation of supercontinents (Hoffman, 1992) and may be similar to continental growth during Archean tectonic amalgamation.

Figure 1.2. Regional map of the Baffin Island-Northern Labrador-West Greenland segment of the Trans-Hudson orogen with ages of crustal amalgamation and proposed suture locations. Abbreviations: BaS, Baffin suture; BeS, Bergeron suture; DBS Disko Bugt suture; NIS, Nordre Isortoq steep belt; SRS, Soper River suture; TgS, Tasiuyak gneiss structure. Map modified from St-Onge et al. (2009).

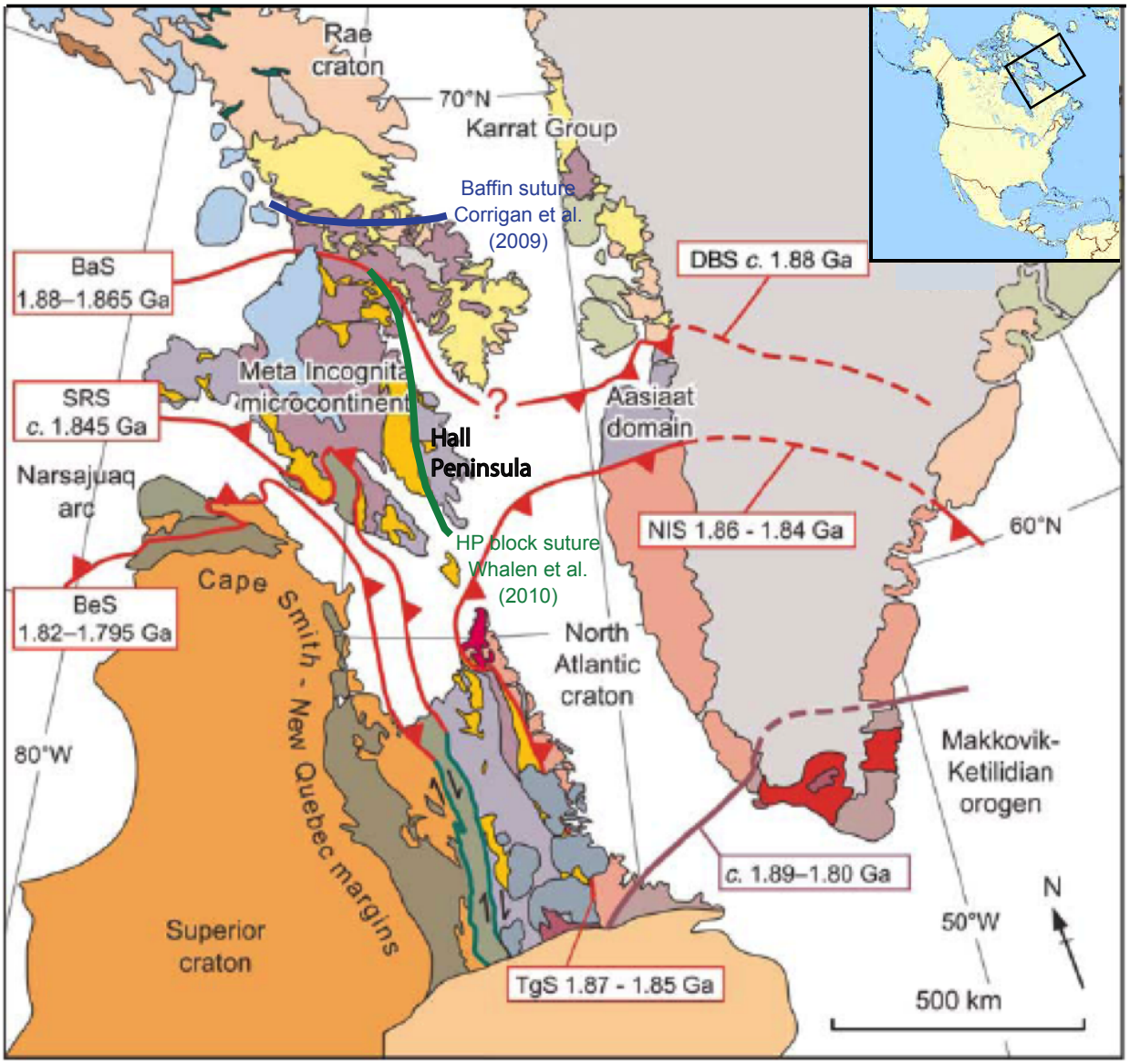

Figure 1.3. Cartoon map illustrating the geological evolution of the THO during the time interval 1.83–1.80 Ga. The location of the Sugluk Block is within the current day Hudson Bay, just prior to it's accretion to Meta Incognita microcontinent. Crustal sutures are shown with thin black lines: BeS, Bergeron suture; BS, Baffin suture; BiS, Big Island suture; Sugluk suture. Abbreviations; GFtz, Great Falls tectonic zone; GLsz, Granville Lake structural zone, LTsz, Lac Tudor shear zone; MHB, Medicine Hat block; PT, Pelican thrust. Modified from Corrigan et al. (2009).

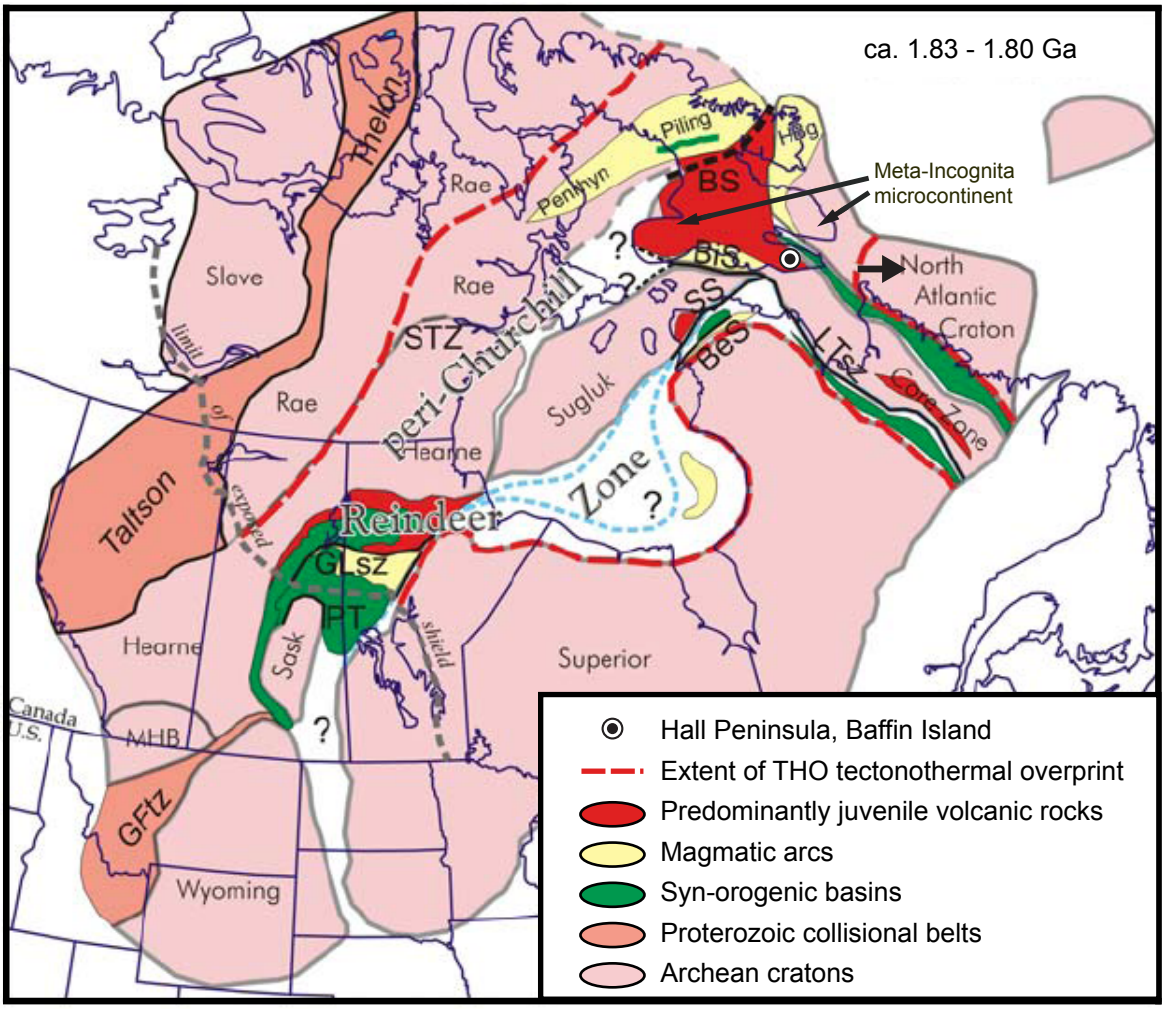

Figure 1.4. Regional geological maps of northeast Laurentia and southeast Asia showing a similar size, shape and extent of crustal constituents and intervening sutures (St-Onge et al., 2009).

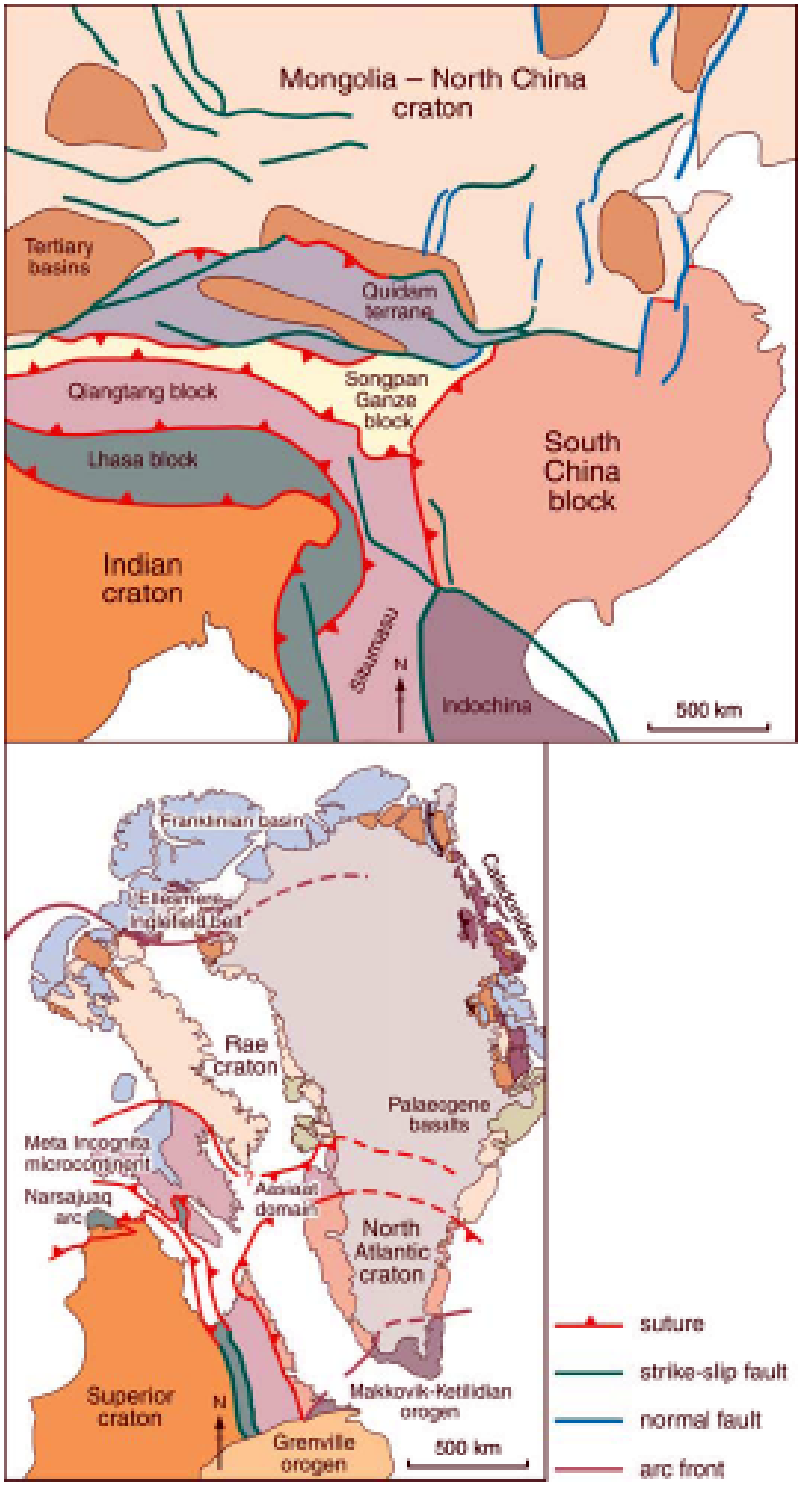

1.1.2. What was Hall Peninsula's role in the history of tectonic amalgamation?

Hall Peninsula has remained an enigmatic crustal domain in the Quebec-Baffin segment of the THO (e.g., Scott and Campbell, 1993; van Gool et al., 2004; Hollis et al., 2006). Some studies have inferred the presence of crustal sutures either:

1. striking north-south through central Hall Peninsula (Figure 1.2; Grocott and Davies, 1999; Whalen et al., 2010), or
2. striking east-west in the north of Hall Peninsula, grouping it as part of Meta Incognita microcontinent (Figure 1.2; Corrigan et al., 2009; St-Onge et al., 2009).

These interpretations were based on reconnaissance-scale mapping of Hall Peninsula by Blackadar in the 1960's (Blackadar, 1967) and along a narrow E-W transect across central Hall Peninsula by Scott in the late 1990's. Scott (1996; 1999) documented Archean gneissic basement rocks on eastern Hall Peninsula with crystallization ages ranging from ca. 2920 to 2700 Ma and Paleoproterozoic supracrustal and plutonic rocks on western Hall Peninsula towards the Meta Incognita microcontinent. These ages are quite different from U-Pb ages of Meta Incognita basement gneisses that have interpreted crystallization ages of ca. 2680, 2630-2600, 2400, 2340-2310 Ma, with only sporadic ages from ca. 3000 to 2850 Ma (Wodicka et al., 2010).

Paleoproterozoic metamorphism on Hall Peninsula has been documented as three events: pre-, syn- and post-deformational (Skipton et al., 2016). On eastern Hall Peninsula, this Paleoproterozoic metamorphism largely overprinted the Archean metamorphic assemblages from granulite-facies to upper amphibolite-facies, with an exception of mafic to ultramafic pods that preserve granulite-facies assemblages in their insulated cores (From et al., 2013; Steenkamp and St-Onge, 2014). The majority of the

gneissic fabric on Hall Peninsula was transposed during Paleoproterozoic deformation, except for local preservation within the Archean orthogneiss complex of at least two orientations of a pervasive, gneissic fabric indicating the presence of a cryptic Archean gneissosity (From et al., 2013).

Airborne magnetic data outline strongly linear features, striking roughly north to south along central Hall Peninsula (Figure 1.5). With an orientation perpendicular to maximum Paleoproterozoic shortening these linear features likely indicate a zone of strong transpressional deformation on Hall Peninsula approximates a separation between Paleoproterozoic rocks to the west and Archean rocks to the east. If correct, this tectonic zone could represent a large-scale structure such as a crustal suture that separates different cratonic blocks that were amalgamated during Paleoproterozoic tectonism (i.e. Meta Incognita micorcontinent to the west, Hall Peninsula to the east).

The Paleoproterozoic supracrustal and intrusive rocks on western Hall Peninsula are lithologically similar to Lake Harbour Group and Cumberland Batholith of Meta Incognita microcontinent, respectively (Scott, 1999). Alternatively, the Paleoproterozoic supracrustal rocks of Hall Peninsula have been correlated to supracrustal rocks within the Tasiuyak gneisses, northern Labrador (Scott, 1999) or within the Aasiaat domain, West Greenland (St-Onge et al., 2009). The eastern Archean basement rocks of Hall Peninsula have also been correlated with the Aasiaat domain, west Greenland. (St-Onge et al., 2009; Garde and Hollis, 2010). However, a definitive correlation to West Greenland is complicated by the fact that the Archean crust of West Greenland has an unknown number of distinct tectonostratigraphic terranes or microcontinents varying in size from tens to hundreds of kilometers (Friend and Nutman, 2005). These crustal terranes have

different geological histories and amalgamated at ca. 2700 Ma (Hollis et al., 2006). The Aasiaat domain has been recently interpreted as one of these microcontinent, separate from the Rae craton to the north and the North Atlantic craton to the south (Kolb, 2014). After recording a structural history different from the eastern coast of Greenland this microcontinent was sandwiched in between the Rae craton, Meta Incognita microcontinent and North Atlantic craton during Paleoproterozoic tectonic amalgamation (Kolb, 2014). Eastern Hall Peninsula is of a comparable size to the Aasiaat domain and shares a similar location within a tectonic zone of amalgamation. These two fragments of Archean crust, amongst others, will continue to be compared throughout this thesis to discern any definitive correlations.

Figure 1.5. Total-field magnetic susceptibility of southern Hall Peninsula in NTS areas 025O, P, I and J (Dumont and Dostaler, 2010a–q), highlighting strongly linear features (in purple) trending approximately north-south down central Hall Peninsula.

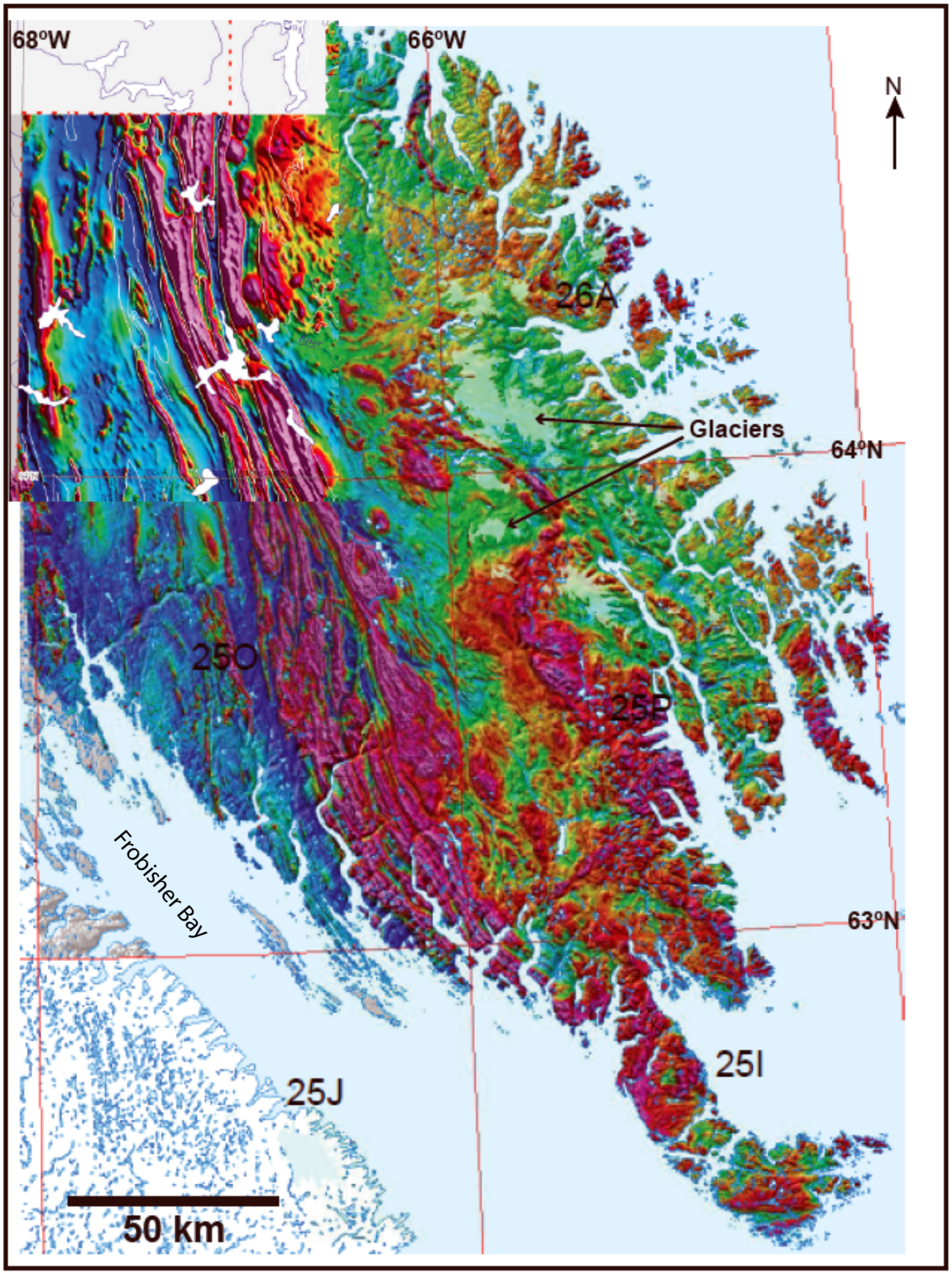

1.2. Objectives and Significance of Research

The objective of this thesis is to provide a lithological, geochemical and geochronological framework for the eastern Archean block of Hall Peninsula, an area that has lacked substantial detailed mapping and isotopic analytical work. This has implications for reconstructing the regional assembly of the Churchill province and contributes to a growing dataset within the Quebec-Baffin segment of the THO. Moreover, a more complete characterization of the geologic history will allow for better informed mineral exploration opportunities given the presence of diamonds (Pell et al., 2013; Nichols et al., 2013), base metals, gem-quality minerals including spinel, apatite, garnet and carvingstone already established on eastern Hall Peninsula (Senkow, 2013; Steenkamp et al., 2014), all of which may be important for Nunavut's future economic development.

Three broad hypotheses and related objectives are as follows:

i) The eastern Archean block of Hall Peninsula is lithologically, geochemically and geochronologically unique from the western portion of Hall Peninsula and potentially to the rest of the Meta-Incognita microcontinent to the west.

- Characterize the lithologic units present throughout the Archean orthogneiss complex of eastern Hall Peninsula.
- Evaluate the complex geology of Archean orthogneisses through detailed mapping of a well-exposed study area.
- Establish an age range for Archean magmatism and metamorphism on eastern Hall Peninsula using U-Pb and Lu-Hf isotopes on zircon.

- Asses the magmatic provence of different units timing of protolith extraction from the mantle and the degreet o which crust has been recycled during the formation of different crustal units.

ii) Relatively undeformed magnetite-bearing plutonic intrusions act as crustal probes into the character of the underlying crust, which may not be exposed at surface.

- Determine crystallization and metamorphic ages of a suite of magnetite-bearing granites.
- Use whole rock Sm-Nd isotopes on magnetite-bearing granitoids along two roughly east-west trending transects to examine spatial trends within the Archean orthogneiss complex and along the boundary with Paleoproterozoic rocks to the west.
- Compare whole-rock Sm-Nd and zircon Lu-Hf data, indentifying any patterns in εNd, εHf and model ages.
- Compare these new Sm-Nd isotopic data to existing data immediately adjacent to the west of Hall Peninsula, on Meta Incognita microcontinent, to determine whether Hall Peninsula and Meta Incognita microcontinent are different crustal blocks.

iii) The Archean orthogneiss complex of Hall Peninsula is related to the Aasiaat domain of west Greenland and potentially other adjacent Archean cratons that may share an Archean geologic history.

- Review literature and make comparisons with the new U-Pb, Lu-Hf and Sm-Nd isotope data from this thesis project.

- Propose a new model of updated crustal correlations within the Quebec-Baffin segment of the THO incorporating recent research in adjacent regions and the results of this thesis project.

1.3. Structure of the thesis

This thesis contains four chapters that are published manuscripts, manuscripts currently under review or manuscripts soon to be submitted for peer review. Together they represent the trajectory of research conducted to ultimately elucidate the Archean geologic history of eastern Hall Peninsula as outlined in Chapter 1.

Chapter 2: *"From, R.E., St-Onge, M. R. and Camacho, A.L. 2014: Preliminary characterization of the Archean orthogneiss complex of Hall Peninsula, Baffin Island, Nunavut: Insights from the "snow bowl" study area; in Summary of Activities 2013, Canada-Nunavut Geoscience Office, p. 53–62"* documents the geology of the Archean orthogneiss complex of eastern Hall Peninsula based on field observations during Hall Peninsula Integrated Geoscience Project geological mapping in 2012 and 2013. This article includes a structural and metamorphic analysis, and economic considerations establishing a framework upon which studies presented in Chapters 3, 4 and 5 are built upon.

Chapter 3: *"From, R.E., Rayner, N. and Camacho, A. 2016: Archean magmatism and metamorphism of eastern Hall Peninsula, southern Baffin Island, Nunavut; in Summary of Activities 2015, Canada-Nunavut Geoscience Office, p. 73–88"* presents the results from detailed mapping and U-Pb geochronological study within the snow bowl area in central Hall peninsula. Eight rock types were identified along a 600m transect,

highlighting the previously unrecognized heterogeneity of the Archean orthogneiss complex of eastern Hall Peninsula. Zircons from six orthogneiss samples were analyzed with the SHRIMP II housed at the Geological Survey of Canada. Crystallization ages range between ca. 2.98 to 2.75 Ga and metamorphic-overprint ages range between ca. 2.74 to 2.68 Ga.

Chapter 4: *"From, R.E., Camacho, A., Pearson, D.G. and Luo, Y. In review. U-Pb and Lu-Hf isotopes of the Archean orthogneiss complex on eastern Hall Peninsula, southern Baffin Island, Nunavut: identification of exotic Paleo- to Mesoarchean crust beneath eastern Hall Peninsula. Precambrian Research"* builds upon the work in Chapter 3 by analyzing the same zircon grains used for U-Pb geochronology for Lu-Hf isotopes to assess the magmatic provenance of the rocks from the snow bowl area and regionally representative samples. The rocks of the orthogneiss complex, eastern Hall Peninsula appear to be well-represented in the snow bowl area with tonalitic to monzogranitic rock units having crystallization ages from ca. 2975 to 2720 Ma. Further evidence of Archean metamorphism was documented as unzoned zircon rims and single grains throughout the orthogneiss complex further narrowing the time of metamorphism to ca. 2.74 to 2.70 Ga. εHf(t) data indicate that magmatic rocks older than ca. 2.74 Ga were likely derived from the recycling of crust whose protolith melt was extracted from the depleted mantle at ca. 3.1 Ga. Two orthogneiss samples with negative εHf(t) and older mean model ages of ca. 3.4 to 3.3 Ga indicate derivation from the recycling of older, potentially exotic, crust not observed on eastern Hall Peninsula.

Chapter 5: *"From, R.E., Camacho, A., Pearson, D.G. and Luo, in preparation. Eastern Hall Peninsula as an Archean microcontinent fragment unique from Meta*

Incognita microcontinent: an integrated study using U-Pb, Lu-Hf and Sm-Nd isotopes. Chemical Geology". Whole rock Sm-Nd isotopes are used to test whether relatively undeformed, magnetite-bearing monzogranites probe the underlying basement rocks. The εNd(t) signatures show a definite trend from west to east across central and eastern Hall Peninsula indicating significant crustal recycling or magma mixing in the west along a boundary zone between Paleoproterozoic and Archean rocks and more juvenile, mantle-derived rocks towards the east within the Archean orthogneiss complex. This could indicate the presence of a cryptic suture zone where partial melting and crustal contamination may have occurred during an Archean crustal amalgamation event or during Paleoproterozoic accretion of eastern Hall Peninsula and the Meta Incognita microcontinent. This paper will be submitted to the journal of Chemical Geology in October, 2017.

Finally, Chapter 6 provides a summary of this Ph.D. thesis research, highlights it's significance and synthesizes the data to further develop the geologic history of eastern Hall Peninsula in a regional context and it's role in regional tectonic assembly. Opportunities for future work are also discussed.

An list of useful definitions and equations used for data calculations has been assembled in APPENDIX 1A for reference throughout this thesis.

1.4. References

Bethune, K.M., Berman, R.G., Rayner, N. and Ashton, K.E. 2013. Structural, petrological and U–Pb SHRIMP geochronological study of the western Beaverlodge domain: Implications for crustal architecture, multi-stage orogenesis and the extent of the Taltson orogen in the SW Rae craton, Canadian Shield. Precambrian Research, v. 232, p. 89-118.

Berman, R.G., Sanborn-Barrie, M., Rayner, N. and Whalen, J. 2013. The tectonometamorphic evolution of Southampton Island, Nunavut: Insight from petrologic modeling and in situ SHRIMP geochronology of multiple episodes of monazite growth. Precambrian Research, v. 232, p. 140–166.

Blackadar, R.G. 1967. Geological reconnaissance, southern Baffin Island, District of Franklin. Geological Survey of Canada, Paper p. 66–47.

Card, K.D. 1990. A review of the Superior Province of the Canadian Shield, a product of Archean accretion. Precambrian Research, v. 48, p. 99-156.

Condie, K.C. and Kröner, A. 2013. The building blocks of continental crust: evidence for a major change in the tectonic setting of continental growth at the end of the Archean. Gondwana Research, v. 23, p. 394-402.

Connelly, J. N. 2001. Constraining the timing of metamorphism: U–Pb and Sm–Nd ages from a transect across the northern Torngat Orogen, Labrador, Canada. Journal of Geology, v. 109, p. 57–77.

Corrigan, D., Pehrsson, S., Wodicka, N., and Kemp, E. 2009. The Palaeoproterozoic Trans-Hudson Orogen: a prototype of modern accretionary processes. Geological Society, London, Special Publication, v. 327, p. 457–479.

Friend, C. R. L. and Nutman, A. P. 2005. New pieces to the Archaean terrane puzzle in the Nuuk region, southern West Greenland: Steps in transforming a simple insight into a complex

regional tectonothermal model, Journal of the Geological Society, London, v. 162, p. 147-162.

Garde, A.A. and Hollis, J.A. 2010. A buried Palaeoproterozoic spreading ridge in the northern Nagssugtoqidian orogen, West Greenland. Geological Society, London, Special Publications, v. 338, p. 213-234.

Grocott, J., Davies, S.C. 1999. Deformation at the southern boundary of the late Archaean Atâ tonalite and the extent of Proterozoic reworking of the Disko terrane, West Greenland. Precambrian geology of the Disko Bugt region, West Greenland. Geology of Greenland Survey Bulletin, v. 181, p. 155-169.

Hoffman, P.F. 1988. United Plates of America, the birth of a craton: Early Proterozoic assembly and growth of Laurentia. Annual Review of Earth and Planetary Sciences, v. 16, p. 543–603.

Hoffman, P.F., 1989. Precambrian geology and tectonic history of North America. The Geology of North America (textbook), p. 447-512.

Hoffman, P. F. 1992. Supercontinents. In: Brekhovs- Kikh, L., Turekian, K. K., Emery, K. and Tseng, C. K. (eds) Encyclopedia of Earth System Science, 4, Academic Press, London, p. 323–328.

Hollis, J. A., Keiding, M., Møller Stensgaard, B., Van Gool, J. A. M. and Garde, A. A. 2006. Evolution of Neoarcheaean supracrustal belts at the northern margin of the North Atlantic craton, West Greenland, Geological Survey of Denmark and Greenland Bulletin, v. 11, p. 9-31.

Kolb, J. 2014. Structure of the Palaeoproterozoic Nagssugtoqidian Orogen, South-East Greenland: model for the tectonic evolution. Precambrian Research, v. 255, p. 809-822.

Lewry, J.F. and Collerson, K.D. 1990. The Trans-Hudson Orogen: extent, subdivisions and problems. in Lewry, J.F. and Stauffer, M.R. (Eds.), The Early Proterozoic Trans-Hudson Orogen of North America, Geological Association of Canada, Special Paper 37, p. 1–14.

Nichols, K.M.A., Stachel, T., Stern, R.A., Pell, J.A. and Mate, D.J. 2014. Diamond sources beneath the Hall Peninsula, Baffin Island, Nunavut: an update of the preliminary assessment. in Summary of Activities 2013, Canada-Nunavut Geoscience Office, p. 20-26.

Pell, J., Grütter, H., Neilson, S., Lockhart, G., Dempsey, S. and Grenon, H. 2013. Exploration and discovery of the Chidliak kimberlite province, Baffin Island, Nunavut: Canada's newest diamond district. in Proceedings of 10th International Kimberlite Conference (pp. 209-227). Springer India.

Scott, D.J. 1999. U-Pb geochronology of the eastern Hall Peninsula, southern Baffin Island, Canada: a northern link between the Archean of West Greenland and the Paleoproterozoic Torngat Orogen of northern Labrador. Precambrian Research, v. 93, p. 5–26.

Scott, D.J. and Campbell, L.M. 1993. Evolution of the Paleoproterozoic Torngat orogen, Labrador Canada: recent advances using U–Pb geochronology and Nd isotopic systematics (abstr); Geological Society of America Abstract with Programs, v. 25, A237

Senkow, M.D. 2013. Characterization of ultramafic occurrences on southern Hall Peninsula, Baffin Island, Nunavut, and evaluation of their potential as a source of carving stone. in Summary of Activities 2012, Canada-Nunavut Geoscience Office, p. 163–168.

Skipton, D.R., Schneider, D.A., McFarlane, C.R.M., St-Onge, M.R. and Jackson, S.E. 2016. Multi-stage zircon and monazite growth revealed by depth profiling and in situ U–Pb geochronology: Resolving the Paleoproterozoic tectonics of the Trans-Hudson Orogen on southeastern Baffin Island, Canada. Precambrian Research, v. 285, p. 272-298.

St-Onge, M.R., Searle, M.P. and Wodicka, N. 2006. Trans-Hudson Orogen of North America and Himalaya–Karakorum–Tibetan Orogen of Asia: structural and thermal characteristics of the lower and upper plates. Tectonics, v. 25, p. 1–22.

St-Onge, M.R., Wodicka, N. and Ijewliw, O. 2007. Polymetamorphic evolution of the Trans-Hudson Orogen, Baffin Island, Canada: integration of petrological, structural and geochronological data. Journal of Petrology, v. 48, p. 271–302.

St-Onge, M.R., Van Gool, J.A.M., Garde, A.A. and Scott, D.J. 2009. Correlation of Archaean and Palaeoproterozoic units between northeastern Canada and western Greenland: constraining the pre-collisional upper plate accretionary history of the Trans-Hudson Orogen. Geological Society of London Special Publication 318, p. 193–235.

Steenkamp, H.M., Bros, E.R. and St-Onge, M.R. 2014. Altered ultramafic and layered mafic-ultramafic intrusions: new economic and carving stone potential on northern Hall Peninsula, Baffin Island, Nunavut. in Summary of Activities 2013, Canada-Nunavut Geoscience Office, p. 11-20.

Thrane, K. and Connelly J.N. 2006. Zircon geochronology from the Kangatsiaq-Qasigiannguit region, the northern part of the 1.9–1.8 Ga Nagssugtoqidian orogen, West Greenland; Geological Survey of Denmark and Greenland, Bulletin 11, p. 87–99.

Van Gool, J.A.M., Garde, A.A. and Larsen, L. M. 2004. Correlation of Precambrian geology in Labrador and southern Greenland; Danmarks og Grønlands Geologiske Under- søgelse Rapport, 2004/29, 30 p.

Wardle, R.J., James D.T., Scott, D.J. and Hall, J. 2002. The southeastern Churchill Province: synthesis of a Palaeoproterozoic transpressional orogen; Canadian Journal of Earth Sciences, v. 39, p. 639–663. doi:10.1139/E02-004

Whalen, J.B., Wodicka, N., Taylor, B.E. and Jackson, G.D. 2010. Cumberland Batholith, Trans-Hudson Orogen, Canada: Petrogenesis and implications for Paleoproterozoic crustal and orogenic processes. Lithos, v. 117, p. 99-118.

White, D.J., Musacchio, G., Helmstaedt, H.H., Harrap, R.M., Thurston, P.C., Van der Velden, A. and Hall, K. 2003. Images of a lower-crustal oceanic slab: Direct evidence for tectonic accretion in the Archean western Superior province. Geology, v. 31, p. 997-1000.

Wodicka, N., Scott, D.J. 1997. A preliminary report on the U–Pb geochronology of the Meta Incognita Peninsula, southern Baffin Island, Northwest Territories. Geological Survey of Canada Paper 1997-C, p. 167–178.

Wodicka, N., St-Onge, M.R., Corrigan, D., Scott, D.J. and Whalen, J.B. 2014. Did a proto-ocean basin form along the southeastern Rae cratonic margin? Evidence from U-Pb geochronology, geochemistry (Sm-Nd and whole-rock), and stratigraphy of the Paleoproterozoic Piling Group, northern Canada. Geological Society of America Bulletin, v. 126, p. 1625-1653.

Wodicka, N., Whalen, J., St-Onge, M.R., Corrigan, D. 2010. Meta Incognita microcontinent revisited: insights from U–Pb geochronology and Nd isotopes. Geological Association of Canada – Mineralogical Association of Canada Abstract Volume 35.

Yin, A. and Harrison, T.M. 2000. Geologic evolution of the Himalayan-Tibetan orogen. Annual Review of Earth and Planetary Sciences, v. 28, p. 211-280.

1.5. *Data appendices*

APPENDIX 1A - Reference list of useful definitions and equations.

APPENDIX 1A - Reference list of useful definitions and equations.

mantle: Highly viscous layer directly under the crust, and generated directly from the convecting mantle.

crust: outermost layer of solid rocks creating a shell around planet Earth or of any other planet or moon. Crust can be further differentiated into continental or oceanic type based on composition and geologic setting.

juvenile magma: Generated directly from the convecting mantle.

crustal recycling / recycled magma: generated from the re-melting of older crust.

mantle extraction: The process by which a partial melt from separates from the depleted mantle reservoir and ascends into the middle to lower crust.

crustal recycling: The process by which existing crust is re-melted and incorporated in the process of subsequent crust production.

parental magma: A volume of magma with a specific composition that eventually crystallizes into crust (continental or oceanic).

crustal residence age: The time elapsed since a piece of crust was formed from its parental magma

CHUR: An acronym for Chondritic Uniform Reservoir which is the experimentally derived composition of meteorites thought to represent the original composition of the Earth-Mantle system at initial formation.

εHf and εNd : A specific notation comparing the measured $^{176}Hf/^{177}Hf$ or $^{143}Nd/^{144}Nd$ to known CHUR values.

$$\varepsilon Hf = [\ (^{176}Hf/^{177}Hf)_{sample} / (^{176}Hf/^{177}Hf)_{chondrites} - 1\ ] \times 10^4$$

$$\varepsilon Nd = [\ (^{143}Nd/^{144}Nd)_{sample} / (^{143}Nd/^{144}Nd)_{chondrites} - 1\ ] \times 10^4$$

+ ε results: A result of high $^{176}Hf/^{177}Hf$ or $^{143}Nd/^{144}Nd$ values typically interpreted to imply a juvenile origin for the magma.

- ε results: A result of high $^{176}Hf/^{177}Hf$ or $^{143}Nd/^{144}Nd$ values typically interpreted to imply the reworking of older crustal material.

magma mixing: An interaction between juvenile and recycled magmas, which may crystallize into crust, giving rise to a mixed Hf signature.

Nd Depleted Mantle model age (T_{DM}Nd): An age representing the time elapsed between the formation of crust and the time at which it's parental magma was extracted from the mantle.

$$\mathbf{T_{DM}Nd} = 1/\lambda * LN(((^{143}Nd/^{144}Nd)_{sample} - {}^{143}Nd/^{144}Nd)_{DM})/((^{147}Sm/^{144}Nd)_{sample} - (^{147}Sm/^{144}Nd)_{DM}) + 1)$$

Hf Depleted Mantle "crustal" model age (T_{DM}Hf): An age representing the time elapsed between the crystallization of a zircon from it's parental magma, which is presumed to have been produced from a volume of average continental crust that was originally derived from the depleted mantle.

$$\mathbf{T_{DM}Hf} = ((1/\lambda * LN((((^{176}Hf/^{177}Hf)_{DM(t)} - (^{176}Hf/^{177}Hf)_{SAMPLE(t)})/((^{176}Lu/^{177}Hf)_{DM} - 0.0113)) + 1)/t)/1000$$

2. Chapter 2. Preliminary characterization of the Archean orthogneiss complex of Hall Peninsula, Baffin Island, Nunavut: Insights from the "snow bowl" study area.°

This chapter is based on fieldwork within the Archean orthogneiss complex of Hall Peninsula, Baffin Island during the 2012-13 Hall Peninsula Integrated Geoscience Project (HPIGP). Regional scale mapping (1:250 000) and detailed mapping (1:6000) in a well-exposed study area (termed the snow bowl area) documented seven different Archean rock units. In addition to lithological descriptions of orthogneiss units, the structural and metamorphic characteristics of the snow bowl area give insight into the Archean geologic history of eastern Hall Peninsula. Presented here is an essential framework of geological observations from which further studies are built upon. I was responsible for sample collection and analyses, creation of all figures, and the writing. My co-authors assisted with fieldwork and sample collection and reviewed drafts of the article, which is published in the 2013 edition of the CNGO Summary of Activities volume (see citation below) and is reproduced herein with express permission from the CNGO and NRCAN. This version of the article is re-formatted and in some cases re-written for consistency of the thesis.

From, R.E., St-Onge, M. R. and Camacho, A.L. 2014: Preliminary characterization of the Archean orthogneiss complex of Hall Peninsula, Baffin Island, Nunavut: Insights from the "snow bowl" study area; *in* Summary of Activities 2013, Canada-Nunavut Geoscience Office, p. 53–62

2.1. Abstract

Archean gneissic rocks of the "snow bowl" study area, Hall Peninsula, Baffin Island, were mapped at a scale of 1:6000 along a 600-metre transect. The snow bowl area was selected for its spectacular exposures of continuous, lichen free outcrops within the Archean orthogneiss complex of Hall Peninsula. Mapping delineated seven distinct lithological units within the orthogneiss complex. Unequivocal cross-cutting relationships observed in the field were vital in establishing age relationships. A unit of porphyroclastic monzogranite dominates the snow bowl area, entraining older units of magnetite-bearing monzogranite, ribbon granite, mafic monzogranite, leopard gneiss, grey tonalite gneiss and pyroxene diorite. The dominance of monzogranite in this locality is unique from the general character of the Hall Peninsula orthogneiss complex, which was previously mapped as mostly tonalite with monzogranite gneiss (Blackadar, 1967; Scott, 1996). Petrography, petrology, geochemistry, geochronology and Lu-Hf isotopic work will be the first stage in developing a fingerprint for the Archean orthogneiss complex of Hall Peninsula allowing comparison to adjacent Archean terrains and providing insight into paleo-plate reconstructions for the Baffin Island and sub-Arctic region.

2.2. Introduction

This study is part of the Canada-Nunavut Geoscience Office's (CNGO) Hall Peninsula Integrated Geoscience Program (HPIGP), a multiyear bedrock and surficial geology mapping program with associated thematic studies (e.g., Creason et al., 2012;

Leblanc-Dumas et al., 2012; MacKay et al., 2012; Skipton et al., 2012). In the summer of 2013, the northern portion of Hall Peninsula (NTS 26A, B) was mapped at 1:250 000-scale completing the 2-year HPIGP field work (Figure 2.1).

A transition in dominant rock types from the eastern to the western portion of Hall Peninsula was documented during the 2012 and 2013 field seasons. Steenkamp et al., (2014) provide an overview of the geology of Hall Peninsula and a brief outline is presented herein. The eastern portion of Hall Peninsula is dominated by an Archean TTG (tonalite-trondhjemite-granodiorite) plutonic suite that hosts tectonically interleaved panels of Paleoproterozoic metasedimentary rocks (Scott, 1999; Rayner, 2014). The western portion of Hall Peninsula is dominated by a plutonic suite of granodiorite to orthopyroxene-bearing monzogranite with intervening metasedimentary panels; the plutonic suite and the metasedimentary rocks are both inferred to be Paleoproterozoic (Scott, 1999; Rayner, 2014).

This article focuses on the multitude of metamorphosed, plutonic units that dominate the geographically eastern portion of Hall Peninsula referred to herein as the Archean orthogneiss complex of Hall Peninsula. The Archean orthogneiss complex is very similar in age and appearance to Archean tonalitic to granitic gneiss found elsewhere throughout Baffin Island and the sub-Arctic region (St-Onge et al., 2009). Characterizing the Archean rocks of Hall Peninsula will allow comparison and correlation with similar age rocks in the surrounding cratonic blocks (e.g., Rae craton, Meta Incognita microcontinent, Aasiaat domain, North Atlantic craton) and better define the regional tectonic assembly of northeastern Laurentia. This work will include petrography,

Figure 2.1. Compilation map of Hall Peninsula from mapping during the 2012 and 2013 field seasons showing the distribution of principal tectonostratigraphic units. The snow bowl area is shown with a white star in red circle.

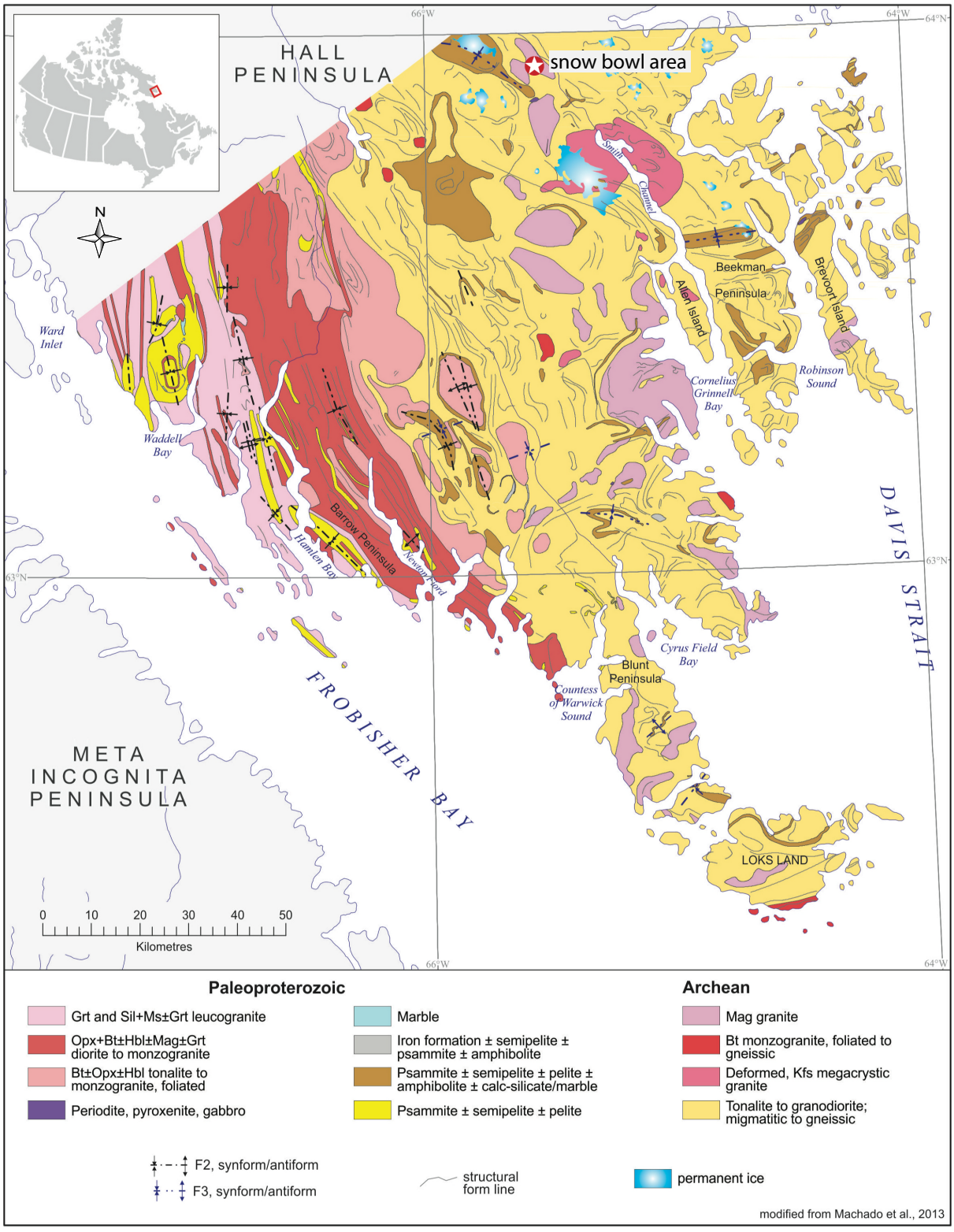

petrology, geochronology, whole-rock and isotope geochemistry of selected samples and is the first stage in characterizing this Archean terrain.

2.3. Geological background and previous work

The Archean orthogneiss complex of Hall Peninsula was previously described by Blackadar (1965), Scott (1996, 1999) and From et al. (2013). These orthogneisses are broadly similar in U-Pb ages, lithological characteristics and texture to Archean tonalitic to granitic gneiss found elsewhere throughout Baffin Island and the surrounding sub-Arctic region (St-Onge et al., 2009). Previous work in adjacent terranes has elucidated the nature of different crustal blocks, although there are multiple working hypotheses on the location of intervening sutures (Figure 2.2) due to, in part, the absence of detailed geological work on Hall Peninsula (Corrigan et al., 2009; St-Onge et al., 2009; Whalen et al., 2010). Based on lithological similarities, geochronology, geochemistry and aeromagnetic characteristics, the Archean rocks of central and northern Baffin Island have been correlated with the Rae craton of the north-central Canadian Shield and northwestern Greenland (Hoffman, 1988). Archean rocks of the Meta Incognita microcontinent documented in southern Baffin Island may correlate with the Aasiaat domain of west-central Greenland (Hollis et al., 2006; Thrane and Connelly, 2006; St-Onge et al., 2009). Other correlations between the Nain craton of northern Labrador and the North Atlantic craton of southern Greenland have also been proposed (van Gool et al., 2004). In addition, Paleoproterozoic Lake Harbour Group metasedimentary rocks have been correlated from the Meta Incognita microcontinent to the south and into the core zone of northern Labrador and northeastern Quebec (Knight and Morgan, 1981; Scott and

Figure 2.2. Compilation map of Baffin Island, which predates the initiation of the CNGO Hall Peninsula project, showing the alternative hypotheses for suture locations on Baffin Island with specific convergence on Hall Peninsula. Abbreviations: B, Borden basin; F, Franklinian basin; FH, Fury and Hecla basin; HP, Hall Peninsula. Map modified from St-Onge et al., 2009).

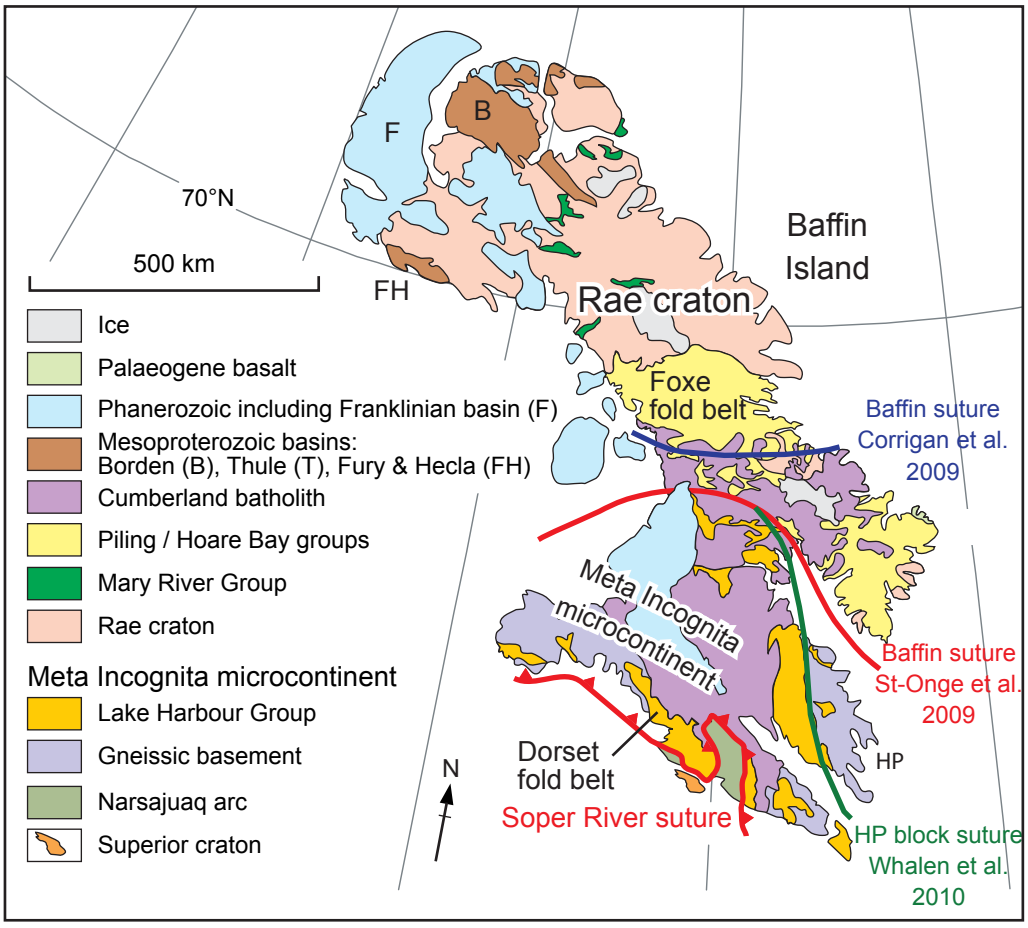

Gauthier, 1996, Scott, 1999). Archean rocks of eastern Hall Peninsula have yet to be unequivocally correlated with any of the surrounding crustal blocks and remain enigmatic in terms of how they fit into the regional tectonic assembly of the Baffin Island region. Correlating the Archean orthogneiss complex of Hall Peninsula with the adjacent crustal blocks, such as the Meta Incognita microcontinent to the west (St-Onge et al., 2009), the Rae craton to the north, the Aasiaat domain of central West Greenland to the east (Hollis et al., 2006; Thrane and Connelly, 2006), the Nain craton to the south (Scott and Campbell, 1993; Scott, 1999; Connelly, 2001; Wardle et al., 2002) or presenting it as a unique and distinct microcontinent will directly assess its role in the continually developing story of tectonic assembly for the sub-Arctic region.

Analytical work on the Hall Peninsula orthogneiss complex has been carried out by Scott (1999) and Rayner (2014). U-Pb zircon geochronology by Scott (1999) produced U-Pb ages ranging from 2920 to 2797 +8/-15 Ma, which were interpreted as magmatic. Geochronology by Rayner (2014) utilized the Sensitive High Resolution Ion MicroProbe (SHRIMP) U-Pb technique on zircon grain separates from a tonalite gneiss and K-feldspar porphyritic granite located on the Beekman Peninsula (Figure 2.1). Zircons from the tonalite gneiss sample yielded a weighted mean age of 2841 ±3 Ma, which is interpreted to be the crystallization age of the rock (Rayner, 2014). In contrast, a sample of strongly deformed, K-feldspar porphyritic granite collected about 40 km west of Allen Island (Figure 2.1) has a crystallization age of 2701±2 Ma (Rayner, 2014). These preliminary results confirm the general extent of Archean U-Pb ages for the eastern orthogneiss complex. In addition, Scott (1999) and Rayner (2014) indicate the possibility of tectonothermal overprints at ca. 2770, 2700 and between ca. 1856 and 1736 Ma.

2.4. Geology of the "snow bowl" study area

The "snow bowl" study area, herein referred to as the snow bowl area, is located in the central region of Hall Peninsula wholly within the orthogneiss complex of Hall Peninsula as described by From et al. (2013) (Figure 2.1). The majority of rocks are metamorphosed, pervasively deformed and gneissic in character and the term meta is omitted from the rock names for brevity. The snow bowl area was chosen due to the absence of lichen over most of the bedrock. One day was dedicated to mapping a 1:6000-scale transect in a SW to NE direction, which documented eight plutonic units within the orthogneiss complex (Figure 2.3). The lithological units are described from oldest to youngest below based on field observations and thin section analysis.

2.4.1. Description of lithological units

2.4.1.1. Unit 1: Pyroxene diorite

Unit 1 consists of clinopyroxene ± orthopyroxene bearing diorite that is locally varied to quartz diorite. The rocks are grey to reddish brown on the weathered surface and have a dark grey to black fresh surface. Typically, the rocks are fine grained having local concentrations of clinopyroxene ± orthopyroxene. This unit occurs as centimeter-scale enclaves to metre-scale panels within some of the younger, units (Figure 2.4a).

2.4.1.2. Unit 2: Grey tonalite gneiss

Unit 2 consists of a grey, biotite and hornblende-bearing tonalite. The rocks are distinctly grey weathering and have a salt-and-pepper fresh surface. The rocks are fine to medium grained having thin (mm scale) trondhjemitic segregations (Figure 2.4b) and

Figure 2.3. Preliminary geological map of the snow bowl area; regional location shown in Figure 2.1. The legend lists units from oldest (1) to youngest (7). The numbered locations refer to locations of outcrops shown in Figures 2.4 and 2.5.

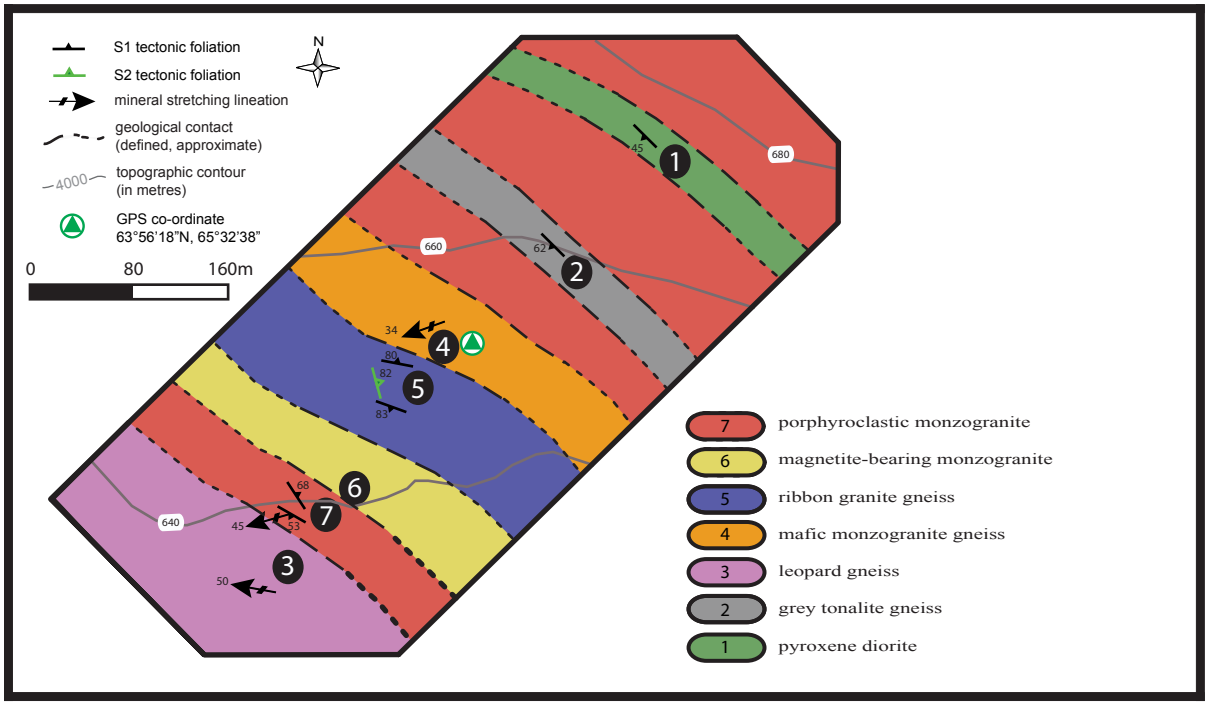

Figure 2.4. Field photographs from the study area. Unit numbers and color codes correspond to those of Figure 2.3 and are shown in the bottom right of each photograph. a) Unit 1 fine grained pyroxene diorite that occurs as a 5-10m wide panel within Unit 7; b) Unit 2 medium grained grey tonalite gneiss with thin trondhjemitic segregations. c) Unit 2 medium grained grey tonalite gneiss intruded by monzogranitic veining mm to 10's of cm in width. d) Unit 3 medium grained leopard gneiss with plagioclase phenocrysts. e) Unit 3 leopard gneiss characterized by fine-grained enclaves of hornblende + biotite + epidote quartz diorite. f) Mafic monzogranite of Unit 4 containing abundant clinopyroxene and orthopyroxene-bearing mafic enclaves and discontinuous layering.

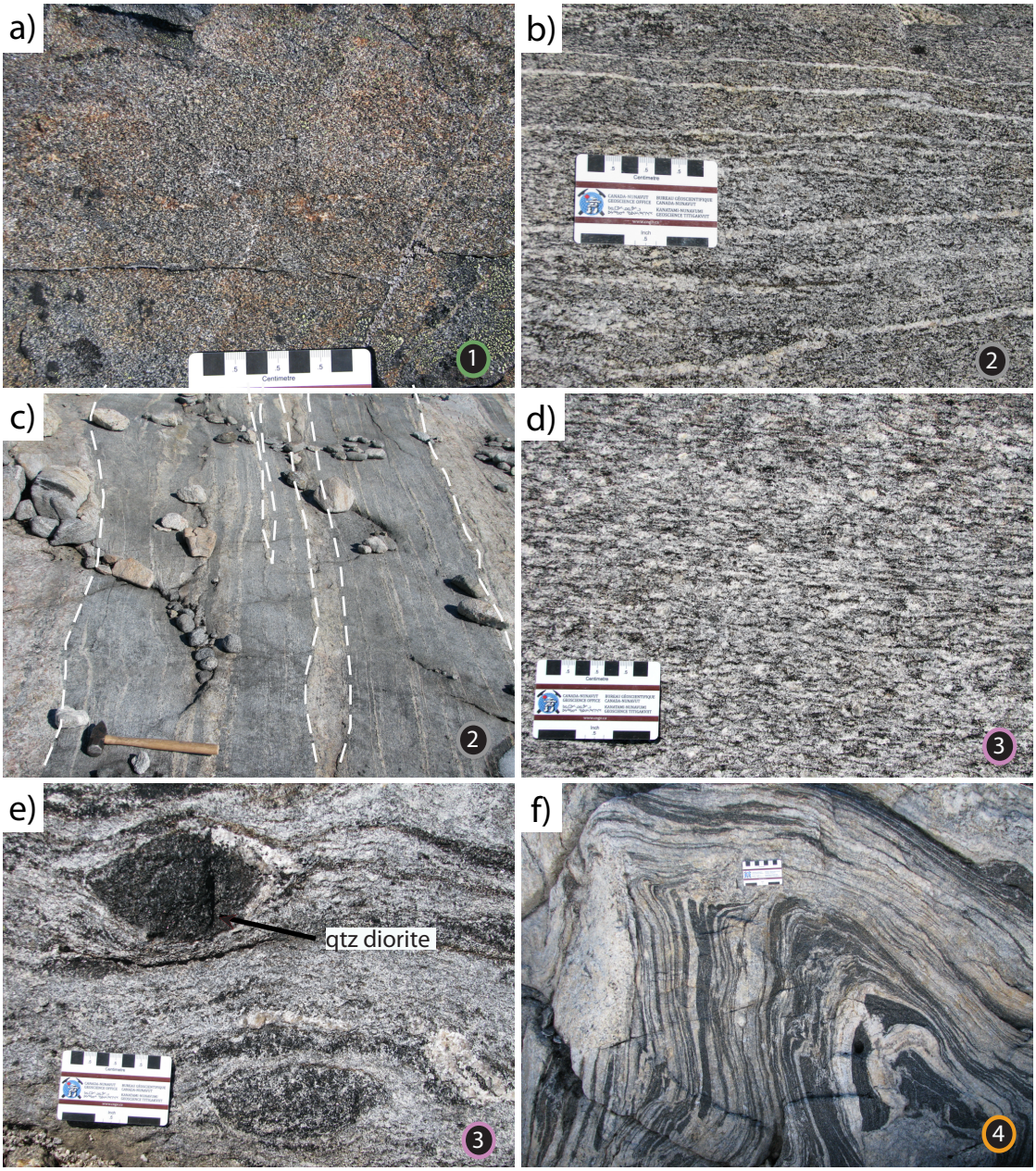

boudinaged relicts of Unit 1 pyroxene diorite. Monzogranitic to syenogranitic rocks, (units 7 and 8), intrude Unit 2 tonalite gneiss parallel to gneissosity (Figure 2.4c).

2.4.1.3. Unit 3: Leopard gneiss

Unit 3 consists of a hornblende + biotite + epidote megacrystic granodiorite that is informally named the "Leopard gneiss" based on its archetypal leopard-like spotted appearance. The rocks are black and white on the weathered and fresh surfaces. They are medium to coarse grained and commonly have an L-tectonite fabric defined by elongated, relict plagioclase phenocrysts (Figure 2.4d). The plagioclase phenocrysts are commonly surrounded by hornblende and locally by K-feldspar phenocrysts. This unit is further characterized by entrained, fine-grained enclaves of hornblende + biotite + epidote quartz diorite very similar to the composition of Unit 1 (Figure 2.4e).

2.4.1.4. Unit 4: Mafic monzogranite gneiss

Unit 4 consists of biotite and hornblende-bearing monzogranite containing abundant mafic enclaves. The rocks are typically whitish grey to black on the weathered and fresh surfaces and are fine to medium grained. Unit 4 is distinguished by an abundance of mafic material occurring as angular enclaves and discrete layers creating a black-and-white stripped gneissosity. The mafic material is biotite ± clinopyroxene ± orthopyroxene quartz diorite that is provisionally correlated with Unit 1. The gneissosity in Unit 4 rocks is irregularly and complexly deformed (Figure 2.4f).

2.4.1.5. Unit 5 : Ribbon granite gneiss

Unit 5 consists of a hornblende and biotite-bearing monzogranite. The rocks are reddish grey to black on the weathered and fresh surfaces. The rocks ares fine to medium

grained and have hornblende quartz diorite schlieren similar to Unit 1 in composition and cross-cutting felsic monzogranite and syenogranite veins (cm-scale). As its name suggests, the unit is characterized by a "ribbon" layering texture defined by alternating pinkish, grey and black layers of K-feldspar, plagioclase and hornblende rich layers (Figure 2.5a). Thin red layers (mm scale) contain minor amounts of pyrite, which have produced a deep red stain on quartz. Unit 5 rocks cut the gneissic layering of the Unit 4 mafic monzogranite gneiss (Figure 2.5b)

2.4.1.6. Unit 6: Magnetite-bearing monzogranite

Unit 6 consists of a greyish white and pinkish weathering biotite and magnetite-bearing monzogranite. Typically, Unit 6 rocks are fine grained and characterized by melt segregations that have depletion halos enriched in mafic minerals. The melt segregations also contain magnetite and are syn-deformational as they locally cross-cut the foliation but are in turn folded (Figure 2.5c).

2.4.1.7. Unit 7: Porphyroclastic monzogranite

Unit 7 rocks are typically greyish white on the weathered and fresh surfaces. The rocks are mainly fine grained and commonly contain biotite, hornblende and epidote. The unit is characteristic by a K-feldspar porphyroclastic texture (Figure 2.5d) that is demonstrably derived from the disaggregation of syenogranitic veins. Locally, the rocks contain mineral clots consisting of relict orthopyroxene + clinopyroxene + hornblende and elsewhere by abundant mineral clots of biotite ± hornblende ± magnetite. The clots of both compositions have light coloured depletion halos (Figure 5e). Locally,

Figure 2.5. Field photographs from the study area. Unit numbers and color codes correspond to those of Figure 2.3 and are shown in the bottom right of each photograph. a) Typical field aspects of the Unit 5 Ribbon granite gneiss with alternating bands of differential mineral composition giving a "ribbon" textured appearance; b) Unit 5 ribbon granite gneiss crosscutting the foliation and layering in the Unit 4 mafic monzogranite gneiss; c) Unit 6 magnetite-bearing monzogranite characterized by syn-tectonic melt segregations and depletion halos enriched in mafic minerals.; d) Unit 7 fine grained porphyroclastic monzogranite characterized by K-feldspar porphyroclasts (disaggregated syenogranite veins); e) Clots of biotite + hornblende with light-coloured depletion halos within Unit 7 biotite + epidote + hornblende monzogranite; f) Weakly defomed syenogranite vein of Unit 8 crosscutting foliation (parallel to the direction of the hammer) in Unit 2 grey tonalite gneiss.

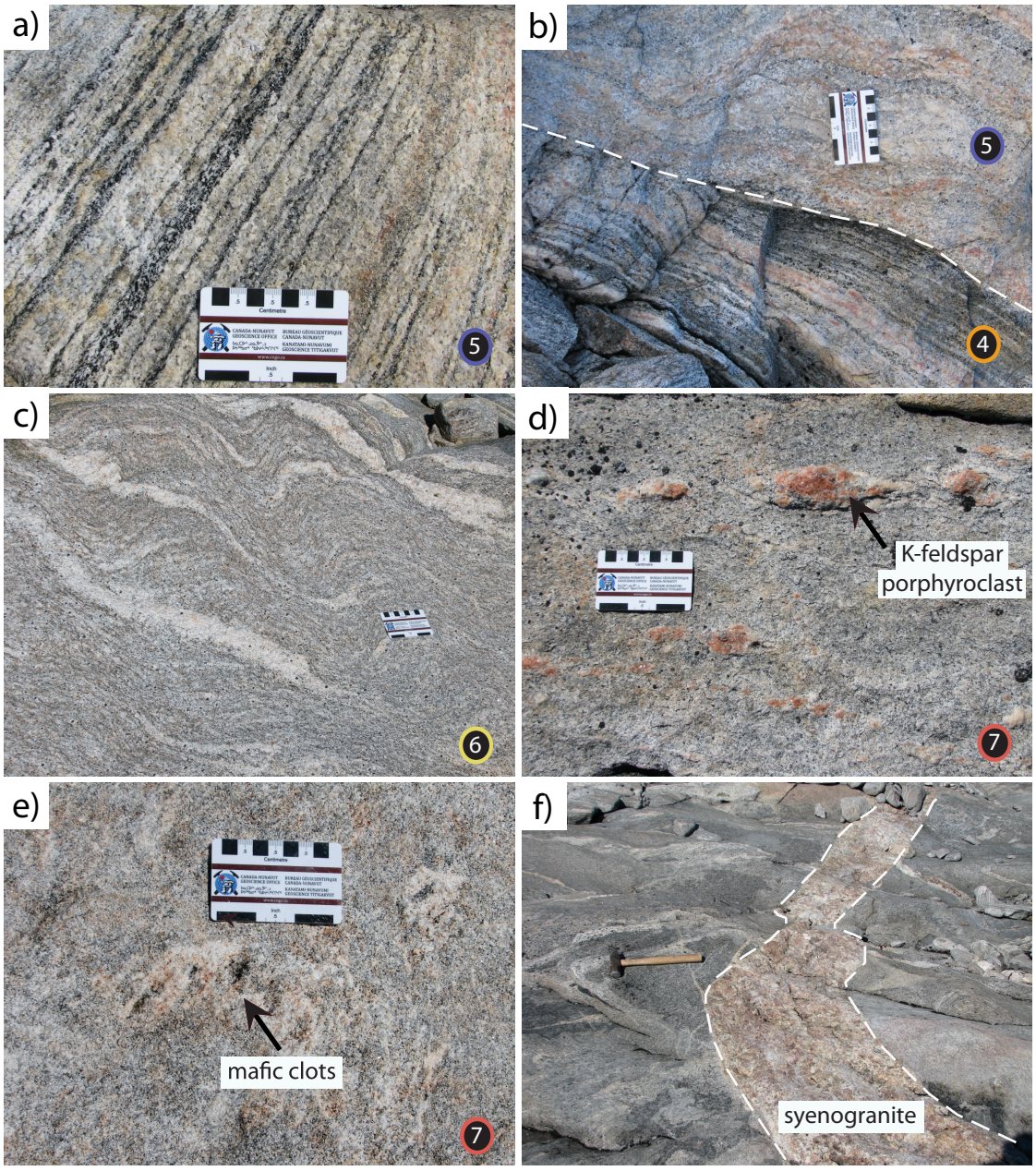

hornblende appears to be breaking down to biotite, and the biotite breaking down to epidote.

2.4.1.8. Unit 8: Syenogranite

The snow bowl area contains abundant occurrences of pegmatitic syenogranite, which forms dykes that cross cut all rock units in the area. The width of these pegmatite dykes are around 20 cm and are not quite large enough to be shown on the scale of the snow bowl area map (Figure 2.3). The pegmatites are distinctively reddish pink in weathered and fresh surfaces. The rocks are coarse to very coarse grained and dominated by K-feldspar with lesser amounts of quartz and biotite. That these dykes cut Unit 1 to Unit 7 rocks demonstrates that they are the youngest rock type in the snow bowl area. The pegmatite dykes have a varied structure. Principally they are undeformed although locally some dykes are weakly folded (Figure 2.5f).

2.4.2. Structural and metamorphic character of the snow bowl area

The snow bowl area lies within the regionally extensive, Archean orthogneiss complex that dominates eastern Hall Peninsula. The gneissic rocks in the snow bowl area broadly possess similar structural characteristics to the entirety of the Archean orthogneiss complex of eastern Hall Peninsula as described by From et al. (2013). A summary of the structural context with emphasis on observations made within the snow bowl area is given here.

Field observations, including complex, superposed folding of gneissosity, demonstrate that multiple deformation events affected the gneissic rocks across Hall Peninsula during the Archean. In the snow bowl area, the deformational fabric, folding

and metamorphism is labeled starting with the oldest recognizable deformation event. None of the structures in the snow bowl area have been constrained by geochronology and their relative chronology is established based upon field observations. The pervasive gneissic fabric (S1) developed in Units 1 to 7 strikes to the east to southeast and dips moderately to steeply to the south and southwest. A mineral lineation (L1), common in all Units in the snow bowl area plunges moderately to the west. This lineation is a common feature in Archean orthogneiss units of Hall Peninsula. F1 folds, defined by folded S1 gneissosity, are observed only in rare, low-strain zones throughout the complex and were not observed in the snow bowl area. Some rocks in the snow bowl area contain an S2 fabric that strikes north-northwest to northwest and is defined as a local, axial planar foliation in F2 folds of gneissosity. F2 folds have a hinge-parallel, shallowly plunging mineral stretching lineation (L2) defined by quartz + feldspar ± hornblende ± biotite. A quartz + feldspar rodding lineation (L2) is also observed at the same orientation plunging shallowly to the northwest.

The metamorphic assemblage seen most commonly throughout the snow bowl area is biotite + hornblende + epidote indicating lower amphibolite grade metamorphism. However, the epidote is seen locally to be growing at the expense of biotite indicating that epidote is not a part of the peak metamorphic assemblage. The presence of clots, that contain relict orthopyroxene + clinopyroxene + hornblende where hornblende is observed to be breaking down to biotite and subsequently epidote, is indicative of a previous metamorphic grade at granulite facies. Other localities throughout the orthogneiss complex contain larger mafic enclaves or pods that also preserve a granulite grade metamorphic assemblage of orthopyroxene + clinopyroxene + hornblende. These

observations indicate that the orthogneiss complex was previously at Granulite facies metamorphic grade during the Archean. During subsequent metamorphism in the Paleoproterozoic (Scott, 1999; Rayner. 2014) Amphibolite facies metamorphism overprinted the Granulite facies as shown by the retrogression of mineral assemblages.

Migmatitic textures are observed locally throughout the snow bowl area appearing as layers of mineral segregation, leucosome development and irregular bodies of leucocratic material centimeters to several meters in size. It is possible that some of the monzogranitic to syenogranitic phases within these lithological units and within the orthogneiss complex are a result of partial melting and remobilization.

2.5. Conclusions

Previous regional-scale mapping within the Archean orthogneiss complex of Hall Peninsula grouped a vast area of gneissic rocks as tonalite and monzogranite gneiss. Contributing factors of felsenmeer erosion, inaccessibility, snow cover and lichen coated outcrops left the tonalite and monzogranite units mainly undifferentiated at a regional scale. However, the subtle yet distinct lithologies mapped in the snow bowl area demonstrate the complexity of Archean rock units in the region. The snow bowl area is dominated by porphyroclastic monzogranite (Unit 7) that intrudes and entrains other older phases of plutonic rocks (Units 1-6) including a small amount of truly grey tonalite gneiss of Unit 2 (Figures 2.3, 2.4 and 2.5). Each of these eight units has a pervasive S1 gneissosity and fairly consistent L1 mineral lineations with no crosscutting units having a significantly different texture (e.g., grain size, strength of gneissosity), therefore all of these Units are presumably Archean in age. Further detailed analytical work, including

isotope geochronology will be required to allow the correlation of Units across the Archean orthogneiss complex and the plutonic history of the complex to emerge. Future work will further characterize the Archean Hall Peninsula block, developing a fingerprint for comparison to adjacent Archean terrains and provide insight into the paleo-plate reconstruction for the Baffin Island and sub-Arctic region as a whole.

2.6. Future work

Excellent exposure and well-defined cross-cutting relationships between the plutonic phases within the snow bowl area makes this locality ideal for future detailed work to fully characterize the geological history of these rocks. Petrography on each phase will provide full mineral assemblage characterization. U-Pb geochronology using the SHRIMP technique on selected Units will constrain the crystallization ages of these intrusive phases and provide data to corroborate observed cross-cutting relationships. Lu-Hf isotopic ratios in zircon grains having a known U-Pb crystallization age from will provide insight into the magmatic history of the plutonic rocks. The field and analytical work will then provide a baseline from which to assess the spatial extent of plutonic units across the Archean orthogneiss complex. In addition, regional-scale sampling transects across eastern Hall Peninsula analyzing for Sm-Nd isotopes will provide an assessment of any underlying crust not exposed at surface on Hall Peninsula and comparisons of εNd values to data from adjacent crustal blocks can be made.

2.7. Acknowledgements

The authors thank M.D. Young, A.L. Camacho, M.R. St-Onge, B.J. Dyck, N.M. Rayner, D.J. Mate, D.R. Skipton, C.B. MacKay, Z.M. Braden and H. Steencamp for enlightening discussions and enthusiastic field collaboration and everyone involved in making this field season possible. Reviews of this manuscript by N. Rayner and D. James improved the focus, clarity and content of this manuscript and are much appreciated.

2.8. References

Blackadar, R.G. 1967. Geological reconnaissance, southern Baffin Island, District of Franklin; Geological Survey of Canada, Paper 66-47.

Connelly, J. N. 2001. Constraining the timing of metamorphism: U–Pb and Sm–Nd ages from a transect across the northern Torngat Orogen, Labrador, Canada. Journal of Geology; v. 109, p. 57–77.

Creason C.G., Gosse, J.C. and Young, M.D. 2013. Rift flank uplift and landscape evolution of Hall Peninsula, Baffin Island, Nunavut: an exhumation model based on low-temperature thermochronology; *in* Summary of Activities 2012, Canada-Nunavut Geoscience Office, p. 75–84.

From, R.E., Camacho, A.L. and St-Onge, M.R. 2013. Preliminary observations on the nature and origin of the eastern orthogneiss complex of southern Hall Peninsula, Baffin Island, Nunavut. *in* Summary of Activities 2012, Canada Nunavut Geoscience Office, p. 43-54.

Hoffman, P.F. 1988. United Plates of America, the birth of a craton: Early Proterozoic assembly and growth of Laurentia; Annual Review of Earth and Planetary Sciences, v. 16, p. 543–603.

Hollis, J. A., Frei, D., Van Gool, J. A. M., Garde A. A. and Persson, M. 2006. Using zircon geochronology to resolve the Archaean geology of southern West Greenland; Geological Survey of Denmark and Greenland, Bulletin 10, p. 49–52.

Knight, I. and Morgan, W.C. 1981. The Aphebian Ramah Group, northern Labrador; *in* Proterozoic Basins of Canada, F.H.A. Campbell (ed.), Geological Survey of Canada, Paper 81-10, p. 313–330.

Leblanc-Dumas, J., Allard, M. and Tremblay, T. 2013. Quaternary geology and permafrost characteristics in central Hall Peninsula, Baffin Island, Nunavut; *in* Summary of Activities 2012, Canada-Nunavut Geoscience Office, p. 101–106.

MacKay, C.B., Ansdell, K.M., St-Onge, M.R., Machado, G. and Bilodeau, C. 2013. Geological relationships in the Qaqqanittuaq area, southern Hall Peninsula, Baffin Island, Nunavut; *in* Summary of Activities 2012, Canada-Nunavut Geoscience Office, p. 55–64.

Rayner, N.M. 2013. New U-Pb geochronological results from Hall Peninsula, Baffin Island, Nunavut; *in* Summary of Activities 2013, Canada Nunavut Geoscience Office, p. 39–52.

Senkow, M.D. 2013. Characterization of ultramafic occurrences on southern Hall Peninsula, Baffin Island, Nunavut, and evaluation of their potential as a source of carving stone; in Summary of Activities 2012, Canada-Nunavut Geoscience Office, p. 163–168.

Scott, D.J. 1996. Geology of the Hall Peninsula east of Iqaluit, southern Baffin Island; *in* Current Research 1996-C, Geological Survey of Canada, p. 83–91.

Scott, D.J. 1999. U–Pb geochronology of the eastern Hall Peninsula, southern Baffin Island, Canada: a northern link between the Archean of West Greenland and the Paleoproterozoic Torngat orogen of northern Labrador; Precambrian Research, v. 93, p. 5–26.

Scott, D.J. and Gauthier, G. 1996. Comparison of TIMS (U-Pb) and laser ablation microprobe ICP-MS (Pb) techniques for age determination of detrital zircons from Paleoproterozoic

metasedimentary rocks from northeastern Laurentia, Canada, with tectonic implications; Chemical Geology, v. 131, p. 127–142.

Scott, D.J., Campbell, L.M. 1993. Evolution of the Paleoproterozoic Torngat orogen, Labrador Canada: recent advances using U–Pb geochronology and Nd isotopic systematics (abstr); Geological Society of America Abstract with Programs, V. 25, p. A237

Skipton, D.R., Schneider, D.A. and St-Onge, M.R. 2013. Preliminary observations on Archean and Paleoproterozoic metamorphism and deformation of the southern Hall Peninsula, Baffin Island, Nunavut; *in* Summary of Activities 2012, Canada-Nunavut Geoscience Office, p. 29–42.

Steenkamp, H., and St-Onge, M.R. 2013. Overview of 2013 regional mapping on Hall Peninsula, Nunavut; *in* Summary of Activities 2013, Canada Nunavut Geoscience Office, p. 27–38.

St-Onge, M.R., Van Gool, J., Garde, A.A. and Scott, D.J. 2009. Correlation of Archaean and Palaeoproterozoic units between northeastern Canada and western Greenland: constraining the pre-collisional upper plate accretionary history of the Trans-Hudson orogen; Geological Society of London, Special Publications, v. 318, p. 193–235.

Thrane, K. and Connelly J. N. 2006. Zircon geochronology from the Kangatsiaq–Qasigiannguit region, the northern part of the 1.9–1.8 Ga Nagssugtoqidian orogen, West Greenland; Geological Survey of Denmark and Greenland Bulletin, no. 11, p. 87–99.

Van Gool, J. A. M., Garde, A. A. and Larsen, L. M. 2004. Correlation of Precambrian geology in Labrador and southern Greenland; Danmarks og Grønlands Geologiske Undersøgelse Rapport, 2004/29, 30 p.

Wardle, R. J., and Hall, J. 2002. Proterozoic evolution of the northeastern Canadian Shield: Lithoprobe Eastern Canadian Shield Onshore-Offshore Transect (ECSOOT) introduction and summary; Canadian Journal of Earth Sciences, v. 39, p. 563–567.

3. Chapter 3. Archean magmatism and metamorphism of eastern Hall Peninsula, southern Baffin Island, Nunavut

This chapter is an article published in the 2015 edition of the CNGO Summary of Activities volume in co-authorship with my Ph.D. thesis advisor Dr. Alfredo Camacho and HPIGP collaborator Nicole Rayner. This article details an in-depth mapping and geochronological study that provides robust U-Pb age constraints on six lithologically distinct rock units from the snow bowl area previously characterized in Chapter 2. I was responsible for the sample collection, U-Pb isotopic analysis and data collection, data interpretation, literature review, figure drafting, and the writing. My collaborator N. Rayner and the lab staff at the SHRIMP laboratory at the GSC provided assistance with sample preparation, data acquisition and processing. My co-authors assisted with fieldwork and sample collection and reviewed drafts of the article, which is published in the 2013 edition of the CNGO Summary of Activities volume (see citation below) and is reproduced herein with express permission from the CNGO and NRCAN. This version of the article is re-formatted and in some cases re-written for consistency of the thesis.

From, R.E., Rayner, N. and Camacho, A. 2016: Archean magmatism and metamorphism of eastern Hall Peninsula, southern Baffin Island, Nunavut; *in* Summary of Activities 2015, Canada-Nunavut Geoscience Office, p. 73–88.

3.1. Abstract

Zircon U-Pb geochronology was conducted on six distinct crustal units within a well-constrained study area on eastern Hall Peninsula, Baffin Island. U-Pb isotopic ages range from ca. 3209 to 2682 Ma, outlining a protracted period of Archean magmatic activity and highlighting the previously unrecognized heterogeneity of this orthogneiss suite. Integrating the U-Pb isotopic age data with high-resolution zircon imaging and Th/U ratios, several samples were interpreted to have both an Archean crystallization age and an Archean metamorphic-overprint age. Crystallization ages, characterized by prismatic zircon grains with well-defined oscillatory-growth zoning, range from ca. 2.98 to 2.75 Ga. Archean metamorphic ages, characterized by rounded zircon grains that are commonly unzoned or sector zoned, or have an irregular internal structure, range from ca. 2.74 to 2.68 Ga. Constraining the timing of Archean crystallization and metamorphism is a key step in fingerprinting the Archean orthogneiss complex of Hall Peninsula. The data can be used for comparison with adjacent Archean terrains, and may allow correlations critical for paleoplate reconstructions for the Baffin Island and subarctic regions.

3.2. Introduction

This study is part of the Hall Peninsula Integrated Geoscience Project (HPIGP), led by the Canada-Nunavut Geoscience Office (CNGO) in collaboration with the Geological Survey of Canada (GSC) and a number of Canadian universities. While the broad focus of the HPIGP is the production of bedrock and surficial geological maps, this study targets the Archean geological history of Hall Peninsula.

An overview of the geology of Hall Peninsula can be found in Machado et al. (2013) and Steenkamp and St-Onge (2014). The Archean rocks of Hall Peninsula are a complex assortment of polydeformed and polymetamorphosed rocks collectively termed "the Archean orthogneiss complex" (From et al., 2013). The Archean orthogneiss complex dominates eastern Hall Peninsula (Figure 3.1) and is composed mostly of gneissic to migmatitic tonalite to monzogranite with subsidiary components of syenogranite and localized ultramafic pods. Paleoproterozoic metasedimentary units disconformably overlie the Archean orthogneiss complex (Steenkamp and St-Onge, 2014) and are tectonically interleaved in thick-skinned imbricate folds and thrusts as slivers and panels ranging from ~2 m to several kilometres in thickness (Machado et al., 2013).

The Archean orthogneiss complex is very heterogeneous; seven distinct units along a 700 m transect (snow bowl area) on east-central Hall Peninsula were recognized (Figure 3.2) and are documented in Chapter 2. In brief, the snow bowl area is dominated by porphyroclastic monzogranite gneiss that intrudes several older orthogneiss units, each with distinct characteristics. Relatively undeformed, coarse-grained syenogranite intrudes all units. In this study, uranium-lead (U-Pb) geochronology was completed on six of these rock units to determine the time span of Archean magmatism, confirm the field relationships observed in the snow bowl area and provide a temporal framework for the Archean orthogneiss complex.

3.3. Previous age determinations

Previous reconnaissance-scale U-Pb age determinations of the Archean orthogneiss complex were carried out by Scott (1999) and Rayner (2014, 2015). Scott (1999) analyzed zircon and titanite in four samples of foliated tonalite along the eastern coast of

Figure 3.1. Geology of southern Hall Peninsula, Nunavut from data collected during the 2012 and 2013 field seasons, showing the distribution of the principal units and the locations of previous U-Pb age determinations (modified from Machado et al., 2013). Location of the study area (snow bowl area) is shown with a red star. Abbreviations: grt, garnet; bt, biotite; mag, magnetite; opx, orthopyroxene; cpx, clinopyroxene.

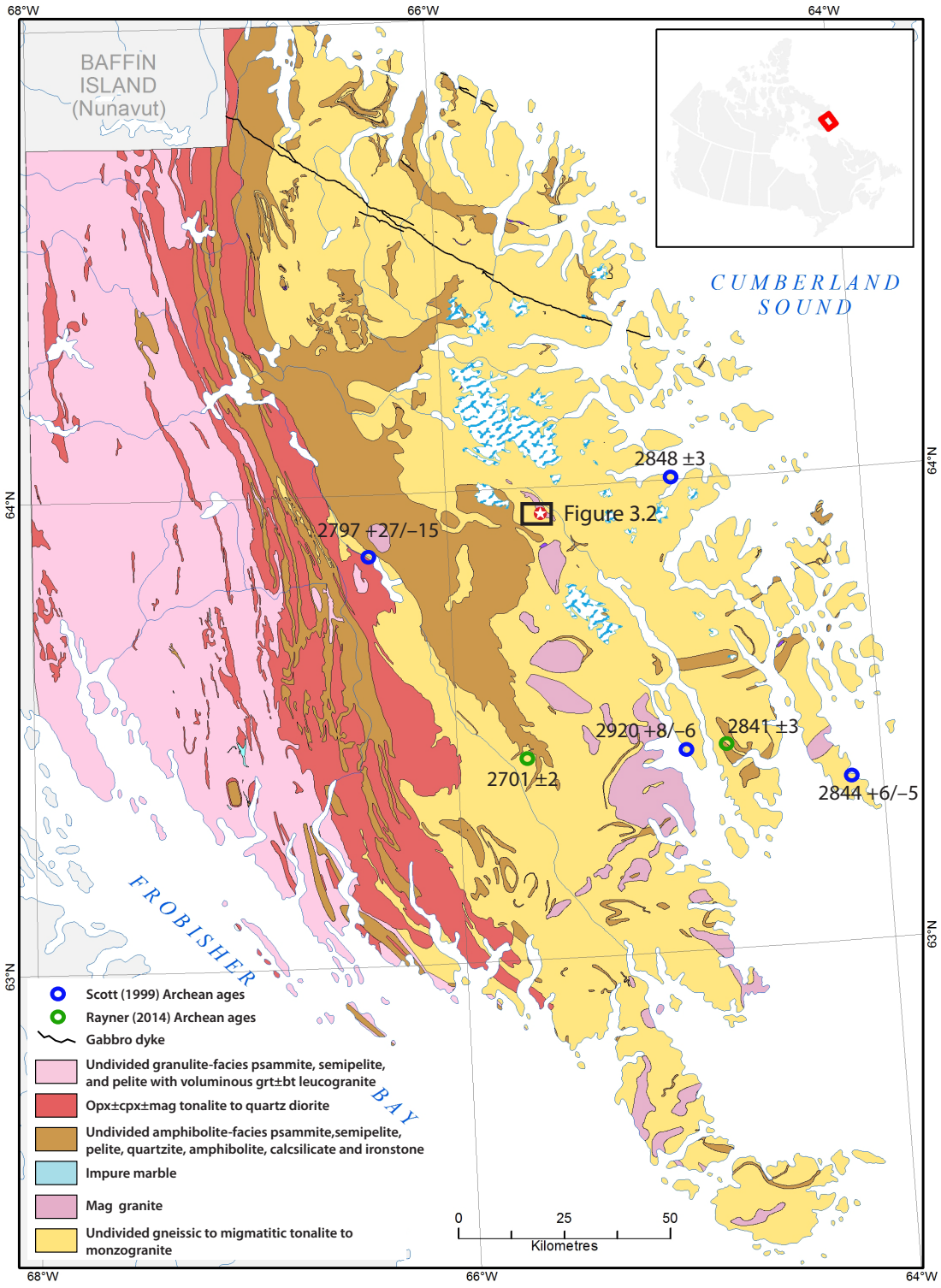

Figure 3.2. Detailed geology of the snow bowl area on east-central Hall Peninsula, Nunavut, with inset schematic map showing the general geology of the surrounding area. The geological unit legend of the study area lists units from oldest to youngest (from top to bottom), as interpreted in From et al. (2014), with black dots and sample numbers indicating the positions of samples analyzed for U-Pb geochronology.

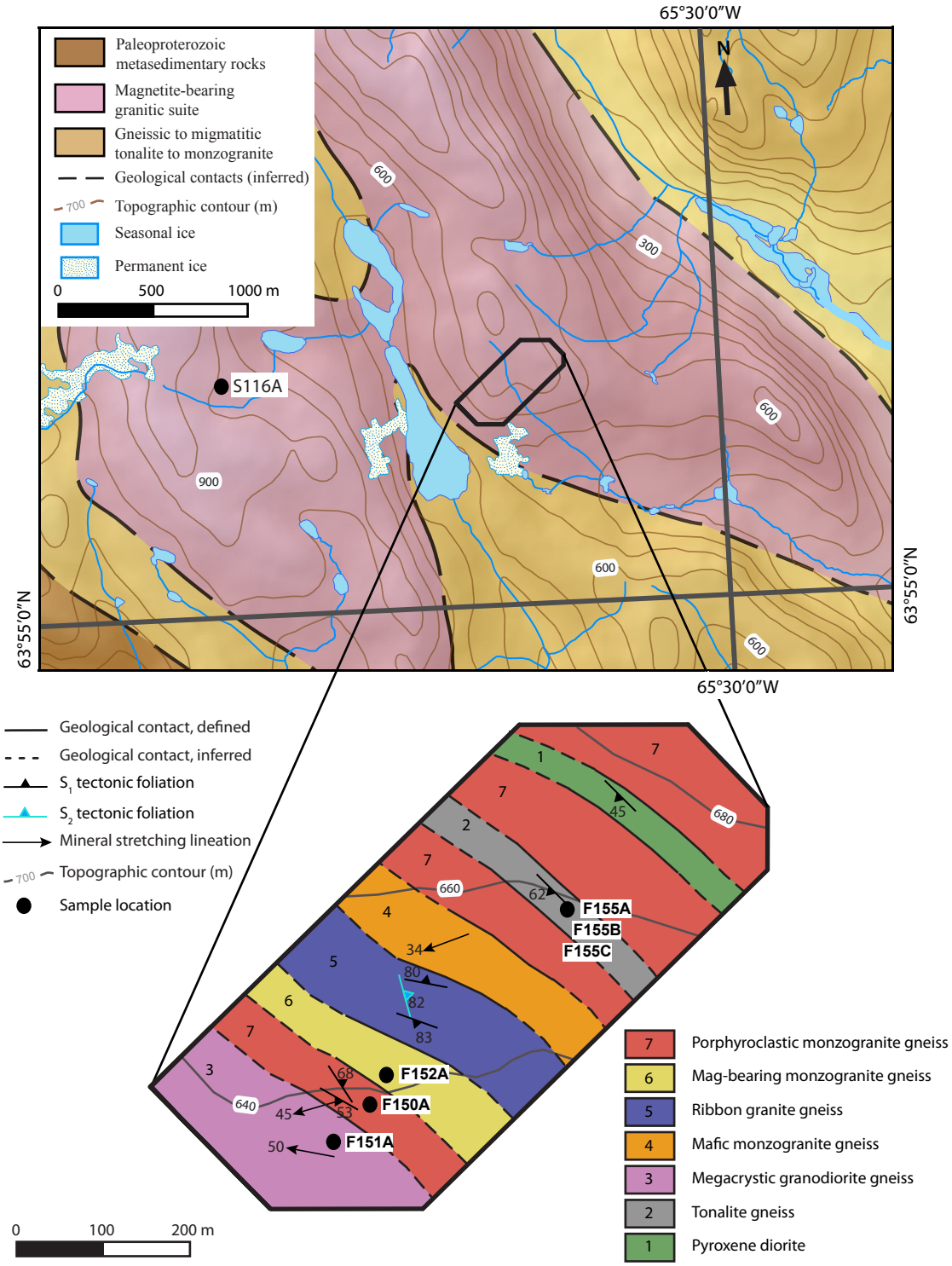

Hall Peninsula and one foliated tonalite along a narrow east-west transect on central Hall Peninsula (Figure 3.1) using the isotope dilution–thermal ionization mass spectrometry (ID-TIMS) method. The resulting upper intercept regression ages of 2920 +8/–6, 2848 ±3, 2844 +6/–5 and 2797 +27/–15 Ma were interpreted as magmatic crystallization ages. In addition, zircon from three separate granitic dykes that intrude the gneisses along the eastern coast yielded crystallization ages of 2835 ±11, 2768 ±13 and 2820 ±5 Ma. Analyses of titanite from the same granitic dykes returned much younger ages between ca. 1730 and 1842 Ma. Consequently, the Archean zircons from the intrusive granitic dykes are interpreted to have either grown during initial emplacement of the veins or been inherited as xenocrysts within Paleoproterozoic granitic dykes (Scott, 1999).

Subsequent investigations (Rayner, 2014, 2015) used the sensitive high-resolution ion microprobe (SHRIMP) technique to determine the ages of four foliated tonalite gneiss samples and one deformed megacrystic monzogranite collected across central and eastern Hall Peninsula (Figure 3.1) in order to calibrate the regional geological map legend. The U-Pb isotopic ages of these samples were interpreted to represent crystallization ages between 2701 ±2 and 2841 ±3 Ma (Rayner, 2014, 2015). This work provided an initial framework of the broad temporal extent of Archean rock emplacement on eastern Hall Peninsula and sets the stage for further, more detailed geochronological investigations.

3.4. Hypothesis for further investigation

The crustal provenance of the Archean orthogneiss complex on eastern Hall Peninsula remains enigmatic. Based on lithological similarities, geochronology and aeromagnetic characteristics, these rocks have been previously interpreted to correlate

with the Rae craton of northern Baffin Island and western Greenland (Hoffman, 1988), the Meta Incognita microcontinent of southern Baffin Island and northern Labrador (St-Onge et al., 2009), the Aasiaat domain of central western Greenland (Hollis et al., 2006; Thrane and Connelly, 2006; St-Onge et al., 2009) and the Nain craton of northern Labrador (Scott and Campbell, 1993; Scott, 1999; Connelly, 2001; Wardle et al., 2002), and as a unique and distinct microcontinent (Whalen et al., 2010).

U-Pb geochronology has proven to be an effective method to identify and delineate unique pieces of crust that may have been tectonically amalgamated in this region during the Trans-Hudson orogen (e.g., St-Onge et al., 2002; Connelly et al., 2006; Corrigan et al., 2009). Previous reconnaissance-scale geochronology in the Archean orthogneiss complex has targeted mainly the tonalitic gneiss, which was believed to be a significant component of the complex. Recent detailed mapping of the snow bowl area on east-central Hall Peninsula characterized seven distinct units within the Archean orthogneiss complex (Chapter 2), with monzogranite gneiss being the dominant component (Figure 3.2). Therefore, further geochronological investigation of the previously unidentified heterogeneity of gneisses within the Archean orthogneiss complex is warranted.

Zircon was selected to use for U-Pb isotopic analyses because it is refractory and consequently rresistant to most magmatic, metamorphic and erosional processes that may destroy or alter other common U-bearing accessory minerals (Williams, 1992). The closure temperature of Pb in zircon is very high (950 to >1000°C) and is not easily reset (Lee et al., 1997; Möller et al., 2002). Within a single zircon grain, it is not uncommon to observe distinct chemical and structural domains, each preserving the chemical conditions of a particular period of zircon crystallization. Therefore, both the external

morphology and the internal chemical and structural zoning of each zircon grain must be carefully considered when interpreting the relationship between particular domains and specific stages of the rocks' history (e.g., Hanchar and Miller, 1993). Whole-rock lithogeochemical data (APPENDIX 3A) was used to select samples with adequate zirconium to be candidates for further U-Pb zircon analyses and to confirm the lithologic classifications of samples that were based on field observation and thin section analysis.

This study presents SHRIMP U-Pb zircon results for a suite of seven samples from distinct rock types documented within the Archean basement complex, as defined in Chapter 2. The SHRIMP instrument specializes in isotopic analysis of mineral grains at the micrometre scale and is an ideal tool to help unravel the timing of past geological events in complex and polydeformed rocks, such as those of Hall Peninsula. If the distinct rock units in question are all Archean in age, then they may provide a more detailed age range for the formation of the Archean orthogneiss complex and help to identify any recorded Archean tectonothermal events. Furthermore, refinement of the timing of Archean crustal genesis may provide insight into discriminating different geological processes active during the Archean.

3.5. Analytical methods

Seven samples were disaggregated (fine to medium sand size) using standard crushing and pulverizing techniques followed by density separation using a Wilfley table. The crushed material was further separated by density using heavy liquids (methylene iodide) and subsequently a magnetic separator to isolate the zircon separate. Details

regarding the procedure, or any deviations from it, are noted in the sections describing specific samples.

The SHRIMP analytical procedures are described in Stern (1997), with reference material and U-Pb calibration methodology following Stern and Amelin (2003). In brief, zircons were set in 2.5 cm diameter epoxy mounts (GSC epoxy mounts #733 and #690) along with fragments of the GSC zircon laboratory standards (z6266 with $^{206}Pb/^{238}U$ age of 559 Ma; z1242 with $^{207}Pb/^{206}Pb$ age of 2679 Ma). The epoxy mounts were polished and cores of the zircons were exposed using 9, 6 and 1 μm diamond polishing compounds. The internal structure and features of the zircons were then characterized in backscattered electron (BSE) mode and cathodoluminescence (CL) mode using a Zeiss Evo® 50 scanning electron microscope. Details of the SHRIMP analytical session, including spot size, number of scans, age/error of standard, calibration error and the application of any intra-element fractionation corrections are given in the footnotes of the accompanying data table (APPENDIX 3B). The count rates of 11 masses including background were sequentially measured with a single electron multiplier. Offline data processing was accomplished using SQUID2 (version 2.22.08.04.30, revised April 30, 2008). The 1σ external errors of $^{206}Pb/^{238}U$ ratios reported in the data table incorporate the error in calibrating the standard. Common Pb correction used the Pb composition of the surface blank (Stern, 1997). Isoplot version 3.00 (Ludwig, 2003) was used to generate concordia plots and calculate weighted means. The error ellipses on the concordia diagrams and the weighted-mean errors in the text and on the figures are reported at the 2σ uncertainty level.

3.6. U-Pb results

A separate section for each sample is presented here, and contains lithology and zircon descriptions, mineralogy based on thin section analysis, a summary of the geochronological results and a geological interpretation. All U-Pb analytical results can be found in the accompanying data table (APPENDIX 3B).

3.6.1. 12MBC-S116A – monzogranite gneiss

The monzogranite gneiss is typically greyish white on both weathered and fresh surfaces, and is intruded by coarse-grained leucocratic veins. A sample was collected, carefully avoiding the veins, just west-northwest of the snow bowl area as part of a larger scale traverse in 2012. The sample is fine grained and has a mineral foliation defined by hornblende and biotite. The mineralogy is 30% quartz, 20% K-feldspar, 20% plagioclase, 20% biotite, 5% titanite and 5% hornblende.

Zircon grains separated from this sample are generally subrounded, prismatic to ovoid, and slightly elongate (aspect ratios up to 3:1; <200 μm long). The zircons show well-defined, fine- to medium-scale oscillatory-growth zoning in BSE and CL images (Figure 3.3a, b). A few grains have overgrowths that are unzoned or irregularly zoned (Figure 3.3b).

Thirty-two analyses were conducted on 25 separate zircon grains, yielding $^{207}Pb/^{206}Pb$ ages between ca. 2988 and 2716 Ma (APPENDIX 3B). A cluster of the thirteen oldest ages, ranging from ca. 2988 to 2969 Ma, is characterized by well-defined, fine-scale growth zonation and has a weighted-mean $^{207}Pb/^{206}Pb$ age of 2976 ±4 Ma (n = 10; mean square of weighted deviates [MSWD] = 2.0; Figure 3.3c), interpreted as the

Figure 3.3. Representative zircon images and concordia diagrams for a-c) sample 13SUB-S166A; d-f) sample 13SUB-F151A; dark grey ellipses correspond to ages used to calculate the crystallization age; light grey ellipses are ages excluded from the crystallization-age calculation; unfilled ellipses denote ages used to calculate the weighted-mean age of metamorphism (see text for discussion). Back scattered electron (BSE) images show spot analyses (correspond to analyses in APPENDIX 3B; errors given at 1σ); white scale bars all 50 μm; mean ages reported at the 2σ confidence level.

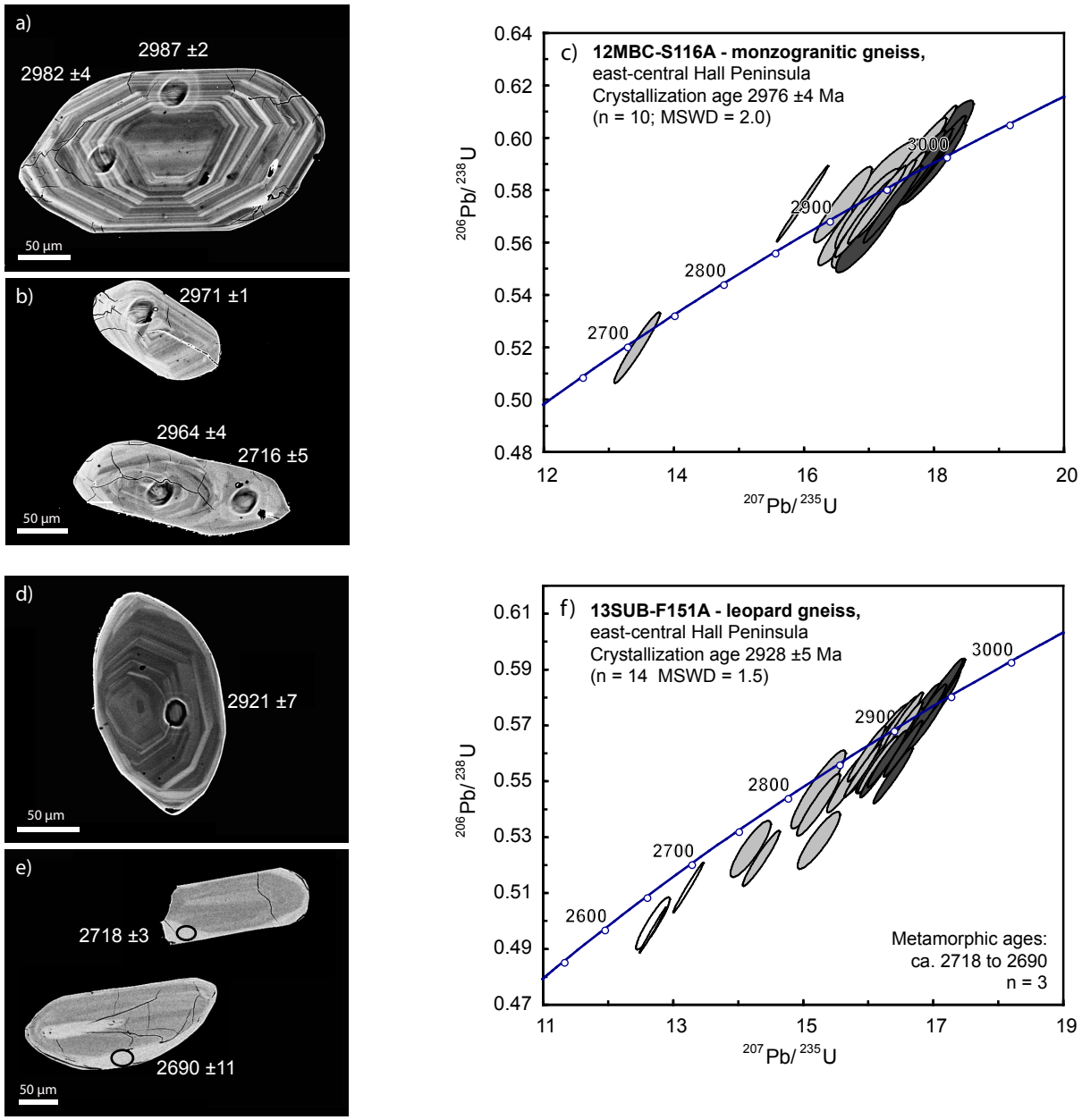

crystallization age of this monzogranite. The remaining younger ages (n = 11), ranging from ca. 2964 to 2943 Ma, cascade toward three even younger ages of ca. 2901, 2837 and 2716 Ma. Two of these young results (ca. 2901 and 2837 Ma) are from homogeneous overgrowth rims that have relatively high U values (673 to 3834 ppm) and low Th/U values (0.12 to 0.16), compared to the older zircon grains. These dates may be related to non-zero-age Pb loss where Pb is leaked from the zircon during open-system behaviour (e.g. during recrystallization of zircon due to tectonothermal activity associated with the emplacement of younger magmatic rocks). The youngest date of ca. 2716 Ma comes from a zircon with a particularly clean core and rim relationship that can be interpreted to represent initial crystallization (core) and subsequent metamorphism (rim) of this sample. However, with only one example of this relationship, an alternative interpretation is that there was Pb loss due to later tectonothermal events (after ca. 2716 Ma) that may have partially reset the isotope systematics of the older, oscillatory-zoned zircon (e.g., Pb loss through partial recrystallization), resulting in the age scatter.

3.6.2. 13SUB-F151A – megacrystic granodiorite gneiss

The megacrystic granodiorite gneiss is medium to coarse grained and characterized by a pervasive L-tectonite fabric defined by elongate, relict plagioclase phenocrysts that are commonly surrounded by hornblende. There are fine-grained mafic lenses composed of hornblende+biotite+epidote quartz diorite. A homogeneous sample without mafic material was collected from the southwestern edge of the snow bowl area (Figure 3.2). The dated sample is medium grained with 40% quartz, 30% plagioclase, 15% hornblende, 10% biotite and 5% titanite.

Zircon grains separated from this sample are dominantly ovoid with rounded grain edges, while only a few grains are elongate and prismatic (aspect ratios 3:1; <200 μm long). Images (BSE and CL) of the zircon show that most grains have fine-scale oscillatory-growth zonation throughout the entire grain (Figure 3.3d), with a few grains having more diffuse oscillatory zones toward the outer edges. All of the grains have a thin, unzoned, high-U rim (bright in BSE images), but only three of these unzoned rims were large enough for a spot analysis (Figure 3.3e).

Thirty-six analyses were conducted on 31 separate zircon grains, yielding $^{207}Pb/^{206}Pb$ ages between ca. 2945 and 2690 Ma (APPENDIX 3B). The nine oldest $^{207}Pb/^{206}Pb$ ages, from ca. 2945 to 2917 Ma, were collected in areas of zircon grains with fine-scale oscillatory-growth zoning and are interpreted as the crystallization age of the megacrystic granodiorite gneiss. These data yield a weighted-mean $^{207}Pb/^{206}Pb$ age of 2928 ±5 Ma (n = 14, MSWD = 1.5; Figure 3.3f). Younger ages (n = 17), from ca. 2913 to 2718 Ma, appear to scatter towards a small cluster of analyses collected from the unzoned overgrowths. The three overgrowths produced ages between ca. 2718 and 2690 Ma, and are characterized by high U (563 to 1497 ppm) and low Th/U (0.07 to 0.18) compared to the analyses with older ages (U concentrations of 55 to 259 ppm and Th/U ratios of 0.39 to 0.73). These three zircon overgrowths are interpreted to have formed during a separate episode of metamorphism and zircon growth. This metamorphic event may have partially reset the isotope systematics of the older, oscillatory-zoned zircon (e.g., Pb loss through partial recrystallization), resulting in the scatter toward younger ages.

3.6.3. 13SUB-F155B – grey tonalite gneiss

The grey tonalite gneiss is found only as a semicontinuous raft (5 m wide by 25 m long) in monzogranite gneiss (13SUB-F155A) and has a distinct grey weathering surface and a black and white fresh surface. There are local discontinuous mafic lenses (13SUB-F155C) and thin (millimetre-scale) trondhjemitic segregations that define the gneissic foliation. The tonalite gneiss is intruded by centimetre- to metre-scale dykes of the monzogranitic gneiss (13SUB-F155A) concordant to, but locally crosscutting, the gneissic fabric. A homogeneous sample of the grey tonalite gneiss, excluding stringers and other crosscutting components, was collected from the northeastern edge of the snow bowl area (Figure 3.2). The dated sample is fine grained with a mineral foliation defined by hornblende and biotite. The mineralogy is 40% quartz, 30% plagioclase, 15% hornblende, 10% biotite, 3% K-feldspar and 2% apatite.

Zircon grains separated from this sample have varied morphological and zonation characteristics. In general, the majority of grains are mostly ovoid, while a minor population is elongate and prismatic (aspect ratios up to 3:1; <220 μm long). Most of the zircons have fine-scale oscillatory-growth zonation (Figure 3.4a). These zircons may have cores (Figure 3.4b) and unzoned overgrowth domains (Figure 3.4c). There is a separate population of stubby, generally rounded zircon that is unzoned or sector zoned (Figure 3.4d).

Forty-three analyses were conducted on 37 separate zircon grains, yielding $^{207}Pb/^{206}Pb$ ages between ca. 3209 and 2671 Ma (APPENDIX 3B). The oldest ages, ca. 3209 to 2846 Ma, are from the cores of zircon grains that are overgrown by oscillatory-zoned zircon material (Figure 3.4d) and are interpreted as inherited cores. A tight cluster of ages, between ca. 2820 and 2806 Ma, with well-defined, fine-scale oscillatory-growth

Figure 3.4. Representative zircon images and concordia diagrams for a-e) sample 13SUB-F155B; f-h) sample 13SUB-F155C; i-k) sample 13SUB-F155A; dark grey ellipses correspond to ages used to calculate the crystallization age; light grey ellipses are ages excluded from the crystallization-age calculation; unfilled ellipses denote ages used to calculate the weighted-mean age of metamorphism (see text for discussion). Back scattered electron (BSE) images show spot analyses (correspond to analyses in APPENDIX 3B; errors given at 1σ); white scale bars all 50 µm; mean ages reported at the 2σ confidence level.

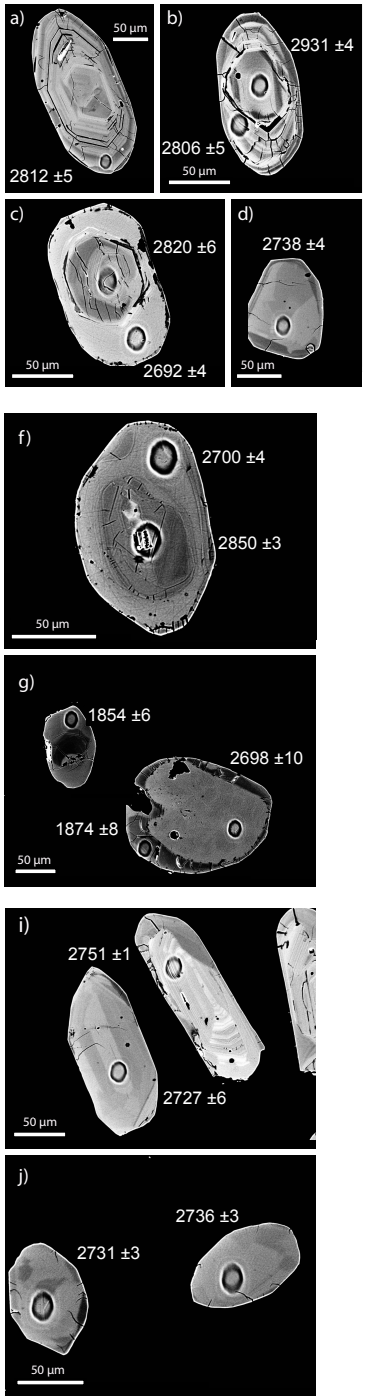

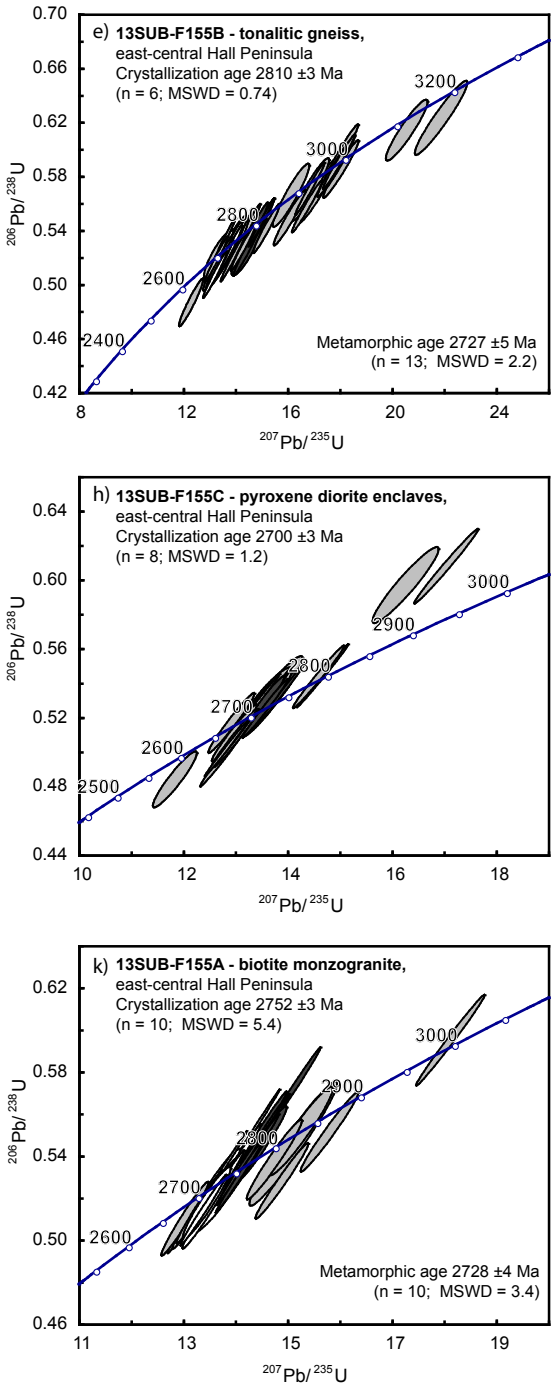

zonation and consistent Th/U values (0.33 to 0.53) are interpreted to represent the crystallization age of the grey tonalite gneiss. These data give a $^{207}Pb/^{206}Pb$ weighted-mean age of 2810 ±3 Ma (n = 6, MSWD = 0.74; Figure 3.4e). Four younger ages, from ca. 2794 to 2766 Ma, are from oscillatory-zoned zircon with high U and low Th/U values (0.05 to 0.39), and may represent scatter of ages due to Pb loss (see below). The youngest zircon ages, from ca. 2738 to 2671 Ma, are from zircon overgrowth rims and stubby single grains. Many of these zircons are unzoned and have Th/U ratios that are two to four times higher than the Th/U values from all other zircons previously mentioned (0.69 to 1.36). These ages suggest a separate episode of zircon growth with a weighted-mean $^{207}Pb/^{206}Pb$ age of 2727 ±5 (n = 13, MSWD = 2.2). This separate episode of zircon growth is likely from an Archean tectonothermal event that may have partially reset the isotope systematics of the older, oscillatory-zoned zircon (e.g., Pb loss through partial recrystallization), resulting in the scatter toward younger ages.

3.6.4. 13SUB-F155C – mafic lenses

The discontinuous hornblende diorite lenses occur within the tonalite gneiss (13SUB-F155B) and are generally elongate parallel to the gneissosity. The mineralogy of these mafic lenses is homogeneous, comprising 55% hornblende, 15% biotite, 15% plagioclase, 10% quartz, and 5% accessory allanite and apatite. Initially, these mafic lenses were thought to be boudins of a nearby pyroxene diorite unit (From et al., 2014), but the mafic lenses within the grey tonalite gneiss do not contain any pyroxene and have a significantly different texture than the pyroxene diorite, based on petrographic analyses, making it unlikely that these mafic lenses are derived from the pyroxene diorite. A

sample was collected from the largest mafic horizon (40 cm wide by 80 cm long), observed just a few metres from the grey tonalite gneiss sample (Figure 3.2).

Zircon grains separated from this sample are ovoid with rounded edges. Images (BSE and CL) show that most of the grains are unzoned, with a few grains containing sector zoning (Figure 3.4f, g). In several unzoned grains, there are visible internal cores that are darker in BSE images. Several grains have thin, unzoned overgrowth rims that appear dark in BSE images (Figure 3.4g).

Thirty-four analyses were conducted on 22 zircon grains, yielding a range of $^{207}Pb/^{206}Pb$ ages between ca. 2850 and 1825 Ma (APPENDIX 3B). The four oldest ages, between ca. 2850 and 2777 Ma, are from zircon cores with low Th/U values (0.02 to 0.07); these zircon domains are interpreted as a xenocrystic component. Sixteen $^{207}Pb/^{206}Pb$ ages between ca. 2724 and 2621 Ma are all from the ovoid, unzoned zircon with Th/U values of 0.07 to 0.31. Within this grouping, a cluster of eight analyses gives a $^{207}Pb/^{206}Pb$ weighted-mean age of 2700 ±3 Ma (MSWD = 1.2; Figure 3.4h). This cluster excludes four outlier ages of ca. 2724 to 2714 Ma. The remaining Archean ages, from ca. 2693 to 2621 Ma, likely represent scatter due to non-zero Pb loss. The seven youngest ages, from ca. 1882 to 1826 Ma, are from the thin, unzoned overgrowth rims, which appear black in BSE images and have distinct, low Th/U values (0.01). These zircon rims are interpreted to have grown due to metamorphism during the Paleoproterozoic Trans-Hudson orogeny (St-Onge et al., 2007), which may have also been the thermotectonic event responsible for the non-zero Pb loss of the slightly older ages.

As these mafic lenses were observed only within the tonalite gneiss, they were inferred in the field to be xenoliths or rafts and consequently older than their host

(13SUB-F155B, with a crystallization age of 2810 ±3 Ma). The resulting younger age (2700 ±3 Ma) was unexpected. The revised age relationships among all the samples in the detailed transect will be dealt with in the 'Discussion' section.

3.6.5. 13SUB-F155A – porphyroclastic monzogranite gneiss

The porphyroclastic monzogranite gneiss is fine grained with greyish-white weathered and fresh surfaces, and commonly contains biotite, hornblende and epidote. There is a characteristic porphyroclastic texture in which K-feldspar porphyroclasts of various sizes (0.5 to 5 cm) are commonly sheared and interconnected by recrystallized bands of finer grained K-feldspar. Filed observations led to the interpretation that the porphyroclasts were derived from the disaggregation of coarse-grained syenogranitic veins. The monzogranite gneiss entrains and intrudes into the tonalite gneiss (13SUB-F155B). A representative sample of homogeneous monzogranite gneiss, with minimal porphyroclastic material and mineral segregations, was collected on the northeastern edge of the snow bowl area (Figure 3.2). The sample is medium to coarse grained with a well-developed mineral foliation defined by biotite and hornblende. The mineralogy is 40% quartz, 35% K-feldspar, 10% plagioclase, 5% biotite, 5% hornblende, 2% epidote, 2% chlorite and 1% magnetite.

Zircon separated from this sample is divided into two morphological groups: elongate prismatic (aspect ratios up to 4:1; <200 μm long) grains and ovoid grains with rounded edges. Images (BSE and CL) show that the elongate prismatic zircon grains have well-defined, fine-scale, oscillatory-zoned cores (Figure 3.4i) and homogeneous

overgrowths (Figure 3.4i). The population of ovoid, rounded grains is generally unzoned or sector zoned (Figure 3.4j).

Forty-three analyses were conducted on 37 zircon grains, yielding $^{207}Pb/^{206}Pb$ ages between 2984 and 2687 Ma (APPENDIX 3B). The six oldest ages, between ca. 2984 and 2810 Ma, were from domains with irregular zonation that are interpreted as xenocrystic components. Ten ages between ca. 2761 and 2742 Ma have well-defined, fine-scale oscillatory-growth zonation and high U concentrations (689 to 3639 ppm), and yield a weighted-mean $^{207}Pb/^{206}Pb$ age of 2752 ±3 Ma (MSWD = 5.4; Figure 3.4k), interpreted to represent the crystallization age. The remaining younger ages (n = 25), from ca. 2737 to 2687 Ma, have distinctly lower U concentrations, typically between 200 and 650 ppm, and are generally ovoid with sector zoning, or are unzoned. These ages are interpreted to record a separate episode of zircon growth with a weighted-mean age of 2728 ±4 Ma (n = 10, MSWD = 3.4). Several zircons in this youngest cluster (ca. 2737 to 2687 Ma) show oscillatory zonation; therefore, these data are interpreted to be scatter of the oscillatory-zoned zircon population ca. 2761 to 2742 Ma and are not included in the weighted mean of the youngest zircon-growth episode defined by the ovoid, unzoned grains.

3.6.6. 13SUB-F152A – magnetite-bearing monzogranite gneiss

The magnetite-bearing monzogranite gneiss is medium grained with greyish-white fresh and weathered surfaces. This rock is characterized by abundant melt segregations (leucosomes) that have haloes enriched in mafic minerals (melanosomes). These leucosomes are a prominent feature of this unit, as they locally crosscut the gneissic foliation but are also folded themselves. Magnetite is pervasive throughout the unit, with

a slight concentration along leucosome-melanosome boundaries. A homogeneous sample of magnetite-bearing monzogranite gneiss containing minimal felsic material was collected from the central portion of the snow bowl area (Figure 3.2). The sample is medium grained with a mineral foliation defined by hornblende and biotite. The mineralogy is 25% quartz, 20% K-feldspar, 20% plagioclase, 15% biotite, 10% titanite and 10% hornblende.

Zircon grains separated from this sample are dominantly ovoid, with some being prismatic and elongate (aspect ratios up to 4:1; <200 μm long). Images (BSE and CL) show faint and slightly irregular oscillatory-growth zonation, sometimes with internal discontinuities that truncate zonation (Figure 3.5a, b). All grains have thin, unzoned overgrowth rims (dark in BSE images), but only three of these unzoned rims were large enough for a spot analysis (Figure 3.5b).

Twenty-five analyses were conducted on 20 zircon grains. Twenty analyses yielded $^{207}Pb/^{206}Pb$ ages between ca. 2746 and 2709 Ma (APPENDIX 3B). These ages are indistinguishable chemically or by zonation characteristics and yield a weighted-mean age of 2728 ±5 Ma (n = 20, MSWD = 1.2; Figure 3.5c) that is interpreted as the crystallization age of the magnetite-bearing monzogranite. The three youngest ages, between ca. 1838 to 1740 Ma, are preserved in thin, unzoned rims that have low Th/U values (0.01 to 0.12) compared to the Archean zircon (0.33 to 3.52) and are dark in BSE images. These zircon domains are interpreted to have grown due to metamorphism during the Paleoproterozoic Trans-Hudson orogeny (St-Onge et al., 2007).

Figure 3.5. Representative zircon images and concordia diagrams for a-c) sample 13SUB-F152A; d-f) sample 13SUB-F150A; dark grey ellipses correspond to ages used to calculate the crystallization age; light grey ellipses are ages excluded from the crystallization-age calculation; unfilled ellipses denote ages used to calculate the weighted-mean age of metamorphism (see text for discussion). Back scattered electron (BSE) images show spot analyses (correspond to analyses in APPENDIX 3B; errors given at 1σ); white scale bars all 50 μm; mean ages reported at the 2σ confidence level.

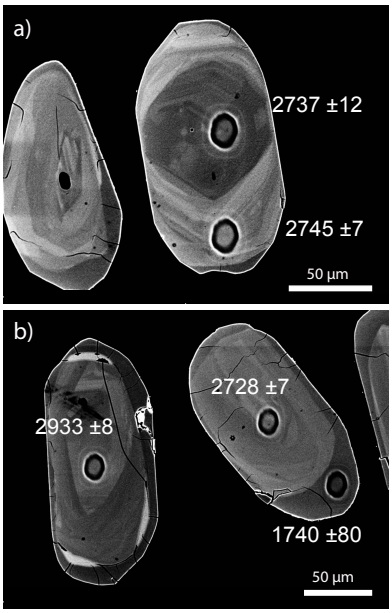

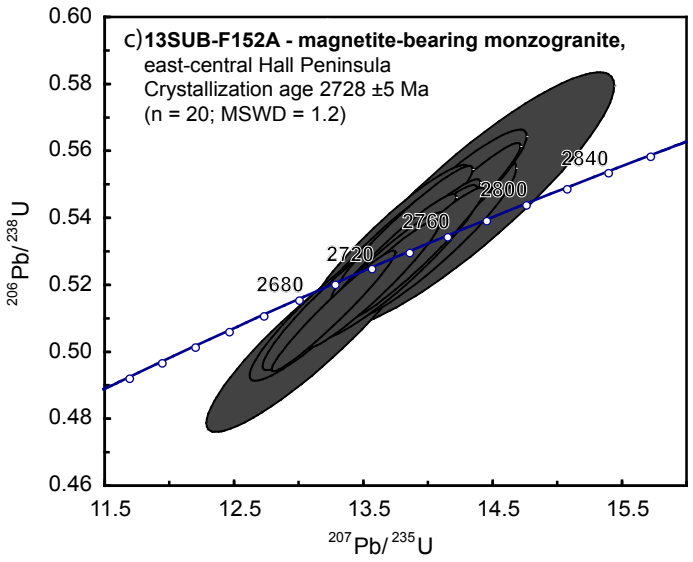

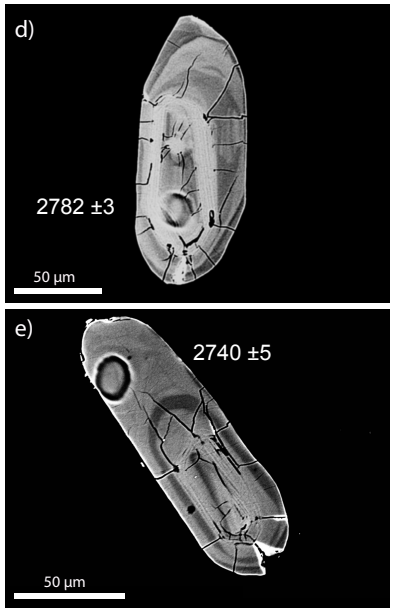

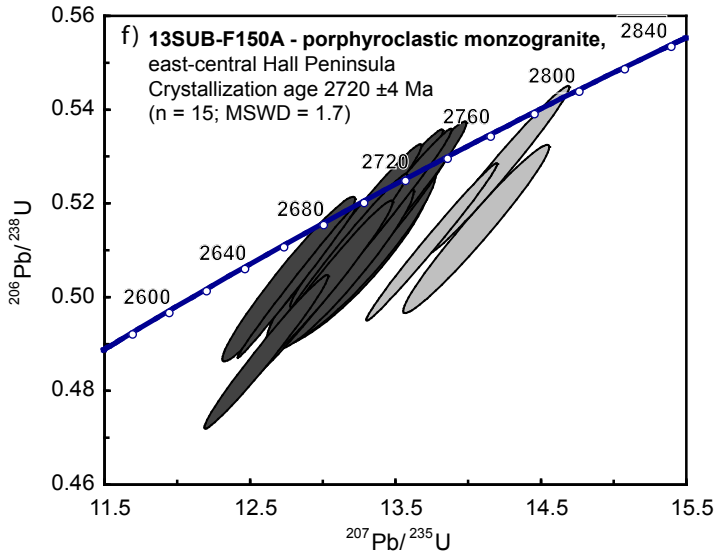

3.6.7. 13SUB-F150A – porphyroclastic monzogranite gneiss

The monzogranite gneiss is characterized by a K-feldspar–porphyroclastic texture similar to that of 13SUB-F155A. The gneiss is fine grained with abundant mineral clots of biotite±hornblende±magnetite and local mineral clots consisting of relict orthopyroxene+clinopyroxene+hornblende. A sample was collected with minimal porphyroclastic material and mineral segregations from the western side of the snow bowl area (Figure 3.2). It is fine grained with a moderate foliation defined by biotite. The mineralogy is 30% quartz, 25% plagioclase, 25% K-feldspar, 10% biotite, 5% titanite, 3% apatite and 2% allanite.

Zircon grains separated from this sample are generally elongate (aspect ratios up to 3:1; <200 μm long), with most grains having subrounded rather than prismatic grain edges. There are several ovoid grains. Images (BSE and CL) of the zircon grains show cores with faint, fine-scale oscillatory-growth zoning (Figure 3.5d, e) and overgrowth rims that are generally unzoned. A few of the rims have faint oscillatory zoning at a broad scale (Figure 3.5a). There are also several equant to ovoid, single grains that are unzoned.

Twenty-seven analyses were conducted on 26 zircon grains, yielding $^{207}Pb/^{206}Pb$ ages between 2810 and 1732 Ma (APPENDIX 3B). The three oldest ages, between ca. 2810 and 2782 Ma, are from zircon cores, which are interpreted to be xenocrystic components. A cluster of 15 ages between ca. 2731 and 2708 Ma is interpreted as the crystallization age of the monzogranite. These ages have a weighted-mean $^{207}Pb/^{206}Pb$ age of 2720 ±4 Ma (n = 15, MSWD = 1.7; Figure 3.5f). Two zircon analyses with younger ages of ca. 2695 and 2686 Ma are interpreted to have been the result of non-zero Pb loss (see below). The two youngest results, ca. 1843 and 1732 Ma, are derived from

unzoned rims that are dark in BSE images and have low Th/U values (0.05 to 0.08). The rims are interpreted to have grown due to metamorphism during the Paleoproterozoic Trans-Hudson orogeny (St-Onge et al., 2007) and may explain the scattered Archean ages that are interpreted to have experienced non-zero Pb loss.

3.7. Discussion

3.7.1. Magmatic versus metamorphic zircon ages

The U-Pb data show that the snow bowl area within the Archean orthogneiss complex of Hall Peninsula has a wide range of Archean $^{207}Pb/^{206}Pb$ spot ages: ca. 3209 to 2682 Ma. However, the detailed assessment of zircon morphology and zonation characteristics allows the discernment between magmatic versus metamorphic zircon-growth events.

The ages of zircon grains from the snow bowl area and two additional Archean orthogneiss samples from eastern Hall Peninsula (12MBC-F105A, 12MBC-F096A; Rayner, 2014) can be grouped based on the zircon domain characteristics as having oscillatory, irregular or no zonation (Figure 3.6). Analyses from several samples with oscillatory-growth zoning (12MBC-S116A, 13SUB-F151A, 13SUB-F155B, 13SUB-F155A, 13SUB-F150A) provide crystallization ages ranging from 2976 ±4 to 2752 ±3 Ma. Unzoned, and irregular- and sector-zoned zircon ages define a consistent range of ca. 2.74 to 2.68 Ga in every sample (Figure 3.6). The unzoned zircons are generally ovoid with rounded grain edges and show Th/U values that are unique (typically lower) from the oscillatory-growth zoned zircons that yielded older ages.

Figure 3.6. Summary of zircon U-Pb ^{207}Pb / ^{206}Pb age data for each sample analyzed from the snow bowl area and two samples (12MBC-F105A, 12MBC-F096A) from the eastern Hall Peninsula orthogneiss complex dated by Rayner (2014). General zonation characteristics associated with age clusters are shown in the legend. Zircon zonation is based purely on characterization from BSE images independent of U-Pb isotopic age interpretation.

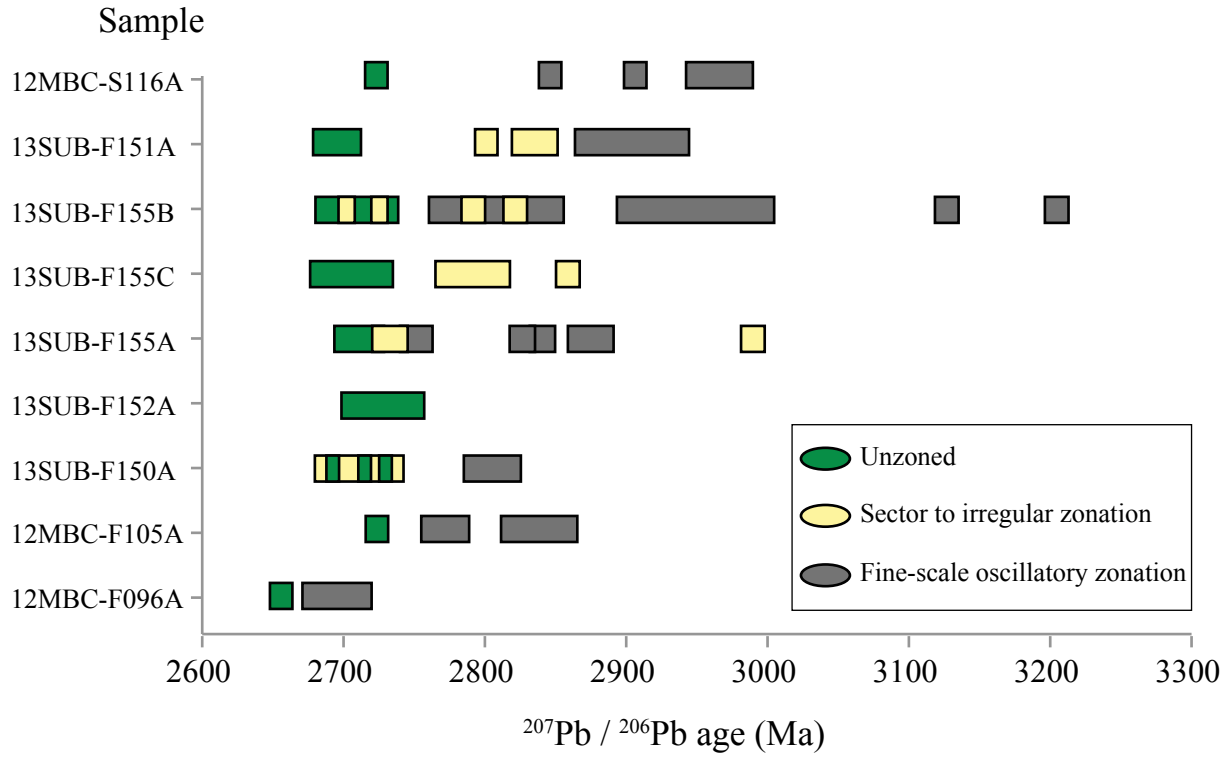

Three samples demonstrate clearly that the Th/U values of the igneous zircon interpreted to represent crystallization ages are distinct from the Th/U values of metamorphic zircon. In the tonalite gneiss (13SUB-F155B), the distinct oscillatory-zoned zircons used to interpret the crystallization age have consistent Th/U values (0.33 to 0.53), whereas the irregularly zoned and unzoned zircons show a broad range of Th/U values (0.05 to 1.36), with most of the values greater than 0.53. Typically, zircon that has grown or been modified after initial magmatic crystallization of the rock has a lower Th/U value than magmatic zircon (see Pidgeon, 1992). Although zircon with Th/U values <0.1 is usually thought to be melt precipitated after initial crystallization, it has been shown that magmatic zircon can have a large Th/U value range of 0.1 to 1.0 and higher (Rubatto, 2002), precluding interpretations based solely on Th/U values. Therefore, the consistency between the zonation characteristics, Th/U values and $^{207}Pb/^{206}Pb$ ages is critical for identifying the different zircon-growth processes. In the megacrystic granodiorite gneiss (13SUB-F151A), the three unzoned zircons with ages between ca. 2.72 and 2.69 Ga have Th/U values (0.07 to 0.18) that are clearly distinguished from the larger Th/U values (0.39 to 0.73) of the fine-scale oscillatory-growth zoned zircons with ages between ca. 2.95 and 2.79 Ga. In the biotite monzogranite (13SUB-F155A), the zircons displaying fine-scale oscillatory-growth zoning have high U and Th values of 689 to 3639 ppm and 277 to 3477 ppm, respectively. The homogeneous, unzoned zircon rims have distinctly lower U and Th values of 206 to 619 ppm and 107 to 620 ppm, respectively, except for two zircons that have U values of 2145 and 3062 ppm, sharing the distinctly high U values of the oscillatory-zoned zircons (APPENDIX 3B). These two zircons may have initially crystallized with the oscillatory-zoned group at ca. 2752 ±3 Ma

but underwent non-zero Pb loss due to recrystallization and yet preserved their initial anomalous U and Th content.

Interestingly, the remaining three samples that do not record multiple Archean zircon-growth events (13SUB-F155C, 13SUB-F152A, 13SUB-F150A) instead record Paleoproterozoic ages that are synchronous with the terminal collision of the Trans-Hudson orogen, which occurred from ca. 1.88 to 1.80 Ga (St-Onge et al., 2009). All of the Paleoproterozoic zircon ages have low Th/U ratios of 0.01 to 0.12 and are clearly distinguished from the older Archean zircon ages, which have Th/U ratios of 0.21 to 3.52.

3.7.2. Revised age relations between units

Relative emplacement ages of eight rock units were interpreted from field observations in Chapter 2 based on crosscutting relationships. The new U-Pb ages on six of these units provide absolute constraints on the relationships observed in the field (Table 3.1). There is an interesting comparison between the absolute ages and the field relationships of the three samples collected from the 13SUB-F155 locality. Here, monzogranitic gneiss (13SUB-F155A) entrains a raft of tonalite gneiss (13SUB-F155B) that has discontinuous mafic lenses (13SUB-F155C). The mafic lenses were observed only within the tonalite gneiss and initially interpreted to be older than the tonalite gneiss. Surprisingly, the majority of U-Pb ages from zircon within the mafic lenses cluster at ca. 2700 Ma, which is much younger than the tonalite gneiss that has an interpreted crystallization age of 2810 ±3 Ma. There are two possible interpretations of the data:

1) The mafic lenses are older than the tonalite gneiss, crystallizing initially as a coherent plutonic rock without primary zircon.

Table 3.1: Summary of the field relationships presented in Chapter 2 compared to the zircon U-Pb age data for six samples from the snow bowl area.

sample	weighted $^{207}Pb/^{206}Pb$ age	lithology	**relative age interpreted in From et al. (2013)**	**revised age relationships**	Figure reference
12MBC-S116A	2976±4	monzogranite gneiss	-	2a	Figure 2.3
13SUB-F151A	2928±5	leopard gneiss	3	2b	Figure 2.3
13SUB-F155B	2810±3	tonalte gneiss	2	3	Figure 2.4
13SUB-F155C	2700±3	mafic lenses	1	1	Figure 2.4
13SUB-F155A	2751±3	monzogranite gneiss	5	4	Figure 2.4
13SUB-F152A	2728±5	magnetite-bearing gneiss	4	5	Figure 2.5
13SUB-F150A	2720±5	monzogranite gneiss	5	6	Figure 2.5

2) The mafic lenses crystallized at ca. 2700 Ma and were subsequently dismembered into discontinuous mafic lenses during the later emplacement of the tonalite gneiss.

Whole-rock geochemistry of the mafic lenses shows silica undersaturation (APPENDIX 3A), which has been linked with crystallization of baddeleyite rather than zircon (Allibon et al., 2011) and supports the notion of an initial crystallization void of zircon crystals. Subsequent partial melting during a tectonometamorphic event at ca. 2700 Ma would then have caused the breakdown of baddeleyite and subsequent crystallization of unzoned, metamorphic zircon.

Additional considerations stem from the relationship between the entraining tonalite gneiss (13SUB-F155B) and the cross-cutting monzogranite gneiss (13SUB-F155A). Ages collected from the fine-scale oscillatory-growth zoning domains of the zircons from the monzogranite gneiss range from ca. 2761 to 2742 Ma. This age range is noticeably absent from the wide spectrum of ages found in the tonalite gneiss. This absence of ages rules out the possibility that those dated zircons are xenocrysts derived from the tonalite gneiss. This also suggests that the younger ages in the tonalite gneiss, ranging from ca. 2738 to 2671 Ma, must be from a later episode of zircon crystallization, interpreted here as an Archean tectonothermal event. Moreover, ovoid, unzoned zircon single grains and overgrowth rims with ages ~2700 Ma were documented in all three of these related units. Therefore, the first interpretation of the mafic lenses being older xenoliths within the tonalite gneiss is preferred.

Sample 12MBC-S116A, a biotite monzogranite gneiss, was taken just northwest of the snow bowl area and has the oldest interpreted crystallization age (2976 ±4 Ma) found so far on Hall Peninsula. This age is closest to the megacrystic granodiorite gneiss

(13SUB-F151A), which has an interpreted crystallization age of 2928 ±5 Ma, but the lithological characteristics and overall textures of these two rock units are very different. Therefore, the biotite monzogranite gneiss does not correlate with any other rock unit documented within the snow bowl area.

This study shows that a small area (700 m transect) within the Archean orthogneiss complex records a complicated and prolonged geological history. Considering the large spatial extent of Archean rocks on eastern Hall Peninsula (>20 000 km^2; Figure 3.1), there likely remain many more undocumented geological complexities that could be revealed upon further, in-depth analysis.

3.8. Conclusions

The seven distinct units from within and around the snow bowl area on east-central Hall Peninsula delineate the episodic crystallization of Archean rocks at ca. 2.98, 2.97, 2.92 and 2.75 Ga. The timing of these crystallization events corresponds to previous work completed on eastern Hall Peninsula that documented emplacement of Archean units from ca. 2.92 to 2.70 Ga (Scott, 1999; Rayner, 2014). Detailed analyses of zircon morphology, structural and chemical zoning characteristics, and Th/U ratios have elucidated a period of subsolidus zircon modification from ca. 2.74 to 2.68 Ga. Zircon overgrowth domains, and new homogeneous and ovoid zircon grains crystallized during this time period are likely due to metamorphism and are consistent with the observed development of partial melt and migmatization throughout the Archean orthogneiss complex of eastern Hall Peninsula.

3.9. Future work

These newly presented U-Pb zircon ages set the stage for further isotopic studies on the same rock units using lutetium-hafnium (Lu-Hf) isotopes. Lu-Hf data can help to provide a more detailed understanding of the magmatic history of the rocks from the snow bowl area. Because zircon effectively preserves the $^{176}Hf/^{177}Hf$ ratio at the time of melt extraction from the mantle, information can be gained about whether rock units in the study area were derived from 1) juvenile crust in episodic melt extraction from the mantle or 2) the recycling of older crust during partial melting and magma mixing events. The same combination of isotopic techniques can then be applied to samples collected from across the Archean orthogneiss complex of Hall Peninsula and the results compared with the dataset from this study.

3.10. Economic considerations

The Archean orthogneiss complex of eastern Hall Peninsula is known to host diamondiferous kimberlites, base metals, gem-quality minerals (spinel, apatite and garnet) and carving stone. The ages of Archean magmatism on eastern Hall Peninsula presented here, and the identification of Archean metamorphism allow for a more detailed correlation and paleotectonic reconstruction with nearby crustal blocks that may have other economic commodities yet to be discovered on Hall Peninsula. In addition, information from this study may help minimize investment risk for diamond exploration by defining the spatial extent of Archean rocks and providing further understanding of tectonic reworking during the Paleoproterozoic.

3.11. Acknowledgments

The authors thank H. Steenkamp, M. St-Onge, D. Mate, G. Machado and the CNGO staff and crew who made the two fields seasons on Hall Peninsula possible. T. Pestaj, R. Chung, R. Christie and P. Hunt at the GSC are thanked for their assistance with sample preparation, SHRIMP instrumentation and data reduction. Reviews of this paper by D. Schneider greatly improved the content, focus and clarity, and are much appreciated. The Canadian Northern Economic Development Agency's (CanNor) Strategic Investments in Northern Economic Development (SINED) program is also thanked for providing financial support for the HPIGP as a whole.

3.12. References

Allibon, J., Ovtcharova, M., Bussy, F., Cosca, M., Schaltegger, U., Bussien, D. and Lewin, É. 2011. Lifetime of an ocean island volcano feeder zone: constraints from U-Pb dating on coexisting zircon and baddeleyite, and 40Ar/39Ar age determinations, Fuerteventura, Canary Islands; Canadian Journal of Earth Sciences, v. 48, p. 567–592.

Connelly, J.N. 2001. Degree of preservation of igneous zonation in zircon as a signpost for concordancy in U/Pb geochronology; Chemical Geology, v. 172, p. 25–39.

Connelly, J.N., Thrane, K., Krawiec, A.W. and Garde, A.A. 2006. Linking the Palaeoproterozoic Nagssugtoqidian and Rinkian orogens through the Disko Bugt region of West Greenland; Journal of the Geological Society, v. 163, p. 319–335.

Corfu, F., Hanchar, J.M., Hoskin, P.W. and Kinny, P. 2003. Atlas of zircon textures; Reviews in Mineralogy and Geochemistry, v. 53, no. 1, p. 469–500. doi:10.2113/0530469

Corrigan, D., Pehrsson, S., Wodicka, N. and De Kemp, E. 2009. The Palaeoproterozoic Trans-Hudson Orogen: a prototype of modern accretionary processes; Geological Society of London, Special Publications, v. 327, p. 457–479. doi: 10.1144/SP327.19

From, R.E., Camacho, A.L. and St-Onge, M.R. 2013. Preliminary observations on the nature and origin of the eastern orthogneiss complex of southern Hall Peninsula, Baffin Island, Nunavut; in Summary of Activities 2012, Canada-Nunavut Geoscience Office, p. 43–54.

From, R.E., St-Onge, M.R. and Camacho, A.L. 2014. Preliminary characterization of the Archean orthogneiss complex of Hall Peninsula, Baffin Island, Nunavut; in Summary of Activities 2013, Canada-Nunavut Geoscience Office, p. 53–62.

Hanchar, J.M. and Miller, C.F. 1993. Zircon zonation patterns as revealed by cathodoluminescence and backscattered electron images: implications for interpretation of complex crustal histories; Chemical Geology, v. 110, p. 1–13

Hollis, J.A., Frei, D., Van Gool, J.A.M., Garde A.A. and Persson, M. 2006. Using zircon geochronology to resolve the Archaean geology of southern West Greenland; Geological Survey of Denmark and Greenland, Bulletin 10, p. 49–52.

Lee, J.K., Williams, I.S. and Ellis, D.J. 1997. Pb, U and Th diffusion in natural zircon; Nature, v. 390, p. 159–162. doi:10.1038/36554

Ludwig, K.R. 2003. User's manual for Isoplot 3.00: a geochronological toolkit for Microsoft® Excel®; Berkeley Geochronology Center, Special Publication 4, 70 p.

Machado, G., Bilodeau, C., Takpanie, R., St-Onge, M.R., Rayner, N.M., Skipton, D.R., From, R.E., MacKay, C.B., Creason, C.G. and Braden, Z.M. 2013. Hall Peninsula regional bedrock mapping, Baffin Island, Nunavut: summary of fieldwork; in Summary of Activities 2012, Canada-Nunavut Geoscience Office, p. 13–22.

Möller A., O'Brien P.J., Kennedy A. and Kröner A. 2002. Polyphase zircon in ultrahigh-temperature granulites (Rogaland, SW Norway): constraints for Pb diffusion in zircon; Journal of Metamorphic Geology, v. 20, p. 727–740.

Pidgeon, R.T. 1992. Recrystallization of oscillatory zoned zircon: some geochronological and petrological implications; Contributions to Mineralogy and Petrology, v. 110, p. 463–472.

Rayner, N.M. 2014. New U-Pb geochronological results from Hall Peninsula, Baffin Island, Nunavut; in Summary of Activities 2013, Canada-Nunavut Geoscience Office, p. 39–52, URL <http://cngo.ca/summary-of-activities/2013/> [March 2015].

Rayner, N.M. 2015. New (2013–2014) U-Pb geochronological results from northern Hall Peninsula, southern Baffin Island, Nunavut; in Summary of Activities 2014, Canada-Nunavut Geoscience Office, p. 31–44 URL <http://cngo.ca/summary-of-activities/2014/> [March 2015].

Rubatto, D. 2002. Zircon trace element geochemistry: partitioning with garnet and the link between U-Pb ages and metamorphism; Chemical Geology, v. 184, p. 123–138.

Scott, D.J. 1999. U-Pb geochronology of the eastern Hall Peninsula, southern Baffin Island, Canada: a northern link between the Archean of West Greenland and the Paleoproterozoic Torngat Orogen of northern Labrador; Precambrian Research, v. 93, p. 5–26.

Scott, D.J. and Campbell, L.M. 1993. Evolution of the Paleoproterozoic Torngat orogen, Labrador, Canada: recent advances using U-Pb geochronology and Nd isotopic systematics (abstract); Geological Society of America, Annual Meeting 1993, Boston, Massachusetts, Program with Abstracts, v. 25, p. A23.

Steenkamp, H.M. and St-Onge, M.R. 2014. Overview of the 2013 regional bedrock mapping program on northern Hall Peninsula, Baffin Island, Nunavut; in Summary of Activities 2013,

Canada-Nunavut Geoscience Office, p. 27–38, URL <http://cngo.ca/summary-of-activities/2013/> [March 2015].

St-Onge, M.R., Scott, D.J. and Wodicka, N. 2002. Review of crustal architecture and evolution in the Ungava Peninsula–Baffin Island area: connection to the Lithoprobe ECSOOT transect; Canadian Journal of Earth Sciences, v. 39, p. 589–610.

St-Onge, M.R., Van Gool, J.A.M., Garde, A.A. and Scott, D.J. 2009. Correlation of Archaean and Palaeoproterozoic units between northeastern Canada and western Greenland: constraining the pre-collisional upper plate accretionary history of the Trans-Hudson orogen; Geological Society of London, Special Publications, v. 318, p. 193–235. doi:10.1144/SP318.7

St-Onge, M.R., Wodicka, N. and Ijewliw, O. 2007. Polymetamorphic evolution of the Trans-Hudson Orogen, Baffin Island, Canada: integration of petrological, structural and geochronological data; Journal of Petrology, v. 48, p. 271–302.

Stern, R.A. 1997. The GSC sensitive high resolution ion microprobe (SHRIMP): analytical techniques of zircon U-Th-Pb age determinations and performance evaluation; in Radiogenic Age and Isotopic Studies: Report 10, Geological Survey of Canada, Current Research 1997-F, p. 1–31.

Stern, R.A. and Amelin, Y. 2003. Assessment of errors in SIMS zircon U-Pb geochronology using a natural zircon standard and NIST SRM 610 glass; Chemical Geology, v. 197, p. 111–146.

Thrane, K. and Connelly J.N. 2006. Zircon geochronology from the Kangatsiaq-Qasigiannguit region, the northern part of the 1.9–1.8 Ga Nagssugtoqidian orogen, West Greenland; Geological Survey of Denmark and Greenland, Bulletin 11, p. 87–99.

Wardle, R.J., James D.T., Scott, D.J. and Hall, J. 2002. The southeastern Churchill Province: synthesis of a Palaeoproterozoic transpressional orogen; Canadian Journal of Earth Sciences, v. 39, p. 639–663. doi:10.1139/E02-004

Whalen, J.B., Wodicka, N., Taylor, B.E. and Jackson, G.D. 2010. Cumberland batholith, Trans-Hudson Orogen, Canada: petrogenesis and implications for Paleoproterozoic crustal and orogenic processes; Lithos, v. 117, p. 99–118.

Williams, I.S. 1992. Some observations on the use of zircon U-Pb geochronology in the study of granitic rocks; Transactions of the Royal Society of Edinburgh: Earth Sciences, v. 83, no. 1-2, p. 447–458. doi:10.1017/S0263593300008129

3.13. Data appendices

APPENDIX 3A - Lithogeochemical data for selected Hall Peninsula samples from the 2012 (12MBC) and 2013 (13SUB) field seasons.
APPENDIX 3B - SHRIMP U-Pb isotopic data.

APPENDIX 3A - Lithogeochemical data for selected Hall Peninsula samples from the 2012 (12MBC) and 2013 (13SUB) field seasons

SampleID	Latitude	Longitude	Field Lithology	Q	Ab	Or	SiO2	Al2O3	Fe2O3(T)	MnO	MgO	CaO
12MBC-B011D	63.21071	-66.02407	tonalite	46.7	49.0	4.2	75.04	14.51	0.94	0.01	0.27	3.37
12MBC-B022A	62.27223	-64.22208	granite	47.5	46.1	6.5	74.78	13.75	1.83	0.013	0.46	3.08
12MBC-B025A	62.32330	-64.37124	granite	31.5	57.5	11.0	69.09	16.33	2.9	0.039	0.92	3.59
12MBC-B031A1	63.28452	-65.55452	tonalite	33.5	43.2	23.4	71.91	15.13	0.94	0.014	0.21	2.21
12MBC-B056A1	63.31075	-64.55559	porphyritic granite	33.0	28.8	38.1	68.82	14.4	4.12	0.05	0.97	2.14
12MBC-B076A1	63.30342	-64.22356	tonalite	32.9	56.4	10.7	70.97	16.31	2.32	0.024	0.83	2.99
12MBC-B082A1	63.31521	-65.38102	tonalite	40.7	50.2	9.1	66.68	16.03	3.56	0.05	1.25	4.62
12MBC-B107A1	63.48300	-65.18076	porphyritic granite	27.7	37.6	34.6	68.84	14.08	4.78	0.061	1.02	2.44
12MBC-B108A	63.50467	-64.58487	tonalite	37.0	48.1	14.9	66.35	16.01	3.85	0.057	1.92	4.56
12MBC-B117A1	63.41310	-65.29168	mzgranite	30.2	49.0	20.8	72.5	14.13	1.44	0.017	0.42	1.93
12MBC-B117C1	63.41310	-65.29168	charnockite	42.0	51.6	6.4	70.96	16.29	2.22	0.026	0.8	4.6
12MBC-B127A1	63.11565	-65.27345	tonalite	42.4	48.2	9.5	72.65	15	1.64	0.021	0.68	3.04
12MBC-B155A1	62.52331	-65.09362	mzgranite	22.2	65.9	12.0	63.77	18.38	2.84	0.043	1.59	5.3
12MBC-B157A1	63.38031	-64.49371	diorite	31.4	53.2	15.4	64.05	16.21	5.91	0.102	2.32	5.13
12MBC-C038A1	63.31445	-65.32481	tonalite/mzgr	34.3	49.2	16.5	71.87	16.14	0.86	0.01	0.13	2.95
12MBC-C077A2	62.48320	-65.07265	diorite	48.8	43.9	7.2	71.18	14.48	3.58	0.052	1.32	4.64
12MBC-F018A1	63.02347	-65.34204	porphyritic granite	31.0	30.6	38.4	68.17	14.51	4.65	0.058	1.29	2.62
12MBC-F037A1	63.25201	-64.32239	tonalite	40.7	38.6	20.7	71.37	14.37	2.78	0.045	0.72	2.4
12MBC-F096A1	63.21534	-65.32384	porphyritic granite	34.7	28.6	36.6	70.87	13.65	4.3	0.038	1.01	1.44
12MBC-F105A1	63.26186	-64.42458	tonalite	36.9	30.1	33.0	69.58	14.29	2.98	0.047	1.07	2.22
12MBC-K021A2	63.22504	-66.59329	mzgranite	46.8	42.1	11.1	74.11	15.62	0.8	0.01	0.21	2.64
12MBC-K051A1	63.09370	-65.25308	porphyritic granite	23.5	37.2	39.3	64.44	15.82	5.16	0.063	1.41	3
12MBC-K058A1	63.09423	-65.53519	tonalite	27.4	60.7	12.0	66.77	18.2	2.74	0.034	1.14	4.16
12MBC-K103A1	63.45287	-65.09348	porphyritic granite	27.9	40.5	31.6	66.45	14.85	5.45	0.065	1.29	3.36
12MBC-K107A1	63.34229	-65.27457	mzgranite	40.0	27.5	32.5	75.26	13.56	1.74	0.024	0.3	1.48
12MBC-K111A1	63.32301	-65.31031	mzgranite	36.1	29.0	34.9	71.1	14.34	1.48	0.022	0.55	1.82
12MBC-K111B1	63.32301	-65.31031	mzgranite	40.4	34.7	24.9	73.79	14.53	2	0.022	0.59	2.23
12MBC-M027A1	63.38409	-65.27319	mzgranite	35.5	30.1	34.4	73.47	14.52	1.92	0.022	0.38	1.59
12MBC-S018A1	62.56170	-65.13159	mzgranite	49.0	45.2	5.8	74.52	14.44	0.92	0.008	0.31	3.24
12MBC-S116A1	63.56141	-65.36139	mzgranite	43.9	49.0	7.1	73.64	15.12	2.18	0.022	0.58	2.87
12MBC-S119A1	63.55377	-65.37257	mzgranite	35.1	51.2	13.7	64.19	16.16	5.78	0.075	2.21	4.97
12MBC-S130A1	63.07205	-64.50339	mzgranite	33.5	55.6	11.0	70.21	16.97	2.19	0.028	0.82	3.18
12MBC-S170A1	63.40443	-64.47132	tonalite	40.9	30.7	28.4	73.11	15.66	0.51	0.006	0.12	2.63

Na2O	K2O	TiO2	P2O5	LOI	Total	Sc	Be	V	Cr	Co	Ni	Cu	Zn	Ga	Ge	As	Rb	Sr	Y	Zr	Nb	Mo	Ag
4.7	0.58	0.081	0.01	0.22	99.72	1	1	16	40	8	30	20	30	17	1.7	5	7	418	0.6	44	0.4	2	0.5
4.42	0.89	0.151	0.05	0.2	99.62	1	1	13	20	5	20	10	30	18	1.9	5	18	343	1.3	124	0.8	5	1.1
5.23	1.43	0.333	0.1	0.25	100.2	6	1	38	20	8	20	10	60	21	1.7	5	45	341	5.6	146	2.8	2	1
4.36	3.38	0.081	0.01	0.13	98.36	1	1	7	20	2	20	20	30	18	1.7	5	55	442	1.3	64	0.9	2	0.5
2.78	5.27	0.687	0.17	0.34	99.76	9	2	42	20	7	20	10	60	21	1.4	5	147	292	28.4	366	21.6	2	2.2
5.38	1.46	0.294	0.05	0.24	100.9	2	1	30	20	7	20	10	60	22	1.6	5	54	412	1	119	2	2	1
4.05	1.05	0.429	0.14	0.26	98.12	6	1	53	20	8	20	10	50	19	0.9	5	29	399	5.4	140	3.4	2	1
3.66	4.83	0.755	0.18	0.27	100.9	8	2	42	20	9	20	10	80	24	2.9	5	138	214	31.3	478	21.3	3	3.4
3.85	1.71	0.421	0.16	1.2	100.1	8	2	56	20	10	20	10	60	20	1.2	5	106	546	7	126	6.1	2	0.7
5.08	3.09	0.191	0.05	0.17	99.03	2	1	18	20	3	20	10	50	24	2.1	5	90	498	2.7	108	2.6	2	0.7
4.48	0.8	0.318	0.06	0.07	100.6	3	1	32	20	5	20	20	30	19	0.7	5	19	392	1.8	118	2.3	2	0.7
4.55	1.28	0.193	0.03	0.37	99.46	2	2	23	20	4	20	10	30	19	0.8	5	46	319	1.3	73	2.1	2	0.5
5.26	1.37	0.403	0.27	0.59	99.81	4	2	40	20	8	30	10	60	21	1	5	44	706	6.2	95	4.8	2	0.5
4.04	1.67	0.645	0.16	0.4	100.6	10	2	93	30	16	30	10	90	22	1.4	5	66	333	14.8	157	5.8	2	0.8
4.83	2.32	0.054	0.02	0.14	99.32	1	1	12	20	1	20	10	30	20	1.8	5	52	469	1.2	111	0.2	2	0.7
3.68	0.87	0.273	0.02	0.44	100.5	10	1	76	50	14	40	80	70	15	0.9	5	6	355	5.2	49	1.4	2	0.5
2.86	5.13	0.766	0.21	0.23	100.5	7	2	54	20	9	20	10	70	21	1.3	5	128	338	20.1	361	14.7	2	2.2
3.7	2.84	0.321	0.07	0.22	98.83	5	1	34	130	5	20	10	50	18	1.2	5	94	253	9.8	163	5.2	2	1
2.89	5.3	0.53	0.17	0.59	100.8	6	2	31	20	5	20	10	70	22	1.5	5	174	140	14.9	320	17.7	2	1.7
2.86	4.5	0.335	0.09	0.3	98.27	4	2	38	20	6	20	10	30	17	1	5	128	284	10.3	122	5.1	2	0.6
4.09	1.54	0.079	0.01	0.24	99.35	1	1	9	20	1	20	10	30	19	0.7	5	24	505	0.5	92	0.7	2	0.5
3.35	5.06	0.74	0.29	0.38	99.72	12	2	60	20	9	20	20	70	22	1.4	5	145	521	31.6	383	14.4	2	3.2
5.28	1.49	0.347	0.14	0.42	100.7	5	1	38	20	8	20	20	50	21	1.8	5	47	725	4.4	154	2.2	2	1.1
3.65	4.07	0.91	0.27	0.2	100.6	9	2	55	90	10	20	10	80	23	1.4	5	100	315	27.2	458	19.6	2	2.6
2.92	4.94	0.134	0.05	0.14	100.6	1	1	25	20	2	20	10	30	16	0.9	5	152	373	2.2	166	2.1	2	1
2.9	5	0.174	0.06	0.31	97.78	2	1	21	20	3	20	10	30	15	0.8	5	96	347	2.4	125	1.6	2	0.6
3.49	3.58	0.208	0.05	0.29	100.8	1	1	27	20	4	20	10	40	17	0.8	5	78	292	2.6	176	1.6	2	1
3.16	5.17	0.23	0.06	0.16	100.7	1	1	17	20	2	20	80	40	19	0.8	5	152	150	2.4	198	3.5	2	1.2
4.28	0.78	0.097	0.01	0.15	98.77	1	1	14	20	2	20	10	30	18	0.9	5	18	518	0.5	60	0.7	2	0.5
4.71	0.98	0.25	0.06	0.2	100.6	1	1	30	20	4	20	10	40	20	0.8	5	23	378	1.7	100	1.4	2	0.5
3.86	1.48	0.578	0.12	0.3	99.71	11	1	89	130	15	30	10	70	20	1	5	50	377	9.5	137	3.1	2	0.8
5.2	1.47	0.247	0.07	0.23	100.6	2	1	24	20	5	20	10	100	23	0.8	5	54	460	2	79	1.9	2	0.5
3.29	4.36	0.034	0.01	0.12	99.85	1	1	11	20	1	20	10	30	19	1.1	5	102	150	0.5	27	0.2	2	0.5

In	Sn	Sb	Cs	Ba	La	Ce	Pr	Nd	Sm	Eu	Gd	Tb	Dy	Ho	Er	Tm	Yb	Lu	Hf	Ta
0.1	1	0.6	0.1	270	7.61	10.2	0.99	2.94	0.4	0.574	0.4	0.04	0.12	0.02	0.05	0.009	0.08	0.02	1.3	0.01
0.1	1	0.5	0.7	228	12.8	21.1	2.18	7.43	1.06	0.491	0.75	0.07	0.3	0.05	0.16	0.025	0.18	0.034	3.3	0.01
0.1	1	0.6	1.7	260	15.5	29.5	3.4	12.6	2.29	0.605	1.99	0.25	1.21	0.22	0.59	0.079	0.49	0.078	3.6	0.27
0.1	2	0.8	0.4	1067	9.21	17.3	1.96	6.56	1.13	0.422	0.79	0.07	0.33	0.05	0.14	0.02	0.13	0.023	1.8	0.01
0.1	3	0.2	1.6	1262	79.4	181	17	58.7	9.5	1.52	6.77	1.07	6.16	1.15	3.22	0.455	2.91	0.461	8.4	2.2
0.1	1	0.4	1.1	244	5	11.4	1.07	3.86	0.75	0.401	0.53	0.06	0.26	0.05	0.14	0.02	0.13	0.021	2.7	0.08
0.1	1	0.2	0.5	304	22.2	47.4	4.93	18	2.61	0.674	1.75	0.24	1.24	0.22	0.6	0.08	0.5	0.079	3	0.17
0.1	1	0.5	0.6	839	40.5	100	13.4	53.5	10.6	1.43	8	1.16	6.21	1.17	3.12	0.429	2.69	0.425	10.1	0.99
0.1	1	0.2	10.4	448	36.5	75.6	7.74	28.1	3.66	0.838	2.2	0.29	1.46	0.26	0.7	0.095	0.59	0.098	3	0.98
0.1	1	0.6	0.5	738	22.4	41.8	4.71	15.5	2	0.576	1.44	0.15	0.57	0.09	0.22	0.029	0.18	0.033	2.6	0.07
0.1	1	0.2	0.1	259	11.3	17.2	1.66	5.62	0.8	0.456	0.61	0.08	0.39	0.07	0.17	0.026	0.2	0.039	2.6	0.1
0.1	1	0.2	0.9	136	10.5	11.3	1.63	5.62	0.75	0.497	0.52	0.06	0.25	0.05	0.12	0.016	0.1	0.017	1.9	0.07
0.1	1	0.2	0.6	424	38.5	80.8	9.35	36.4	5.3	1.06	2.74	0.3	1.39	0.25	0.66	0.092	0.59	0.099	2.6	0.92
0.1	1	0.2	1.9	324	21.2	41.8	4.33	17.3	3.27	0.833	2.87	0.48	2.8	0.56	1.63	0.249	1.72	0.304	3.4	11.1
0.1	1	0.4	0.3	736	5.88	16.3	0.91	2.96	0.35	0.446	0.43	0.05	0.21	0.04	0.14	0.029	0.26	0.055	4.2	0.01
0.1	1	0.2	0.1	149	4.44	7.98	0.91	3.87	0.85	0.342	0.83	0.16	1.01	0.21	0.61	0.088	0.57	0.099	1.3	0.23
0.1	3	0.2	0.6	1563	77.5	184	15.6	54.4	8.19	1.42	5.52	0.81	4.29	0.77	2.02	0.29	1.97	0.343	8	0.77
0.1	1	0.2	2.7	860	38.6	76.6	7.61	26.7	3.73	0.732	2.47	0.33	1.95	0.38	1.11	0.166	1.15	0.202	3.9	0.47
0.1	1	0.2	1.8	788	63.4	139	10.8	35	4.91	0.844	3.4	0.51	2.97	0.58	1.61	0.235	1.53	0.251	7.7	1
0.1	1	0.2	2.3	1286	35.2	62.4	6.42	22.2	3.18	0.946	2.27	0.35	2.03	0.4	1.1	0.156	1	0.163	2.8	0.44
0.1	1	0.2	0.1	624	6.07	6.84	0.63	1.97	0.16	0.559	0.09	0.01	0.06	0.01	0.03	0.006	0.05	0.011	2.5	0.02
0.1	3	0.2	0.9	2685	98.2	191	21.4	81.8	13.4	2.23	9.15	1.25	6.56	1.14	3.02	0.41	2.47	0.397	8.6	1.44
0.1	1	0.4	0.4	542	20.1	35.8	4.13	13.9	2.52	0.739	1.71	0.22	1.06	0.18	0.48	0.065	0.42	0.078	3.9	0.08
0.1	1	0.2	0.3	1004	57.7	141	15.5	59.6	9.61	1.59	6.77	1.03	5.74	1.07	2.88	0.407	2.58	0.399	9.6	0.91
0.1	1	0.2	1.4	1486	14.4	54.5	2.2	6.64	1.02	0.392	0.7	0.09	0.46	0.08	0.23	0.033	0.24	0.053	4.5	0.09
0.1	1	0.2	0.2	1729	20.7	30.5	2.97	9.93	1.24	0.807	0.88	0.1	0.52	0.09	0.24	0.033	0.23	0.047	3.2	0.06
0.1	1	0.2	0.2	904	50.3	86.1	7.49	23.6	2.5	0.558	1.33	0.14	0.62	0.1	0.28	0.039	0.27	0.054	4.4	0.03
0.1	1	0.2	0.3	779	26.6	93.4	5.04	15.5	2.08	0.477	1.17	0.13	0.58	0.1	0.25	0.036	0.26	0.048	5.1	0.1
0.1	1	0.2	0.2	185	7.68	12	1.05	3.2	0.3	0.534	0.16	0.01	0.07	0.01	0.04	0.006	0.06	0.017	2	0.01
0.1	1	0.2	0.2	314	13.7	24.7	2.42	8.83	1.23	0.49	0.77	0.08	0.39	0.06	0.16	0.022	0.14	0.025	2.5	0.04
0.1	1	0.2	2.8	393	14.4	34.3	3.59	14.2	2.75	0.723	2.27	0.35	2.06	0.38	1.06	0.156	1.07	0.179	3.3	0.18
0.1	1	0.2	1.8	399	6.5	12.6	1.31	5.26	0.97	0.389	0.81	0.09	0.44	0.08	0.19	0.026	0.15	0.021	2.1	0.12
0.1	1	0.2	0.4	228	1.17	2.11	0.2	0.73	0.12	0.307	0.09	0.01	0.06	0.01	0.03	0.006	0.06	0.017	1.1	0.02

W	Tl	Pb	Bi	Th	U
1.4	0.05	8	0.1	0.3	0.1
1.1	0.09	5	0.1	1.25	0.27
1.3	0.25	6	0.1	2.9	0.43
0.9	0.32	17	0.1	3.52	0.24
0.6	0.61	16	0.1	13.1	1.96
1.3	0.24	5	0.1	0.75	0.15
0.5	0.23	5	0.1	2.6	0.17
0.9	0.56	16	0.1	6.3	1.44
0.8	0.55	8	0.9	6.29	0.6
1.5	0.54	15	0.1	3.7	0.42
2.4	0.07	5	0.1	0.14	0.13
0.5	0.2	10	0.1	0.98	0.18
0.5	0.15	10	0.1	7.61	0.99
0.5	0.28	7	0.2	2.24	0.59
0.9	0.27	18	0.1	0.78	0.74
0.5	0.05	7	0.1	1.67	0.44
0.5	0.52	17	0.1	16.4	0.58
0.5	0.43	12	0.1	10.6	1.35
0.5	0.8	20	0.1	19.8	1.27
0.5	0.54	13	0.1	6.52	0.87
0.5	0.05	11	0.1	0.05	0.15
0.5	0.66	18	0.1	15.9	1.46
0.8	0.29	8	0.1	2.3	0.2
0.5	0.39	12	0.1	2.89	0.98
0.5	0.64	18	0.1	15.7	0.47
0.5	0.45	12	0.1	0.96	0.21
0.5	0.3	11	0.1	11.2	0.33
0.5	0.79	17	0.1	14.5	0.59
0.5	0.14	9	0.1	0.48	0.24
0.5	0.1	5	0.1	0.57	0.14
0.5	0.2	6	0.3	2.65	0.86
0.5	0.19	6	0.1	0.19	0.12
0.5	0.39	30	0.1	8.49	1.54

APPENDIX 3A - Lithogeochemical data for selected Hall Peninsula samples from the 2012 (12MBC) and 2013 (13SUB) field seasons

SampleID	Latitude	Longitude	Field Lithology	Q	Ab	Or	SiO2	Al2O3	Fe2O3(T)	MnO	MgO	CaO
12MBC-Y007B1	63.06333	65.38174	mzgranite	55.6	38.4	5.9	77.29	12.81	1.74	0.013	0.36	2.71
12MBC-Y079A1	62.54209	-64.36290	charnockite	40.0	27.8	32.3	75.91	13.29	1.28	0.013	0.34	1.5
12MBC-R011A3	63.21508	-66.22483	charnockite	38.3	52.4	9.3	71.35	16.07	2.34	0.021	0.85	3.31
13SUB-B007A	62.57463	-65.47266	granite	46.0	44.2	9.9	71.34	15.42	2.96	0.026	0.97	3.84
13SUB-K015A	63.21033	-65.08147	mafic tonalite	12.9	54.5	32.6	57.6	15.5	8.23	0.142	3.17	5.7
13SUB-K015B	63.21033	-65.08147	syenogranite	31.6	32.4	36.0	71.19	14.54	2.72	0.032	0.54	1.4
13SUB-S154A	63.14063	-65.14280	mt mzgranite	38.6	49.8	11.6	68.49	15.83	4	0.057	1.36	4.01
13SUB-S154B	63.14063	-65.14280	syenogranite	38.4	29.5	32.1	76.45	13.61	0.75	0.01	0.12	1.36
13SUB-T027A	63.09442	-65.14440	mt syenogranite	35.1	32.6	32.3	72.28	14.46	2.77	0.03	0.53	1.85
13SUB-F150A	63.56133	-65.32457	bt ep mzgranite	34.9	49.1	16.0	69.49	16.03	2.43	0.029	0.79	3.23
13SUB-F151A	63.56121	-65.32480	hbl bt granodiorite	33.0	53.2	13.8	64.93	16.38	5.59	0.089	2.18	4.94
13SUB-F151B	63.56121	-65.32480	bt hbl diorite	34.8	60.4	4.8	64.26	16.44	4.9	0.051	1.58	6.17
13SUB-F152A	63.56140	-65.32440	mt mzgranite	29.1	48.0	22.8	64.64	15.16	6.73	0.062	1.51	3.44
13SUB-F153C	63.56165	-65.32399	ribbon monzogranite	36.9	26.8	36.3	76.03	13.75	0.77	0.008	0.16	1.03
13SUB-F154B	63.56175	-65.32381	gabbro	-	-	-	46.96	15.29	13.43	0.2	8.82	10.36
13SUB-F154C	63.56175	-65.32381	mzgranite	39.8	30.6	29.6	75.23	14.51	0.55	0.006	0.04	1.91
13SUB-F155A	63.56195	-65.32301	bt hbl ep mzgranite	35.0	36.1	28.8	72.3	14.77	1.72	0.027	0.49	2
13SUB-F155B	63.56195	-65.32301	bt hbl tonalite	33.0	52.0	15.0	66	15.16	4.95	0.091	3.2	4.81
13SUB-F155C	63.56195	-65.32301	hbl pl qtz diorite	-	-	-	48.65	11.88	13.15	0.294	10.21	10.35
13SUB-F156B	63.56222	-65.32238	qtz diorite	8.2	84.6	7.1	49.16	15.69	10.85	0.283	4.84	14.23
13SUB-F157A	64.32447	-66.26187	monzogranite	37.1	52.2	10.6	69.94	15.91	3.53	0.04	1.12	3.44
13SUB-H055A	63.54237	-66.20385	monzogranite	76.2	20.3	3.5	70.6	16.36	2.72	0.022	0.77	3.08
13SUB-H056A	63.57199	-65.33526	granite	31.2	67.6	1.2	72.28	13.9	1.57	0.018	0.47	0.81
13SUB-H086A	64.07242	-64.28481	tonalite	39.4	23.2	37.3	74.57	13.37	2.11	0.019	0.38	1.5
13SUB-H090A	64.09482	-64.57223	tonalite	37.1	47.4	15.5	72.07	15.42	2.06	0.027	0.58	2.7
13SUB-H098A	64.27474	-65.00092	tonalite	37.1	45.9	16.9	72.05	15.59	2.08	0.021	0.72	2.63
13SUB-K037A	64.33518	-66.45530	tonalite	43.5	39.3	17.2	73.58	14.36	2.37	0.053	0.56	2.28
13SUB-Y032A	64.33472	-66.58162	granodiorite	16.8	52.4	30.8	58.74	16.28	7.4	0.087	3.03	5.43
13SUB-Y033A	64.33360	-67.00033	qtz diorite to tonalite	41.9	52.1	6.0	64.46	13.38	7.57	0.12	3.91	7.23
13SUB-Z108A	64.11139	-65.39338	monzogranite	38.7	48.3	13.0	70.96	15.37	2.26	0.036	0.6	3.05

Na2O	K2O	TiO2	P2O5	LOI	Total	Sc	Be	V	Cr	Co	Ni	Cu	Zn	Ga	Ge	As	Rb	Sr	Y	Zr	Nb	Mo	Ag
3.76	0.83	0.169	0.04	0.2	99.92	1	1	16	20	3	20	10	30	16	1.9	5	20	284	0.9	107	0.2	2	1
2.97	4.94	0.145	0.04	0.1	100.5	1	1	14	20	2	20	10	30	16	1.9	5	102	218	2.3	123	0.6	2	0.8
4.87	1.24	0.291	0.07	0.24	100.7	3	1	33	20	6	20	30	50	22	1.8	5	38	588	1.6	115	0.8	2	1.8
3.91	1.25	0.321	0.09	0.67	100.8	2	1	41	30	6	< 20	10	50	19	0.7	< 5	482	< 0.1	540	< 0.2	1.4	31.3	2.9
3.76	3.22	1.448	0.37	0.56	99.71	15	3	105	50	19	50	< 10	140	24	1.6	< 5	320	< 0.1	866	< 0.2	22.6	116	14.9
3.34	5.32	0.329	0.09	0.48	99.97	3	1	28	30	3	< 20	10	40	22	1.4	< 5	212	< 0.1	1356	< 0.2	9	228	24.8
4.27	1.42	0.438	0.12	0.44	100.4	6	2	52	40	9	< 20	< 10	70	20	1.3	< 5	400	< 0.1	338	< 0.2	3.8	35.9	4.39
3.22	5.02	0.039	0.01	0.24	100.8	< 1	1	7	< 20	< 1	< 20	< 10	< 30	16	1.1	< 5	153	< 0.1	790	< 0.2	0.5	26.4	3.99
3.34	4.73	0.232	0.13	0.44	100.8	1	1	41	30	4	< 20	10	50	19	1.3	< 5	342	< 0.1	1225	< 0.2	2.8	175	17.9
4.53	2.11	0.327	0.1	0.72	99.79	2	2	28	< 20	4	< 20	< 10	40	20	0.9	< 5	356	< 0.1	578	< 0.2	3	59.9	6.35
4.13	1.54	0.614	0.17	0.42	101	12	1	84	30	14	20	< 10	80	21	1.3	< 5	352	< 0.1	386	< 0.2	4.8	35.6	4.93
4.43	0.5	0.788	0.21	0.34	99.67	8	1	69	< 20	12	< 20	40	50	19	0.9	< 5	317	< 0.1	83	< 0.2	4.1	14.4	2.05
4.17	2.84	1.337	0.53	0.41	100.8	8	2	84	20	11	< 20	20	90	21	1.5	< 5	374	< 0.1	1348	< 0.2	22.7	221	23
2.96	5.74	0.053	0.02	0.36	100.9	< 1	< 1	9	< 20	< 1	< 20	< 10	< 30	12	0.7	< 5	508	< 0.1	2227	< 0.2	< 0.2	8.28	0.91
2.56	1.33	0.874	0.07	0.73	100.6	39	< 1	274	260	51	180	< 10	90	16	2.3	< 5	87	< 0.1	33	< 0.2	1.7	7.63	1.19
3.22	4.45	0.019	< 0.01	0.21	100.2	< 1	< 1	< 5	< 20	< 1	< 20	< 10	< 30	17	1	< 5	218	< 0.1	996	< 0.2	< 0.2	14.1	0.98
3.67	4.19	0.125	0.06	0.27	99.62	2	1	24	< 20	3	< 20	< 10	30	19	1.2	< 5	304	< 0.1	881	< 0.2	1.1	39.3	3.36
4.03	1.66	0.448	0.18	0.41	100.9	12	2	87	120	14	50	< 10	70	18	1.3	< 5	430	< 0.1	534	< 0.2	3.4	57.6	7.64
2.02	1.65	0.772	0.58	1.19	100.8	33	3	222	610	38	140	< 10	210	23	2.7	< 5	148	< 0.1	171	< 0.2	7.6	216	26.6
2.81	0.34	1.095	0.1	0.31	99.71	41	2	298	240	43	140	70	90	16	2	< 5	121	< 0.1	58	< 0.2	2.5	8.67	1.4
4.73	1.38	0.38	0.11	0.31	100.9	5	1	47	< 20	6	< 20	< 10	50	20	0.9	< 5	550	< 0.1	415	< 0.2	1.9	46.9	5.1
5.05	1.44	0.354	0.09	0.09	100.6	2	1	35	< 20	5	< 20	< 10	50	22	0.9	< 5	504	< 0.1	564	< 0.2	< 0.2	26.1	2.9
2.63	6.81	0.176	0.03	0.08	98.77	1	< 1	12	< 20	3	< 20	< 10	< 30	15	0.8	< 5	268	< 0.1	1401	< 0.2	< 0.2	68.5	7.15
2.45	5.64	0.221	0.08	0.53	100.9	5	< 1	31	40	2	< 20	< 10	40	15	1.4	< 5	148	< 0.1	953	< 0.2	6	139	14.4
4.61	2.16	0.241	0.08	0.3	100.3	3	1	24	< 20	4	< 20	< 10	50	19	0.9	< 5	367	< 0.1	535	< 0.2	2.6	13.2	1.08
4.47	2.36	0.26	0.08	0.31	100.6	3	1	29	< 20	4	< 20	< 10	40	19	0.8	< 5	501	< 0.1	815	< 0.2	3.1	22.5	2.05
3.87	2.43	0.199	0.07	0.07	99.85	3	2	17	< 20	3	< 20	< 10	40	16	1.3	< 5	146	< 0.1	580	< 0.2	6.4	34.4	3.46
3.69	3.11	0.624	0.28	0.31	98.97	19	2	133	50	19	30	30	110	26	1.6	9	442	< 0.1	1194	< 0.2	4.8	153	17.8
3.27	0.54	0.475	0.05	-0.3	100.7	21	< 1	143	60	27	30	10	50	15	1.7	< 5	177	< 0.1	132	< 0.2	1.7	18	2.06
4.54	1.75	0.23	0.11	0.37	99.28	2	< 1	19	< 20	3	< 20	< 10	40	18	1	< 5	347	< 0.1	536	< 0.2	3.4	26.8	4.45

In	Sn	Sb	Cs	Ba	La	Ce	Pr	Nd	Sm	Eu	Gd	Tb	Dy	Ho	Er	Tm	Yb	Lu	Hf	Ta
0.1	1	0.4	0.1	276	17.9	26.7	2.75	7.83	0.93	0.541	0.61	0.05	0.18	0.03	0.08	0.013	0.11	0.024	2.8	0.01
0.1	1	0.2	1.4	1296	5.27	14.7	1.25	4.21	0.97	0.533	0.95	0.12	0.56	0.09	0.24	0.035	0.27	0.053	3.9	0.08
0.1	1	0.3	0.1	472	11.7	21.1	2.36	8.03	1.25	0.538	0.75	0.08	0.35	0.06	0.15	0.02	0.12	0.023	2.5	0.01
8.54	1.11	0.755	0.5	1.4	< 2	0.9	0.06	< 1	0.25	0.04	0.12	0.019	0.13	0.019	3.8	0.04	< 0.5	0.16	5	< 0.1
56.3	9.51	2.09	6.85	28.8	< 2	1.4	0.98	3	5.01	0.96	2.56	0.375	2.53	0.356	5.7	1.17	< 0.5	0.48	13	< 0.1
76.5	8.95	1.01	4.87	11.7	< 2	1.6	0.57	< 1	2.43	0.4	0.99	0.114	0.59	0.086	6.4	0.41	< 0.5	0.69	15	< 0.1
16	2.5	0.794	1.79	6.9	2	0.7	0.24	< 1	1.26	0.23	0.65	0.088	0.61	0.08	3.3	0.26	< 0.5	0.33	7	< 0.1
12.4	1.77	0.401	1	1.4	< 2	< 0.5	0.09	< 1	0.29	0.04	0.12	0.015	0.07	0.01	1.1	0.08	< 0.5	0.69	20	< 0.1
54.4	6.43	0.888	3.06	6.4	< 2	1.7	0.33	< 1	1.37	0.22	0.62	0.084	0.47	0.07	8.2	0.12	< 0.5	0.66	20	< 0.1
20	2.44	0.608	1.27	2.1	< 2	0.9	0.13	< 1	0.46	0.08	0.2	0.028	0.15	0.024	3.8	0.08	< 0.5	0.34	10	< 0.1
19.2	3.72	0.997	3.02	13	< 2	0.7	0.46	< 1	2.59	0.5	1.36	0.217	1.29	0.168	3.4	0.4	< 0.5	0.25	< 5	< 0.1
8.88	2.14	0.773	1.99	7.3	< 2	1.2	0.3	< 1	1.52	0.29	0.75	0.099	0.63	0.102	5.5	0.41	< 0.5	< 0.05	< 5	< 0.1
77.8	11.5	1.97	7.54	22	< 2	4.8	0.97	3	4.64	0.78	2.06	0.255	1.42	0.204	17.5	0.63	< 0.5	0.25	7	< 0.1
2.64	0.29	0.306	0.16	< 0.5	< 2	< 0.5	0.02	< 1	0.08	0.01	0.04	0.006	0.04	0.006	1.1	< 0.01	< 0.5	0.37	12	< 0.1
6.12	2.04	0.76	2.55	18.6	< 2	< 0.5	0.5	< 1	3.3	0.69	2	0.326	2.07	0.299	1.5	0.21	< 0.5	0.38	< 5	0.4
2.49	0.25	0.614	0.15	< 0.5	< 2	< 0.5	0.02	< 1	0.08	0.02	0.05	0.007	0.04	0.005	1.6	0.01	2	0.46	17	< 0.1
10.7	1.5	0.57	1.06	3.4	< 2	0.8	0.14	< 1	0.77	0.14	0.38	0.053	0.33	0.045	4.3	0.05	< 0.5	0.52	17	< 0.1
31.1	5.59	1.21	3.77	14.1	< 2	0.5	0.52	1	2.61	0.47	1.31	0.187	1.22	0.187	2.7	0.17	< 0.5	0.31	12	< 0.1
99.7	16.7	3.27	11	38.1	< 2	0.6	1.38	5	7.08	1.31	3.67	0.498	3.33	0.472	3.4	0.36	< 0.5	0.25	6	< 0.1
6.93	2.37	0.822	3.02	20.6	9	< 0.5	0.53	< 1	3.4	0.71	2.07	0.334	2.14	0.327	1.5	0.15	< 0.5	0.06	< 5	1.1
17.3	2.36	0.701	1.45	3.5	< 2	0.6	0.16	< 1	0.7	0.12	0.33	0.04	0.24	0.038	2.9	0.05	14.7	0.23	6	< 0.1
10.2	1.47	0.538	0.84	2.7	< 2	< 0.5	0.11	< 1	0.55	0.09	0.24	0.03	0.2	0.028	2.1	0.04	< 0.5	0.31	< 5	< 0.1
22	2.32	0.766	0.53	1.4	< 2	< 0.5	0.05	< 1	0.28	0.05	0.13	0.018	0.1	0.012	1	0.1	11.5	0.55	15	< 0.1
46.5	5.54	0.959	2.96	5.6	2	1	0.3	< 1	1.18	0.2	0.63	0.09	0.56	0.092	5.1	5.52	16.7	0.67	28	< 0.1
3.63	0.79	0.414	0.65	2.1	< 2	0.5	0.09	< 1	0.4	0.08	0.18	0.025	0.17	0.025	2.8	0.56	< 0.5	0.26	8	< 0.1
6.81	0.96	0.53	0.68	1.6	< 2	0.6	0.08	< 1	0.33	0.05	0.15	0.02	0.13	0.019	2.4	0.09	< 0.5	0.27	7	< 0.1
11.8	1.96	0.468	1.56	8.1	< 2	0.6	0.23	< 1	1.32	0.25	0.77	0.107	0.74	0.115	3.4	0.68	< 0.5	0.53	12	< 0.1
64.4	10.8	1.42	6.57	24.1	< 2	1.6	0.93	< 1	4.73	0.9	2.34	0.317	1.93	0.246	4.8	0.13	< 0.5	0.32	9	< 0.1
7.82	1.8	0.592	1.92	10.2	< 2	< 0.5	0.32	< 1	1.8	0.36	1.03	0.158	1.04	0.151	1.4	0.16	< 0.5	0.07	< 5	< 0.1
16.3	2.79	0.539	2.15	5.9	< 2	0.6	0.25	< 1	1.15	0.2	0.54	0.066	0.36	0.047	3.1	0.16	< 0.5	0.34	7	< 0.1

W	Tl	Pb	Bi	Th	U
0.5	0.14	6	0.1	4.03	0.32
0.6	0.45	17	0.1	12.7	0.43
1.2	0.22	8	0.1	0.16	0.1
0.47	0.12	36	0.1	0.3	0.1
2.79	1.25	106	0.1	3.52	0.24
24.1	0.97	178	0.1	13.1	1.96
2.34	0.2	63	0.1	2.6	0.17
2.32	0.17	146	0.1	1.08	0.22
26.7	0.82	146	0.1	1.32	0.25
11.2	0.3	69	0.5	0.23	0.21
1.54	0.78	54	0.1	0.37	0.24
0.4	0.46	3	0.1	0.43	0.08
11.2	0.24	64	0.1	0.05	0.15
0.94	0.13	83	0.1	15.9	1.46
0.57	0.13	55	0.1	2.3	0.2
3.24	1.5	118	0.1	2.89	0.98
4.97	0.66	123	0.1	15.7	0.47
0.89	0.36	63	0.1	0.96	0.21
13.1	1.56	53	0.1	11.2	0.33
0.54	0.45	6	1.4	0.75	0.72
4.56	0.11	46	0.4	0.53	1
0.43	0.1	41	-	-	-
6.44	0.17	140	-	-	-
27.7	0.82	148	0.2	2.24	0.59
3.61	0.31	64	0.2	0.78	0.46
0.88	0.15	63	0.1	16.4	0.58
8.15	1.63	108	0.1	8.49	1.54
1.81	0.25	59	-	-	-
0.72	0.1	4	-	-	-
2.81	0.25	67	0.1	9.56	0.56

APPENDIX 3B - SHRIMP U-Pb isotopic data

Spot name	U (ppm)	Th (ppm)	Th/U	Yb (ppm)	Hf (ppm)	$^{204}Pb/^{206}Pb$	% ±	$^{206}Pb^*$ (ppm)	$f(206)^{204}$ %	$^{208*}Pb/^{206*}Pb$	% ±	$^{207*}Pb/^{235}U$
12MBC-S116A, monzogranite												
713778 7041607 NAD 1983 UTM Zone 19N												
11001-002.1	216	57	0.27	227	11554	1.8E-5	18	105	0.003	0.075	1.9	16.9
11001-007.1	206	43	0.21	191	13572	5.9E-5	21	102	0.012	0.056	2.2	17.4
11001-008.1	214	60	0.29	206	11501	3.4E-5	48	106	0.120	0.079	1.8	17.3
11001-009.1	196	77	0.40	222	10998	---	100	97	0.411	0.116	1.6	17.1
11001-010.1	195	52	0.27	189	11915	9.3E-5	17	97	0.018	0.075	1.9	17.4
11001-011.1	673	86	0.13	344	15443	3.7E-6	28	329	0.028	0.037	1.5	16.7
11001-011.2	1268	153	0.12	421	16896	1.8E-5	19	626	0.029	0.034	1.1	16.6
11001-012.1	234	71	0.31	234	10843	3.2E-5	16	118	0.012	0.087	1.6	17.8
11001-014.1	73	18	0.25	113	9701	2.0E-4	34	36	0.042	0.067	3.3	17.0
11001-014.2	143	34	0.25	157	11864	1.4E-4	18	69	0.113	0.068	3.8	17.0
11001-015.1	206	27	0.13	159	12674	5.6E-5	46	104	0.095	0.036	2.6	17.7
11001-016.1	138	25	0.19	142	11865	5.9E-5	36	69	0.010	0.051	3.6	17.3
11001-016.2	166	34	0.21	166	11840	1.5E-4	19	84	-0.023	0.058	2.5	17.7
11001-017.1	237	56	0.24	250	11995	7.0E-5	18	122	0.072	0.069	1.8	17.8
11001-019.1	213	30	0.15	174	12632	2.0E-5	31	108	-0.001	0.041	2.6	17.8
11001-020.1	51	24	0.48	111	8107	1.5E-4	34	26	0.019	0.135	2.8	18.1
11001-020.2	75	28	0.39	81	10026	8.8E-4	10	37	0.138	0.110	2.5	17.0
11001-021.1	196	60	0.32	216	10899	6.1E-5	33	99	0.234	0.091	1.8	17.8
11001-022.1	158	42	0.28	199	10614	1.3E-4	17	77	0.222	0.077	2.1	16.9
11001-024.1	127	18	0.14	134	14302	1.2E-4	24	65	0.060	0.041	3.1	18.1
11001-025.1	272	59	0.22	219	12158	6.1E-5	21	137	-0.001	0.065	1.8	17.6
11001-026.1	191	93	0.50	148	12074	7.6E-5	32	85	0.113	0.142	1.5	13.4
11001-026.2	205	50	0.25	189	11031	9.6E-5	18	102	0.051	0.074	3.3	17.4
11001-038.1	191	13	0.07	88	11259	8.3E-5	20	98	0.033	0.019	3.7	17.9
11001-038.2	68	21	0.32	146	9189	9.1E-5	19	35	0.023	0.093	5.3	17.7
11001-051.1	180	65	0.37	189	11438	1.3E-4	19	91	0.054	0.103	3.1	17.9
11001-052.1	215	55	0.26	229	11411	1.1E-4	18	107	0.099	0.075	1.9	17.3
11001-068.1	3134	476	0.16	802	15958	3.3E-6	36	1548	0.015	0.047	0.6	16.0
11001-109.1	156	48	0.32	194	11026	4.5E-5	62	79	0.033	0.088	2.1	18.0
11001-109.2	251	76	0.31	297	10570	3.0E-5	67	128	0.015	0.091	1.6	18.0

						age (Ma)				
% ±	$^{206*}Pb/^{238}U$	% ±	Corr Coeff	$^{207*}Pb/^{206*}Pb$	% ±	$^{206*}Pb/^{238}U$	±	$^{207*}Pb/^{206*}Pb$	±	Disc. %
12MBC-S116A, monzogranite										
713778 7041607 NAD 1983 UTM Zone 19N										
1.19	0.57	1.06	0.890	0.217	0.5	2888	25	2958	9	2.93
1.07	0.57	1.05	0.980	0.219	0.2	2928	25	2973	3	1.89
1.07	0.58	1.05	0.979	0.217	0.2	2936	25	2958	4	0.91
1.07	0.57	1.05	0.980	0.216	0.2	2927	25	2951	3	1.03
1.08	0.58	1.05	0.977	0.218	0.2	2949	25	2964	4	0.64
1.28	0.57	1.20	0.941	0.214	0.4	2901	28	2933	7	1.38
1.10	0.57	1.02	0.935	0.209	0.4	2927	24	2901	6	-1.11
1.06	0.59	1.05	0.983	0.220	0.2	2984	25	2978	3	-0.24
1.23	0.57	1.11	0.907	0.215	0.5	2920	26	2943	8	0.99
1.17	0.56	1.06	0.908	0.218	0.5	2881	25	2969	8	3.65
1.08	0.59	1.05	0.974	0.218	0.2	2981	25	2969	4	-0.50
1.37	0.58	1.08	0.787	0.215	0.8	2965	26	2943	14	-0.93
1.11	0.59	1.07	0.965	0.217	0.3	2998	26	2957	5	-1.75
1.13	0.60	1.11	0.984	0.217	0.2	3014	27	2960	3	-2.28
1.24	0.59	1.22	0.985	0.219	0.2	2993	29	2970	3	-0.99
1.25	0.60	1.14	0.918	0.219	0.5	3019	28	2975	8	-1.87
1.66	0.57	1.12	0.675	0.216	1.2	2904	26	2954	20	2.09
1.08	0.59	1.05	0.976	0.220	0.2	2975	25	2980	4	0.22
1.09	0.57	1.06	0.969	0.215	0.3	2906	25	2946	4	1.72
1.13	0.60	1.08	0.963	0.221	0.3	3011	26	2988	5	-0.97
1.18	0.58	1.18	0.997	0.219	0.1	2968	28	2971	1	0.12
1.09	0.52	1.05	0.964	0.187	0.3	2700	23	2716	5	0.73
1.15	0.58	1.12	0.978	0.218	0.2	2954	27	2964	4	0.41
1.10	0.59	1.07	0.977	0.218	0.2	3006	26	2969	4	-1.55
1.12	0.60	1.11	0.991	0.215	0.1	3014	27	2944	2	-3.00
1.09	0.59	1.06	0.971	0.220	0.3	2987	25	2982	4	-0.19
1.12	0.58	1.10	0.978	0.218	0.2	2942	26	2963	4	0.88
1.03	0.57	1.02	0.995	0.201	0.1	2928	24	2837	2	-3.99
1.13	0.59	1.06	0.940	0.221	0.4	2991	25	2987	6	-0.13
1.07	0.59	1.05	0.979	0.220	0.2	3003	25	2982	4	-0.88

APPENDIX 3B - SHRIMP U-Pb isotopic data

Spot name	U (ppm)	Th (ppm)	Th/U	Yb (ppm)	Hf (ppm)	$^{204}Pb/^{206}Pb$	% ±	$^{206}Pb^*$ (ppm)	$f(206)^{204}$ %	$^{208*}Pb/^{206*}Pb$	% ±	$^{207*}Pb/^{235}U$
13SUB-F151A, granodiorite												
669300 7094544 NAD1983, UTM Zone 19N												
11187-005.1	94	39	0.43	206	9319	-3.1E-5	58	46	-0.053	0.126	3.1	16.85
11187-006.1	96	48	0.52	217	9139	4.9E-5	45	46	0.085	0.138	2.9	16.13
11187-012.1	148	67	0.47	238	8535	5.5E-5	35	71	0.095	0.128	4.8	16.15
11187-016.1	73	47	0.66	185	9416	8.1E-5	41	36	0.140	0.178	3.0	16.55
11187-017.1	103	39	0.39	188	10298	4.2E-5	45	49	0.072	0.104	3.0	16.18
11187-018.1	139	73	0.54	127	10260	1.8E-5	58	67	0.032	0.148	2.2	16.54
11187-021.1	107	53	0.51	77	11444	-3.1E-5	58	49	-0.053	0.140	7.8	15.24
11187-038.1	874	107	0.13	120	12283	2.0E-5	23	375	0.035	0.036	1.9	12.68
11187-039.1	563	97	0.18	123	12067	4.8E-5	20	248	0.084	0.049	4.0	13.22
11187-051.1	150	72	0.49	270	8831	6.7E-5	30	72	0.116	0.141	2.2	15.98
11187-051.2	109	43	0.41	156	10875	9.2E-6	100	53	0.016	0.103	3.1	16.69
11187-052.1	100	66	0.68	232	8968	---	---	49	0.000	0.199	5.2	16.54
11187-053.1	76	47	0.64	181	9373	3.9E-5	58	36	0.068	0.191	2.8	15.23
11187-053.2	55	19	0.36	116	10194	5.6E-5	58	26	0.097	0.105	7.2	15.23
11187-055.1	84	38	0.46	172	8903	7.3E-5	41	38	0.127	0.134	3.4	14.19
11187-055.2	91	52	0.59	195	9223	2.4E-5	71	41	0.041	0.173	2.8	14.35
11187-058.1	127	89	0.73	283	9235	-2.2E-5	58	60	-0.039	0.197	2.0	16.38
11187-059.1	527	13	0.03	151	12545	8.6E-5	18	228	0.149	0.004	17.9	13.51
11187-063.1	259	3	0.01	99	13542	1.2E-5	58	123	0.020	0.004	13.8	15.91
11187-069.1	76	31	0.42	152	9060	6.2E-5	45	37	0.108	0.115	3.6	16.24
11187-070.1	84	34	0.42	123	9342	1.9E-5	71	41	0.033	0.124	2.9	16.78
11187-081.1	110	48	0.46	185	9612	7.1E-5	33	54	0.124	0.126	2.8	16.48
11187-083.1	88	43	0.50	184	9984	---	---	43	0.000	0.144	2.7	16.68
11187-084.1	115	59	0.53	194	9146	2.3E-5	58	54	0.040	0.155	2.4	15.66
11187-084.2	147	103	0.72	294	9706	6.7E-6	100	72	0.012	0.204	1.9	16.54
11187-094.1	80	53	0.68	226	8754	3.2E-5	58	39	0.056	0.194	2.5	16.28
11187-098.1	95	57	0.62	222	10076	8.9E-5	32	48	0.154	0.170	4.5	17.16
11187-102.1	81	32	0.41	183	9250	1.0E-5	100	40	0.018	0.121	3.1	17.07
11187-106.1	116	48	0.43	197	10128	5.1E-5	38	58	0.089	0.113	2.7	17.14
11187-108.1	124	60	0.50	254	9602	2.8E-5	50	61	0.049	0.142	2.4	16.53
11187-116.1	72	33	0.47	120	9945	----	---	35	0.000	0.135	3.1	16.00
11187-116.2	73	29	0.40	162	10213	1.6E-4	30	35	0.274	0.102	4.4	15.69
11187-117.1	66	15	0.24	81	12441	1.5E-5	100	32	0.026	0.065	5.2	16.23
11187-122.1	114	46	0.41	216	9655	6.5E-5	33	55	0.113	0.117	2.8	16.29

						age (Ma)				
% ±	$^{206*}Pb/^{238}U$	% ±	Corr Coeff	$^{207*}Pb/^{206*}Pb$	% ±	$^{206*}Pb/^{238}U$	±	$^{207*}Pb/^{206*}Pb$	±	Disc. %
13SUB-F151A, granodiorite										
669300 7094544 NAD1983, UTM Zone 19N										
1.61	0.570	1.54	0.953	0.2143	0.5	2910	36	2938	8	1.2
1.60	0.556	1.52	0.952	0.2103	0.5	2851	35	2908	8	2.4
1.54	0.556	1.49	0.964	0.2106	0.4	2851	34	2910	7	2.5
1.70	0.567	1.60	0.940	0.2115	0.6	2897	37	2917	9	0.8
1.54	0.555	1.48	0.966	0.2117	0.4	2844	34	2918	6	3.1
1.48	0.562	1.44	0.974	0.2135	0.3	2874	33	2932	5	2.5
1.76	0.529	1.57	0.892	0.2089	0.8	2738	35	2897	13	6.7
1.66	0.500	1.53	0.920	0.1840	0.7	2612	33	2690	11	3.5
1.42	0.512	1.41	0.989	0.1872	0.2	2667	31	2718	3	2.3
1.48	0.560	1.44	0.972	0.2069	0.3	2867	33	2882	6	0.6
1.75	0.569	1.50	0.859	0.2129	0.9	2902	35	2928	15	1.1
1.56	0.566	1.51	0.965	0.2120	0.4	2891	35	2921	7	1.3
2.25	0.547	2.08	0.922	0.2018	0.9	2814	47	2841	14	1.2
1.77	0.542	1.67	0.939	0.2039	0.6	2791	38	2858	10	2.8
1.78	0.526	1.55	0.870	0.1956	0.9	2725	34	2790	14	2.8
1.61	0.523	1.54	0.955	0.1991	0.5	2711	34	2819	8	4.7
1.51	0.552	1.47	0.970	0.2151	0.4	2835	34	2945	6	4.6
1.37	0.505	1.35	0.983	0.1942	0.2	2634	29	2778	4	6.3
1.42	0.554	1.39	0.978	0.2083	0.3	2842	32	2892	5	2.2
2.13	0.564	1.97	0.925	0.2087	0.8	2885	46	2896	13	0.5
1.58	0.574	1.51	0.961	0.2119	0.4	2925	36	2920	7	-0.2
1.60	0.570	1.48	0.923	0.2096	0.6	2909	35	2902	10	-0.3
1.58	0.568	1.52	0.958	0.2130	0.5	2900	35	2928	7	1.2
1.52	0.548	1.47	0.968	0.2072	0.4	2818	34	2884	6	2.8
1.49	0.572	1.45	0.973	0.2098	0.3	2915	34	2904	6	-0.5
1.60	0.562	1.54	0.960	0.2101	0.5	2874	36	2907	7	1.4
1.56	0.583	1.50	0.962	0.2134	0.4	2962	36	2932	7	-1.3
1.69	0.579	1.53	0.907	0.2136	0.7	2947	36	2933	11	-0.6
1.52	0.583	1.47	0.969	0.2131	0.4	2962	35	2930	6	-1.4
1.50	0.568	1.46	0.971	0.2110	0.4	2901	34	2913	6	0.5
1.64	0.556	1.57	0.958	0.2085	0.5	2852	36	2894	8	1.8
1.70	0.550	1.60	0.941	0.2069	0.6	2825	37	2882	9	2.4
1.73	0.564	1.63	0.938	0.2089	0.6	2881	38	2897	10	0.7
1.51	0.558	1.46	0.968	0.2117	0.4	2859	34	2918	6	2.5

APPENDIX 3B - SHRIMP U-Pb isotopic data

Spot name	U (ppm)	Th (ppm)	Th/U	Yb (ppm)	Hf (ppm)	$^{204}Pb/^{206}Pb$	% ±	$^{206}Pb^*$ (ppm)	$f(206)^{204}$ %	$^{208*}Pb/^{206*}Pb$	% ±	$^{207*}Pb/^{235}U$
11187-124.1	1497	107	0.07	119	13232	2.7E-5	37	639	0.046	0.020	2.8	12.68
11187-125.1	108	62	0.59	195	10344	8.0E-6	100	53	0.014	0.164	3.9	16.89
13SUB-F155B, tonalite												
669461 7094784 NAD1983, UTM Zone 19N												
11189-001.1	230	243	1.09	292	11109	-9.4E-6	71	104	-0.016	0.314	1.3	13.73
11189-008.1	198	97	0.51	457	9576	3.8E-5	38	90	0.065	0.143	3.7	14.36
11189-015.1	272	103	0.39	195	10483	3.6E-6	100	126	0.006	0.108	1.9	14.36
11189-015.2	123	63	0.53	130	11723	4.3E-5	45	54	0.075	0.147	2.6	13.21
11189-016.1	198	230	1.20	304	11303	1.1E-5	71	88	0.019	0.335	1.3	13.32
11189-020.1	315	195	0.64	463	5713	2.5E-5	33	155	0.044	0.180	1.3	16.81
11189-020.2	242	92	0.39	152	11622	6.5E-5	24	112	0.112	0.107	2.0	14.68
11189-023.1	118	87	0.76	197	11505	7.6E-5	33	53	0.132	0.208	2.2	13.38
11189-025.1	284	175	0.64	354	9143	---	100	145	0.000	0.172	1.4	17.91
11189-030.1	199	74	0.38	239	8432	8.5E-6	71	96	0.015	0.104	2.1	16.68
11189-030.2	94	63	0.69	149	12113	---	---	43	0.000	0.194	2.5	13.86
11189-034.1	173	198	1.19	239	11775	4.4E-5	38	76	0.076	0.329	1.5	13.27
11189-041.1	155	181	1.20	132	12479	5.6E-5	35	70	0.097	0.340	1.5	13.54
11189-042.1	331	86	0.27	238	11504	2.7E-6	100	148	0.005	0.078	2.0	13.85
11189-043.1	175	97	0.57	346	8709	5.8E-6	100	88	0.010	0.164	2.0	17.73
11189-045.1	115	15	0.14	135	11416	7.8E-6	100	61	0.014	0.040	4.7	20.51
11189-046.1	56	36	0.67	226	10080	7.4E-5	50	28	0.128	0.192	3.3	17.05
11189-048.1	197	186	0.97	356	11838	-1.7E-5	58	89	-0.029	0.274	1.5	13.77
11189-049.1	45	25	0.57	244	8405	2.2E-5	100	24	0.038	0.148	6.8	21.84
11189-050.1	813	419	0.53	461	10961	1.5E-5	29	382	0.025	0.152	0.9	14.93
11189-055.1	194	86	0.46	147	11805	-5.0E-6	100	88	-0.009	0.132	2.1	14.37
11189-057.1	3190	158	0.05	382	16834	3.0E-6	32	1458	0.005	0.014	1.5	13.47
11189-057.2	325	134	0.43	132	12423	5.2E-5	24	142	0.091	0.123	2.8	13.15
11189-058.1	118	70	0.62	305	8547	4.5E-5	45	56	0.077	0.175	2.4	16.02
11189-063.1	177	222	1.30	289	11790	2.6E-5	50	80	0.045	0.369	1.4	13.72
11189-065.1	297	100	0.35	224	11115	5.6E-5	24	135	0.097	0.094	2.0	14.25
11189-071.1	180	162	0.93	346	11389	-1.2E-5	71	81	-0.022	0.272	1.6	13.60
11189-072.1	270	133	0.51	230	10686	4.2E-5	30	120	0.073	0.143	1.7	13.37
11189-072.2	72	65	0.93	233	12042	---	100	33	0.000	0.269	2.4	13.71
11189-076.1	50	25	0.52	42	10328	1.1E-4	41	24	0.193	0.144	4.0	16.08
11189-081.1	112	66	0.61	410	8802	5.9E-5	35	56	0.102	0.165	2.3	18.00

						age (Ma)				
% ±	$^{206*}Pb/^{238}U$	% ±	Corr Coeff	$^{207*}Pb/^{206*}Pb$	% ±	$^{206*}Pb/^{238}U$	±	$^{207*}Pb/^{206*}Pb$	±	Disc. %
1.33	0.497	1.32	0.994	0.1849	0.1	2602	28	2697	2	4.3
1.53	0.574	1.48	0.970	0.2132	0.4	2926	35	2930	6	0.2
13SUB-F155B, tonalite										
669461 7094784 NAD1983, UTM Zone 19N										
1.44	0.527	1.40	0.978	0.1891	0.3	2727	31	2735	5	0.3
1.61	0.526	1.42	0.884	0.1981	0.8	2723	32	2811	12	3.8
1.56	0.540	1.54	0.986	0.1928	0.3	2784	35	2766	4	-0.8
1.54	0.515	1.48	0.961	0.1861	0.4	2678	32	2708	7	1.4
1.45	0.517	1.42	0.975	0.1867	0.3	2688	31	2713	5	1.1
1.39	0.571	1.37	0.987	0.2133	0.2	2914	32	2931	4	0.7
1.41	0.539	1.38	0.980	0.1976	0.3	2778	31	2806	5	1.2
1.54	0.523	1.48	0.959	0.1855	0.4	2711	33	2703	7	-0.4
1.40	0.591	1.38	0.986	0.2196	0.2	2995	33	2978	4	-0.7
1.42	0.559	1.40	0.981	0.2166	0.3	2861	32	2956	4	4.0
1.71	0.532	1.52	0.890	0.1889	0.8	2750	34	2733	13	-0.8
1.48	0.514	1.43	0.969	0.1872	0.4	2675	31	2717	6	1.9
1.50	0.523	1.45	0.966	0.1876	0.4	2714	32	2721	6	0.3
1.38	0.521	1.36	0.987	0.1929	0.2	2702	30	2767	4	2.9
1.47	0.586	1.44	0.977	0.2194	0.3	2974	34	2977	5	0.1
1.61	0.615	1.49	0.928	0.2420	0.6	3089	37	3133	10	1.8
1.80	0.569	1.69	0.943	0.2172	0.6	2905	40	2960	10	2.3
1.46	0.527	1.42	0.974	0.1894	0.3	2731	32	2737	5	0.3
1.88	0.624	1.79	0.950	0.2539	0.6	3125	44	3209	9	3.3
1.34	0.547	1.33	0.994	0.1980	0.2	2812	30	2810	2	-0.1
1.44	0.526	1.41	0.978	0.1983	0.3	2723	31	2812	5	3.9
1.37	0.532	1.36	0.989	0.1837	0.2	2750	30	2686	3	-2.9
1.39	0.508	1.37	0.983	0.1877	0.3	2649	30	2722	4	3.3
1.55	0.550	1.50	0.964	0.2113	0.4	2825	34	2916	7	3.8
1.49	0.529	1.44	0.970	0.1881	0.4	2736	32	2726	6	-0.5
1.40	0.529	1.37	0.981	0.1955	0.3	2737	31	2789	4	2.3
1.48	0.522	1.44	0.972	0.1890	0.3	2708	32	2733	6	1.1
1.41	0.516	1.38	0.980	0.1878	0.3	2683	30	2723	5	1.8
1.67	0.527	1.58	0.950	0.1886	0.5	2729	35	2730	9	0.1
1.80	0.567	1.69	0.936	0.2057	0.6	2894	39	2872	10	-0.9
1.52	0.586	1.47	0.970	0.2227	0.4	2973	35	3000	6	1.1

APPENDIX 3B - SHRIMP U-Pb isotopic data

Spot name	U (ppm)	Th (ppm)	Th/U	Yb (ppm)	Hf (ppm)	$^{204}Pb/^{206}Pb$	% ±	$^{206}Pb^*$ (ppm)	$f(206)^{204}$ %	$^{208*}Pb/^{206*}Pb$	% ±	$^{207*}Pb/^{235}U$
11189-082.1	149	81	0.56	372	9056	2.8E-5	45	76	0.049	0.151	4.0	18.01
11189-085.1	140	114	0.84	167	12550	4.3E-5	41	63	0.074	0.240	1.8	13.46
11189-087.1	323	103	0.33	232	12300	1.2E-4	17	152	0.216	0.092	2.1	14.91
11189-089.1	2313	109	0.05	185	17020	1.5E-6	50	1079	0.003	0.014	1.7	14.68
11189-091.1	109	49	0.46	149	12557	1.0E-4	29	46	0.175	0.142	4.2	12.24
11189-093.1	273	359	1.36	392	11475	3.6E-6	100	125	0.006	0.380	1.0	13.93
11189-095.1	201	117	0.60	323	8123	4.0E-5	35	99	0.069	0.160	1.9	16.82
11189-096.1	119	145	1.26	264	11237	9.9E-5	29	53	0.172	0.362	1.6	13.34
11189-099.1	131	79	0.63	488	9373	4.7E-5	38	66	0.082	0.177	2.1	17.89
11189-100.1	404	159	0.41	290	11040	4.8E-5	22	188	0.084	0.114	1.5	15.14
11189-104.1	463	168	0.37	290	10426	7.6E-6	50	211	0.013	0.107	3.3	14.57
11189-104.2	1544	190	0.13	114	13726	4.6E-6	35	689	0.008	0.036	1.3	13.21
13SUB-155C, mafic lenses												
669461 7094784 NAD1983, UTM Zone 19N												
11217-005.1	194	4	0.02	141	11143	1.1E-4	28	57	0.186	0.004	37.2	5.92
11217-006.1	1983	185	0.10	106	11152	3.8E-6	38	872	0.007	0.028	1.5	12.95
11217-008.1	305	4	0.01	189	10350	2.3E-5	50	88	0.040	0.004	17.6	5.32
11217-009.1	413	4	0.01	112	10661	----	---	118	0.000	0.003	12.0	5.21
11217-014.1	1678	347	0.21	286	15353	6.6E-6	29	734	0.011	0.060	1.0	12.95
11217-014.2	2131	633	0.31	387	13412	3.8E-6	35	968	0.007	0.087	0.8	13.39
11217-020.1	1138	166	0.15	50	8315	5.8E-6	35	520	0.010	0.043	1.4	13.57
11217-020.2	187	2	0.01	85	11375	----	---	54	0.000	0.004	15.7	5.27
11217-021.1	1633	105	0.07	144	16757	1.5E-5	19	732	0.025	0.018	1.9	13.21
11217-021.2	1579	115	0.08	72	10458	6.7E-6	32	657	0.012	0.022	3.3	11.80
11217-023.1	421	5	0.01	117	10222	1.9E-5	45	118	0.033	0.002	20.4	5.19
11217-024.1	277	3	0.01	64	10702	3.4E-5	41	79	0.058	0.002	31.5	5.17
11217-024.2	1010	83	0.08	247	10892	1.1E-4	10	422	0.191	0.022	5.7	12.20
11217-026.1	1121	121	0.11	143	16198	5.5E-6	38	511	0.010	0.033	1.6	13.56
11217-026.2	1776	223	0.13	166	17237	1.5E-5	46	767	0.026	0.038	1.5	12.81
11217-036.1	1975	499	0.26	340	15097	5.0E-6	30	895	0.009	0.074	0.8	13.47
11217-040.1	397	9	0.02	408	11862	1.4E-5	41	186	0.024	0.006	8.1	14.56
11217-040.2	1570	260	0.17	184	13812	5.7E-6	32	721	0.010	0.049	1.1	13.85
11217-041.1	2893	269	0.10	221	18877	1.9E-6	41	1339	0.003	0.028	1.1	13.78
11217-046.1	86	1	0.01	77	11234	2.4E-4	28	24	0.409	-0.005	53.3	5.03
11217-057.1	1108	148	0.14	40	6493	1.6E-6	71	505	0.003	0.042	3.9	13.69

						age (Ma)				
	$^{206*}Pb$		Corr	$^{207*}Pb$		$^{206*}Pb$		$^{207*}Pb$		Disc.
% ±	^{238}U	% ±	Coeff	$^{206*}Pb$	% ±	^{238}U	±	$^{206*}Pb$	±	%
1.47	0.598	1.44	0.976	0.2184	0.3	3021	35	2969	5	-2.2
1.77	0.520	1.65	0.936	0.1876	0.6	2701	36	2721	10	0.9
1.39	0.546	1.37	0.981	0.1980	0.3	2809	31	2810	4	0.0
1.41	0.543	1.37	0.976	0.1961	0.3	2796	31	2794	5	-0.1
1.53	0.488	1.47	0.955	0.1820	0.5	2560	31	2671	7	5.0
1.40	0.533	1.38	0.983	0.1895	0.3	2754	31	2738	4	-0.7
1.76	0.571	1.66	0.942	0.2136	0.6	2912	39	2933	10	0.9
1.79	0.522	1.47	0.820	0.1853	1.0	2708	33	2701	17	-0.4
1.50	0.590	1.46	0.972	0.2200	0.4	2988	35	2981	6	-0.3
1.39	0.542	1.35	0.972	0.2024	0.3	2793	31	2846	5	2.3
1.55	0.530	1.50	0.970	0.1993	0.4	2742	34	2820	6	3.4
1.33	0.520	1.31	0.984	0.1844	0.2	2697	29	2692	4	-0.2
13SUB-155C, diorite										
669461 7094784 NAD1983, UTM Zone 19N										
1.64	0.343	1.42	0.866	0.1251	0.8	1902	23	2030	14	7.3
1.35	0.512	1.31	0.975	0.1836	0.3	2664	29	2685	5	1.0
1.44	0.335	1.38	0.956	0.1151	0.4	1863	22	1882	8	1.2
1.39	0.334	1.35	0.973	0.1134	0.3	1855	22	1854	6	-0.1
1.33	0.509	1.31	0.989	0.1845	0.2	2653	29	2693	3	1.8
1.31	0.529	1.31	0.997	0.1836	0.1	2737	29	2686	2	-2.3
1.45	0.532	1.32	0.910	0.1849	0.6	2751	30	2698	10	-2.5
1.82	0.334	1.75	0.965	0.1146	0.5	1856	28	1874	9	1.1
1.37	0.522	1.35	0.984	0.1835	0.2	2707	30	2685	4	-1.0
1.45	0.485	1.36	0.937	0.1766	0.5	2548	29	2621	8	3.4
1.49	0.328	1.35	0.909	0.1148	0.6	1827	22	1877	11	3.0
1.44	0.331	1.38	0.955	0.1133	0.4	1844	22	1853	8	0.6
1.35	0.487	1.33	0.982	0.1819	0.3	2556	28	2670	4	5.2
1.38	0.530	1.37	0.996	0.1855	0.1	2743	31	2703	2	-1.8
1.32	0.503	1.31	0.996	0.1847	0.1	2626	28	2696	2	3.1
1.35	0.528	1.31	0.975	0.1851	0.3	2732	29	2699	5	-1.5
1.37	0.544	1.35	0.988	0.1941	0.2	2801	31	2777	3	-1.1
1.35	0.535	1.34	0.996	0.1879	0.1	2761	30	2724	2	-1.7
1.42	0.539	1.32	0.928	0.1855	0.5	2778	30	2703	9	-3.4
1.88	0.327	1.54	0.818	0.1116	1.1	1824	24	1826	20	0.1
1.40	0.530	1.37	0.977	0.1872	0.3	2743	31	2718	5	-1.1

APPENDIX 3B - SHRIMP U-Pb isotopic data

Spot name	U (ppm)	Th (ppm)	Th/U	Yb (ppm)	Hf (ppm)	$^{204}Pb/^{206}Pb$	% ±	$^{206}Pb^*$ (ppm)	$f(206)^{204}$ %	$^{208*}Pb/^{206*}Pb$	% ±	$^{207*}Pb/^{235}U$
11217-057.2	1543	207	0.14	76	5849	4.5E-6	38	697	0.008	0.039	1.3	13.54
11217-064.1	904	25	0.03	672	11405	1.4E-5	23	473	0.024	0.008	3.5	17.02
11217-064.2	1639	139	0.09	136	15972	8.0E-6	28	716	0.014	0.024	1.7	12.99
11217-087.1	1571	181	0.12	141	15387	3.4E-6	41	707	0.006	0.033	2.4	13.23
11217-087.2	2108	317	0.16	196	16860	4.7E-6	32	962	0.008	0.043	1.1	13.57
11217-094.1	409	4	0.01	98	10720	1.9E-5	45	118	0.033	0.002	23.1	5.21
11217-100.1	1001	48	0.05	178	11719	4.5E-6	45	448	0.008	0.013	2.8	13.75
11217-106.1	1484	228	0.16	71	8671	3.6E-6	41	672	0.006	0.046	1.2	13.58
11217-106.2	1435	365	0.26	103	12579	3.6E-6	45	642	0.006	0.074	1.0	13.23
11217-110.1	1165	47	0.04	546	13319	6.2E-6	35	545	0.011	0.011	2.9	14.64
11217-110.2	1888	197	0.11	167	17945	7.4E-6	28	807	0.013	0.031	1.4	12.72
11217-111.1	2241	190	0.09	105	12842	3.7E-6	33	996	0.006	0.025	1.3	12.89
11217-111.2	3541	242	0.07	349	4544	3.6E-6	24	1817	0.006	0.021	3.5	16.25
13SUB-F155A, Bt monzogranite												
669461 7094784 NAD 1983 UTM Zone 19N												
11216-001.1	1246	1064	0.88	387	9408	3.4E-5	16	572	0.059	0.251	0.6	14.06
11216-005.1	221	160	0.75	170	12517	2.9E-5	38	98	0.050	0.209	1.5	13.45
11216-008.1	322	334	1.07	322	13306	2.8E-6	100	145	0.005	0.301	1.0	13.58
11216-011.1	316	121	0.39	194	12271	4.9E-5	24	140	0.085	0.112	1.7	13.29
11216-012.1	2036	1373	0.70	655	11611	---	71	980	0.001	0.198	0.9	14.77
11216-012.2	3290	3340	1.05	487	13216	---	50	1561	0.002	0.296	0.6	14.47
11216-014.1	242	175	0.75	187	12995	1.5E-5	50	108	0.026	0.207	1.4	13.53
11216-017.1	193	99	0.53	450	7965	1.4E-5	58	91	0.024	0.149	1.9	15.77
11216-020.1	595	411	0.71	309	15020	1.2E-5	35	266	0.021	0.201	0.9	13.36
11216-021.1	263	204	0.80	178	12178	2.5E-5	38	119	0.043	0.221	1.3	13.66
11216-022.1	592	223	0.39	258	14231	1.1E-5	38	273	0.019	0.107	1.3	14.00
11216-023.1	137	84	0.63	307	8491	2.6E-5	50	64	0.045	0.179	2.0	14.71
11216-025.1	230	111	0.50	301	9552	1.6E-5	50	105	0.027	0.141	1.7	14.87
11216-026.1	200	181	0.93	244	12411	1.9E-5	50	89	0.032	0.262	1.4	13.42
11216-030.1	2068	1325	0.66	642	11914	5.0E-6	28	979	0.009	0.187	0.5	14.52
11216-031.1	1641	1747	1.10	433	11142	3.1E-6	41	771	0.005	0.307	0.4	14.37
11216-036.1	547	179	0.34	281	14128	1.6E-6	100	242	0.003	0.096	1.3	13.35
11216-041.1	191	44	0.24	101	13518	8.4E-4	24	81	1.463	0.081	9.7	12.46
11216-041.2	456	100	0.23	193	13949	-5.7E-6	58	206	-0.010	0.065	1.8	13.61
11216-043.1	363	187	0.53	234	15399	---	---	163	0.000	0.152	1.3	13.65

						age (Ma)				
% ±	$^{206*}Pb/^{238}U$	% ±	Corr Coeff	$^{207*}Pb/^{206*}Pb$	% ±	$^{206*}Pb/^{238}U$	±	$^{207*}Pb/^{206*}Pb$	±	Disc. %
1.33	0.526	1.32	0.990	0.1868	0.2	2724	29	2714	3	-0.4
1.46	0.608	1.45	0.990	0.2029	0.2	3064	35	2850	3	-9.4
1.36	0.509	1.34	0.987	0.1852	0.2	2651	29	2700	4	2.2
1.39	0.524	1.37	0.984	0.1832	0.2	2716	30	2682	4	-1.6
1.35	0.531	1.35	0.997	0.1854	0.1	2746	30	2702	2	-2.0
1.40	0.336	1.36	0.969	0.1126	0.3	1866	22	1842	6	-1.5
1.33	0.521	1.32	0.995	0.1915	0.1	2702	29	2755	2	2.4
1.43	0.527	1.37	0.959	0.1868	0.4	2730	30	2714	7	-0.7
1.36	0.521	1.35	0.995	0.1840	0.1	2704	30	2690	2	-0.7
1.38	0.545	1.37	0.995	0.1949	0.1	2803	31	2784	2	-0.9
1.39	0.498	1.38	0.990	0.1854	0.2	2603	29	2702	3	4.4
1.41	0.518	1.37	0.977	0.1806	0.3	2689	30	2658	5	-1.4
1.60	0.597	1.50	0.943	0.1973	0.5	3019	36	2804	9	-9.6
13SUB-F155A, Bt monzogranite										
669461 7094784 NAD 1983 UTM Zone 19N										
1.32	0.535	1.32	0.996	0.1908	0.1	2761	30	2749	2	-0.5
1.46	0.519	1.39	0.953	0.1880	0.4	2694	31	2725	7	1.4
1.60	0.523	1.55	0.971	0.1883	0.4	2712	34	2727	6	0.7
1.38	0.516	1.36	0.984	0.1867	0.2	2684	30	2713	4	1.3
1.47	0.560	1.47	0.998	0.1911	0.1	2868	34	2752	2	-5.3
1.39	0.552	1.38	0.991	0.1900	0.2	2836	32	2742	3	-4.2
1.41	0.522	1.38	0.981	0.1880	0.3	2706	30	2725	4	0.8
1.43	0.552	1.40	0.979	0.2072	0.3	2833	32	2884	5	2.2
1.39	0.519	1.38	0.992	0.1865	0.2	2696	30	2712	3	0.7
1.40	0.525	1.38	0.982	0.1888	0.3	2719	31	2732	4	0.6
1.35	0.538	1.34	0.991	0.1888	0.2	2776	30	2731	3	-2.0
1.48	0.539	1.44	0.971	0.1980	0.4	2778	32	2810	6	1.4
1.41	0.529	1.38	0.982	0.2039	0.3	2736	31	2858	4	5.2
1.44	0.517	1.40	0.977	0.1882	0.3	2687	31	2726	5	1.7
1.36	0.551	1.36	0.998	0.1910	0.1	2831	31	2751	1	-3.6
1.34	0.547	1.34	0.997	0.1906	0.1	2812	30	2748	2	-2.9
1.35	0.515	1.33	0.992	0.1881	0.2	2678	29	2726	3	2.2
2.04	0.492	1.44	0.709	0.1838	1.4	2578	31	2687	24	4.9
1.36	0.526	1.34	0.990	0.1879	0.2	2723	30	2724	3	0.0
1.47	0.523	1.45	0.989	0.1894	0.2	2712	32	2737	4	1.1

APPENDIX 3B - SHRIMP U-Pb isotopic data

Spot name	U (ppm)	Th (ppm)	Th/U	Yb (ppm)	Hf (ppm)	$^{204}Pb/^{206}Pb$	% ±	$^{206}Pb^*$ (ppm)	$f(206)^{204}$ %	$^{208*}Pb/^{206*}Pb$	% ±	$^{207*}Pb/^{235}U$
11216-045.1	867	535	0.64	476	11415	1.0E-6	100	395	0.002	0.182	0.8	14.04
11216-047.1	203	148	0.75	152	12619	9.1E-6	71	90	0.016	0.216	1.5	13.23
11216-054.1	811	417	0.53	294	11694	----	---	378	0.000	0.151	0.8	14.34
11216-059.1	2154	223	0.11	311	18612	3.9E-6	32	990	0.007	0.031	2.4	13.74
11216-061.1	282	174	0.64	196	12723	1.0E-4	21	124	0.180	0.181	1.5	13.40
11216-063.1	244	187	0.79	173	12718	7.9E-6	71	111	0.014	0.232	1.4	13.70
11216-068.1	362	261	0.74	259	13368	1.6E-5	41	160	0.027	0.214	1.2	13.15
11216-069.1	619	350	0.58	404	14990	9.0E-6	41	280	0.016	0.165	1.0	13.69
11216-070.1	588	620	1.09	419	12583	3.3E-6	71	267	0.006	0.311	0.8	13.82
11216-083.1	3639	3477	0.99	520	12908	---	58	1788	0.001	0.275	0.3	15.07
11216-086.1	1383	838	0.63	436	10516	6.6E-5	51	649	0.115	0.179	1.2	14.49
11216-087.1	491	287	0.60	614	10118	3.2E-6	71	251	0.005	0.165	1.0	18.10
11216-089.1	609	149	0.25	313	10945	7.2E-6	45	286	0.012	0.071	3.3	15.09
11216-089.2	3062	147	0.05	857	18555	3.0E-6	30	1456	0.005	0.014	1.5	14.34
11216-096.1	89	26	0.30	193	9251	5.8E-5	45	42	0.101	0.086	4.1	15.23
11216-096.2	241	161	0.69	170	12185	-2.7E-5	41	109	-0.046	0.200	1.6	13.65
11216-102.1	206	143	0.72	167	13260	1.3E-5	58	90	0.023	0.201	1.6	13.00
11216-103.1	689	277	0.41	187	11836	8.9E-6	38	316	0.015	0.118	1.1	14.15
11216-103.2	447	107	0.25	94	11686	3.2E-5	25	200	0.056	0.067	3.2	13.58
11216-107.1	471	237	0.52	314	15193	5.9E-6	58	210	0.010	0.146	1.2	13.42
11216-108.1	602	186	0.32	243	13891	6.1E-6	50	271	0.011	0.090	1.4	13.49
11216-108.2	446	274	0.64	283	14158	2.0E-6	100	199	0.004	0.180	1.1	13.55
11216-113.1	262	196	0.77	238	12262	4.1E-5	30	118	0.071	0.222	1.4	13.57
13SUB-F152A, Mt monzogranite												
669280 7094606 NAD1983 UTM Zone 19N												
11188-001.1	80	69	0.89	106	13097	1.2E-5	100	37	0.020	0.255	2.3	13.85
11188-003.1	125	61	0.51	114	10720	3.1E-5	50	57	0.054	0.139	2.6	13.92
11188-003.2	8	0	0.01	39	9640	3.9E-4	71	2	0.681	0.006	212.6	5.02
11188-012.1	90	59	0.68	106	10501	6.7E-5	41	41	0.116	0.193	2.6	13.83
11188-013.1	46	95	2.11	150	8436	2.2E-5	100	21	0.038	0.598	2.0	13.70
11188-014.1	98	60	0.63	105	11534	1.5E-4	27	44	0.253	0.170	2.7	13.58
11188-033.1	67	120	1.86	181	9890	6.8E-5	45	31	0.118	0.514	1.8	14.32
11188-035.1	32	66	2.11	120	8542	1.5E-4	45	15	0.266	0.579	2.5	13.97
11188-038.1	99	143	1.49	94	10397	3.0E-5	58	46	0.052	0.424	1.6	14.16
11188-044.1	65	123	1.95	173	8454	1.2E-4	35	30	0.212	0.555	3.6	13.66

						age (Ma)				
% ±	$^{206*}Pb/^{238}U$	% ±	Corr Coeff	$^{207*}Pb/^{206*}Pb$	% ±	$^{206*}Pb/^{238}U$	±	$^{207*}Pb/^{206*}Pb$	±	Disc. %
1.33	0.531	1.32	0.994	0.1919	0.1	2744	30	2759	2	0.7
1.43	0.514	1.40	0.978	0.1866	0.3	2675	31	2712	5	1.7
1.33	0.543	1.32	0.995	0.1917	0.1	2795	30	2757	2	-1.7
1.34	0.535	1.34	0.998	0.1864	0.1	2761	30	2710	1	-2.3
1.40	0.514	1.37	0.979	0.1892	0.3	2673	30	2735	5	2.8
1.41	0.528	1.39	0.981	0.1883	0.3	2732	31	2728	5	-0.2
1.49	0.513	1.47	0.988	0.1859	0.2	2670	32	2706	4	1.6
1.34	0.526	1.33	0.992	0.1888	0.2	2725	30	2731	3	0.3
1.43	0.529	1.42	0.992	0.1893	0.2	2739	32	2736	3	-0.1
1.43	0.572	1.42	0.995	0.1911	0.1	2916	33	2752	2	-7.5
1.36	0.546	1.32	0.968	0.1922	0.3	2811	30	2761	6	-2.2
1.49	0.595	1.48	0.992	0.2205	0.2	3012	35	2984	3	-1.1
2.28	0.546	2.20	0.966	0.2003	0.6	2810	50	2828	10	0.8
1.36	0.554	1.36	0.999	0.1879	0.1	2840	31	2724	1	-5.3
1.63	0.552	1.55	0.954	0.2000	0.5	2835	36	2826	8	-0.4
1.43	0.524	1.40	0.978	0.1890	0.3	2715	31	2734	5	0.8
1.43	0.511	1.39	0.978	0.1845	0.3	2660	30	2694	5	1.5
1.34	0.534	1.33	0.993	0.1921	0.2	2759	30	2760	3	0.0
1.53	0.520	1.34	0.876	0.1892	0.7	2701	30	2735	12	1.5
1.41	0.518	1.34	0.952	0.1878	0.4	2692	30	2723	7	1.4
1.42	0.524	1.41	0.991	0.1868	0.2	2716	31	2714	3	-0.1
1.38	0.520	1.35	0.974	0.1889	0.3	2701	30	2732	5	1.4
1.45	0.526	1.38	0.952	0.1872	0.4	2724	31	2718	7	-0.3
13SUB-F152A, Mt monzogranite										
669280 7094606 NAD1983 UTM Zone 19N										
1.62	0.532	1.55	0.955	0.1890	0.5	2748	35	2733	8	-0.7
1.84	0.536	1.79	0.976	0.1884	0.4	2766	40	2728	7	-1.7
5.33	0.342	3.02	0.567	0.1065	4.4	1896	50	1740	80	-10.3
1.61	0.530	1.53	0.952	0.1893	0.5	2741	34	2736	8	-0.2
1.85	0.533	1.72	0.933	0.1862	0.7	2756	39	2709	11	-2.1
1.60	0.522	1.52	0.947	0.1886	0.5	2708	34	2730	8	0.9
3.18	0.546	2.84	0.895	0.1904	1.4	2807	65	2746	23	-2.8
2.06	0.533	1.86	0.903	0.1901	0.9	2754	42	2743	15	-0.5
1.58	0.542	1.52	0.958	0.1895	0.5	2793	34	2737	7	-2.5
1.73	0.530	1.62	0.935	0.1869	0.6	2742	36	2715	10	-1.2

APPENDIX 3B - SHRIMP U-Pb isotopic data

Spot name	U (ppm)	Th (ppm)	Th/U	Yb (ppm)	Hf (ppm)	$^{204}Pb/^{206}Pb$	% ±	$^{206}Pb^*$ (ppm)	$f(206)^{204}$ %	$^{208*}Pb/^{206*}Pb$	% ±	$^{207*}Pb/^{235}U$
11188-046.1	15	2	0.12	66	9614	4.7E-4	45	4	0.821	0.025	40.7	5.12
11188-046.2	154	49	0.33	103	10759	-3.2E-5	45	68	-0.055	0.093	2.8	13.26
11188-057.1	14	2	0.18	38	9808	-4.3E-4	50	4	-0.753	0.072	15.8	5.79
11188-059.1	46	79	1.79	148	9434	1.6E-4	35	21	0.281	0.490	2.2	14.12
11188-059.2	20	2	0.08	61	10606	1.5E-4	71	6	0.259	0.022	28.2	5.19
11188-068.1	88	83	0.97	91	11401	2.1E-5	71	40	0.037	0.281	2.0	13.68
11188-077.1	76	71	0.97	106	10012	4.7E-5	50	35	0.082	0.272	2.2	13.79
11188-079.1	92	87	0.98	119	10382	1.0E-4	30	41	0.181	0.275	2.0	13.56
11188-080.1	34	64	1.93	131	8307	4.9E-5	71	16	0.085	0.566	3.9	13.75
11188-080.2	90	65	0.74	77	10598	3.0E-5	58	41	0.053	0.208	2.3	13.89
11188-086.1	50	95	1.95	75	10084	1.3E-4	38	22	0.229	0.555	2.0	13.19
11188-103.1	60	115	1.97	92	10164	7.5E-5	45	27	0.130	0.552	3.9	13.26
11188-113.1	8	1	0.10	54	9790	-5.6E-4	58	2	-0.963	0.072	20.7	5.78
11188-113.2	47	106	2.34	102	9982	1.7E-4	35	20	0.290	0.681	1.9	13.09
11188-121.1	37	125	3.52	91	9487	1.9E-4	35	17	0.336	0.974	1.7	13.73
13SUB-F150A, monzogranite												
669259 7094583 NAD1983, UTM Zone 19N												
11186-005.1	150	128	0.88	128	12108	3.7E-5	41	66	0.065	0.246	1.7	13.08
11186-007.1	163	113	0.72	102	12519	6.0E-5	32	70	0.104	0.204	1.8	12.76
11186-010.1	108	92	0.88	101	11900	8.3E-5	32	47	0.144	0.251	1.9	13.25
11186-016.1	297	118	0.41	111	12247	1.3E-5	50	129	0.022	0.112	1.8	13.08
11186-018.1	474	58	0.13	121	12628	3.1E-5	24	211	0.053	0.035	4.9	13.48
11186-023.1	89	82	0.95	91	11805	3.1E-5	58	39	0.054	0.249	2.2	13.16
11186-025.1	151	70	0.48	195	11638	5.7E-6	100	67	0.010	0.128	2.3	14.05
11186-027.1	299	62	0.21	106	10207	1.2E-5	50	135	0.021	0.064	7.9	14.20
11186-028.1	569	366	0.67	226	8687	3.2E-5	22	250	0.055	0.187	1.0	13.74
11186-030.1	84	47	0.58	106	11955	9.2E-5	38	31	0.160	0.200	10.6	9.85
11186-031.1	268	204	0.79	113	12643	2.4E-5	38	119	0.041	0.227	1.3	13.22
11186-039.1	86	88	1.05	94	12292	6.7E-5	41	38	0.115	0.288	3.7	13.18
11186-048.1	951	96	0.10	231	14744	1.3E-5	25	421	0.023	0.031	8.3	13.41
11186-051.1	365	86	0.24	135	12328	3.2E-4	9	158	0.559	0.073	2.5	13.04
11186-055.1	262	155	0.61	102	13041	5.0E-5	27	114	0.087	0.178	2.8	13.15
11186-057.1	236	169	0.74	108	13094	1.0E-5	58	105	0.018	0.210	1.3	13.36
11186-058.1	186	8	0.05	60	11556	3.9E-4	15	59	0.679	0.019	14.6	7.74
11186-058.2	67	5	0.08	43	10066	-2.0E-5	100	19	-0.034	0.026	9.8	5.03

						age (Ma)				
% ±	$^{206*}Pb/^{238}U$	% ±	Corr Coeff	$^{207*}Pb/^{206*}Pb$	% ±	$^{206*}Pb/^{238}U$	±	$^{207*}Pb/^{206*}Pb$	±	Disc. %
3.93	0.337	2.35	0.596	0.1100	3.2	1875	38	1800	57	-4.8
1.48	0.512	1.43	0.970	0.1877	0.4	2667	31	2722	6	2.5
3.75	0.342	2.42	0.645	0.1228	2.9	1897	40	1998	51	5.8
1.85	0.544	1.70	0.918	0.1883	0.7	2799	39	2728	12	-3.2
2.88	0.335	2.12	0.736	0.1123	1.9	1861	34	1838	35	-1.5
1.60	0.527	1.53	0.957	0.1881	0.5	2731	34	2725	8	-0.2
1.62	0.535	1.54	0.952	0.1869	0.5	2764	35	2715	8	-2.2
1.57	0.520	1.50	0.954	0.1890	0.5	2701	33	2733	8	1.4
1.92	0.527	1.78	0.923	0.1894	0.7	2728	39	2737	12	0.4
1.57	0.529	1.51	0.958	0.1903	0.4	2739	34	2745	7	0.3
1.80	0.512	1.66	0.924	0.1867	0.7	2667	36	2713	11	2.1
1.70	0.515	1.60	0.940	0.1867	0.6	2678	35	2713	10	1.6
4.99	0.331	3.03	0.609	0.1267	4.0	1844	49	2053	70	11.7
2.56	0.505	2.32	0.909	0.1880	1.1	2636	50	2724	18	3.9
1.95	0.532	1.77	0.907	0.1873	0.8	2748	40	2718	13	-1.3
13SUB-F150A, monzogranite										
669259 7094583 NAD1983, UTM Zone 19N										
1.47	0.509	1.43	0.970	0.1864	0.4	2652	31	2711	6	2.6
1.47	0.504	1.42	0.969	0.1836	0.4	2631	31	2686	6	2.5
1.61	0.509	1.47	0.917	0.1886	0.6	2654	32	2730	11	3.4
1.50	0.507	1.37	0.915	0.1873	0.6	2642	30	2719	10	3.4
1.35	0.517	1.34	0.990	0.1889	0.2	2688	29	2733	3	2.0
2.89	0.517	2.28	0.790	0.1847	1.8	2686	50	2695	29	0.4
1.46	0.515	1.42	0.973	0.1980	0.3	2676	31	2810	6	5.8
1.40	0.527	1.38	0.984	0.1954	0.2	2730	31	2788	4	2.6
1.35	0.512	1.34	0.991	0.1947	0.2	2665	29	2782	3	5.2
5.59	0.429	4.35	0.779	0.1665	3.5	2301	84	2523	59	10.5
1.40	0.515	1.37	0.982	0.1861	0.3	2679	30	2708	4	1.3
1.75	0.509	1.53	0.873	0.1879	0.9	2651	33	2724	14	3.3
1.50	0.515	1.41	0.939	0.1890	0.5	2677	31	2733	9	2.5
1.38	0.504	1.35	0.978	0.1876	0.3	2631	29	2721	5	4.1
1.45	0.506	1.38	0.951	0.1884	0.4	2641	30	2728	7	3.9
1.40	0.518	1.37	0.983	0.1870	0.3	2692	30	2716	4	1.1
2.65	0.367	2.01	0.758	0.1530	1.7	2016	35	2380	29	17.8
1.73	0.324	1.54	0.893	0.1127	0.8	1810	24	1843	14	2.1

APPENDIX 3B - SHRIMP U-Pb isotopic data

Spot name	U (ppm)	Th (ppm)	Th/U	Yb (ppm)	Hf (ppm)	$^{204}Pb/^{206}Pb$	% ±	$^{206}Pb^*$ (ppm)	$f(206)^{204}$ %	$^{208*}Pb/^{206*}Pb$	% ±	$^{207*}Pb/^{235}U$
11186-059.1	138	116	0.86	115	12495	1.7E-5	58	61	0.030	0.235	1.6	13.42
11186-061.1	228	134	0.60	94	12890	8.9E-6	71	98	0.015	0.174	1.7	12.90
11186-062.1	319	365	1.18	202	12556	2.5E-5	35	134	0.044	0.329	1.0	12.60
11186-064.1	17	1	0.05	26	10213	9.5E-4	30	5	1.652	-0.014	81.8	4.68
11186-065.1	1059	47	0.05	137	12086	6.1E-6	35	458	0.011	0.012	2.9	12.82
11186-071.1	362	339	0.97	182	12894	1.4E-5	45	158	0.023	0.274	1.0	13.13
11186-072.1	421	109	0.27	153	12415	1.8E-5	35	188	0.030	0.079	1.8	13.43
11186-075.1	217	161	0.77	123	12845	1.7E-5	50	97	0.030	0.222	1.5	13.51
11186-077.1	275	124	0.47	117	12048	2.5E-5	38	121	0.043	0.129	1.8	13.30

table notes:
spot name follows the convention x-y.z; where x = sample number, y = grain number and z = spot number.
multiple analyses in an individual spot are labelled as x-y.z.z; nd = not determined
$f(206)^{204}$ refers to mole percent of total ^{206}Pb that is due to common Pb, calculated using the ^{204}Pb-method; common Pb composition used is the surface blank (4/6: 0.05770; 7/6: 0.89500; 8/6: 2.13840)
* refers to radiogenic Pb (corrected for common Pb)
errors are reported at 1σ uncertainty level unless otherwise noted

						age (Ma)				
% ±	$^{206*}Pb/^{238}U$	% ±	Corr Coeff	$^{207*}Pb/^{206*}Pb$	% ±	$^{206*}Pb/^{238}U$	±	$^{207*}Pb/^{206*}Pb$	±	Disc. %
1.46	0.516	1.42	0.973	0.1887	0.3	2682	31	2731	6	2.2
1.43	0.499	1.40	0.979	0.1874	0.3	2610	30	2720	5	4.9
1.39	0.489	1.36	0.983	0.1871	0.3	2564	29	2717	4	6.8
4.71	0.320	2.24	0.475	0.1060	4.1	1791	35	1732	76	-3.9
1.32	0.504	1.32	0.996	0.1846	0.1	2629	28	2695	2	3.0
1.38	0.509	1.36	0.986	0.1869	0.2	2654	30	2715	4	2.7
1.36	0.519	1.35	0.988	0.1878	0.2	2694	30	2723	3	1.3
1.42	0.520	1.39	0.979	0.1886	0.3	2698	31	2730	5	1.4
1.40	0.514	1.38	0.982	0.1876	0.3	2675	30	2721	4	2.1

table notes:
spot name follows the convention x-y.z; where x = sample number, y = grain number and z = spot number.
multiple analyses in an individual spot are labelled as x-y.z.z; nd = not determined
$f(206)^{204}$ refers to mole percent of total ^{206}Pb that is due to common Pb, calculated using the ^{204}Pb-method; common Pb composition used is the surface blank (4/6: 0.05770; 7/6: 0.89500; 8/6: 2.13840)
* refers to radiogenic Pb (corrected for common Pb)
errors are reported at 1σ uncertainty level unless otherwise noted

4. Chapter 4. U-Pb and Pb and Lu-Hf isotopes of the Archean orthogneiss complex on eastern Hall Peninsula, southern Baffin Island, Nunavut: identification of exotic Paleo- to Mesoarchean crust beneath eastern Hall Peninsula, southern Baffin Island, Nunavut

This chapter is published with the journal *Precambrian Research* and is co-authored with my thesis advisor Dr. Alfredo Camacho and research colleagues Dr. Graham Pearson and Dr. Yan Luo. This chapter is a continuation of work from Chapters 2 and 3 and now includes paired U-Pb and Lu-Hf isotopic analyses of zircons from orthogneiss units previously characterized in chapter 2 and 3. I was responsible for the sample collection, U-Pb and Lu-Hf isotopic analysis and data collection and interpretation, figure creation, and the writing. My collaborators G. Pearson and Y. Luo along with their lab staff at the Arctic research laboratory at the University of Alberta, provided assistance with sample preparation, data acquisition and processing. My co-authors reviewed drafts of the article and this is reproduced herein with the kind permission of my co-authors. Re-formatting and minor re-writing was done to maintain continuity within this Ph.D. thesis.

From, R.E., Camacho, A., Pearson, D.G. and Luo, Y. *2017*. U-Pb and Pb and Lu-Hf isotopes of the Archean orthogneiss complex on eastern Hall Peninsula, southern Baffin Island, Nunavut: identification of exotic Paleo- to Mesoarchean crust beneath eastern Hall Peninsula, southern Baffin Island, Nunavut. Precambrian Research.

4.1. Abstract

Eastern Hall Peninsula on southeastern Baffin Island, lies at the junction of a complex Paleoproterozoic collision between the Rae craton, Meta Incognita microcontinent and the North Atlantic craton from ca. 1.88 to 1.80 Ga. Several different interpretations of crustal correlations and the location of intervening sutures have been proposed based on reconnaissance-scale geologic investigation. Therefore, in this study, complex zircon grains from Archean orthogneiss units on eastern Hall Peninsula were analyzed in-situ to elucidate the detailed magmatic history of the region and assess crustal provenance.

Magmatic zircons yielded U-Pb crystallization ages between ca. 2976 to 2720 Ma and metamorphic zircons record tectonothermal disturbances between ca. 2740 to 2700 Ma, a period coinciding with metamorphism documented in adjacent crustal blocks (e.g., west Greenland and northern Labrador). Magmatic rocks older than ca. 2740 Ma generally have positive **ε**Hf(t) signatures between 0 to 7 (±2) and depleted mantle model ages of ca. 3.1 to 3.0 Ga indicating the time that protolith melt was extracted from the mantle. The oldest, granodioritic crust crystallized at ca. 2976 Ma and was then reworked periodically at ca. 2.93, 2.84-2.81 and 2.77-2.69 Ma. Zircons from two orthogneiss samples, with U-Pb crystallization ages younger than ca. 2740 Ma, yielded negative **ε**Hf(t) values ranging from -4 to -12 and mean depleted mantle model ages of ca. 3.4 and 3.3 Ga respectively, indicating derivation from an older, potentially exotic, crustal source yet to be identified in outcrop on Hall Peninsula.

Synthesizing regional U-Pb data we propose a new regional correlation model that retains the essentials of previous models and incorporates new data from eastern Hall

Peninsula and other recent studies. This new tectonic correlation model groups eastern Hall Peninsula, southern Cumberland Peninsula and the Aasiaat domain into a "Core zone" that shared a geologic history prior to 1.90 Ga and potentially prior to 2.75 Ga.

4.2. Introduction

The Archean orthogneiss complex of eastern Hall Peninsula, which is situated on the southeastern edge of Baffin Island, Nunavut, Canada, was involved in a two-stage Paleoproterozoic collision with at least three other crustal blocks (Figure 4.1). The three main crustal blocks involved, the Rae craton, Meta Incognita microcontinent and North Atlantic craton, were amalgamated over an area that presently underlies northern Labrador to Baffin Island to west Greenland during a period of progressive accretionary tectonism within the Trans-Hudson orogen, ca. 1.88-1.80 Ga (Figure 4.1; St-Onge et al., 2009 *and references therein*). To briefly summarize the sequence of events, at ca. 1.88 Ga Meta-Incognita microcontinent accreted onto the Rae craton's southern margin (Baffin Suture) with concurrent accretion of the Aasiaat domain to the southern margin of Rae craton of west Greenland (Disko Bugt suture) creating the Rinkian fold belt (Figure 4.1). Next, the Torngat orogen developed between ca. 1.87-1.85 Ga as the North Atlantic craton collided with the eastern margin of Meta-Incognita microcontinent in northern Labrador. Shortly after, between ca. 1.86-1.84 Ga, the North Atlantic craton collided with the composite Rae craton and Aasiaat domain. Subsequent accretion of juvenile material and arc terranes led to terminal collision of the Superior craton with the now composite Churchill domain between 1.82-1.80 Ga (Figure 4.1).

Figure 4.1: Regional map of the Quebec-Baffin segment of the Trans-Hudson orogen with ages of crustal amalgamation and proposed suture locations. Abbreviations: BaS, Baffin suture; BeS, Bergeron suture; DBS Disko Bugt suture; NIS, Nordre Isortoq steep belt; SRS, Soper River suture; TgS, Tasiuyak gneiss structure. Map modified from St-Onge et al. (2009).

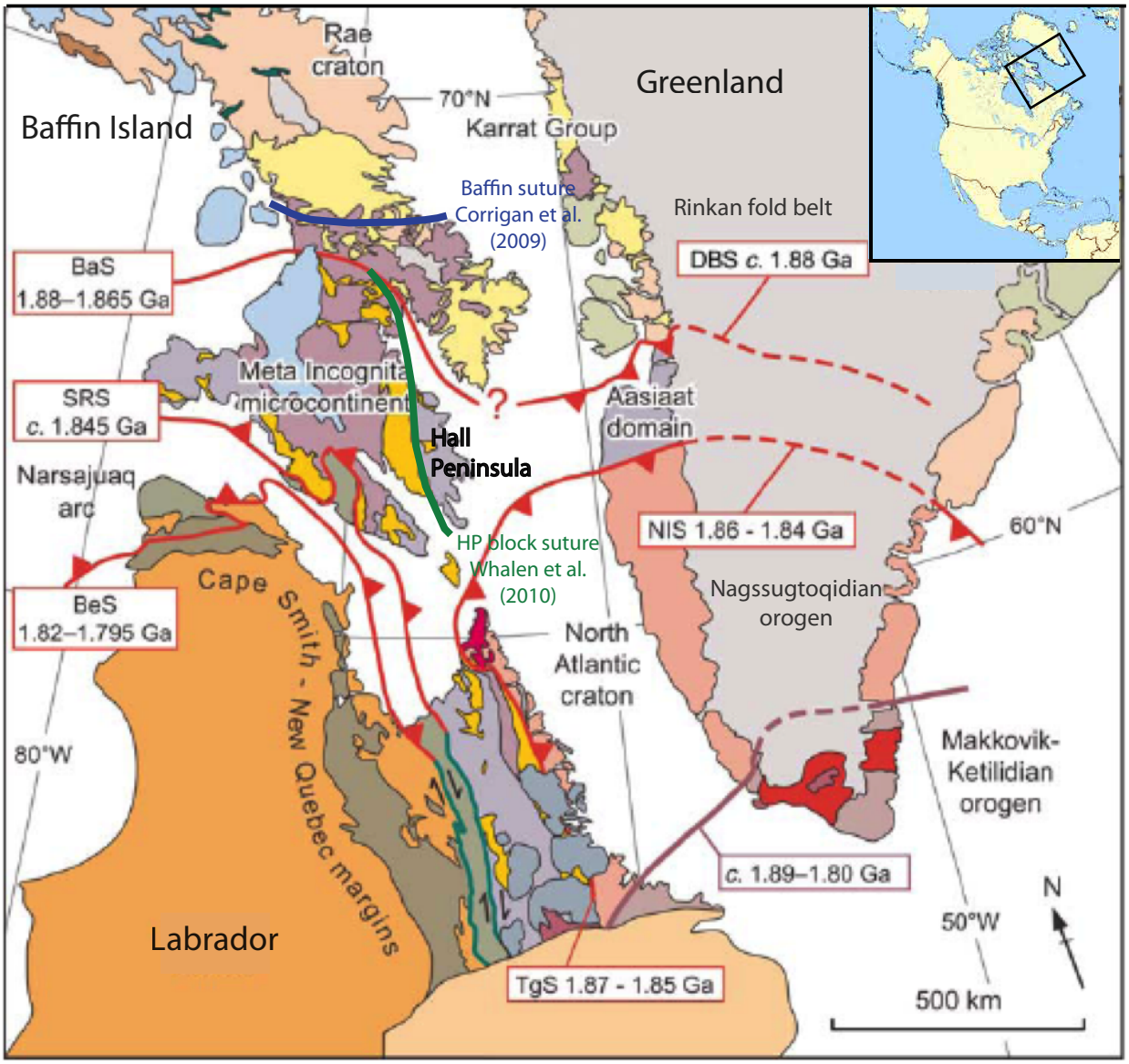

While the geology of these crustal blocks has been well documented and the location of their intervening sutures largely delineated through field based studies and isotopic work, the cratonic affinity of the eastern Hall Peninsula block has remained enigmatic due to a lack of detailed mapping and isotopic work. Nevertheless, tentative correlations between eastern Hall Peninsula and the Aasiaat domain (also termed the Disko craton) of West Greenland have been proposed in several studies (e.g., Grocott and Davies, 1999; van Gool et al., 2002). The Archean Aasiaat domain, initially thought to be a transition zone between the Nagssugtoqidian Orogen and Rinkian fold belts of West Greenland (Connelly et al., 2006), has now been determined to be a unique crustal fragment that was caught between the Rae craton and North Atlantic craton of West Greenland during north-south shortening (Kolb, 2014). However, a potential crustal correlation with the North Atlantic craton of northern Labrador and southwestern Greenland based on lithological characteristics and U-Pb ages has also been argued for and cannot be ruled out (Scott, 1997a; Connelly and Mengel, 2000).

Recent regional synthesis studies propose various locations for the crustal sutures separating the Rae craton from Meta Incognita microcontinent on southern Baffin Island and suggest correlations of these cratons across Davis Strait to west Greenland (e.g., Corrigan et al., 2009; St-Onge et al., 2009; Whalen et al., 2010). With the interpreted geology of Hall Peninsula being a critical piece of the puzzle correlating rocks of southern Baffin Island to west Greenland, field mapping of Hall Peninsula was conducted in 2012-13 as part of an integrated geoscience project (Machado et al., 2013; Steenkamp and St-Onge, 2014). Now, follow-up analytical work on the Archean rocks of Eastern

Hall Peninsula has been undertaken with the aim of further elucidating the geologic history and crustal provenance of this enigmatic crustal block.

In this study, U-Pb and Lu-Hf isotopic studies were carried out on zircon separates from seven orthogneiss samples (ranging from syenogranitic to tonalitic in composition) from a small area of heterogeneous metamorphic gneisses on eastern Hall Peninsula (herein termed the "snow bowl area"). The Sensitive High Resolution Ion MicroProbe (SHRIMP) was used to obtain U-Pb dates while Lu-Hf isotopes on the same zircon grains were measured using Laser Ablation Inductively Coupled Plasma Mass Spectroscopy (LA-ICPMS) to effectively link crystallization ages to magmatic evolution (e.g., Kemp et al., 2005; Wooden et al., 2013). The results from the snow bowl area were compared with those of zircon separates from seven samples of Archean orthogneiss that are compositionally and spatially representative of the widely distributed Archean rocks of eastern Hall Peninsula. These regional samples were analyzed using split stream LA(SS)-ICPMS to collect simultaneously U-Pb and Lu-Hf isotopes in zircon grains.

Results of this study expand upon the magmatic and metamorphic history of Archean orthogneisses on eastern Hall Peninsula. New U-Pb crystallization ages between ca. 2975 and 2700 Ma and metamorphic ages from ca. 2740 to 2700 Ma provide key information for comparisons with adjacent Archean crust. Coupled Lu-Hf isotopic data gives more detailed information on when the parental magmas were extracted from the depleted mantle and how much crustal recycling took place. Ultimately, this study adds to the isotopic database for Hall Peninsula and southeastern Baffin Island, allowing for detailed comparisons of eastern Hall Peninsula to the neighbouring Archean blocks in this region of the THO to test the extent that various blocks shared a common history. This has

implications for re-examining how various blocks were assembled in the Paleoproterozoic within this segment of the THO and leads to a newly proposed crustal correlation model that hybridizes several aspects from previous models that are typically considered as mutually exclusive. Since previous correlation models have been used within subsequent geologic investigations, a re-evaluation of opposing hypotheses surrounding the accretionary tectonics during the THO is in order. The results of this study also expand upon a cryptic Archean geologic history for eastern Hall Peninsula and a comparison of the ages of Archean magmatic pulses and subsequent metamorphism can be compared with the adjacent regions to examine the extent that now independent crustal blocks shared a Neoarchean or earlier geologic history.

4.3. Geological setting

On the basis of similar lithological, geochronological and aeromagnetic characteristics, the Archean rocks on Hall Peninsula have been variably correlated with the Rae craton of northern Baffin Island and western Greenland (Hoffman, 1988), the Meta Incognita microcontinent of southern Baffin Island and northern Labrador (St-Onge et al., 2009), the Aasiaat domain of central-western Greenland (Hollis et al., 2006; Thrane and Connelly, 2006; St-Onge et al., 2009), the North Atlantic craton of northern Labrador (also termed "Nain craton"; Scott and Campbell, 1993; Scott, 1999; Connelly, 2001; Wardle et al., 2002), or presented as a separate and unique microcontinent fragment (Whalen et al., 2010).

Geological investigation by Scott (1996) along a narrow E-W transect of the western and central portions of Hall Peninsula, combined with previous reconnaissance-scale

work by Blackadar (1967), led to the initial recognition of three principal lithological domains on Hall Peninsula: a western plutonic domain, a central metasedimentary domain and an eastern plutonic domain. Subsequent work in 2012-2013 by the Hall Peninsula Integrated Geoscience Project led by the Canada-Nunavut Geoscience Office resulted in updated geologic maps (1:250,000) of the southern (Machado et al., 2013) and northern (Steenkamp and St-Onge, 2014) portions of Hall Peninsula, and the broad division of two distinct geologic domains on Hall Peninsula. The eastern portion of Hall Peninsula is dominated by polydeformed and polymetamorphosed Archean gneissic to migmatitic tonalite to monzogranite with subsidiary components of syenogranite and locally ultramafic pods (Scott, 1999; From et al., 2013). The western portion of Hall Peninsula is dominated by a polydeformed and polymetamorphosed Paleoproterozoic plutonic suite of granodiorite to orthopyroxene-bearing monzogranite with intervening panels of metasedimentary rocks (Scott, 1999; Rayner, 2014). The plutonic rocks of the western Hall Peninsula are interpreted as a continuation of the ca. 1.865-1.845 Ga Cumberland Batholith, a post accretion batholith including granites of arc, A-type (within plate) and post-collisional affinity (Jackson and Taylor, 1972; Scott, 1996; Whalen et al., 2010). The central region of Hall Peninsula is dominated by Paleoproterozoic metasedimentary units historically interpreted to be part of the Lake Harbour group of Meta Incognita microcontinent and the northern continuation of the Tasiuyak gneiss complex of the Torngat orogen (Figure 4.1; Hoffman, 1989; Scott and Machado, 1995; Scott 1997b, 1999). These metasedimentary rocks are interpreted to unconformably overlie the Archean orthogneiss complex (Steenkamp and St-Onge, 2014) and are

interleaved in imbricate folds and thrusts as slivers and panels ranging from 2 m to several kilometres in thickness (Machado et al., 2013).

Within the eastern domain of Hall Peninsula, zircon $^{207}Pb/^{206}Pb$ ages ranging from 2920 +8/-6 to 2797 +27/-15 Ma were interpreted to represent magmatic crystallization of tonalite (Figure 4.2, Table 4.1, Scott, 1999). Zircon rims from all samples analyzed yielded $^{207}Pb/^{206}Pb$ ages between ca. 1844 and 1736 Ma and one rim at ca. 2770 interpreted as representing metamorphic events (Scott, 1999). Granitic dykes intruding these Archean gneisses along the eastern coast yielded zircon $^{207}Pb/^{206}Pb$ ages ranging from ca. 2835 to 2768 Ma and titanite $^{207}Pb/^{206}Pb$ ages from ca. 1736 to 1730 Ma (Scott, 1999). Subsequent reconnaissance-scale U-Pb investigations of the Archean rocks on eastern Hall Peninsula by Rayner (2014, 2015) determined $^{207}Pb/^{206}Pb$ ages between 2841 and 2701 Ma, interpreted as representing the magmatic crystallization ages of tonalitic and granitic gneiss (Figure 4.2, Table 4.1). Complete summary data of previous U-Pb geochronology on Archean rocks of Hall Peninsula is presented in Table 4.1.

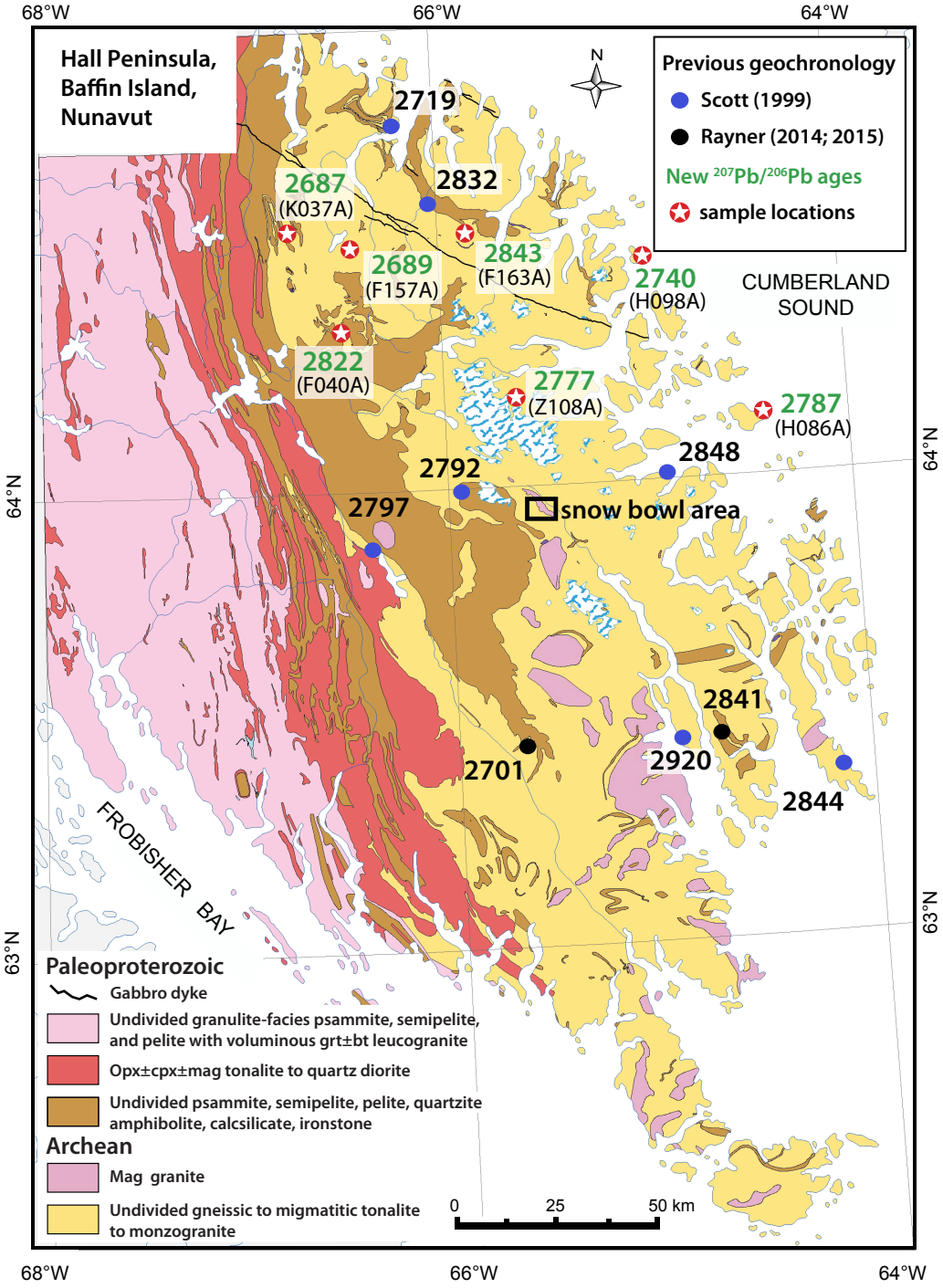
Hall Peninsula,
Baffin Island,
Nunavut
N
Previous geochronology
Scott (1999)
Rayner (2014; 2015)
New 207Pb/206Pb ages
sample locations
2719
2687
(K037A)
2832
2689
(F157A)
2843
(F163A)
2740
(H098A)
CUMBERLAND
SOUND
2822
(F040A)
2777
(Z108A)
2787
(H086A)
2848
2792
2797
snow bowl area
2841
2920
2701
2844
FROBISHER BAY
68°W
66°W
64°W
64°N
63°N
Paleoproterozoic
Gabbro dyke
Undivided granulite-facies psammite, semipelite, and pelite with voluminous grt±bt leucogranite
Opx±cpx±mag tonalite to quartz diorite
Undivided psammite, semipelite, pelite, quartzite amphibolite, calcsilicate, ironstone
Archean
Mag granite
Undivided gneissic to migmatitic tonalite to monzogranite
0
25
50 km

Table 4.1. Summary of previous U-Pb geochronology work on eastern Hall Peninsula organized by age.

Age (Ma)	± 2σ	Interpretation	Rock Type	Mineral	Method	Reference
2920	+8/-6	crystallization	foliated tonalite	zircon	ID-TIMS	Scott (1999)
2848	3	crystallization	foliated tonalite	zircon	ID-TIMS	Scott (1999)
2844	+6/-5	crystallization	foliated tonalite	zircon	ID-TIMS	Scott (1999)
2841	3	crystallization	tonalite gneiss (713778 7041607, 19N)	zircon	SHRIMP	Rayner (2014)
2835	11	crystallization	granitic dyke	zircon	ID-TIMS	Scott (1999)
2832	5	crystallization	bt-cpx tonalite (642985 7168148, 19N)	zircon	SHRIMP	Rayner (2015)
2820	5	age of xenocrysts	granitic dyke	zircon	ID-TIMS	Scott (1999)
2797	+27/-15	crystallization	opx-bt tonalite	zircon	ID-TIMS	Scott (1999)
2792	9	crystallization	bt tonalite (355848 7101089, 20N)	zircon	SHRIMP	Rayner (2015)
2768	13	crystallization or age of xenocrysts	granitic dyke	zircon	ID-TIMS	Scott (1999)
2719	4	crystallization	monzogranite (632654, 7187186, 19N)	zircon	SHRIMP	Rayner (2015)
2701	2	crystallization	megacrystic granite (672804 7030899, 19N)	zircon	SHRIMP	Rayner (2014)
1742	3	metamorphism	foliated tonalite	titanite	ID-TIMS	Scott (1999)
1736	2	post-metamorphic	granitic dyke	titanite	ID-TIMS	Scott (1999)
1730	3	cooling	granitic dyke	titanite	ID-TIMS	Scott (1999)

Abbreviations: bt = biotite; cpx = clinopyroxene; opx = orthopyroxene; ID-TIMS = Isotope Dilution Thermal Ionization Mass Spectrometry; SHRIMP = Sensitive High Resolution Ion Microprobe

4.4. Geology of the snow bowl area

A study area on central Hall Peninsula was chosen in a location where long-standing ice exposed pristine, lichen-free outcrops and is informally named 'snow bowl' area based on a translation from the traditional Inuktitut place name for this locality. The snow bowl area covers an area of approximately 700 x 200 m that preserves eight plutonic units (seven of which are represented in Figure 4.3) and reveals that the Archean orthogneiss complex is more heterogeneous than previously thought. Overall, porphyroclastic monzogranite gneiss intrudes several older orthogneiss units ranging from tonalitic to granitic in composition, each with distinct characteristics. Relatively small (cm to m scale), undeformed, coarse-grained syenogranite dykes intrude all units.

A pervasive gneissic fabric (S_1) strikes east-southeast and dips moderately to steeply (~50-80°) to the southwest. A mineral lineation (L_1) defined by biotite and hornblende, common in all units in the snow bowl area and throughout Hall Peninsula, plunges moderately (35-50°) to the west. F_1 folds were not observed in the snow bowl area but are documented in rare, low-strain zones throughout eastern Hall Peninsula. A less pervasive S_2 gneissic fabric transects S_1; it strikes north-northwest to northwest and is axial-planar to F_2 folds. Parallel to F_2 fold hinges there is a mineral-stretching lineation (L_2) defined by quartz + feldspar ± hornblende ± biotite shallowly plunging (~20°) to the northwest. A quartz + feldspar rodding lineation (L_2) also has the same orientation.

The metaplutonic gneisses in the snow bowl area typically contain biotite + hornblende, diagnostic of amphibolite facies metamorphism. However, mafic silicate clots within the gneissic fabric locally contain hornblende, together with orthopyroxene + clinopyroxene indicating transitional granulite-facies conditions. Clinopyroxene ±

Figure 4.3. Geology of the snow bowl area on east-central Hall Peninsula, Nunavut. Units are presented from oldest (1) to youngest (7), as interpreted in From et al. (2014). The majority of rocks are pervasively deformed and gneissic; the prefix 'meta' is omitted from rock units for brevity. Samples locations analyzed with SHRIMP U-Pb geochronology are shown with a black dot and their ages of crystallization in green.

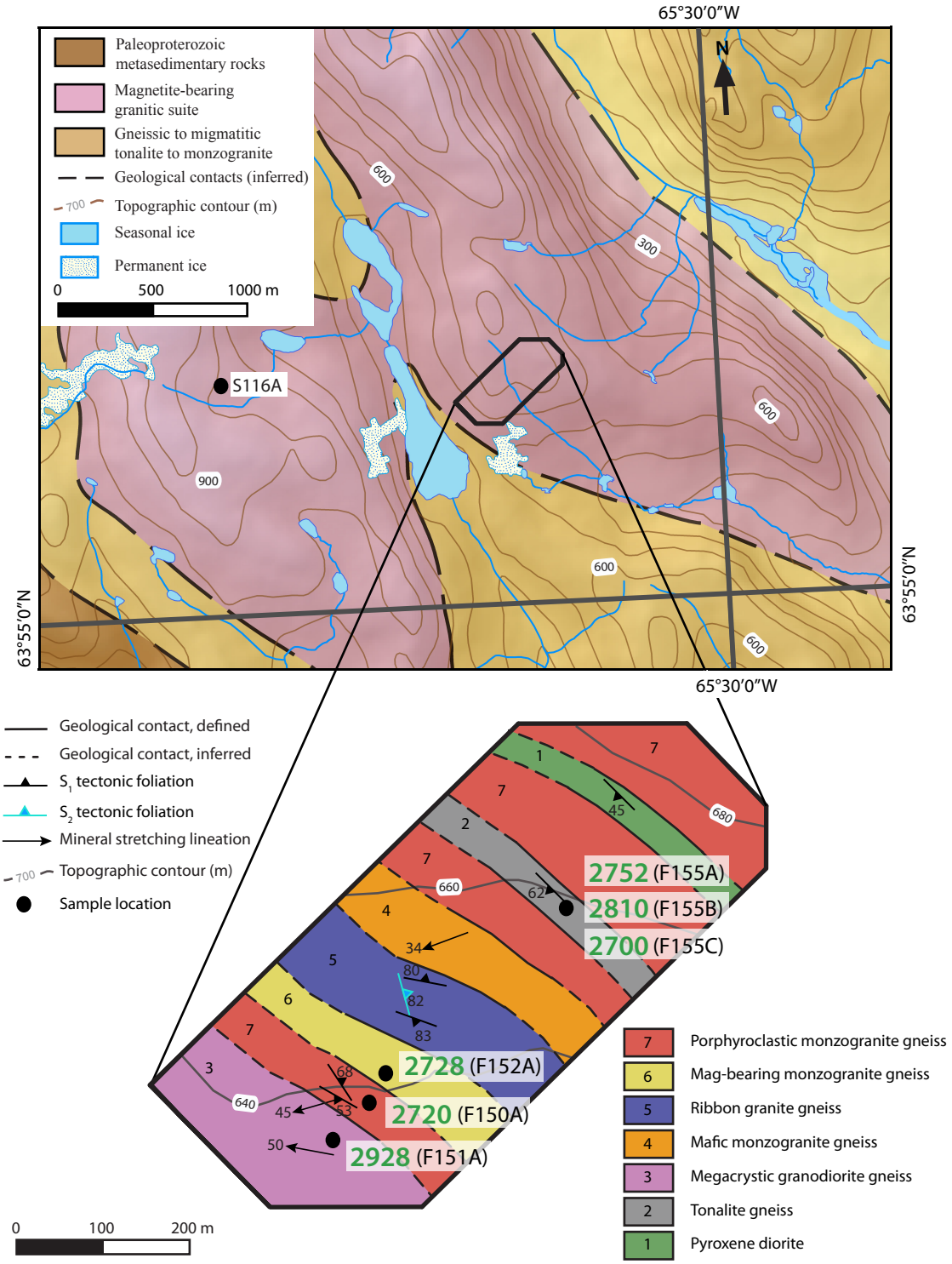

orthopyroxene in the centre of pods, and are replaced or rimmed by hornblende towards the margins indicating regional amphibolite-facies retrogression on an older granulite-facies assemblage. Other localities throughout eastern Hall Peninsula have large mafic enclaves or pods that also preserve granulite-facies assemblages.

4.5. Analytical Techniques

4.5.1. Sample Collection

Samples from the snow bowl area were collected along a transect during detailed mapping (Figure 4.3) while regional-scale samples were collected by collaborating geologists of the Hall Peninsula Project during helicopter-assisted mapping traverses (Figure 4.2). Large homogeneous samples were collected, avoiding veins, dykes or mineral aggregates. Petrography and whole-rock geochemistry were used to select samples with adequate zircon for U-Pb geochronology.

4.5.2. U-Pb SHRIMP

Seven samples from the snow bowl area were analyzed using the SHRIMP II instrument at the Geological Survey of Canada in Ottawa, Canada. The complete methodology and results are presented in From et al. (2015), and related U-Pb SHRIMP results are summarized herein for cross-referencing to newly presented Hf data that were collected by multi collector LA-ICPMS on the same SHRIMP sputter pits. Time-resolved ablation traces were examined to check that there were no significant changes in measured $^{176}Hf/^{177}Hf$ during ablation.

4.5.3. U-Pb and Lu-Hf LASS-ICPMS:

Separated zircons were analyzed by a the LASS-ICPMS technique that was first described by Yuan et al. (2008) and Xie et al. (2008) and further refined by Fisher et al. (2011, 2014). Simultaneous Hf and U-Pb isotope measurements on a single ablation spot were made in the Arctic Resources Laboratory at the University of Alberta using a Resolution Excimer 193 nm laser operating with an energy fluence of 5 J/cm^2 and 10 Hz, using a 33 μm diameter spot size. Ablated aerosols were entrained in a He cell gas flow of 1.0 L/min and subsequently mixed with N_2 (10mL/min) and Ar (in total 1.8 L/min) prior to the total gas flow being split. The ablated sample + He^+ $N2^+$ Ar mixture was then split after the laser cell using a Y-piece, diverting the ablation product into two independent mass spectrometers. Note that the length of tubing in this device was set as equal such that the ablated sample materials arrived simultaneously at both mass spectrometers. The U-Pb isotope measurements were performed on a Thermo Element-XR 2 mass spectrometer using a single secondary electron multiplier (SEM) detector in peak hopping mode. Lu-Hf isotope measurements were made on a Thermo Fisher Neptune Plus using multiple Faraday detectors with 10^{11} Ω amplifiers operating in static collection mode. Analysis time was typically 140 seconds consisting of 30 seconds of background followed by 70 seconds of ablation and 40 seconds of sample washout. Both Hf and U-Pb data were processed offline using Iolite v3.32 software (http://iolite-software.com/).

Hf and U-Pb analytical biases were calibrated using the Plesovîce zircon as a primary reference material (Aftalion et al., 1989). Due to the large corrections necessary for the isobaric interference of ^{176}Yb (and ^{176}Lu) on the ^{176}Hf mass, each run includes a variety of secondary standards of known age and Hf isotope composition interspersed

with unknowns in order to evaluate the accuracy of the interference correction. In this study we monitored the Yb interference correction by analysis of a variety of natural and synthetic zircons with a wide range of Yb/Hf. Synthetic HREE-doped zircons (MUN1 and MUN3 – Fisher et al., 2011) were evaluated, along with zircon standard 91500 (Blichert-Toft, 2008). The measured $^{176}Yb/^{173}Yb$ was iteratively calibrated to optimize the Yb-interference correction, monitored by zircon reference materials with variable Yb contents (91500, MUN1, MUN3). The mean $^{176}Hf/^{177}Hf$ for the calibration standard Plesovîce zircon (0.282482 ± 47 [2 SD], n = 242) is in close agreement with the solution MC-ICPMS values of 0.282482 (Sláma et al., 2008). Multiple analyses (n=194) of the 91500 zircon standard (Blichert-Toft, 2008) by LASS yielded a weighted mean $^{206}Pb/^{238}U$ age of 1068 ± 12 Ma (2 SE) and a mean $^{176}Hf/^{177}Hf$ of 0.282313 ± 72 (2 SD). The results agree well with the U-Pb age of 1063.4 ±1.4 (Schoene et al., 2006) and $^{176}Hf/^{177}Hf$ value of 0.282308 ± 6 (2SD; Blichert-Toft, 2008). The mean $^{176}Hf/^{177}Hf$ for MUN1 and MUN3 (0.282130 ± 59 [2 SD], n = 15; 0.282154 ± 42 [2 SD], n = 5) are in good agreement with the solution MC-ICPMS values of 0.282135 ± 31 (2SD) for MUNZirc 1 and 3 (Fisher et al., 2011). The decay constant and parameters used for Hf model age calculations are $^{176}Lu/^{177}Hf$ (chondrite) = 0.0336, $^{176}Hf/^{177}Hf$ = 0.282785 (chondrite) after Bouvier et al. (2008) and $^{176}Lu/^{177}Hf$ (DM) = 0.038, $^{176}Hf/^{177}Hf$ = 0.283223 (DM) after Vervoort and Blichert-Toft (1999). An average $^{176}Lu/^{177}Hf$ value of 0.0113 for Archean crust was used for model age calculations (Taylor and McLennan, 1985; Wedepohl, 1995). Uncertainties on initial Hf ratios and epsilon Hf values were calculated using full error propagation, outlined by Ickert (2013). Uncertainties on Hf depleted mantle model ages ($T_{DM}Hf$) have σ1 errors of ~5%.

4.6. Results

Accompanying data APPENDICES A-D contain complete U-Pb and Lu-Hf results and descriptions of zircon characteristics. Concordia diagrams for all samples are presented in APPENDIX 4E and Th/U diagrams in APPENDIX 4F. A summary of U-Pb and Hf magmatic zircon results are given in Table 4.2. The results of seven samples from the snow bowl area, on central Hall Peninsula (Figure 4.3) will be presented first with the U-Pb SHRIMP results from From et al. (2015) followed by the Lu-Hf results obtained through multi-collector LA-ICPMS. Following this, seven regional samples (Figure 4.2) will be presented where both the U-Pb and Lu-Hf isotopes were collected by LASS-ICPMS. Rocks samples are discussed individually, first classifying the lithology, then presenting the U-Pb ($^{207}Pb/^{206}Pb$ ages) and Lu-Hf results with reference to the type of zircon material they were derived from.

On the basis of morphology and internal structures, three types of zircons were classified: inherited, magmatic or metamorphic. Inherited zircons are interpreted to represent "inherited" material; this includes zircon cores that are overgrown by either magmatic or metamorphic zircon. Inherited cores typically have a well-defined discontinuity between the core and overgrowth material or show truncation by subsequent zircon material (Figure 4.4A). Magmatic zircons are interpreted to represent crystallization from a melt, i.e., "magmatic"; these zircons have well-defined, oscillatory growth zonation, typically at a fine scale (Figure 4.4B). Metamorphic zircons typically occur as unzoned rims on inherited or magmatic zircons (Figure 4.4C) or as single, unzoned grains with different U and Pb contents or U/Th compared to the other zircon types (Figure 4.4D).

Figure 4: Representative zircon grains from orthogneiss units outlining the characteristics of inherited, magmatic and metamorphic zircons as defined in the text; A) inherited cores with a well-defined discontinuity between the core and overgrowth material; B) magmatic zircon with well-defined, oscillatory growth zonation, typically at a fine scale; C) metamorphic zircon as unzoned overgrowths on domain 1 zircon; D) metamorphic zircon as ovoid, single weakly sector zoned grains. $^{207}Pb/^{206}Pb$ ages shown in red are interpreted as metamorphic.

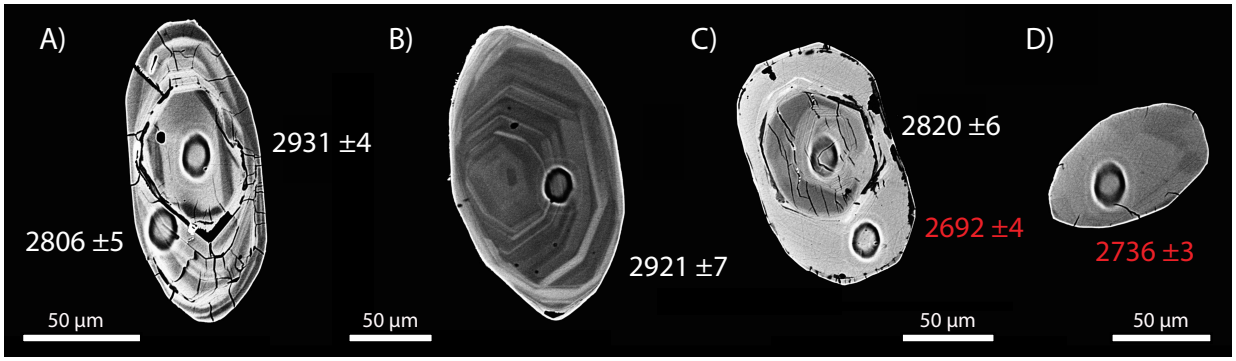

4.6.1. snow bowl area

4.6.1.1. Monzogranite gneiss (S116A)

This monzogranite gneiss sample was collected from just outside the snow bowl area (Figure 4.3) and appears to be volumetrically significant in that region. The gneiss has a strong foliation defined by hornblende and biotite and is texturally homogeneous with minor veins of syenogranite and coarse-grained leucogranite that sub-parallel gneissosity but locally crosscut it at shallow angles. Thirty U-Pb isotopic analyses were conducted on 23 separate zircon grains from sample S116A (APPENDIX 4A).

As summarized in Table 4.2, From et al. (2015) reported a 2976 ±4 Ma crystallization age based on 10 analyses of oscillatory-zoned zircon. Younger zircon dates range from ca. 2964 to 2716 Ma. Two, outlying young dates (ca. 2901 and 2837 Ma) are from homogeneous zircon material with low Th/U (0.12 to 0.16) and interpreted to be related to non-zero-age Pb recrystallization of zircon (partial Pb loss). A ca. 2716 Ma date on an unzoned zircon rim is interpreted to be metamorphic.

The Lu-Hf analyses of ten magmatic zircons (U-Pb ages, ca. 2988 to 2933 Ma) yielded relative homogeneous **ε**Hf(t) between 3 and 5. Depleted mantle model ages (T_{DM}Hf) range between between ca. 3.10 and 3.02 Ga. The metamorphic zircon rim (U-Pb age, ca. 2716 Ma) has a **ε**Hf(t) of -2.

4.6.1.2. Megacrystic granodiorite gneiss (F151A)

This megacrystic granodiorite gneiss from the southwest margin of the snow bowl area (Figure 4.3) is characterized by a pervasive L-tectonite fabric defined by elongate, relict plagioclase phenocrysts that are commonly surrounded by hornblende. Locally, the gneiss has fine-grained quartz diorite lenses composed of hornblende + biotite + epidote.

Thirty-six U-Pb isotopic analyses were conducted on 31 separate zircon grains from sample F151A (APPENDIX 4A).

As summarized in Table 4.2, From et al. (2015) reported a 2928 ±5 crystallization age based on 14 analyses of oscillatory-zoned zircon. Younger zircon dates, derived from largely oscillatory-zoned zircons, range from ca. 2913 to 2718 Ma and cascade (due to partial Pb loss) towards three younger dates from unzoned zircon rims interpreted to be metamorphic (ca. 2718 to 2690 Ma). These metamorphic rims have low Th/U (0.07 to 0.18) compared to the magmatic zircon (0.39 to 0.73).

Fifteen Lu-Hf analyses of magmatic zircon from the oldest age cluster (U-Pb ages, ca. 2945 to 2917 Ma) yielded **ε**Hf(t) between 1 and 5 and T_{DM}Hf between 2.99 and 3.13 Ga. Fifteen Lu-Hf analyses of the younger oscillatory-zoned zircon (U-Pb ages, ca. 2913 to 2790 Ma) yielded similar **ε**Hf(t) between -1 and 4 and model ages between T_{DM}Hf = 2.82 and 3.02 Ga.

4.6.1.3. Tonalite gneiss (F155B)

In the snow bowl area, tonalite gneiss was observed only as a semi-continuous raft (5 m wide by 25 m long) in porphyroclastic monzogranite gneiss. The tonalite gneiss has a strong gneissic fabric defined by thin (mm-scale) trondhjemitic segregations. Discrete, mm- to cm-scale injections of porphyroclastic monzogranite and syenogranite parallel, but locally crosscut, the gneissosity. Mineral segregation banding concentrates hornblende in mm- to cm-wide bands. There are also discontinuous lenses of quartz diorite (see next sample section). Forty-three U-Pb isotopic analyses were conducted on 37 separate zircon grains from sample F155B (APPENDIX 4A).

As summarized in Table 4.2, From et al. (2015) reported a 2810 ±3 Ma crystallization age based on six analyses of oscillatory-zoned zircon. The oldest dates from ca. 3209 to 2846 Ma were derived from zircons interpreted to be inherited. Younger zircon dates range from ca. 2794 to 2766 Ma cascading towards younger ages derived from metamorphic zircon. The youngest dates of ca. 2738 to 2671 Ma were derived from largely unzoned or irregularly zoned zircons, with most grains having Th/U (0.69-1.36) that are two to four times higher than the Th/U (0.05-0.63) from all other zircons (APPENDIX 4F). Nineteen zircons interpreted to be metamorphic provide a $^{207}Pb/^{206}Pb$ weighted mean age of 2727 ±5 Ma.

The Lu-Hf analyses of seven inherited zircons (U-Pb ages, ca. 3209 to 2931 Ma) yielded **ε**Hf(t) between -4 and 6 and $T_{DM}Hf$ between 3.10 and 3.48 Ga. The Lu-Hf analyses of the five magmatic zircons (U-Pb ages, ca. 2820 to 2806 Ma) that represent the time of crystallization of the tonalite gneiss, have **ε**Hf(t) between 0 and 2 and $T_{DM}Hf$ between 2.98 and 3.07 Ga. The Lu-Hf analyses of nine stubby, single zircon grains, most of which are interpreted to be metamorphic, (U-Pb ages, ca. 2766 to 2692 Ma) yielded **ε**Hf(t) between -8 and 2.

4.6.1.4. Quartz diorite lenses (F155C)

Discontinuous hornblende quartz diorite lenses ("mafic lenses" in From et al. 2015) occur within the tonalite gneiss, generally with their long axes parallel to the gneissosity. These lenses have a homogeneous composition, consisting of 55% hornblende, 15% biotite, 15% plagioclase, 10% quartz, and 5% accessory allanite and apatite. Thirty-four

U-Pb isotopic analyses were conducted on 22 zircon grains from sample F155C (APPENDIX 4A).

As summarized in Table 4.2, From et al. (2015) reported a 2700 ±3 Ma crystallization age based on eight analyses of ovoid and unzoned zircon. However, this age represents the growth of zircon and not necessarily the original emplacement of this rock unit (see discussion 1.7.3 below). Zircon cores with indistinct zonation, yielded the oldest dates from ca. 2850 to 2777 Ma. Unzoned zircon material that surrounds these indistinct cores yielded younger zircon dates from ca. 2693 to 2621 Ma. Additionally, seven unzoned zircon single grains or rims with low Th/U (0.01) and dates ranging from ca. 1882 to 1826 Ma are interpreted as metamorphic.

The Lu-Hf analyses of three inherited zircons (U-Pb ages, ca. 2804 to 2777 Ma) yielded **ε**Hf(t) between -3 and 3 and T_{DM}Hf between 2.94 and 3.20 Ga. The Lu-Hf analyses of ten metamorphic zircons (U-Pb ages, ca. 2724 to 2621) yielded **ε**Hf(t) between 3 and 5.

4.6.1.5. Porphyroclastic monzogranite gneiss (F155A, F150A)

Porphyroclastic monzogranite gneiss is characterized by K-feldspar porphyroclasts of various sizes (0.5 to 5 cm) that are commonly sheared and interconnected by recrystallized bands of finer grained K-feldspar. The porphyroclasts are demonstrably derived from the disaggregation of coarse-grained syenogranitic veins. A well-developed mineral foliation is defined by biotite and hornblende. A porphyroclastic monzogranite (F155A) entrains and intrudes the tonalite gneiss in the eastern portion of the snow bowl area, and another, very similar porphyroclastic monzogranite (F150A) occurs in the

western portion of the snow bowl area, not associated with tonalite gneiss. Forty-three U-Pb isotopic analyses were conducted on 37 zircon grains from sample F155A and twenty-seven analyses were conducted on 26 zircon grains from sample F150A (APPENDIX 4A).

4.6.1.5.1. Sample F155A

As summarized in Table 4.2, From et al. (2015) reported a 2752 ±3 Ma crystallization age based on ten analyses of oscillatory-zoned zircon. Older dates from ca. 2984 to 2810 Ma are from zircon cores interpreted to be inherited. Younger zircon dates range from ca. 2737 to 2687 Ma with the majority of these dates derived from unzoned zircon rims interpreted to be metamorphic. Ten zircons interpreted to be metamorphic provide a $^{207}Pb/^{206}Pb$ weighted mean age of 2728 ±4 Ma, identical to the age of metamorphism derived from F155B above.

The Lu-Hf analyses of five inherited zircon cores (U-Pb ages, ca. 2984 to 2810 Ma) yielded $\varepsilon Hf(t)$ of -3 to 1 and $T_{DM}Hf$ of 3.05 to 3.31 Ga. Eight magmatic zircons interpreted to represent crystallization of the monzogranite at 2752 ±3 Ma yielded $\varepsilon Hf(t)$ between -3 and 2 and slightly younger $T_{DM}Hf$ between 2.95 and 3.16 Ga. Fifteen metamorphic zircon rims and stubby grains yielded $\varepsilon Hf(t)$ between -3 and 2.

4.6.1.5.2. F150A

As summarized in Table 4.2, From et al. (2015) reported a 2720 ±4 Ma crystallization based on 15 analyses of irregular, sector zoned or unzoned zircon grains. Older zircon cores, interpreted to be inherited due to a clear discontinuity between subsequent overgrowth, have dates ranging from ca. 2810 to 2782 Ma. Younger zircon dates range from ca. 2695 and 2686 Ma, which are interpreted to have been affected by

Pb loss. Two unzoned zircon rims interpreted to be metamorphic have dates of ca. 1843 and 1732 Ma.

The Lu-Hf analyses of three inherited zircon grains (U-Pb ages, ca. 2810 to 2782 Ma), yielded **ε**Hf(t) between 3 and 7 and T_{DM}Hf between 2.80 and 2.98 Ga. The Lu-Hf analyses of ten zircons interpreted to represent the crystallization of this monzogranite at 2720 ±4 yielded **ε**Hf(t) between 0 and 4 and T_{DM}Hf = 2.85 and 3.02 Ga. Three zircon grains interpreted to be the result of non-zero Pb loss (U-Pb ages, ca. 2695 and 2686 Ma) yielded **ε**Hf(t) of -1 and 2 and T_{DM}^{Hf} = 2.89 to 3.00 Ga.

4.6.1.6. Magnetite-bearing monzogranite gneiss (F152A)

Magnetite-bearing monzogranite gneiss is characterized by abundant melt segregations (leucosomes) that have haloes enriched in mafic minerals (melanosomes). These leucosomes locally crosscut the gneissic foliation but are also folded themselves. Magnetite is pervasive throughout the unit, with a slight concentration along leucosome-melanosome boundaries. The foliation is defined by hornblende and biotite. Twenty-five U-Pb isotopic analyses were conducted on 20 zircon grains from sample F152A (APPENDIX 4A).

As summarized in Table 4.2, From et al. (2015) reported a 2728 ±5 Ma crystallization age based on 20 analyses of zircon grains that are indistinguishable from one another by elemental concentrations or zonation characteristics. Younger dates range from 1838 to 1740 Ma and are interpreted to be metamorphic.

The Lu-Hf analyses of 19 zircon grains interpreted to represent the crystallization of this magnetite-bearing monzogranite at 2728 ±5 Ma yielded **ε**Hf(t) between -12 and -8,

significantly more negative than the other rock samples. Depleted mantle model ages are also older with T_{DM}Hf between 3.39 and 3.61 Ga. The Lu-Hf analyses of three metamorphic zircon rims (U-Pb ages, ca. 1830 to 1800 Ma) yielded **ε**Hf(t) of -31 to -28.

4.6.2. Regional samples (LASS for U-Pb and Lu-Hf)

4.6.2.1. Tonalite gneiss (H098A, H086A, F040A, K037A)

Two tonalite gneiss samples (H098A and H086A) collected from the northeastern coastal islands of Hall Peninsula (Figure 4.2) have local discontinuous mafic lenses and discrete, mm- to cm-scale injections of monzogranite generally parallel to the gneissosity. Twenty-one U-Pb isotopic analyses were conducted on 19 separate zircon grains from sample H098A. Twenty-seven analyses were conducted on 23 separate zircon grains from sample H086A (APPENDIX 4B). Two other tonalite samples (F040A and K037A) collected from outcrops farther west, immediately adjacent to the western domain of Paleoproterozoic metasediments (Figure 4.2), have a weaker gneissic fabric compared to H098A and H086A and do not have monzogranite injections. Twenty-three analyses were conducted on 22 separate zircon grains from sample F040A and twenty-five analyses were conducted on separate zircon grains from sample K037A (APPENDIX 4B).

4.6.2.1.1. Sample H098A

Two analyses of inherited zircons yielded dates of ca. 2814 and 2811 Ma with **ε**Hf(t) of 4 and 1 and T_{DM}Hf = 2.92 and 3.04 Ga, respectively. Six analyses of magmatic zircons yielded a cluster of dates between 2745 and 2708 Ma interpreted to represent the crystallization age of this tonalite gneiss (weighted-mean $^{207}Pb/^{206}Pb$ age of 2740 ±5 Ma;

MSWD = 1.11). These zircons yielded **ε**Hf(t) between 1 and 4 and T_{DM}Hf between 2.87 and 3.00 Ga. Six metamorphic zircons have younger dates between ca. 2702 to 2590 Ma and **ε**Hf(t) between -5 and 4.

4.6.2.1.2. Sample H086A

Four analyses of inherited zircon yielded dates from ca. 2911 to 2812 Ma, **ε**Hf(t) of 3 to 9 and T_{DM}Hf between 2.89 and 3.02 Ga. Eleven analyses of magmatic zircon yielded a cluster of dates between 2801 and 2758 Ma interpreted to represent the crystallization age of this tonalite gneiss (weighted-mean $^{207}Pb/^{206}Pb$ age of 2783 ±10 Ma; MSWD = 6.4). These zircons yielded **ε**Hf(t) between 3 and 7 and T_{DM}Hf between 2.84 and 2.96 Ga. Six metamorphic zircons have Th/U (0.02-0.34) that are generally twice as low as the Th/U of all other zircon analyses (0.20-0.87) and yielded dates ranging from ca. 2684 to 2470 Ma with **ε**Hf(t) between -5 and 1.

4.6.2.1.3. Sample F040A

Two analyses of inherited zircon cores yielded dates of ca. 2853 and 2845 Ma, **ε**Hf(t) of 4 and 6 and T_{DM}Hf of 2.90 and 2.99 Ga, respectively. Ten analyses of magmatic zircon yielded a cluster of dates between ca. 2836 and 2804 Ma that are interpreted to represent the crystallization age of this tonalite gneiss (weighted-mean $^{207}Pb/^{206}Pb$ age of 2822 ±8 Ma, MSWD = 3.5). These zircons yielded **ε**Hf(t) between -1 and 5 and T_{DM}Hf of 2.93 to 3.13 Ga. Eight, younger dates derived from magmatic zircon cascade from ca. 2791 to 2723 Ma and have associated **ε**Hf(t) between -3 and 2 with T_{DM}Hf between 2.85 and 3.17 Ga. Three of these zircon grains have elevated U (524-750 ppm), Th (288-750 ppm) and Pb (372-392 ppm) compared to the rest of the zircon grains from this sample (U=179-420 ppm, Th=63-271 ppm, Pb=96-302 ppm) and have the youngest dates ages

ranging from ca. 2767 to 2723 Ma; however, compelling textural or chemical evidence for these zircon being metamorphic is lacking. Most likely, these three dates represent scatter due to partial Pb loss.

4.6.2.1.4. Sample K037A

Eleven analyses of magmatic zircon grains yielded only five (sub)concordant Archean dates from ca. 2692 to 2563 Ma. These Archean zircons yielded εHf(t) of -10 to -4 and T_{DM}Hf between 3.12 and 3.36 Ga. The three most concordant dates between ca. 2692 and 2663 Ma are interpreted as the crystallization age of this tonalite gneiss (weighted mean $^{207}Pb/^{206}Pb$ age of 2687 ±26 Ma, MSWD = 8.9). However, this age represents the growth of zircon and not necessarily the original emplacement of this rock unit (see discussion 1.7.3 below). Eleven unzoned metamorphic single grains or rims yielded dates between ca. 1870 to 1773 Ma with **ε**Hf(t) between -20 and -16. With a majority of Paleoproterozoic dates, this tonalite gneiss could have been emplaced in the Paleoproterozoic (weighted mean $^{207}Pb/^{206}Pb$ age of 1863 Ma) and simply inherited Archean zircon grains; this possibility is discussed in more detail in section 1.7.3 below.

4.6.2.2. Monzogranite gneiss (F163B, Z108A, F157A)

Monzogranite gneiss has a moderate foliation defined by hornblende and biotite. The gneiss is homogeneous in composition with minor veins of syenogranite, which locally disaggregates into K-feldspar porphyroclasts. The syenogranite veins along with minor coarse-grained leucogranite are parallel to gneissosity but locally crosscut it at shallow angles. Sample F163A is boundinaged within tonalite gneiss; twenty-three U-Pb isotopic analyses were conducted on 22 separate zircon grains (APPENDIX 4A). Sample Z108A

contains large clots of magnetite; twenty-two analyses were conducted on 20 separate zircon grains (APPENDIX 4A). Sample F157A contains epidote, along with mafic clots associated with magnetite; twenty-five analyses were conducted on 23 separate zircon grains (APPENDIX 4A).

4.6.2.2.1. Sample F163B

Three analyses of zircon cores with indistinct zonation yielded dates from ca. 2984 to 2970 Ma, **ε**Hf(t) between 2 and 5 and T_{DM}Hf between 3.04 and 3.14 Ga. Nine analyses of magmatic zircon yielded a cluster of dates between ca. 2866 and 2833 Ma that are interpreted to represent the crystallization age of this monzogranite gneiss (weighted-mean $^{207}Pb/^{206}Pb$ age of 2843 ±9 Ma; MSWD = 3.4). These zircons yielded **ε**Hf(t) between 0 and 4 and T_{DM}Hf between 2.94 and 3.13 Ga. Three magmatic zircons with dates cascading from ca. 2826 to 2815 Ma towards even younger dates derived from metamorphic zircon are interpreted to have been affected by partial Pb loss; these zircons yielded **ε**Hf(t) between -1 and 3 and T_{DM}Hf between 2.99 and 3.11 Ga. Five analyses of unzoned metamorphic rims with elevated U content (134-333 ppm) compared to the rest of the zircon from this sample (U=65-165ppm) yielded dates between 2813 to 2731 Ma and **ε**Hf(t) between -2 and 1. These metamorphic dates are older than those recorded from all other samples (ca. 2730 to 2700 Ma) and raises the possibility for multiple or locally prolonged Archean tectonothermal disturbances.

4.6.2.2.2. Sample Z108A

Three analyses of inherited zircon grains yielded sporadic dates from ca. 2925 to 2861 Ma, **ε**Hf(t) ranging from 0 to 3 and T_{DM}Hf between 3.06 to 3.13 Ga. These zircons have lower $^{176}Hf/^{177}Hf$ (0.28096 – 0.28105) compared to the $^{176}Hf/^{177}Hf$ of rest of the

zircons from this sample (0.28107 to 0.28112). Eight analyses of magmatic zircon grains yielded dates from ca. 2801 to 2727 Ma that are interpreted to represent the crystallization age of this rock (weighted-mean $^{207}Pb/^{206}Pb$ age of 2777 ±20 Ma; MSWD = 9.4). These zircon grains yielded **ε**Hf(t) ranging between 0 to 3 and T_{DM}Hf between 2.95 to 3.04 Ga. Five analyses of largely unzoned zircon yielded $^{207}Pb/^{206}Pb$ ages between ca. 2612 to 2521 Ma and are interpreted to be metamorphic. These zircon grains yielded **ε**Hf(t) between -5 and 2.

4.6.2.2.3. Sample F157A

Three analyses of inherited zircon yielded sporadic dates from ca. 2924 to 2788 Ma, **ε**Hf(t) ranging from -1 to 9 and T_{DM}Hf between 2.83 to 3.10 Ga. Thirteen analyses of zircon grains that have variability in zonation between oscillatory and irregular cores to unzoned rims yielded dates from 2711 to 2630 Ma. With no obvious geochemical signatures to discriminate between magmatic and metamorphic zircon, the five oldest zircon with a cluster of dates between ca. 2711 and 2684 Ma are interpreted to represent the age of crystallization (weighted-mean $^{207}Pb/^{206}Pb$ age of 2689 ±10 Ma; MSWD = 2.4). These zircons yielded **ε**Hf(t) between 0 and 1 and T_{DM}Hf between 2.92 and 2.97 Ga. The remaining nine Archean zircons have dates that cascade from 2668 to 2597 Ma, **ε**Hf(t) between -1 and 9, T_{DM}Hf between 2.60 and 2.97 Ga, and are interpreted to have been affected by partial Pb loss. Two analyses of metamorphic rims yielded dates of ca. 1877 and 1819 Ma and **ε**Hf(t) of -18 and -16, respectively.

4.7. Discussion

4.7.1. SHRIMP versus LASS-ICPMS U-Pb results

SHRIMP $^{207}Pb/^{206}Pb$ zircon dates from all analyzed zircon in the snow bowl area range from ca. 3209 to 2621 Ma while LASS-ICPMS $^{207}Pb/^{206}Pb$ zircon dates of all analyzed zircon from regional samples collected throughout eastern Hall Peninsula range from ca. 2984 to 2470 Ma (Figure 4.5). Aside from sporadic older $^{207}Pb/^{206}Pb$ dates from the snow bowl area and slightly younger $^{207}Pb/^{206}Pb$ ages from the regional dataset the main concentration of dates that would represent magmatic and tectonometamorphic episodes are in fairly close agreement (Figure 4.5).

In an independent test to compare the U-Pb results of these two analytical techniques, Archean detrital zircons from a quartzite sample basal to the Paleoproterozoic metasedimentary rocks of Hall Peninsula, analyzed by the SHRIMP, were analyzed using LASS-ICPMS overtop the same SHRIMP analytical spots (Sample 10914; APPENDIX 4G). The SHRIMP results ($^{207}Pb/^{206}Pb$ ages of 3277 ±9 to 2615 ±10 Ma; Rayner, 2014) and LASS-ICPMS results ($^{207}Pb/^{206}Pb$ ages of 3236 ±9 to 2495 ±11 Ma) yield comparable dates, however, slightly younger dates using the LASS-ICPMS technique are outside analytical uncertainty from the SHRIMP results (APPENDIX 4G). These younger LASS-ICPMS dates likely result from sampling scale and volume. LASS-ICPMS uses a larger spot size (~33μm) and ablates a significantly larger volume of material than SHRIMP (spot size ~16-25μm). Consequently, the likelihood of ablating zones of zircon of different age (likely to be younger since we typically target core areas of zircon) is increased. The LASS-ICPMS dates have an average 2σ error twice that of the SHRIMP dates (APPENDIX 4G) and may also be influenced by higher degrees of Pb loss and discordance. Accuracy is best judged from secondary standards and each of these techniques produces results within error of the standards. Nevertheless, we have

Figure 4.5: Summary of $^{207}Pb/^{206}Pb$ dates from all analyzed zircon from the snow bowl area (SHRIMP) and regional samples (LASS-ICPMS) across the northern portion of the eastern Hall Peninsula orthogneiss complex. Dates used to calculate the weighted mean crystallization age are shown in blue. Zircon zonation is based purely on characterization from BSE images independent of U-Pb date.

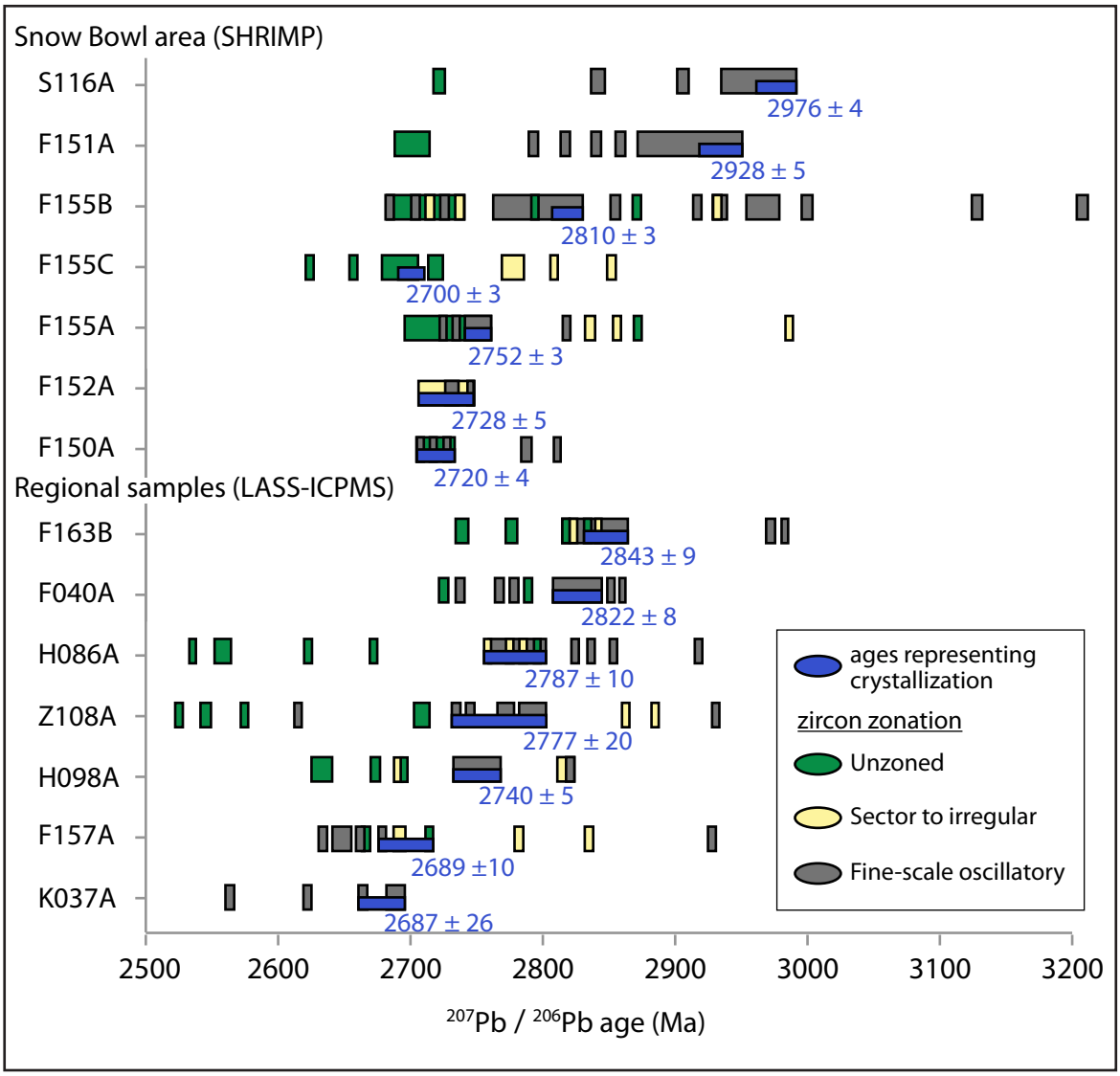

preferentially used pre-existing SHRIMP dates over LASS-ICPMS dates, when available, because they are more precise and sample a smaller and potentially less complex region of a zircon grain.

4.7.2. Archean magmatism and metamorphism on eastern Hall Peninsula

In the snow bowl area, the rock units range in composition from tonalitic to monzogranitic with crystallization ages from 2976 ±4 to 2720 ±4 (Table 4.2, Figure 4.5), with no apparent link between rock composition and crystallization age. For the regional samples, the crystallization ages of rock units range from 2843 ±9 to 2689 ±10 (Table 4.2, Figure 4.5), also with no apparent link between rock composition and crystallization ages. The ca. 250 Ma range in crystallization ages, suggests at least two pulses of magmatic activity during the formation of this Archean orthogneiss complex rather than a single, protracted period of magmatism (see discussion 1.7.3 below).

Archean metamorphic $^{207}Pb/^{206}Pb$ ages were derived from unzoned zircon rims and single grains that are typically ovoid or round and are almost exclusively younger than 2750 Ma (Figure 4.5). A large portion of these metamorphic rims have Th/U that are significantly lower compared to Th/U from the older, magmatic zircons, with few exceptions (e.g., F155B, F155C; APPENDIX 4F). While post-magmatic growth or modification usually produces zircon with lower Th/U than zircon crystallization from a melt (Pidgeon, 1992), it has been shown that magmatic zircon can have a large Th/U range of 0.1 to >1.0 (Rubatto, 2002). On eastern Hall Peninsula, when there was no discernable difference in Th/U between zircons interpreted as metamorphic versus

Table 4.2. Summary of zircon characteristics, U-Pb geochronology and Lu-Hf isotopic data results from eastern Hall Peninsula.

Rock Type	Zircon Characteristics				$\frac{^{207*}Pb}{^{206*}Pb}$ crystallization age ± 2σ (Ma)	εHf	$T_{DM}Hf$	$\frac{^{207*}Pb}{^{206*}Pb}$ metamorphic ages (Ma)
	Morphology	Zonation						
		Cores	Rims	Unzoned Single Grains				
Snow bowl area samples (SHRIMP)								
S116A - monzogranite gneiss (713778 7041607, 19N)	subrounded, prismatic to ovoid, and slightly elongate	fine scale oscillatory	unzoned	yes, rare	2976 ± 4	3 to 5	3.02-3.10	2716
F151A - granodiorite gneiss (669300 7094544, 19N)	ovoid with rounded edges, rare prismatic	fine scale oscillatory	thin, unzoned, high U	no	2928 ± 5	1 to 5	2.99-3.13	2718-2690
F155B - tonalite gneiss (669461 7094784, 19N)	mostly ovoid, minor elongate and prismatic	fine scale oscillatory	unzoned or oscillatory	yes	2810 ± 3	0 to 2	2.98-3.07	2738-2671
F155C - quartz diorite lenses (669461 7094784,19N)	all grains-ovoid with rounded edges	unzoned	none	yes, almost all	2700 ± 3	0	2.94-3.20	1882-1826
F155A - porphyroclastic monzogranite gneiss (669461 7094784, 19N)	elongate prismatic and ovoid with rounded edges	prismatic grains: fine scale oscillatory	unzoned	yes, ovoid	2752 ± 3	-3 to 2	2.95-3.16	2737-2687
F150A - porphyroclastic monzogranite gneiss (669259 7094583, 19N)	elongate and subrounded, some ovoid	fine scale oscillatory	unzoned	yes	2720 ± 4	0 to 4	2.85-3.02	1843-1732
F152A - mag-bearing monzogranite gneiss (669280 7094606, 19N)	dominantly ovoid, some prismatic and elongate	irregular oscillatory with internal discontinuities	none	no	2728 ± 5	-12 to -8	3.39-3.61	1838-1740

Table 4.2 cont'd. Summary of zircon characteristics, U-Pb geochronology and Lu-Hf isotopic data results from eastern Hall Peninsula.

Rock Type	Zircon Characteristics				$^{207*}Pb/^{206*}Pb$ crystallization age ± 2σ (Ma)	εHf	$T_{DM}Hf$	$^{207*}Pb/^{206*}Pb$ metamorphic ages (Ma)
	Morphology	Zonation						
		Cores	Rims	Unzoned Single Grains				
Regional samples (LASS-ICPMS)								
F163B - monzogranite gneiss (669461 7094784, 19N)	ovoid with rounded edges, rare prismatic	irregular to fine scale oscillatory zoned	unzoned	no	2843 ± 9	0 to 4	2.94-3.13	2813-2784, 2740-2731
F040A - tonalite gneiss (620333 7136294, 19N)	dominantly ovoid, some prismatic and elongate	fine scale to irregular oscillatory	unzoned	no	2822 ± 8	-1 to 5	2.93-3.13	2723
H086A - tonalite gneiss (719964 7118577, 19N)	elongate and subrounded, some ovoid	unzoned or irregular and faint oscillatory	unzoned to faint oscillatory	yes, rare	2787 ± 10	3 to 7	2.84-2.96	2684-2470
Z108A - monzogranite gneiss (662246 7122133, 19N)	elongate and subrounded, some ovoid	fine scale oscillatory, unzoned or irregular	unzoned	no	2777 ± 20	0 to 3	2.95-3.04	2612-2521
H098A - tonalite gneiss (692183 7154679, 19N)	elongate, prismatic, subrounded edges, rare ovoid	oscillatory, some unzoned, rare irregular	unzoned	yes, rare	2740 ± 5	0 to 4	2.87-3.00	2702-2620
F157A - monzogranite gneiss (622813 7160311, 19N)	mostly ovoid, minor elongate and prismatic	fine scale oscillatory	unzoned	no	2689 ±10	0 to 1	2.92-2.97	1877-1819
K037A - tonalite gneiss (607104 7161794, 19N)	dominantly round, some stubby	irregular to faint oscillatory	unzoned	yes, almost all	2687 ± 26	-10 to -4	3.12-3.36	1870-1774

tables notes:

Abbreviations: mag = magnetite; SHRIMP = Sensitive High Resolution Ion Microprobe; LASS-ICPMS = Laser Ablation Split Stream Inductively Coupled Plasma Mass Spectrometry

Hf depleted mantle model ages ($T_{DM}Hf$) have σ1 errors of ~5%

* refers to radiogenic Pb (corrected for common Pb)

magmatic, groupings of U, Pb or Th contents were sometimes used to reinforce interpretations (e.g., F040A, F163B).

Using the textural and chemical classification criteria established above, the majority of Archean metamorphic zircon $^{207}Pb/^{206}Pb$ ages are within the range ca. 2740 to 2660 Ma with just a few outlying dates at ca. 2810 and 2780 Ma. These dates could be significant and represent earlier tectonometamorphic overprints recorded in older gneisses, however, the overwhelming majority of data indicates a sustained period of Archean metamorphism that initiated at ca. 2740 and continued until at least ca. 2700 Ma.

Sample F155 and F155B provided identical $^{207}Pb/^{206}Pb$ weighted means of metamorphism at ca. 2728 ±4 Ma (n=10) and 2727 ±5 Ma (n=19) respectively.

There are rare concordant $^{207}Pb/^{206}Pb$ ages as young as ca. 2525 Ma but no distinct age populations and the majority of samples do not yield any $^{207}Pb/^{206}Pb$ ages younger than ca. 2700 Ma. The rare $^{207}Pb/^{206}Pb$ ages younger than ca. 2700 Ma, whether they exhibit characteristics consistent with a metamorphic or magmatic origin, are believed to have been affected by partial Pb loss due to isotopic disturbance from subsequent tectonothermal events and/or accidental overlap of the analytical spot with younger age domains in the zircon crystal.

4.7.3. εHf(t), magmatic provenance and model ages

Studies of Hf isotopes in zircon have been successful in delineating unique geologic histories of Archean crustal domains within regions that have experienced significant tectonic amalgamation, especially in highly deformed and metamorphosed Archean rocks

(e.g., Amelin et al., 2000; Griffin et al., 2004; Davis et al., 2005). Recently, the ability to measure U-Pb and Lu-Hf isotopes simultaneously on a single analytical spot using LASS-ICPMS creates an invaluable link between these two isotope systems within complex zircons. This allows for more robust interpretations of magmatic provenance since the time at which Lu-Hf isotopes were incorporated into the zircon crystal is well constrained (Vervoort and Kemp, 2016). Moreover, the coupled isotopic data provides enhanced discrimination between magmatic and metamorphic zircon by assessing any deviations from the $^{177}Hf/^{176}Hf$ initially recorded during magmatic crystallization (e.g., Chen et al., 2010).

On eastern Hall Peninsula, the **ε**Hf(t) of magmatic zircon from both the snow bowl area and the regional samples have a similar range between 0 to 7 with an mean propagated error of ±2 (Figure 4.6). There are two outliers to this range with F152A and K037A having negative **ε**Hf(t) of -4 to -10 and -8 to -12 respectively (discussed separately below). In the snow bowl area, there is an overall trend of **ε**Hf(t) becoming less positive as magmatic ages become younger. This trend begins with the oldest samples S116A ($\varepsilon Hf_{(t)}$ of 3 to 5) and F151A ($\varepsilon Hf_{(t)}$ of 1 to 5) that plot very close to the depleted mantle **ε**Hf(t) composition line (Figure 4.6). The remaining samples, aside from F152 with highly negative **ε**Hf(t), all plot along a trajectory emanating from S116A and F151A with a slope very similar to the average crustal evolution line (Figure 4.6). S116A and F151A both have mean $T_{DM}Hf$ of ca. 3.1 Ga with the remaining samples having mean $T_{DM}Hf$ of ca. 3.0 (F155A, B, C) and ca. 2.9 Ga (F150A). Therefore, the protolith magma for all of these rock units was extracted from the mantle at ca. 3.1 Ga initially forming monzogranite at ca. 2976 Ma and granodiorite at ca. 2928 Ma. Subsequent

Figure 4.6: εHf(t) vs. magmatic $^{207}Pb/^{206}Pb$ ages interpreted to represent crystallization age A) for samples from the Snow Bowl area (SHRIMP $^{207}Pb/^{206}Pb$ ages); B) for regional samples (LASS-ICPMS $^{207}Pb/^{206}Pb$ ages) across the northern portion of the eastern Hall Peninsula orthogneiss complex.

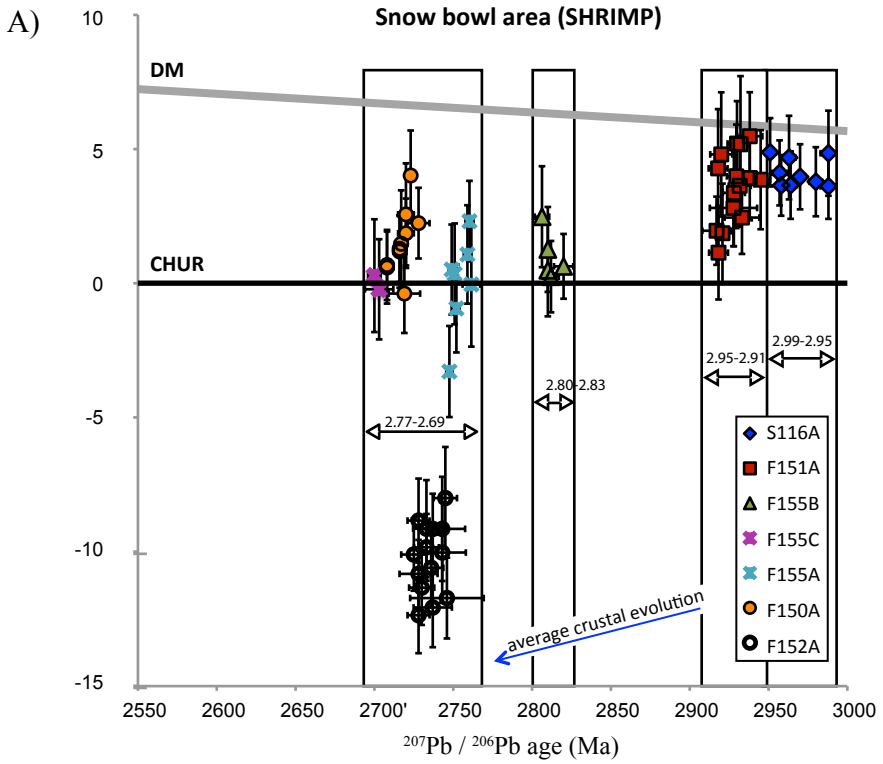

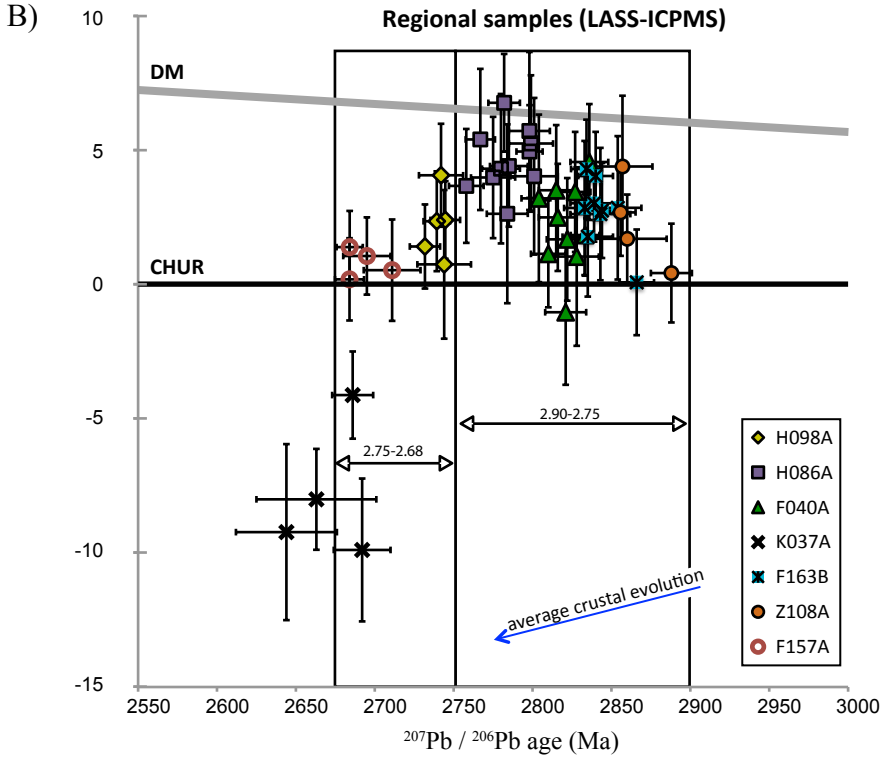

monzogranitic rocks were derived from this same protolith magma or recycled crust from the same parental source, crystallizing at ca. 2810, 2752 and 2720 Ma. Based on the ranges of $^{207}Pb/^{206}Pb$ dates, three main pulses of magmatic emplacement can be delineated at ca. 2.99-2.91, 2.83-2.80 and 2.77-2.69 Ga (Figure 4.6).

Sample F152A is completely different with negative **ε**Hf(t) values between -12 to -8 and a much older mean $T_{DM}Hf$ of ca. 3.4 Ga. F152A also shows significant enrichment in K and several rare-earth elements (Ce, Er, Tm) relative to all the other rock units from the snow bowl area, indicating it is magmatically more evolved (APPENDIX 4H). Therefore, F152A must have been derived from the recycling of Paleoarchean crust whereas the majority of snow bowl area rock units were derived from Mesoarchean juvenile magma and/or recycled crust.

The regional samples, aside from K037A with highly negative **ε**Hf(t), show a very similar trend of $\varepsilon Hf_{(t)}$ versus $^{207}Pb/^{206}Pb$ age as outlined above for the snow bowl area but the larger propagated errors for the regional samples yield a overlapping group of data (Figure 4.6). There is still a cascading of $\varepsilon Hf_{(t)}$ along a trajectory of average crustal evolution but this crustal evolution starts from ca. 2.86 Ga rather than 3.00 Ga for snow bowl area samples. Samples F163B and F040 are the oldest othogneisses from the regional sample set with U-Pb crystallization age of ca. 2843 and 2822 Ma respectively and a common mean $T_{DM}Hf$ of ca. 3.0 Ga. The remaining regional samples have slightly younger mean $T_{DM}Hf$ of ca. 2.9 (H086A, Z108A, H098A, F157). Consequently, it is likely that all of these rock units were derived from the same protolith magma extracted from the mantle at ca. 3.0 Ga with monzogranitic and granodioritic rocks crystallizing intermittently from ca. 2843 to 2689 Ma but ultimately derived from the same protolith

magma or recycled crust from the same parental source. No discrete pulses of magmatic emplacement can be delineated from this data (Figure 4.6).

Sample K037A, one of the tonalite gneisses from the northwest corner of eastern Hall Peninsula (Figure 4.2), yielded significantly negative **ε**Hf(t) values of -10 to -4 and a much older mean T_{DM}Hf model age of 3.3 Ga. Geochemically, K037A is enriched in SiO_2 (74%) and U (1.54ppm) relative to all of the other rock units from the regional sample set (SiO_2<=72%; U<0.58ppm; APPENDIX 4F). Zircons from K037A are also unusual, with a uniquely round morphology, sometimes with small euhedral fragments of inherited, oscillatory-zoned zircon. Similar to F152A from the now Bowl area, K037A must have been derived from the recycling of Paleoarchean crust compared to the majority of all other samples that were derived from Mesoarchean juvenile magma and/or recycled crust.

Examining sample K037A further, it stands out from the others by having a majority of Paleoproterozoic $^{207}Pb/^{206}Pb$ ages (n = 11; ca. 1870 to 1773 Ma) compared to Archean $^{207}Pb/^{206}Pb$ ages (n = 5; ca. 2692 and 2663 Ma). The combined U-Pb and Lu-Hf data imply that this rock is either (1) a Paleoproterozoic gneiss that inherited Archean zircon during its emplacement, or (2) the product of an Archean partial melt derived from older Paleoarchean crust. In the latter case, primary, magmatic zircon was simply not crystallized or preserved in this rock but subsequent partial melting during Paleoproterozoic metamorphism and deformation enabled the crystallization of a population of round, Paleoproterozoic zircon grains.

4.7.4. Paleoproterozoic metamorphism

There is an interesting trend of the preferential preservation of Paleoproterozoic zircon rims linked to U-Pb crystallization ages. Zircon grains from Archean orthogneisses with crystallization ages younger than 2740 Ma have Paleoproterozoic rims ranging in age from ca. 1882 to 1732 Ma (Table 4.2). Conversely, Archean orthogneisses with crystallization ages of ca. 2740 Ma or older contain zircon grains that exclusively record Archean metamorphic ages, with no dateable Paleoproterozoic zircon rims (aside from F155C, which is discussed below). For the orthogneisses that record Paleoproterozoic metamorphism, this observation has several possible explanations: (1) the gneisses are Paleoproterozoic in age and incorporated zircons from the surrounding Archean rocks that they intrude, (2) the gneisses are Archean in age and crystallized after ca. 2740 Ma, synchronous with Archean metamorphism, or (3) the gneisses crystallized prior to ca. 2740 Ma but with no growth or preservation of primary zircon; the presence of zircon younger than ca. 2740 Ma records late Archean tectonometamorphism, which partially melted and deformed the rock providing the necessary constituents and conditions for zircon growth.

Since the zircon grains that were used to constrain the crystallization ages younger than ca. 2740 Ma are distinctively ovoid, rounded and unzoned compared to the zircon from the rest of the ≥2740 Ma Archean rocks units, we prefer the latter interpretation.

This age dependent, preferential zircon growth is best observed in sheared quartz diorite lenses (F155C) that are entrained within ca. 2810 Ma tonalite gneiss (F155B), subsequently intruded by the ca. 2752 Ma monzogranite gneiss (F155A). The intrusive contacts of the monzogranite gneiss with the tonalite gneiss are clear and supported with the crystallization ages of the tonalite gneiss being 2810 ±3 Ma and the monzogranite

gneiss 2752 ±3 Ma. Zircon cores within the quartz diorite lenses (n=4) have $^{207}Pb/^{206}Pb$ ages ranging from ca. 2850 to 2777 Ma and have both Archean metamorphic overgrowth material (n =16; ca. 2724 to 2621 Ma) and Paleoproterozoic metamorphic rims (n = 7; ca. 1882 to 1826 Ma). Therefore, the quartz diorite lenses represent either (1) an intrusive phase to the tonalite gneiss, which became dismembered during subsequent deformation; in this case the zircons experienced significant resorption and subsequent overgrowth during Archean tectonometamorphism, or (2) xenoliths of an older rock, entrained in the tonalite gneiss; in this case the four, partially resorbed, zircon cores that preserve older $^{207}Pb/^{206}Pb$ ages represent the age of the parental rock that likely underwent partial melting during subsequent Archean tectonometamorphism.

The latter interpretation is preferred but in either case, these zircon grains that crystallized after 2740 Ma, synchronous with Archean metamorphism, then had the requisite compositions to preferentially grow thicker, dateable Paleoproterozoic zircon rims compared to the other Archean units older than ca. 2740 Ma.

In an assessment of Th/U of Paleoproterozoic zircon rims and single grains, they have low Th/U (0.01-0.12) that are clearly distinguished from the older Archean zircons, in which the vast majority have Th/U = 0.18-3.52. Exceptions to this occur within the regional U-Pb data where several Archean $^{207}Pb/^{206}Pb$ ages have Th/U as low as 0.02 (e.g. H098A, H086A, Z108A; APPENDICES E, F); however, most of these $^{207}Pb/^{206}Pb$ ages are younger than 2700 Ma and these zircon are interpreted to be secondary or metamorphic growth and/or experienced Pb loss due to partial recrystallization.

4.7.5. Regional tectonic synthesis

New U-Pb and Lu-Hf data for the Archean orthogneisses of eastern Hall Peninsula provides an opportunity to further test crustal correlations proposed in recent studies (e.g., Corrigan et al., 2009; St-Onge et al., 2009; Whalen et al., 2010). U-Pb data from the Archean cratons within the Quebec-Baffin segment of the Trans-Hudson orogen indicates that there is a collective, overlapping metamorphic history from ca. 2.75 and 2.69 Ga (St-Onge et al., 2009). This ca. 60 Ma interval has previously been interpreted as a period of tectonic accretion and juvenile crustal production, potentially on a global scale (Nutman et al., 1989; Friend et al., 1996; Condie, 1998). However, correlations between all of the Archean terranes that experienced common geologic histories prior to ca. 2.75 Ga within this region have remained elusive. Archean rocks from eastern Hall Peninsula share an abundance of geological characteristics with rocks from adjacent crustal domains, below we summarize relevant data for each of them.

Aasiaat domain

The Aasiaat domain of West Greenland is juxtaposed between the Rinkian orogen of the Rae craton to the north and the Nagssugtoqidian orogen of the North Atlantic craton to the south (Figure 4.1). Connelly et al. (2006) suggested that the southern portion of the Aasiaat domain was likely a northward extension of Archean orthogneisses of the North Atlantic Craton that underlies the Nagssugtoqidian Orogen. However, there have been 4 subdomains recognized within the Aasiaat domain. In the northern portion, the Nuussuaq and Atâ subdomains are composed of Archean supracrustal rocks and basement orthogneisses older than ca. 3030 Ma, similar to the age of orthogneisses to the north in the Rinkian orogen (Thrane et al., 2003). In the southern portion, the Rodebay and Nunatarsuaq subdomains have orthogneisses dated at ca. 2791 Ma to 2785 Ma. These

rocks were metamorphosed during an Archean thermal event that lasted until at least ca. 2725 Ma. The southern portion of the Aasiaat domain has rocks with a much narrower, but overlapping, age range compared to orthogneisses from eastern Hall Peninsula.

Kolb (2014) concluded that the Aasiaat domain is a unique Archean crustal fragment present only on the western flank of Greenland, which opens the possiblilty that eastern Hall Peninsula could be a similar crustal fragment, especially given that it share a similar geologic history.

Nagssugtoquidian orogen and Rinkian orogen of West Greenland

In the Nagssugtoquidian orogen, emplacement of magmatic rocks between ca. 2.87 to 2.80 Ga was followed by deformation and metamorphism at ca. 2.80 to 2.73 (Connelly and Mengel, 2000). This Archean history is very similar to eastern Hall Peninsula, however, cross cutting tonalitic sheets (2.50 Ga) and Kangamiut dikes (2.04 Ga; Kalsbeek and Nutman, 1996) that are not observed on eastern Hall Peninsula indicate that these cratons did no share the same Paleoproterozoic history. The Rinkian orogeny, to the north of the Nagssugtoquidian orogeny, has been correlated with the Foxe fold belt of northern Canada (Jackson and Taylor 1972; Pulvertaft 1986) and is not likely to be correlative to eastern Hall Peninsula.

Nain craton of Northern Labrador

Magmatism in the Nain province of northern Labrador is constrained by U-Pb geochronology to mostly older than 2.96 Ga (Schiøtte et al., 1989; Wardle et al., 2002) and doesn't correlate with the new U-Pb magmatic crystallization ages derived from eastern Hall Peninsula. Moreover, metasedimentary packages of the Nain province, tectonically interleaved with tonalitic orthogneisses dated between ca. 3.86 and 3.73 Ga

(Bridgwater and Schiøtte, 1991), do not have any potential correlative Archean metasedimentary rocks on eastern Hall Peninsula. There are U-Pb ages for gneissic rocks on the eastern margin of the Torngat orogen that are similar to gneisses of eastern Hall Peninsula, ranging in age from ca. 2832 to 2802 Ma, with zircon overgrowths dated at ca. 2770 Ma, but they correlate with known magmatic and metamorphic events in the Saglek and Hopedale blocks of the Nain province (e.g., Kanairiktok Plutonic Suite). Moreover, two late, mildly foliated granitic intrusions range in age from ca. 2587 to ca. 2564 Ma, falling within the range of ages for similar late granitic intrusions identified near Saglek Fiord, Okak Bay, and in the vicinity of the community of Nain (Baadsgaard et al., 1979; Scott, 1995). No known correlatives for this suite exist on eastern Hall Peninsula. Scott (1997) documented tonalitic gneisses north of Nachvak Fiord, Labrador with crystallization ages ranging from 2.83 to 2.75 Ga and postulated a correlation with gneisses from southeast Baffin Island. However, with the expanded age range of magmatism documented in this study on eastern Hall Peninsula, to as old as 2.92 Ga, this correlation remains speculative and would require further investigation of the Nachvak fiord gneisses using Lu-Hf isotopes.

Cumberland Peninsula

The geology of Cumberland Peninsula, north of Hall Peninsula, is dominated by Archean tonalitic to granodioritic orthogneisses with interleaved Archean metasedimentary rocks (Keim et al., 2011). In that region, existing U-Pb crystallization ages (SHRIMP) of orthogneiss units are 2991 ± 4 Ma, 2938 ± 4 Ma, and 2782 ± 4 Ma (Rayner et al., 2012), which are generally within the range found in our study of the eastern Hall Peninsula. Additionally, a group of discrete plutons on Cumberland

Peninsula have U-Pb crystallization ages of 2772 ± 6 Ma, 2759 ± 3 Ma, and 2700 ± 4 Ma (Rayner et al., 2012), similar to the crystallization ages of several rock units on eastern Hall Peninsula. However, eastern Hall Peninsula lacks the Archean metasedimentary rocks and distinctive komatiitic suite rocks documented on central and northern Cumberland Peninsula (Keim et al., 2011; Rayner et al., 2012).

Geophysical studies of magnetotelluric (MT) character of the crustal architecture of southern Cumberland Peninsula identified a substantial change in the MT character indicating a crustal scale boundary (Craven et al., 2013). If this abrupt change in MT character is geologically significant, then at depth it may represent a separate crustal block from the Rae craton, namely the Meta Incognita microcontinent (Craven et al., 2013). Overall, the Archean basement of Cumberland Peninsula is comparable in age and lithology to the Rae craton of northern Baffin Island and parts of western Greenland, north of the Isua gneisses. Additionally, the Qikiqtarjuaq suite of Cumberland Peninsula (ca. 1.92–1.87 Ga) is proposed to be correlative to the Sisimiut and Arfersiorfik suites in West Greenland (Jackson et al., 1990; Wodicka et al., 2002; Bethune and Scammell, 2003; Connelly et al., 2006; Rayner et al., 2012), which would argue for the juxtaposition of these crust across these regions during the Archean and Paleoproterozoic.

Meta Incognita microcontinent

Comparing eastern Hall Peninsula with Meta Incognita microcontinent, (Figure 4.1), Archean orthogneiss in Meta Incognita microcontinent has slightly younger Archean crystallization ages and Paleoproterozoic intrusive ages of ca. 2680, 2630-2600, 2400, 2340-2310 Ma, with only sporadic ages from ca. 3000 to 2850 Ma (Wodicka et al., 2010). The metasedimentary rocks of Hall Peninsula have interpreted as correlative with

Lake Harbour Group, which outcrops on much of Meta Incognita microcontinent, however, this correlation only signifies that these two cratons were juxtaposed in the Paleoproterozoic, prior to the deposition of the ca. ≤1.93 to 1.88 Ga Lake Harbour sequence. This interpretation is still open to speculation because, as outlined in Chapter 5, the source of Neoarchean and Paleoproterozoic zircon detritus documented in Hall Peninsula supracrustal sequences is still an unresolved question. A likely, nearby source could be the composite Rae craton to the north (which includes Cumberland Peninsula). Nevertheless, Hall Peninsula and Meta Incognita microcontinent do share a common Paleoproterozoic tectonothermal history between ca. 1.87 Ga and 1.83 Ga, and even from ca. 1.80 to 1.75 Ga (Skipton et al., 2017).

4.8. Conclusions

- Archean tonalitic to monzogranitic rock units on eastern Hall Peninsula crystallized from ca. 2975 to 2720 Ma with Archean metamorphism from ca. 2740 to 2700 Ma recorded as zircon rims and single grains throughout the orthogneiss complex.
- **ε**Hf(t) data on the same zircons analyzed for U-Pb geochronology indicate that the majority of magmatic rock units were derived from the recycling of crust whose protolith magma was extracted from the mantle at ca. 3.1 Ga.
- Two Archean orthogneiss samples with mean **ε**Hf(t) values of -7 and -10 (±2) yielded mean depleted mantle model ages of ca. 3.3 and 3.4 Ga respectively indicating derivation from the recycling of older Paleoarchean crust compared to the majority of Archean orthogneisses. There are no documented

source rocks on eastern Hall Peninsula but a potential source of this exotic crust could be the North Atlantic craton or the Rae craton.

- Synthesizing data from Archean crustal provinces adjacent to eastern Hall Peninsula indicates a likely correlation with Archean crust within the southern block of the Aasiaat domain in West Greenland. However, these two Archean blocks may also be independent crustal fragments with unique geologic histories that were caught in the complex Paleoproterozoic collision between the Rae craton, Meta Incognita microcontinent and the North Atlantic craton.

4.9. Acknowledgements

Special thanks to D. Mate, G. Machado, H. Steenkamp, M. St-Onge, and the CNGO staff and crew who collaborated on the Hall Peninsula Integrated Geoscience Project. N. Rayner, T. Pestaj, R. Chung, R. Christie and P. Hunt at the GSC assisted with sample preparation, SHRIMP instrumentation and data reduction. At the University of Alberta, R. Stern and K. Nichols assisted with zircon mounting and imaging, while Qiao Shu, Chirajeeb Sarkar and Chris Fisher assisted with running the LA-ICP-MS unit and data reduction. Reviews of this paper by K. Ferreira greatly improved the content, focus and clarity, and are much appreciated. The Canadian Northern Economic Development Agency's (CanNor) Strategic Investments in Northern Economic Development (SINED) program provided financial support for the HPIGP as a whole.

4.10. References Cited

Aftalion, M., Bowes, D.R., Vrána, S., 1989. Early Carboniferous U–Pb zircon age of garnetiferous, perpotassic granulites, Blanský les massif, Czechoslovakia. Neues Jahrbuch für Mineralogie, Monatsheft 4, 145–152.

Amelin, Y., Lee, D. C., Halliday, A. N., 2000. Early-middle Archaean crustal evolution deduced from Lu-Hf and U-Pb isotopic studies of single zircon grains. Geochimica et Cosmochimica Acta 64, 4205-4225.

Baadsgaard, H., Collerson, K.D., Bridgwater, D., 1979. The Archean gneiss complex of northern Labrador: 1. Preliminary U -Th- Pb geochronology. Canadian Journal of Earth Sciences 16, 951-961.

Berman, R G, Sanborn-Barrie, M, Hamilton, B M, Rayner, N, Young, M., 2013. Preliminary in situ SHRIMP geochronological constraints on the tectonometamorphic evolution of Cumberland Peninsula, Baffin Island, Nunavut. Geological Survey of Canada, Current Research article no. 2013-7, 23 p.

Bethune, K.M., Scammell, R.J., 2003. Geology, geochronology, and geochemistry of Archean rocks in the Eqe Bay area, north-central Baffin Island, Canada: constraints on the depositional and tectonic history of the Mary River Group of northeastern Rae Province. Canadian Journal of Earth Sciences 40, 1137-1167.

Blackadar, R.G., 1967. Geological reconnaissance, southern Baffin Island, District of Franklin. Geological Survey of Canada, Paper 66–47.

Blichert-Toft, J., 2008. The Hf isotopic composition of zircon reference material 91500. Chemical Geology 253, 252-257.

Bridgwater, D., Watson, J., Windley, B.F., 1973. The Archaean craton of the North Atlantic region. Philosophical Transactions for the Royal Society of London. Series A, Mathematical and Physical Sciences, 493-512.

Bouvier, A., Vervoort, J.D., Patchett, P.J., 2008. The Lu–Hf and Sm–Nd isotopic composition of CHUR: constraints from unequilibrated chondrites and implications for the bulk composition of terrestrial planets. Earth and Planetary Science Letters 273, 48-57.

Bridgwater, D., Schiøtte,L., 1991. The Archean gneiss complex of northern Labrador. A review of current results, ideas and problems. Bulletin of the Geological Society of Denmark 39, 153-166.

Chen, R. X., Zheng, Y. F., Xie, L., 2010. Metamorphic growth and recrystallization of zircon: distinction by simultaneous in-situ analyses of trace elements, U–Th–Pb and Lu–Hf isotopes in zircons from eclogite-facies rocks in the Sulu orogen. Lithos 114, 132-154.

Condie, K.C., 1998. Episodic continental growth and supercontinents: a mantle avalanche connection?. Earth and Planetary Science Letters 163, 97-108.

Connelly, J.N., 2001. Degree of preservation of igneous zonation in zircon as a signpost for concordancy in U/Pb geochronology; Chemical Geology 172, 25–39.

Connelly, J.N., Thrane, K., Krawiec, A.W., Garde, A.A., 2006: Linking the Palaeoproterozoic Nagssugtoqidian and Rinkian orogens through the Disko Bugt region of West Greenland; Journal of the Geological Society 163, 319–335.

Connelly, J.N., Mengel, F.C., 2000. Evolution of Archaean components in the Palaeoproterozoic Nagssugtoqidian Orogen, West Greenland. Geological Society of America Bulletin 112, 747–763.

Corrigan, D., Pehrsson, S., Wodicka, N., De Kemp, E., 2009. The Palaeoproterozoic Trans-Hudson Orogen: a prototype of modern accretionary processes; Geological Society of London, Special Publications 327, 457-479.

Craven, J.A., Sanborn-Barrie, M., Roberts, B.J., Stefanescu, M., Young, M., 2013. Preliminary in- sights into the architecture of southern Cumberland Peninsula from magnetotelluric data; Geological Survey of Canada, Current Research 2013-3, 11 p.

Davis, D.W., Amelin, Y., Nowell, G.M., Parrish, R.R., 2005. Hf isotopes in zircon from the western Superior province, Canada: Implications for Archean crustal development and evolution of the depleted mantle reservoir. Precambrian Research 140, 132-156.

Fisher M. C., Vervoort, D. J., DuFrane, A. S., 2014. Accurate Hf isotope determinations of complex zircons using the ‘‘laser ablation split stream’’ method; Geochemistry Geophysics Geosystems 15, 121-139.

Fisher, C. M., Hanchar, J. M., Samson, S. D., Dhuime, B., Blichert-Toft, J., Vervoort, J. D., Lam, R., 2011. Synthetic zircon doped with hafnium and rare earth elements: a reference material for in situ hafnium isotope analysis. Chemical Geology 286, 32-47.

Friend, C.R.L., Nutman, A.P., Baadsgaard, H., Kinny, P.D., McGregor, V.R., 1996. Timing of late Archaean terrane assembly, crustal thickening and granite emplacement in the Nuuk region, southern West Greenland. Earth and Planetary Science Letters 142, 353-365.

From, R.E., Rayner, N.M., Camacho, A., 2016. Archean magmatism and metamorphism of eastern Hall Peninsula, southern Baffin Is- land, Nunavut. in Canada-Nunavut Geoscience Office Summary of Activities 2015, 73–88.

From, R.E., St-Onge, M.R., Camacho, A., 2014. Preliminary characterization of the Archean orthogneiss complex of Hall Peninsula, Baffin Island, Nunavut. in Canada-Nunavut Geoscience Office Summary of Activities 2013, 53-62.

From, R.E., Camacho, A., St-Onge, M.R., 2013. Preliminary observations on the nature and origin of the eastern orthogneiss complex of southern Hall Peninsula, Baffin Island, Nunavut. in Canada-Nunavut Geoscience Office Summary of Activities 2012, , p. 43-54.

Garde, A.A., Hollis, J.A., 2010. A buried Palaeoproterozoic spreading ridge in the northern Nagssugtoqidian orogen, West Greenland. Geological Society, London, Special Publications 338, 213-234.

Grocott, J., Davies, S.C., 1999. Deformation at the southern boundary of the late Archaean Atâ tonalite and the extent of Proterozoic reworking of the Disko terrane, West Greenland. Precambrian geology of the Disko Bugt region, West Greenland. Geology of Greenland Survey Bulletin 181, 155-169.

Griffin, W. L., Belousova, E. A., Shee, S. R., Pearson, N. J. O'reilly, S. Y., 2004. Archean crustal evolution in the northern Yilgarn Craton: U–Pb and Hf-isotope evidence from detrital zircons. Precambrian Research 131, 231-282.

Hoffman, P.F., 1988. United Plates of America, the birth of a craton: Early Proterozoic assembly and growth of Laurentia. Annual Review of Earth and Planetary Sciences 16, 543–603.

Hoffman, P.F., 1989. Precambrian geology and tectonic history of North America. The Geology of North America, 447-512.

Hollis, J.A., Frei, D., Van Gool, J.A.M., Garde A.A., Persson, M., 2006. Using zircon geochronology to resolve the Archaean geology of southern West Greenland; Geological Survey of Denmark and Greenland, Bulletin 10, 49–52.

Hosseinpour, M., Müller, R.D., Williams, S.E., Whittaker, J.M., 2013. Full-fit reconstruction of the Labrador Sea and Baffin Bay. Solid Earth 4, 461-479.

Ickert, R.B., 2013. Algorithms for estimating uncertainties in initial radiogenic isotope ratios and model ages. Chemical Geology 340, 131-138.

Jackson G. D., Hunt, P. A., Loveridge, W. D., Parrish, R. R., 1990. Reconnaissance geochronology of Baffin Island, N. W. T. In: Radiogenic age and isotopic studies: report 2. Geological Survey of Canada Paper 89-2, 123–148.

Jackson, G.D., Taylor, F.C., 1972. Correlation of major Aphebian rock units in the northeastern Canadian Shield. Canadian Journal of Earth Sciences 9, 1650-1669.

Kalsbeek, F., Nutman, A.P., 1996. Anatomy of the Early Proterozoic Nagssugtoqidian orogen, West Greenland, explored by reconnaissance SHRIMP U-Pb zircon dating. Geology 24, 515-518.

Kemp, A.I.S., Wormald, J.R., Whitehouse, M.J., Price, C.R., 2005. Hf isotopes in zircon reveal contrasting sources and crystallization histories for alkaline to peralkaline granites of Temora, southeastern Australia; Geology 33, 797-800.

Kolb, J., 2014. Structure of the Palaeoproterozoic Nagssugtoqidian Orogen, South-East Greenland: model for the tectonic evolution. Precambrian Research 255, 809-822.

Machado, G., Bilodeau, C., Takpanie, R., St-Onge, M.R., Rayner, N.M., Skipton, D.R., From, R.E., MacKay, C.B., Creason, C.G., Braden, Z.M., 2013. Hall Peninsula regional bedrock mapping, Baffin Island, Nunavut: summary of field-work. in Canada-Nunavut Geoscience Office Summary of Activities 2012, 13-22.

Nutman, A.P., Friend, C.R., Baadsgaard, H., McGregor, V.R., 1989. Evolution and assembly of Archean gneiss terranes in the Godthåbsfjord region, southern West Greenland: structural, metamorphic, and isotopic evidence. Tectonics 8, 573-589.

Pidgeon, R.T., 1992: Recrystallization of oscillatory zoned zircon: some geochronological and petrological implications; Contributions to Mineralogy and Petrology 110, 463–472.

Rayner, N.M., 2015. New (2013–2014) U-Pb geochronological results from northern Hall Peninsula, southern Baffin Island, Nunavut. in Canada-Nunavut Geoscience Office Summary of Activities 2014, 31–44.

Rayner, N.M., 2014. New U-Pb geochronological results from Hall Peninsula, Baffin Island, Nunavut. in Canada-Nunavut Geoscience Office Summary of Activities 2013, 39-52.

Rayner, N.M., Sanborn-Barrie, M., Young, M.D., Whalen, J.B., 2012. U-Pb ages of Archean basement and Paleoproterozoic plutonic rocks, southern Cumberland Peninsula, eastern Baffin Island, Nunavut; Geological Survey of Canada, Current Research 2012-8, 24 p.

Rubatto, D., 2002. Zircon trace element geochemistry: partitioning with garnet and the link between U–Pb ages and metamorphism. Chemical Geology 184, 123-138.

Sanborn-Barrie, M., St-Onge, M. R., Young, M., 2009. Bedrock geology of southwestern Baffin Island: Expanding the tectonostratigraphic framework with relevance to base metal mineralization. Geological Survey of Canada Paper 2008-6, 1–16.

Schiøtte, L., Compston, W., Bridgwater, D., 1989. Ion probe U-Th-Pb zircon dating of polymetamorphic orthogneisses from northern Labrador, Canada. Canadian Journal of Earth Sciences 26, 1533- 1556.

Schoene, B., Crowley, J.L., Condon, D.J., Schmitz, M.D., Bowring, S.A., 2006. Reassessing the uranium decay constants for geochronology using ID-TIMS U–Pb data. Geochimica et Cosmochimica Acta 70, 426-445.

Scott, D.J., 1999. U-Pb geochronology of the eastern Hall Peninsula, southern Baffin Island, Canada: a northern link between the Archean of West Greenland and the Paleoproterozoic Torngat Orogen of northern Labrador; Precambrian Research 93, 5-26.

Scott, D.J., 1997a. Preliminary U-Pb geochronology of the Hall Peninsula east of Iqaluit, southern Baffin Island, in Radiogenic age and isotopic studies: Report 10: Geological Survey of Canada, Current Research 1997-F, 67–78.

Scott, D.J., 1997b. Geology, U–Pb, and Pb–Pb geochronology of the Lake Harbour area, southern Baffin Island: implications for the Paleoproterozoic tectonic evolution of northeastern Laurentia. Canadian Journal of Earth Sciences 34, 140-155.

Scott, D.J., 1995. U–Pb geochronology of the Nain craton on the eastern margin of the Torngat Orogen, Labrador. Canadian Journal of Earth Sciences 32, 1859-1869.

Scott, D.J., Stern, R.A., St-Onge, M.R., McMullen, S.M., 2002. U-Pb geochronology of detrital zircons in metasedimentary rocks from southern Baffin Island: implications for the Paleoproterozoic tectonic evolution of Northeastern Laurentia. Canadian Journal of Earth Sciences 39, 611–623.

Scott, D.J., Gauthier, G., 1996. Comparison of TIMS (U-Pb) and laser ablation microprobe ICP-MS (Pb) techniques for age determination of detrital zircons from Paleoproterozoic metasedimentary rocks from northeastern Laurentia, Canada, with tectonic implications. Chemical Geology 131, 127–142.

Scott, D.J., Machado, N., 1995. U Pb geochronology of the northern Torngat Orogen, Labrador, Canada: a record of Palaeoproterozoic magmatism and deformation. Precambrian Research 70, 69-190.

Scott, D.J., Campbell, L.M., 1993. Evolution of the Paleoproterozoic Torngat orogen, Labrador, Canada: recent advances using U-Pb geochronology and Nd isotopic systematics (abstract); Geological Society of America, Annual Meeting 1993, Boston, Massachusetts, Program with Abstracts 25, p. A23.

Skipton, D.R., St-Onge, M.R., 2014. Paleoproterozoic deformation and metamorphism in metasedimentary rocks west of Okalik Bay: a field template for the evolution of eastern Hall Peninsula, Baffin Island, Nunavut. in Canada-Nunavut Geoscience Office Summary of Activities 2013, 63-72.

Sláma, J., Košler, J., Condon, D.J., Crowley, J.L., Gerdes, A., Hanchar, J.M., Horstwood, M.S., Morris, G.A., Nasdala, L., Norberg, N., Schaltegger, U., 2008. Plešovice zircon—a new natural reference material for U–Pb and Hf isotopic microanalysis. Chemical Geology 249, 1-35.

St-Onge, M.R., Scott, D.J., Wodicka, N., 2002. Review of crustal architecture and evolution in the Ungava Peninsula–Baffin Island area: connection to the Lithoprobe ECSOOT transect; Canadian Journal of Earth Sciences 39, 589-610.

St-Onge, M.R., Van Gool, J.A.M., Garde, A.A., Scott, D.J., 2009. Correlation of Archaean and Palaeoproterozoic units between northeastern Canada and western Greenland: constraining the pre-collisional upper plate accretionary history of the Trans-Hudson orogen; Geological Society of London, Special Publications 318, 193-235.

St-Onge, M.R., Wodicka, N., Ijewliw, O., 2007. Polymetamorphic evolution of the Trans-Hudson Orogen, Baffin Island, Canada: integration of petrological, structural and geochronological data; Journal of Petrology 48, 271-302.

Steenkamp, H.M., St-Onge, M.R., 2014. Overview of the 2013 regional bedrock mapping program on northern Hall Peninsula, Baffin Island, Nunavut, in Canada-Nunavut Geoscience Office Summary of Activities 2013, 27-38.

Taylor, S. R., McLennan, S. M., 1985. The continental crust: its composition and evolution.

Thrane, K., Connelly J.N., 2006. Zircon geochronology from the Kangatsiaq-Qasigiannguit region, the northern part of the 1.9–1.8 Ga Nagssugtoqidian orogen, West Greenland; Geological Survey of Denmark and Greenland, Bulletin 11, 87–99.

Thrane, K., Connelly, J.N., Garde, A.A., Grocott, J., Krawiec, A., 2003. Linking the Palaeoproterozoic Rinkian and Nagssugtoqidian belts of central W.Greenland: implications of new U–Pb and Pb–Pb ages. European Union of Geosciences Meeting, Geophysical Research Abstracts CD, 5, Abstract 09275.

van Gool J. A. M., Connelly, J. N., Marker, M., Mengel , F. C., 2002. The Nagssugtoqidian Orogen of West Greenland: Tectonic evolution and regional correlations from a West Greenland perspective. Canadian Journal of Earth Sciences 39, 665-686.

Van Kranendonk, M.J., 1996. Tectonic evolution of the Paleoproterozoic Torngat Orogen: Evidence from pressure‐temperature‐time‐deformation paths in the North River map area, Labrador. Tectonics 15, 843-869.

Vervoort, J.D., Kemp, A.I.S., 2016. Clarifying the zirconHf isotope record of crust-mantle evolution. Chemical Geology 425, 65-75.

Vervoort, J.D., Blichert-Toft, J., 1999. Evolution of the depleted mantle: Hf isotope evidence from juvenile rocks through time. Geochimica et Cosmochimica Acta 63, 533-556.

Wardle, R.J., James D.T., Scott, D.J., Hall, J., 2002. The southeastern Churchill Province: synthesis of a Palaeoproterozoic transpressional orogen; Canadian Journal of Earth Sciences 39, 639-663.

Wedepohl, H. K., 1995. The composition of the continental crust. Geochimica et cosmochimica Acta 59, 1217-1232.

Whalen, J.B., Wodicka, N., Taylor, B.E., Jackson, G.D., 2010. Cumberland batholith, Trans-Hudson Orogen, Canada: petrogenesis and implications for Paleoproterozoic crustal and orogenic processes. Lithos 117, 99-118.

Wodicka, N., Whalen, J., St-Onge, M.R., Corrigan, D., 2010. Meta Incognita microcontinent revisited: insights from U–Pb geochronology and Nd isotopes. Geological Association of Canada – Mineralogical Association of Canada Abstract Volume 35.

Wodicka, N., St-Onge, M. R., Scott, D. J., Corrigan, D., 2002. Preliminary report on the U–Pb geochronology of the northern margin of the Trans Hudson Orogen, central Baffin Island, Nunavut. Geological Survey of Canada Paper, 2002-F7.

Wooden, L. J., Barth, P.A., Mueller, A. P., 2013. Crustal growth and tectonic evolution of the Mojave crustal province: Insights from hafnium isotope systematics in zircons, Lithosphere 5, 17-28.

Xie, l., Zhang, Y., Zhang, H., Sun, J., Wu, F., 2008. In situ simultaneous determination of trace elements, U–Pb and Lu–Hf isotopes in zircon and baddeleyite. Chinese Science Bulletin 53, 1565-1573.

Yuan, H.L., Gao, S., Dai, M.N., Zong, L., Gunther, G.H., Fontaine, X.M., Liu, C.D., 2008. Simultaneous determinations of U–Pb age, Hf isotopes and trace element compositions of zircon by excimer laser-ablation quadrupole and multiple-collector ICP-MS, Chemical Geology 247, 100–118.

4.11. *Data appendices*

APPENDIX 4A - SHRIMP U-Pb isotopic data from snow bowl area samples
APPENDIX 4B - LASS-ICPMS U-Pb isotopic data from regional samples
APPENDIX 4C - LASS-ICPMS Lu-Hf isotopic data from snow bowl area samples
APPENDIX 4D - LASS-ICPMS Lu-Hf isotopic data from regional samples
APPENDIX 4E - Concordia diagrams for snow bowl area and regional samples from eastern Hall Peninsula.
APPENDIX 4F - Th/U versus $^{207}Pb/^{206}Pb$ age diagrams for snow bowl area and regional samples from eastern Hall Peninsula
APPENDIX 4G - SHRIMP and LASS-ICPMS U-Pb zircon dates from the same zircons from basal quartzite sample 10914 from eastern Hall Peninsula.
APPENDIX 4H - Lithogeochemical data for snow bowl area and regional samples from eastern Hall Peninsula.

APPENDIX 4A - SHRIMP U-Pb isotopic data from snow bowl area samples

Spot name	U (ppm)	Th (ppm)	Yb (ppm)	$^{204}Pb/^{206}Pb$	% ±	$^{206}Pb^*$ (ppm)	$f(206)^{204}$ %	$^{208*}Pb/^{206*}Pb$	% ±	$^{207*}Pb/^{235}U$	% ±	$^{206*}Pb/^{238}U$	% ±	Corr Coeff
S116A, monzogranite gneiss														
713778 7041607 NAD 1983 UTM Zone 19N														
11001-026.1	191	93	148	7.6E-5	32	85	0.113	0.142	1.5	13.4	1.09	0.52	1.05	0.964
11001-068.1	3134	476	802	3.3E-6	36	1548	0.015	0.047	0.6	16.0	1.03	0.57	1.02	0.995
11001-011.2	1268	153	421	1.8E-5	19	626	0.029	0.034	1.1	16.6	1.10	0.57	1.02	0.935
11001-011.1	673	86	344	3.7E-6	28	329	0.028	0.037	1.5	16.7	1.28	0.57	1.20	0.941
11001-014.1	73	18	113	2.0E-4	34	36	0.042	0.067	3.3	17.0	1.23	0.57	1.11	0.907
11001-016.1	138	25	142	5.9E-5	36	69	0.010	0.051	3.6	17.3	1.37	0.58	1.08	0.787
~~11001-038.2~~	~~68~~	~~21~~	~~146~~	~~9.1E-5~~	~~19~~	~~35~~	~~0.023~~	~~0.093~~	~~5.3~~	~~17.7~~	~~1.12~~	~~0.60~~	~~1.11~~	~~0.991~~
11001-022.1	158	42	199	1.3E-4	17	77	0.222	0.077	2.1	16.9	1.09	0.57	1.06	0.969
11001-009.1	196	77	222	---	100	97	0.411	0.116	1.6	17.1	1.07	0.57	1.05	0.980
~~11001-020.2~~	~~75~~	~~28~~	~~81~~	~~8.8E-4~~	~~10~~	~~37~~	~~0.138~~	~~0.110~~	~~2.5~~	~~17.0~~	~~1.66~~	~~0.57~~	~~1.12~~	~~0.675~~
11001-016.2	166	34	166	1.5E-4	19	84	-0.023	0.058	2.5	17.7	1.11	0.59	1.07	0.965
11001-008.1	214	60	206	3.4E-5	48	106	0.120	0.079	1.8	17.3	1.07	0.58	1.05	0.979
11001-002.1	216	57	227	1.8E-5	18	105	0.003	0.075	1.9	16.9	1.19	0.57	1.06	0.890
11001-017.1	237	56	250	7.0E-5	18	122	0.072	0.069	1.8	17.8	1.13	0.60	1.11	0.984
11001-052.1	215	55	229	1.1E-4	18	107	0.099	0.075	1.9	17.3	1.12	0.58	1.10	0.978
11001-026.2	205	50	189	9.6E-5	18	102	0.051	0.074	3.3	17.4	1.15	0.58	1.12	0.978
11001-010.1	195	52	189	9.3E-5	17	97	0.018	0.075	1.9	17.4	1.08	0.58	1.05	0.977
11001-015.1	*206*	*27*	*159*	*5.6E-5*	*46*	*104*	*0.095*	*0.036*	*2.6*	*17.7*	*1.08*	*0.59*	*1.05*	*0.974*
11001-014.2	*143*	*34*	*157*	*1.4E-4*	*18*	*69*	*0.113*	*0.068*	*3.8*	*17.0*	*1.17*	*0.56*	*1.06*	*0.908*
~~11001-038.1~~	~~191~~	~~13~~	~~88~~	~~8.3E-5~~	~~20~~	~~98~~	~~0.033~~	~~0.019~~	~~3.7~~	~~17.9~~	~~1.10~~	~~0.59~~	~~1.07~~	~~0.977~~
11001-019.1	*213*	*30*	*174*	*2.0E-5*	*31*	*108*	*-0.001*	*0.041*	*2.6*	*17.8*	*1.24*	*0.59*	*1.22*	*0.985*
11001-025.1	*272*	*59*	*219*	*6.1E-5*	*21*	*137*	*-0.001*	*0.065*	*1.8*	*17.6*	*1.18*	*0.58*	*1.18*	*0.997*
11001-007.1	*206*	*43*	*191*	*5.9E-5*	*21*	*102*	*0.012*	*0.056*	*2.2*	*17.4*	*1.07*	*0.57*	*1.05*	*0.980*
11001-020.1	*51*	*24*	*111*	*1.5E-4*	*34*	*26*	*0.019*	*0.135*	*2.8*	*18.1*	*1.25*	*0.60*	*1.14*	*0.918*
11001-012.1	*234*	*71*	*234*	*3.2E-5*	*16*	*118*	*0.012*	*0.087*	*1.6*	*17.8*	*1.06*	*0.59*	*1.05*	*0.983*
11001-021.1	*196*	*60*	*216*	*6.1E-5*	*33*	*99*	*0.234*	*0.091*	*1.8*	*17.8*	*1.08*	*0.59*	*1.05*	*0.976*
11001-109.2	*251*	*76*	*297*	*3.0E-5*	*67*	*128*	*0.015*	*0.091*	*1.6*	*18.0*	*1.07*	*0.59*	*1.05*	*0.979*
11001-051.1	*180*	*65*	*189*	*1.3E-4*	*19*	*91*	*0.054*	*0.103*	*3.1*	*17.9*	*1.09*	*0.59*	*1.06*	*0.971*
11001-109.1	*156*	*48*	*194*	*4.5E-5*	*62*	*79*	*0.033*	*0.088*	*2.1*	*18.0*	*1.13*	*0.59*	*1.06*	*0.940*
~~11001-024.1~~	~~127~~	~~18~~	~~134~~	~~1.2E-4~~	~~24~~	~~65~~	~~0.060~~	~~0.041~~	~~3.1~~	~~18.1~~	~~1.13~~	~~0.60~~	~~1.08~~	~~0.963~~

			Age (Ma)						
Th/U	$^{207*}Pb/^{206*}Pb$	% ±	$^{206*}Pb/^{238}U$	±	$^{207*}Pb/^{206*}Pb$	±	Disc. %	zonation	notes
12MBC-S116A, monzogranite									
713778 7041607 NAD 1983 UTM Zone 19N									
0.50	0.187	0.3	2700	23	2716	5	0.73	unzoned	
0.16	0.201	0.1	2928	24	2837	2	-3.99	unzoned	
0.12	0.209	0.4	2927	24	2901	6	-1.11	unzoned	
0.13	0.214	0.4	2901	28	2933	7	1.38	unzoned	
0.25	0.215	0.5	2920	26	2943	8	0.99	osc	
0.19	0.215	0.8	2965	26	2943	14	-0.93	osc	
~~0.32~~	~~0.215~~	~~0.1~~	~~3014~~	~~27~~	~~2944~~	~~2~~	~~-3.00~~	~~mixed~~	~~incidental overlap of domains~~
0.28	0.215	0.3	2906	25	2946	4	1.72	osc	
0.40	0.216	0.2	2927	25	2951	3	1.03	osc	
~~0.39~~	~~0.216~~	~~1.2~~	~~2904~~	~~26~~	~~2954~~	~~20~~	~~2.09~~	~~mixed~~	~~incidental overlap of domains~~
0.21	0.217	0.3	2998	26	2957	5	-1.75	osc	
0.29	0.217	0.2	2936	25	2958	4	0.91	osc	
0.27	0.217	0.5	2888	25	2958	9	2.93	osc	
0.24	0.217	0.2	3014	27	2960	3	-2.28	osc	
0.26	0.218	0.2	2942	26	2963	4	0.88	osc	
0.25	0.218	0.2	2954	27	2964	4	0.41	osc	
0.27	0.218	0.2	2949	25	2964	4	0.64	osc	
0.13	*0.218*	*0.2*	*2981*	*25*	*2969*	*4*	*-0.50*	*osc*	
0.25	*0.218*	*0.5*	*2881*	*25*	*2969*	*8*	*3.65*	*osc*	
~~0.07~~	~~0.218~~	~~0.2~~	~~3006~~	~~26~~	~~*2969*~~	~~*4*~~	~~-1.55~~	~~mixed~~	~~incidental overlap of domains~~
0.15	*0.219*	*0.2*	*2993*	*29*	*2970*	*3*	*-0.99*	*osc*	
0.22	*0.219*	*0.1*	*2968*	*28*	*2971*	*1*	*0.12*	*osc*	
0.21	*0.219*	*0.2*	*2928*	*25*	*2973*	*3*	*1.89*	*osc*	
0.48	*0.219*	*0.5*	*3019*	*28*	*2975*	*8*	*-1.87*	*irregular*	
0.31	*0.220*	*0.2*	*2984*	*25*	*2978*	*3*	*-0.24*	*osc*	
0.32	*0.220*	*0.2*	*2975*	*25*	*2980*	*4*	*0.22*	*osc*	
0.31	*0.220*	*0.2*	*3003*	*25*	*2982*	*4*	*-0.88*	*osc*	
0.37	*0.220*	*0.3*	*2987*	*25*	*2982*	*4*	*-0.19*	*osc*	
0.32	*0.221*	*0.4*	*2991*	*25*	*2987*	*6*	*-0.13*	*osc*	
~~0.14~~	~~0.221~~	~~0.3~~	~~3011~~	~~26~~	~~*2988*~~	~~*5*~~	~~-0.97~~	~~unzoned~~	~~odd unzoned domain~~

APPENDIX 4A - SHRIMP U-Pb isotopic data from snow bowl area samples

Spot name	U (ppm)	Th (ppm)	Yb (ppm)	$^{204}Pb/^{206}Pb$	% ±	$^{206}Pb^*$ (ppm)	$f(206)^{204}$ %	$^{208*}Pb/^{206*}Pb$	% ±	$^{207*}Pb/^{235}U$	% ±	$^{206*}Pb/^{238}U$	% ±	Corr Coeff
F151A, granodiorite gneiss														
669300 7094544 NAD1983, UTM Zone 19N														
11187-038.1	874	107	120	2.0E-5	23	375	0.035	0.036	1.9	12.68	1.66	0.500	1.53	0.920
11187-124.1	1497	107	119	2.7E-5	37	639	0.046	0.020	2.8	12.68	1.33	0.497	1.32	0.994
11187-039.1	563	97	123	4.8E-5	20	248	0.084	0.049	4.0	13.22	1.42	0.512	1.41	0.989
~~11187-059.1~~	~~527~~	~~13~~	~~151~~	~~8.6E-5~~	~~18~~	~~228~~	~~0.149~~	~~0.004~~	~~17.9~~	~~13.51~~	~~1.37~~	~~0.505~~	~~1.35~~	~~0.983~~
11187-055.1	84	38	172	7.3E-5	41	38	0.127	0.134	3.4	14.19	1.78	0.526	1.55	0.870
11187-055.2	91	52	195	2.4E-5	71	41	0.041	0.173	2.8	14.35	1.61	0.523	1.54	0.955
11187-053.1	76	47	181	3.9E-5	58	36	0.068	0.191	2.8	15.23	2.25	0.547	2.08	0.922
11187-053.2	55	19	116	5.6E-5	58	26	0.097	0.105	7.2	15.23	1.77	0.542	1.67	0.939
11187-116.2	73	29	162	1.6E-4	30	35	0.274	0.102	4.4	15.69	1.70	0.550	1.60	0.941
11187-051.1	150	72	270	6.7E-5	30	72	0.116	0.141	2.2	15.98	1.48	0.560	1.44	0.972
~~11187-084.1~~	~~115~~	~~59~~	~~194~~	~~2.3E-5~~	~~58~~	~~54~~	~~0.040~~	~~0.155~~	~~2.4~~	~~15.66~~	~~1.52~~	~~0.548~~	~~1.47~~	~~0.968~~
11187-063.1	259	3	99	1.2E-5	58	123	0.020	0.004	13.8	15.91	1.42	0.554	1.39	0.978
11187-116.1	72	33	120	----	---	35	0.000	0.135	3.1	16.00	1.64	0.556	1.57	0.958
11187-069.1	76	31	152	6.2E-5	45	37	0.108	0.115	3.6	16.24	2.13	0.564	1.97	0.925
11187-021.1	107	53	77	-3.1E-5	58	49	-0.053	0.140	7.8	15.24	1.76	0.529	1.57	0.892
11187-117.1	66	15	81	1.5E-5	100	32	0.026	0.065	5.2	16.23	1.73	0.564	1.63	0.938
11187-081.1	110	48	185	7.1E-5	33	54	0.124	0.126	2.8	16.48	1.60	0.570	1.48	0.923
11187-084.2	147	103	294	6.7E-6	100	72	0.012	0.204	1.9	16.54	1.49	0.572	1.45	0.973
11187-094.1	80	53	226	3.2E-5	58	39	0.056	0.194	2.5	16.28	1.60	0.562	1.54	0.960
11187-006.1	96	48	217	4.9E-5	45	46	0.085	0.138	2.9	16.13	1.60	0.556	1.52	0.952
11187-012.1	148	67	238	5.5E-5	35	71	0.095	0.128	4.8	16.15	1.54	0.556	1.49	0.964
11187-108.1	124	60	254	2.8E-5	50	61	0.049	0.142	2.4	16.53	1.50	0.568	1.46	0.971
11187-016.1	*73*	*47*	*185*	*8.1E-5*	*41*	*36*	*0.140*	*0.178*	*3.0*	*16.55*	*1.70*	*0.567*	*1.60*	*0.940*
11187-017.1	*103*	*39*	*188*	*4.2E-5*	*45*	*49*	*0.072*	*0.104*	*3.0*	*16.18*	*1.54*	*0.555*	*1.48*	*0.966*
11187-122.1	*114*	*46*	*216*	*6.5E-5*	*33*	*55*	*0.113*	*0.117*	*2.8*	*16.29*	*1.51*	*0.558*	*1.46*	*0.968*
11187-070.1	*84*	*34*	*123*	*1.9E-5*	*71*	*41*	*0.033*	*0.124*	*2.9*	*16.78*	*1.58*	*0.574*	*1.51*	*0.961*
11187-052.1	*100*	*66*	*232*	*---*	*---*	*49*	*0.000*	*0.199*	*5.2*	*16.54*	*1.56*	*0.566*	*1.51*	*0.965*
11187-051.2	*109*	*43*	*156*	*9.2E-6*	*100*	*53*	*0.016*	*0.103*	*3.1*	*16.69*	*1.75*	*0.569*	*1.50*	*0.859*
11187-083.1	*88*	*43*	*184*	*---*	*---*	*43*	*0.000*	*0.144*	*2.7*	*16.68*	*1.58*	*0.568*	*1.52*	*0.958*
11187-106.1	*116*	*48*	*197*	*5.1E-5*	*38*	*58*	*0.089*	*0.113*	*2.7*	*17.14*	*1.52*	*0.583*	*1.47*	*0.969*

			Age (Ma)						
Th/U	$^{207*}Pb/^{206*}Pb$	% ±	$^{206*}Pb/^{238}U$	±	$^{207*}Pb/^{206*}Pb$	±	Disc. %	zonation	notes
13SUB-F151A, granodiorite									
669300 7094544 NAD1983, UTM Zone 19N									
0.13	0.1840	0.7	2612	33	2690	11	3.5	unzoned	
0.07	0.1849	0.1	2602	28	2697	2	4.3	unzoned	
0.18	0.1872	0.2	2667	31	2718	3	2.3	unzoned	
~~0.03~~	~~0.1942~~	~~0.2~~	~~2634~~	~~29~~	~~2778~~	~~4~~	~~6.3~~	~~mixed~~	~~incidental overlap of domains~~
0.46	0.1956	0.9	2725	34	2790	14	2.8	osc	
0.59	0.1991	0.5	2711	34	2819	8	4.7	osc	
0.64	0.2018	0.9	2814	47	2841	14	1.2	osc	
0.36	0.2039	0.6	2791	38	2858	10	2.8	osc	
0.40	0.2069	0.6	2825	37	2882	9	2.4	osc	
0.49	0.2069	0.3	2867	33	2882	6	0.6	irregular	
~~0.53~~	~~0.2072~~	~~0.4~~	~~2818~~	~~34~~	~~2884~~	~~6~~	~~2.8~~	~~mixed~~	~~incidental overlap of domains~~
0.01	0.2083	0.3	2842	32	2892	5	2.2	irregular	
0.47	0.2085	0.5	2852	36	2894	8	1.8	osc	
0.42	0.2087	0.8	2885	46	2896	13	0.5	osc	
0.51	0.2089	0.8	2738	35	2897	13	6.7	osc	
0.24	0.2089	0.6	2881	38	2897	10	0.7	osc	
0.46	0.2096	0.6	2909	35	2902	10	-0.3	osc	
0.72	0.2098	0.3	2915	34	2904	6	-0.5	osc	
0.68	0.2101	0.5	2874	36	2907	7	1.4	osc	
0.52	0.2103	0.5	2851	35	2908	8	2.4	osc	
0.47	0.2106	0.4	2851	34	2910	7	2.5	osc	
0.50	0.2110	0.4	2901	34	2913	6	0.5	irregular	
0.66	*0.2115*	*0.6*	*2897*	*37*	*2917*	*9*	*0.8*	*osc*	
0.39	*0.2117*	*0.4*	*2844*	*34*	*2918*	*6*	*3.1*	*osc*	
0.41	*0.2117*	*0.4*	*2859*	*34*	*2918*	*6*	*2.5*	*osc*	
0.42	*0.2119*	*0.4*	*2925*	*36*	*2920*	*7*	*-0.2*	*osc*	
0.68	*0.2120*	*0.4*	*2891*	*35*	*2921*	*7*	*1.3*	*osc*	
0.41	*0.2129*	*0.9*	*2902*	*35*	*2928*	*15*	*1.1*	*irregular*	
0.50	*0.2130*	*0.5*	*2900*	*35*	*2928*	*7*	*1.2*	*osc*	
0.43	*0.2131*	*0.4*	*2962*	*35*	*2930*	*6*	*-1.4*	*osc*	

APPENDIX 4A - SHRIMP U-Pb isotopic data from snow bowl area samples

Spot name	U (ppm)	Th (ppm)	Yb (ppm)	$^{204}Pb/^{206}Pb$	% ±	$^{206}Pb^*$ (ppm)	$f(206)^{204}$ %	$^{208*}Pb/^{206*}Pb$	% ±	$^{207*}Pb/^{235}U$	% ±	$^{206*}Pb/^{238}U$	% ±	Corr Coeff
11187-125.1	*108*	*62*	*195*	*8.0E-6*	*100*	*53*	*0.014*	*0.164*	*3.9*	*16.89*	*1.53*	*0.574*	*1.48*	*0.970*
11187-098.1	*95*	*57*	*222*	*8.9E-5*	*32*	*48*	*0.154*	*0.170*	*4.5*	*17.16*	*1.56*	*0.583*	*1.50*	*0.962*
11187-018.1	*139*	*73*	*127*	*1.8E-5*	*58*	*67*	*0.032*	*0.148*	*2.2*	*16.54*	*1.48*	*0.562*	*1.44*	*0.974*
11187-102.1	*81*	*32*	*183*	*1.0E-5*	*100*	*40*	*0.018*	*0.121*	*3.1*	*17.07*	*1.69*	*0.579*	*1.53*	*0.907*
11187-005.1	*94*	*39*	*206*	*-3.1E-5*	*58*	*46*	*-0.053*	*0.126*	*3.1*	*16.85*	*1.61*	*0.570*	*1.54*	*0.953*
11187-058.1	*127*	*89*	*283*	*-2.2E-5*	*58*	*60*	*-0.039*	*0.197*	*2.0*	*16.38*	*1.51*	*0.552*	*1.47*	*0.970*
F155B, tonalite gneiss														
669461 7094784 NAD1983, UTM Zone 19N														
11189-091.1	109	49	149	1.0E-4	29	46	0.175	0.142	4.2	12.24	1.53	0.488	1.47	0.955
11189-057.1	3190	158	382	3.0E-6	32	1458	0.005	0.014	1.5	13.47	1.37	0.532	1.36	0.989
11189-104.2	1544	190	114	4.6E-6	35	689	0.008	0.036	1.3	13.21	1.33	0.520	1.31	0.984
11189-096.1	119	145	264	9.9E-5	29	53	0.172	0.362	1.6	13.34	1.79	0.522	1.47	0.820
11189-023.1	118	87	197	7.6E-5	33	53	0.132	0.208	2.2	13.38	1.54	0.523	1.48	0.959
11189-015.2	123	63	130	4.3E-5	45	54	0.075	0.147	2.6	13.21	1.54	0.515	1.48	0.961
11189-016.1	198	230	304	1.1E-5	71	88	0.019	0.335	1.3	13.32	1.45	0.517	1.42	0.975
11189-034.1	173	198	239	4.4E-5	38	76	0.076	0.329	1.5	13.27	1.48	0.514	1.43	0.969
11189-085.1	140	114	167	4.3E-5	41	63	0.074	0.240	1.8	13.46	1.77	0.520	1.65	0.936
11189-041.1	155	181	132	5.6E-5	35	70	0.097	0.340	1.5	13.54	1.50	0.523	1.45	0.966
11189-057.2	325	134	132	5.2E-5	24	142	0.091	0.123	2.8	13.15	1.39	0.508	1.37	0.983
11189-072.1	270	133	230	4.2E-5	30	120	0.073	0.143	1.7	13.37	1.41	0.516	1.38	0.980
11189-063.1	177	222	289	2.6E-5	50	80	0.045	0.369	1.4	13.72	1.49	0.529	1.44	0.970
11189-072.2	72	65	233	---	100	33	0.000	0.269	2.4	13.71	1.67	0.527	1.58	0.950
11189-030.2	94	63	149	---	---	43	0.000	0.194	2.5	13.86	1.71	0.532	1.52	0.890
11189-071.1	180	162	346	-1.2E-5	71	81	-0.022	0.272	1.6	13.60	1.48	0.522	1.44	0.972
11189-001.1	230	243	292	-9.4E-6	71	104	-0.016	0.314	1.3	13.73	1.44	0.527	1.40	0.978
11189-048.1	197	186	356	-1.7E-5	58	89	-0.029	0.274	1.5	13.77	1.46	0.527	1.42	0.974
11189-093.1	273	359	392	3.6E-6	100	125	0.006	0.380	1.0	13.93	1.40	0.533	1.38	0.983
11189-015.1	272	103	195	3.6E-6	100	126	0.006	0.108	1.9	14.36	1.56	0.540	1.54	0.986
11189-042.1	331	86	238	2.7E-6	100	148	0.005	0.078	2.0	13.85	1.38	0.521	1.36	0.987
11189-065.1	297	100	224	5.6E-5	24	135	0.097	0.094	2.0	14.25	1.40	0.529	1.37	0.981
11189-089.1	2313	109	185	1.5E-6	50	1079	0.003	0.014	1.7	14.68	1.41	0.543	1.37	0.976

			Age (Ma)						
Th/U	$^{207*}Pb/^{206*}Pb$	% ±	$^{206*}Pb/^{238}U$	±	$^{207*}Pb/^{206*}Pb$	±	Disc. %	zonation	notes
0.59	*0.2132*	*0.4*	*2926*	*35*	*2930*	*6*	*0.2*	*osc*	
0.62	*0.2134*	*0.4*	*2962*	*36*	*2932*	*7*	*-1.3*	*osc*	
0.54	*0.2135*	*0.3*	*2874*	*33*	*2932*	*8*	*2.5*	*osc*	
0.41	*0.2136*	*0.7*	*2947*	*36*	*2933*	*11*	*-0.6*	*osc*	
0.43	*0.2143*	*0.5*	*2910*	*36*	*2938*	*8*	*1.2*	*osc*	
0.73	*0.2151*	*0.4*	*2835*	*34*	*2945*	*6*	*4.6*	*osc*	
13SUB-F155B, tonalite									
669461	***7094784***	***NAD1983, UTM Zone 19N***							
0.46	0.1820	0.5	2560	31	2671	7	5.0	osc	
0.05	0.1837	0.2	2750	30	2686	3	-2.9	unzoned	
0.13	0.1844	0.2	2697	29	2692	4	-0.2	unzoned	
1.26	0.1853	1.0	2708	33	2701	17	-0.4	unzoned	
0.76	0.1855	0.4	2711	33	2703	7	-0.4	osc	
0.53	0.1861	0.4	2678	32	2708	7	1.4	osc	
1.20	0.1867	0.3	2688	31	2713	5	1.1	irregular	
1.19	0.1872	0.4	2675	31	2717	6	1.9	irregular	
0.84	0.1876	0.6	2701	36	2721	10	0.9	osc	
1.20	0.1876	0.4	2714	32	2721	6	0.3	unzoned	
0.43	0.1877	0.3	2649	30	2722	4	3.3	osc	
0.51	0.1878	0.3	2683	30	2723	5	1.8	osc	
1.30	0.1881	0.4	2736	32	2726	6	-0.5	irr	
0.93	0.1886	0.5	2729	35	2730	9	0.1	osc	
0.69	0.1889	0.8	2750	34	2733	13	-0.8	osc	
0.93	0.1890	0.3	2708	32	2733	6	1.1	irregular	
1.09	0.1891	0.3	2727	31	2735	5	0.3	irregular	
0.97	0.1894	0.3	2731	32	2737	5	0.3	irregular	
1.36	0.1895	0.3	2754	31	2738	4	-0.7	irregular	
0.39	0.1928	0.3	2784	35	2766	4	-0.8	osc	
0.27	0.1929	0.2	2702	30	2767	4	2.9	osc	
0.35	0.1955	0.3	2737	31	2789	4	2.3	osc	
0.05	0.1961	0.3	2796	31	2794	5	-0.1	unzoned	

APPENDIX 4A - SHRIMP U-Pb isotopic data from snow bowl area samples

Spot name	U (ppm)	Th (ppm)	Yb (ppm)	$^{204}Pb/^{206}Pb$	% ±	$^{206}Pb^*$ (ppm)	$f(206)^{204}$ %	$^{208*}Pb/^{206*}Pb$	% ±	$^{207*}Pb/^{235}U$	% ±	$^{206*}Pb/^{238}U$	% ±	Corr Coeff
11189-020.2	*242*	*92*	*152*	*6.5E-5*	*24*	*112*	*0.112*	*0.107*	*2.0*	*14.68*	*1.41*	*0.539*	*1.38*	*0.980*
11189-050.1	*813*	*419*	*461*	*1.5E-5*	*29*	*382*	*0.025*	*0.152*	*0.9*	*14.93*	*1.34*	*0.547*	*1.33*	*0.994*
11189-087.1	*323*	*103*	*232*	*1.2E-4*	*17*	*152*	*0.216*	*0.092*	*2.1*	*14.91*	*1.39*	*0.546*	*1.37*	*0.981*
11189-008.1	*198*	*97*	*457*	*3.8E-5*	*38*	*90*	*0.065*	*0.143*	*3.7*	*14.36*	*1.61*	*0.526*	*1.42*	*0.884*
11189-055.1	*194*	*86*	*147*	*-5.0E-6*	*100*	*88*	*-0.009*	*0.132*	*2.1*	*14.37*	*1.44*	*0.526*	*1.41*	*0.978*
11189-104.1	*463*	*168*	*290*	*7.6E-6*	*50*	*211*	*0.013*	*0.107*	*3.3*	*14.57*	*1.55*	*0.530*	*1.50*	*0.970*
11189-100.1	404	159	290	4.8E-5	22	188	0.084	0.114	1.5	15.14	1.39	0.542	1.35	0.972
11189-076.1	50	25	42	1.1E-4	41	24	0.193	0.144	4.0	16.08	1.80	0.567	1.69	0.936
11189-058.1	118	70	305	4.5E-5	45	56	0.077	0.175	2.4	16.02	1.55	0.550	1.50	0.964
11189-020.1	315	195	463	2.5E-5	33	155	0.044	0.180	1.3	16.81	1.39	0.571	1.37	0.987
11189-095.1	201	117	323	4.0E-5	35	99	0.069	0.160	1.9	16.82	1.76	0.571	1.66	0.942
11189-030.1	199	74	239	8.5E-6	71	96	0.015	0.104	2.1	16.68	1.42	0.559	1.40	0.981
11189-046.1	56	36	226	7.4E-5	50	28	0.128	0.192	3.3	17.05	1.80	0.569	1.69	0.943
11189-082.1	149	81	372	2.8E-5	45	76	0.049	0.151	4.0	18.01	1.47	0.598	1.44	0.976
11189-043.1	175	97	346	5.8E-6	100	88	0.010	0.164	2.0	17.73	1.47	0.586	1.44	0.977
11189-025.1	284	175	354	---	100	145	0.000	0.172	1.4	17.91	1.40	0.591	1.38	0.986
11189-099.1	131	79	488	4.7E-5	38	66	0.082	0.177	2.1	17.89	1.50	0.590	1.46	0.972
11189-081.1	112	66	410	5.9E-5	35	56	0.102	0.165	2.3	18.00	1.52	0.586	1.47	0.970
11189-045.1	115	15	135	7.8E-6	100	61	0.014	0.040	4.7	20.51	1.61	0.615	1.49	0.928
11189-049.1	45	25	244	2.2E-5	100	24	0.038	0.148	6.8	21.84	1.88	0.624	1.79	0.950
F155C, quartz diorite lenses														
669461 7094784 NAD1983, UTM Zone 19N														
11217-046.1	86	1	77	2.4E-4	28	24	0.409	-0.005	53.3	5.03	1.88	0.327	1.54	0.818
11217-094.1	409	4	98	1.9E-5	45	118	0.033	0.002	23.1	5.21	1.40	0.336	1.36	0.969
11217-024.1	277	3	64	3.4E-5	41	79	0.058	0.002	31.5	5.17	1.44	0.331	1.38	0.955
11217-009.1	413	4	112	----	---	118	0.000	0.003	12.0	5.21	1.39	0.334	1.35	0.973
11217-020.2	187	2	85	----	---	54	0.000	0.004	15.7	5.27	1.82	0.334	1.75	0.965
11217-023.1	421	5	117	1.9E-5	45	118	0.033	0.002	20.4	5.19	1.49	0.328	1.35	0.909
11217-008.1	305	4	189	2.3E-5	50	88	0.040	0.004	17.6	5.32	1.44	0.335	1.38	0.956
~~11217-005.1~~	~~194~~	~~4~~	~~141~~	~~1.1E-4~~	~~28~~	~~57~~	~~0.186~~	~~0.004~~	~~37.2~~	~~5.92~~	~~1.64~~	~~0.343~~	~~1.42~~	~~0.866~~
11217-021.2	1579	115	72	6.7E-6	32	657	0.012	0.022	3.3	11.80	1.45	0.485	1.36	0.937

			Age (Ma)						
$\frac{Th}{U}$	$\frac{^{207*}Pb}{^{206*}Pb}$	% ±	$\frac{^{206*}Pb}{^{238}U}$	±	$\frac{^{207*}Pb}{^{206*}Pb}$	±	Disc. %	zonation	notes
0.39	*0.1976*	*0.3*	*2778*	*31*	*2806*	*5*	*1.2*	*osc*	
0.53	*0.1980*	*0.2*	*2812*	*30*	*2810*	*2*	*-0.1*	*osc*	
0.33	*0.1980*	*0.3*	*2809*	*31*	*2810*	*4*	*0.0*	*osc*	
0.51	*0.1981*	*0.8*	*2723*	*32*	*2811*	*12*	*3.8*	*osc*	
0.46	*0.1983*	*0.3*	*2723*	*31*	*2812*	*5*	*3.9*	*osc*	
0.37	*0.1993*	*0.4*	*2742*	*34*	*2820*	*6*	*3.4*	*osc*	
0.41	0.2024	0.3	2793	31	2846	5	2.3	osc	
0.52	0.2057	0.6	2894	39	2872	10	-0.9	unzoned	
0.62	0.2113	0.4	2825	34	2916	7	3.8	osc	
0.64	0.2133	0.2	2914	32	2931	4	0.7	irregular	
0.60	0.2136	0.6	2912	39	2933	10	0.9	osc	
0.38	0.2166	0.3	2861	32	2956	4	4.0	osc	
0.67	0.2172	0.6	2905	40	2960	10	2.3	osc	
0.56	0.2184	0.3	3021	35	2969	5	-2.2	osc	
0.57	0.2194	0.3	2974	34	2977	5	0.1	osc	
0.64	0.2196	0.2	2995	33	2978	4	-0.7	osc	
0.63	0.2200	0.4	2988	35	2981	6	-0.3	osc	
0.61	0.2227	0.4	2973	35	3000	6	1.1	osc	
0.14	0.2420	0.6	3089	37	3133	10	1.8	irregular	
0.57	0.2539	0.6	3125	44	3209	9	3.3	irregular	
13SUB-155C, diorite									
669461 7094784 NAD1983, UTM Zone 19N									
0.01	0.1116	1.1	1824	24	1826	20	0.1	unzoned	
0.01	0.1126	0.3	1866	22	1842	6	-1.5	unzoned	
0.01	0.1133	0.4	1844	22	1853	8	0.6	unzoned	
0.01	0.1134	0.3	1855	22	1854	6	-0.1	unzoned	
0.01	0.1146	0.5	1856	28	1874	9	1.1	unzoned	
0.01	0.1148	0.6	1827	22	1877	11	3.0	unzoned	
0.01	0.1151	0.4	1863	22	1882	8	1.2	unzoned	
~~0.02~~	~~0.1251~~	~~0.8~~	~~1902~~	~~23~~	~~2030~~	~~14~~	~~7.3~~	~~mxed~~	~~incidental overlap of domains~~
0.08	0.1766	0.5	2548	29	2621	8	3.4	unzoned	

APPENDIX 4A - SHRIMP U-Pb isotopic data from snow bowl area samples

Spot name	U (ppm)	Th (ppm)	Yb (ppm)	$^{204}Pb/^{206}Pb$	% ±	$^{206}Pb^*$ (ppm)	$f(206)^{204}$ %	$^{208*}Pb/^{206*}Pb$	% ±	$^{207*}Pb/^{235}U$	% ±	$^{206*}Pb/^{238}U$	% ±	Corr Coeff
11217-111.1	2241	190	105	3.7E-6	33	996	0.006	0.025	1.3	12.89	1.41	0.518	1.37	0.977
~~11217-024.2~~	~~1010~~	~~83~~	~~247~~	~~1.1E-4~~	~~10~~	~~422~~	~~0.191~~	~~0.022~~	~~5.7~~	~~12.20~~	~~1.35~~	~~0.487~~	~~1.33~~	~~0.982~~
11217-087.1	1571	181	141	3.4E-6	41	707	0.006	0.033	2.4	13.23	1.39	0.524	1.37	0.984
11217-021.1	1633	105	144	1.5E-5	19	732	0.025	0.018	1.9	13.21	1.37	0.522	1.35	0.984
11217-006.1	1983	185	106	3.8E-6	38	872	0.007	0.028	1.5	12.95	1.35	0.512	1.31	0.975
11217-014.2	2131	633	387	3.8E-6	35	968	0.007	0.087	0.8	13.39	1.31	0.529	1.31	0.997
11217-106.2	1435	365	103	3.6E-6	45	642	0.006	0.074	1.0	13.23	1.36	0.521	1.35	0.995
11217-014.1	1678	347	286	6.6E-6	29	734	0.011	0.060	1.0	12.95	1.33	0.509	1.31	0.989
11217-026.2	*1776*	*223*	*166*	*1.5E-5*	*46*	*767*	*0.026*	*0.038*	*1.5*	*12.81*	*1.32*	*0.503*	*1.31*	*0.996*
11217-020.1	*1138*	*166*	*50*	*5.8E-6*	*35*	*520*	*0.010*	*0.043*	*1.4*	*13.57*	*1.45*	*0.532*	*1.32*	*0.910*
11217-036.1	*1975*	*499*	*340*	*5.0E-6*	*30*	*895*	*0.009*	*0.074*	*0.8*	*13.47*	*1.35*	*0.528*	*1.31*	*0.975*
11217-064.2	*1639*	*139*	*136*	*8.0E-6*	*28*	*716*	*0.014*	*0.024*	*1.7*	*12.99*	*1.36*	*0.509*	*1.34*	*0.987*
11217-087.2	*2108*	*317*	*196*	*4.7E-6*	*32*	*962*	*0.008*	*0.043*	*1.1*	*13.57*	*1.35*	*0.531*	*1.35*	*0.997*
11217-110.2	*1888*	*197*	*167*	*7.4E-6*	*28*	*807*	*0.013*	*0.031*	*1.4*	*12.72*	*1.39*	*0.498*	*1.38*	*0.990*
11217-026.1	*1121*	*121*	*143*	*5.5E-6*	*38*	*511*	*0.010*	*0.033*	*1.6*	*13.56*	*1.38*	*0.530*	*1.37*	*0.996*
11217-041.1	*2893*	*269*	*221*	*1.9E-6*	*41*	*1339*	*0.003*	*0.028*	*1.1*	*13.78*	*1.42*	*0.539*	*1.32*	*0.928*
11217-057.2	1543	207	76	4.5E-6	38	697	0.008	0.039	1.3	13.54	1.33	0.526	1.32	0.990
11217-106.1	1484	228	71	3.6E-6	41	672	0.006	0.046	1.2	13.58	1.43	0.527	1.37	0.959
11217-057.1	1108	148	40	1.6E-6	71	505	0.003	0.042	3.9	13.69	1.40	0.530	1.37	0.977
11217-040.2	1570	260	184	5.7E-6	32	721	0.010	0.049	1.1	13.85	1.35	0.535	1.34	0.996
~~11217-100.1~~	~~1001~~	~~48~~	~~178~~	~~4.5E-6~~	~~45~~	~~448~~	~~0.008~~	~~0.013~~	~~2.8~~	~~13.75~~	~~1.33~~	~~0.521~~	~~1.32~~	~~0.995~~
11217-040.1	397	9	408	1.4E-5	41	186	0.024	0.006	8.1	14.56	1.37	0.544	1.35	0.988
11217-110.1	1165	47	546	6.2E-6	35	545	0.011	0.011	2.9	14.64	1.38	0.545	1.37	0.995
11217-111.2	3541	242	349	3.6E-6	24	1817	0.006	0.021	3.5	16.25	1.60	0.597	1.50	0.943
11217-064.1	904	25	672	1.4E-5	23	473	0.024	0.008	3.5	17.02	1.46	0.608	1.45	0.990
F155A, prophyroclastic monzogranite gneiss														
669461 7094784 NAD 1983 UTM Zone 19N														
~~11216-041.1~~	~~191~~	~~44~~	~~101~~	~~8.4E-4~~	~~24~~	~~81~~	~~1.463~~	~~0.081~~	~~9.7~~	~~12.46~~	~~2.04~~	~~0.492~~	~~1.44~~	~~0.709~~
11216-102.1	206	143	167	1.3E-5	58	90	0.023	0.201	1.6	13.00	1.43	0.511	1.39	0.978
11216-068.1	362	261	259	1.6E-5	41	160	0.027	0.214	1.2	13.15	1.49	0.513	1.47	0.988
11216-059.1	2154	223	311	3.9E-6	32	990	0.007	0.031	2.4	13.74	1.34	0.535	1.34	0.998

			Age (Ma)						
Th/U	$^{207*}Pb/^{206*}Pb$	% ±	$^{206*}Pb/^{238}U$	±	$^{207*}Pb/^{206*}Pb$	±	Disc. %	zonation	notes
0.09	0.1806	0.3	2689	30	2658	5	-1.4	unzoned	
~~0.08~~	~~0.1819~~	~~0.3~~	~~2556~~	~~28~~	~~2670~~	~~4~~	~~5.2~~	~~mixed~~	~~incidental overlap of domains~~
0.12	0.1832	0.2	2716	30	2682	4	-1.6	unzoned	
0.07	0.1835	0.2	2707	30	2685	4	-1.0	unzoned	
0.10	0.1836	0.3	2664	29	2685	5	1.0	unzoned	
0.31	0.1836	0.1	2737	29	2686	2	-2.3	unzoned	
0.26	0.1840	0.1	2704	30	2690	2	-0.7	unzoned	
0.21	0.1845	0.2	2653	29	2693	3	1.8	unzoned	
0.13	*0.1847*	*0.1*	*2626*	*28*	*2696*	*2*	*3.1*	*unzoned*	
0.15	*0.1849*	*0.6*	*2751*	*30*	*2698*	*10*	*-2.5*	*unzoned*	
0.26	*0.1851*	*0.3*	*2732*	*29*	*2699*	*5*	*-1.5*	*unzoned*	
0.09	*0.1852*	*0.2*	*2651*	*29*	*2700*	*4*	*2.2*	*unzoned*	
0.16	*0.1854*	*0.1*	*2746*	*30*	*2702*	*2*	*-2.0*	*unzoned*	
0.11	*0.1854*	*0.2*	*2603*	*29*	*2702*	*3*	*4.4*	*unzoned*	
0.11	*0.1855*	*0.1*	*2743*	*31*	*2703*	*2*	*-1.8*	*unzoned*	
0.10	*0.1855*	*0.5*	*2778*	*30*	*2703*	*9*	*-3.4*	*unzoned*	
0.14	0.1868	0.2	2724	29	2714	3	-0.4	unzoned	
0.16	0.1868	0.4	2730	30	2714	7	-0.7	unzoned	
0.14	0.1872	0.3	2743	31	2718	5	-1.1	unzoned	
0.17	0.1879	0.1	2761	30	2724	2	-1.7	unzoned	
~~0.05~~	~~0.1915~~	~~0.1~~	~~2702~~	~~29~~	~~2755~~	~~2~~	~~2.4~~	~~mixed~~	~~incidental overlap of domains~~
0.02	0.1941	0.2	2801	31	2777	3	-1.1	irregular	
0.04	0.1949	0.1	2803	31	2784	2	-0.9	irregular	
0.07	0.1973	0.5	3019	36	2804	9	-9.6	irregular	
0.03	0.2029	0.2	3064	35	2850	3	-9.4	irregular	

13SUB-F155A, Bt monzogranite

669461 7094784 NAD 1983 UTM Zone 19N

~~0.24~~	~~0.1838~~	~~1.4~~	~~2578~~	~~31~~	~~2687~~	~~24~~	~~4.9~~	~~osc~~	
0.72	0.1845	0.3	2660	30	2694	5	1.5	unzoned	
0.74	0.1859	0.2	2670	32	2706	4	1.6	unzoned	
0.11	0.1864	0.1	2761	30	2710	1	-2.3	unzoned	

APPENDIX 4A - SHRIMP U-Pb isotopic data from snow bowl area samples

Spot name	U (ppm)	Th (ppm)	Yb (ppm)	$^{204}Pb/^{206}Pb$	% ±	$^{206}Pb^*$ (ppm)	$f(206)^{204}$ %	$^{208*}Pb/^{206*}Pb$	% ±	$^{207*}Pb/^{235}U$	% ±	$^{206*}Pb/^{238}U$	% ±	Corr Coeff
11216-020.1	595	411	309	1.2E-5	35	266	0.021	0.201	0.9	13.36	1.39	0.519	1.38	0.992
11216-047.1	203	148	152	9.1E-6	71	90	0.016	0.216	1.5	13.23	1.43	0.514	1.40	0.978
11216-011.1	316	121	194	4.9E-5	24	140	0.085	0.112	1.7	13.29	1.38	0.516	1.36	0.984
11216-108.1	602	186	243	6.1E-6	50	271	0.011	0.090	1.4	13.49	1.42	0.524	1.41	0.991
11216-113.1	262	196	238	4.1E-5	30	118	0.071	0.222	1.4	13.57	1.45	0.526	1.38	0.952
11216-107.1	471	237	314	5.9E-6	58	210	0.010	0.146	1.2	13.42	1.41	0.518	1.34	0.952
~~11216-041.2~~	~~456~~	~~100~~	~~193~~	~~-5.7E-6~~	~~58~~	~~206~~	~~-0.010~~	~~0.065~~	~~1.8~~	~~13.61~~	~~1.36~~	~~0.526~~	~~1.34~~	~~0.990~~
11216-089.2	3062	147	857	3.0E-6	30	1456	0.005	0.014	1.5	14.34	1.36	0.554	1.36	0.999
11216-014.1	242	175	187	1.5E-5	50	108	0.026	0.207	1.4	13.53	1.41	0.522	1.38	0.981
11216-005.1	221	160	170	2.9E-5	38	98	0.050	0.209	1.5	13.45	1.46	0.519	1.39	0.953
11216-036.1	547	179	281	1.6E-6	100	242	0.003	0.096	1.3	13.35	1.35	0.515	1.33	0.992
11216-026.1	200	181	244	1.9E-5	50	89	0.032	0.262	1.4	13.42	1.44	0.517	1.40	0.977
11216-008.1	322	334	322	2.8E-6	100	145	0.005	0.301	1.0	13.58	1.60	0.523	1.55	0.971
11216-063.1	244	187	173	7.9E-6	71	111	0.014	0.232	1.4	13.70	1.41	0.528	1.39	0.981
11216-022.1	592	223	258	1.1E-5	38	273	0.019	0.107	1.3	14.00	1.35	0.538	1.34	0.991
11216-069.1	619	350	404	9.0E-6	41	280	0.016	0.165	1.0	13.69	1.34	0.526	1.33	0.992
11216-021.1	263	204	178	2.5E-5	38	119	0.043	0.221	1.3	13.66	1.40	0.525	1.38	0.982
11216-108.2	446	274	283	2.0E-6	100	199	0.004	0.180	1.1	13.55	1.38	0.520	1.35	0.974
11216-096.2	241	161	170	-2.7E-5	41	109	-0.046	0.200	1.6	13.65	1.43	0.524	1.40	0.978
11216-103.2	447	107	94	3.2E-5	25	200	0.056	0.067	3.2	13.58	1.53	0.520	1.34	0.876
11216-061.1	282	174	196	1.0E-4	21	124	0.180	0.181	1.5	13.40	1.40	0.514	1.37	0.979
11216-070.1	588	620	419	3.3E-6	71	267	0.006	0.311	0.8	13.82	1.43	0.529	1.42	0.992
11216-043.1	363	187	234	---	---	163	0.000	0.152	1.3	13.65	1.47	0.523	1.45	0.989
11216-012.2	*3290*	*3340*	*487*	*---*	*50*	*1561*	*0.002*	*0.296*	*0.6*	*14.47*	*1.39*	*0.552*	*1.38*	*0.991*
11216-031.1	*1641*	*1747*	*433*	*3.1E-6*	*41*	*771*	*0.005*	*0.307*	*0.4*	*14.37*	*1.34*	*0.547*	*1.34*	*0.997*
11216-001.1	*1246*	*1064*	*387*	*3.4E-5*	*16*	*572*	*0.059*	*0.251*	*0.6*	*14.06*	*1.32*	*0.535*	*1.32*	*0.996*
11216-030.1	*2068*	*1325*	*642*	*5.0E-6*	*28*	*979*	*0.009*	*0.187*	*0.5*	*14.52*	*1.36*	*0.551*	*1.36*	*0.998*
11216-083.1	*3639*	*3477*	*520*	*---*	*58*	*1788*	*0.001*	*0.275*	*0.3*	*15.07*	*1.43*	*0.572*	*1.42*	*0.995*
11216-012.1	*2036*	*1373*	*655*	*---*	*71*	*980*	*0.001*	*0.198*	*0.9*	*14.77*	*1.47*	*0.560*	*1.47*	*0.998*
11216-054.1	*811*	*417*	*294*	*----*	*---*	*378*	*0.000*	*0.151*	*0.8*	*14.34*	*1.33*	*0.543*	*1.32*	*0.995*
11216-045.1	*867*	*535*	*476*	*---*	*100*	*395*	*0.002*	*0.182*	*0.8*	*14.04*	*1.33*	*0.531*	*1.32*	*0.994*
11216-103.1	*689*	*277*	*187*	*8.9E-6*	*38*	*316*	*0.015*	*0.118*	*1.1*	*14.15*	*1.34*	*0.534*	*1.33*	*0.993*

			Age (Ma)						
Th/U	$^{207*}Pb/^{206*}Pb$	% ±	$^{206*}Pb/^{238}U$	±	$^{207*}Pb/^{206*}Pb$	±	Disc. %	zonation	notes
0.71	0.1865	0.2	2696	30	2712	3	0.7	unzoned	
0.75	0.1866	0.3	2675	31	2712	5	1.7	unzoned	
0.39	0.1867	0.2	2684	30	2713	4	1.3	unzoned	
0.32	0.1868	0.2	2716	31	2714	3	-0.1	unzoned	
0.77	0.1872	0.4	2724	31	2718	7	-0.3	unzoned	
0.52	0.1878	0.4	2692	30	2723	7	1.4	unzoned	
~~0.23~~	~~0.1879~~	~~0.2~~	~~2723~~	~~30~~	~~2724~~	~~3~~	~~0.0~~	~~mixed~~	
0.05	0.1879	0.1	2840	31	2724	1	-5.3	unzoned	
0.75	0.1880	0.3	2706	30	2725	4	0.8	osc	
0.75	0.1880	0.4	2694	31	2725	7	1.4	osc	
0.34	0.1881	0.2	2678	29	2726	3	2.2	unzoned	
0.93	0.1882	0.3	2687	31	2726	5	1.7	unzoned	
1.07	0.1883	0.4	2712	34	2727	6	0.7	osc	
0.79	0.1883	0.3	2732	31	2728	5	-0.2	osc	
0.39	0.1888	0.2	2776	30	2731	3	-2.0	unzoned	
0.58	0.1888	0.2	2725	30	2731	3	0.3	unzoned	
0.80	0.1888	0.3	2719	31	2732	4	0.6	unzoned	
0.64	0.1889	0.3	2701	30	2732	5	1.4	unzoned	
0.69	0.1890	0.3	2715	31	2734	5	0.8	osc	
0.25	0.1892	0.7	2701	30	2735	12	1.5	osc	
0.64	0.1892	0.3	2673	30	2735	5	2.8	osc	
1.09	0.1893	0.2	2739	32	2736	3	-0.1	unzoned	
0.53	0.1894	0.2	2712	32	2737	4	1.1	unzoned	
1.05	*0.1900*	*0.2*	*2836*	*32*	*2742*	*3*	*-4.2*	*osc*	
1.10	*0.1906*	*0.1*	*2812*	*30*	*2748*	*2*	*-2.9*	*osc*	
0.88	*0.1908*	*0.1*	*2761*	*30*	*2749*	*2*	*-0.5*	*osc*	
0.66	*0.1910*	*0.1*	*2831*	*31*	*2751*	*1*	*-3.6*	*osc*	
0.99	*0.1911*	*0.1*	*2916*	*33*	*2752*	*2*	*-7.5*	*osc*	
0.70	*0.1911*	*0.1*	*2868*	*34*	*2752*	*2*	*-5.3*	*osc*	
0.53	*0.1917*	*0.1*	*2795*	*30*	*2757*	*2*	*-1.7*	*osc*	
0.64	*0.1919*	*0.1*	*2744*	*30*	*2759*	*2*	*0.7*	*osc*	
0.41	*0.1921*	*0.2*	*2759*	*30*	*2760*	*3*	*0.0*	*osc*	

APPENDIX 4A - SHRIMP U-Pb isotopic data from snow bowl area samples

Spot name	U (ppm)	Th (ppm)	Yb (ppm)	$^{204}Pb/^{206}Pb$	% ±	$^{206}Pb^*$ (ppm)	$f(206)^{204}$ %	$^{208*}Pb/^{206*}Pb$	% ±	$^{207*}Pb/^{235}U$	% ±	$^{206*}Pb/^{238}U$	% ±	Corr Coeff
11216-086.1	*1383*	*838*	*436*	*6.6E-5*	*51*	*649*	*0.115*	*0.179*	*1.2*	*14.49*	*1.36*	*0.546*	*1.32*	*0.968*
11216-023.1	137	84	307	2.6E-5	50	64	0.045	0.179	2.0	14.71	1.48	0.539	1.44	0.971
11216-096.1	89	26	193	5.8E-5	45	42	0.101	0.086	4.1	15.23	1.63	0.552	1.55	0.954
11216-089.1	609	149	313	7.2E-6	45	286	0.012	0.071	3.3	15.09	2.28	0.546	2.20	0.966
11216-025.1	230	111	301	1.6E-5	50	105	0.027	0.141	1.7	14.87	1.41	0.529	1.38	0.982
11216-017.1	193	99	450	1.4E-5	58	91	0.024	0.149	1.9	15.77	1.43	0.552	1.40	0.979
11216-087.1	491	287	614	3.2E-6	71	251	0.005	0.165	1.0	18.10	1.49	0.595	1.48	0.992
F150A, prophyroclastic monzogranite gneiss														
669259 7094583 NAD1983, UTM Zone 19N														
11186-064.1	17	1	26	9.5E-4	30	5	1.652	-0.014	81.8	4.68	4.71	0.320	2.24	0.475
11186-058.2	67	5	43	-2.0E-5	100	19	-0.034	0.026	9.8	5.03	1.73	0.324	1.54	0.893
~~11186-058.1~~	~~186~~	~~8~~	~~60~~	~~3.9E-4~~	~~15~~	~~59~~	~~0.679~~	~~0.019~~	~~14.6~~	~~7.74~~	~~2.65~~	~~0.367~~	~~2.01~~	~~0.758~~
~~11186-030.1~~	~~84~~	~~47~~	~~106~~	~~9.2E-5~~	~~38~~	~~31~~	~~0.160~~	~~0.200~~	~~10.6~~	~~9.85~~	~~5.59~~	~~0.429~~	~~4.35~~	~~0.779~~
11186-007.1	163	113	102	6.0E-5	32	70	0.104	0.204	1.8	12.76	1.47	0.504	1.42	0.969
11186-065.1	1059	47	137	6.1E-6	35	458	0.011	0.012	2.9	12.82	1.32	0.504	1.32	0.996
~~11186-023.1~~	~~89~~	~~82~~	~~91~~	~~3.1E-5~~	~~58~~	~~39~~	~~0.054~~	~~0.249~~	~~2.2~~	~~13.16~~	~~2.89~~	~~0.517~~	~~2.28~~	~~0.790~~
11186-031.1	*268*	*204*	*113*	*2.4E-5*	*38*	*119*	*0.041*	*0.227*	*1.3*	*13.22*	*1.40*	*0.515*	*1.37*	*0.982*
11186-005.1	*150*	*128*	*128*	*3.7E-5*	*41*	*66*	*0.065*	*0.246*	*1.7*	*13.08*	*1.47*	*0.509*	*1.43*	*0.970*
11186-071.1	*362*	*339*	*182*	*1.4E-5*	*45*	*158*	*0.023*	*0.274*	*1.0*	*13.13*	*1.38*	*0.509*	*1.36*	*0.986*
11186-057.1	*236*	*169*	*108*	*1.0E-5*	*58*	*105*	*0.018*	*0.210*	*1.3*	*13.36*	*1.40*	*0.518*	*1.37*	*0.983*
11186-062.1	*319*	*365*	*202*	*2.5E-5*	*35*	*134*	*0.044*	*0.329*	*1.0*	*12.60*	*1.39*	*0.489*	*1.36*	*0.983*
11186-016.1	*297*	*118*	*111*	*1.3E-5*	*50*	*129*	*0.022*	*0.112*	*1.8*	*13.08*	*1.50*	*0.507*	*1.37*	*0.915*
11186-061.1	*228*	*134*	*94*	*8.9E-6*	*71*	*98*	*0.015*	*0.174*	*1.7*	*12.90*	*1.43*	*0.499*	*1.40*	*0.979*
11186-077.1	*275*	*124*	*117*	*2.5E-5*	*38*	*121*	*0.043*	*0.129*	*1.8*	*13.30*	*1.40*	*0.514*	*1.38*	*0.982*
11186-051.1	*365*	*86*	*135*	*3.2E-4*	*9*	*158*	*0.559*	*0.073*	*2.5*	*13.04*	*1.38*	*0.504*	*1.35*	*0.978*
11186-072.1	*421*	*109*	*153*	*1.8E-5*	*35*	*188*	*0.030*	*0.079*	*1.8*	*13.43*	*1.36*	*0.519*	*1.35*	*0.988*
11186-039.1	*86*	*88*	*94*	*6.7E-5*	*41*	*38*	*0.115*	*0.288*	*3.7*	*13.18*	*1.75*	*0.509*	*1.53*	*0.873*
11186-055.1	*262*	*155*	*102*	*5.0E-5*	*27*	*114*	*0.087*	*0.178*	*2.8*	*13.15*	*1.45*	*0.506*	*1.38*	*0.951*
11186-075.1	*217*	*161*	*123*	*1.7E-5*	*50*	*97*	*0.030*	*0.222*	*1.5*	*13.51*	*1.42*	*0.520*	*1.39*	*0.979*
11186-010.1	*108*	*92*	*101*	*8.3E-5*	*32*	*47*	*0.144*	*0.251*	*1.9*	*13.25*	*1.61*	*0.509*	*1.47*	*0.917*
11186-059.1	*138*	*116*	*115*	*1.7E-5*	*58*	*61*	*0.030*	*0.235*	*1.6*	*13.42*	*1.46*	*0.516*	*1.42*	*0.973*

			Age (Ma)						
Th/U	$^{207*}Pb/^{206*}Pb$	% ±	$^{206*}Pb/^{238}U$	±	$^{207*}Pb/^{206*}Pb$	±	Disc. %	zonation	notes
0.63	*0.1922*	*0.3*	*2811*	*30*	*2761*	*6*	*-2.2*	*osc*	
0.63	0.1980	0.4	2778	32	2810	6	1.4	osc	
0.30	0.2000	0.5	2835	36	2826	8	-0.4	irregular	
0.25	0.2003	0.6	2810	50	2828	10	0.8	irregular	
0.50	0.2039	0.3	2736	31	2858	4	5.2	irregular	
0.53	0.2072	0.3	2833	32	2884	5	2.2	unzoned	
0.60	0.2205	0.2	3012	35	2984	3	-1.1	irregular	
13SUB-F150A, monzogranite									
669259 7094583 NAD1983, UTM Zone 19N									
0.05	0.1060	4.1	1791	35	1732	76	-3.9	rim	
0.08	0.1127	0.8	1810	24	1843	14	2.1	rim	
~~0.05~~	~~0.1530~~	~~1.7~~	~~2016~~	~~35~~	~~2380~~	~~29~~	~~17.8~~	~~rim~~	~~incidental overlap of domains~~
~~0.58~~	~~0.1665~~	~~3.5~~	~~2301~~	~~84~~	~~2523~~	~~59~~	~~10.5~~	~~unzoned~~	~~fracture rich area~~
0.72	0.1836	0.4	2631	31	2686	6	2.5	irregular	
0.05	0.1846	0.1	2629	28	2695	2	3.0	osc	
~~0.95~~	~~0.1847~~	~~1.8~~	~~2686~~	~~50~~	~~2695~~	~~29~~	~~0.4~~	~~unzoned~~	~~incidental overlap of domains~~
0.79	*0.1861*	*0.3*	*2679*	*30*	*2708*	*4*	*1.3*	*osc*	
0.88	*0.1864*	*0.4*	*2652*	*31*	*2711*	*6*	*2.6*	*unzoned*	
0.97	*0.1869*	*0.2*	*2654*	*30*	*2715*	*4*	*2.7*	*unzoned*	
0.74	*0.1870*	*0.3*	*2692*	*30*	*2716*	*4*	*1.1*	*osc*	
1.18	*0.1871*	*0.3*	*2564*	*29*	*2717*	*4*	*6.8*	*unzoned*	
0.41	*0.1873*	*0.6*	*2642*	*30*	*2719*	*10*	*3.4*	*unzoned*	
0.60	*0.1874*	*0.3*	*2610*	*30*	*2720*	*5*	*4.9*	*unzoned*	
0.47	*0.1876*	*0.3*	*2675*	*30*	*2721*	*4*	*2.1*	*unzoned*	
0.24	*0.1876*	*0.3*	*2631*	*29*	*2721*	*5*	*4.1*	*osc*	
0.27	*0.1878*	*0.2*	*2694*	*30*	*2723*	*3*	*1.3*	*osc*	
1.05	*0.1879*	*0.9*	*2651*	*33*	*2724*	*14*	*3.3*	*unzoned*	
0.61	*0.1884*	*0.4*	*2641*	*30*	*2728*	*7*	*3.9*	*osc*	
0.77	*0.1886*	*0.3*	*2698*	*31*	*2730*	*5*	*1.4*	*unzoned*	
0.88	*0.1886*	*0.6*	*2654*	*32*	*2730*	*11*	*3.4*	*osc*	
0.86	*0.1887*	*0.3*	*2682*	*31*	*2731*	*6*	*2.2*	*osc*	

APPENDIX 4A - SHRIMP U-Pb isotopic data from snow bowl area samples

Spot name	U (ppm)	Th (ppm)	Yb (ppm)	$^{204}Pb/^{206}Pb$	% ±	$^{206}Pb^*$ (ppm)	$f(206)^{204}$ %	$^{208*}Pb/^{206*}Pb$	% ±	$^{207*}Pb/^{235}U$	% ±	$^{206*}Pb/^{238}U$	% ±	Corr Coeff
~~11186-018.1~~	~~474~~	~~58~~	~~121~~	~~3.1E-5~~	~~24~~	~~211~~	~~0.053~~	~~0.035~~	~~4.9~~	~~13.48~~	~~1.35~~	~~0.517~~	~~1.34~~	~~0.990~~
~~11186-048.1~~	~~951~~	~~96~~	~~231~~	~~1.3E-5~~	~~25~~	~~421~~	~~0.023~~	~~0.031~~	~~8.3~~	~~13.41~~	~~1.50~~	~~0.515~~	~~1.41~~	~~0.939~~
11186-028.1	569	366	226	3.2E-5	22	250	0.055	0.187	1.0	13.74	1.35	0.512	1.34	0.991
11186-027.1	299	62	106	1.2E-5	50	135	0.021	0.064	7.9	14.20	1.40	0.527	1.38	0.984
11186-025.1	151	70	195	5.7E-6	100	67	0.010	0.128	2.3	14.05	1.46	0.515	1.42	0.973
F152A, mag-bearing monzogranite gneiss														
669280 7094606 NAD1983 UTM Zone 19N														
11188-003.2	8	0	39	3.9E-4	71	2	0.681	0.006	212.6	5.02	5.33	0.342	3.02	0.567
11188-046.1	15	2	66	4.7E-4	45	4	0.821	0.025	40.7	5.12	3.93	0.337	2.35	0.596
11188-059.2	20	2	61	1.5E-4	71	6	0.259	0.022	28.2	5.19	2.88	0.335	2.12	0.736
~~11188-057.1~~	~~14~~	~~2~~	~~38~~	~~-4.3E-4~~	~~50~~	~~4~~	~~-0.753~~	~~0.072~~	~~15.8~~	~~5.79~~	~~3.75~~	~~0.342~~	~~2.42~~	~~0.645~~
~~11188-113.1~~	~~8~~	~~1~~	~~54~~	~~-5.6E-4~~	~~58~~	~~2~~	~~-0.963~~	~~0.072~~	~~20.7~~	~~5.78~~	~~4.99~~	~~0.331~~	~~3.03~~	~~0.609~~
11188-013.1	*46*	*95*	*150*	*2.2E-5*	*100*	*21*	*0.038*	*0.598*	*2.0*	*13.70*	*1.85*	*0.533*	*1.72*	*0.933*
11188-086.1	*50*	*95*	*75*	*1.3E-4*	*38*	*22*	*0.229*	*0.555*	*2.0*	*13.19*	*1.80*	*0.512*	*1.66*	*0.924*
11188-103.1	*60*	*115*	*92*	*7.5E-5*	*45*	*27*	*0.130*	*0.552*	*3.9*	*13.26*	*1.70*	*0.515*	*1.60*	*0.940*
11188-077.1	*76*	*71*	*106*	*4.7E-5*	*50*	*35*	*0.082*	*0.272*	*2.2*	*13.79*	*1.62*	*0.535*	*1.54*	*0.952*
11188-044.1	*65*	*123*	*173*	*1.2E-4*	*35*	*30*	*0.212*	*0.555*	*3.6*	*13.66*	*1.73*	*0.530*	*1.62*	*0.935*
11188-121.1	*37*	*125*	*91*	*1.9E-4*	*35*	*17*	*0.336*	*0.974*	*1.7*	*13.73*	*1.95*	*0.532*	*1.77*	*0.907*
11188-046.2	*154*	*49*	*103*	*-3.2E-5*	*45*	*68*	*-0.055*	*0.093*	*2.8*	*13.26*	*1.48*	*0.512*	*1.43*	*0.970*
11188-113.2	*47*	*106*	*102*	*1.7E-4*	*35*	*20*	*0.290*	*0.681*	*1.9*	*13.09*	*2.56*	*0.505*	*2.32*	*0.909*
11188-068.1	*88*	*83*	*91*	*2.1E-5*	*71*	*40*	*0.037*	*0.281*	*2.0*	*13.68*	*1.60*	*0.527*	*1.53*	*0.957*
11188-059.1	*46*	*79*	*148*	*1.6E-4*	*35*	*21*	*0.281*	*0.490*	*2.2*	*14.12*	*1.85*	*0.544*	*1.70*	*0.918*
11188-003.1	*125*	*61*	*114*	*3.1E-5*	*50*	*57*	*0.054*	*0.139*	*2.6*	*13.92*	*1.84*	*0.536*	*1.79*	*0.976*
11188-014.1	*98*	*60*	*105*	*1.5E-4*	*27*	*44*	*0.253*	*0.170*	*2.7*	*13.58*	*1.60*	*0.522*	*1.52*	*0.947*
11188-001.1	*80*	*69*	*106*	*1.2E-5*	*100*	*37*	*0.020*	*0.255*	*2.3*	*13.85*	*1.62*	*0.532*	*1.55*	*0.955*
11188-079.1	*92*	*87*	*119*	*1.0E-4*	*30*	*41*	*0.181*	*0.275*	*2.0*	*13.56*	*1.57*	*0.520*	*1.50*	*0.954*
11188-012.1	*90*	*59*	*106*	*6.7E-5*	*41*	*41*	*0.116*	*0.193*	*2.6*	*13.83*	*1.61*	*0.530*	*1.53*	*0.952*
11188-080.1	*34*	*64*	*131*	*4.9E-5*	*71*	*16*	*0.085*	*0.566*	*3.9*	*13.75*	*1.92*	*0.527*	*1.78*	*0.923*
11188-038.1	*99*	*143*	*94*	*3.0E-5*	*58*	*46*	*0.052*	*0.424*	*1.6*	*14.16*	*1.58*	*0.542*	*1.52*	*0.958*
11188-035.1	*32*	*66*	*120*	*1.5E-4*	*45*	*15*	*0.266*	*0.579*	*2.5*	*13.97*	*2.06*	*0.533*	*1.86*	*0.903*
11188-080.2	*90*	*65*	*77*	*3.0E-5*	*58*	*41*	*0.053*	*0.208*	*2.3*	*13.89*	*1.57*	*0.529*	*1.51*	*0.958*

			Age (Ma)						
Th/U	$^{207*}Pb/^{206*}Pb$	% ±	$^{206*}Pb/^{238}U$	±	$^{207*}Pb/^{206*}Pb$	±	Disc. %	zonation	notes
~~0.13~~	~~0.1889~~	~~0.2~~	~~2688~~	~~29~~	~~2733~~	~~3~~	~~2.0~~	~~osc~~	~~incidental overlap of domains~~
~~0.10~~	~~0.1890~~	~~0.5~~	~~2677~~	~~31~~	~~2733~~	~~9~~	~~2.5~~	~~osc~~	~~incidental overlap of domains~~
0.67	0.1947	0.2	2665	29	2782	3	5.2	osc	
0.21	0.1954	0.2	2730	31	2788	4	2.6	osc	
0.48	0.1980	0.3	2676	31	2810	6	5.8	osc	
13SUB-F152A, Mt monzogranite									
669280 7094606 NAD1983 UTM Zone 19N									
0.01	0.1065	4.4	1896	50	1740	80	-10.3	rim	
0.12	0.1100	3.2	1875	38	1800	57	-4.8	rim	
0.08	0.1123	1.9	1861	34	1838	35	-1.5	rim	
~~0.18~~	~~0.1228~~	~~2.9~~	~~1897~~	~~40~~	~~1998~~	~~51~~	~~5.8~~	~~mixed~~	~~incidental overlap of domains~~
~~0.10~~	~~0.1267~~	~~4.0~~	~~1844~~	~~49~~	~~2053~~	~~70~~	~~11.7~~	~~mixed~~	~~incidental overlap of domains~~
2.11	*0.1862*	*0.7*	*2756*	*39*	*2709*	*11*	*-2.1*	*irregular*	
1.95	*0.1867*	*0.7*	*2667*	*36*	*2713*	*11*	*2.1*	*irregular*	
1.97	*0.1867*	*0.6*	*2678*	*35*	*2713*	*10*	*1.6*	*irregular*	
0.97	*0.1869*	*0.5*	*2764*	*35*	*2715*	*8*	*-2.2*	*irregular*	
1.95	*0.1869*	*0.6*	*2742*	*36*	*2715*	*10*	*-1.2*	*irregular*	
3.52	*0.1873*	*0.8*	*2748*	*40*	*2718*	*13*	*-1.3*	*irregular*	
0.33	*0.1877*	*0.4*	*2667*	*31*	*2722*	*6*	*2.5*	*irregular*	
2.34	*0.1880*	*1.1*	*2636*	*50*	*2724*	*18*	*3.9*	*irregular*	
0.97	*0.1881*	*0.5*	*2731*	*34*	*2725*	*8*	*-0.2*	*irregular*	
1.79	*0.1883*	*0.7*	*2799*	*39*	*2728*	*12*	*-3.2*	*irregular*	
0.51	*0.1884*	*0.4*	*2766*	*40*	*2728*	*7*	*-1.7*	*irregular*	
0.63	*0.1886*	*0.5*	*2708*	*34*	*2730*	*8*	*0.9*	*osc*	
0.89	*0.1890*	*0.5*	*2748*	*35*	*2733*	*8*	*-0.7*	*osc*	
0.98	*0.1890*	*0.5*	*2701*	*33*	*2733*	*8*	*1.4*	*osc*	
0.68	*0.1893*	*0.5*	*2741*	*34*	*2736*	*8*	*-0.2*	*osc*	
1.93	*0.1894*	*0.7*	*2728*	*39*	*2737*	*12*	*0.4*	*osc*	
1.49	*0.1895*	*0.5*	*2793*	*34*	*2737*	*7*	*-2.5*	*irregular*	
2.11	*0.1901*	*0.9*	*2754*	*42*	*2743*	*15*	*-0.5*	*osc*	
0.74	*0.1903*	*0.4*	*2739*	*34*	*2745*	*7*	*0.3*	*osc*	

APPENDIX 4A - SHRIMP U-Pb isotopic data from snow bowl area samples

Spot name	U (ppm)	Th (ppm)	Yb (ppm)	$^{204}Pb/^{206}Pb$	% ±	$^{206}Pb^*$ (ppm)	$f(206)^{204}$ %	$^{208*}Pb/^{206*}Pb$	% ±	$^{207*}Pb/^{235}U$	% ±	$^{206*}Pb/^{238}U$	% ±	Corr Coeff
11188-033.1	*67*	*120*	*181*	*6.8E-5*	*45*	*31*	*0.118*	*0.514*	*1.8*	*14.32*	*3.18*	*0.546*	*2.84*	*0.895*

table notes:

Italicized and lighter toned data were used to calculate the weighted mean $^{207}Pb/^{206}Pb$ age.

Strikethrough data indicate analyses that were excluded from further calculations and discussion. These analyses had overlapping domains, were from fracture rich areas or otherwise yielded anomalous results (see individual notes for each instance).

Spot name follows the convention x-y-z; where x = sample number, y = grain number and z = spot number.

Errors are reported at 2σ uncertainty level unless otherwise noted.

			Age (Ma)						
$\frac{Th}{U}$	$\frac{^{207*}Pb}{^{206*}Pb}$	% ±	$\frac{^{206*}Pb}{^{238}U}$	±	$\frac{^{207*}Pb}{^{206*}Pb}$	±	Disc. %	zonation	notes
1.86	*0.1904*	*1.4*	*2807*	*65*	*2746*	*23*	*-2.8*	*irregular*	

table notes:

Italicized and lighter toned data were used to calculate the weighted mean $^{207}Pb/^{206}Pb$ age.

Strikethrough data indicate analyses that were excluded from further calculations and discussion. These analyses had overlapping domains, were from fracture rich areas or otherwise yielded anomalous results (see individual notes for each instance).

Spot name follows the convention x-y-z; where x = sample number, y = grain number and z = spot number.

Errors are reported at 2σ uncertainty level unless otherwise noted.

APPENDIX 4B - LASS-ICPMS U-Pb isotopic data from regional samples

spot name	U (ppm)	Th (ppm)	Pb (ppm)	$^{207}Pb/^{235}U$	±	$^{206}Pb/^{238}U$	±	$^{207}Pb/^{206}Pb$	$^{206}Pb/^{208}Pb$	±	Th/U	age (Ma) $^{206}Pb/^{238}U$	±	age (Ma) $^{207}Pb/^{206}Pb$	±	disc. %
H098A, tonalite gneiss																
692183 7154679 NAD 1983 UTM Zone 19N																
~~H098A - 11~~	~~1040~~	~~185~~	~~208~~	~~11.08~~	~~0.8~~	~~0.495~~	~~0.026~~	~~0.1629~~	~~0.1371~~	~~0.0062~~	~~0.18~~	~~2590~~	~~110~~	~~2481~~	~~49~~	~~-4.4~~
~~H098A - 20~~	~~1171~~	~~286~~	~~333~~	~~8.91~~	~~0.77~~	~~0.373~~	~~0.032~~	~~0.1734~~	~~0.1329~~	~~0.0022~~	~~0.23~~	~~2020~~	~~160~~	~~2590~~	~~11~~	~~22.0~~
H098A - 11 - 2	462	41.2	75.1	12.3	0.41	0.51	0.016	0.1766	0.1888	0.0067	0.09	2656	66	2620	11	-1.4
H098A - 9	678	17.96	56.7	11.7	0.14	0.4817	0.0062	0.177	0.352	0.043	0.03	2534	27	2624	14	3.4
H098A - 6	590	95	131	13.78	0.38	0.559	0.015	0.1786	0.177	0.013	0.13	2860	62	2639	15	-8.4
H098A - 15	141	85.5	106.1	12.71	0.2	0.5048	0.0088	0.1827	0.1357	0.0021	0.60	2633	38	2677	16	1.6
~~H098A - 17~~	~~685~~	~~136.2~~	~~175.3~~	~~10.51~~	~~0.39~~	~~0.417~~	~~0.017~~	~~0.1846~~	~~0.1391~~	~~0.0061~~	~~0.19~~	~~2243~~	~~77~~	~~2694~~	~~17~~	~~16.7~~
H098A - 8	231.1	61.8	95.6	14.18	0.18	0.5594	0.0074	0.1848	0.1637	0.0045	0.27	2863	31	2696	11	-6.2
H098A - 5	271	45.7	63.6	13.66	0.42	0.532	0.017	0.1855	0.157	0.01	0.15	2750	71	2702	24	-1.8
H098A - 12	*332*	*78*	*101*	*14.13*	*0.15*	*0.5469*	*0.0058*	*0.1889*	*0.1354*	*0.0038*	*0.22*	*2812*	*24*	*2732*	*9.6*	*-2.9*
H098A - 3	*272*	*75*	*60.8*	*14.39*	*0.16*	*0.55*	*0.0057*	*0.1896*	*0.0906*	*0.0047*	*0.23*	*2824*	*24*	*2739*	*8.4*	*-3.1*
H098A - 16	*468*	*124*	*160*	*12.95*	*0.3*	*0.4943*	*0.0096*	*0.1901*	*0.1461*	*0.0032*	*0.26*	*2587*	*42*	*2742*	*14*	*5.7*
H098A - 10 - 2	*291*	*32.3*	*59.4*	*13.23*	*0.8*	*0.508*	*0.029*	*0.1903*	*0.215*	*0.021*	*0.09*	*2640*	*130*	*2744*	*17*	*3.8*
H098A - 13	*227*	*42.9*	*70.9*	*14.3*	*0.21*	*0.5491*	*0.0072*	*0.1904*	*0.1825*	*0.0084*	*0.17*	*2820*	*30*	*2745*	*9.4*	*-2.7*
H098A - 1	*377*	*37*	*88.2*	*13.61*	*0.68*	*0.514*	*0.031*	*0.1924*	*0.38*	*0.11*	*0.07*	*2670*	*130*	*2761*	*37*	*3.3*
~~H098A - 7~~	~~285~~	~~19.1~~	~~65.4~~	~~13.43~~	~~0.68~~	~~0.502~~	~~0.023~~	~~0.1943~~	~~0.396~~	~~0.034~~	~~0.07~~	~~2619~~	~~99~~	~~2778~~	~~20~~	~~5.7~~
~~H098A - 19~~	~~530~~	~~64.8~~	~~100.6~~	~~8.19~~	~~0.35~~	~~0.307~~	~~0.014~~	~~0.1944~~	~~0.191~~	~~0.017~~	~~0.11~~	~~1721~~	~~71~~	~~2781~~	~~14~~	~~38.1~~
~~H098A - 2~~	~~192~~	~~46.9~~	~~91~~	~~16.7~~	~~1.2~~	~~0.615~~	~~0.041~~	~~0.196~~	~~0.209~~	~~0.014~~	~~0.27~~	~~3120~~	~~150~~	~~2792~~	~~18~~	~~-11.7~~
~~H098A - 4~~	~~142.5~~	~~53.2~~	~~76.8~~	~~15.54~~	~~0.17~~	~~0.5681~~	~~0.0062~~	~~0.1982~~	~~0.153~~	~~0.0027~~	~~0.36~~	~~2899~~	~~26~~	~~2811~~	~~12~~	~~-3.1~~
H098A - 10	157	62	79	15.65	0.48	0.576	0.017	0.1983	0.1495	0.0058	0.37	2929	72	2811	21	-4.2
H098A - 18	177	43.8	66.1	15.93	0.35	0.582	0.012	0.1986	0.1677	0.004	0.24	2956	48	2814	14	-5.0
H086A, tonalite gneiss																
719964 7118577 NAD1983, UTM Zone 19N																
~~H086A - 17~~	~~1625~~	~~41.8~~	~~57~~	~~11.92~~	~~0.59~~	~~0.552~~	~~0.032~~	~~0.1561~~	~~0.1528~~	~~0.0041~~	~~0.02~~	~~2820~~	~~130~~	~~2411~~	~~26~~	
H086A - 17 - 2	1145	26.5	39.9	10.9	0.18	0.4908	0.009	0.1614	0.1523	0.0033	0.02	2573	39	2470	11	
H086A - 11	1118	28.5	50	11.25	0.2	0.489	0.01	0.167	0.19	0.014	0.03	2563	45	2527	18	-1.4
H086A - 9	822	269	374	11.92	0.17	0.5096	0.0054	0.17	0.1536	0.0027	0.31	2654	23	2557	12	-3.8
H086A - 18	696	251	356	12.17	0.18	0.5162	0.0062	0.1712	0.1521	0.0039	0.34	2682	27	2568	12	-4.4
H086A - 14	537	43.4	61.5	11.77	0.23	0.4854	0.0079	0.1768	0.1619	0.0061	0.08	2550	35	2623	17	2.8

spot location	zonation	notes

H098A, tonalite gneiss

692183 7154679 NAD 1983 UTM Zone 19N

~~core~~	~~mixed~~	~~incidental overlap of domains~~
~~core~~	~~irregular~~	~~discordant - abundant cracks~~
core	unzoned	
rim	unzoned	
core	unzoned	
rim	unzoned	
~~core~~	~~unzoned~~	~~discordant~~
core	irregular	
single grain	unzoned	
core	*osc*	
core	*osc*	
core	*osc*	
core	*osc*	
core	*osc*	
core	*osc*	
~~rim~~	~~mixed~~	~~incidental overlap of domains~~
~~core~~	~~mixed~~	~~incidental overlap of domains~~
~~core~~	~~osc~~	~~discordant~~
~~core~~	~~mixed~~	~~incidental overlap of domains~~
core	irregular	
core	osc	

H086A, tonalite gneiss

719964 7118577 NAD1983, UTM Zone 19N

~~rim~~	~~unzoned~~
rim	unzoned
rim	unzoned
rim	unzoned
single grain	unzoned
rim	unzoned

APPENDIX 4B - LASS-ICPMS U-Pb isotopic data from regional samples

spot name	U (ppm)	Th (ppm)	Pb (ppm)	$^{207}Pb/^{235}U$	±	$^{206}Pb/^{238}U$	±	$^{207}Pb/^{206}Pb$	$^{206}Pb/^{208}Pb$	±	Th/U	age (Ma) $^{206}Pb/^{238}U$	±	age (Ma) $^{207}Pb/^{206}Pb$	±	disc. %
~~H086A - 4~~	~~515~~	~~16.9~~	~~57.5~~	~~15.41~~	~~0.49~~	~~0.626~~	~~0.018~~	~~0.17825~~	~~0.341~~	~~0.024~~	~~0.03~~	~~3128~~	~~70~~	~~2636~~	~~9.1~~	~~-18.7~~
~~H086A - 21 - 2~~	~~590~~	~~19~~	~~33.1~~	~~15.58~~	~~0.72~~	~~0.636~~	~~0.025~~	~~0.1784~~	~~0.208~~	~~0.016~~	~~0.02~~	~~3170~~	~~100~~	~~2637~~	~~23~~	~~-20.2~~
~~H086A - 22 - 2~~	~~302~~	~~19.2~~	~~31.2~~	~~13.05~~	~~0.48~~	~~0.519~~	~~0.019~~	~~0.1824~~	~~0.1639~~	~~0.006~~	~~0.06~~	~~2689~~	~~79~~	~~2674~~	~~17~~	~~-0.6~~
H086A - 7	254	34.2	53	13.16	0.15	0.5209	0.0073	0.1835	0.1629	0.0041	0.13	2702	31	2684	9.7	-0.7
~~H086A - 14 - 2~~	~~308.5~~	~~15~~	~~62.6~~	~~12.16~~	~~0.19~~	~~0.4694~~	~~0.0054~~	~~0.1884~~	~~0.425~~	~~0.03~~	~~0.05~~	~~2481~~	~~24~~	~~2727~~	~~15~~	~~9.0~~
H086A - 16	*189.4*	*84.5*	*116.6*	*13.65*	*0.16*	*0.5171*	*0.0054*	*0.1919*	*0.1457*	*0.0021*	*0.41*	*2686*	*23*	*2758*	*11*	*2.6*
H086A - 8	*189*	*108.4*	*141.5*	*14.27*	*0.12*	*0.5376*	*0.0045*	*0.193*	*0.1372*	*0.0021*	*0.55*	*2773*	*19*	*2767*	*9.3*	*-0.2*
H086A - 19	*123.8*	*57.4*	*77.9*	*13.59*	*0.32*	*0.508*	*0.011*	*0.194*	*0.1467*	*0.0048*	*0.42*	*2644*	*45*	*2775*	*14*	*4.7*
H086A - 15	*207.9*	*68*	*94*	*14.37*	*0.36*	*0.536*	*0.013*	*0.1945*	*0.1441*	*0.0034*	*0.20*	*2766*	*53*	*2780*	*12*	*0.5*
H086A - 13	*271.2*	*177.9*	*234.1*	*14.16*	*0.09*	*0.5277*	*0.0035*	*0.1947*	*0.1388*	*0.0014*	*0.64*	*2731*	*15*	*2782*	*10*	*1.8*
H086A - 22 - 1	*232*	*114*	*152*	*15.2*	*0.33*	*0.563*	*0.011*	*0.1946*	*0.1462*	*0.0025*	*0.48*	*2879*	*46*	*2784*	*13*	*-3.4*
H086A - 20	*220*	*96*	*137*	*15.38*	*0.22*	*0.5725*	*0.0067*	*0.1951*	*0.1536*	*0.002*	*0.36*	*2917*	*27*	*2785*	*12*	*-4.7*
H086A - 10	*148.8*	*144*	*188*	*14.25*	*0.16*	*0.5266*	*0.0053*	*0.1967*	*0.1366*	*0.0026*	*0.87*	*2727*	*22*	*2798*	*13*	*2.5*
H086A - 6	*217*	*127.8*	*166.4*	*14.76*	*0.09*	*0.5454*	*0.0032*	*0.1966*	*0.14*	*0.0014*	*0.57*	*2806*	*14*	*2798*	*8.3*	*-0.3*
H086A - 21	*271*	*170*	*221*	*14.63*	*0.35*	*0.5445*	*0.0093*	*0.1967*	*0.1535*	*0.0058*	*0.56*	*2801*	*39*	*2799*	*14*	*-0.1*
H086A - 12	*249*	*224*	*306*	*14.46*	*0.24*	*0.5327*	*0.0091*	*0.1971*	*0.1666*	*0.0096*	*0.45*	*2751*	*38*	*2801*	*15*	*1.8*
H086A - 5	139	60.9	82.4	14.39	0.19	0.528	0.0078	0.1986	0.1513	0.0043	0.41	2737	34	2812	17	2.7
H086A - 3	148.1	98	132.7	15.56	0.15	0.5607	0.0053	0.2011	0.1466	0.0022	0.62	2869	22	2836	8.5	-1.2
H086A - 23	84.1	40.3	57	15.44	0.18	0.5508	0.0068	0.2039	0.1541	0.0035	0.47	2827	28	2856	13	1.0
~~H086A - 1~~	~~165.8~~	~~93.9~~	~~143.6~~	~~12.38~~	~~0.14~~	~~0.4376~~	~~0.0048~~	~~0.2049~~	~~0.1647~~	~~0.0045~~	~~0.53~~	~~2339~~	~~22~~	~~2867~~	~~12~~	~~18.4~~
H086A - 2	117.5	89.2	130.3	15.99	0.2	0.5498	0.0042	0.2109	0.1594	0.0044	0.75	2824	17	2911	15	3.0
F040A, tonalite gneiss																
620333 7136294 NAD 1983 UTM Zone 19N																
~~F040 - 3~~	~~1050~~	~~515~~	~~373~~	~~5.58~~	~~0.45~~	~~0.224~~	~~0.016~~	~~0.1804~~	~~0.0912~~	~~0.0083~~	~~0.46~~	~~1297~~	~~85~~	~~2655~~	~~25~~	51.1
F040 - 15	750	370	392	10.85	0.45	0.421	0.021	0.188	0.1303	0.005	0.36	2257	94	2723	23	17.1
F040 - 14	528	335	372	13.65	0.42	0.519	0.014	0.1904	0.134	0.0061	0.57	2691	57	2744	13	1.9
~~F040 - 12~~	~~434~~	~~264~~	~~336~~	~~14.06~~	~~0.31~~	~~0.53~~	~~0.011~~	~~0.1921~~	~~0.1429~~	~~0.0042~~	~~0.54~~	~~2738~~	~~47~~	~~2759~~	~~11~~	0.8
F040 - 23	524	288	392	14.83	0.25	0.5588	0.0088	0.193	0.152	0.003	0.55	2860	36	2767	9.7	-3.4
F040 - 6	322.5	113	158.5	15.11	0.27	0.563	0.011	0.1945	0.1487	0.0046	0.34	2878	46	2780	8.6	-3.5
F040 - 10	315	139	181	14	0.24	0.5196	0.0084	0.195	0.1418	0.0026	0.44	2696	36	2784	13	3.2
~~F040 - 13~~	~~420~~	~~175~~	~~186~~	~~9.85~~	~~0.33~~	~~0.363~~	~~0.0097~~	~~0.1951~~	~~0.1105~~	~~0.003~~	~~0.40~~	~~1995~~	~~46~~	~~2784~~	~~24~~	~~28.3~~

spot location	zonation	notes
~~rim~~	~~mixed~~	~~incidental overlap of domains~~
~~rim~~	~~mixed~~	~~incidental overlap of domains~~
~~rim~~	~~mixed~~	~~incidental overlap of domains~~
rim	unzoned	
~~core~~	~~mixed~~	~~incidental overlap of domains~~
core	*irregular osc*	
core	*osc*	
core	*osc*	
core	*irregular osc*	
core	*osc*	
core	*iregular osc*	
core	*irregular osc*	
core	*unzoned*	
core	*osc*	
core	*osc*	
core	*osc*	
core	iregular osc	
core	osc	
core	osc	
~~core~~	~~osc~~	
core	osc	

F040A, tonalite gneiss

620333 7136294 NAD 1983 UTM Zone 19N

~~single grain~~	~~osc~~	~~discordant - abundant cracks~~
core	unzoned	
rim	osc	
~~core~~	~~mixed~~	~~incidental overlap of domains~~
core	osc	
outer	osc	
core	osc	
~~core~~	~~unzoned~~	~~discordant~~

APPENDIX 4B - LASS-ICPMS U-Pb isotopic data from regional samples

spot name	U (ppm)	Th (ppm)	Pb (ppm)	$^{207}Pb/^{235}U$	±	$^{206}Pb/^{238}U$	±	$^{207}Pb/^{206}Pb$	$^{206}Pb/^{208}Pb$	±	Th/U	age (Ma) $^{206}Pb/^{238}U$	±	age (Ma) $^{207}Pb/^{206}Pb$	±	disc. %
F040 - 7	224	116.9	161.8	15.92	0.39	0.588	0.013	0.1954	0.1437	0.0032	0.51	2980	52	2787	20	-6.9
F040 - 1	336	76.2	107.4	15.64	0.31	0.58	0.011	0.1958	0.1625	0.0065	0.23	2949	43	2791	22	-5.7
F040 - 5	259.3	85.1	106	13.02	0.51	0.481	0.019	0.1958	0.1338	0.0048	0.33	2526	83	2791	12	9.5
F040 - 2	*242*	*138*	*197*	*14.06*	*0.24*	*0.5157*	*0.0079*	*0.1973*	*0.1422*	*0.0069*	*0.49*	*2680*	*33*	*2804*	*11*	*4.4*
F040 - 11	*351*	*149*	*196*	*14.82*	*0.24*	*0.5412*	*0.0072*	*0.1981*	*0.1443*	*0.0022*	*0.42*	*2787*	*30*	*2810*	*11*	*0.8*
F040 - 20	*283*	*125*	*171.5*	*15.26*	*0.27*	*0.558*	*0.011*	*0.1988*	*0.1465*	*0.0033*	*0.44*	*2856*	*45*	*2815*	*11*	*-1.5*
F040 - 16	*283*	*156*	*220.7*	*14.83*	*0.27*	*0.5415*	*0.0091*	*0.1989*	*0.1572*	*0.0031*	*0.54*	*2788*	*38*	*2816*	*12*	*1.0*
F040 - 8	*321*	*139*	*196*	*14.9*	*0.24*	*0.5412*	*0.0092*	*0.1995*	*0.1567*	*0.0038*	*0.40*	*2787*	*39*	*2821*	*13*	*1.2*
F040 - 18	*356*	*208*	*250*	*14.58*	*0.16*	*0.5301*	*0.0059*	*0.1996*	*0.1291*	*0.0018*	*0.52*	*2741*	*25*	*2822*	*13*	*2.9*
F040 - 17	*264*	*174*	*214*	*14.34*	*0.38*	*0.519*	*0.013*	*0.2002*	*0.1433*	*0.0055*	*0.55*	*2692*	*53*	*2827*	*9.7*	*4.8*
F040 - 1 - 2	*193*	*63.3*	*95.6*	*16.08*	*0.51*	*0.58*	*0.018*	*0.2003*	*0.1567*	*0.0045*	*0.33*	*2946*	*75*	*2828*	*14*	*-4.2*
F040 - 9	*241*	*147*	*197*	*14.58*	*0.14*	*0.5227*	*0.0051*	*0.2009*	*0.1413*	*0.002*	*0.61*	*2710*	*22*	*2833*	*9.1*	*4.4*
F040 - 19	*292*	*271*	*302*	*14.53*	*0.27*	*0.5214*	*0.0097*	*0.2014*	*0.1227*	*0.0057*	*0.85*	*2703*	*42*	*2836*	*12*	*4.7*
F040 - 4	179	98	130	14.95	0.23	0.535	0.0077	0.2024	0.1318	0.0044	0.51	2762	33	2845	15	2.9
F040 - 22	215	113.1	163	15	0.23	0.5362	0.0078	0.2034	0.157	0.0024	0.50	2766	33	2853	9.9	3.1
K037A, tonalite gneiss																
607104 7161794 NAD1983, UTM Zone 19N																
~~K037A - 21~~	~~1545~~	~~325~~	~~254~~	~~4.9~~	~~0.21~~	~~0.36~~	~~0.017~~	~~0.09863~~	~~0.0888~~	~~0.0015~~	~~0.21~~	~~1977~~	~~80~~	~~1598~~	~~14~~	~~-23.7~~
~~K037A - 22~~	~~992~~	~~110.7~~	~~96.7~~	~~4.49~~	~~0.12~~	~~0.3136~~	~~0.0097~~	~~0.1035~~	~~0.0922~~	~~0.0016~~	~~0.11~~	~~1755~~	~~47~~	~~1686~~	~~18~~	~~-4.1~~
K037A - 11	575	74	60	4.74	0.22	0.318	0.012	0.1083	0.1049	0.0057	0.10	1776	59	1774	21	-0.1
~~K037A - 7~~	~~532~~	~~29~~	~~31.2~~	~~3.91~~	~~0.15~~	~~0.261~~	~~0.011~~	~~0.10901~~	~~0.1238~~	~~0.006~~	~~0.04~~	~~1489~~	~~54~~	~~1782~~	~~12~~	~~16.4~~
K037A - 16	610	61.9	52.2	4.542	0.06	0.3024	0.0035	0.10907	0.0923	0.0016	0.10	1703	17	1783	12	4.5
K037A - 9	393	32.3	29.4	4.727	0.04	0.3127	0.0023	0.1098	0.0985	0.002	0.08	1754	11	1795	13	2.3
K037A - 8	305.4	35.12	30.27	4.804	0.05	0.3159	0.0036	0.11036	0.0945	0.0019	0.11	1769	18	1805	13	2.0
K037A - 19	310	22.41	20.35	4.883	0.03	0.318	0.0018	0.11091	0.0958	0.0019	0.07	1779.7	8.9	1814	11	1.9
K037A - 20	301	15.36	15.05	5.01	0.04	0.3252	0.0023	0.1115	0.1026	0.0024	0.05	1815	11	1823	13	0.4
K037A - 10	317.2	24.52	22.43	4.915	0.05	0.3209	0.0036	0.11184	0.0999	0.0024	0.07	1794	18	1828	14	1.9
K037A - 24	344	11.58	10.89	5.072	0.05	0.3289	0.0031	0.11208	0.103	0.0042	0.03	1833	15	1832	13	-0.1
K037A - 18	169	10.53	10.98	5.159	0.07	0.3331	0.0043	0.1131	0.1036	0.0046	0.06	1853	21	1848	23	-0.3
K037A - 12	466	53.5	49	4.778	0.07	0.3049	0.003	0.11417	0.098	0.0021	0.11	1715	15	1865	15	8.0
K037A - 25	260	18.85	17.74	5.453	0.07	0.3438	0.0034	0.1145	0.1007	0.0027	0.07	1905	16	1870	18	-1.9

spot location	zonation	notes
core	osc	
core	unzoned	
core	unzoned	
core	*osc*	
core	*osc*	
core	*osc*	
core	*osc*	
core	*osc*	
core	*unzoned*	
core	*osc*	
core	*osc*	
core	*osc*	
core	*osc*	
core	osc - truncated	
core	osc - truncated	

K037A, tonalite gneiss

607104 7161794 NAD1983, UTM Zone 19N

~~single grain~~	~~unzoned~~	~~discordant~~
~~single grain~~	~~unzoned~~	~~same grain as spot 21~~
core	unzoned	
~~single grain~~	~~unzoned~~	
single grain	unzoned	
single grain	unzoned	
single grain	unzoned	
rim	sector	
single grain	sector	
single grain	sector	
single grain	sector	
core	osc	
core	unzoned	
core	irregular	

APPENDIX 4B - LASS-ICPMS U-Pb isotopic data from regional samples

spot name	U (ppm)	Th (ppm)	Pb (ppm)	$^{207}Pb/^{235}U$	±	$^{206}Pb/^{238}U$	±	$^{207}Pb/^{206}Pb$	$^{206}Pb/^{208}Pb$	±	Th/U	age (Ma) $^{206}Pb/^{238}U$	±	age (Ma) $^{207}Pb/^{206}Pb$	±	disc. %
~~K037A - 2~~	~~74.1~~	~~41.9~~	~~49.6~~	~~11.2~~	~~0.13~~	~~0.4926~~	~~0.0051~~	~~0.1636~~	~~0.1295~~	~~0.0022~~	~~0.54~~	~~2581~~	~~22~~	~~2492~~	~~13~~	~~-3.6~~
~~K037A - 4~~	~~121.6~~	~~70.4~~	~~85.6~~	~~10.96~~	~~0.11~~	~~0.48~~	~~0.0039~~	~~0.1646~~	~~0.1325~~	~~0.0015~~	~~0.56~~	~~2527~~	~~17~~	~~2503~~	~~11~~	~~-1.0~~
K037A - 6	67.5	55	64.3	11.74	0.29	0.5003	0.0092	0.1708	0.1369	0.0031	0.76	2614	40	2563	33	-2.0
~~K037A - 14~~	~~67.3~~	~~39.4~~	~~48.7~~	~~10.1~~	~~0.21~~	~~0.4342~~	~~0.0099~~	~~0.171~~	~~0.1328~~	~~0.0038~~	~~0.57~~	~~2322~~	~~44~~	~~2565~~	~~21~~	~~9.5~~
~~K037A - 1~~	~~253.9~~	~~205~~	~~244.9~~	~~11.93~~	~~0.06~~	~~0.5004~~	~~0.0026~~	~~0.17168~~	~~0.1307~~	~~0.001~~	~~0.77~~	~~2615~~	~~11~~	~~2574~~	~~8~~	~~-1.6~~
~~K037A - 26~~	~~700~~	~~67.1~~	~~84.3~~	~~8.23~~	~~0.65~~	~~0.339~~	~~0.026~~	~~0.1755~~	~~0.1343~~	~~0.0049~~	~~0.10~~	~~1870~~	~~130~~	~~2610~~	~~16~~	~~28.4~~
K037A - 17	230	265	268	11.34	0.36	0.466	0.015	0.1775	0.1216	0.0033	1.12	2463	69	2627	27	6.2
~~*K037A - 23*~~	~~*62.1*~~	~~*43.1*~~	~~*62.6*~~	~~*13.14*~~	~~*0.4*~~	~~*0.531*~~	~~*0.011*~~	~~*0.1794*~~	~~*0.1504*~~	~~*0.0046*~~	~~*0.68*~~	~~*2758*~~	~~*52*~~	~~*2644*~~	~~*32*~~	~~*-4.3*~~
K037A - 5	*44.4*	*40.3*	*48.1*	*13.65*	*0.4*	*0.548*	*0.012*	*0.1815*	*0.142*	*0.0036*	*0.86*	*2814*	*51*	*2663*	*38*	*-5.7*
K037A - 15	*92.9*	*55.3*	*67.3*	*11.68*	*0.12*	*0.4607*	*0.0051*	*0.1838*	*0.1327*	*0.0028*	*0.58*	*2442*	*22*	*2686*	*13*	*9.1*
K037A - 3	*66.4*	*69.3*	*86.1*	*13.97*	*0.23*	*0.5479*	*0.0083*	*0.1844*	*0.1422*	*0.0029*	*1.00*	*2816*	*34*	*2692*	*18*	*-4.6*
Z108A, monzogranite gneiss																
662246 7122133 NAD1983 UTM Zone 19N																
~~Z108A_21~~	~~709~~	~~37~~	~~37~~	~~9.7~~	~~0.16~~	~~0.425~~	~~0.006~~	~~0.1647~~	~~76~~	~~3.3~~	~~0.05~~	~~2282~~	~~27~~	~~2504~~	~~16~~	~~8.87~~
~~Z108A_13~~	~~1151~~	~~426~~	~~330~~	~~7.46~~	~~0.41~~	~~0.326~~	~~0.017~~	~~0.1659~~	~~9.96~~	~~0.37~~	~~0.36~~	~~1815~~	~~83~~	~~2516~~	~~19~~	~~27.86~~
Z108A_22	762	30	43	12.05	0.34	0.524	0.012	0.1665	88.8	5.2	0.04	2712	50	2521	18	-7.58
Z108A_8	780	55	99	11.42	0.14	0.4928	0.0078	0.1689	43.3	3.1	0.06	2582	33	2546	12	-1.41
Z108A_14	639	50	43	10.95	0.19	0.471	0.0085	0.1689	64.6	2	0.08	2487	37	2546	10	2.32
Z108A_6	742	50	98	11.69	0.23	0.4926	0.0085	0.1722	38.8	4.2	0.06	2581	37	2578	16	-0.12
Z108A_5	1104	558	507	12.16	0.37	0.504	0.019	0.1759	9.86	0.39	0.47	2628	79	2612	26	-0.61
Z108A_7	*292*	*67*	*97*	*13.85*	*0.4*	*0.531*	*0.012*	*0.1885*	*20.4*	*3.6*	*0.16*	*2751*	*54*	*2727*	*17*	*-0.88*
Z108A_12	*572*	*196*	*226*	*13.76*	*0.33*	*0.524*	*0.011*	*0.1903*	*12.25*	*0.72*	*0.33*	*2716*	*45*	*2743*	*22*	*0.98*
Z108A_11	*243*	*82*	*109*	*14.47*	*0.39*	*0.542*	*0.012*	*0.1933*	*11.11*	*0.42*	*0.33*	*2792*	*52*	*2769*	*16*	*-0.83*
Z108A_10	*346*	*147*	*182*	*14.67*	*0.3*	*0.5488*	*0.0098*	*0.1934*	*9.53*	*0.41*	*0.41*	*2820*	*41*	*2771*	*17*	*-1.77*
~~*Z108A_19*~~	~~*285*~~	~~*166*~~	~~*183*~~	~~*12.26*~~	~~*0.55*~~	~~*0.463*~~	~~*0.02*~~	~~*0.1936*~~	~~*7.9*~~	~~*0.48*~~	~~*0.52*~~	~~*2445*~~	~~*91*~~	~~*2772*~~	~~*17*~~	~~*11.80*~~
Z108A_20	*333*	*81*	*124*	*14.9*	*0.27*	*0.554*	*0.012*	*0.1941*	*14.1*	*1.1*	*0.22*	*2842*	*51*	*2777*	*18*	*-2.34*
Z108A_16	*340*	*156*	*198*	*14.73*	*0.16*	*0.5464*	*0.0075*	*0.1957*	*9.1*	*0.66*	*0.43*	*2810*	*31*	*2790*	*11*	*-0.72*
Z108A_4	*160*	*54*	*72*	*14.53*	*0.29*	*0.536*	*0.011*	*0.1964*	*11.87*	*0.89*	*0.31*	*2777*	*50*	*2795*	*15*	*0.64*
Z108A_18	*238*	*15*	*25*	*14.44*	*0.22*	*0.5312*	*0.009*	*0.197*	*51*	*5.5*	*0.06*	*2745*	*38*	*2801*	*16*	*2.00*
~~Z108A_2~~	~~160~~	~~65~~	~~93~~	~~16.38~~	~~0.94~~	~~0.596~~	~~0.032~~	~~0.1997~~	~~9.02~~	~~0.28~~	~~0.41~~	~~3010~~	~~130~~	~~2823~~	~~19~~	~~-6.62~~
~~Z108A_15~~	~~140~~	~~48~~	~~86~~	~~17.17~~	~~0.24~~	~~0.6134~~	~~0.0084~~	~~0.2037~~	~~10.06~~	~~0.39~~	~~0.33~~	~~3082~~	~~33~~	~~2856~~	~~10~~	~~-7.92~~

spot location	zonation	notes
~~core fragmen~~	~~faint osc~~	~~incidental overlap of cracks~~
~~core~~	~~faint osc~~	~~incidental overlap of domains~~
core	faint osc	
~~core~~	~~osc~~	~~discordant~~
~~core~~	~~light~~	~~discordant~~
~~core~~	~~faint osc~~	~~incidental overlap of cracks~~
core	faint osc	
~~core~~	~~faint osc~~	~~discordant~~
core	faint osc	
core	osc	
core	faint osc	

Z108A, monzogranite gneiss

662246 7122133 NAD1983 UTM Zone 19N

~~rim~~	~~mixed~~	~~incidental overlap of domains~~
~~core~~	~~osc~~	~~discordant~~
rim	unzoned	
rim	unzoned	
rim	unzoned	
rim	unzoned	
rim	faint osc	
core	*osc*	
core	*osc*	
core	*osc*	
core	*osc*	
~~*core*~~	~~*osc*~~	~~discordant~~
core	*osc*	
core	*osc*	
core	*osc*	
outer core	*osc*	
~~core~~	~~osc~~	
~~core~~	~~osc~~	

APPENDIX 4B - LASS-ICPMS U-Pb isotopic data from regional samples

spot name	U (ppm)	Th (ppm)	Pb (ppm)	$^{207}Pb/^{235}U$	±	$^{206}Pb/^{238}U$	±	$^{207}Pb/^{206}Pb$	$^{206}Pb/^{208}Pb$	±	Th/U	age (Ma) $^{206}Pb/^{238}U$	±	age (Ma) $^{207}Pb/^{206}Pb$	±	disc. %
~~Z108A_9~~	~~122~~	~~56~~	~~80~~	~~15.83~~	~~0.52~~	~~0.56~~	~~0.018~~	~~0.204~~	~~7.81~~	~~0.38~~	~~0.47~~	~~2862~~	~~72~~	~~2857~~	~~19~~	~~-0.18~~
Z108A_3	101	38	55	17.38	0.7	0.618	0.02	0.2045	10.32	0.74	0.35	3101	80	2861	26	-8.39
Z108A_1	80	36	55	17.19	0.15	0.6024	0.0057	0.2079	8.47	0.12	0.46	3039	23	2888	13	-5.23
Z108A_17	135	120	160	16.45	0.46	0.562	0.013	0.2127	4.268	0.079	0.87	2874	55	2925	16	1.74
F163B, tonalite gneiss																
669461 7094784 NAD1983, UTM Zone 19N																
F163B - 3	260	111.2	139	13.8	0.28	0.53	0.011	0.1888	0.1399	0.0024	0.44	2741	45	2731	11	-0.4
F163B - 12	333	150.4	178.6	13.16	0.33	0.5035	0.0087	0.1898	0.1396	0.0016	0.46	2628	37	2740	17	4.1
~~F163B - 4_1~~	~~303~~	~~236~~	~~258~~	~~11.16~~	~~0.17~~	~~0.4248~~	~~0.0045~~	~~0.1914~~	~~0.1168~~	~~0.0015~~	~~0.75~~	~~2282~~	~~21~~	~~2753~~	~~15~~	~~17.1~~
F163B - 14	195	105.2	137.9	15.23	0.12	0.5627	0.0042	0.1949	0.1487	0.0016	0.56	2881	18	2784	8.9	-3.5
F163B - 16	151	42.2	56.6	15.95	0.2	0.5889	0.0066	0.195	0.1518	0.0021	0.28	2984	27	2784	11	-7.2
~~F163B - 19~~	~~109~~	~~30.3~~	~~42.2~~	~~16.86~~	~~0.28~~	~~0.621~~	~~0.013~~	~~0.1978~~	~~0.1663~~	~~0.0067~~	~~0.25~~	~~3111~~	~~51~~	~~2807~~	~~18~~	~~-10.8~~
F163B - 8	134	65.08	83.8	14.9	0.25	0.5435	0.0085	0.1985	0.1464	0.0031	0.50	2797	35	2813	15	0.6
F163B - 21	110	33.1	46.6	14.56	0.4	0.532	0.015	0.1987	0.1569	0.0049	0.29	2748	64	2815	14	2.4
F163B - 15	80.9	34.2	45.2	16.36	0.43	0.595	0.016	0.1994	0.1715	0.0091	0.38	3001	62	2820	13	-6.4
F163B - 18	106	52.3	66.4	15.82	0.28	0.5732	0.0098	0.2002	0.1571	0.0072	0.35	2918	40	2826	13	-3.3
F163B - 11	*109.4*	*52.3*	*78.7*	*16.13*	*0.34*	*0.587*	*0.014*	*0.2009*	*0.1774*	*0.0075*	*0.48*	*2971*	*54*	*2833*	*13*	*-4.9*
F163B - 1	*165*	*118.3*	*164.9*	*15.88*	*0.12*	*0.5736*	*0.0049*	*0.2011*	*0.1524*	*0.0024*	*0.73*	*2922*	*20*	*2834*	*9.8*	*-3.1*
F163B - 17	*94.8*	*33.2*	*48.8*	*16.08*	*0.38*	*0.576*	*0.013*	*0.2013*	*0.1676*	*0.0052*	*0.32*	*2930*	*54*	*2835*	*16*	*-3.4*
F163B - 22	*80.2*	*36.6*	*49.5*	*14.35*	*0.21*	*0.5177*	*0.0072*	*0.2014*	*0.1445*	*0.0028*	*0.45*	*2688*	*31*	*2839*	*15*	*5.3*
F163B - 5	*88.8*	*41.8*	*54.3*	*16.59*	*0.44*	*0.599*	*0.017*	*0.2018*	*0.1524*	*0.0035*	*0.41*	*3019*	*67*	*2840*	*11*	*-6.3*
F163B - 13	*72*	*24.3*	*34.5*	*15.43*	*0.22*	*0.5536*	*0.0085*	*0.202*	*0.1601*	*0.0047*	*0.34*	*2838*	*35*	*2843*	*19*	*0.2*
F163B - 7	*97*	*45.2*	*74*	*17.24*	*0.36*	*0.617*	*0.012*	*0.2023*	*0.2021*	*0.0074*	*0.44*	*3096*	*48*	*2844*	*13*	*-8.9*
F163B - 4_2	*80.2*	*33.2*	*46.4*	*17*	*0.43*	*0.609*	*0.016*	*0.2035*	*0.152*	*0.0073*	*0.40*	*3063*	*64*	*2854*	*15*	*-7.3*
~~*F163B - 2*~~	~~*153*~~	~~*46.7*~~	~~*71.6*~~	~~*17.73*~~	~~*0.38*~~	~~*0.631*~~	~~*0.013*~~	~~*0.2037*~~	~~*0.1914*~~	~~*0.0089*~~	~~*0.30*~~	~~*3148*~~	~~*50*~~	~~*2855*~~	~~*11*~~	~~*-10.3*~~
F163B - 20	*157*	*53.9*	*70.6*	*16.15*	*0.16*	*0.571*	*0.006*	*0.2051*	*0.1505*	*0.0044*	*0.25*	*2911*	*25*	*2866*	*11*	*-1.6*
F163B - 6	65.3	26.2	36.9	18.93	0.39	0.625	0.0096	0.2187	0.166	0.0052	0.41	3129	38	2970	20	-5.4
F163B - 9	112	64.4	80.5	17.15	0.27	0.5671	0.0089	0.2189	0.1481	0.0034	0.55	2894	37	2972	16	2.6
F163B - 10	118	58.6	82.9	18.89	0.22	0.6171	0.0068	0.2206	0.164	0.0026	0.50	3098	27	2984	14	-3.8

spot location	zonation	notes
~~core~~	~~osc~~	
core	irregular	
core	irregular	
core	osc	

Mean = 2877 ± 20 [0.72%] 95% conf.
Wtd by data-pt errs only, 0 of 8 rej.
MSWD = 9.4, probability = 0.000

F163B, tonalite gneiss

669461 7094784 NAD1983, UTM Zone 19N

rim	unzoned	
rim	unzoned	
~~core~~	~~mixed~~	~~incidental overlap of domains~~
rim	unzoned	
rim	unzoned	
~~core~~	~~unzoned~~	
rim	unzoned	
core	irregular	
core	irregular	
core	osc	
core	*unzoned*	
core	*osc*	
core	*osc*	
core	*irregular*	
core	*osc*	
core	*osc*	
core	*irregular*	
core	*irregular*	
~~*core*~~	~~*unzoned*~~	
core	*osc*	
core	osc	
core	osc	
mid	osc	

APPENDIX 4B - LASS-ICPMS U-Pb isotopic data from regional samples

spot name	U (ppm)	Th (ppm)	Pb (ppm)	$^{207}Pb/^{235}U$	±	$^{206}Pb/^{238}U$	±	$^{207}Pb/^{206}Pb$	$^{206}Pb/^{208}Pb$	±	Th/U	age (Ma) $^{206}Pb/^{238}U$	±	age (Ma) $^{207}Pb/^{206}Pb$	±	disc. %
F157A, monzogranite gneiss																
622813 7160311 NAD1983, UTM Zone 19N																
F157A - 14 - 2	325	104.2	89.3	4.925	0.09	0.3187	0.0057	0.11123	0.0893	0.0014	0.32	1782	28	1819	15	2.0
F157A - 20 - 1	97.3	28.1	23.5	5.032	0.09	0.3185	0.0053	0.1147	0.093	0.003	0.29	1781	26	1877	24	5.1
~~F157A - 14 - 1~~	~~445~~	~~119.3~~	~~138~~	~~10.23~~	~~0.23~~	~~0.4657~~	~~0.0069~~	~~0.1605~~	~~0.1331~~	~~0.0054~~	~~0.26~~	~~2464~~	~~31~~	~~2459~~	~~33~~	~~-0.2~~
~~F157A - 13 - 1~~	~~561~~	~~212~~	~~248~~	~~11.85~~	~~0.14~~	~~0.4905~~	~~0.0051~~	~~0.1741~~	~~0.1288~~	~~0.0023~~	~~0.33~~	~~2572~~	~~22~~	~~2597~~	~~12~~	~~1.0~~
~~F157A -7 - 1~~	~~453~~	~~266~~	~~166~~	~~11.34~~	~~0.25~~	~~0.461~~	~~0.01~~	~~0.1769~~	~~0.0773~~	~~0.0069~~	~~0.45~~	~~2443~~	~~45~~	~~2623~~	~~12~~	~~6.9~~
~~F157A - 16 - 1~~	~~604~~	~~74~~	~~79.2~~	~~11.77~~	~~0.09~~	~~0.4805~~	~~0.004~~	~~0.1775~~	~~0.1268~~	~~0.0067~~	~~0.11~~	~~2529~~	~~18~~	~~2629~~	~~15~~	~~3.8~~
F157A - 4 - 1	184	170	197	12.99	0.28	0.527	0.0086	0.1776	0.1278	0.0025	0.93	2728	37	2630	19	-3.7
F157A - 6 - 1	326	94.9	125.6	11.59	0.11	0.4654	0.0034	0.1795	0.139	0.0026	0.31	2463	15	2648	12	7.0
F157A - 11 - 1	623	225	267	12	0.29	0.482	0.01	0.1798	0.155	0.013	0.24	2532	44	2650	15	4.5
F157A - 12 - 1	339	97.5	128	12.47	0.1	0.4989	0.0042	0.1798	0.1435	0.0038	0.24	2608	18	2651	9.6	1.6
F157A - 8 - 1	331	94	118	13.3	0.31	0.529	0.01	0.1803	0.1555	0.0091	0.15	2734	43	2655	11	-3.0
F157A -5 - 1	428	458	304	11.8	0.22	0.4708	0.0078	0.18046	0.0885	0.0062	0.75	2485	35	2657	9	6.5
F157A - 1 - 1	416	139	192	12.44	0.23	0.4971	0.0091	0.181	0.1571	0.0037	0.23	2599	40	2661	9.6	2.3
F157A - 9 - 1	358	216	164	13.01	0.29	0.5137	0.0088	0.1819	0.0954	0.0048	0.49	2670	37	2668	14	-0.1
~~F157A - 22 - 1~~	~~297~~	~~305~~	~~343~~	~~12.49~~	~~0.12~~	~~0.4962~~	~~0.0045~~	~~0.1824~~	~~0.1256~~	~~0.0023~~	~~1.01~~	~~2597~~	~~19~~	~~2674~~	~~12~~	~~2.9~~
F157A - 2 - 1	*328*	*132*	*152*	*12.89*	*0.22*	*0.5068*	*0.0082*	*0.1835*	*0.1322*	*0.0041*	*0.25*	*2641*	*35*	*2684*	*9.2*	*1.6*
F157A - 19 - 1	*234*	*228*	*274*	*13.07*	*0.13*	*0.5169*	*0.0055*	*0.18347*	*0.137*	*0.0024*	*0.96*	*2685*	*23*	*2684*	*8.3*	*0.0*
~~*F157A - 10 - 1*~~	~~*928*~~	~~*484*~~	~~*594*~~	~~*9.11*~~	~~*0.43*~~	~~*0.357*~~	~~*0.017*~~	~~*0.1843*~~	~~*0.1387*~~	~~*0.0052*~~	~~*0.53*~~	~~*1963*~~	~~*79*~~	~~*2691*~~	~~*14*~~	~~*27.1*~~
F157A - 23 - 1	123.5	185.4	242	13.53	0.17	*13.29*	*0.28*	*0.5233*	*0.0065*	*0.1844*	1.42	*2712*	*28*	*2692*	*11*	-0.7
F157A - 15 - 1	*297*	*58.6*	*75.5*	*13.47*	*0.12*	*0.5257*	*0.004*	*0.1847*	*0.1461*	*0.0029*	*0.18*	*2723*	*17*	*2695*	*15*	*-1.0*
F157A - 3 - 1	*100.6*	*66*	*83.9*	*12.74*	*0.35*	*0.493*	*0.014*	*0.1866*	*0.1418*	*0.0072*	*0.61*	*2580*	*63*	*2711*	*18*	*4.8*
~~F157A - 21 - 2~~	~~273~~	~~67~~	~~90~~	~~16.21~~	~~0.39~~	~~0.626~~	~~0.019~~	~~0.189~~	~~0.175~~	~~0.016~~	~~0.15~~	~~3130~~	~~74~~	~~2732~~	~~23~~	~~-14.6~~
F157A - 18 - 1	171	85.3	100.8	13.75	0.2	0.5085	0.007	0.1954	0.1317	0.0023	0.50	2649	30	2788	11	5.0
F157A - 17 - 1	118.7	59.4	79.5	15.37	0.14	0.5516	0.005	0.2009	0.1486	0.0032	0.46	2831	21	2833	11	0.1
F157A - 21 - 1	257	95	116	16.51	0.41	0.565	0.012	0.2125	0.1482	0.0039	0.37	2886	51	2924	18	1.3

spot location	zonation	notes
F157A, monzogranite gneiss		
622813 7160311 NAD1983, UTM Zone 19N		
core	irregular	
rim	unzoned	
~~core~~	~~irregular~~	
~~core~~	~~osc~~	
~~core-rim~~	~~mixed~~	~~incidental overlap of domains~~
~~core-rim~~	~~mixed~~	~~incidental overlap of domains~~
rim	osc	
rim	osc	
core	osc	
rim	osc	
core	osc	
core	unzoned	
core	osc	
rim	unzoned	
~~core~~	~~mixed~~	~~incidental overlap of domains~~
core	*osc*	
core	*unzoned*	
~~*mid*~~	~~*osc*~~	
core	irregular	
core	*irregular*	
rim	*unzoned*	
~~core~~	~~mixed~~	
rim	irregular	
core	irregular	
core	osc	

APPENDIX 4B - LASS-ICPMS U-Pb isotopic data from regional samples

spot name	U (ppm)	Th (ppm)	Pb (ppm)	$^{207}Pb/^{235}U$	±	$^{206}Pb/^{238}U$	±	$^{207}Pb/^{206}Pb$	$^{206}Pb/^{208}Pb$	±	Th/U	age (Ma) $^{206}Pb/^{238}U$	±	age (Ma) $^{207}Pb/^{206}Pb$	±	disc. %

table notes:

Italicized and lighter toned data were used to calculate the weighted mean $^{207}Pb/^{206}Pb$ age.

Strikethrough data indicate analyses that were excluded from further calculations and discussion. These analyses had overlapping domains, were from fracture rich areas or otherwise yielded anomalous results (see individual notes for each instance).

Spot name follows the convention x-y-z; where x = sample number, y = grain number and z = spot number.

Errors are reported at 2σ uncertainty level unless otherwise noted.

spot location	zonation	notes

table notes:

Italicized and lighter toned data were used to calculate the weighted mean $^{207}Pb/^{206}Pb$ age.

Strikethrough data indicate analyses that were excluded from further calculations and discussion. These analyses had overlapping domains, were from fracture rich areas or otherwise yielded anomalous results (see individual notes for each instance).

Spot name follows the convention x-y-z; where x = sample number, y = grain number and z = spot number.

Errors are reported at 2σ uncertainty level unless otherwise noted.

APPENDIX 4C - LASS-ICPMS Lu-Hf isotopic data from snow ball area samples

Spot name	$^{176}Yb/^{177}Hf$	±2s	$^{176}Lu/^{177}Hf$	±2s	$^{178}Hf/^{177}Hf$	$^{180}Hf/^{177}Hf$	$^{176}Hf/^{177}Hf$	±2s	$^{176}Hf/^{177}Hf$	εHf(t)[1]	±2s	age (Ma) T_{DM}[2]	age (Ma) $^{207}Pb/^{206}Pb$
S116A, monzogranite gneiss													
713778 7041607 NAD 1983 UTM Zone 19N													
S116-26.1	0.012217	0.001143	0.000369	0.000030	1.4670	1.8866	0.280992	0.000035	0.280973	-2	1.5	3084	2716
S116-11.1	0.027003	0.002350	0.000814	0.000060	1.4670	1.8864	0.281023	0.000033	0.280978	3	1.4	3078	2933
S116-09-1	0.017107	0.001466	0.000503	0.000032	1.4670	1.8865	0.281047	0.000028	0.281019	5	1.3	3021	2951
S116-16-1	0.014388	0.001198	0.000435	0.000028	1.4671	1.8865	0.281018	0.000026	0.280993	4	1.2	3055	2957
S116-02-1	0.020116	0.002016	0.000582	0.000047	1.4670	1.8866	0.281013	0.000023	0.280980	4	1.1	3074	2958
S116-52-1	0.014224	0.001289	0.000419	0.000029	1.4671	1.8866	0.281029	0.000038	0.281005	5	1.6	3039	2963
S116-10-1	0.018303	0.001542	0.000529	0.000033	1.4670	1.8866	0.281006	0.000028	0.280976	4	1.3	3079	2964
S116-19-1	0.016484	0.001562	0.000483	0.000037	1.4670	1.8866	0.281008	0.000026	0.280981	4	1.2	3072	2970
S116-21-1	0.019779	0.001710	0.000575	0.000038	1.4670	1.8865	0.281002	0.000029	0.280969	4	1.3	3088	2980
S116-24.1	0.012553	0.002064	0.000380	0.000059	1.4671	1.8867	0.280981	0.000026	0.280959	4	1.2	3101	2988
S116-24.2	0.012976	0.001068	0.000455	0.000028	1.4667	1.8865	0.281020	0.000039	0.280993	5	1.6	3055	2988
F151A, granodiorite gneiss													
669300 7094544 NAD1983, UTM Zone 19N													
F151A_55.1	0.012693	0.001104	0.000453	0.000038	1.4670	1.8865	0.280996	0.000035	0.280972	-1	1.4	3086	2790
F151A_51.1	0.008277	0.000759	0.000327	0.000024	1.4671	1.8866	0.281040	0.000043	0.281022	3	1.7	3017	2882
F151A_116.2	0.024438	0.003958	0.000618	0.000090	1.4671	1.8865	0.281012	0.000035	0.280978	2	1.5	3078	2882
F151A_84-1	0.019686	0.002221	0.000491	0.000038	1.4670	1.8865	0.281032	0.000087	0.281005	3	3.2	3040	2884
F151A_63.1	0.006508	0.000555	0.000287	0.000019	1.4669	1.8865	0.281061	0.000042	0.281045	4	1.7	2985	2892
F151A_116.1	0.020136	0.001977	0.000531	0.000038	1.4671	1.8864	0.281054	0.000044	0.281024	4	1.7	3015	2894
F151A_69	0.005808	0.000584	0.000223	0.000018	1.4671	1.8866	0.280990	0.000035	0.280978	2	1.5	3076	2896
F151A_21	0.005772	0.000559	0.000224	0.000017	1.4670	1.8866	0.280980	0.000047	0.280967	2	1.9	3090	2897
F151A_117	0.010109	0.000831	0.000287	0.000022	1.4671	1.8867	0.281003	0.000049	0.280987	2	1.9	3064	2897
F151A_81	0.006239	0.000852	0.000245	0.000028	1.4671	1.8866	0.281031	0.000057	0.281017	4	2.2	3023	2902
F151A_84-2	0.007539	0.000988	0.000199	0.000023	1.4671	1.8867	0.281034	0.000036	0.281023	4	1.5	3015	2904
F151A_94	0.022114	0.001822	0.000553	0.000035	1.4669	1.8864	0.281026	0.000035	0.280995	3	1.5	3054	2907
F151A_6	0.005315	0.000560	0.000205	0.000018	1.4672	1.8868	0.280998	0.000057	0.280986	3	2.2	3064	2908
F151A_12	0.019455	0.001847	0.000689	0.000055	1.4671	1.8865	0.281026	0.000027	0.280987	3	1.2	3065	2910
F151A_108	0.026060	0.002276	0.000666	0.000055	1.4670	1.8866	0.280985	0.000041	0.280948	1	1.7	3118	2913
F151A_16	0.019238	0.001575	0.000701	0.000043	1.4671	1.8864	0.280999	0.000028	0.280959	2	1.3	3103	2917

APPENDIX 4C - LASS-ICPMS Lu-Hf isotopic data from snow ball area samples

Spot name	$^{176}Yb/^{177}Hf$	±2s	$^{176}Lu/^{177}Hf$	±2s	$^{178}Hf/^{177}Hf$	$^{180}Hf/^{177}Hf$	$^{176}Hf/^{177}Hf$	±2s	$^{176}Hf/^{177}Hf$	εHf(t)[1]	±2s	age (Ma) T_{DM}[2]	age (Ma) $^{207}Pb/^{206}Pb$
F151A_122	0.018660	0.004090	0.000482	0.000090	1.4671	1.8865	0.281051	0.000058	0.281024	4	2.2	3014	2918
F151A_17	0.006852	0.000618	0.000266	0.000023	1.4671	1.8866	0.280950	0.000044	0.280936	1	1.7	3132	2918
F151A_70	0.014571	0.002644	0.000561	0.000091	1.4671	1.8866	0.281069	0.000061	0.281037	5	2.3	2997	2920
F151A_52.1	0.017025	0.002347	0.000619	0.000068	1.4672	1.8866	0.280989	0.000047	0.280954	2	1.8	3109	2921
F151A_51.2	0.019942	0.001621	0.000717	0.000044	1.4671	1.8866	0.281016	0.000034	0.280976	3	1.4	3080	2928
F151A_83	0.007860	0.000804	0.000219	0.000019	1.4671	1.8866	0.281004	0.000051	0.280992	3	2.0	3057	2928
F151A_106	0.016324	0.002160	0.000427	0.000049	1.4671	1.8864	0.281032	0.000050	0.281008	4	1.9	3036	2930
F151A_125	0.013147	0.001055	0.000366	0.000022	1.4669	1.8864	0.281063	0.000039	0.281042	5	1.6	2990	2930
F151A_98	0.016857	0.002325	0.000430	0.000051	1.4671	1.8865	0.281021	0.000037	0.280997	4	1.5	3051	2932
F151A_18	0.011919	0.002003	0.000446	0.000066	1.4670	1.8867	0.281065	0.000068	0.281040	5	2.5	2993	2932
F151A_102	0.021312	0.001773	0.000562	0.000037	1.4671	1.8867	0.280994	0.000031	0.280962	2	1.4	3098	2933
F151A_5.1	0.011695	0.002323	0.000445	0.000087	1.4670	1.8864	0.281069	0.000040	0.281044	5	1.6	2987	2938
F151A_5.2	0.004391	0.000355	0.000169	0.000013	1.4670	1.8867	0.281010	0.000038	0.281001	4	1.6	3045	2938
F151A_58.1	0.013801	0.001171	0.000513	0.000044	1.4671	1.8866	0.281023	0.000047	0.280994	4	1.8	3054	2945
F155B, tonalite gneiss													
669461 7094784 NAD1983, UTM Zone 19N													
F155B_104.2	0.007709	0.000734	0.000298	0.000025	1.4668	1.8865	0.281062	0.000076	0.281047	0	2.8	2985	2692
F155B-23	0.045417	0.009954	0.001021	0.000191	1.4672	1.8867	0.280956	0.000058	0.280903	-5	2.2	3186	2703
F155B-15.2	0.019789	0.001728	0.000543	0.000045	1.4670	1.8867	0.281115	0.000041	0.281087	2	1.6	2932	2708
F155B-16	0.034849	0.003421	0.000741	0.000053	1.4670	1.8866	0.281016	0.000044	0.280977	-2	1.7	3083	2713
F155B_34	0.016446	0.002100	0.000493	0.000050	1.4672	1.8867	0.281056	0.000046	0.281030	0	1.8	3009	2717
F155B_85.1	0.010678	0.000862	0.000337	0.000020	1.4671	1.8868	0.281015	0.000033	0.280998	-1	1.4	3051	2721
F155B_85.2	0.042914	0.004672	0.001341	0.000130	1.4672	1.8866	0.280890	0.000036	0.280820	-8	1.5	3305	2721
F155B_63	0.020488	0.001761	0.000628	0.000040	1.4671	1.8868	0.280997	0.000035	0.280965	-2	1.5	3098	2726
F155B-1	0.039099	0.003253	0.000813	0.000053	1.4671	1.8867	0.280988	0.000031	0.280945	-3	1.3	3126	2735
F155B-15.1	0.025586	0.003386	0.000563	0.000064	1.4671	1.8864	0.281111	0.000050	0.281082	3	1.9	2939	2766
F155B-20.2	0.018115	0.001489	0.000508	0.000039	1.4671	1.8866	0.281075	0.000049	0.281047	2	1.9	2984	2806
F155B_50.1	0.021452	0.002876	0.000699	0.000083	1.4672	1.8868	0.281026	0.000043	0.280989	0	1.7	3065	2810
F155B_50.2	0.013424	0.001452	0.000428	0.000035	1.4671	1.8867	0.281034	0.000039	0.281011	1	1.6	3033	2810
F155B_55	0.012830	0.001089	0.000427	0.000028	1.4672	1.8868	0.281004	0.000031	0.280981	0	1.3	3074	2812
F155B_104.1	0.014533	0.002174	0.000501	0.000064	1.4671	1.8866	0.281013	0.000026	0.280986	1	1.2	3067	2820

APPENDIX 4C - LASS-ICPMS Lu-Hf isotopic data from snow ball area samples

Spot name	$^{176}Yb/^{177}Hf$	±2s	$^{176}Lu/^{177}Hf$	±2s	$^{178}Hf/^{177}Hf$	$^{180}Hf/^{177}Hf$	$^{176}Hf/^{177}Hf$	±2s	$^{176}Hf/^{177}Hf$	εHf(t)[1]	±2s	age (Ma) T_{DM}[2]	age (Ma) $^{207}Pb/^{206}Pb$
F155B-20.1	0.019655	0.003183	0.000510	0.000074	1.4670	1.8866	0.280988	0.000035	0.280959	2	1.5	3102	2931
F155b_30.1	0.025175	0.002983	0.000773	0.000078	1.4671	1.8865	0.280902	0.000049	0.280858	-1	1.9	3240	2956
F155B_46	0.006964	0.001351	0.000230	0.000043	1.4672	1.8866	0.280868	0.000037	0.280855	-1	1.5	3240	2960
F155B_43	0.031743	0.006085	0.000986	0.000168	1.4672	1.8869	0.280995	0.000082	0.280939	3	3.1	3131	2977
F155B_81	0.044340	0.005166	0.001314	0.000130	1.4670	1.8866	0.280803	0.000034	0.280727	-4	1.4	3422	3000
F155B_45	0.010570	0.001102	0.000423	0.000028	1.4672	1.8867	0.280704	0.000040	0.280678	-3	1.6	3476	3133
F155B_49	0.015780	0.002813	0.000495	0.000077	1.4673	1.8868	0.280900	0.000046	0.280870	6	1.9	3219	3209
F155C, quartz diorite lenses													
669461 7094784 NAD1983, UTM Zone 19N													
F155C-20	0.008160	0.000968	0.000319	0.000039	1.4670	1.8867	0.281352	0.000040	0.281341	-9	1.5	2596	1874
F155C-23	0.009929	0.000925	0.000411	0.000031	1.4671	1.8869	0.281345	0.000061	0.281331	-9	2.2	2611	1877
F155C-111.1	0.009189	0.001104	0.000309	0.000036	1.4671	1.8867	0.281079	0.000054	0.281063	0	2.1	2964	2658
F155C-21	0.007315	0.001103	0.000236	0.000030	1.4671	1.8867	0.281081	0.000049	0.281069	0	1.9	2955	2685
F155C-64.2	0.008668	0.000745	0.000295	0.000022	1.4669	1.8867	0.281071	0.000055	0.281056	0	2.1	2973	2700
F155C-41	0.009453	0.000827	0.000304	0.000021	1.4671	1.8866	0.281055	0.000048	0.281040	0	1.9	2995	2703
F155C-40.1	0.012876	0.001278	0.000406	0.000032	1.4669	1.8868	0.281091	0.000120	0.281070	3	4.3	2954	2777
F155C-110.1	0.009413	0.001440	0.000297	0.000041	1.4671	1.8870	0.281098	0.000078	0.281082	3	2.9	2937	2784
F155C-111.2	0.042385	0.010146	0.001590	0.000345	1.4671	1.8867	0.280980	0.000044	0.280894	-3	1.8	3203	2804
F155A, porphyroclastic monzogranite gneiss													
669461 7094784 NAD 1983 UTM Zone 19N													
F155A-20	0.023910	0.002270	0.000521	0.000042	1.4671	1.8866	0.281056	0.000027	0.281029	0	1.2	3011	2712
F155A-47	0.021432	0.001865	0.000459	0.000039	1.4670	1.8864	0.281047	0.000035	0.281023	-1	1.4	3019	2712
F155A-11	0.022098	0.002013	0.000505	0.000051	1.4671	1.8865	0.281114	0.000038	0.281088	2	1.5	2931	2713
F155A-89.2	0.023647	0.002667	0.000620	0.000049	1.4665	1.8864	0.281079	0.000087	0.281046	0	3.2	2988	2724
F155A-5	0.017378	0.001526	0.000371	0.000023	1.4671	1.8867	0.281045	0.000055	0.281026	0	2.1	3014	2725
F155A-14	0.018858	0.001526	0.000410	0.000031	1.4670	1.8866	0.281021	0.000038	0.281000	-1	1.6	3049	2725
F155A-36	0.024327	0.001977	0.000524	0.000032	1.4671	1.8867	0.281045	0.000034	0.281018	0	1.4	3025	2726
F155A-26	0.024791	0.002065	0.000547	0.000040	1.4671	1.8869	0.280969	0.000035	0.280941	-3	1.4	3130	2726
F155A-8	0.031329	0.002765	0.000680	0.000047	1.4671	1.8867	0.281030	0.000033	0.280995	-1	1.4	3058	2727
F155A-22	0.030214	0.002724	0.000671	0.000059	1.4670	1.8865	0.281049	0.000044	0.281014	0	1.7	3032	2731

APPENDIX 4C - LASS-ICPMS Lu-Hf isotopic data from snow ball area samples

Spot name	$^{176}Yb/^{177}Hf$	±2s	$^{176}Lu/^{177}Hf$	±2s	$^{178}Hf/^{177}Hf$	$^{180}Hf/^{177}Hf$	$^{176}Hf/^{177}Hf$	±2s	$^{176}Hf/^{177}Hf$	εHf(t)[1]	±2s	age (Ma) T_{DM}[2]	age (Ma) $^{207}Pb/^{206}Pb$
F155A-21	0.019143	0.001567	0.000407	0.000025	1.4671	1.8867	0.281016	0.000028	0.280995	-1	1.2	3056	2732
F155A-96.2	0.017355	0.001430	0.000431	0.000028	1.4669	1.8865	0.281042	0.000035	0.281020	0	1.5	3022	2734
F155A-61.1	0.016456	0.001396	0.000387	0.000033	1.4671	1.8867	0.281082	0.000047	0.281062	1	1.8	2965	2735
F155A-61.2	0.031675	0.002703	0.000741	0.000050	1.4670	1.8867	0.281046	0.000042	0.281007	-1	1.7	3042	2735
F155A-70	0.037705	0.003794	0.000777	0.000062	1.4671	1.8866	0.281011	0.000035	0.280970	-2	1.4	3092	2736
F155A-31	0.079922	0.007333	0.001663	0.000120	1.4671	1.8867	0.281012	0.000043	0.280924	-3	1.7	3164	2748
F155A-1	0.033588	0.003067	0.000734	0.000051	1.4671	1.8866	0.281069	0.000042	0.281030	1	1.7	3010	2749
F155A-30	0.035531	0.006800	0.000766	0.000137	1.4671	1.8866	0.281064	0.000048	0.281024	0	1.9	3018	2751
F155A-12	0.040188	0.007984	0.000870	0.000170	1.4671	1.8867	0.281033	0.000040	0.280987	-1	1.6	3070	2752
F155A-45	0.041793	0.005761	0.000930	0.000103	1.4671	1.8868	0.281088	0.000047	0.281039	1	1.8	2999	2759
F155A-103	0.020897	0.002883	0.000477	0.000057	1.4671	1.8865	0.281098	0.000037	0.281073	2	1.5	2950	2760
F155A-86	0.053159	0.009645	0.001122	0.000183	1.4670	1.8867	0.281065	0.000061	0.281006	0	2.3	3046	2761
F155A-23	0.042913	0.007211	0.000972	0.000143	1.4671	1.8867	0.280980	0.000068	0.280928	-2	2.5	3150	2810
F155A-96.1	0.049692	0.006514	0.001050	0.000120	1.4672	1.8866	0.281061	0.000036	0.281004	1	1.5	3046	2826
F155A-89.1	0.023447	0.002397	0.000558	0.000049	1.4671	1.8866	0.281016	0.000051	0.280986	1	2.0	3067	2828
F155A-25	0.051700	0.005003	0.001152	0.000087	1.4672	1.8866	0.280924	0.000047	0.280861	-3	1.8	3242	2858
F155A-17	0.049258	0.005194	0.001042	0.000093	1.4671	1.8865	0.280887	0.000057	0.280829	-3	2.2	3283	2884
F155A-87	0.065058	0.008884	0.001358	0.000154	1.4672	1.8866	0.280889	0.000057	0.280811	-2	2.2	3307	2984
F150A, porphyroclastic monzogranite gneiss													
669259 7094583 NAD1983, UTM Zone 19N													
F150A_07	0.010337	0.000872	0.000268	0.000018	1.4670	1.8867	0.281052	0.000044	0.281038	-1	1.7	2997	2686
F150A_23	0.010088	0.001338	0.000246	0.000023	1.4671	1.8868	0.281062	0.000037	0.281049	0	1.5	2981	2695
F150A_65	0.009648	0.000925	0.000235	0.000017	1.4670	1.8867	0.281130	0.000032	0.281118	2	1.4	2889	2695
F150A_31.2	0.013185	0.001601	0.000333	0.000031	1.4670	1.8865	0.281079	0.000031	0.281062	1	1.3	2965	2708
F150A_31	0.007753	0.000756	0.000212	0.000024	1.4669	1.8864	0.281070	0.000032	0.281059	1	1.3	2968	2708
F150A_57	0.011209	0.001818	0.000287	0.000033	1.4671	1.8869	0.281085	0.000032	0.281071	1	1.3	2953	2716
F150A_57	0.011405	0.001442	0.000296	0.000030	1.4671	1.8869	0.281089	0.000028	0.281073	1	1.2	2949	2716
F150A_62	0.011162	0.001754	0.000275	0.000032	1.4669	1.8866	0.281092	0.000052	0.281078	1	2.0	2943	2717
F150A_16	0.012862	0.001391	0.000314	0.000026	1.4670	1.8867	0.281041	0.000036	0.281024	0	1.5	3015	2719
F150A_60.2	0.013153	0.001349	0.000315	0.000036	1.4671	1.8864	0.281123	0.000049	0.281107	3	1.9	2904	2720
F150A_60	0.005916	0.000483	0.000158	0.000010	1.4671	1.8866	0.281095	0.000030	0.281087	2	1.3	2930	2720

APPENDIX 4C - LASS-ICPMS Lu-Hf isotopic data from snow ball area samples

Spot name	$^{176}Yb/^{177}Hf$	±2s	$^{176}Lu/^{177}Hf$	±2s	$^{178}Hf/^{177}Hf$	$^{180}Hf/^{177}Hf$	$^{176}Hf/^{177}Hf$	±2s	$^{176}Hf/^{177}Hf$	εHf(t)[1]	±2s	age (Ma) T_{DM}[2]	age (Ma) $^{207}Pb/^{206}Pb$
~~F150A_77~~	~~0.009676~~	~~0.000881~~	~~0.000293~~	~~0.000030~~	~~1.4647~~	~~1.8857~~	~~0.281427~~	~~0.000038~~	~~0.281411~~	~~13~~	~~1.5~~	~~2493~~	~~2721~~
F150A_72	0.011278	0.001030	0.000272	0.000019	1.4659	1.8862	0.281160	0.000042	0.281146	4	1.7	2852	2723
F150A_55	0.009542	0.000774	0.000254	0.000017	1.4668	1.8862	0.281106	0.000031	0.281092	2	1.3	2923	2728
~~F150A_10.2~~	~~0.003980~~	~~0.000539~~	~~0.000133~~	~~0.000019~~	~~1.4662~~	~~1.8867~~	~~0.281294~~	~~0.000039~~	~~0.281287~~	~~9~~	~~1.6~~	~~2661~~	~~2730~~
F150A_28.2	0.006329	0.000994	0.000185	0.000020	1.4669	1.8869	0.281132	0.000048	0.281122	5	1.9	2882	2782
F150A_28.1	0.009667	0.001235	0.000242	0.000022	1.4669	1.8867	0.281155	0.000050	0.281142	5	1.9	2856	2782
F150A_27	0.007379	0.000998	0.000215	0.000024	1.4655	1.8856	0.281194	0.000037	0.281182	7	1.5	2802	2788
F150A_25	0.012792	0.001257	0.000310	0.000024	1.4671	1.8866	0.281066	0.000033	0.281050	3	1.4	2980	2810
F152A, mag-bearing monzogranite gneiss													
669280 7094606 NAD1983 UTM Zone 19N													
F152A-46.1	0.005803	0.000566	0.000191	0.000022	1.4670	1.8868	0.280810	0.000032	0.280804	-30	1.2	3313	1800
F152A-46.2	0.009513	0.000871	0.000234	0.000015	1.4670	1.8867	0.280769	0.000035	0.280761	-31	1.3	3372	1800
F152A-59.2	0.002925	0.000237	0.000091	0.000006	1.4670	1.8866	0.280831	0.000031	0.280828	-28	1.2	3277	1838
F152A-13	0.016605	0.002203	0.000374	0.000036	1.4670	1.8865	0.280749	0.000037	0.280730	-11	1.5	3411	2709
F152A-86	0.006597	0.000539	0.000160	0.000010	1.4670	1.8866	0.280797	0.000030	0.280789	-9	1.3	3329	2713
F152A-103	0.009808	0.001541	0.000239	0.000027	1.4670	1.8866	0.280784	0.000052	0.280772	-10	2.0	3352	2713
F152A-77	0.010853	0.000893	0.000249	0.000015	1.4670	1.8866	0.280750	0.000051	0.280737	-11	2.0	3398	2715
F152A-121.1	0.014387	0.001379	0.000323	0.000024	1.4671	1.8866	0.280756	0.000032	0.280739	-11	1.4	3397	2718
F152A-121.2	0.019086	0.003037	0.000407	0.000054	1.4671	1.8864	0.280778	0.000040	0.280757	-10	1.6	3375	2718
F152A-68	0.004909	0.000796	0.000133	0.000015	1.4671	1.8868	0.280754	0.000032	0.280747	-10	1.4	3383	2725
F152A-3.1	0.017484	0.002181	0.000377	0.000038	1.4671	1.8867	0.280701	0.000034	0.280682	-12	1.4	3475	2728
F152A-3.2	0.003858	0.000523	0.000129	0.000019	1.4670	1.8867	0.280788	0.000039	0.280781	-9	1.6	3338	2728
F152A-59.1	0.015517	0.001832	0.000338	0.000030	1.4671	1.8869	0.280743	0.000029	0.280725	-11	1.3	3416	2728
F152A-14	0.010793	0.001060	0.000252	0.000019	1.4670	1.8867	0.280723	0.000033	0.280709	-11	1.4	3435	2730
F152A-1	0.013574	0.001383	0.000300	0.000023	1.4671	1.8866	0.280785	0.000047	0.280769	-9	1.8	3357	2733
F152A-79	0.018826	0.002380	0.000407	0.000041	1.4671	1.8866	0.280771	0.000028	0.280750	-10	1.2	3385	2733
F152A-12	0.015562	0.001683	0.000347	0.000029	1.4671	1.8866	0.280744	0.000036	0.280726	-11	1.5	3415	2736
F152A-38	0.013851	0.001682	0.000308	0.000029	1.4671	1.8865	0.280782	0.000031	0.280766	-9	1.3	3361	2737
F152A-80.1	0.012361	0.001092	0.000269	0.000018	1.4670	1.8866	0.280698	0.000036	0.280684	-12	1.5	3470	2737
F152A-35.1	0.012614	0.001981	0.000286	0.000031	1.4670	1.8868	0.280753	0.000048	0.280737	-10	1.9	3398	2743
F152A-35.2	0.009932	0.001269	0.000270	0.000024	1.4668	1.8867	0.280776	0.000050	0.280762	-9	1.9	3365	2743

APPENDIX 4C - LASS-ICPMS Lu-Hf isotopic data from snow ball area samples

Spot name	$\frac{^{176}Yb}{^{177}Hf}$	±2s	$\frac{^{176}Lu}{^{177}Hf}$	±2s	$\frac{^{178}Hf}{^{177}Hf}$	$\frac{^{180}Hf}{^{177}Hf}$	$\frac{^{176}Hf}{^{177}Hf}$	±2s	$\frac{^{176}Hf}{^{177}Hf}$	εHf(t)[1]	±2s	age (Ma) T_{DM}[2]	age (Ma) $\frac{^{207}Pb}{^{206}Pb}$
F152A-80.2	0.007943	0.000815	0.000217	0.000025	1.4669	1.8867	0.280805	0.000049	0.280793	-8	1.9	3323	2745
F152A-33	0.025113	0.003396	0.000523	0.000059	1.4672	1.8866	0.280715	0.000037	0.280688	-12	1.5	3469	2746

Footnotes:

(1) Initial $^{176}Hf/^{177}Hf$ and εHf calculated using the 206/207Pb age determined by SHRIMP dating (see column f), and the CHUR parameters: $^{176}Lu/^{177}Hf = 0.0336$, and $^{176}Hf/^{177}Hf = 0.282785$ (Bouvier *et al*., 2008).

(2) depleted mantle model ages were calculated using the measured $^{176}Lu/^{177}Hf$ of each spot and a depleted mantle (DM) $^{176}Lu/^{177}Hf$ and $^{176}Hf/^{177}Hf$ of 0.038 and 0.283223, respectively (Vervoort and Blichert-Toft, 1999).

- data in grey are from magmatic zircon used to calculated the crystallization age of the unit

- strikethrough data did not meet minimum percision requirements or yielded T_{DM} ages younger than the $^{207}Pb/^{206}Pb$ age and were not used in further calculations, plots or discussed in the text

APPENDIX 4D - LASS-ICPMS Lu-Hf isotopic data from regional samples

Spot name	$^{176}Yb/^{177}Hf$	±2s	$^{176}Lu/^{177}Hf$	±2s	$^{178}Hf/^{177}Hf$	$^{180}Hf/^{177}Hf$	$^{176}Hf/^{177}Hf$	±2s	$^{176}Hf/^{177}Hf$	εHf(t)[1]	±2s	age (Ma) T_{DM}[2]	age (Ma) $^{207}Pb/^{206}Pb$
H098A, tonalite gneiss													
692183 7154679 NAD 1983 UTM Zone 19N													
~~H098A - 12~~	~~0.029400~~	~~0.004500~~	~~0.000780~~	~~0.000100~~	~~1.4673~~	~~1.8867~~	~~0.281131~~	~~0.000057~~	~~0.281094~~	~~-3~~	~~2.1~~	~~2929~~	~~2481~~
~~H098A - 11_1~~	~~0.041200~~	~~0.004600~~	~~0.001062~~	~~0.000085~~	~~1.4672~~	~~1.8867~~	~~0.281205~~	~~0.000300~~	~~0.281154~~	~~-1~~	~~10.7~~	~~2849~~	~~2481~~
~~H098A - 20~~	~~0.070700~~	~~0.001200~~	~~0.001849~~	~~0.000047~~	~~1.4673~~	~~1.8867~~	~~0.281415~~	~~0.000110~~	~~0.281323~~	~~7~~	~~4.0~~	~~2614~~	~~2590~~
H098A - 11 - 2	0.017000	0.001100	0.000501	0.000026	1.4674	1.8868	0.281033	0.000041	0.281008	-3	1.6	3041	2620
H098A - 9	0.013170	0.000380	0.000402	0.000012	1.4674	1.8870	0.281138	0.000053	0.281117	1	2.0	2891	2624
H098A - 6	0.027000	0.012000	0.000710	0.000280	1.4674	1.8868	0.280996	0.000094	0.280960	-5	3.5	3107	2639
H098A - 15	0.011560	0.000300	0.000324	0.000005	1.4674	1.8870	0.281091	0.000017	0.281074	0	0.9	2949	2677
~~H098A - 17~~	~~0.042600~~	~~0.001100~~	~~0.001099~~	~~0.000041~~	~~1.4673~~	~~1.8868~~	~~0.281230~~	~~0.000098~~	~~0.281173~~	~~4~~	~~3.6~~	~~2818~~	~~2694~~
H098A - 8	0.028310	0.000900	0.000832	0.000025	1.4673	1.8868	0.281159	0.000058	0.281116	2	2.2	2895	2696
H098A - 5	0.000000	0.000000	0.000000	0.000000	0.0000	0.0000	0.000000	0.000000	0.000000	0	0.0	0	2702
H098A - 13	0.018800	0.001400	0.000542	0.000033	1.4674	1.8868	0.281095	0.000039	0.281066	1	1.6	2960	2732
H098A - 3	0.015400	0.002500	0.000474	0.000058	1.4673	1.8868	0.281113	0.000048	0.281088	2	1.9	2930	2739
H098A - 16	0.044100	0.002100	0.001133	0.000027	1.4673	1.8868	0.281194	0.000050	0.281134	4	1.9	2870	2742
H098A - 10 - 2	0.017900	0.003100	0.000497	0.000072	1.4672	1.8868	0.281066	0.000075	0.281040	1	2.8	2996	2744
H098A - 14	0.013400	0.001000	0.000401	0.000033	1.4673	1.8868	0.281107	0.000035	0.281086	2	1.4	2933	2745
H098A - 1	0.000000	0.000000	0.000000	0.000000	0.0000	0.0000	0.000000	0.000000	0.000000	0	0.0	0	2761
~~H098A - 7~~	~~0.000000~~	~~0.000000~~	~~0.000000~~	~~0.000000~~	~~0.0000~~	~~0.0000~~	~~0.000000~~	~~0.000000~~	~~0.000000~~	~~0~~	~~0.0~~	~~0~~	~~2778~~
~~H098A - 19~~	~~0.013600~~	~~0.000800~~	~~0.000374~~	~~0.000022~~	~~1.4674~~	~~1.8868~~	~~0.281228~~	~~0.000043~~	~~0.281208~~	~~8~~	~~1.7~~	~~2768~~	~~2781~~
~~H098A - 2~~	~~0.010800~~	~~0.001100~~	~~0.000309~~	~~0.000027~~	~~1.4674~~	~~1.8868~~	~~0.281072~~	~~0.000064~~	~~0.281055~~	~~2~~	~~2.4~~	~~2973~~	~~2792~~
~~H098A - 4~~	~~0.032500~~	~~0.001700~~	~~0.000962~~	~~0.000057~~	~~1.4673~~	~~1.8868~~	~~0.281107~~	~~0.000047~~	~~0.281055~~	~~3~~	~~1.8~~	~~2976~~	~~2811~~
H098A - 10	0.026500	0.005900	0.000700	0.000150	1.4673	1.8870	0.281045	0.000110	0.281007	1	4.0	3040	2811
H098A - 18	0.023400	0.002100	0.000659	0.000053	1.4673	1.8868	0.281130	0.000047	0.281094	4	1.8	2922	2814
H086A, tonalite gneiss													
719964 7118577 NAD1983, UTM Zone 19N													
~~H086A - 17~~	~~0.032500~~	~~0.002300~~	~~0.000938~~	~~0.000042~~	~~1.4674~~	~~1.8868~~	~~0.281138~~	~~0.000052~~	~~0.281095~~	~~-5~~	~~2.0~~	~~2931~~	~~2411~~
H086A - 17 - 2	0.030800	0.001700	0.000949	0.000043	1.4673	1.8870	0.281105	0.000076	0.281060	-5	2.8	2977	2470
H086A - 11	0.020600	0.001200	0.000642	0.000026	1.4673	1.8870	0.281104	0.000051	0.281073	-3	1.9	2955	2527
H086A - 9	0.018110	0.000830	0.000499	0.000020	1.4673	1.8869	0.281077	0.000033	0.281053	-3	1.4	2980	2557
H086A - 18	0.027500	0.002400	0.000762	0.000060	1.4673	1.8869	0.281105	0.000045	0.281068	-2	1.7	2963	2568

APPENDIX 4D - LASS-ICPMS Lu-Hf isotopic data from regional samples

Spot name	$^{176}Yb/^{177}Hf$	±2s	$^{176}Lu/^{177}Hf$	±2s	$^{178}Hf/^{177}Hf$	$^{180}Hf/^{177}Hf$	$^{176}Hf/^{177}Hf$	±2s	$^{176}Hf/^{177}Hf$	εHf(t)[1]	±2s	age (Ma) T_{DM}[2]	age (Ma) $^{207}Pb/^{206}Pb$
H086A - 14	0.010650	0.000400	0.000298	0.000005	1.4674	1.8870	0.281079	0.000047	0.281064	-1	1.8	2962	2623
~~H086A - 4~~	~~0.013500~~	~~0.001900~~	~~0.000401~~	~~0.000059~~	~~1.4673~~	~~1.8868~~	~~0.281061~~	~~0.000043~~	~~0.281041~~	~~-2~~	~~1.7~~	~~2994~~	~~2636~~
~~H086A - 21 - 2~~	~~0.017500~~	~~0.003100~~	~~0.000570~~	~~0.000110~~	~~1.4673~~	~~1.8868~~	~~0.281119~~	~~0.000067~~	~~0.281090~~	~~0~~	~~2.5~~	~~2929~~	~~2637~~
~~H086A - 22~~	~~0.053200~~	~~0.006100~~	~~0.001480~~	~~0.000110~~	~~1.4673~~	~~1.8868~~	~~0.281152~~	~~0.000079~~	~~0.281076~~	0	2.9	2954	~~2674~~
H086A - 7	0.013120	0.000380	0.000393	0.000011	1.4673	1.8868	0.281094	0.000051	0.281074	1	2.0	2949	2684
~~H086A - 14 - 2~~	~~0.010150~~	~~0.000600~~	~~0.000312~~	~~0.000015~~	~~1.4674~~	~~1.8871~~	~~0.281052~~	~~0.000100~~	~~0.281036~~	~~0~~	~~3.6~~	~~2999~~	~~2727~~
H086A - 16	0.044000	0.002200	0.001245	0.000072	1.4673	1.8869	0.281178	0.000056	0.281112	4	2.1	2900	2758
H086A - 8	0.049400	0.002400	0.001377	0.000073	1.4673	1.8868	0.281228	0.000071	0.281155	5	2.6	2841	2767
H086A - 19	0.028600	0.002300	0.000850	0.000069	1.4673	1.8870	0.281155	0.000060	0.281110	4	2.3	2901	2775
H086A - 15	0.023900	0.005800	0.000700	0.000160	1.4672	1.8867	0.281153	0.000075	0.281116	4	2.8	2893	2780
H086A - 13	0.056300	0.001300	0.001531	0.000029	1.4673	1.8868	0.281265	0.000047	0.281184	7	1.8	2801	2782
H086A - 22 - 2	0.025100	0.005400	0.000790	0.000150	1.4671	1.8868	0.281108	0.000091	0.281066	3	3.3	2961	2784
H086A - 20	0.045200	0.004000	0.001252	0.000090	1.4674	1.8869	0.281182	0.000060	0.281115	4	2.3	2895	2785
H086A - 10	0.020090	0.000390	0.000591	0.000011	1.4673	1.8868	0.281175	0.000080	0.281144	6	2.9	2855	2798
H086A - 6	0.048700	0.001500	0.001329	0.000033	1.4673	1.8866	0.281193	0.000044	0.281122	5	1.7	2886	2798
H086A - 21	0.054800	0.006800	0.001500	0.000150	1.4674	1.8869	0.281210	0.000068	0.281130	5	2.5	2875	2799
H086A - 12	0.048000	0.010000	0.001380	0.000280	1.4672	1.8868	0.281168	0.000078	0.281094	4	2.9	2924	2801
H086A - 5	0.023500	0.003400	0.000683	0.000088	1.4673	1.8868	0.281149	0.000049	0.281112	5	1.9	2897	2812
H086A - 3	0.023900	0.001600	0.000702	0.000044	1.4674	1.8870	0.281105	0.000037	0.281067	4	1.5	2958	2836
H086A - 23	0.027000	0.001700	0.000792	0.000049	1.4674	1.8870	0.281122	0.000038	0.281079	5	1.6	2942	2856
~~H086A - 1~~	~~0.021090~~	~~0.000920~~	~~0.000664~~	~~0.000033~~	~~1.4673~~	~~1.8869~~	~~0.281060~~	~~0.000050~~	~~0.281024~~	3	1.9	3016	~~2867~~
H086A - 2	0.059300	0.001800	0.001724	0.000040	1.4673	1.8868	0.281251	0.000076	0.281155	9	2.8	2835	2911
F040A, tonalite gneiss													
620333 7136294 NAD 1983 UTM Zone 19N													
F040 - 21	0.051000	0.019000	0.001420	0.000490	1.4674	1.8870	0.281001	0.000065	0.281001	-63	2.3	3158	-
F040 - 24	0.015100	0.001000	0.000462	0.000034	1.4673	1.8868	0.281234	0.000038	0.281234	-55	1.4	2765	-
~~F040 - 3~~	~~0.035600~~	~~0.002900~~	~~0.000973~~	~~0.000081~~	~~1.4673~~	~~1.8869~~	~~0.281260~~	~~0.000076~~	~~0.281211~~	~~5~~	~~2.8~~	~~2767~~	~~2655~~
F040 - 15	0.040000	0.012000	0.001160	0.000290	1.4674	1.8869	0.281092	0.000130	0.281032	0	4.7	3012	2723
F040 - 14	0.020800	0.002000	0.000639	0.000064	1.4673	1.8869	0.281078	0.000040	0.281045	1	1.6	2990	2744
~~F040 - 12~~	~~0.036800~~	~~0.004800~~	~~0.001070~~	~~0.000120~~	~~1.4674~~	~~1.8870~~	~~0.281096~~	~~0.000079~~	~~0.281040~~	~~1~~	~~2.9~~	~~2999~~	~~2759~~
F040 - 23	0.036800	0.004400	0.001090	0.000120	1.4674	1.8869	0.281120	0.000067	0.281061	2	2.5	2968	2767

APPENDIX 4D - LASS-ICPMS Lu-Hf isotopic data from regional samples

Spot name	$^{176}Yb/^{177}Hf$	±2s	$^{176}Lu/^{177}Hf$	±2s	$^{178}Hf/^{177}Hf$	$^{180}Hf/^{177}Hf$	$^{176}Hf/^{177}Hf$	±2s	$^{176}Hf/^{177}Hf$	εHf(t)[1]	±2s	age (Ma) T_{DM}[2]	age (Ma) $^{207}Pb/^{206}Pb$
F040 - 6	0.023380	0.000690	0.000735	0.000025	1.4673	1.8867	0.281024	0.000049	0.280985	0	1.9	3071	2780
F040 - 10	0.034000	0.003800	0.001015	0.000097	1.4673	1.8868	0.281136	0.000061	0.281082	3	2.3	2940	2784
~~F040 - 13~~	~~0.024600~~	~~0.009200~~	~~0.000690~~	~~0.000220~~	~~1.4672~~	~~1.8869~~	~~0.281182~~	~~0.000100~~	~~0.281145~~	~~5~~	~~3.7~~	~~2852~~	~~2784~~
F040 - 7	0.026400	0.003100	0.000830	0.000100	1.4673	1.8867	0.281070	0.000085	0.281026	1	3.1	3016	2787
F040 - 1	0.014800	0.001300	0.000449	0.000022	1.4673	1.8870	0.280930	0.000074	0.280906	-3	2.7	3174	2791
F040 - 5	0.014200	0.001000	0.000430	0.000029	1.4674	1.8869	0.281036	0.000072	0.281013	1	2.7	3030	2791
F040 - 2	0.027400	0.004200	0.000860	0.000120	1.4673	1.8867	0.281115	0.000085	0.281069	3	3.1	2957	2804
F040 - 11	0.028630	0.000940	0.000859	0.000022	1.4673	1.8868	0.281053	0.000052	0.281007	1	2.0	3041	2810
F040 - 20	0.026700	0.000720	0.000797	0.000014	1.4673	1.8869	0.281113	0.000065	0.281070	4	2.4	2954	2815
F040 - 16	0.034900	0.003000	0.001039	0.000069	1.4673	1.8869	0.281097	0.000052	0.281041	2	2.0	2995	2816
F040 - 8	0.025400	0.002200	0.000771	0.000053	1.4674	1.8870	0.280980	0.000073	0.280939	-1	2.7	3133	2821
F040 - 18	0.037200	0.006000	0.001110	0.000180	1.4674	1.8868	0.281074	0.000060	0.281014	2	2.3	3032	2822
F040 - 17	0.029600	0.004200	0.000880	0.000110	1.4674	1.8871	0.281108	0.000059	0.281061	3	2.2	2968	2827
F040 - 1 - 2	0.018500	0.001300	0.000591	0.000047	1.4673	1.8868	0.281024	0.000091	0.280993	1	3.3	3059	2828
F040 - 9	0.030100	0.001400	0.000902	0.000046	1.4674	1.8869	0.281060	0.000037	0.281011	2	1.5	3035	2833
F040 - 19	0.044800	0.006900	0.001330	0.000200	1.4674	1.8871	0.281158	0.000056	0.281086	5	2.2	2934	2836
F040 - 4	0.029700	0.003200	0.000950	0.000100	1.4673	1.8869	0.281162	0.000130	0.281110	6	4.7	2899	2845
F040 - 22	0.026500	0.001400	0.000822	0.000037	1.4673	1.8870	0.281090	0.000037	0.281046	4	1.5	2988	2853
K037A, tonalite gneiss													
607104 7161794 NAD1983, UTM Zone 19N													
~~K037A - 21~~	~~0.000660~~	~~0.000180~~	~~0.000012~~	~~0.000003~~	~~1.4674~~	~~1.8869~~	~~0.281098~~	~~0.000045~~	~~0.281098~~	~~-24~~	~~1.7~~	~~2915~~	~~1598~~
~~K037A - 22~~	~~0.001410~~	~~0.000730~~	~~0.000027~~	~~0.000014~~	~~1.4673~~	~~1.8868~~	~~0.281113~~	~~0.000028~~	~~0.281112~~	~~-21~~	~~1.1~~	~~2896~~	~~1686~~
K037A - 11	0.000289	0.000030	0.000005	0.000001	1.4674	1.8869	0.281092	0.000052	0.281092	-20	1.9	2923	1774
~~K037A - 7~~	~~0.001160~~	~~0.000260~~	~~0.000024~~	~~0.000005~~	~~1.4673~~	~~1.8868~~	~~0.281153~~	~~0.000039~~	~~0.281152~~	~~-18~~	~~1.5~~	~~2842~~	~~1782~~
K037A - 16	0.002000	0.001600	0.000054	0.000046	1.4673	1.8869	0.281133	0.000054	0.281131	-18	2.0	2871	1783
K037A - 9	0.000095	0.000032	0.000001	0.000000	1.4674	1.8868	0.281116	0.000033	0.281116	-19	1.3	2890	1795
K037A - 8	0.000074	0.000037	0.000001	0.000000	1.4673	1.8869	0.281067	0.000040	0.281067	-20	1.5	2956	1805
K037A - 19	0.000597	0.000026	0.000011	0.000000	1.4673	1.8868	0.281163	0.000037	0.281163	-17	1.4	2828	1814
K037A - 20	0.000325	0.000040	0.000005	0.000000	1.4673	1.8868	0.281120	0.000029	0.281120	-18	1.2	2885	1823
K037A - 10	0.000170	0.000064	0.000004	0.000002	1.4673	1.8869	0.281142	0.000037	0.281142	-17	1.4	2856	1828
K037A - 24	0.000630	0.000170	0.000017	0.000005	1.4673	1.8869	0.281156	0.000042	0.281156	-16	1.6	2838	1832

APPENDIX 4D - LASS-ICPMS Lu-Hf isotopic data from regional samples

Spot name	$^{176}Yb/^{177}Hf$	±2s	$^{176}Lu/^{177}Hf$	±2s	$^{178}Hf/^{177}Hf$	$^{180}Hf/^{177}Hf$	$^{176}Hf/^{177}Hf$	±2s	$^{176}Hf/^{177}Hf$	εHf(t)[1]	±2s	age (Ma) T_{DM}[2]	age (Ma) $^{207}Pb/^{206}Pb$
K037A - 18	0.002100	0.001400	0.000054	0.000041	1.4673	1.8868	0.281142	0.000060	0.281140	-17	2.2	2859	1848
K037A - 12	0.006500	0.002400	0.000182	0.000070	1.4672	1.8868	0.281116	0.000036	0.281110	-17	1.4	2904	1865
K037A - 25	0.001260	0.000530	0.000034	0.000015	1.4674	1.8869	0.281135	0.000043	0.281134	-16	1.6	2867	1870
~~K037A - 11 - 2~~	~~0.012100~~	~~0.002100~~	~~0.000347~~	~~0.000056~~	~~1.4673~~	~~1.8868~~	~~0.281110~~	~~0.000099~~	~~0.281095~~	~~-7~~	~~3.6~~	~~2924~~	~~2322~~
~~K037A - 2~~	~~0.013230~~	~~0.000250~~	~~0.000359~~	~~0.000006~~	~~1.4673~~	~~1.8868~~	~~0.280824~~	~~0.000057~~	~~0.280807~~	~~-13~~	~~2.1~~	~~3309~~	~~2492~~
K037A - 4	0.014850	0.000680	0.000398	0.000020	1.4673	1.8868	0.280842	0.000031	0.280823	-13	1.3	3288	2503
K037A - 6	0.026300	0.002400	0.000666	0.000047	1.4673	1.8868	0.280894	0.000064	0.280862	-10	2.4	3241	2563
K037A - 14	0.017590	0.000350	0.000469	0.000009	1.4674	1.8869	0.280874	0.000050	0.280851	-10	1.9	3251	2565
K037A - 1	0.038160	0.000590	0.000957	0.000022	1.4673	1.8868	0.281009	0.000052	0.280962	-6	2.0	3109	2574
~~K037A - 26~~	~~0.017600~~	~~0.002100~~	~~0.000496~~	~~0.000044~~	~~1.4673~~	~~1.8869~~	~~0.281202~~	~~0.000085~~	~~0.281177~~	~~3~~	~~3.1~~	~~2811~~	~~2610~~
K037A - 17	0.039800	0.005000	0.000990	0.000130	1.4673	1.8868	0.281003	0.000080	0.280953	-5	2.9	3120	2627
K037A - 23	0.014200	0.001100	0.000399	0.000031	1.4673	1.8867	0.280845	0.000090	0.280825	-9	3.3	3284	2644
K037A - 5	0.041300	0.002200	0.001027	0.000032	1.4673	1.8869	0.280899	0.000049	0.280847	-8	1.9	3265	2663
K037A - 15	0.021480	0.000530	0.000570	0.000012	1.4673	1.8869	0.280970	0.000041	0.280941	-4	1.6	3130	2686
K037A - 3	0.025900	0.002600	0.000669	0.000065	1.4674	1.8870	0.280809	0.000072	0.280775	-10	2.7	3356	2692
F163B, tonalite gneiss													
669461 7094784 NAD1983, UTM Zone 19N													
F163B - 3	0.004310	0.000660	0.000152	0.000029	1.4675	1.8869	0.280986	0.000070	0.280978	-2	2.6	3075	2731
F163B - 12	0.006187	0.000060	0.000197	0.000002	1.4674	1.8870	0.281006	0.000069	0.280996	-1	2.6	3052	2740
~~F163B - 4~~	~~0.020000~~	~~0.001000~~	~~0.000571~~	~~0.000021~~	~~1.4674~~	~~1.8869~~	~~0.281086~~	~~0.000058~~	~~0.281056~~	~~2~~	~~2.2~~	~~2974~~	~~2753~~
F163B - 14	0.006200	0.000120	0.000208	0.000006	1.4673	1.8869	0.281014	0.000057	0.281003	0	2.2	3042	2784
F163B - 16	0.003330	0.000150	0.000110	0.000005	1.4674	1.8870	0.280997	0.000040	0.280991	0	1.6	3057	2784
~~F163B - 19~~	~~0.014400~~	~~0.003000~~	~~0.000443~~	~~0.000078~~	~~1.4672~~	~~1.8869~~	~~0.281098~~	~~0.000082~~	~~0.281074~~	~~3~~	~~3.0~~	~~2948~~	~~2807~~
F163B - 8	0.003750	0.000120	0.000119	0.000005	1.4673	1.8868	0.281000	0.000022	0.280994	1	1.1	3054	2813
F163B - 21	0.013200	0.002500	0.000409	0.000069	1.4674	1.8873	0.280975	0.000053	0.280953	-1	2.0	3111	2815
F163B - 15	0.011700	0.003400	0.000347	0.000095	1.4673	1.8869	0.281023	0.000043	0.281004	1	1.7	3041	2820
F163B - 18	0.011700	0.001100	0.000357	0.000036	1.4674	1.8869	0.281061	0.000044	0.281042	3	1.7	2991	2826
F163B - 11	0.025980	0.000850	0.000764	0.000036	1.4674	1.8868	0.281081	0.000067	0.281040	3	2.5	2995	2833
F163B - 1	0.016600	0.002600	0.000487	0.000069	1.4674	1.8869	0.281106	0.000047	0.281080	4	1.8	2940	2834
F163B - 17	0.007610	0.000670	0.000255	0.000023	1.4673	1.8868	0.281022	0.000059	0.281008	2	2.2	3035	2835
F163B - 22	0.014000	0.002000	0.000432	0.000056	1.4673	1.8869	0.281064	0.000034	0.281041	3	1.4	2993	2839

APPENDIX 4D - LASS-ICPMS Lu-Hf isotopic data from regional samples

Spot name	$^{176}Yb/^{177}Hf$	±2s	$^{176}Lu/^{177}Hf$	±2s	$^{178}Hf/^{177}Hf$	$^{180}Hf/^{177}Hf$	$^{176}Hf/^{177}Hf$	±2s	$^{176}Hf/^{177}Hf$	εHf(t)[1]	±2s	age (Ma) T_{DM}[2]	age (Ma) $^{207}Pb/^{206}Pb$
F163B - 5	0.009280	0.000750	0.000287	0.000024	1.4674	1.8869	0.281084	0.000041	0.281069	4	1.6	2955	2840
F163B - 13	0.020000	0.001300	0.000614	0.000033	1.4674	1.8870	0.281060	0.000066	0.281027	3	2.5	3012	2843
F163B - 7	0.017720	0.000790	0.000539	0.000015	1.4674	1.8870	0.281059	0.000045	0.281030	3	1.8	3008	2844
F163B - 4 - 2	0.022800	0.001400	0.000698	0.000041	1.4674	1.8871	0.281064	0.000072	0.281026	3	2.7	3013	2854
~~F163B - 2~~	~~0.017100~~	~~0.002100~~	~~0.000510~~	~~0.000055~~	~~1.4674~~	~~1.8870~~	~~0.281090~~	~~0.000070~~	~~0.281062~~	~~4~~	~~2.6~~	~~2964~~	~~2855~~
F163B - 20	0.012750	0.000800	0.000385	0.000022	1.4673	1.8871	0.280961	0.000051	0.280940	0	2.0	3128	2866
F163B - 6	0.018900	0.003200	0.000522	0.000070	1.4673	1.8871	0.280960	0.000062	0.280930	2	2.3	3140	2970
F163B - 9	0.041100	0.005500	0.001120	0.000130	1.4673	1.8869	0.281068	0.000063	0.281004	5	2.4	3041	2972
F163B - 10	0.023680	0.000600	0.000653	0.000012	1.4674	1.8870	0.280989	0.000037	0.280952	3	1.5	3111	2984
Z108A, monzogranite gneiss													
662246 7122133 NAD1983 UTM Zone 19N													
~~Z108A - 21~~	~~0.022360~~	~~0.000850~~	~~0.000695~~	~~0.000030~~	~~1.4673~~	~~1.8868~~	~~0.281037~~	~~0.000046~~	~~0.281003~~	~~-6~~	~~1.8~~	~~3051~~	~~2504~~
~~Z108A - 13~~	~~0.053300~~	~~0.001400~~	~~0.001321~~	~~0.000048~~	~~1.4673~~	~~1.8867~~	~~0.281255~~	~~0.000110~~	~~0.281191~~	~~1~~	~~4.0~~	~~2800~~	~~2516~~
Z108A - 22	0.025500	0.002200	0.000772	0.000062	1.4673	1.8868	0.281069	0.000053	0.281031	-5	2.0	3013	2521
Z108A - 8	0.026520	0.000450	0.000772	0.000018	1.4674	1.8868	0.281080	0.000044	0.281042	-4	1.7	2998	2546
Z108A - 14	0.024700	0.001600	0.000736	0.000034	1.4673	1.8867	0.281066	0.000030	0.281030	-4	1.3	3014	2546
~~Z108A - 13 - 2~~	~~0.026500~~	~~0.001200~~	~~0.000791~~	~~0.000017~~	~~1.4672~~	~~1.8865~~	~~0.281095~~	~~0.000130~~	~~0.281056~~	~~-3~~	~~4.7~~	~~2979~~	~~2572~~
Z108A - 6	0.024670	0.000950	0.000707	0.000037	1.4674	1.8867	0.281089	0.000066	0.281054	-3	2.4	2981	2578
Z108A - 5	0.045700	0.006400	0.001170	0.000140	1.4673	1.8866	0.281185	0.000100	0.281125	2	3.6	2885	2650
Z108A - 19 - 2	0.025600	0.004200	0.000730	0.000120	1.4673	1.8867	0.281131	0.000094	0.281093	2	3.4	2926	2712
~~Z108A - 7~~	~~0.027700~~	~~0.002500~~	~~0.000745~~	~~0.000067~~	~~1.4673~~	~~1.8868~~	~~0.281067~~	~~0.000061~~	~~0.281028~~	~~0~~	~~2.3~~	~~3014~~	~~2727~~
Z108A - 12	0.025900	0.001600	0.000689	0.000028	1.4673	1.8866	0.281084	0.000083	0.281047	1	3.0	2986	2743
Z108A - 11	0.029500	0.004300	0.000820	0.000130	1.4672	1.8867	0.281116	0.000053	0.281072	2	2.0	2953	2769
Z108A - 10	0.053800	0.007400	0.001430	0.000210	1.4674	1.8867	0.281120	0.000090	0.281044	2	3.3	2995	2771
~~Z108A - 19~~	~~0.034200~~	~~0.005500~~	~~0.000870~~	~~0.000120~~	~~1.4673~~	~~1.8867~~	~~0.281109~~	~~0.000082~~	~~0.281062~~	~~2~~	~~3.0~~	~~2966~~	~~2772~~
Z108A - 20	0.027400	0.002000	0.000756	0.000039	1.4674	1.8869	0.281049	0.000044	0.281008	0	1.7	3039	2777
Z108A - 16	0.027000	0.002300	0.000743	0.000076	1.4673	1.8868	0.281105	0.000061	0.281065	3	2.3	2962	2790
Z108A - 4	0.020800	0.003300	0.000559	0.000084	1.4674	1.8867	0.281103	0.000064	0.281073	3	2.4	2950	2795
Z108A - 18	0.013500	0.001200	0.000373	0.000030	1.4673	1.8865	0.281066	0.000068	0.281046	2	2.5	2986	2801
Z108A - 2	0.022500	0.002100	0.000579	0.000049	1.4672	1.8867	0.281133	0.000075	0.281101	5	2.8	2911	2827
Z108A - 15	0.013600	0.002400	0.000395	0.000064	1.4673	1.8866	0.281042	0.000040	0.281020	3	1.6	3020	2856

APPENDIX 4D - LASS-ICPMS Lu-Hf isotopic data from regional samples

Spot name	$^{176}Yb/^{177}Hf$	±2s	$^{176}Lu/^{177}Hf$	±2s	$^{178}Hf/^{177}Hf$	$^{180}Hf/^{177}Hf$	$^{176}Hf/^{177}Hf$	±2s	$^{176}Hf/^{177}Hf$	εHf(t)[1]	±2s	age (Ma) T_{DM}[2]	age (Ma) $^{207}Pb/^{206}Pb$
Z108A - 9	0.036400	0.002100	0.000974	0.000052	1.4672	1.8867	0.281121	0.000071	0.281067	4	2.6	2958	2857
Z108A - 3	0.011700	0.002500	0.000292	0.000044	1.4672	1.8867	0.281006	0.000041	0.280990	2	1.6	3060	2860
Z108A - 1	0.011850	0.000480	0.000387	0.000018	1.4674	1.8869	0.280957	0.000047	0.280935	0	1.8	3134	2888
Z108A - 17	0.040200	0.004700	0.001150	0.000110	1.4673	1.8868	0.281051	0.000066	0.280986	3	2.5	3068	2925
F157A, monzogranite gneiss													
622813 7160311 NAD1983, UTM Zone 19N													
F157A - 14 - 2	0.020700	0.002300	0.000642	0.000068	1.4673	1.8868	0.281194	0.000046	0.281172	-16	1.7	2832	1819
F157A - 20 - 1	0.006350	0.000610	0.000200	0.000020	1.4673	1.8868	0.281099	0.000044	0.281092	-18	1.7	2928	1877
~~F157A - 14 - 1~~	~~0.013270~~	~~0.000490~~	~~0.000394~~	~~0.000018~~	~~1.4673~~	~~1.8870~~	~~0.281148~~	~~0.000047~~	~~0.281130~~	~~-3~~	~~1.8~~	~~2876~~	~~2459~~
F157A - 13 - 1	0.019500	0.002900	0.000566	0.000076	1.4673	1.8868	0.281139	0.000039	0.281111	0	1.6	2901	2597
~~F157A -7 - 1~~	~~0.016200~~	~~0.002000~~	~~0.000451~~	~~0.000050~~	~~1.4673~~	~~1.8866~~	~~0.281288~~	~~0.000059~~	~~0.281266~~	~~6~~	~~2.2~~	~~2691~~	~~2623~~
~~F157A - 16 - 1~~	~~0.009450~~	~~0.000450~~	~~0.000277~~	~~0.000007~~	~~1.4673~~	~~1.8868~~	~~0.281081~~	~~0.000037~~	~~0.281067~~	~~-1~~	~~1.5~~	~~2958~~	~~2629~~
F157A - 4 - 1	0.012600	0.001100	0.000363	0.000026	1.4673	1.8870	0.281154	0.000048	0.281136	1	1.8	2866	2630
F157A - 6 - 1	0.007350	0.000170	0.000215	0.000004	1.4673	1.8868	0.281079	0.000037	0.281068	0	1.5	2956	2648
F157A - 11 - 1	0.020800	0.003300	0.000584	0.000072	1.4673	1.8868	0.281172	0.000089	0.281143	2	3.2	2858	2650
F157A - 12 - 1	0.009260	0.000440	0.000274	0.000016	1.4673	1.8868	0.281084	0.000033	0.281070	0	1.4	2954	2651
F157A - 8 - 1	0.013120	0.000910	0.000401	0.000021	1.4673	1.8868	0.281081	0.000036	0.281061	-1	1.5	2967	2655
F157A -5 - 1	0.024500	0.001500	0.000652	0.000026	1.4673	1.8868	0.281365	0.000084	0.281332	9	3.1	2600	2657
F157A - 1 - 1	0.015000	0.001800	0.000449	0.000050	1.4673	1.8867	0.281087	0.000048	0.281064	0	1.9	2963	2661
F157A - 9 - 1	0.013370	0.000540	0.000400	0.000006	1.4673	1.8868	0.281150	0.000052	0.281130	2	2.0	2874	2668
~~F157A - 22 - 1~~	~~0.009753~~	~~0.000080~~	~~0.000277~~	~~0.000005~~	~~1.4673~~	~~1.8869~~	~~0.281081~~	~~0.000042~~	~~0.281067~~	~~0~~	~~1.7~~	~~2958~~	~~2674~~
F157A - 2 - 1	0.014000	0.001700	0.000424	0.000045	1.4673	1.8867	0.281085	0.000038	0.281063	0	1.5	2964	2684
F157A - 19 - 1	0.011000	0.001000	0.000313	0.000025	1.4673	1.8868	0.281113	0.000032	0.281097	1	1.3	2918	2684
~~F157A - 10 - 1~~	~~0.026900~~	~~0.001400~~	~~0.000754~~	~~0.000041~~	~~1.4673~~	~~1.8869~~	~~0.281290~~	~~0.000053~~	~~0.281251~~	~~7~~	~~2.0~~	~~2710~~	~~2691~~
F157A - 23 - 1	0.009360	0.000810	0.000283	0.000028	1.4674	1.8870	0.281088	0.000050	0.281074	1	1.9	2949	2715
F157A - 15 - 1	0.010340	0.000320	0.000302	0.000011	1.4673	1.8868	0.281096	0.000035	0.281081	1	1.4	2940	2695
F157A - 3 - 1	0.008910	0.000220	0.000270	0.000007	1.4673	1.8868	0.281069	0.000049	0.281055	1	1.9	2973	2711
~~F157A - 21 - 2~~	~~0.010800~~	~~0.001800~~	~~0.000348~~	~~0.000054~~	~~1.4674~~	~~1.8869~~	~~0.281059~~	~~0.000063~~	~~0.281041~~	~~1~~	~~2.4~~	~~2993~~	~~2732~~
F157A - 18 - 1	0.004940	0.000270	0.000174	0.000016	1.4674	1.8867	0.280971	0.000035	0.280962	-1	1.5	3097	2788
F157A - 17 - 1	0.010000	0.000960	0.000308	0.000029	1.4673	1.8868	0.281017	0.000033	0.281001	1	1.4	3046	2833
F157A - 21 - 1	0.051000	0.014000	-	-	-	1.8871	0.281162	0.000140	0.281081	9	5.0	2829	2924

APPENDIX 4D - LASS-ICPMS Lu-Hf isotopic data from regional samples

Spot name	$\frac{^{176}Yb}{^{177}Hf}$	±2s	$\frac{^{176}Lu}{^{177}Hf}$	±2s	$\frac{^{178}Hf}{^{177}Hf}$	$\frac{^{180}Hf}{^{177}Hf}$	$\frac{^{176}Hf}{^{177}Hf}$	±2s	$\frac{^{176}Hf}{^{177}Hf}$	εHf(t)[1]	±2s	age (Ma) T_{DM}[2]	age (Ma) $\frac{^{207}Pb}{^{206}Pb}$

Footnotes:

(1) Initial $^{176}Hf/^{177}Hf$ and eHf calculated using the 206/207Pb age determined by SHRIMP dating (see column f), and the CHUR parameters: $^{176}Lu/^{177}Hf$ = 0.0336, and $^{176}Hf/^{177}Hf$ = 0.282785 (Bouvier *et al*., 2008).

(2) depleted mantle model ages were calculated using the measured 176Lu/177Hf of each spot and a depleted mantle (DM) 176Lu/177Hf and 176Hf/177Hf of 0.038 and 0.283223, respectively (Vervoort and Blichert-Toft, 1999).

- data in grey are from magmatic zircon used to calculated the crystallization age of the unit

- strikethrough data did not meet minimum percision requirements or yielded T_{DM} ages younger than the $^{207}Pb/^{206}Pb$ age and were not used in further calculations, plots or discussed in the text

APPENDIX 4E. Concordia diagrams for snow bowl area and regional samples from eastern Hall Peninsula. Dark grey ellipses correspond to ages used to calculate the crystallization age; light grey ellipses are ages excluded from the crystallization-age calculation; Crystallization ages are weighted mean $^{207}Pb/^{206}Pb$ ages reported at the 2σ confidence level.

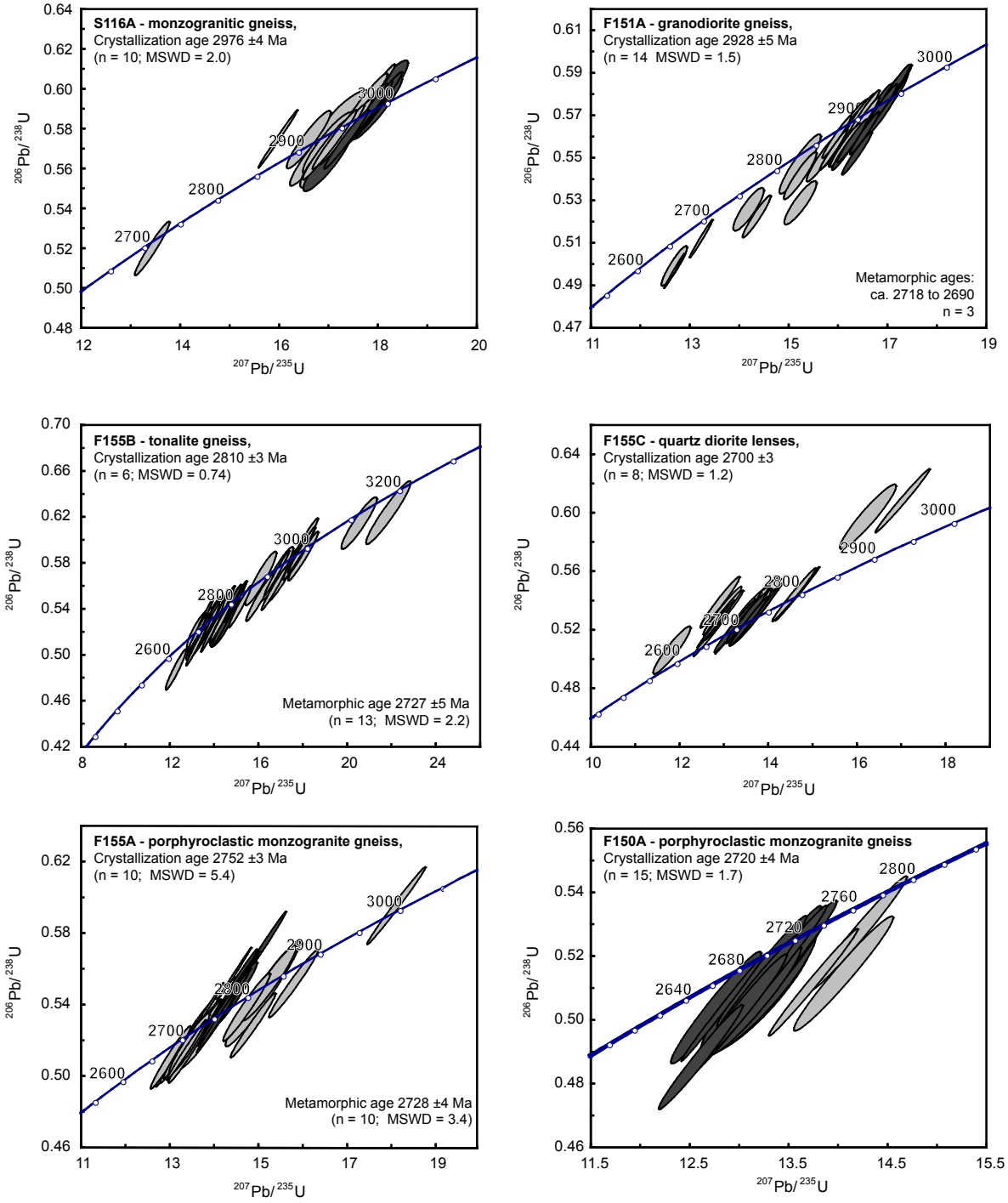

APPENDIX 4E cont'd. Concordia diagrams for snow bowl area and regional samples from eastern Hall Peninsula. Dark grey ellipses correspond to ages used to calculate the crystallization age; light grey ellipses are ages excluded from the crystallization-age calculation; Crystallization ages are weighted mean $^{207}Pb/^{206}Pb$ ages reported at the 2σ confidence level.

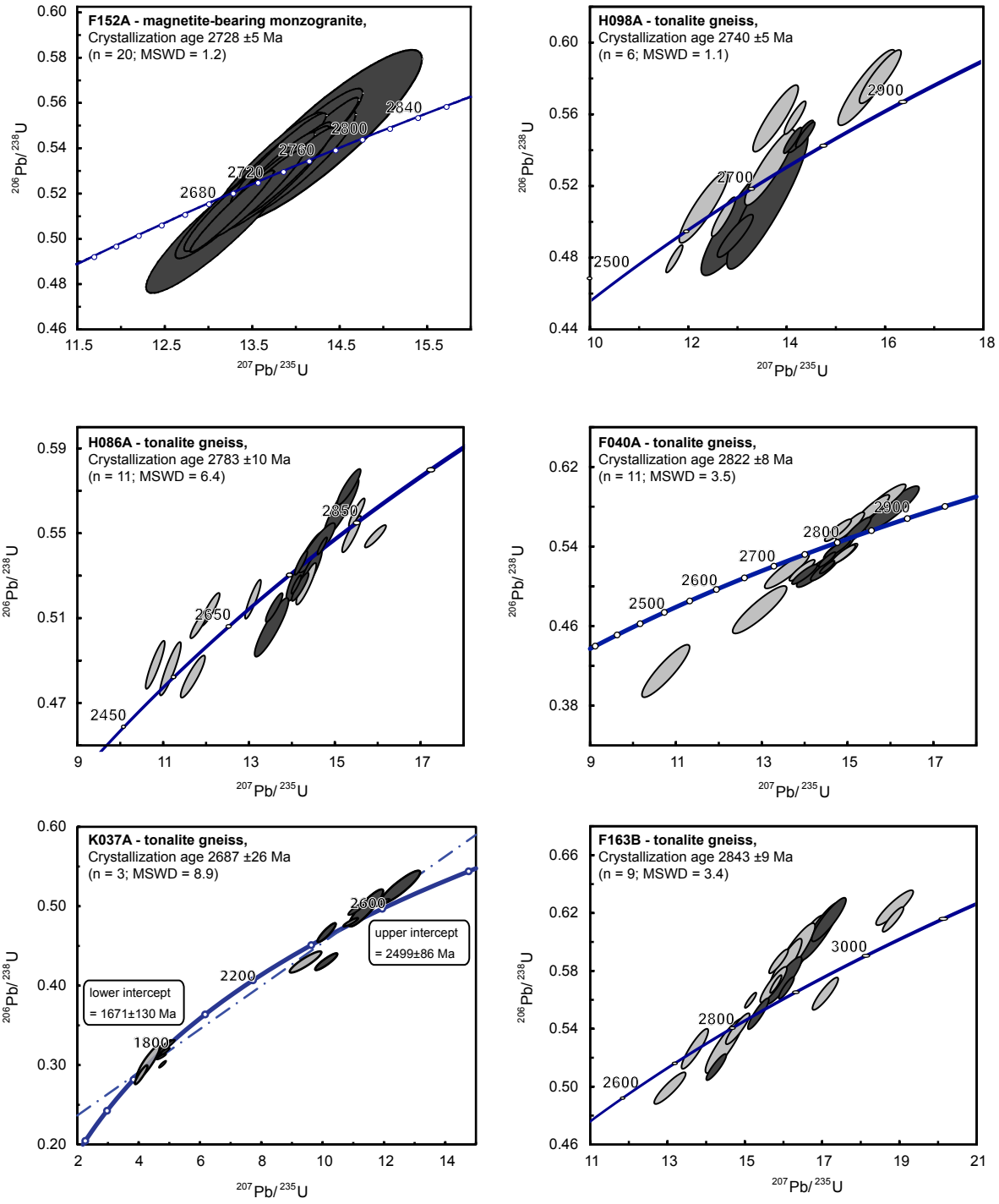

APPENDIX 4E cont'd. Concordia diagrams for snow bowl area and regional samples from eastern Hall Peninsula. Dark grey ellipses correspond to ages used to calculate the crystallization age; light grey ellipses are ages excluded from the crystallization-age calculation; Crystallization ages are weighted mean $^{207}Pb/^{206}Pb$ ages reported at the 2σ confidence level.

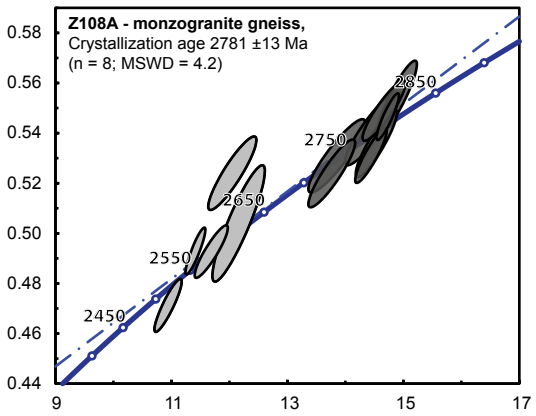

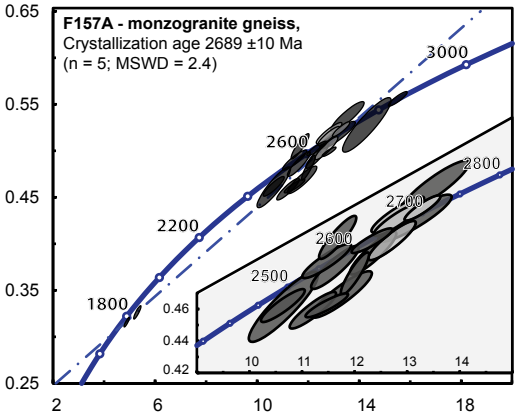

APPENDIX 4F. Th/U versus $^{207}Pb/^{206}Pb$ age diagrams for snow bowl area and regional samples from eastern Hall Peninsula.

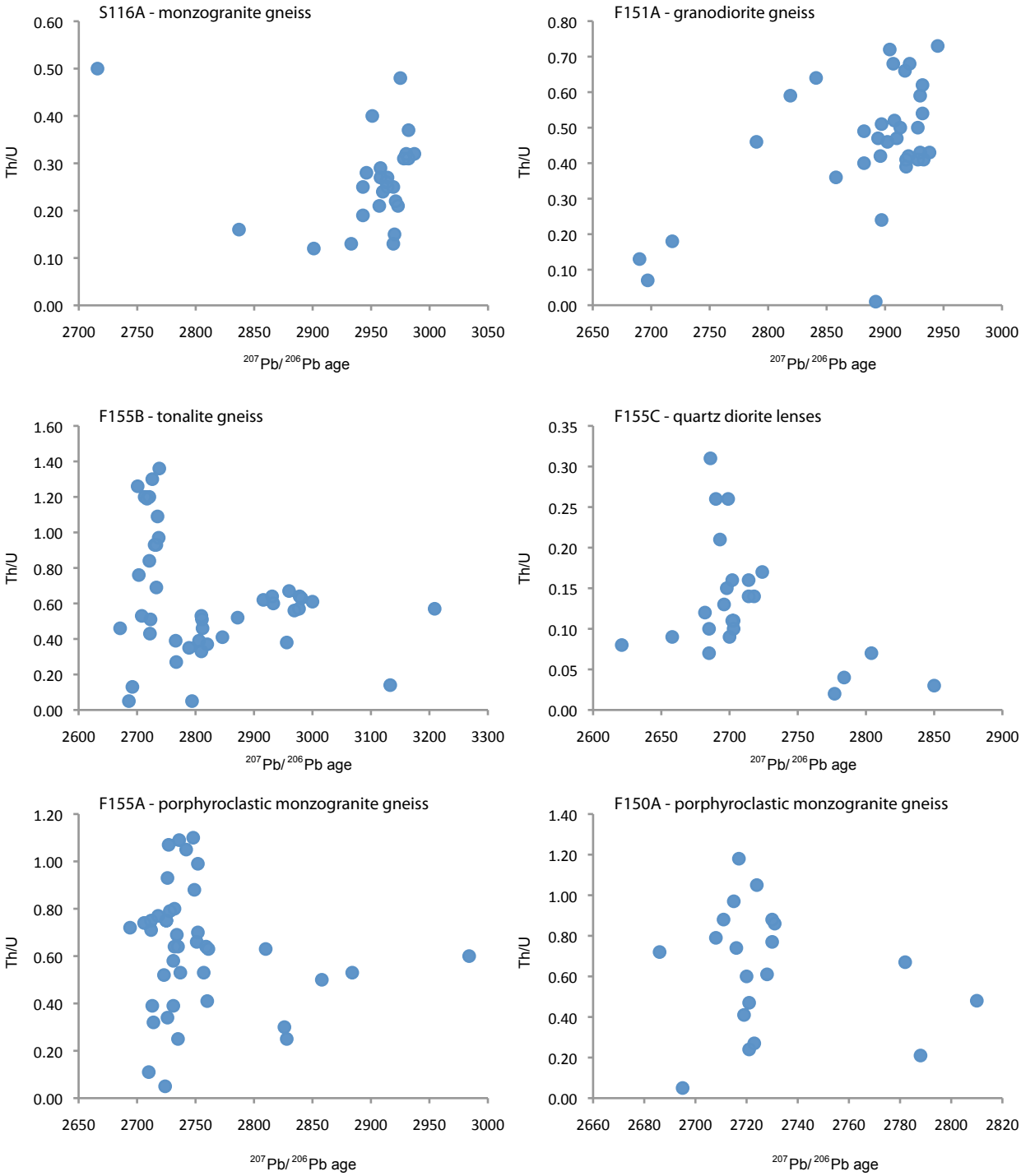

APPENDIX 4F cont'd. Th/U versus $^{207}Pb/^{206}Pb$ age diagrams for snow bowl area and regional samples from eastern Hall Peninsula.

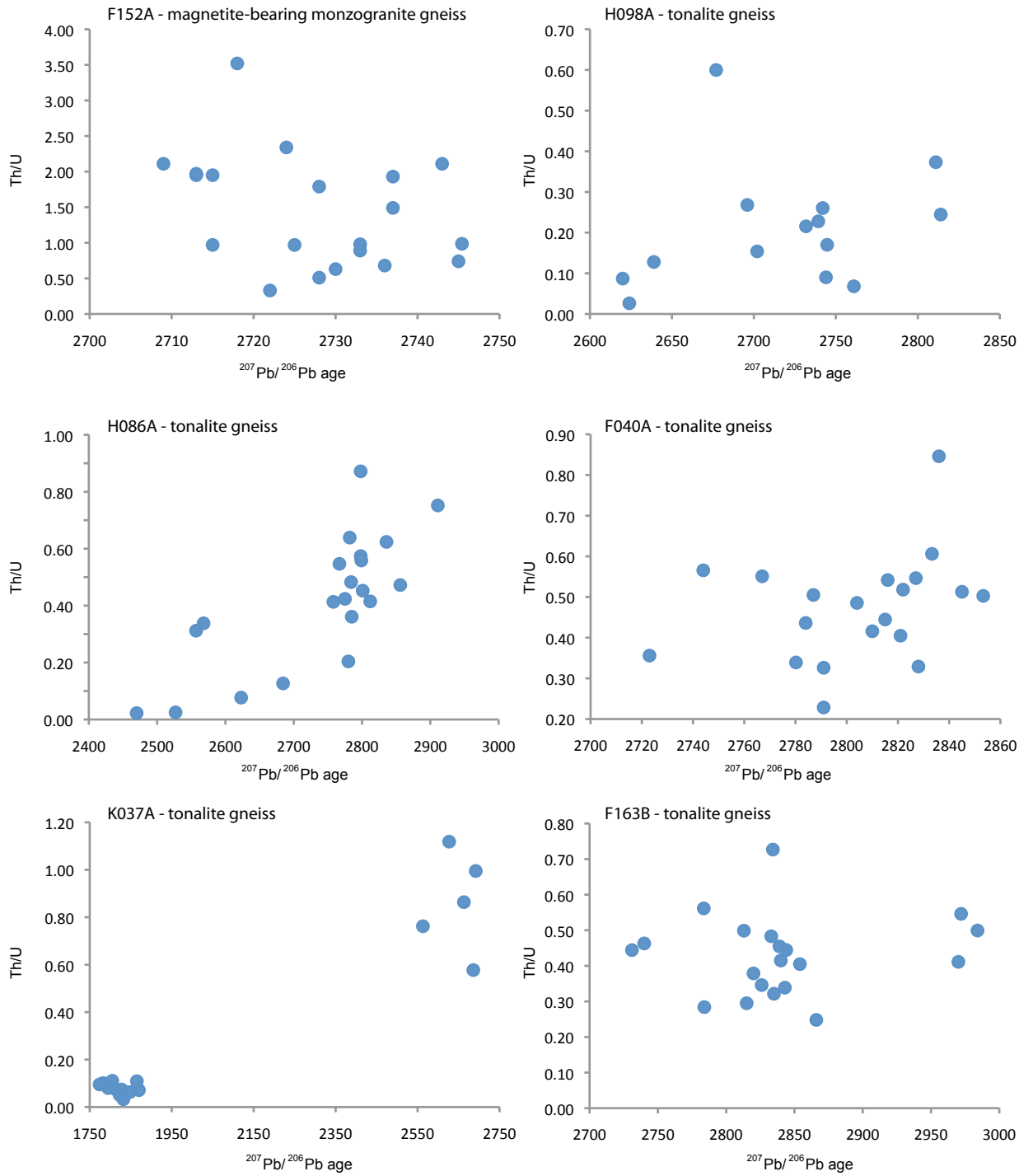

APPENDIX 4F cont'd. Th/U versus $^{207}Pb/^{206}Pb$ age diagrams for snow bowl area and regional samples from eastern Hall Peninsula.

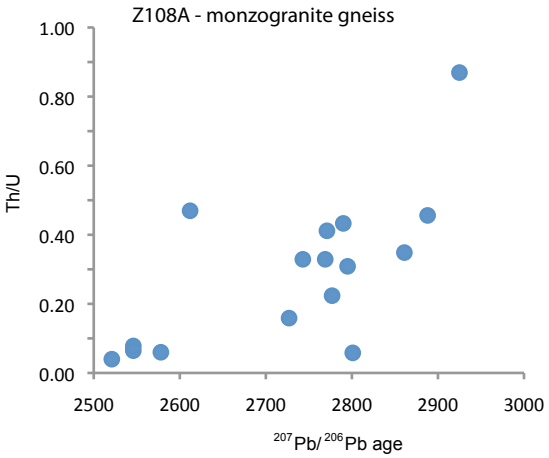

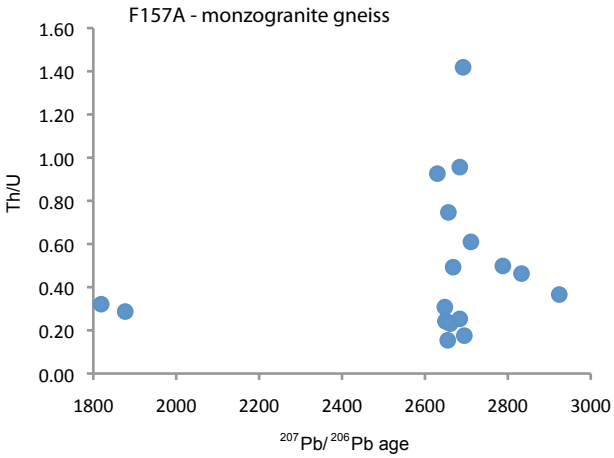

APPENDIX 4G - SHRIMP and LASS-ICPMS U-Pb zircon dates from the same zircons from basal quartzite sample 10914 from eastern Hall Peninsula.

Spot name	SHRIMP $\frac{^{207*}Pb}{^{206*}Pb}$	± 2σ	LASS round 1 (2015) $\frac{^{207*}Pb}{^{206*}Pb}$	± 2σ	LASS round2 (2016 re-run) $\frac{^{207*}Pb}{^{206*}Pb}$	± 2σ
10914-2.1	2985	7	3002	22		
10914-4.1	2816	5	2644	17		
10914-6.1	2727	55	2803	92		
10914-7.1	2871	5	1857	43		
10914-8.1	2832	17	2850	13		
10914-9.1	2813	10	2148	26		
10914-10.1	2615	10	2836	16		
10914-11.1	2865	9	2840	17		
10914-12.1	2709	3	2869	31		
10914-14.1	2815	6	2619	10		
10914-16.1	2684	3	2495	11		
10914-18.1	2704	6	3208	12		
10914-20.1	2781	5	2739	21	2782	14
10914-21.1	3277	9	2803	10		
10914-22.1	2618	6	3228	17	2724	12
10914-23.1	2777	3	2754	12	2714	7
10914-24.1	3219	6	2762	11	3183	10
10914-25.1	2714	6	3236	9	2491	20
10914-26.1	2864	7	2708	12	2023	29
10914-27.1	2842	5	2891	16	2799	17
10914-28.1	2849	10	2843	13	2805	14
10914-29.1	3202	6	2863	19		
10914-30.1	2751	18	3221	16		
10914-31.1	2778	5	2592	13		
10914-32.1	2743	5	2762	11		
10914-33.1	3113	57	2654	11		
10914-34.1	2835	8	3090	16		
10914-35.1	2828	5	2775	10		
10914-36.1	2791	14	2783	10		
10914-37.1	2881	11	2801	31	2672	9
10914-38.1	2878	11	2644	11	2833	23
10914-39.1	2720	7	2847	20	2698	9
10914-40.1	2854	10	2674	13	2494	32
10914-41.1	3236	6	2816	18		
10914-42.1	2722	6	3212	9	2683	13
10914-43.1	2815	8	2672	22		
10914-45.1	3222	7	2848	20		
10914-47.1	3126	5	3224	14	3067	11
10914-49.1	2688	8	3126	11	2679	12
10914-50.1	2780	7	2657	16	2784	9
10914-52.1	2791	5	2802	12	2735	18
10914-54.1	2774	9	2794	14	2809	12
10914-55.1	2697	4	2775	19	2671	7
10914-56.1	2858	14	2631	9	2677	51
10914-57.1	3127	7	2857	20	3101	13
10914-58.1	2789	11	3035	24	2757	12
10914-59.1	2820	6	2459	54	2762	14
10914-60.1	2786	6	2772	11	2797	8

APPENDIX 4G - SHRIMP and LASS-ICPMS U-Pb zircon dates from the same zircons from basal quartzite sample 10914 from eastern Hall Peninsula.

Spot name	**SHRIMP**		**LASS round 1 (2015)**		**LASS round2 (2016 re-run)**	
	$\frac{^{207*}Pb}{^{206*}Pb}$	± 2σ	$\frac{^{207*}Pb}{^{206*}Pb}$	± 2σ	$\frac{^{207*}Pb}{^{206*}Pb}$	± 2σ
10914-61.1	2720	4	2809	17	2709	8
10914-62.1	2718	3	2745	13	2650	7
10914-63.1	2734	6	2713	12	2618	10
10914-64.1	2861	6	2532	9	2845	11
10914-65.1	2761	10	2605	10		
10914-66.1	2833	14	2849	14	2762	12
10914-67.1	2856	10	2733	16		
10914-68.1	2838	12	2760	16		
10914-69.1	2847	15	2847	12	2744	53
10914-71.1	2823	8	2815	12	2806	16
10914-72.1	2736	7	2804	23	2786	10
AVERAGE	2842	9	2792	18	2739	16

table notes:
Spot name follows the convention x-y-z; where x = sample number, y = grain number and z = spot

APPENDIX 4H - Lithogeochemical data for snow bowl area and regional samples from eastern Hall Peninsula.

snow bowl samples

SampleID	Latitude	Longitude	Field Lithology	Q	Ab	Or	SiO2	Al2O3	Fe2O3(T)	MnO	MgO	CaO	Na2O	K2O	TiO2	P2O5	LOI
S116A	63.56141	-65.36139	monzogranite	43.9	49.0	7.1	73.64	15.12	2.18	0.022	0.58	2.87	4.71	0.98	0.25	0.06	0.2
F151A	63.56121	-65.32480	granodiorite	33.0	53.2	13.8	64.93	16.38	5.59	0.089	2.18	4.94	4.13	1.54	0.614	0.17	0.42
F155B	63.56195	-65.32301	tonalite	33.0	52.0	15.0	66	15.16	4.95	0.091	3.2	4.81	4.03	1.66	0.448	0.18	0.41
F155C	63.56195	-65.32301	quartz diorite	-	-	-	48.65	11.88	13.15	0.294	10.21	10.35	2.02	1.65	0.772	0.58	1.19
F155A	63.56195	-65.32301	monzogranite	35.0	36.1	28.8	72.3	14.77	1.72	0.027	0.49	2	3.67	4.19	0.125	0.06	0.27
F150A	63.56133	-65.32457	monzogranite	34.9	49.1	16.0	69.49	16.03	2.43	0.029	0.79	3.23	4.53	2.11	0.327	0.1	0.72
F152A	63.56140	-65.32440	monzogranite	29.1	48.0	22.8	64.64	15.16	6.73	0.062	1.51	3.44	4.17	2.84	1.337	0.53	0.41

regional samples

Sample ID	Latitude	Longitude	Field Lithology	Q	Ab	Or	SiO2	Al2O3	Fe2O3(T)	MnO	MgO	CaO	Na2O	K2O	TiO2	P2O5	LOI
H098A	64.27474	-65.00092	tonalite	37.1	45.9	16.9	72.05	15.59	2.08	0.021	0.72	2.63	4.47	2.36	0.26	0.08	0.31
H086A	64.07242	-64.28481	tonalite	39.4	23.2	37.3	74.57	13.37	2.11	0.019	0.38	1.5	2.45	5.64	0.221	0.08	0.53
F040A	64.19528	-66.30353	tonalite	44.0	44.7	11.3	70.57	14.82	2.91	0.031	0.99	3.49	3.99	1.44	0.298	0.09	0.33
K037A	64.33518	-66.45530	tonalite	43.5	39.3	17.2	73.58	14.36	2.37	0.053	0.56	2.28	3.87	2.43	0.199	0.07	0.07
F163B	64.33293	-65.51066	monzogranite	23.9	55.8	20.2	62.73	18.46	4.67	0.048	2.6	3.52	4.53	2.35	0.588	0.16	0.74
Z108A	64.11139	-65.39338	monzogranite	38.7	48.3	13.0	70.96	15.37	2.26	0.036	0.6	3.05	4.54	1.75	0.23	0.11	0.37
F157A	64.32447	-66.26187	monzogranite	37.1	52.2	10.6	69.94	15.91	3.53	0.04	1.12	3.44	4.73	1.38	0.38	0.11	0.31

APPENDIX 4H - Lithogeochemical data for snow bowl area and regional samples from eastern Hall Peninsula.

snow bowl samples

SampleID	Total	Sc	Be	V	Cr	Co	Ni	Cu	Zn	Ga	Ge	As	Rb	Sr	Y	Zr	Nb	Mo	Ag	In
S116A	100.6	1	1	30	20	4	20	10	40	20	0.8	5	23	378	1.7	100	1.4	2	0.5	0.1
F151A	101	12	1	84	30	14	20	< 10	80	21	1.3	< 5	352	< 0.1	386	< 0.2	4.8	35.6	4.93	19.2
F155B	100.9	12	2	87	120	14	50	< 10	70	18	1.3	< 5	430	< 0.1	534	< 0.2	3.4	57.6	7.64	31.1
F155C	100.8	33	3	222	610	38	140	< 10	210	23	2.7	< 5	148	< 0.1	171	< 0.2	7.6	216	26.6	99.7
F155A	99.62	2	1	24	< 20	3	< 20	< 10	30	19	1.2	< 5	304	< 0.1	881	< 0.2	1.1	39.3	3.36	10.7
F150A	99.79	2	2	28	< 20	4	< 20	< 10	40	20	0.9	< 5	356	< 0.1	578	< 0.2	3	59.9	6.35	20
F152A	100.8	8	2	84	20	11	< 20	20	90	21	1.5	< 5	374	< 0.1	1348	< 0.2	22.7	221	23	77.8

regional samples

Sample ID	Total	Sc	Be	V	Cr	Co	Ni	Cu	Zn	Ga	Ge	As	Rb	Sr	Y	Zr	Nb	Mo	Ag	In
H098A	100.6	3	1	29	< 20	4	< 20	< 10	40	19	0.8	< 5	501	< 0.1	815	< 0.2	3.1	22.5	2.05	6.81
H086A	100.9	5	< 1	31	40	2	< 20	< 10	40	15	1.4	< 5	148	< 0.1	953	< 0.2	6	139	14.4	46.5
F040A	98.96	3	2	35	30	6	< 20	10	40	19	1	< 5	248	< 0.1	298	< 0.2	3.1	43.5	4.1	13.4
K037A	99.85	3	2	17	< 20	3	< 20	< 10	40	16	1.3	< 5	146	< 0.1	580	< 0.2	6.4	34.4	3.46	11.8
F163B	100.4	10	1	80	30	14	30	< 10	70	21	1	< 5	470	< 0.1	702	< 0.2	1.9	18.6	2.48	10.5
Z108A	99.28	2	< 1	19	< 20	3	< 20	< 10	40	18	1	< 5	347	< 0.1	536	< 0.2	3.4	26.8	4.45	16.3
F157A	100.9	5	1	47	< 20	6	< 20	< 10	50	20	0.9	< 5	550	< 0.1	415	< 0.2	1.9	46.9	5.1	17.3

APPENDIX 4H - Lithogeochemical data for snow bowl area and regional samples from eastern Hall Peninsula.

snow bowl samples

SampleID	Sn	Sb	Cs	Ba	La	Ce	Pr	Nd	Sm	Eu	Gd	Tb	Dy	Ho	Er	Tm	Yb	Lu	Hf
S116A	1	0.2	0.2	314	13.7	24.7	2.42	8.83	1.23	0.49	0.77	0.08	0.39	0.06	0.16	0.022	0.14	0.025	2.5
F151A	3.72	0.997	3.02	13	< 2	0.7	0.46	< 1	2.59	0.5	1.36	0.217	1.29	0.168	3.4	0.4	< 0.5	0.25	< 5
F155B	5.59	1.21	3.77	14.1	< 2	0.5	0.52	1	2.61	0.47	1.31	0.187	1.22	0.187	2.7	0.17	< 0.5	0.31	12
F155C	16.7	3.27	11	38.1	< 2	0.6	1.38	5	7.08	1.31	3.67	0.498	3.33	0.472	3.4	0.36	< 0.5	0.25	6
F155A	1.5	0.57	1.06	3.4	< 2	0.8	0.14	< 1	0.77	0.14	0.38	0.053	0.33	0.045	4.3	0.05	< 0.5	0.52	17
F150A	2.44	0.608	1.27	2.1	< 2	0.9	0.13	< 1	0.46	0.08	0.2	0.028	0.15	0.024	3.8	0.08	< 0.5	0.34	10
F152A	11.5	1.97	7.54	22	< 2	4.8	0.97	3	4.64	0.78	2.06	0.255	1.42	0.204	17.5	0.63	< 0.5	0.25	7

regional samples

Sample ID	Sn	Sb	Cs	Ba	La	Ce	Pr	Nd	Sm	Eu	Gd	Tb	Dy	Ho	Er	Tm	Yb	Lu	Hf
H098A	0.96	0.53	0.68	1.6	< 2	0.6	0.08	< 1	0.33	0.05	0.15	0.02	0.13	0.019	2.4	0.09	< 0.5	0.27	7
H086A	5.54	0.959	2.96	5.6	2	1	0.3	< 1	1.18	0.2	0.63	0.09	0.56	0.092	5.1	5.52	16.7	0.67	28
F040A	1.91	0.623	0.85	2.5	< 2	< 0.5	0.1	< 1	0.5	0.08	0.22	0.032	0.17	0.029	3.1	0.38	< 0.5	0.33	8
K037A	1.96	0.468	1.56	8.1	< 2	0.6	0.23	< 1	1.32	0.25	0.77	0.107	0.74	0.115	3.4	0.68	< 0.5	0.53	12
F163B	2.17	0.674	1.73	5.5	< 2	0.8	0.24	< 1	1.1	0.2	0.54	0.078	0.42	0.063	3	0.11	< 0.5	0.66	9
Z108A	2.79	0.539	2.15	5.9	< 2	0.6	0.25	< 1	1.15	0.2	0.54	0.066	0.36	0.047	3.1	0.16	< 0.5	0.34	7
F157A	2.36	0.701	1.45	3.5	< 2	0.6	0.16	< 1	0.7	0.12	0.33	0.04	0.24	0.038	2.9	0.05	14.7	0.23	6

APPENDIX 4H - Lithogeochemical data for snow bowl area and regional samples from eastern Hall Peninsula.

snow bowl samples

SampleID	Ta	W	Tl	Pb	Bi	Th	U
S116A	0.04	0.5	0.1	5	0.1	0.57	0.14
F151A	< 0.1	1.54	0.78	54	0.1	0.37	0.24
F155B	< 0.1	0.89	0.36	63	0.1	0.96	0.21
F155C	< 0.1	13.1	1.56	53	0.1	11.2	0.33
F155A	< 0.1	4.97	0.66	123	0.1	15.7	0.47
F150A	< 0.1	11.2	0.3	69	0.5	0.23	0.21
F152A	< 0.1	11.2	0.24	64	0.1	0.05	0.15

regional samples

Sample ID	Ta	W	Tl	Pb	Bi	Th	U
H098A	< 0.1	0.88	0.15	63	0.1	16.4	0.58
H086A	< 0.1	27.7	0.82	148	0.2	2.24	0.59
F040A	< 0.1	4.35	0.41	69	-	-	-
K037A	< 0.1	8.15	1.63	108	0.1	8.49	1.54
F163B	< 0.1	0.58	0.17	66	0.1	0.57	0.14
Z108A	< 0.1	2.81	0.25	67	0.1	9.56	0.56
F157A	< 0.1	4.56	0.11	46	0.4	0.53	1

5. Chapter 5. Eastern Hall Peninsula, as an Archean microcontinent fragment unique from Meta Incognita microcontinent: an integrated study using U-Pb, Lu-Hf and Sm-Nd isotopes

This article, to be submitted to the journal *Chemical Geology* in, is co-authored with my thesis advisor Dr. Alfredo Camacho and research colleagues Dr. Graham Pearson and Dr. Yan Luo. In this work I was responsible for the sample collection, U-Pb and Lu-Hf isotopic analysis and data collection and interpretation, figure creation, and the writing. My collaborators G. Pearson and Y. Luo along with their lab staff at the Arctic research laboratory at the University of Alberta, provided assistance with U-Pb and Lu-Hf sample preparation, data acquisition and processing. Collaborators Dr. Chris Holmden and Dr. Sandra Timsic were responsible for Sm-Nd data acquisition at the University of Saskatchewan Isotope Laboratory and did not wish to be co-authors on the resulting manuscript. I carried out further Sm-Nd isotopic data calculations and interpretation. My co-authors made suggestions on data interpretations and reviewed final drafts of the manuscript.

This chapter builds upon the framework of Chapters 2, 3 and 4. During fieldwork on Hall Peninsula in 2013, one day was dedicated to a helicopter-assisted sample collection along a generally E-W transect across eastern Hall Peninsula. Plutonic rocks were targeted due to their circular, highly magnetic geophysical signatures and were commensurately found to contain high-amounts of magnetite. These rocks are also relatively undeformed compared to the majority of the rocks comprising the Archean orthogneiss complex of eastern Hall Peninsula. A sample suite of similar rocks from the northern region of eastern Hall Peninsula was also collected (through collaborative foot traverses) and will allow any contrasting isotopic variations from south to north (and the delineation of any associated crustal sutures) to be identified. Ten samples were analyzed using U-Pb, Lu-Hf and Sm-Nd isotopes to further characterize the Archean geologic history of eastern Hall Peninsula. This paper is reproduced with permission of my co-authors

---

From, R.E., Camacho, A., Pearson, D.G. and Luo, Y. *in preparation*. Eastern Hall Peninsula, Baffin Island as an independent Archean microcontinent fragment: an integrated study using U-Pb, Lu-Hf and Sm-Nd isotopes. Chemical Geology

5.1. Abstract

On eastern Hall Peninsula, Baffin Island, a series of magnetite-bearing granites were sampled along two transects across an Archean orthogneiss complex. These granites were targeted by their circular aeromagnetic anomalies and are proposed to represent the latest phase of plutonism in the area. As such, they may have inherited the isotopic signatures of underlying basement rocks and can provide insight into the crustal architecture and paleo-plate reconstructions of the region.

U-Pb and Lu-Hf isotopes were analyzed simultaneously in zircon grains from 10 samples using Laser Ablation Split Stream Inductively Coupled Mass Spectrometry (LASS-ICPMS). Sm-Nd isotopes were also analyzed from whole-rock powder from each sample. U-Pb isotopic data delineate a relatively young phase of magmatism from ca. 2750 to 2612 Ma. Southern and northern transects both document a west to east spatial trend of negative to positive $\varepsilon Nd_{(t)}$ indicating increased magma/mixing or crustal contamination in the west along the boundary between Paleoproterozoic and Archean rocks and more mantle-derived, juvenile Nd isotopic character towards the east within the Archean orthogneiss complex. Zircon $\varepsilon Hf_{(t)}$ data yields a similar spatial trend to that of the whole rock $\varepsilon Nd_{(t)}$ data and $T_{DM}Hf$ further outline three main age ranges of crustal protoliths: (1) from ca. 3.1 to 3.0 Ga for six of the samples (2); from ca. 3.0 to 2.9 Ga for three samples, all from the northern transect; and (3) from ca. 2.9 to 2.7 Ga.

Our combined multi-isotopic results indicate that the Archean rocks of eastern Hall Peninsula constitute a unique and separate microcontinent fragment that was potentially part of the composite Rae craton and/or the Aasiaat domain before subsequent rifting and

accretion to the Meta Incognita microcontinent during Paleoproterozoic tectonic amalgamation.

5.2. Introduction

Within the Paleoproterozoic Trans-Hudson orogen (THO) of North America and Greenland sporadically preserved fragments of Archean crust have largely been obscured by deformation and metamorphism during tectonic amalgamation. As a result, the Archean geologic histories of these crustal fragments and their boundaries are typically cryptic, obscured by subsequent tectonothermal events.

Historically, Sm-Nd isotopes have proven to be an important geological tool for identifying unique crustal blocks within regions that have experienced complex regional tectonic amalgamation (e.g., Blewett et al., 1998; Böhm et al., 2000; Hartlaub et al., 2005; Sá et al., 2014). This has been effectively done in several locations within the THO including regions in northern Manitoba (Böhm et al., 2007), West Greenland (Hamilton et al., 1983) and Baffin Island (Whalen et al., 2010). Now, with further technological advances in microanalytical techniques, Lu-Hf isotopes in zircon can be used in conjunction with whole-rock Sm-Nd isotopes to further elucidate the geologic history of magma generation and evolution.

A multi-faceted approach utilizing U-Pb, Lu-Hf and Sm-Nd isotopes can yield important information regarding magmatism, metamorphism, ages of crustal protoliths and regional correlations to adjacent crustal blocks. During the Paleoproterozoic, Hall Peninsula was at the junction of a two-stage Paleoproterozoic collision between three main cratonic blocks, the Rae craton, Meta Incognita microcontinent and the North Atlantic craton. Accretion during ca. 1.88 to 1.80 Ga (St-Onge et al., 2009) amalgamated

these three blocks and trapped a small microcontinental fragment in between them termed the Aasiaat domain (Figure 5.1; Kolb, 2014). The eastern Hall Peninsula has been tentatively correlated with the Aasiaat domain (also termed the Disko craton; Grocott and Davies, 1999; van Gool et al., 2002) but it may also represent a separate unique microcontinent fragment similar to the Aasiaat domain (Whalen et al., 2010; Chapter 4). Correlations have also been proposed between Paleoproterozoic metasedimentary rocks on Hall Peninsula to those on the North Atlantic craton (also termed the Nain craton) of northern Labrador (Scott, 1997; Connelly and Mengel 2000) raising the possibility of a link between the Archean basement rocks.

To investigate the various hypotheses on the nature and provenance of crust beneath Hall Peninsula and its relationship to Meta Incognita microcontinent to the west and the Davis Strait to the east, a series of granitic rocks associated with circular, positive aeromagnetic anomalies were investigated (Figure 5.2). It is proposed that these granites could be a late-stage of plutonism (potentially Paleoproterozoic) that may serve as a probe to the basement rocks underlying Hall Peninsula and allow the recognition of crustal blocks with unique isotopic signatures. To accomplish this goal, a transect of magnetite-bearing granitic rocks trending north-northeast were sampled in southern Hall Peninsula and five, similar, magnetite-bearing granites were sampled in northern Hall Peninsula along an east trending transect (Figure 5.3). In each transect, the westernmost sampled rock unit is mapped as Paleoproterozoic meta-igneous rocks that are in a region of south-southeast trending aeromagnetic lineations, much different than the more uniform and circular signatures in the Archean orthogneiss complex to the east (Figure 5.2, 5.3). U-Pb and Lu-Hf isotopes were measured on zircon separates from ten granitic

rock samples using Laser Ablation Split Stream Inductively Coupled Plasma Mass Spectroscopy (LASS-ICPMS) at the Arctic Research Laboratory at the University of Alberta. These ten rock samples were also analyzed for whole-rock Sm-Nd isotopes at the University of Saskatchewan Isotope laboratory. This study adds to the growing isotopic database for the Quebec-Baffin segment of the THO, assesses the strength of using in-situ Hf isotope analyses of zircon versus whole rock isotopic signatures using the Sm-Nd system, and discusses the delineation of a potential terrane boundary separating Meta Incognita microcontinent and the Archean Hall Peninsula block.

Figure 5.1. Regional map of the Quebec-Baffin segment of the Trans-Hudson orogen with ages of crustal amalgamation and proposed suture locations. Hall Peninsula is outlined with a blue polygon. Map modified from Kolb, (2014).

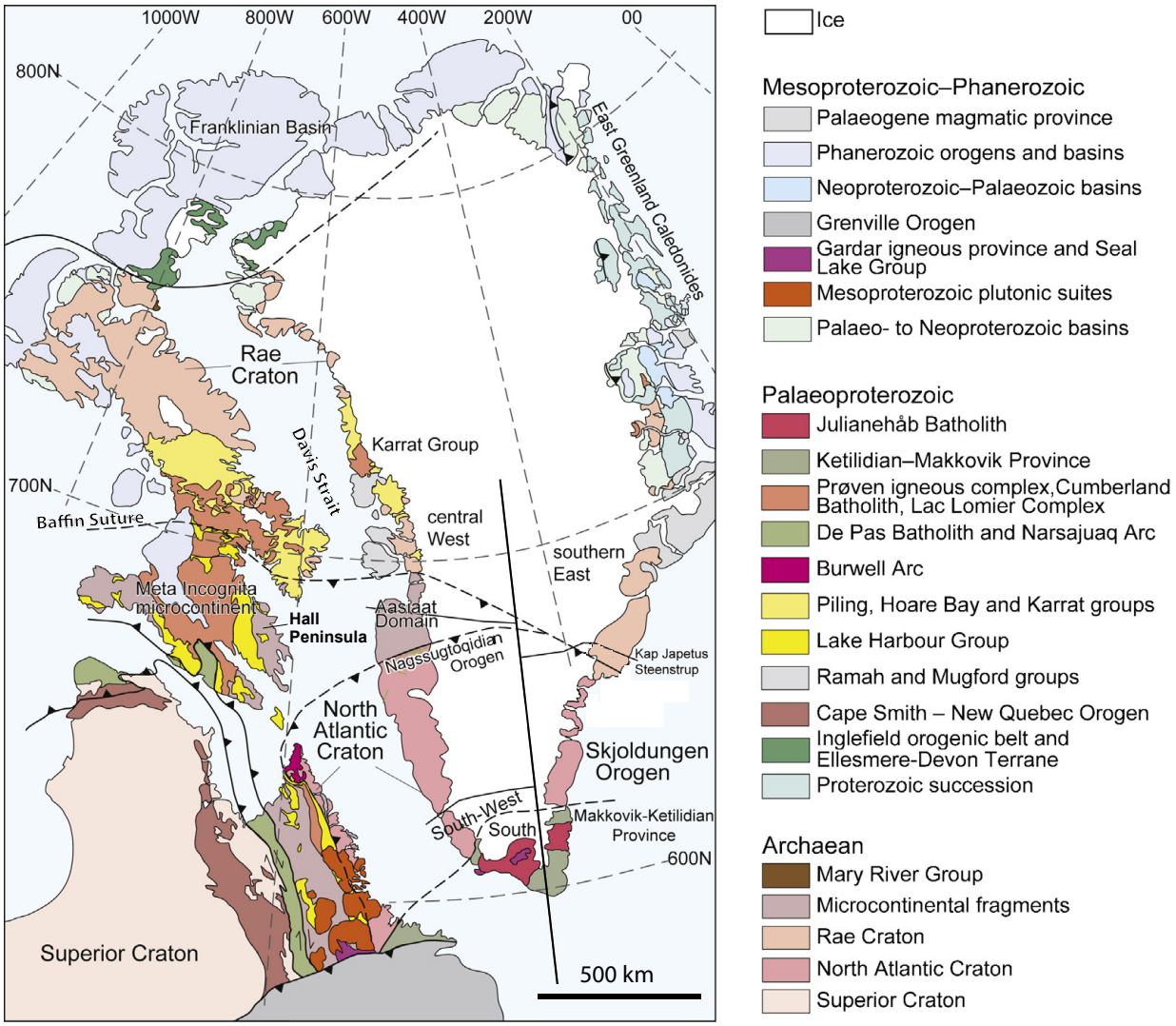

Figure 5.2. Total-field magnetic susceptibility of southern Hall Peninsula in NTS areas 025O, P, I and J (Dumont and Dostaler, 2010a–l), highlighting defined domains and trends reflected in the bedrock geology. Locations of Sm-Nd samples from the southern transect are shown with white circles.

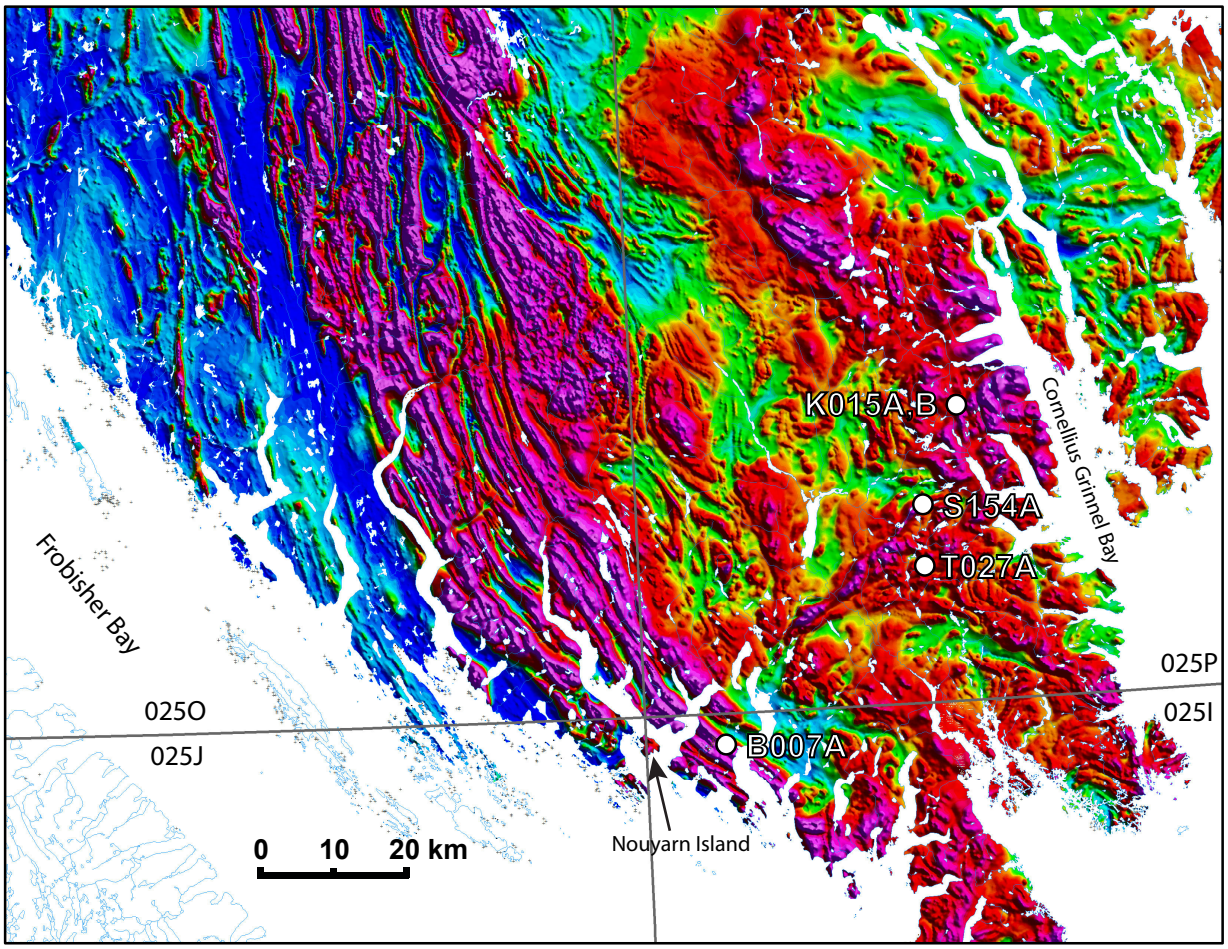

Figure 5.3. Geology of southern Hall Peninsula, Baffin Island, Nunavut showing the distribution of the principal geologic units and the locations of U-Pb age determinations and Sm-Nd isotopic data. The locations of southern and northern transect samples are shown by black circles with their ages of crystallization in green and Nd data in orange and black. Abbreviations: grt, garnet; bt, biotite; mag, magnetite; opx, orthopyroxene; cpx, clinopyroxene. Map modified from Machado et al. (2013).

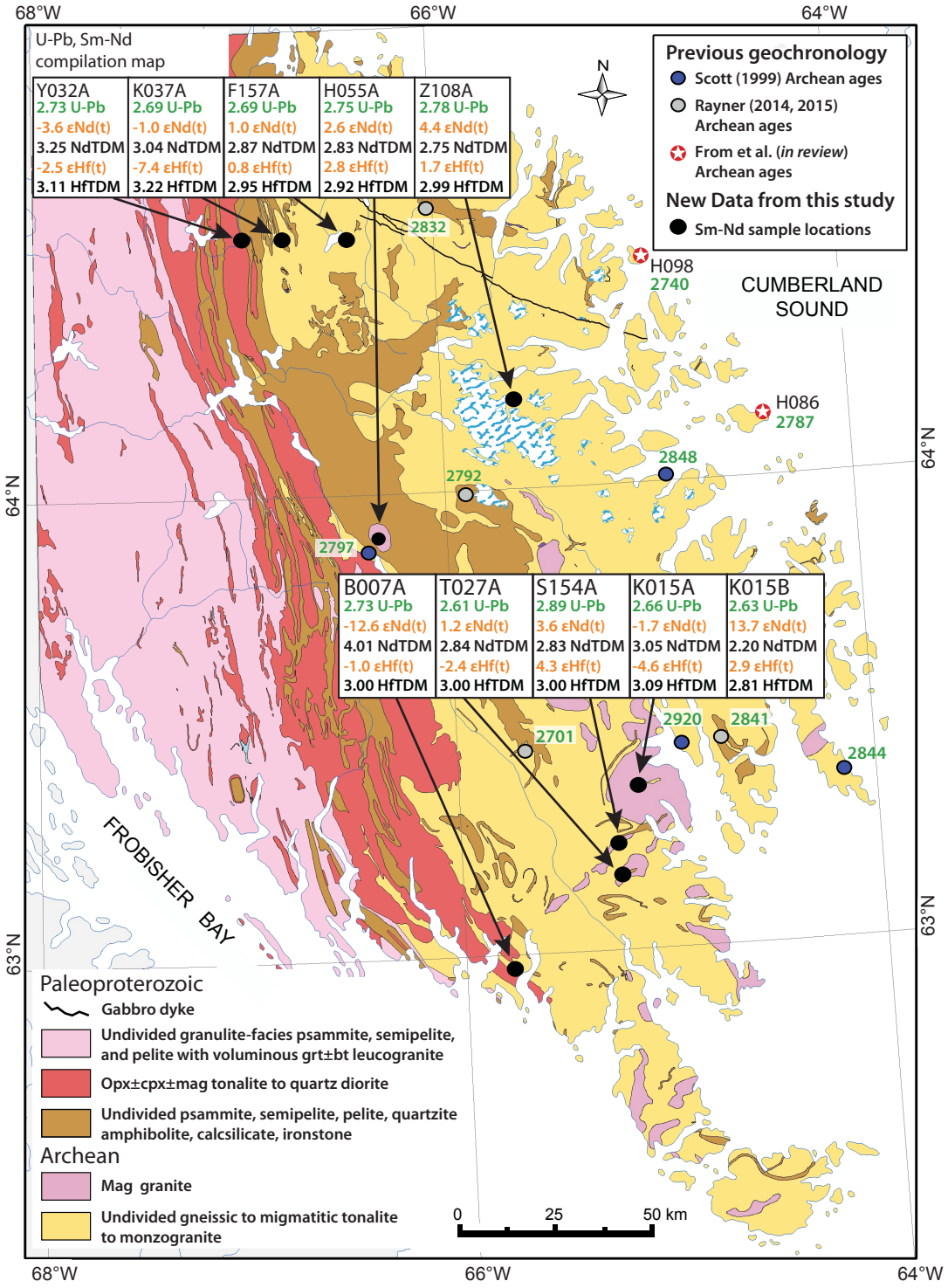

5.3. Previous work and geological setting

Geological mapping of Hall Peninsula was first carried out by Blackadar (1967), followed by a reconnaissance scale east-west transect across central Hall Peninsula with U-Pb geochronology (Scott, 1996, 1999; Figure 5.3). New geological mapping at 1:250,000 through a project led by the Canada-Nunavut Geoscience Office in collaboration with the Geological Survey of Canada led to additional reconnaissance-scale U-Pb geochronology by Rayner (2014, 2015; Figure 5.3). Further detailed mapping within a small study area in the central portion of the Archean orthogneiss complex of eastern Hall Peninsula and correlations with regional samples using U-Pb and Lu-Hf isotopes is presented in Chapter 4. Lithological descriptions and units of the Archean orthogneiss complex can be found in these previous works but in general the western portion of Hall Peninsula is dominated by a Paleoproterozoic plutonic suite of granodiorite to orthopyroxene-bearing monzogranite with intervening Paleoproterozoic metasedimentary panels whereas the eastern portion of Hall Peninsula is dominated by Archean tonalitic to syenogranitic migmatitic gneisses (Figure 5.3; Scott, 1999; From et al., 2013). The entirety of Hall Peninsula is poly-deformed and poly-metamorphosed aside from pegmatites, ultramafic pods and late mafic dykes, all of which are largely undeformed. Paleoproterozoic metasedimentary rocks have been interpreted to unconformably overlie the Archean orthogneiss complex (Steenkamp and St-Onge, 2014) and are interleaved in east-verging imbricate folds and thrusts as slivers and panels ranging from 2 m to several kilometres in thickness (Machado et al., 2013).

Archean magmatism on eastern Hall Peninsula occurred from ca. 2975 to 2720 Ma with metamorphism recorded from ca. 2740 to 2700 Ma and 1860 to 1820 Ma (Chapter 3, 4; Skipton et al., 2016). Hf isotopic analyses from a small study area indicate that orthogneisses older than ca. 2740 Ma were derived from the recycling of crust whose protolith magma was extracted from the mantle at ca. 3.1 Ga. Two Archean orthogneisses younger than ca. 2740 Ma had negative mean εHf(t) values of -7 and -10 (±2) and protolith ages of ca. 3.3 to 3.4 Ga indicating the recycling of a much older crustal source, potentially exotic to Hall Peninsula (Chapter 4).

Paleoproterozoic plutonic and supracrustal rocks of western Hall Peninsula have been investigated by Rayner (2014, 2015) and Skipton et al. (2016), elucidating the deformational and metamorphic history. In brief, the western portion of Hall Peninsula is dominated by garnet-bearing leucogranite, interpreted to be a result of muscovite and biotite-dehydration melting during anatexis associated with the thermal peak metamorphic conditions in the Paleoproterozoic (Dyck and St-Onge, 2014). Deformation related to Paleoproterozoic metamorphism occurred in three discernible stages at mid-amphibolite to granulite facies, decreasing in grade towards the west (Steenkamp and St-Onge, 2014). Monazite and zircon growth from 1860 to 1820 Ma bracket peak metamorphism, and subsequent dissolution and re-precipitation of monazite and zircon material occur from 1800 to 1750 Ma during slow cooling (Skipton et al., 2016). Peak metamorphic estimates derived from equilibrium phase diagram modeling constrained by garnet compositions in pelitic rocks increase from ~720–740°C on the eastern peninsula to ~850°C further west, with pressures of ~6.25–7.35 Kbar (Skipton et al., 2016).

5.4. Magnetite-bearing granites

A series of granitic rocks associated with circular to ovoid aeromagnetic anomalies, were sampled along two generally east-northeast transects, perpendicular to the dominant foliation, across eastern Hall Peninsula (Figure 5.3). This suite of granitoids may represent a late phase of magmatism that may have passed through or is partially derived from underlying basement rocks, consequently inheriting the isotopic character of any underlying rocks. Five granitoid samples in both the southern and northern transect were chosen for U-Pb, Lu-Hf and Sm-Nd isotopic analyses. Samples from the southern transect were collected along a domain of high magnetic susceptibility, which has an arcuate shape that initially trends northeast across eastern Hall Peninsula from Nouyarn Island (Figure 5.2). In more detailed aeromagnetic maps, a series of circular, high aeromagnetic signatures thought to delineate late-stage plutons were targeted and the best quality outcrops were sampled along this trend. Samples from the northern transect were not associated with significant aeromagnetic signatures but were selected from a suite of magnetite-bearing rock, similar to the magnetite-bearing granites from the southern transect. Two control samples of tonalite gneiss considered to be representative of the dominant rock type throughout eastern Hall Peninsula were also selected within the northern transect. Overall, the majority of these magnetite-bearing granites have a very weak foliation with two samples (e.g., K015A, K015B) having a moderate strength gneissic fabric. Individual sample descriptions can be found in the results section.

5.5. Analytical Methods

5.5.1. Sample Collection

The southern transect trending east-northeast was completed by helicopter-assisted sampling of previously described mapping stations. A northern east-west transect was sampled collaboratively during foot traverses targeting magnetite-bearing monzogranites that appeared to be relatively undeformed, interpreted as late-stage plutonic rocks that may have intruded through the Archean orthogneiss complex and any underlying basement rocks (Figure 5.3). Large, representative, homogeneous, unaltered and fresh samples were collected, avoiding veins, dykes or mineral clusters. Thin section examination and whole rock geochemistry were used to select a final sample suite, which contained enough zircon of adequate size for zircon geochronology.

5.5.2. Zircon seperation and imaging

All samples were disaggregated using a Spark 2 electric-pulse disaggregator. The Spark 2 employs high-voltage electrical pulses to fragment a rock sample along zones of weakness (e.g. mineral grain boundaries and fractures). The disaggregated sample was then run through a shaking table that produced a low-grade, minus 1mm concentrate. This concentrate was refined by micropanning to produce a zircon-rich separate that was isolated to individual conical vials. Handpicked zircon grains were separated from the zircon-rich separate and cast in 2.5 cm diameter epoxy mounts. The midsections of the mounted zircons were then exposed using 9, 6, and 1 μm diamond compound, and the internal features of the zircons (such as zoning, structures and alteration) were characterized in back-scattered electron (BSE) and cathodoluminescence

(CL) utilizing a Zeiss EVO MA15 scanning electron microscope with a broadband CL detector in the Canadian Centre for Isotopic Microanalysis at the University of Alberta. The images were taken with a working distance of 5.5 mm, an accelerating voltage of 20 kV and a current of 3.1 to 4.0 nA.

5.5.3. U-Pb and Lu-Hf Laser Ablation Split-Stream (LASS)

Separated zircons were analyzed with a technique first described by Yuan et al. (2008) and Xie et al. (2008) and further refined by Fisher et al. (2011, 2014a). Simultaneous Hf and U-Pb isotope measurements were made in the Arctic Resources Laboratory at the University of Alberta using a Resolution LR50 Excimer 193 nm laser operating with fluence of 5 J/cm^2 and 10 Hz, using a 33 μm diameter spot size. Ablated aerosols were entrained in a He cell gas flow of 1.0 L/min and subsequently mixed with N_2 (10mL/min) and Ar (in total 1.8 L/min) prior to the total gas flow being split. The ablated sample+He+N_2+Ar mixture was then split after the laser cell using a Y-piece, diverting the ablation product to two independent mass spectrometers. The length of tubing is equalized such that the ablated sample materials arrive simultaneously at both mass spectrometers. The U-Pb isotope measurements were performed on a Thermo Element-XR 2 mass spectrometer using a single secondary electron multiplier (SEM) detector in peak hopping mode. Lu-Hf isotope measurements were made on a Thermo Fisher Neptune Plus using multiple Faraday detectors with 10^{11} Ω amplifiers operating in static collection mode. Analysis time was typically 140 seconds consisting of 30 seconds of background followed by 70 seconds of ablation and 40 seconds of sample washout.

Both Hf and U-Pb data were processed offline using Iolite v3.32 software (http://iolite-software.com/).

Both Hf and U-Pb analytical biases were calibrated using the Plesovîce zircon as a primary reference material. Due to the large corrections necessary for the isobaric interference of ^{176}Yb and ^{176}Lu on the ^{176}Hf/^{177}Hf mass each run includes a variety of secondary standards of known age and Hf isotope composition interspersed with unknowns in order to evaluate the accuracy of the interference correction. In this study we monitored the Yb interference correction by analysis of a variety of natural and synthetic zircons, with a wide range of Yb/Hf. Synthetic HREE-doped zircons (MUN1 and MUN3 – Fisher et al., 2011) were evaluated, along with zircon 91500. The modelled ^{176}Yb/^{173}Yb ratio was iteratively calibrated to optimize the Yb-interference correction, monitored by zircon reference materials with variable Yb contents (91500, MUN1, MUN3). The mean ^{176}Hf/^{177}Hf for the calibration standard Plesovîce zircon [0.282482 ± 47 (2 SD), n = 242] is in close agreement with solution MC-ICPMS values of 0.282482 (Slama et al., 2008). Multiple analyses (n=194) of the 91500 zircon standard by LASS yielded a weighted mean ^{206}Pb/^{238}U age of 1068 ± 12 Ma (2 SE) and a mean ^{176}Hf/^{177}Hf of 0.282313 ± 72 (2 SD). The results agree well with the compiled U-Pb age of 1063.4± 1.4 (Schoene et al., 2006) and ^{176}Hf/^{177}Hf value of 0.282308±6 (2SD; Blichert-Toft, 2008). The mean ^{176}Hf/^{177}Hf for MUN1 and MUN3 [0.282130 ± 59 (2 SD), n = 15; 0.282154 ± 42 (2 SD), n = 5] are in good agreement with the solution MC-ICPMS values of 0.282135±31 (2 SD) for MUNZirc 1 and 3 (Fisher et al., 2011). The decay constant and parameters used for Hf model age calculations are ^{176}Lu/^{177}Hf (chondrite) = 0.0336, ^{176}Hf/^{177}Hf = 0.282785 (chondrite) after Bouvier et al. (2008) and ^{176}Lu/^{177}Hf (DM) =

0.038, $^{176}Hf/^{177}Hf$ (DM) = 0.283223 after Vervoort and Blichert-Toft (1999). Uncertainties on initial Hf ratios and Hf model ages were calculated using full error propagation, outlined by Ikert (2014).

5.5.4. Sm-Nd analyses

Whole rock samples were powdered using standard shatterbox techniques. Approximately 50–100 mg of powder were spiked with a ^{149}Sm–^{150}Nd tracer and placed in an HF–HNO_3 mix in Teflon pressure vessels at 220℃ for 4–5 days, then reacted with 6 M HCl and placed back in oven at 180℃ for 24 h to reach complete sample dissolution. Separation of Sm and Nd was done using standard two-stage HDEHP ion chromatography. Isotopic measurements were made on the MIT Isoprobe-T mass spectrometer and both elements were analyzed as the metal. Nd was loaded on triple Re filaments in 1 µl of 0.1 M H_3PO_4 and analyzed using a three-sequence dynamic multicollector Faraday routine with an ~2 V signal of ^{143}Nd. Sm was loaded on single Ta filaments in 1 µl of 1 M H_3PO_4 and analyzed using a static multicollector Faraday routine with an ~400 mV signal of ^{149}Sm. Sm and Nd were corrected for mass fractionation using an exponential law normalizing to $^{152}Sm/^{147}Sm$ = 1.783 and $^{146}Nd/^{144}Nd$ = 0.7219, respectively. $^{143}Nd/^{144}Nd$ measurements of the Ames and Shinetsu (a.k.a. JNdi-1) standards on the Isoprobe-T over the study period were 0.5120786 ±0.0000096 (2SD; n=38) and 0.5121019 ±0.0000102 (2SD; n=43), respectively. Our best estimate for the true $^{143}Nd/^{144}Nd$ value for the Ames and Shinetsu standard in use at MIT is about 0.512095, based on cross-calibration of the La Jolla Nd standard at a $^{143}Nd/^{144}Nd$ value of 0.511850. The quoted uncertainties (~20 ppm) correspond to a conservative estimate of ±0.5 εNd units for Archean ages. Duplicate analyses from this study were reproducible to

<0.1 εNd units. εNd is calculated from the present day composition of the chondritic uniform reservoir (CHUR) of $^{147}Sm/^{144}Nd = 0.1967$ and $^{143}Nd/^{144}Nd = 0.512638$ using the equation $\varepsilon Nd(t) = [(^{143}Nd/^{144}Nd)_{sample}(t)/(^{143}Nd/^{144}Nd)_{CHUR}(t)-1]\times10^4$ (DePaolo and Wasserburg, 1976).

5.6. Results

Rocks analyzed in the study are discussed individually with southern transect samples presented first from west to east followed by the northern transect samples in the same geographic trend (Figure 5.3). The U-Pb, Lu-Hf and Sm-Nd data are summarized in Table 5.1. Complete U-Pb, Lu-Hf and Sm-Nd data can be found in the accompanying data APPENDICES 5A-E.

On the basis of morphology and internal structures, zircons were classified as inherited, magmatic or metamorphic (Figure 5.4). Inherited zircons are typically cores that have overgrowths of magmatic or metamorphic zircon and may show a well-defined discontinuity between the core and subsequent zircon growth (Figure 5.4). Magmatic zircons are interpreted to represent crystallization from a melt and typically have well-defined, oscillatory growth zonation, typically at a fine scale (Figure 5.4). Metamorphic zircons are either unzoned zircon overgrowth rims or single, unzoned grains that will generally have different U and Pb contents or U/Th compared to the zircon it overgrows (Figure 5.4). Each spot analysis of zircon includes a spot location (e.g., core, outer core, rim), zonation characteristics (e.g., irregular, oscillatory, sector, unzoned) and color coded interpretation (e.g., inherited, magmatic, metamorphic) given in APPENDICES 5A,B. Additionally, for each sample a zircon image that best represents the zircon characteristics present throughout the population is shown with the concordia diagrams in

Figure 5.5. Zircon images are BSE images unless otherwise labeled. The $^{207}Pb/^{206}Pb$ ages are color-coded on the concordia diagrams in coordination with the color of the individual analyses in the data repository (see APPENDIX A,B). Light grey ellipses represent $^{207}Pb/^{206}Pb$ ages derived from inherited zircon, dark grey ellipses represent $^{207}Pb/^{206}Pb$ ages derived from magmatic zircon and dark grey ellipses represent $^{207}Pb/^{206}Pb$ ages derived from metamorphic zircon. In several cases, only the $^{207}Pb/^{206}Pb$ ages derived from magmatic zircon appear in the field of view of the concordia diagram.

5.6.1. Southern transect

5.6.1.1. Epidote-biotite hornblende granodiorite (B007A)

Biotite hornblende granodiorite (B007A) is the westernmost intrusive analyzed along the southern transect, located in map unit Paleoproterozoic orthopyroxene ± clinopyroxene ± magnetite tonalite to quartz diorite (Figure 5.3). This granodiorite is fine to medium grained with a weak foliation defined by biotite and hornblende. The composition is quartz (35%), plagioclase (35%), K-feldspar (8%), biotite (7%), hornblende (5%) with an unusual amount of epidote (~10%).

Twenty-seven analyses were conducted on 24 separate zircon grains yielding two distinct $^{207}Pb/^{206}Pb$ age populations. Five $^{207}Pb/^{206}Pb$ ages from ca. 2905 to 2804 Ma were derived from zircon cores interpreted to be inherited (Figure 5.5a). A cluster of $^{207}Pb/^{206}Pb$ ages (n=12) ranging from ca. 2752 to 2708 Ma, plot the closest to concordia (Figure 5.5a) and are interpreted to represent the crystallization age of this rock (weighted mean of 2727 ±9 Ma, MSWD = 4.7). These ages were derived from both oscillatory-zoned zircon cores and unzoned outer cores and rims (whose previous zonation may have been homogenized). These zircons have εHf(t) of -2.6 to 0.5 and depleted mantle model

Table 5.1. Summary of Sm-Nd and U-Pb, Lu-Hf results from southern and northern transects across Hall Peninsula

Sample	lithology	$^{207}Pb/^{206}Pb$ crystallization age ± 2σ (Ma)	$\varepsilon Nd_{(t)}$	± 2 s.e.	$T_{DM}Nd$ (Ga)	$\varepsilon Hf_{(t)}$ (magmatic crystallization zircon)	$T_{DM}Hf$ (Ga) (magmatic crystallization zircon)
South Transect							
B007A	ep-bt-hbl granodiorite	2727 ±9	-12.7	0.6	4.01	-2.6 to 0.7	2.97-3.13
T027A	mt-bt syenogranite	2612 ±15	0.0	0.8	2.84	-3.7 to -1.1	2.96-3.05
S154A	bt-mt monzogranite	2899 ±17	4.7	0.7	2.83	2.7 to 5.4	2.97-3.06
K015A	hbl bt tonalite	2661 ±39	-1.4	0.6	3.05	-6.0 to -2.7	3.02-3.13
K015B	syenogranite	2626 ±12	12.5	0.8	2.20	1.8 to 4.8	2.73-2.89
North Transect							
Y032A	bt-hbl-opx granodiorite	2729 ±9	-3.7	0.6	3.25	-5.4 to 1.0	2.97-3.22
K037A	bt tonalite	2687±26	-1.0	0.6	3.04	-9.9 to -4.1	3.12-3.36
F157A	bt-mt-ep monzogranite	2689 ±10	1.1	0.7	2.87	0.2 to 1.4	2.92-2.97
H055A	bt-mt-hbl monzogranite	2750 ±8	2.7	0.7	2.83	1.6 to 3.4	2.90-2.97
Z108A	bt-mt monzogranite	2777 ±20	4.3	0.7	2.75	-0.1 to 3.1	2.95-3.04

Abbreviations: bt, biotite; ep, epidote; hbl, hornblende; opx, orthopyroxene; mt, magnetite.

Figure 5.4. Back-Scatter Electron images showing representative zircons from the three types recognized consistently throughout the zircon populations: inherited, magmatic and metamorphic.

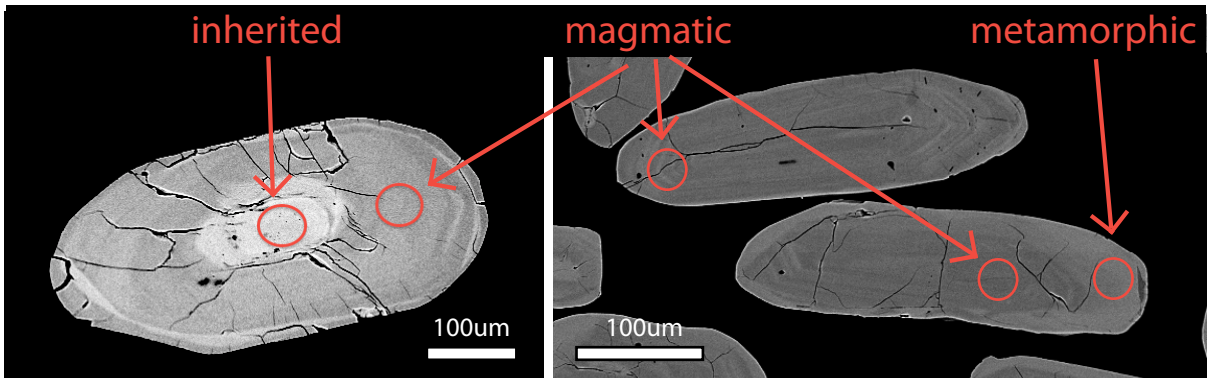

Figure 5.5. U-Pb Concordia diagrams with examples of zircon morphology and zonation for a-e) southern transect samples. Light grey ellipses represent $^{207}Pb/^{206}Pb$ ages derived from inherited zircon, medium grey ellipses with black rims represent $^{207}Pb/^{206}Pb$ ages derived from magmatic zircon and dark greyish black ellipses represent $^{207}Pb/^{206}Pb$ ages derived from metamorphic zircon. Data point error ellipses are 2σ.

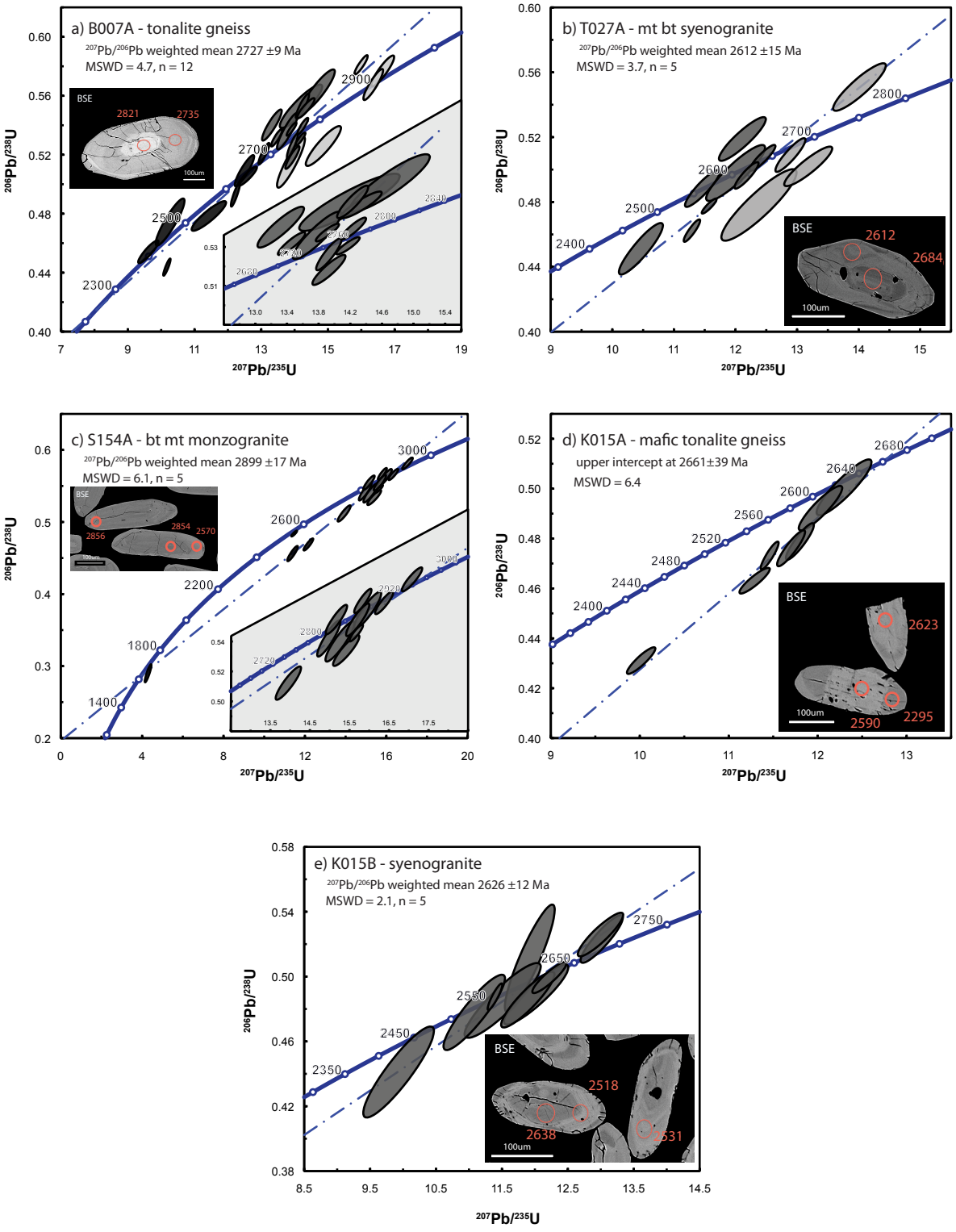

Figure 5.5 cont'd. U-Pb Concordia diagrams with examples of zircon morphology and zonation for f-j) northern transect samples. Light grey ellipses represent $^{207}Pb/^{206}Pb$ ages derived from inherited zircon, medium grey ellipses with black rims represent $^{207}Pb/^{206}Pb$ ages derived from magmatic zircon and dark greyish black ellipses represent $^{207}Pb/^{206}Pb$ ages derived from metamorphic zircon. Data point error ellipses are 2σ.

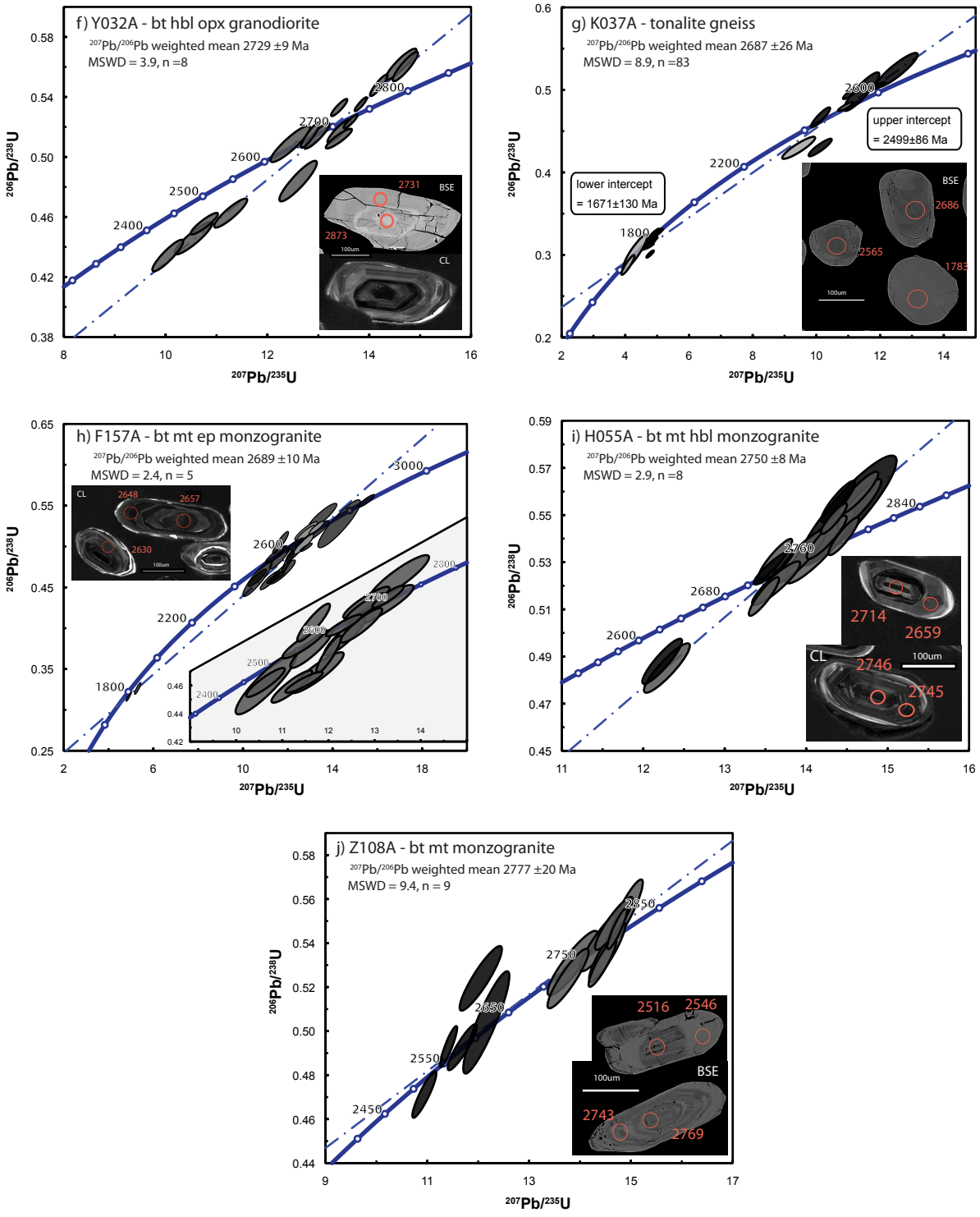

ages (T_{DM}Hf) between 3.1 and 3.0 Ga. The remaining $^{207}Pb/^{206}Pb$ ages, ranging from ca. 2675 to 2426 Ma, are variably discordant towards a poorly defined lower discordia intercept ~2.2 Ga, interpreted as a period of partial Pb loss. Whole rock Sm-Nd analysis yielded a εNd(t) of -12.7 ±0.6 and T_{DM}Nd of 4.0 Ga.

5.6.1.2. Magnetite biotite syenogranite (T027A)

Magnetite biotite syenogranite (T027A) is coarse grained (up to 2.5mm equant grains) and has a weak foliation defined by biotite and clusters of K-feldspar. The composition of this rock is quartz (45%), plagioclase (20%), K-feldspar (15%), biotite (10%), magnetite (<10%) and trace allanite. The location of this rock falls within a region of high total-field aeromagnetic susceptibility (Figure 5.2).

Twenty-one U-Pb isotopic analyses were conducted on 20 separate zircon grains yielding $^{207}Pb/^{206}Pb$ ages from ca. 2756 Ma to 2539 Ma. The four oldest $^{207}Pb/^{206}Pb$ ages between ca. 2756 and 2682 Ma were derived from unzoned or oscillatory zoned zircon cores interpreted to be inherited. A cluster of five concordant $^{207}Pb/^{206}Pb$ ages, from ca. 2628 to 2593 Ma were derived from zircon cores or single grains that are sector or homogenously zoned and are interpreted to represent the magmatic crystallization age of this rock (weighted mean of 2612 ±15 Ma; MSWD = 3.7; Figure 5.5b). These zircons have εHf(t) of -3.7 to -1.1 and T_{DM}Hf from 3.0 to 3.1 Ga. The remaining, three zircon analyses are discordant and range in $^{207}Pb/^{206}Pb$ ages within error from ca. 2541 to 2539 Ma but on a $^{238}U/^{206}Pb$ versus $^{235}U/^{207}Pb$ plot lie along a line of discordia with a trajectory towards a poorly defined Proterozoic lower intercept of 1114 ±1200 Ma (Figure 5.5b). Therefore, these three zircons are interpreted to have suffered partial Pb loss either during

or prior to the Proterozoic. Whole rock Sm-Nd analysis yielded a εNd(t) of 0.0 ±0.8 and T_{DM}Nd of 2.8 Ga.

5.6.1.3. Biotite magnetite monzogranite (S154A)

Biotite magnetite monzogranite (S154A) is medium grained, has abundant plagioclase phenocrysts and has a moderate foliation defined by discrete layers of aligned biotite grains. Plagioclase is simply twinned with little evidence for deformation. The composition of this sample is quartz (40%), plagioclase (30%), K-feldspar (15%), biotite (10%) and magnetite (5%). The sample location is associated with high total-field aeromagnetic susceptibility values delineating a circular shape of a pluton (Figure 5.2).

Nineteen U-Pb isotopic analyses were conducted on separate zircon grains yielding a range in $^{207}Pb/^{206}Pb$ ages from ca. 2912 to 2524 Ma. The eleven oldest $^{207}Pb/^{206}Pb$ ages from ca. 2912 to 2810 Ma are from oscillatory zoned zircons that share similar Th/U (0.33 to 0.78), εHf(t) values (1.3 to 6.3) and TDM model ages (3.06 to 2.85 Ga) and are interpreted to be magmatic. The 5 oldest of these chemically similar zircons form a $^{207}Pb/^{206}Pb$ age cluster on concordia and best represent the crystallization age of this rock (weighted mean of 2899 ±17 Ma; MSWD = 6.1; Figure 5.5c). Younger $^{207}Pb/^{206}Pb$ ages cascade along a line of discordia with a lower intercept of 1633 ±180 Ma (Figure 5.5c). The youngest $^{207}Pb/^{206}Pb$ ages of ca. 2722, 2570 and 1766 Ma are derived from unzoned rims, have much lower Th/U (0.00 – 0.06) and more negative εHf(t) (-14.9 to -2.1) that indicate Neoarchean and Paleoproterozoic metamorphic overprints. Whole rock Sm-Nd analysis yielded a εNd(t) of 4.7 ±0.7 and T_{DM}Nd of 2.8 Ga

5.6.1.4. Biotite hornblende tonalite (K015A)

Hornblende biotite tonalite (K015A) is fine to medium grained with thin, mm-scale discrete banding of hornblende that delineates a moderate strength gneissic foliation. This tonalite has a higher proportion of mafic minerals compared to most tonalite gneisses observed throughout eastern Hall Peninsula and has a composition of 45% quartz, 20% hornblende, 15% plagioclase, 10% biotite, 5% K-feldspar and 5% titanite.

Eighteen U-Pb isotopic analyses were conducted on separate zircon grains yielding $^{207}Pb/^{206}Pb$ ages from ca. 2631 to 1750 Ma. Six $^{207}Pb/^{206}Pb$ ages derived from oscillatory or irregularly zoned zircon cores range from ca. 2631 to 2590 Ma and delineate a line of discordia that has a Paleoproterozoic lower intercept of 1664 ±160 Ma, indicating partial Pb loss. Therefore, the magmatic crystallization age of this rock is best represented by the upper intercept on concordia (2661 ±39 Ma; MSWD = 6.4; Figure 5.5d). Archean zircons have εHf(t) of -6.0 to 1.6 and $T_{DM}Hf$ from 3.13 to 2.86 Ga. Two Paleoproterozoic $^{207}Pb/^{206}Pb$ ages of 1755 to 1750 Ma were derived from unzoned zircon rims and plot adjacent to the lower intercept on concordia. Whole rock Sm-Nd analysis yielded a εNd(t) of -1.4 ±0.6 and $T_{DM}Nd$ of 3.1 Ga.

5.6.1.5. Syenogranite (K015B)

Syenogranite (K015B) intrudes the hornblende biotite tonalite (K015A) and is medium grained with mm-scale quartz ribbons and intergranular corridors of medium grained K-feldspar that along with aligned biotite define a moderate strength gneissic foliation. The composition of this rock is quartz (50%), K-feldspar (40%), plagioclase (5%), muscovite (4%) and biotite (1%).

Twenty U-Pb isotopic analyses were conducted on separate zircon grains yielding $^{207}Pb/^{206}Pb$ ages from ca. 2712 to 2493 Ma. The four oldest $^{207}Pb/^{206}Pb$ ages from ca. 2712 to 2682 Ma all have Hf signatures ($^{176}Hf/^{177}Hf$ = 0.28094 – 0.28112) similar to those of zircons in K015A ($^{176}Hf/^{177}Hf$ = 0.28096 – 0.28103) and are interpreted as inheritance from K015A. These zircons have εHf(t) of -5.4 to 1.8 and $T_{DM}Hf$ from 3.2 to 2.9 Ga. Five younger $^{207}Pb/^{206}Pb$ ages from ca. 2638 to 2613 Ma were derived from zircons with oscillatory or faint oscillatory zonation and are interpreted to be magmatic, aside from one $^{207}Pb/^{206}Pb$ age of 2625 Ma that has a $^{176}Hf/^{177}Hf$ more akin to inheritance from K015A. These four $^{207}Pb/^{206}Pb$ ages cluster directly on concordia and are interpreted to best represent the magmatic crystallization of this rock (weighted mean of 2626 ±12 Ma; MSWD = 2.1; Figure 5.5e). The remaining five $^{207}Pb/^{206}Pb$ ages from ca. 2563 to 2493 Ma cascade along a line of discordia towards a poorly defined lower intercept of 1501 ±740 Ma and are thus interpreted to have suffered partial Pb loss. Whole rock Sm-Nd analysis yields a εNd(t) of 12.5 ±0.8 and $T_{DM}Nd$ of 2.2 Ga. With a εNd(t) very similar to the present day value for the depleted mantle this data is geologically questionable or meaningless and will be addressed in the discussion.

5.6.2. Northern transect

5.6.2.1. Biotite-hornblende orthopyroxene granodiorite (Y032A)

Biotite-hornblende orthopyroxene granodiorite (Y032A) is the westernmost intrusive analyzed along the northern transect, located in the map unit Paleoproterozoic opx±cpx±mag tonalite to quartz diorite (Figure 5.3). This biotite-hornblende orthopyroxene granodiorite has a greasy green fresh surface with an orangey brown weathering surface. The crystalline texture is fine to medium grained and there is no

observable fabric apart from very weakly aligned hornblende. This unique color and texture was associated with the field-name "charnockite", and the rock preliminarily interpreted to be part of a Paleoproterozoic plutonic suite.

Twenty-four U-Pb isotopic analyses on individual zircon grains yielded $^{207}Pb/^{206}Pb$ ages between ca. 2873 and 2314 Ma. The two oldest $^{207}Pb/^{206}Pb$ ages of ca. 2873 and 2820 Ma were derived from zircon with $^{176}Lu/^{177}Hf$ of 0.000175 and 0.000181, $^{176}Hf/^{177}Hf$ of 0.28072 and 0.28082, and εHf[t] of -7.8 and -5.5 respectively and are interpreted to be inherited. In comparison, eight younger zircons range in $^{207}Pb/^{206}Pb$ ages from ca. 2747 to 2713 Ma, with a weighted mean age of 2729 ±9 Ma (MSWD = 3.9; Figure 5f) interpreted to best represent the magmatic crystallization of this rock, and these zircons are characterized by distinct Lu-Hf isotopic composition ($^{176}Lu/^{177}Hf$ = 0.000294 to 0.00115, $^{176}Hf/^{177}Hf$ 0.28090 to 0.28108, εHf[t] of -5.4 to 2.0, $T_{DM}Hf$ from 3.22 to 2.97 Ga). The next eight younger zircons yielded $^{207}Pb/^{206}Pb$ ages from 2684 to 2520 Ma and plot below concordia along a line of discordia towards a lower intercept of 1318 ±340 Ma, suggesting a combination of Paleoproterozoic and more recent partial Pb loss. These zircons have more negative εHf(t) of -15 to -4.3. Whole rock Sm-Nd analysis yielded a εNd(t) of -3.7 ±0.6 and $T_{DM}Nd$ of 3.25 Ga.

5.6.2.2. Biotite tonalite (K037A)

Biotite tonalite (K037A) has a weak foliation defined by aligned biotite. This sample was taken adjacent to a proposed contact between metasedimentary rocks to the west and tonalitic basement rocks to the east. While garnet was observed to occur in adjacent metasedimentary rocks and 1m across the contact into the tonalitic basement, this

particular sample contains no garnet and has a composition of quartz, K-feldspar, biotite and plagioclase (no thin section available).

Twenty-five U-Pb isotopic analyses on individual zircon grains yielded sixteen (sub)concordant $^{207}Pb/^{206}Pb$ ages between ca. 2692 and 1774 Ma. All of the zircons in this sample have a subangular to rounded morphology, with Archean $^{207}Pb/^{206}Pb$ ages derived from oscillatory-zoned prismatic core fragments, and Paleoproterozoic $^{207}Pb/^{206}Pb$ ages from unzoned zircon. Five Archean zircons with $^{207}Pb/^{206}Pb$ ages from ca. 2692 to 2563 Ma have εHf(t) of -10.0 to -4.1 and $T_{DM}Hf$ between 3.4 and 3.1 Ga, whereas eleven Paleoproterozoic zircons with $^{207}Pb/^{206}Pb$ ages from ca. 1870 to 1773 Ma have εHf(t) of -20.1 to -16.3 and $T_{DM}Hf$ between 3.0 and 2.8 Ga. Strangely, on concordia, some of the zircons with Archean $^{207}Pb/^{206}Pb$ ages plot closer to Paleoproterozoic concordia while several zircons with Paleoproterozoic $^{207}Pb/^{206}Pb$ ages plot near Archean concordia (Figure 5.5g). Best-fit regression of all analyses results in an upper concordia intercept of 2499 ±86 Ma and a lower concordia intercept of 1671 ±130 Ma, however a weighted mean age of 2687 ±26 Ma (MSWD = 8.9; Figure 5.5g) of the three most concordant analyses ($^{207}Pb/^{206}Pb$ ages between ca. 2692 and 2663 Ma) is interpreted to provide the best estimate for a tonalite crystallization age. Alternative interpretations of a Paleoproterozoic crystallization age of this rock, with the Archean zircons being inherited are presented below in the discussion. Whole rock Sm-Nd analysis yielded a εNd(t) of -1.0 ±0.6 and $T_{DM}Nd$ of 3.0 Ga.

5.6.2.3. Biotite-magnetite epidote monzogranite (F157A)

Biotite-magnetite epidote monzogranite (F157A) is fine to medium grained with well-developed felsic and mafic mineral segregations that define a moderate strength

gneissic foliation. There are local mineral concentrations or "clots" of biotite, hornblende and magnetite. The composition of this rock is quartz (45%), plagioclase (20%), epidote (10%), K-feldspar (5%), biotite (5%), titanite (5%), magnetite (5%) and trace hornblende.

Twenty-five U-Pb isotopic analyses on 23 individual zircon grains yielded $^{207}Pb/^{206}Pb$ ages from ca. 2924 to 2459 Ma. The three oldest zircons range in $^{207}Pb/^{206}Pb$ ages between ca. 2924 and 2788 Ma, in εHf(t) between -1.0 and 6.5, and are interpreted as inherited cores or entire grains. A cluster of five $^{207}Pb/^{206}Pb$ ages ranging from ca. 2711 to 2684 Ma are from zircon cores that have a consistent range in εHf(t) between 0.2 and 1.4 and $T_{DM}Hf$ between 2.97 and 2.92 Ga. These five zircon cores yield a weighted-mean age of 2689 ±10 Ma (MSWD = 2.4; Figure 5.5h) interpreted to best represent the magmatic crystallization of this rock. Eight younger $^{207}Pb/^{206}Pb$ ages from ca. 2668 to 2630 Ma plot just slightly below concordia and likely represent partial Pb loss (Figure 5.5h). Two Paleoproterozoic ages of ca. 1781 and 1782 Ma are from unzoned zircon rims. Whole rock Sm-Nd analysis yielded a εNd(t) of 1.1 ±0.6 and $T_{DM}Nd$ of 2.87 Ga.

5.6.2.4. Biotite-magnetite hornblende monzogranite (H055A)

Biotite-magnetite hornblende monzogranite (H055A) is fine to medium grained with a massive texture delineated by randomly oriented biotite. The sample location is associated with a high aeromagnetic high.

Twenty-three U-Pb isotopic analyses on individual zircon grains yielded $^{207}Pb/^{206}Pb$ ages from ca. 2763 to 2603 Ma. A cluster of eight $^{207}Pb/^{206}Pb$ ages ranging from ca. 2763 to 2745 Ma were derived from oscillatory zoned zircon cores and are interpreted to represent the crystallization age of this rock (weighted mean of 2750 ±8 Ma; MSWD = 2.9; Figure 5.5i). These zircons have εHf(t) of 1.6 to 3.4 and $T_{DM}Hf$ between 3.0 and 2.9

Ga. Younger $^{207}Pb/^{206}Pb$ ages from ca. 2723 to 2659 Ma were derived from unzoned rims and are interpreted to be metamorphic. Whole rock Sm-Nd analysis yielded a εNd(t) of 2.7 ±0.7 and $T_{DM}Nd$ of 2.8 Ga.

5.6.2.5. Magnetite biotite monzogranite (Z108A)

Magnetite biotite monzogranite (Z108A) has an equant, medium to coarse-grained texture with aligned biotite and local quartz ribbons defining a weak to moderate strength gneissic foliation. There are local K-feldspar porphyroclasts and mineral clots of magnetite ± biotite ± hornblende. The composition of this rock is quartz (30%), perthite (30%), K-feldspar (25%), biotite (10%), magnetite (5%) and trace hornblende.

Twenty-two U-Pb isotopic analyses on 20 individual zircon grains yielded $^{207}Pb/^{206}Pb$ ages from ca. 2925 to 2521 Ma. The three oldest zircons, interpreted as inherited, range in $^{207}Pb/^{206}Pb$ ages from ca. 2925 to 2861 Ma and have lower $^{176}Hf/^{177}Hf$ (0.28096 – 0.28105) compared to the rest of the analyzed zircons from this sample ($^{176}Hf/^{177}Hf$ = 0.28107 to 0.28112). Eight younger $^{207}Pb/^{206}Pb$ ages between ca. 2801 and 2727 Ma were derived from oscillatory zoned zircons and are interpreted to represent the crystallization age of this rock (weighted-mean $^{207}Pb/^{206}Pb$ age of 2777 ±20 Ma; MSWD = 9.4; Figure 5.5j). The remaining $^{207}Pb/^{206}Pb$ ages from ca. 2612 to 2521 Ma are derived from zircon rims that are unzoned or show faint oscillatory zonation and are interpreted to be metamorphic. Whole rock Sm-Nd analysis yielded a εNd(t) of 4.3 ±0.7 and $T_{DM}Nd$ of 2.8 Ga.

5.7. Discussion

5.7.1. Archean magmatic suites on eastern Hall Peninsula

In this targeted study of magnetite-bearing granitoids, the interpreted U-Pb crystallization ages (ca. 2899 to 2626 Ma) overlap with, but are mostly younger than, previously dated tonalitic to monzogranitic gneisses (ca. 2980 to 2720 Ma) of eastern Hall Peninsula (Scott, 1999; Rayner, 2014, 2015; Chapter 4). The current study documents crystallization ages of ca. 2899 Ma, ca. 2777 Ma, three between ca. 2750 and 2727 Ma and five between ca. 2689 to 2612 Ma. Seven out of these ten rock units are younger than previously reported crystallization ages of eastern Hall Peninsula orthogneisses on eastern Hall Peninsula (within 2σ error), and four are younger than documented Archean metamorphism (ca. 2740 to 2700 Ma; Chapter 4).

These seven granites with younger crystallization ages ranging from ca. 2729 to 2612 Ma compared to the majority of previously analyzed orthogneisses (ca. 2976 to 2740 Ma), are proposed to represent a previously unrecognized phase or episodes of Archean magmatism throughout eastern Hall Peninsula that is syn- to post-metamorphic.

5.7.2. Late-stage syenogranite magmatism

At station K015, a tonalite (K015A) is crosscut by coarser grained syenogranite (K015B), a common relationship observed throughout eastern Hall Peninsula (Scott, 1996; From et al., 2013). K015A and K015B have U-Pb crystallization ages of 2661 ±39 Ma and 2626 ±12 Ma, respectively, with the zircons from each rock having different $^{176}Hf/^{177}Hf$ and $\varepsilon Nd_{(t)}$ (Table 5.1; APPENDIX 5A) indicating different parental source magmas. With a definitive crosscutting relationship, syenogranite K015B is the youngest identified component of the Archean orthogneiss complex aside from syenogranite

(T027A), which is relatively close to the K015B sample site (~22 km). While T027A is coarser grained and less deformed than K015B their interpreted crystallization ages are similar (2612 ±15 and 2626 ±12 Ma respectively; 2σ error). These results constrain syenogranitic magma emplacement and injection to ca. 2.62 Ga (between ca. 2.64 and 2.60 Ga) as the final stage of Archean magmatic activity on eastern Hall Peninsula.

5.7.3. Paleoproterozoic zircon crystallization

Amongst the Archean rock units in the southern transect, only two samples (K015A, S154A) yielded Paleoproterozoic zircon ages. Zircons from K015A yielded two Paleoproterozoic $^{207}Pb/^{206}Pb$ ages (ca. 1755, 1750 Ma) amongst six $^{207}Pb/^{206}Pb$ Archean ages, while zircons from S154A yielded only one $^{207}Pb/^{206}Pb$ age (ca. 1766 Ma) amongst thirteen Archean $^{207}Pb/^{206}Pb$ ages.

Within the five rocks units in the northern transect, again only two samples (K037A, F157A) yielded Paleoproterozoic zircon ages. Zircons from K037A yielded eleven Paleoproterozoic $^{207}Pb/^{206}Pb$ ages (n=11; ca. 1870 to 1776 Ma) compared to five Archean $^{207}Pb/^{206}Pb$ ages, whereas zircons from F157A yielded two Paleoproterozoic $^{207}Pb/^{206}Pb$ ages (ca. 1877, 1819 Ma) compared to sixteen Archean $^{207}Pb/^{206}Pb$ ages. Overall, these metamorphic overgrowths date to the same time period as documented Paleoproterozoic granulite to mid-amphibolite facies metamorphism across Hall Peninsula constrained between ca. 1860 and 1820 Ma (Skipton et al., 2016). The preferential growth and preservation of Paleoproterozoic zircon material likely relies on the composition of each unit and the amount of Zr and Si liberated during Paleoproterozoic metamorphism.

In the case of K037A, a question can be raised as to whether this rock was: (1) emplaced during the Archean at ca. 2.69 Ga, experiencing tectonometamorphism

between ca. 1870 and 1774 Ma resulting in subsequent, new zircon growth as single grains and overgrowth rims, or (2) emplaced during the Paleoproterozoic and the Archean dates are simply inherited material.

We prefer an interpretation that initial crystallization took place in the Archean due to the location of this sample 10's of kilometres east of the boundary of any previously recognized Paleoproterozoic plutonic units (Figure 5.3). In this scenario, magmatic zircon either did not crystallize during initial rock formation or was later resorbed/destroyed and round, unzoned metamorphic zircon grains crystallized during Paleoproterozoic tectonometamorphism.

5.7.4. Sm-Nd data trends from west to east

There is a spatial trend in the Sm-Nd data within the southern and northern transects across central and eastern Hall Peninsula with $\varepsilon Nd_{(t)}$ values becoming more positive towards the east (Figure 5.3).

Along the southern transect, εNd(t) ranges from -12.7 ±0.6 in the southwest to 12.5 ±0.8 in the northeast. The furthest northeast sample location has two specimens, K015A (-1.4 ±0.6) and K015B (12.5 ±0.8). T_{DM}Nd follows a similar spatial trend, younging from ca. 4.0 Ga in the west to ca. 2.2 Ga in the east (Figure 5.3; Table 5.1). K015A deviates from the trend with an older T_{DM}Nd of ca. 3.1 Ga compared to the previous stations's T_{DM}Nd of ca. 2.83 Ma (S154A). K015B, in comparison, has a very young T_{DM}Nd of ca. 2.2 Ga and an extremely positive εNd(t) value of 12.5 compared to the rest of the southern transect data (Figure 5.6a). This εNd(t) result is unexpected since the depleted mantle has εNd(t) of ~4 at ca. 2.6 Ga so this anomalous result reflects either (1) a

Proterozoic rock with dominantly inherited zircon, (2) a significant disturbance in the Sm-Nd systematics within the minerals in this rock sample or (3) a flawed analysis.

In the first case, the εNd(t) would be much lower as the $^{147}Sm/^{144}Nd$ is very low, therefore, we interpret the Sm-Nd results of K015B to have most likely been affected by Sm-Nd fractionation resulting in a crustal evolution trend outside of Nd model age/evolution parameters (e.g., $^{147}Sm/^{144}Nd$ <0.15). This could have been a result of Archean metamorphism and/or crustal contamination during emplacement and the Sm-Nd results from this sample will not be discussed further.

The northern transect, which has a higher density of samples located close to the interpreted boundary between Paleoproterozoic and Archean map units (Figure 5.3), has $\varepsilon Nd_{(t)}$ of -3.7 ±0.6 in the west that steadily becomes more positive to 4.3 ±0.7 in the east. The $T_{DM}Nd$ follows a similar trend with a ca. 3.3 Ga model age in the west getting steadily younger to ca. 2.8 Ga in the east. This trend demonstrates, even more strikingly than the southern transect, that there has been significant crustal re-working in the west, close to the Paleoproterozoic rock boundary. Towards the east, the rocks show a more mantle-derived, juvenile magma isotopic character.

5.7.5. Lu-Hf in zircon

Lu-Hf data from the same zircon spot locations used for U-Pb yielded valuable information on the timing of parental magma extraction from the mantle and provided a second line of evidence to corroborate the initial discernment of inherited, magmatic and metamorphic zircons using BSE and CL images. Only the εHf(t) and $T_{DM}Hf$ data for zircons interpreted to represent the magmatic crystallization are discussed below.

Figure 5.6. A) εNd(t) vs. $^{207}Pb/^{206}Pb$ age diagram for samples from the southern and the northern transects. B) $^{143}Nd/^{144}Nd$ vs. $^{147}Sm/^{144}Nd$ diagram for samples from the southern and the northern transects.

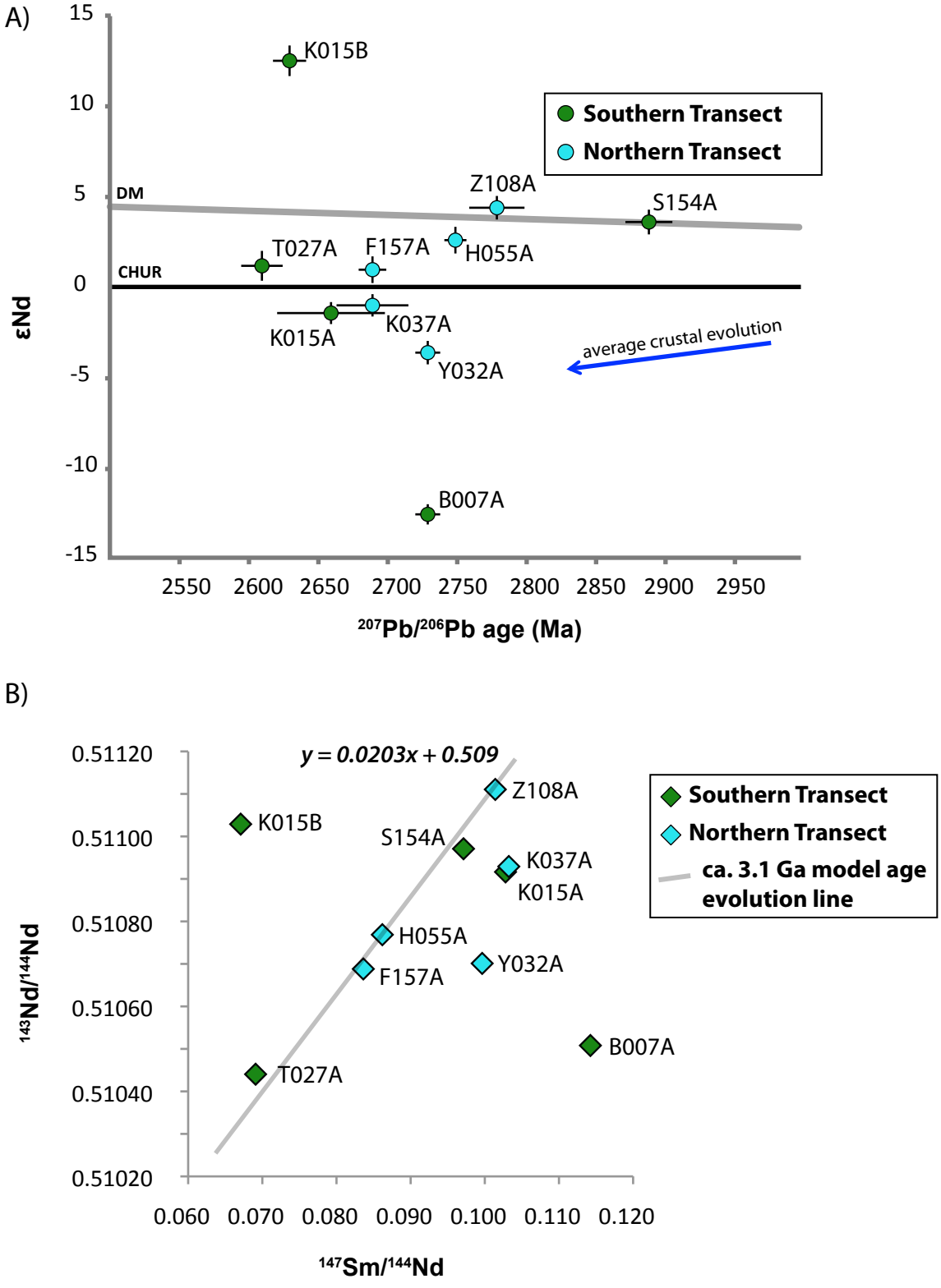

Southern transect

Along the southern transect, εHf(t) ranges from -6.0 to 5.4, but unlike the εNd(t) results, does not yield a well-defined spatial trend from west to east (Figure 5.3). The two westernmost samples, B007A and T027A, both yielded mostly negative εHf(t) from -3.7 to 0.7 indicating some degree of magma mixing or crustal recycling, consistent with the εNd(t) from the same rocks (-12.7 and 0.0, respectively). Continuing northeast along the transect, sample S154A yielded more positive εHf(t) from 2.7 to 5.4 indicating a more juvenile rock forming magma, consistent with its relatively older crystallization age of ca. 2899 Ma. However, all three of the rocks discussed thus far along the southern transect have fairly similar T_{DM}Hf ages ranging from ca. 3.1 to 3.0 Ga, which suggests derivation from the same crust whose protolith melt was extraction from the mantle at ca. 3.1 Ga. Further northeast, sample K015A yielded negative εHf(t) of -6.0 to -2.7 and slightly older T_{DM}Hf of ca. 3.1 to 3.0 Ga compared to crosscutting K015B, which yielded more positive εHf(t) of 1.8 to 4.8 and younger T_{DM}Hf of ca. 2.9 to 2.7 Ga. This data trend from K015A and K015B is very similar to the overall trend seen in the εNd(t) and T_{DM}Nd data, where it is more pronounced. The Lu-Hf data indicate that K015B was derived from a distinct, younger juvenile magmatic source relatively late in the Archean geologic history of eastern Hall Peninsula. However, the Lu-Hf isotope systematics may have been disturbed similar to the Sm-Nd isotopes as discussed above.

Northern transect

Along the northern transect, εHf(t) follows a spatial trend akin to the εNd(t) data with negative εHf(t) in the west (Y032A: -5.4 to 1.0) to more positive in the east (Z108A: -0.1 to 3.1). T_{DM}Hf ages from the westernmost sample Y032A (ca. 3.2 to 3.0 Ga) are

nearly identical to the westernmost sample of the southern transect B007A (ca. 3.1 to 3.0 Ga) but also overlap with the T_{DM}Hf of the easternmost sample in the north, Z108A (ca. 3.0 Ga). The three intervening northern transect samples have slightly younger T_{DM}Hf ranging from ca. 3.0 to 2.9 Ga. Interestingly the T_{DM}Hf of ca. 3.0 Ga is within the upper age range for three samples in the northern transect (K037A, F157A and H055A) and the lower age range of four other samples throughout Hall Peninsula (Y032A, B007A, T027A, S154A; Table 5.1).

In summary, the magmatic εHf(t) data become more positive from west to east suggesting that there was more crustal re-working and the recycling of older crust in the west along the boundary between Archean and Paleoproterozoic rocks. The T_{DM}Hf data show a much more consistent age of protolith melt extraction from the mantle for all of the rocks analyzed (ca. 3.1 to 2.7 Ga) compared to the T_{DM}Nd ages that are more variable across the sample set (ca. 4.0 to 2.2 Ga). While a T_{DM}Nd age of ca. 4.0 Ga indicates the potential recycling of ancient crust, it is puzzling why the T_{DM}Hf age is much younger at ca. 3.1 Ga. One factor in this variability could be the effect of "mixed" Paleoproterozoic and Archean material within a single sample when using the whole-rock sampling method. Overall, the T_{DM}Hf ages agree with previous Hf results from orthogneisses from Chapter 4 with both data sets providing consistent results from ca. 3.1 to 2.9 Ga indicating the time at which parental crust was formed from mantle-derived melts.

5.7.6. Zircon Lu-Hf data versus whole rock Sm-Nd analyses

When elucidating the geologic history of Archean rocks that have seen multiple episodes of deformation and metamorphism, using a highly resistant mineral (e.g., zircon) in order to obtain the most pristine Archean information possible is typically the best option. Moreover, using an in-situ dating technique (e.g., SHRIMP, LA-ICPMS, etc) is essential in order to target single age domains within complex zircon crystals that have multiple age domains (e.g., inherited, magmatic, metamorphic, etc). Poly-phase deformation and metamorphism, as observed on Hall Peninsula (Steenkamp and St-Onge, 2014), can lead to whole-rock samples that contain "mixed" age material. The potential for mixed results from whole-rock Sm-Nd analyses has been well documented, especially in sedimentary provenance studies where this phenomenon is best quantified (e.g., Cattell et al., 1984; McLennan et al., 1993; Frei et al., 1999). In smaller-scale studies with much higher sampling densities compared to this study on eastern Hall Peninsula, T_{DM}Nd ages in between crustal end members (e.g., between ca. 2.75 and ca. 1.85 Ga in the case of Hall Peninsula) have been considered as an indication of mixing due to a remnant fault or ductile shear zone, which formed during juxtaposition of Archean and Paleoproterozoic crustal blocks (Holmden, 1995). However, since this study targeted late-phase plutonic rocks that may have inherited basement signatures or been (partially) derived from underlying crust we employed both zircon and whole-rock analyses in order to compare indications, trends and results from these isotopic systems and techniques.

One benefit of the Lu-Hf zircon data over the Sm-Nd whole-rock data is the ability to discern zircon dates intrinsic to K015B representative of a crystallization age, or inherited from K015A during emplacement (see K015B results section). Moreover, the zircon data from K015B shows a discordant array of U-Pb ages on Concordia (Figure

5.5e) with a trajectory towards a loosely defined lower intercept of 1501 ±740 Ma, which indicates an influence from subsequent metamorphism (likely Paleoproterozoic Pb loss) that would have gone unnoticed by only interpreting whole-rock Sm-Nd data.

In an assessment of all samples from this study plotted on a $^{143}Nd/^{144}Nd$ versus $^{147}Sm/^{144}Nd$ diagram (Figure 5.6a), five of the ten samples scatter around a linear array. Samples T027A, S154A, F157A, H055A and Z108A define a loose array whose slope has an "errorchron" age of ~ ca. 3.1 Ga (Figure 5.6b). These five rocks have different U-Pb crystallization ages (ca. 2899 to 2612 Ma) but very similar mean Nd model ages of ca. 2.9 to 2.8 Ga indicating episodic partial melting events from the same crust. In fact, all εNd from these five samples are positive (0.9 to 4.3) and represent the preservation of the juvenile magma signatures. The remaining five samples have largely negative εNd values (-1.0 to -12.7) aside from K015B (εNd = 12.5) representing derivation from recycled magma and/or crust through the re-melting of older crust.

The $T_{DM}Hf$ and εHf from zircon were examined to evaluate the veracity of the Sm-Nd trend from whole-rock samples. A εHf versus $^{207}Pb/^{206}Pb$ age diagram (Figure 5.7a) shows southern transect samples B007A, S154A, T027A and K015A along an array roughly parallel to an average crustal evolution trajectory that traces back to the depleted mantle line indicating a common age of melt extraction from the depleted mantle (Figure 5.7a). K015B plots outside of this generally linear array (Figure 5.7a). The northern transect samples have tighter clustering of their $^{207}Pb/^{206}Pb$ ages but F157A, H055A and Z108A again define an array roughly parallel to an average crustal evolution trajectory tracing back to the depleted mantle line (Figure 5.7b). Additionally, the five samples that fall outside of the linear array all have Sm-Nd and Lu-Hf data indicative of magma

Figure 5.7. εHf(t) vs. $^{207}Pb/^{206}Pb$ ages A) for samples from the southern transect and B) northern transect.

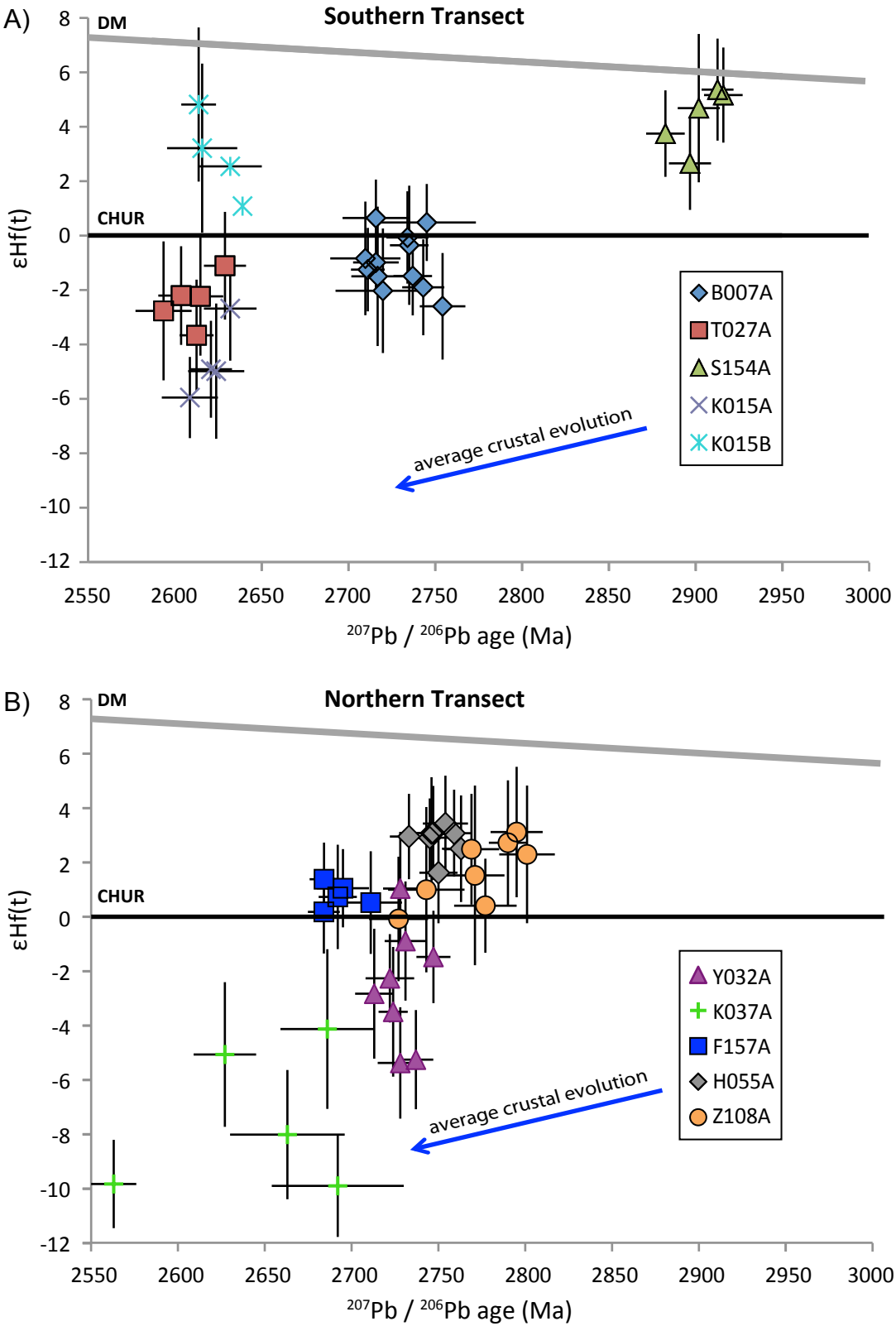

and/or crustal recycling prior to crystallization (as already discussed) by: (1) location on a potential cryptic suture zone (B007A, Y032A; Figure 5.3), (2) disturbed Sm-Nd isotope systematics and/or crustal contamination (K015A, K015B), or (3) a significant component of Paleoproterozoic juvenile magma and disturbed isotopic results (K037A).

5.7.7. A geologic terrane boundary on west-central Hall Peninsula?

The westernmost samples from each transect (B007A and Y032A) were sampled from map units interpreted to be Paleoproterozoic in age (Figure 5.3; Machado et al., 2013), however, their U-Pb isotopic zircon analyses yielded only Archean magmatic $^{207}Pb/^{206}Pb$ ages. These two samples are located within a N-S corridor where Paleoproterozoic and Archean rocks are juxtaposed within a heterogeneous and complex deformational zone. The negative $\varepsilon Nd_{(t)}$ values of B007A and Y032A provide evidence of much higher degrees of magma and/or crustal recycling compared to the majority of other samples towards the east. The Nd and Hf model ages for both of these samples indicate a significantly older age of extraction from the mantle and imply interaction with Mesoarchean crust that has not been found in outcrop on Hall Peninsula. Similar evidence of the re-melting and recycling of Meso- to Paleoarchean crust was documented in previous work on eastern Hall Peninsula within the snow bowl area (Chapter 4). A magnetite-bearing monzogranite with a moderate gneissic fabric, which is very similar to most of the rocks in this study, yielded mean Hf model ages in zircon far older (ca. 3.4 Ga) than those from all other units in the study area. One explanation is that eastern Hall Peninsula once had a thicker, older cratonic root comprised of Meso- to Paleoarchean crust, which has subsequently been delaminated, recycled and/or eroded. Alternatively, during Archean tectonic amalgamation at ca. 2.70 Ga eastern Hall Peninsula may have

been juxtaposed against exotic, Meso- to Paleoarchean crust. The exact origin and history of this potential exotic crust is difficult to ascertain because it has been further obliterated by subsequent Paleoproterozoic deformation and metamorphism. In fact, post-thermal peak, east-west Paleoproterozoic shortening (D_2) produced east-verging, thick skinned imbricate thrusts with thrust slices of Archean basement and Paleoproterozoic supracrustal rocks having strongly-deformed to mylonitic shear zones at the contacts (Steenkamp and St-Onge, 2014). Subsequent Paleoproterozoic magmatism (stitching plutons) then overprinted and likely obscured any field evidence of a remnant Archean or Paleoproterozoic crustal suture along the eastern margin of the Archean orthogneiss complex of eastern Hall Peninsula (e.g., Dickin, 1998; Han et al., 2010; Whalen et al., 2010; Hughes et al., 2014). One remaining clue is the N-S lineaments (as seen on total-field magnetic susceptibility) along the entire length of the "transition zone" on central Hall Peninsula (Figure 5.2), which is markedly different from the aeromagnetic signature of the Archean orthogneiss complex of eastern Hall Peninsula (Figure 5.2). This apparent N-S linear fabric in the "transition zone" may be linked to the direction of maximum shortening (E-W) during Paleoproterozoic deformation. With no additional data available on the nature of this transition zone, more detailed mapping and isotopic work is needed in order to investigate the nature of this tectonic zone and to fully test if Archean rocks extend west beneath the Meta Incognita microcontinent as Archean basement.

5.7.8. Regional tectonic implications

The regional paleo-plate history of the Quebec-Baffin segment of the THO has been investigated through much lithological mapping along with geochemical and isotopic work, but the isolated geography of the area, incomplete rock exposure and the lack of

isotopic data on Hall Peninsula has hindered interpretations of the regional tectonic assembly (e.g., St-Onge et al., 2009; Garde and Hollis, 2010). Moreover, on eastern Hall Peninsula, only the intensely deformed and metamorphosed ancient mid-crustal rocks are preserved. As such, the tectonic processes inferred to have operated at mid-crustal levels during the Archean might differ from processes at work in modern or even Paleoproterozoic collisional plate-tectonic processes (Garde and Hollis, 2010), rendering it difficult to understand and constrain the original crustal architecture of these ancient orogens.

In Chapter 4, it was inferred that Archean crust of eastern Hall Peninsula on Baffin Island is either correlative with Archean crust of the southern block of the Aasiaat domain, West Greenland, or is itself an independent crustal fragment with a unique geologic history. As further detailed studies are conducted throughout similar regions in the THO, new data point towards a number of small Archean crustal fragments with cryptic terrane boundaries that may have amalgamated into larger-scale cratons (e.g., Garde and Hollis, 2010; LaFlamme et al., 2014; Arcuri, 2016). The Aasiaat domain is one such terrane that was caught in the Paleoproterozoic collision between the Rae craton, Meta Incognita microcontinent and the North Atlantic craton (Kolb, 2014), and is directly adjacent to eastern Hall Peninsula across Davis Strait (Figure 5.1). With overlapping U-Pb ages to eastern Hall Peninsula, these two regions of Archean crust may share an Archean geologic history; follow-up studies of Lu-Hf and Sm-Nd isotopes from the Aasiaat domain may further refine a correlation.

There is Sm-Nd data from southern Baffin Island that may be useful in delineating the presence of any cryptic terrane boundaries. Whalen et al. (2010) investigated the

nature of the Cumberland Batholith (CB) using geochemistry and U-Pb and Sm-Nd isotopes along NNE and NNW trending transects across southern Baffin Island. A complete absence of Sm-Nd data on Hall Peninsula, just east of the NNE transect, prompted the present study to include whole-rock Sm-Nd isotopes, in conjunction with U-Pb and Lu-Hf LASS-ICPMS of zircon, to extend the isotopic crustal record across Hall Peninsula. Whalen et al. (2010) postulated that the isotopically more evolved domain defined by CB and post-CB magmas (ca. 1.84–1.82 Ga) images the Archean Sugluk block at depth beneath the southern Meta Incognita microcontinent. In addition, Nd isotopic evidence of at least some assimilation of upper-plate Meta Incognita crustal material with the CB indicates that the Sugluk block and Meta Incognita microcontinent collision occurred prior to CB magmatism. Whalen et al. (2010) also present crystallization ages between ca. 2875 and 2714 Ma for the granitoid rocks of the Rae craton and Big Island (Saglek Bay, North Atlantic craton), which are similar to those of orthogneisses on Hall Peninsula. The granitoid rocks of the Rae craton and Big Island range in $\varepsilon Nd_{(t)}$ (using their interpreted crystallization age as $_{(t)}$) between -4.72 and 1.89 with $T_{DM}Nd$ from ca. 3.0 to 2.8 Ga (one older value of ca 3.4 Ga), also comparable to the Hall Peninsula Sm-Nd data (this Chapter).

With such similar magmatic U-Pb ages on multiple cratons across this segment of the THO, detrital zircon age distributions from Paleoproterozoic metasedimentary rocks may provide additional insight into regional tectonic reconstructions. At least nine metasedimentary samples (psammite and quartzite) taken throughout Hall Peninsula display a wide variation of U-Pb zircon age populations ranging from purely Meso- to Neoarchean (prominent modes at 2.89, 2.81, 2.77 and 2.70 Ga; unit interpreted as a basal

depositional sequence) to ca. 2.50 and 2.25 Ga, with one localized mode at ca. 2.32 Ga, and also an age peak from ca. 2.10 to 1.96 Ga (Rayner, 2014, 2015). Possible source rocks for ca. 2.5 to 2.3 Ga and ca. 1.96 Ga detritus, however, have not been identified on Hall Peninsula and potential candidates have restricted occurrences throughout the Meta Incognita microcontinent and the Rae craton. Interestingly, a hypothesis advanced by Whalen et al. (2010), based on U-Pb age and Sm-Nd isotopic data, postulates that the Meta Incognita microcontinent could be a dominantly ca. 2.4 Ga domain of a composite Rae craton (3.0 and 2.4 Ga domains). This could explain why there is no distinctive Sm-Nd or other isotopic difference across the "Baffin Suture" as proposed by St-Onge at al. (2009), which was thought to separate the Rae craton to the north and the Meta Incognita microcontinent to the south (Figure 5.1). This may also explain the provenance of zircon detritus of the Paleoproterozoic rocks documented across Hall Peninsula (Rayner, 2014, 2015). With the Meta Incognita microcontinent viewed as a fragment rifted from the Rae craton, which contains U-Pb isotopic ages >3.0 Ga, this may also be the source of the Meso- to Paleo-Archean crustal ages documented in granitic rocks from this study along the western boundary of the Archean orthogneiss complex of Hall Peninsula.

Therefore, we postulate that the Archean orthogneiss complex of eastern Hall Peninsula is a unique and separate microcontinent fragment that was potentially once part of the composite Rae craton or the Aasiaat domain but was subsequently rifted and accreted to the Meta Incognita microcontinent during Paleoproterozoic tectonic assembly. In fact, Windley and Garde (2009) interpreted the bulk of Precambrian craton orthogneisses to have been accreted by oceanic arcs, which then evolved into the convergent margins of growing microcontinents. Moreover, these processes are very

similar to those proposed to have operated during Paleoproterozoic assembly and crustal accretion in this segment of the THO (e.g., St-Onge et al., 2009; Garde and Hollis, 2010; Whalen et al., 2010). There is also the possibility that the Archean Hall Peninsula block rifted and re-accreted to the Meta Incognita microcontinent. This notion is supported by Paleoproterozoic supracrustal stratigraphy across Hall Peninsula interpreted as representing a proximal shallow-marine to more distal continental-shelf and slope-rise setting with input of mafic material, possibly from a local rifting environment (Steenkamp and St-Onge, 2014). Further work needs to be focused on the boundary or "transition zone" between Paleoproterozoic and Archean map units along central Hall Peninsula but extant data leads us to propose that the Archean rocks of eastern Hall Peninsula can be considered its own microcontinent fragment termed the Hall Peninsula Block as initially postulated by Whalen et al. (2010).

5.8. Conclusions

- LASS-ICPMS U-Pb and Lu-Hf isotopic data from zircon separated from magnetite-bearing tonalite to syenogranite samples associated with bodies of circular aeromagnetic highs delineate a young phase of plutonic activity from ca. 2750 to 2612 Ma including late-stage syenogranitic magma emplacement and injection at ca. 2626 to 2612 Ma on eastern Hall Peninsula.
- Whole-rock Sm-Nd isotopic data from granitoid samples from transects across southern and northern Hall Peninsula shows a west to east trend of negative $\varepsilon Nd_{(t)}$ to positive $\varepsilon Nd_{(t)}$. This indicates increased crustal re-working and recycling in the west along the boundary between Paleoproterozoic and Archean rocks and more

mantle-derived, juvenile Nd isotopic character towards the east within the Archean orthogneiss complex.

- $\varepsilon Hf_{(t)}$ zircon data yielded a similar spatial trend to that of the whole rock $\varepsilon Nd_{(t)}$ data, and $T_{DM}Hf$ zircon ages outline consistent crustal model ages from ca. 3.1 to 2.9 Ga for all samples aside from the young, crosscutting syenogranites.
- Five granitoid samples have consistently positive εNd (0.0 to 4.3) and nearly identical $T_{DM}Nd$ (ca. 2.8 to 2.9 Ga) indicating they are related although they span ca. 250 Ma in crystallization age. The average εHf are nearly all positive (-2.6 to 2.8) and have nearly identical $T_{DM}Hf$ to one another (ca. 2.9 to 3.0 Ga). Therefore, these five rocks were ultimately derived from the same batch of melt extracted from the mantle at ca. 3.1 Ga.
- Based on existing Sm-Nd data from Meta Incognita micorcontinent to the west and north, Hall Peninsula appears to be a separate Archean block. Further investigation of the Sm-Nd signatures of Paleoproterozoic plutonic and sedimentary rocks along central Hall Peninsula may allow the delineation of a cryptic crustal suture since voluminous Paleoproterozoic magmatism and regional tectono-metamorphism have obliterated any field evidence of such a boundary.

5.9. Acknowledgements

Special thanks to D. Mate, G. Machado, H. Steenkamp, M. St-Onge, and the CNGO staff and crew who collaborated on the Hall Peninsula Integrated Geoscience Project. At the University of Alberta R. Stern and Katie Nichols assisted with zircon mounting and imaging, C. Holmden and S. Timsic at the University of Saskatchewan Isotope laboratory for Sm-Nd analyses. The Canadian Northern Economic Development Agency's (CanNor)

Strategic Investments in Northern Economic Development (SINED) program provided financial support for the HPIGP as a whole.

5.10. References Cited

Arcuri, G.A., 2016. Whole-Rock Pb Isotope Delineation of Archean and Paleoproterozoic Crustal Terranes in the Grenville Province and Adjacent Makkovik Province: Evidence for Juvenile Crustal Growth during the Paleoproterozoic (Doctoral dissertation, McMaster University).

Allibon, J., Ovtcharova, M., Bussy, F., Cosca, M., Schaltegger, U., Bussien, D. and Lewin, É. 2011. Lifetime of an ocean island volcano feeder zone: constraints from U-Pb dating on coexisting zircon and baddeleyite, and 40Ar/39Ar age determinations, Fuerteventura, Canary Islands; Canadian Journal of Earth Sciences, v. 48, p. 567-592.

Blewett, R.S., Black, L.P., Sun, S.S., Knutson, J., Hutton, L.J. and Bain, J.H.C., 1998. U- Pb zircon and Sm-Nd geochronology of the Mesoproterozoic of North Queensland: implications for a Rodinian connection with the Belt supergroup of North America. Precambrian Research, v. 89, p. 101-127.

Böhm, C. O., Heaman, Creaser, R. A., L. M., and Corkery, M. T., 2000. Discovery of pre-3.5 Ga exotic crust at the northwestern Superior Province margin, Manitoba. Geology, v. 28, p. 75–78.

Böhm, C. O., Heaman, L. M., Stern, R. A., Corkery, M. T., and Creaser, R. A. (2003). Nature of Assean lake ancient crust, Manitoba: a combined SHRIMP–ID-TIMS U–Pb geochronology and Sm–Nd isotope study. Precambrian Research, v. 126, p. 55-94.

Böhm, C. O., Zwanzig, H. V., & Creaser, R. A., 2007. Sm-Nd isotope technique as an exploration tool: delineating the northern extension of the Thompson Nickel Belt, Manitoba, Canada. Economic Geology, v. 102, p. 1217-1231.

Cattell, A., Krogh, T.E. and Arndt, N.T., 1984. Conflicting Sm-Nd whole rock and U-Pb zircon ages for Archean lavas from Newton Township, Abitibi belt, Ontario. Earth and Planetary Science Letters, v. 70, p. 280-290.

Connelly, J.N. 2001: Degree of preservation of igneous zonation in zircon as a signpost for concordancy in U/Pb geochronology; Chemical Geology, v. 172, p. 25–39.

Connelly, J.N., Thrane, K., Krawiec, A.W. and Garde, A.A. 2006: Linking the Palaeoproterozoic Nagssugtoqidian and Rinkian orogens through the Disko Bugt region of West Greenland; Journal of the Geological Society, v. 163, p. 319–335.

Corfu, F., Hanchar, J.M., Hoskin, P.W. and Kinny, P. 2003. Atlas of zircon textures; Reviews in Mineralogy and Geochemistry, v. 53, no. 1, p. 469-500. doi:10.2113/0530469

Corrigan, D., Pehrsson, S., Wodicka, N. and De Kemp, E. 2009. The Palaeoproterozoic Trans-Hudson Orogen: a prototype of modern accretionary processes; Geological Society of London, Special Publications, v. 327, p. 457-479. doi: 10.1144/SP327.19

Da Silva Filho, A. F., Guimarães, I. P., Van Schmus, W. R., Armstrong, R. A., Da Silva, J. R., Osako, L. S., and Cocentino, L. M. 2014. SHRIMP U–Pb zircon geochronology and Nd signatures of supracrustal sequences and orthogneisses constrain the Neoproterozoic evolution of the Pernambuco–Alagoas domain, southern part of Borborema Province, NE Brazil. International Journal of Earth Sciences, v. 103, p. 2155-2190.

DePaolo, D.J. and Wasserburg, G.J., 1976. Nd isotopic variations and petrogenetic models. Geophysics Research Letters, v. 3, p. 249–252.

Dickin, A.P. and McNutt, R.H. 1990. Nd model age mapping of Grenville lithotectonic domains: Mid-Proterozoic crustal evolution in Ontario. In Mid-Proterozoic Laurentia-Baltica. Edited by C.F. Gower, T. Rivers, and A.B. Ryan. Geological Association of Canada, Special Paper v. 38, p. 79-94.

Dickin, A.P., 1998. Nd isotope mapping of a cryptic continental suture, Grenville Province of Ontario. Precambrian Research, v. 91, p. 433-444.

Dumont, R., and Dostaler, F. 2010a. Geophysical Series, NTS 25- I/SE and part of 25-I/SW, Aeromagnetic Survey Hall Peninsula, Nunavut; Geological Survey of Canada, Open File 6413, scale 1: 100 000.

Dumont, R. and Dostaler, F. 2010b. Geophysical Series, NTS 25-I/ NE, Aeromagnetic Survey Hall Peninsula, Nunavut; Geo- logical Survey of Canada, Open File 6414, scale 1:100 000.

Dumont, R., and Dostaler, F. 2010c. Geophysical Series, NTS 25- I/NW, Aeromagnetic Survey Hall Peninsula, Nunavut; Geo- logical Survey of Canada, Open File 6415, scale 1:100 000.

Dumont, R., and Dostaler, F. 2010d. Geophysical Series, NTS 25- J/NE, Aeromagnetic Survey Hall Peninsula, Nunavut; Geo- logical Survey of Canada, Open File 6416, scale 1:100 000.

Dumont, R., and Dostaler, F. 2010e. Geophysical Series, NTS 25- O/SE, Aeromagnetic Survey Hall Peninsula, Nunavut; Geo- logical Survey of Canada, Open File 6417, scale 1:100 000.

Dumont, R., and Dostaler, F. 2010f. Geophysical Series, NTS 25- O/SW, Aeromagnetic Survey Hall Peninsula, Nunavut; Geological Survey of Canada, Open File 6418, scale 1: 100 000.

Dumont, R., and Dostaler, F. 2010g. Geophysical Series, NTS 25- O/NE, Aeromagnetic Survey Hall Peninsula, Nunavut; Geological Survey of Canada, Open File 6419, scale 1: 100 000.

Dumont, R., and Dostaler, F. 2010h. Geophysical Series, NTS 25- O/NW, Aeromagnetic Survey Hall Peninsula, Nunavut; Geological Survey of Canada, Open File 6420, scale 1: 100 000.

Dumont, R., and Dostaler, F. 2010i. Geophysical Series, NTS 25- P/SE, Aeromagnetic Survey Hall Peninsula, Nunavut; Geo- logical Survey of Canada, Open File 6421, scale 1: 100 000.

Dumont, R., and Dostaler, F. 2010j. Geophysical Series, NTS 25- P/SW, Aeromagnetic Survey Hall Peninsula, Nunavut; Geo- logical Survey of Canada, Open File 6422, scale 1: 100 000.

Dumont, R., and Dostaler, F. 2010k. Geophysical Series, NTS 25- P/NE, Aeromagnetic Survey Hall Peninsula, Nunavut; Geo- logical Survey of Canada, Open File 6423, scale 1: 100 000.

Dumont, R., and Dostaler, F. 2010l. Geophysical Series, NTS 25- P/NW, Aeromagnetic Survey Hall Peninsula, Nunavut; Geological Survey of Canada, Open File 6424, scale 1: 100 000.

Dyck, B.J., and St-Onge, M.R. 2014. Dehydration-melting reactions, leucogranite emplacement and the Paleoproterozoic structural evolution of Hall Peninsula, Baffin Island, Nunavut; in Summary of Activities 2013, Canada-Nunavut Geoscience Office, p. 73- 84.

Fisher M. C., Vervoort, D. J. and DuFrane, A. S. 2014. Accurate Hf isotope determinations of complex zircons using the ‘‘laser ablation split stream’’ method; Geochemistry Geophysics Geosystems, v. 15, p. 121-139, doi:10.1002/2013GC004962.

Frei, R., Bridgwater, D., Rosing, M. and Stecher, O., 1999. Controversial Pb-Pb and Sm-Nd isotope results in the early Archean Isua (West Greenland) oxide iron formation: Preservation of primary signatures versus secondary disturbances. Geochimica et Cosmochimica Acta, v. 63, p. 473-488.

From, R.E., Rayner, N.M. and Camacho, A. 2015: Archean magmatism and metamorphism of eastern Hall Peninsula, southern Baffin Is- land, Nunavut; in Summary of Activities 2015, Canada-Nunavut Geoscience Office, p. 73–88.

From, R.E., Camacho, A.L. and St-Onge, M.R. 2013. Preliminary observations on the nature and origin of the eastern orthogneiss complex of southern Hall Peninsula, Baffin Island, Nunavut; in Summary of Activities 2012, Canada-Nunavut Geoscience Office, p. 43-54.

Garde, A.A. and Hollis, J.A., 2010. A buried Palaeoproterozoic spreading ridge in the northern Nagssugtoqidian orogen, West Greenland. Geological Society, London, Special Publications, v. 338, p. 213-234.

Goulet, N. and Ciesielski, A., 1990. The Abloviak shear zone and the NW Torngat Orogen, eastern Ungava Bay, Québec. Geoscience Canada, v. 17.

Hamilton, P. J., O'nions, R. K., Bridgwater, D., & Nutman, A. 1983. Sm-Nd studies of Archaean metasediments and metavolcanics from West Greenland and their implications for the Earth's early history. Earth and Planetary Science Letters, v. 62, p. 263-272.

Han, B.F., Guo, Z.J., Zhang, Z.C., Zhang, L., Chen, J.F. and Song, B., 2010. Age, geochemistry, and tectonic implications of a late Paleozoic stitching pluton in the North Tian Shan suture zone, western China. Geological Society of America Bulletin, v. 122, p. 627-640.

Hanchar, J.M. and Miller, C.F. 1993. Zircon zonation patterns as revealed by cathodoluminescence and backscattered electron images: implications for interpretation of complex crustal histories; Chemical Geology, v. 110, p. 1-13

Hartlaub, R.P., Chacko, T., Heaman, L.M., Creaser, R.A., Ashton, K.E. and Simonetti, A., 2005. Ancient (Meso-to Paleoarchean) crust in the Rae Province, Canada: evidence from Sm–Nd and U–Pb constraints. Precambrian Research, v. 141, p. 137-153.

Hinchey, A. M., Davis, W. J., Ryan, J. J., and Nadeau, L. 2011. Neoarchean high-potassium granites of the Boothia mainland area, Rae domain, Churchill Province: U–Pb zircon and Sm–Nd whole rock isotopic constraints This article is one of a series of papers published in this Special Issue on the theme of Geochronology in honour of Tom Krogh. Canadian Journal of Earth Sciences, v. 48, p. 247-279.

Hollis, J.A., Frei, D., Van Gool, J.A.M., Garde A.A. and Persson, M. 2006. Using zircon geochronology to resolve the Archaean geology of southern West Greenland; Geological Survey of Denmark and Greenland, Bulletin 10, p. 49–52.

Holmden, C. and Dickin, A.P., 1995. Paleoproterozoic crustal history of the southwestern Grenville Province: evidence from Nd isotopic mapping. Canadian Journal of Earth Sciences, v. 32, p. 472-485.

Hughes, K.S., Hibbard, J.P., Miller, B.V., Pollock, J.C., Terblanche, A.A., Nance, D.M. and Lewis, D.J. 2014. Does the Chopawamsic fault represent the main Iapetan suture in the southern Appalachians? Geology, geochemistry, and geochronology of the western Piedmont of northern Virginia. Field Guides, v. 35, p. 41-61.

Ickert, R.B. 2013. Algorithms for estimating uncertainties in initial radiogenic isotope ratios and model ages. Chemical Geology v. 340, p. 131-138.

Kemp, S. I. J, Wormald, J. R., Whitehouse, M. J. and Price, C.R. 2005. Hf isotopes in zircon reveal contrasting sources and crystallization histories for alkaline to peralkaline granites of Temora, southeastern Australia; Geology, v. 33, p. 797-800.

Kirkland, C. L., Spaggiari, C. V., Pawley, M. J., Wingate, M. T. D., Smithies, R. H., Howard, H. M. & Poujol, M. 2011. On the edge: U–Pb, Lu–Hf, and Sm–Nd data suggests reworking of the Yilgarn craton margin during formation of the Albany-Fraser Orogen. Precambrian Research, v. 187, p. 223-247.

Kolb, J. 2014. Structure of the Palaeoproterozoic Nagssugtoqidian Orogen, South-East Greenland: model for the tectonic evolution. Precambrian Research, v. 255, p. 809-822.

LaFlamme, C., McFarlane, C.R., Corrigan, D. and Wodicka, N., 2014. Origin and tectonometamorphic history of the Repulse Bay block, Melville Peninsula, Nunavut: exotic

terrane or deeper level of the Rae craton?. Canadian Journal of Earth Sciences, v. 51, p.1097-1122.

Lee, J.K., Williams, I.S. and Ellis, D.J. 1997. Pb, U and Th diffusion in natural zircon; Nature, v. 390, p. 159-162. doi:10.1038/36554

Ludwig, K.R. 2003. User's manual for Isoplot 3.00: a geochronological toolkit for Microsoft® Excel®; Berkeley Geochronology Center, Special Publication 4, 70 p.

Machado, G., Bilodeau, C., Takpanie, R., St-Onge, M.R., Rayner, N.M., Skipton, D.R., From, R.E., MacKay, C.B., Creason, C.G. and Braden, Z.M. 2013. Hall Peninsula regional bedrock mapping, Baffin Island, Nunavut: summary of field-work; in Summary of Activities 2012, Canada-Nunavut Geoscience Office, p. 13-22.

MacKay, C.B. and Ansdell, K.M. 2014. Geochemical study of mafic and ultramafic rocks from southern Hall Peninsula, Baffin Island, Nunavut, in Summary of Activities 2013, Canada-Nunavut Geoscience Office, p. 85-92.

McLennan, S.M., Hemming, S., McDaniel, D.K. and Hanson, G.N., 1993. Geochemical approaches to sedimentation, provenance, and tectonics. Geological Society of America Special Papers, v. 284, p. 21-40.

Mikhalsky, E. V., Henjes-Kunst, F., Belyatsky, B. V., Roland, N. W., and Sergeev, S. A. 2010. New Sm–Nd, Rb–Sr, U–Pb and Hf isotope systematics for the southern Prince Charles Mountains (East Antarctica) and its tectonic implications. Precambrian Research, v. 182, p. 101-123.

Möller A., O'Brien P.J., Kennedy A. and Kröner A. 2002. Polyphase zircon in ultrahigh-temperature granulites (Rogaland, SW Norway): constraints for Pb diffusion in zircon; Journal of Metamorphic Geology, v. 20, p. 727-740.

Peterson, T. D., Pehrsson, S., Skulski, T., & Sandeman, H. 2010. Compilation of Sm-Nd isotope analyses of igneous suites, western Churchill Province. Geological Survey of Canada Open File, 6439, 18p.

Pidgeon, R.T. 1992: Recrystallization of oscillatory zoned zircon: some geochronological and petrological implications; Contributions to Mineralogy and Petrology, v. 110, p. 463–472.

Rayner, N.M. 2015. New (2013–2014) U-Pb geochronological results from northern Hall Peninsula, southern Baffin Island, Nunavut; in Summary of Activities 2014, Canada-Nunavut Geoscience Office, p. 31–44.

Rayner, N.M. 2014. New U-Pb geochronological results from Hall Peninsula, Baffin Island, Nunavut; in Summary of Activities 2013, Canada-Nunavut Geoscience Office, p. 39-52.

Sá, J. M., de Sousa, L. C., Legrand, J. M., Galindo, A. C., Maia, H. N., and Fillippi, R. R. (2014). U-pb and Sm-Nd data of the Rhyacian and Statherian orthogneisses from Rio Piranhas-Seridó and Jaguaribeano terranes, Borborema Province, northeast of Brazil. Geologia USP. Série Científica, v. 14, p. 97-110.

Schoene, B., Crowley, J.L., Condon, D.J., Schmitz, M.D., Bowring, S.A. 2006. Reassessing the uranium decay constants for geochronology using ID-TIMS U–Pb data. Geochimica et Cosmochimica Acta v. 70, p. 426-445.

Scott, D.J. 1999. U-Pb geochronology of the eastern Hall Peninsula, southern Baffin Island, Canada: a northern link between the Archean of West Greenland and the Paleoproterozoic Torngat Orogen of northern Labrador; Precambrian Research, v. 93, p. 5-26.

Scott, D.J. and Campbell, L.M. 1993. Evolution of the Paleoproterozoic Torngat orogen, Labrador, Canada: recent advances using U-Pb geochronology and Nd isotopic systematics (abstract); Geological Society of America, Annual Meeting 1993, Boston, Massachusetts, Program with Abstracts, v. 25, p. A23.

Skipton, D.R., Schneider, D.A., McFarlane, C.R.M., St-Onge, M.R. and Jackson, S.E., 2016. Multi-stage zircon and monazite growth revealed by depth profiling and in situ U–Pb geochronology: Resolving the Paleoproterozoic tectonics of the Trans-Hudson Orogen on southeastern Baffin Island, Canada. Precambrian Research, v. 285, p. 272-298.

Skipton, D.R. and St-Onge, M.R. 2014. Paleoproterozoic deformation and metamorphism in metasedimentary rocks west of Okalik Bay: a field template for the evolution of eastern Hall Peninsula, Baffin Island, Nunavut; in Summary of Activities 2013, Canada-Nunavut Geoscience Office, p. 63-72.

St-Onge, M.R., Van Gool, J.A.M., Garde, A.A. and Scott, D.J. 2009. Correlation of Archaean and Palaeoproterozoic units between northeastern Canada and western Greenland: constraining the pre-collisional upper plate accretionary history of the Trans-Hudson orogen; Geological Society of London, Special Publications, v. 318, p. 193-235. doi:10.1144/SP318.7

St-Onge, M.R., Wodicka, N. and Ijewliw, O. 2007. Polymetamorphic evolution of the Trans-Hudson Orogen, Baffin Island, Canada: integration of petrological, structural and geochronological data; Journal of Petrology, v. 48, p. 271-302.

St-Onge, M.R., Scott, D.J. and Wodicka, N. 2002. Review of crustal architecture and evolution in the Ungava Peninsula–Baffin Island area: connection to the Lithoprobe ECSOOT transect; Canadian Journal of Earth Sciences, v. 39, p. 589-610.

Steenkamp, H.M. and St-Onge, M.R. 2014. Overview of the 2013 regional bedrock mapping program on northern Hall Peninsula, Baffin Island, Nunavut; in Summary of Activities 2013, Canada-Nunavut Geoscience Office, p. 27-38.

Stern, R.A. 1997. The GSC sensitive high resolution ion microprobe (SHRIMP): analytical techniques of zircon U-Th-Pb age determinations and performance evaluation; in Radiogenic

Age and Isotopic Studies: Report 10, Geological Survey of Canada, Current Research 1997-F, p. 1-31.

Stern, R.A. and Amelin, Y. 2003. Assessment of errors in SIMS zircon U-Pb geochronology using a natural zircon standard and NIST SRM 610 glass; Chemical Geology, v. 197, p. 111-146.

Szilas, K., Hoffmann, J., Hansmeier, C., Hollis, J. A., Münker, C., Viehmann, S., & Kasper, H. U. (2015). Sm-Nd and Lu-Hf isotope and trace-element systematics of Mesoarchaean amphibolites, inner Ameralik fjord, southern West Greenland. Mineralogical Magazine, v. 79, p. 857-876.

Vervoort, J.D., Blichert-Toft, J., 1999. Evolution of the depleted mantle: Hf isotope evidence from juvenile rocks through time. Geochimica et Cosmochimica Acta v. 63, p. 533-556.

Wardle, R.J., James D.T., Scott, D.J. and Hall, J. 2002. The southeastern Churchill Province: synthesis of a Palaeoproterozoic transpressional orogen; Canadian Journal of Earth Sciences, v. 39, p. 639-663. doi:10.1139/E02-004

Whalen, J.B., Wodicka, N., Taylor, B.E. and Jackson, G.D. 2010. Cumberland batholith, Trans-Hudson Orogen, Canada: petrogenesis and implications for Paleoproterozoic crustal and orogenic processes; Lithos, v. 117, p. 99-118.

Williams, I.S. 1992. Some observations on the use of zircon U-Pb geochronology in the study of granitic rocks; Transactions of the Royal Society of Edinburgh: Earth Sciences, v. 83, no. 1-2, p. 447-458. doi:10.1017/S0263593300008129

Wodicka, N., St-Onge, M. R., Corrigan, D., Scott, D. J., & Whalen, J. B. (2014). Did a proto-ocean basin form along the southeastern Rae cratonic margin? Evidence from U-Pb geochronology, geochemistry (Sm-Nd and whole-rock), and stratigraphy of the

Paleoproterozoic Piling Group, northern Canada. Geological Society of America Bulletin, v. 126, p. 1625-1653.

Wooden, L. J., Barth, P.A. and Mueller, A. P. 2013. Crustal growth and tectonic evolution of the Mojave crustal province: Insights from hafnium isotope systematics in zircons, Lithosphere, v. 5, p. 17-28.

Xie, l., Zhang, Y., Zhang, H., Sun, J. and Wu, F. 2008. In situ simultaneous determination of trace elements, U–Pb and Lu–Hf isotopes in zircon and baddeleyite. Chinese Science Bulletin, v. 53, p. 1565-1573.

Yuan, H.L., Gao, S., Dai, M.N., Zong, L., Gunther, G. H., Fontaine, X.M. Liu, and C. Diwu (2008), Simultaneous determinations of U–Pb age, Hf isotopes and trace element compositions of zircon by excimer laser-ablation quadrupole and multiple-collector ICP-MS, Chemical Geology, v. 247, p. 100–118.

5.11. *Data appendices*

APPENDIX 5A - LASS-ICPMS U-Pb isotopic data from south transect samples
APPENDIX 5B - LASS-ICPMS U-Pb isotopic data from north transect samples
APPENDIX 5C - LASS-ICPMS Lu-Hf isotopic data from south transect samples
APPENDIX 5D - LASS-ICPMS Lu-Hf isotopic data from north transect samples
APPENDIX 5E - Whole Rock Sm-Nd isotopic data from south and north transect samples
APPENDIX 5F - Lithogeochemical data from south and north transect samples

Appendix 5A - LASS-ICPMS U-Pb isotopic data from south transect samples

Spot name	Pb 206 (counts)	U (ppm)	Th (ppm)	Pb (ppm)	Th / U	$^{207*}Pb/^{235}U$	% ±	$^{206*}Pb/^{238}U$	% ±	$^{207*}Pb/^{206*}Pb$	% ±
B007A, massive pegmatitic granite											
UTM 662715 6985512											
~~B007A - 26_2~~	~~460000~~	~~330~~	~~44~~	~~57~~	~~0.15~~	~~16.5~~	~~2.1~~	~~0.702~~	~~0.091~~	~~0.1741~~	~~0.003~~
~~B007A - 8~~	~~1355000~~	~~638~~	~~19~~	~~35~~	~~0.03~~	~~10.7~~	~~0.25~~	~~0.4133~~	~~0.0098~~	~~0.1751~~	~~0.0019~~
~~B007A - 13_2~~	~~239000~~	~~63~~	~~29~~	~~47~~	~~0.45~~	~~19.7~~	~~1.1~~	~~0.742~~	~~0.038~~	~~0.1862~~	~~0.0023~~
B007A - 25	171200	103	65	71	0.60	9.63	0.25	0.4539	0.0065	0.1576	0.0024
B007A - 27	27400	17	38	42	2.11	10.28	0.35	0.474	0.013	0.1632	0.0044
B007A - 16	448000	207	230	247	1.04	10.181	0.087	0.4434	0.0047	0.16407	0.00093
B007A - 17	79340	34	79	92	2.28	11.44	0.42	0.4784	0.0082	0.17	0.0032
B007A - 10	247000	102	45	59	0.44	12.51	0.23	0.5091	0.0086	0.1782	0.0016
B007A - 6	478000	203	125	156	0.58	12.59	0.23	0.5055	0.0053	0.1798	0.0011
B007A - 2	139900	61	28	34	0.46	12.24	0.11	0.4929	0.0068	0.1804	0.002
B007A - 3	422900	172	147	192	0.85	13.08	0.13	0.5208	0.0059	0.1826	0.0013
B007A - 24	***166400***	***87***	***48***	***63***	***0.54***	***13.32***	***0.24***	***0.5402***	***0.0086***	***0.1862***	***0.0023***
B007A - 1	***473000***	***187***	***89***	***118***	***0.48***	***13.91***	***0.12***	***0.5375***	***0.0037***	***0.1861***	***0.001***
B007A - 9	***66000***	***26***	***57***	***73***	***2.18***	***14.34***	***0.21***	***0.5517***	***0.0056***	***0.187***	***0.0021***
B007A - 12	***287000***	***111***	***42***	***55***	***0.38***	***14.23***	***0.16***	***0.5532***	***0.0068***	***0.1869***	***0.0014***
B007A - 15	***366000***	***151***	***74***	***90***	***0.49***	***13.78***	***0.25***	***0.536***	***0.01***	***0.187***	***0.0017***
B007A - 7	***381000***	***160***	***94***	***125***	***0.61***	***14.19***	***0.52***	***0.553***	***0.012***	***0.1875***	***0.0031***
B007A - 19	***285000***	***121***	***62***	***78***	***0.53***	***14.24***	***0.13***	***0.5395***	***0.0046***	***0.189***	***0.0014***
B007A - 23	***411000***	***217***	***59***	***74***	***0.26***	***13.46***	***0.14***	***0.5316***	***0.0048***	***0.1891***	***0.0012***
B007A - 14	***381000***	***149***	***85***	***104***	***0.57***	***13.93***	***0.13***	***0.5261***	***0.0068***	***0.1892***	***0.0012***
B007A - 21	***263000***	***117***	***65***	***81***	***0.55***	***14.17***	***0.12***	***0.5307***	***0.0036***	***0.19***	***0.0013***
B007A - 5	***68000***	***26***	***65***	***87***	***2.54***	***14.7***	***0.41***	***0.563***	***0.012***	***0.1907***	***0.0032***
B007A - 22	***575000***	***264***	***73***	***90***	***0.14***	***13.93***	***0.17***	***0.5183***	***0.0063***	***0.1913***	***0.0015***
~~***B007A - 26_1***~~	~~***421000***~~	~~***225***~~	~~***26***~~	~~***31***~~	~~***0.11***~~	~~***12.37***~~	~~***0.25***~~	~~***0.461***~~	~~***0.012***~~	~~***0.1875***~~	~~***0.0027***~~
B007A-4_1	208000	90	42	56	0.45	13.89	0.34	0.515	0.014	0.1976	0.0038
B007A - 11	93600	34	13	19	0.38	16	0.16	0.5809	0.0053	0.1993	0.0017
B007A - 4_2_RIM	150000	56	42	55	0.76	14.86	0.43	0.526	0.011	0.2008	0.0027
B007A - 20	166000	69	48	62	0.60	16.64	0.28	0.5767	0.0085	0.2083	0.0024
B007A - 18	234300	87	69	91	0.79	16.35	0.24	0.5677	0.0086	0.21	0.002
~~B007A - 13_1~~	~~4890000~~	~~2326~~	~~630~~	~~705~~	~~0.27~~	~~13.35~~	~~0.12~~	~~0.4889~~	~~0.0058~~	~~0.1994~~	~~0.002~~

			age (Ma)									
$^{206*}Pb$ / $^{208*}Pb$	% ±	Disc. %	$^{206*}Pb$ / ^{238}U	±	$^{207*}Pb$ / $^{206*}Pb$	±	^{176}Lu / ^{177}Hf	^{176}Hf / ^{177}Hf	εHf(t)[1]	±2s	T_{DM}[2] (Ga)	location
B007A, massive pegmatitic granite												
UTM 662715 6985512												
~~0.1433~~	~~0.0045~~	~~-29.82~~	~~3370~~	~~350~~	~~2596~~	~~29~~	~~0.000290~~	~~0.281006~~	~~-4.45~~	~~3.63~~	~~3060~~	~~***core***~~
~~0.1708~~	~~0.0078~~	~~14.50~~	~~2229~~	~~45~~	~~2607~~	~~18~~	~~0.000809~~	~~0.281033~~	~~-4.15~~	~~3.31~~	~~3065~~	~~core~~
~~0.1738~~	~~0.0065~~	~~-31.83~~	~~3570~~	~~140~~	~~2708~~	~~20~~	~~0.000166~~	~~0.281025~~	~~-0.94~~	~~1.76~~	~~3025~~	~~core~~
0.123	0.0026	0.62	2411	29	2426	26	0.000252	0.280964	-9.82	1.67	3114	core
0.1274	0.0055	-0.65	2496	56	2480	45	0.000190	0.281007	-6.93	1.23	3051	rim
0.1167	0.0017	5.30	2365	21	2497	10	0.000686	0.281092	-4.35	1.38	2975	core
0.1246	0.0022	1.25	2519	35	2551	32	0.000352	0.280998	-5.88	1.61	3076	rim
0.1378	0.0022	-0.61	2651	37	2635	15	0.000182	0.281048	-1.86	1.56	2996	core
0.1369	0.0024	0.49	2637	23	2650	10	0.000387	0.281092	-0.31	2.08	2952	core
0.1297	0.0029	2.75	2582	29	2655	18	0.000145	0.281027	-2.07	1.88	3021	core
0.1406	0.0016	-1.01	2702	25	2675	12	0.000635	0.281062	-1.25	1.75	3012	core
0.1474	***0.0037***	***-2.77***	***2783***	***36***	***2708***	***20***	***0.000206***	***0.281030***	***-0.84***	***2.09***	***3022***	***rim***
0.1436	***0.0023***	***-2.35***	***2773***	***16***	***2709***	***10***	***0.000370***	***0.281026***	***-1.25***	***1.53***	***3040***	***outer***
0.1392	***0.002***	***-4.31***	***2831***	***23***	***2714***	***19***	***0.000326***	***0.281074***	***0.65***	***1.41***	***2972***	***rim***
0.1409	***0.0025***	***-4.53***	***2837***	***28***	***2714***	***13***	***0.000170***	***0.281020***	***-0.99***	***1.12***	***3032***	***rim***
0.1333	***0.0032***	***-1.95***	***2768***	***44***	***2715***	***15***	***0.000189***	***0.281006***	***-1.50***	***2.56***	***3052***	***core***
0.1471	***0.0044***	***-4.30***	***2835***	***51***	***2718***	***27***	***0.000456***	***0.281003***	***-2.03***	***2.29***	***3077***	***core***
0.1358	***0.0021***	***-1.79***	***2781***	***19***	***2732***	***12***	***0.000266***	***0.281039***	***-0.07***	***1.70***	***3014***	***core***
0.1408	***0.0038***	***-0.55***	***2748***	***20***	***2733***	***11***	***0.000299***	***0.281032***	***-0.36***	***2.19***	***3026***	***core***
0.1319	***0.0021***	***0.40***	***2724***	***29***	***2735***	***11***	***0.000186***	***0.280993***	***-1.49***	***1.45***	***3069***	***rim***
0.1355	***0.0019***	***-0.11***	***2744***	***15***	***2741***	***12***	***0.000235***	***0.280980***	***-1.90***	***1.76***	***3091***	***rim***
0.1428	***0.002***	***-4.89***	***2877***	***48***	***2743***	***28***	***0.000318***	***0.281050***	***0.48***	***1.42***	***3003***	***rim***
0.137	***0.004***	***2.22***	***2691***	***27***	***2752***	***13***	***0.000459***	***0.280965***	***-2.60***	***1.96***	***3129***	***rim***
~~***0.1215***~~	~~***0.007***~~	~~***10.08***~~	~~***2445***~~	~~***51***~~	~~***2719***~~	~~***24***~~	~~***0.000640***~~	~~***0.280976***~~	~~***-3.31***~~	~~***4.34***~~	~~***3129***~~	~~***core***~~
0.1423	0.0036	4.53	2677	62	2804	31	0.001060	0.281139	3.65	3.03	2940	core
0.1526	0.0033	-4.72	2952	21	2819	14	0.000483	0.281013	0.62	2.06	3066	core
0.136	0.0035	3.75	2724	48	2830	22	0.001133	0.281032	0.29	3.08	3093	core
0.148	0.0047	-1.49	2934	35	2891	19	0.000820	0.280943	-0.87	1.91	3188	core
0.141	0.0023	0.28	2897	36	2905	16	0.001543	0.281118	4.25	2.06	3007	core
~~0.1213~~	~~0.0042~~	~~9.07~~	~~2565~~	~~25~~	~~2821~~	~~16~~	~~0.002454~~	~~0.281137~~	~~1.28~~	~~3.39~~	~~3055~~	~~core~~

zonation	notes
B007A, massive pegmatitic granite	
UTM 662715 6985512	
~~***osc***~~	~~discordant~~
~~osc~~	~~discordant~~
~~faint osc~~	~~discordant~~
faint osc	
homo	
osc	
homo	
osc	
osc	
homo	
homo	
homo	
osc	
homo	
osc	
osc	
osc	
faint osc	
irregular	
homo	
osc	
homo	
osc	
~~***osc***~~	~~***discordant***~~
faint osc	
faint osc	
homo	
osc	
osc	
~~faint osc~~	~~discordant~~

Appendix 5A - LASS-ICPMS U-Pb isotopic data from south transect samples

Spot name	Pb 206 (counts)	U (ppm)	Th (ppm)	Pb (ppm)	Th / U	$^{207*}Pb/^{235}U$	% ±	$^{206*}Pb/^{238}U$	% ±	$^{207*}Pb/^{206*}Pb$	% ±
T027A, mt bt syenogranite											
UTM 689036 7009198											
~~*T027A - 1*~~	~~*383000*~~	~~*271*~~	~~*148*~~	~~*154*~~	~~*0.53*~~	~~*7.88*~~	~~*0.14*~~	~~*0.374*~~	~~*0.0063*~~	~~*0.1512*~~	~~*0.0018*~~
~~*T027A - 16*~~	~~*631000*~~	~~*382*~~	~~*99*~~	~~*114*~~	~~*0.25*~~	~~*10.01*~~	~~*0.13*~~	~~*0.4205*~~	~~*0.0058*~~	~~*0.1712*~~	~~*0.0013*~~
~~*T027A - 5*~~	~~*671000*~~	~~*429*~~	~~*187*~~	~~*210*~~	~~*0.44*~~	~~*9.07*~~	~~*0.28*~~	~~*0.386*~~	~~*0.012*~~	~~*0.1713*~~	~~*0.0031*~~
~~*T027A - 3*~~	~~*1101000*~~	~~*558*~~	~~*394*~~	~~*521*~~	~~*0.69*~~	~~*11.96*~~	~~*0.16*~~	~~*0.4945*~~	~~*0.0069*~~	~~*0.1753*~~	~~*0.0013*~~
~~*T027A - 2*~~	~~*104900*~~	~~*57*~~	~~*84*~~	~~*110*~~	~~*1.23*~~	~~*11.91*~~	~~*0.38*~~	~~*0.479*~~	~~*0.014*~~	~~*0.1806*~~	~~*0.0025*~~
T027A - 19	***1875000***	***941***	***355***	***456***	***0.31***	***12.11***	***0.31***	***0.519***	***0.011***	***0.168***	***0.0016***
T027A - 14	***1772000***	***958***	***670***	***760***	***0.49***	***11.46***	***0.23***	***0.4884***	***0.0093***	***0.1683***	***0.0011***
T027A - 12	***1640000***	***1086***	***1080***	***980***	***0.79***	***10.47***	***0.29***	***0.451***	***0.013***	***0.1685***	***0.0017***
T027A - 15.2	***976000***	***475***	***184***	***244***	***0.38***	***12***	***0.39***	***0.498***	***0.014***	***0.1737***	***0.0017***
T027A - 8	***1354000***	***798***	***86***	***115***	***0.11***	***11.3***	***0.11***	***0.462***	***0.0058***	***0.1747***	***0.0014***
T027A - 21	***620000***	***331***	***110***	***138***	***0.34***	***11.58***	***0.1***	***0.4773***	***0.0037***	***0.1757***	***0.001***
T027A - 15.1	***723000***	***373***	***726***	***794***	***1.90***	***12.44***	***0.17***	***0.5074***	***0.0064***	***0.1759***	***0.0014***
T027A - 11	***1043000***	***639***	***208***	***260***	***0.33***	***12.18***	***0.16***	***0.4966***	***0.0067***	***0.1774***	***0.0012***
~~T027A - 18~~	~~158100~~	~~72~~	~~81~~	~~105~~	~~1.08~~	~~14.38~~	~~0.32~~	~~0.57~~	~~0.013~~	~~0.1815~~	~~0.0021~~
~~T027A - 17~~	~~407000~~	~~253~~	~~413~~	~~448~~	~~1.49~~	~~10.06~~	~~0.75~~	~~0.401~~	~~0.032~~	~~0.1827~~	~~0.004~~
T027A - 6	577000	272	99	141	0.34	14.01	0.35	0.551	0.012	0.1833	0.0012
T027A - 20	542700	258	205	264	0.76	12.89	0.2	0.5091	0.0085	0.1832	0.001
T027A - 4	218000	108	140	193	1.29	12.39	0.5	0.478	0.018	0.1897	0.0029
T027A - 10	115000	65	102	123	1.54	13.18	0.32	0.502	0.01	0.1919	0.0033
~~T027A - 13~~	~~291000~~	~~117~~	~~85~~	~~120~~	~~0.65~~	~~17.23~~	~~0.52~~	~~0.668~~	~~0.021~~	~~0.1852~~	~~0.0025~~
~~T027A - 9~~	~~275000~~	~~136~~	~~80~~	~~100~~	~~0.60~~	~~16.3~~	~~1~~	~~0.638~~	~~0.045~~	~~0.1857~~	~~0.0034~~
~~T027A - 7~~	~~110500~~	~~50~~	~~79~~	~~107~~	~~1.58~~	~~15.49~~	~~0.25~~	~~0.5886~~	~~0.0086~~	~~0.1891~~	~~0.0027~~
S154A, bt mt monzogranite											
UTM 688784 7017312											
~~S154A - 4~~	~~667000~~	~~411~~	~~57~~	~~64~~	~~0.10~~	~~9.93~~	~~0.36~~	~~0.427~~	~~0.013~~	~~0.1667~~	~~0.0012~~
~~S154A - 1~~	~~670000~~	~~358~~	~~74~~	~~104~~	~~0.13~~	~~12.14~~	~~0.46~~	~~0.472~~	~~0.017~~	~~0.1896~~	~~0.0045~~
S154A - 2	1140000	1130	9	23	0.01	4.29	0.13	0.289	0.01	0.1081	0.0013
S154A - 10	1053000	555	42	55	0.06	11.49	0.11	0.484	0.0035	0.17131	0.00091

$^{206*}Pb/^{208*}Pb$	% ±	Disc. %	age (Ma) $^{206*}Pb/^{238}U$	±	age (Ma) $^{207*}Pb/^{206*}Pb$	±	$^{176}Lu/^{177}Hf$	$^{176}Hf/^{177}Hf$	εHf(t)[1]	±2s	T_{DM}[2] (Ga)	location
T027A, mt bt syenogranite												
UTM 689036 7009198												
~~0.112~~	~~0.0039~~	~~13.18~~	~~2048~~	~~29~~	~~2359~~	~~20~~	~~0.000354~~	~~0.281074~~	~~-7.62~~	~~3.16~~	~~2974~~	~~core~~
~~0.1284~~	~~0.0026~~	~~12.02~~	~~2262~~	~~26~~	~~2571~~	~~12~~	~~0.000489~~	~~0.281058~~	~~-3.53~~	~~1.87~~	~~3006~~	~~outer~~
~~0.1194~~	~~0.0041~~	~~18.48~~	~~2104~~	~~55~~	~~2581~~	~~20~~	0.000533	0.281076	-2.74	2.21	2985	~~rim~~
~~0.139~~	~~0.0026~~	~~0.77~~	~~2589~~	~~30~~	~~2609~~	~~13~~	~~0.000774~~	~~0.281168~~	~~0.75~~	~~2.38~~	~~2879~~	~~interior~~
~~0.145~~	~~0.004~~	~~5.41~~	~~2516~~	~~61~~	~~2660~~	~~22~~	~~0.000550~~	~~0.281145~~	~~1.51~~	~~2.50~~	~~2893~~	~~outer~~
0.1457	0.003	-6.07	2693	48	2539	16	0.000906	0.281072	-4.49	2.18	3020	interior
0.149	0.012	-0.91	2563	40	2540	11	0.000880	0.281160	-1.29	2.55	2897	outer
0.0975	0.0015	5.67	2397	55	2541	16	0.001120	0.281162	-1.61	1.55	2913	rim
0.1416	0.0035	-0.46	2605	59	2593	16	0.000768	0.281079	-2.77	2.55	2999	core
0.1476	0.0022	5.95	2448	25	2603	13	0.000357	0.281068	-2.20	1.81	2982	single gr
0.1359	0.0016	3.71	2515	16	2612	10	0.000394	0.281023	-3.66	2.05	3046	outer
0.121	0.0011	-1.19	2645	27	2614	13	0.001038	0.281094	-2.23	2.18	3000	core
0.135	0.0022	1.14	2598	29	2628	12	0.000426	0.281086	-1.11	1.98	2963	core
~~0.1459~~	~~0.0027~~	~~-9.00~~	~~2906~~	~~55~~	~~2666~~	~~19~~	~~0.000333~~	~~0.280979~~	~~-3.86~~	~~1.69~~	~~3100~~	~~core~~
~~0.1204~~	~~0.0073~~	~~18.88~~	~~2170~~	~~150~~	~~2675~~	~~36~~	~~0.000840~~	~~0.281195~~	~~3.11~~	~~5.39~~	~~2847~~	~~core~~
0.1528	0.0049	-5.33	2825	51	2682	11	0.000368	0.281019	-2.14	1.85	3049	core
0.1379	0.0019	1.23	2651	36	2684	10	0.000753	0.281116	0.66	2.90	2948	core
0.1427	0.0052	8.14	2515	79	2738	25	0.000700	0.281072	0.43	1.53	3004	core
0.129	0.004	4.83	2623	44	2756	29	0.000383	0.281101	2.47	5.39	2940	core
~~0.1655~~	~~0.0066~~	~~-22.09~~	~~3294~~	~~82~~	~~2698~~	~~22~~	~~0.000416~~	~~0.281079~~	~~0.29~~	~~2.70~~	~~2972~~	~~core~~
~~0.1415~~	~~0.0033~~	~~-17.28~~	~~3170~~	~~180~~	~~2703~~	~~31~~	~~0.000391~~	~~0.281067~~	~~0.02~~	~~2.70~~	~~2986~~	~~core~~
~~0.1471~~	~~0.0021~~	~~-9.19~~	~~2983~~	~~35~~	~~2732~~	~~24~~	~~0.000496~~	~~0.281100~~	~~1.67~~	~~1.69~~	~~2950~~	~~core~~
S154A, bt mt monzogranite												
UTM 688784 7017312												
~~0.1256~~	~~0.0024~~	~~9.35~~	~~2288~~	~~58~~	~~2524~~	~~12~~	~~0.000342~~	~~0.281036~~	~~-5.15~~	~~1.84~~	~~3024~~	~~rim~~
~~0.1529~~	~~0.0073~~	~~8.92~~	~~2490~~	~~77~~	~~2734~~	~~40~~	~~0.000684~~	~~0.281182~~	~~4.28~~	~~2.06~~	~~2853~~	~~core~~
0.291	0.042	7.53	1633	49	1766	21	0.000386	0.281253	-14.88	2.13	2735	rim
0.1384	0.0023	1.01	2544	15	2570	9	0.000436	0.281054	-3.61	1.21	3007	rim

zonation	notes

T027A, mt bt syenogranite
UTM 689036 7009198

faint osc	***discordant***
faint osc	***discordant***
faint osc	***discordant***
irregular	***incidental overlap of domains***
faint osc	***incidental overlap of domains***
faint osc	
osc	
faint osc	
faint osc	
sector	
irregular	
faint osc	
homo	
homo	discordant
faint osc	discordant
homo	
faint osc	
homo	
sector	
homo	discordant
faint osc	discordant
sector	discordant

S154A, bt mt monzogranite
UTM 688784 7017312

homo	discordant
osc	incidental overlap of domains
homo	
homo	

Appendix 5A - LASS-ICPMS U-Pb isotopic data from south transect samples

Spot name	Pb 206 (counts)	U (ppm)	Th (ppm)	Pb (ppm)	Th / U	$^{207*}Pb/^{235}U$	% ±	$^{206*}Pb/^{238}U$	% ±	$^{207*}Pb/^{206*}Pb$	% ±
~~S154A - 3~~	~~401000~~	~~244~~	~~131~~	~~146~~	~~0.49~~	~~11.41~~	~~0.2~~	~~0.4565~~	~~0.0087~~	~~0.18~~	~~0.0022~~
S154A - 16	1235000	711	3	8	0.00	12.19	0.18	0.4692	0.0068	0.1878	0.0014
S154A - 6	***240000***	***123***	***65***	***85***	***0.46***	***14.98***	***0.24***	***0.542***	***0.0099***	***0.1981***	***0.0021***
S154A - 12	***523000***	***270***	***222***	***279***	***0.78***	***13.96***	***0.26***	***0.512***	***0.0092***	***0.1986***	***0.0019***
S154A - 14	***222000***	***104***	***59***	***83***	***0.52***	***15.17***	***0.22***	***0.5547***	***0.008***	***0.1989***	***0.0016***
S154A - 11	***255100***	***117***	***40***	***59***	***0.33***	***15.84***	***0.18***	***0.5671***	***0.0066***	***0.2028***	***0.0018***
S154A - 9	***315000***	***155***	***98***	***131***	***0.60***	***15.26***	***0.3***	***0.54***	***0.011***	***0.2035***	***0.0014***
S154A - 7	***506000***	***242***	***155***	***218***	***0.59***	***15.71***	***0.24***	***0.5545***	***0.0089***	***0.2037***	***0.001***
S154A - 17	***239000***	***109***	***64***	***93***	***0.55***	***15.96***	***0.28***	***0.561***	***0.01***	***0.2067***	***0.0014***
S154A - 18	***281000***	***130***	***63***	***86***	***0.48***	***15.67***	***0.14***	***0.5458***	***0.0046***	***0.2085***	***0.0015***
S154A - 19	***337000***	***159***	***117***	***152***	***0.67***	***15.42***	***0.27***	***0.5341***	***0.0084***	***0.2091***	***0.0016***
S154A - 15	***286100***	***128***	***64***	***92***	***0.50***	***16.38***	***0.19***	***0.5659***	***0.0062***	***0.2105***	***0.0012***
S154A - 8	***271000***	***122***	***67***	***100***	***0.49***	***17.08***	***0.21***	***0.5815***	***0.0065***	***0.2109***	***0.0014***
~~***S154A - 13***~~	~~***775000***~~	~~***401***~~	~~***363***~~	~~***427***~~	~~***0.88***~~	~~***14.64***~~	~~***0.22***~~	~~***0.5296***~~	~~***0.0095***~~	~~***0.1995***~~	~~***0.0024***~~
K015A, mafic tonalite											
UTM 693209 7030513											
K015A - 3	317600	252	36	33	0.14	4.662	0.043	0.3152	0.0026	0.10712	0.00076
K015A - 11	399000	394	30	24	0.08	4.479	0.066	0.2995	0.0033	0.1074	0.0012
~~***K015A - 16***~~	~~***52900***~~	~~***41***~~	~~***5***~~	~~***14***~~	~~***0.11***~~	~~***7.26***~~	~~***0.57***~~	~~***0.357***~~	~~***0.01***~~	~~***0.1472***~~	~~***0.0085***~~
~~***K015A - 9***~~	~~***45000***~~	~~***27***~~	~~***7***~~	~~***14***~~	~~***0.25***~~	~~***9.3***~~	~~***1.6***~~	~~***0.421***~~	~~***0.051***~~	~~***0.158***~~	~~***0.0098***~~
~~***K015A - 4***~~	~~***1180000***~~	~~***720***~~	~~***412***~~	~~***454***~~	~~***0.54***~~	~~***9.96***~~	~~***0.14***~~	~~***0.4416***~~	~~***0.0075***~~	~~***0.1629***~~	~~***0.0014***~~
~~***K015A - 2***~~	~~***2160000***~~	~~***1188***~~	~~***1230***~~	~~***1110***~~	~~***0.90***~~	~~***12.53***~~	~~***0.52***~~	~~***0.543***~~	~~***0.025***~~	~~***0.166***~~	~~***0.0017***~~
~~***K015A - 6***~~	~~***1290000***~~	~~***793***~~	~~***494***~~	~~***551***~~	~~***0.62***~~	~~***10.02***~~	~~***0.13***~~	~~***0.4308***~~	~~***0.0044***~~	~~***0.168***~~	~~***0.0017***~~
~~***K015A - 8***~~	~~***1490000***~~	~~***810***~~	~~***520***~~	~~***570***~~	~~***0.47***~~	~~***12.77***~~	~~***0.51***~~	~~***0.538***~~	~~***0.023***~~	~~***0.1718***~~	~~***0.0023***~~
K015A - 15	***1587000***	***966***	***1109***	***1137***	***1.15***	***11.461***	***0.083***	***0.4732***	***0.0046***	***0.1734***	***0.0014***
K015A - 14	***992000***	***580***	***200***	***223***	***0.26***	***11.29***	***0.14***	***0.4632***	***0.0042***	***0.1753***	***0.0017***
K015A - 7	***866000***	***473***	***174***	***225***	***0.37***	***12.03***	***0.2***	***0.4922***	***0.0073***	***0.1766***	***0.0013***
K015A - 10	***1020000***	***599***	***395***	***462***	***0.65***	***11.7***	***0.13***	***0.4762***	***0.0059***	***0.1765***	***0.0014***
K015A - 12	***893000***	***541***	***44***	***61***	***0.08***	***11.8***	***0.13***	***0.4789***	***0.006***	***0.1769***	***0.0017***
~~***K015A - 17***~~	~~***854000***~~	~~***506***~~	~~***253***~~	~~***304***~~	~~***0.42***~~	~~***10.99***~~	~~***0.27***~~	~~***0.446***~~	~~***0.011***~~	~~***0.1768***~~	~~***0.0012***~~
K015A - 1	***853000***	***445***	***142***	***192***	***0.33***	***12.3***	***0.25***	***0.5004***	***0.0091***	***0.1777***	***0.0016***

			age (Ma)									
$^{206*}Pb$ / $^{208*}Pb$	% ±	Disc. %	$^{206*}Pb$ / ^{238}U	±	$^{207*}Pb$ / $^{206*}Pb$	±	^{176}Lu / ^{177}Hf	^{176}Hf / ^{177}Hf	εHf(t)[1]	±2s	T_{DM}[2] (Ga)	location
~~0.1268~~	~~0.0031~~	~~8.60~~	~~2423~~	~~38~~	~~2651~~	~~20~~	~~0.000377~~	~~0.281012~~	~~-3.12~~	~~1.82~~	~~3059~~	~~core~~
0.278	0.019	8.89	2480	30	2722	12	0.000191	0.280985	-2.09	1.35	3081	rim
0.1547	*0.0053*	*0.71*	*2790*	*41*	*2810*	*17*	*0.000450*	*0.281078*	*2.78*	*2.17*	*2976*	*core*
0.1359	*0.0033*	*5.33*	*2663*	*39*	*2813*	*15*	*0.001450*	*0.281217*	*5.88*	*2.81*	*2862*	*core*
0.1559	*0.0043*	*-0.96*	*2843*	*33*	*2816*	*13*	*0.000594*	*0.281039*	*1.26*	*1.74*	*3040*	*core*
0.1582	*0.0034*	*-1.69*	*2895*	*27*	*2847*	*14*	*0.000449*	*0.281039*	*2.26*	*1.68*	*3029*	*core*
0.1497	*0.004*	*2.63*	*2779*	*48*	*2854*	*11*	*0.000796*	*0.281127*	*4.87*	*3.05*	*2936*	*core*
0.1582	*0.0041*	*0.48*	*2842*	*36*	*2856*	*8*	*0.000812*	*0.281168*	*6.34*	*2.03*	*2881*	*core*
0.1581	*0.0037*	*0.38*	*2868*	*41*	*2879*	*11*	*0.000611*	*0.281069*	*3.75*	*1.59*	*3001*	*core*
0.1463	*0.0019*	*2.97*	*2807*	*19*	*2893*	*12*	*0.000626*	*0.281030*	*2.65*	*1.71*	*3055*	*outer*
0.1409	*0.0035*	*4.87*	*2757*	*35*	*2898*	*12*	*0.000900*	*0.281099*	*4.68*	*2.73*	*2982*	*core*
0.1525	*0.0029*	*0.64*	*2890*	*25*	*2909*	*9*	*0.000663*	*0.281098*	*5.37*	*1.87*	*2965*	*core*
0.1614	*0.0032*	*-1.44*	*2954*	*27*	*2912*	*11*	*0.000659*	*0.281090*	*5.16*	*1.75*	*2976*	*core*
~~*0.129*~~	~~*0.003*~~	~~*2.94*~~	~~*2739*~~	~~*40*~~	~~*2822*~~	~~*20*~~	~~*0.001230*~~	~~*0.281261*~~	~~*8.07*~~	~~*3.65*~~	~~*2785*~~	~~*core*~~
K015A, mafic tonalite												
UTM 693209 7030513												
0.0967	0.0019	-0.91	1766	13	1750	13	0.000287	0.281172	-18.00	2.02	2837	rim
0.0945	0.004	3.82	1688	17	1755	20	0.000274	0.281179	-17.62	2.40	2827	rim
~~*0.311*~~	~~*0.04*~~	~~*14.38*~~	~~*1965*~~	~~*48*~~	~~*2295*~~	~~*84*~~	~~*0.000086*~~	~~*0.281182*~~	~~*-4.84*~~	~~*2.71*~~	~~*2809*~~	~~*rim*~~
~~*0.208*~~	~~*0.064*~~	~~*7.00*~~	~~*2260*~~	~~*230*~~	~~*2430*~~	~~*100*~~	~~*0.000250*~~	~~*0.280981*~~	~~*-9.12*~~	~~*7.14*~~	~~*3091*~~	~~*rim*~~
~~*0.1211*~~	~~*0.0022*~~	~~*5.19*~~	~~*2357*~~	~~*33*~~	~~*2486*~~	~~*15*~~	~~*0.000710*~~	~~*0.281044*~~	~~*-6.36*~~	~~*2.87*~~	~~*3042*~~	~~*single gr*~~
~~*0.1074*~~	~~*0.0049*~~	~~*-10.85*~~	~~*2790*~~	~~*110*~~	~~*2517*~~	~~*17*~~	~~*0.000640*~~	~~*0.281081*~~	~~*-4.22*~~	~~*5.39*~~	~~*2987*~~	~~*single gr*~~
~~*0.1222*~~	~~*0.0012*~~	~~*8.95*~~	~~*2309*~~	~~*20*~~	~~*2536*~~	~~*17*~~	~~*0.001120*~~	~~*0.281202*~~	~~*-0.31*~~	~~*2.80*~~	~~*2858*~~	~~*core*~~
~~*0.1484*~~	~~*0.0075*~~	~~*-7.66*~~	~~*2770*~~	~~*100*~~	~~*2573*~~	~~*23*~~	~~*0.000690*~~	~~*0.281059*~~	~~*-3.80*~~	~~*3.29*~~	~~*3020*~~	~~*core*~~
0.1175	*0.0022*	*3.59*	*2497*	*20*	*2590*	*14*	*0.001729*	*0.281237*	*1.09*	*1.80*	*2856*	*core*
0.1355	*0.0059*	*5.94*	*2453*	*19*	*2608*	*16*	*0.000389*	*0.280961*	*-5.95*	*1.49*	*3129*	*core*
0.1421	*0.0027*	*1.56*	*2579*	*31*	*2620*	*12*	*0.000381*	*0.280982*	*-4.91*	*1.78*	*3100*	*core*
0.1337	*0.0041*	*4.20*	*2510*	*26*	*2620*	*13*	*0.000960*	*0.281195*	*1.63*	*2.87*	*2856*	*core*
0.1607	*0.0043*	*3.85*	*2522*	*26*	*2623*	*16*	*0.000280*	*0.280973*	*-4.98*	*2.49*	*3104*	*core*
~~*0.1402*~~	~~*0.0064*~~	~~*9.38*~~	~~*2377*~~	~~*48*~~	~~*2623*~~	~~*11*~~	~~*0.000612*~~	~~*0.281053*~~	~~*-2.73*~~	~~*2.35*~~	~~*3022*~~	~~*core*~~
0.1448	*0.0049*	*0.61*	*2615*	*39*	*2631*	*15*	*0.000311*	*0.281034*	*-2.68*	*1.91*	*3024*	*core*

zonation	notes
~~osc~~	~~incidental overlap of domains~~
homo	
osc	
osc	
osc	
osc	
osc	
osc	
osc	
osc	
osc	
osc	
osc	
~~osc~~	***~~unique Hf~~***

K015A, mafic tonalite
UTM 693209 7030513

homo	
homo	
~~homo~~	***~~discordant~~***
~~homo~~	***~~discordant~~***
~~irregular~~	~~incidental overlap of domains~~
~~irregular~~	***~~discordant~~***
~~faint osc~~	
~~irregular~~	***~~discordant~~***
faint osc	
irregular	
faint osc	
osc	
irregular	
~~osc~~	***~~discordant~~***
irregular	

Appendix 5A - LASS-ICPMS U-Pb isotopic data from south transect samples

Spot name	Pb 206 (counts)	U (ppm)	Th (ppm)	Pb (ppm)	Th / U	$^{207*}Pb/^{235}U$	% ±	$^{206*}Pb/^{238}U$	% ±	$^{207*}Pb/^{206*}Pb$	% ±
~~***K015A - 5***~~	~~***592000***~~	~~***348***~~	~~***86***~~	~~***103***~~	~~***0.25***~~	~~***11.51***~~	~~***0.18***~~	~~***0.4579***~~	~~***0.0084***~~	~~***0.1814***~~	~~***0.0015***~~
~~***K015A - 18***~~	~~***310000***~~	~~***177***~~	~~***191***~~	~~***225***~~	~~***0.95***~~	~~***11.4***~~	~~***0.41***~~	~~***0.45***~~	~~***0.016***~~	~~***0.184***~~	~~***0.002***~~
~~***K015A - 13***~~	~~***274000***~~	~~***142***~~	~~***67***~~	~~***83***~~	~~***0.47***~~	~~***13.92***~~	~~***0.37***~~	~~***0.536***~~	~~***0.014***~~	~~***0.1863***~~	~~***0.0022***~~
K015B, massive syenogranite											
UTM 693209 7030513											
~~K015B - 9~~	~~2962000~~	~~1439~~	~~209~~	~~209~~	~~0.13~~	~~13.01~~	~~0.22~~	~~0.586~~	~~0.011~~	~~0.159~~	~~0.0016~~
~~K015B - 13~~	~~3560000~~	~~1689~~	~~1270~~	~~1370~~	~~0.72~~	~~13.27~~	~~0.46~~	~~0.585~~	~~0.021~~	~~0.1629~~	~~0.0036~~
~~K015B - 5~~	~~1770000~~	~~1105~~	~~245~~	~~264~~	~~0.22~~	~~9.75~~	~~0.31~~	~~0.43~~	~~0.015~~	~~0.1631~~	~~0.0012~~
~~K015B - 7~~	~~2770000~~	~~1446~~	~~678~~	~~720~~	~~0.35~~	~~11.68~~	~~0.24~~	~~0.513~~	~~0.012~~	~~0.1633~~	~~0.0019~~
K015B - 16	***1840000***	***1030***	***135***	***144***	***0.12***	***9.94***	***0.44***	***0.441***	***0.023***	***0.1637***	***0.0025***
K015B - 19	***2180000***	***1248***	***417***	***408***	***0.31***	***11.08***	***0.38***	***0.478***	***0.019***	***0.1661***	***0.0015***
K015B - 20	***1756000***	***978***	***443***	***444***	***0.43***	***11.394***	***0.09***	***0.4877***	***0.0067***	***0.1674***	***0.0016***
K015B - 11	***2084000***	***1244***	***326***	***379***	***0.22***	***11.51***	***0.47***	***0.485***	***0.019***	***0.1697***	***0.0016***
K015B - 10	***3840000***	***1880***	***175***	***247***	***0.09***	***11.92***	***0.31***	***0.511***	***0.027***	***0.1715***	***0.0066***
K015B - 8	***1129000***	***738***	***521***	***519***	***0.68***	***11.89***	***0.33***	***0.486***	***0.014***	***0.1758***	***0.0032***
K015B - 4	***396000***	***210***	***178***	***227***	***0.84***	***12.22***	***0.21***	***0.4995***	***0.0077***	***0.1761***	***0.0013***
K015B - 12	***1192000***	***598***	***306***	***328***	***0.43***	***12.99***	***0.28***	***0.526***	***0.011***	***0.1771***	***0.0011***
K015B - 14	***1190000***	***604***	***306***	***410***	***0.45***	***12.02***	***0.4***	***0.489***	***0.015***	***0.1777***	***0.0019***
K015B - 18	***735000***	***359***	***182***	***212***	***0.50***	***13.01***	***0.26***	***0.523***	***0.012***	***0.1784***	***0.0013***
K015B - 6	***767000***	***425***	***468***	***519***	***1.06***	***13.18***	***0.17***	***0.5153***	***0.0088***	***0.1833***	***0.0021***
K015B - 15	***780000***	***426***	***439***	***494***	***0.98***	***13.69***	***0.47***	***0.532***	***0.018***	***0.1834***	***0.002***
K015B - 3	***372000***	***184***	***151***	***206***	***0.82***	***14.14***	***0.29***	***0.545***	***0.011***	***0.1862***	***0.0014***
K015B - 1	***321000***	***170***	***338***	***405***	***1.97***	***13.52***	***0.23***	***0.5188***	***0.0072***	***0.1867***	***0.002***
~~***K015B - 2***~~	~~***943000***~~	~~***547***~~	~~***400***~~	~~***420***~~	~~***0.72***~~	~~***10.19***~~	~~***0.25***~~	~~***0.418***~~	~~***0.01***~~	~~***0.1771***~~	~~***0.0021***~~
~~***K015B - 17***~~	~~***531000***~~	~~***327***~~	~~***270***~~	~~***261***~~	~~***0.82***~~	~~***10.03***~~	~~***0.3***~~	~~***0.396***~~	~~***0.017***~~	~~***0.1837***~~	~~***0.0035***~~

table notes:
normal black font denotes metamorphic zircons, ***bold italics denotes magmatic zircons***, light grey denotes inherited zircons
denotes magmatic zircon ages interpreted to best represent the crystallization age
denotes magmatic zircon inherirted from a different rock unit

			age (Ma)									
$^{206*}Pb$ / $^{208*}Pb$	% ±	Disc. %	$^{206*}Pb$ / ^{238}U	±	$^{207*}Pb$ / $^{206*}Pb$	±	^{176}Lu / ^{177}Hf	^{176}Hf / ^{177}Hf	εHf(t)[1]	±2s	T_{DM}[2] (Ga)	location
0.1312	***0.0026***	***8.86***	***2429***	***37***	***2665***	***14***	***0.000326***	***0.280984***	***-3.70***	***1.95***	***3093***	***core***
0.1293	***0.0038***	***11.01***	***2392***	***73***	***2688***	***19***	***0.001480***	***0.281231***	***3.51***	***5.41***	***2845***	***core***
0.1395	***0.005***	***-1.99***	***2763***	***59***	***2709***	***19***	***0.000333***	***0.280992***	***-2.40***	***2.60***	***3083***	***core***
K015B, massive syenogranite												
UTM 693209 7030513												
0.1178	0.0083	-21.60	2973	46	2445	17	0.000514	0.281049	-6.80	2.00	3020	rim
0.1189	0.0031	-19.43	2963	87	2481	35	0.001218	0.281160	-3.21	2.58	2923	rim
0.1167	0.0024	7.48	2302	69	2488	13	0.000515	0.281134	-2.79	1.80	2905	core
0.1228	0.0043	-7.11	2666	50	2489	20	0.000980	0.281131	-3.66	2.94	2945	single gra
0.1091	***0.0076***	***5.74***	***2350***	***100***	***2493***	***26***	***0.000567***	***0.281106***	***-3.75***	***3.55***	***2947***	***core***
0.1111	***0.0014***	***0.12***	***2515***	***84***	***2518***	***15***	***0.000557***	***0.281088***	***-3.80***	***2.00***	***2971***	***rim***
0.1098	***0.0052***	***-1.15***	***2560***	***29***	***2531***	***16***	***0.000775***	***0.281158***	***-1.39***	***2.89***	***2892***	***rim***
0.136	***0.0043***	***0.39***	***2545***	***81***	***2555***	***16***	***0.000743***	***0.281131***	***-1.75***	***3.97***	***2927***	***core***
0.1493	***0.0029***	***-3.39***	***2650***	***110***	***2563***	***65***	***0.000768***	***0.281167***	***-0.33***	***3.28***	***2880***	***core***
0.119	***0.0035***	***2.33***	***2552***	***60***	***2613***	***31***	***0.000800***	***0.281281***	***4.82***	***10.70***	***2726***	***core***
0.1366	***0.0035***	***0.19***	***2610***	***33***	***2615***	***12***	***0.001167***	***0.281253***	***3.21***	***2.31***	***2791***	***outer***
0.1185	***0.0062***	***-3.76***	***2724***	***45***	***2625***	***10***	***0.000577***	***0.281100***	***-0.94***	***2.83***	***2956***	***core***
0.1433	***0.005***	***2.55***	***2564***	***65***	***2631***	***18***	***0.000710***	***0.281201***	***2.54***	***3.63***	***2829***	***core***
0.1267	***0.0026***	***-2.73***	***2710***	***50***	***2638***	***12***	***0.000563***	***0.281148***	***1.08***	***1.75***	***2890***	***core***
0.1253	***0.0022***	***0.11***	***2679***	***37***	***2682***	***20***	***0.000871***	***0.281119***	***0.50***	***3.11***	***2953***	***core***
0.1327	***0.0059***	***-2.42***	***2749***	***74***	***2684***	***18***	***0.000810***	***0.281151***	***1.80***	***4.68***	***2905***	***core***
0.1504	***0.0041***	***-3.47***	***2803***	***44***	***2709***	***12***	***0.000323***	***0.281039***	***-0.71***	***2.16***	***3019***	***core***
0.1322	***0.002***	***0.70***	***2693***	***31***	***2712***	***17***	***0.000709***	***0.280925***	***-5.41***	***3.18***	***3204***	***core***
0.1092	***0.0031***	***14.25***	***2251***	***47***	***2625***	***20***	***0.000846***	***0.281133***	***-0.26***	***3.14***	***2932***	***core***
0.1018	***0.0034***	***19.89***	***2151***	***77***	***2685***	***32***	***0.000543***	***0.281191***	***3.73***	***3.98***	***2830***	***core***

table notes:
normal black font denotes metamorphic zircons, ***bold italics denotes magmatic zircons***, light grey denotes inherited zircons
denotes magmatic zircon ages interpreted to best represent the crystallization age
denotes magmatic zircon inherirted from a different rock unit

zonation	notes
~~***osc***~~	~~***incidental overlap of cracks***~~
~~***osc***~~	~~***some bright white disturbances***~~
~~***osc***~~	~~***incidental overlap of cracks***~~

K015B, massive syenogranite
UTM 693209 7030513

~~homo~~	~~discordant~~
~~homo~~	~~discordant~~
~~irregular~~	~~incidental overlap of cracks~~
~~homo~~	~~discordant~~
osc	
faint osc	
osc	
osc	
osc	
faint osc	
faint osc	
faint osc	
osc	
faint osc	
osc	***inherited from K015A***
osc	***inherited from K015A***
osc	***inherited from K015A***
osc	***inherited from K015A***
~~***osc***~~	~~discordant~~
~~***osc***~~	~~discordant~~

table notes:
normal black font denotes metamorphic zircons, ***bold italics denotes magmatic zircons***, light grey denotes inherited zircons
denotes magmatic zircon ages interpreted to best represent the crystallization age
denotes magmatic zircon inherirted from a different rock unit

Appendix 5B - LASS-ICPMS U-Pb isotopic data from north transect samples

Spot name	Pb 206 (counts)	U (ppm)	Th (ppm)	Pb (ppm)	Th / U	$^{207*}Pb/^{235}U$	% ±	$^{206*}Pb/^{238}U$	% ±	$^{207*}Pb/^{206*}Pb$	% ±
Y032A, bt hbl opx granodiorite (charnockite)											
UTM 597219 7161320											
~~*Y032A_23*~~	~~*1100000*~~	~~*800*~~	~~*740*~~	~~*770*~~	~~*0.68*~~	~~*8.46*~~	~~*0.13*~~	~~*0.4166*~~	~~*0.0073*~~	~~*0.1473*~~	~~*0.0014*~~
~~*Y032A_9*~~	~~*1990000*~~	~~*1526*~~	~~*1050*~~	~~*1010*~~	~~*0.67*~~	~~*9.27*~~	~~*0.63*~~	~~*0.444*~~	~~*0.032*~~	~~*0.1512*~~	~~*0.0019*~~
~~*Y032A_5*~~	~~*2840000*~~	~~*1543*~~	~~*1850*~~	~~*1930*~~	~~*0.92*~~	~~*11.81*~~	~~*0.37*~~	~~*0.542*~~	~~*0.018*~~	~~*0.1566*~~	~~*0.0012*~~
~~*Y032A_14*~~	~~*196600*~~	~~*135*~~	~~*233*~~	~~*259*~~	~~*1.69*~~	~~*9.55*~~	~~*0.2*~~	~~*0.4414*~~	~~*0.006*~~	~~*0.1579*~~	~~*0.0017*~~
Y032A_8	*802000*	*522*	*389*	*436*	*0.73*	*10.05*	*0.25*	*0.434*	*0.0087*	*0.1663*	*0.0013*
Y032A_21	*242000*	*177*	*275*	*301*	*1.49*	*10.55*	*0.3*	*0.4457*	*0.0089*	*0.17*	*0.0023*
Y032A_16	*118400*	*81*	*90*	*104*	*1.10*	*10.76*	*0.22*	*0.4556*	*0.0058*	*0.172*	*0.0034*
Y032A_24	*622000*	*424*	*582*	*662*	*1.37*	*11.28*	*0.26*	*0.4624*	*0.0081*	*0.1763*	*0.0017*
Y032A_2	*417000*	*252*	*175*	*214*	*0.68*	*12.45*	*0.32*	*0.5088*	*0.0098*	*0.1769*	*0.0018*
Y032A_3	*656000*	*382*	*243*	*323*	*0.63*	*12.97*	*0.2*	*0.5142*	*0.007*	*0.182*	*0.0012*
Y032A_13	*400900*	*235*	*126*	*165*	*0.52*	*12.84*	*0.15*	*0.5146*	*0.0069*	*0.18246*	*0.00099*
Y032A_12	*749000*	*417*	*265*	*361*	*0.62*	*13.41*	*0.13*	*0.533*	*0.0046*	*0.18342*	*0.00092*
Y032A_4	*420000*	*239*	*554*	*662*	*2.23*	*13.41*	*0.19*	*0.5174*	*0.0064*	*0.1868*	*0.0012*
Y032A_7	*288800*	*161*	*231*	*300*	*1.43*	*13.4*	*0.21*	*0.5123*	*0.0054*	*0.1878*	*0.0016*
Y032A_11	*494000*	*272*	*408*	*526*	*1.50*	*13.83*	*0.1*	*0.5352*	*0.0037*	*0.18796*	*0.00096*
Y032A_17	*154700*	*88*	*71*	*99*	*0.81*	*14.19*	*0.14*	*0.5478*	*0.0058*	*0.1885*	*0.0015*
Y032A_1	*306400*	*178*	*248*	*327*	*1.40*	*13.63*	*0.11*	*0.5237*	*0.0037*	*0.1884*	*0.0011*
Y032A_22	*482000*	*312*	*177*	*233*	*0.56*	*12.6*	*0.3*	*0.484*	*0.011*	*0.1888*	*0.0014*
Y032A_18	*443000*	*253*	*150*	*205*	*0.59*	*14.63*	*0.25*	*0.5615*	*0.0084*	*0.1895*	*0.0012*
Y032A_10	*271000*	*141*	*57*	*83*	*0.37*	*14.71*	*0.2*	*0.5601*	*0.008*	*0.1906*	*0.0011*
~~*Y032A_15*~~	~~*129000*~~	~~*69*~~	~~*79*~~	~~*118*~~	~~*1.14*~~	~~*15.72*~~	~~*0.26*~~	~~*0.6026*~~	~~*0.0099*~~	~~*0.1903*~~	~~*0.0017*~~
~~*Y032A_6*~~	~~*342500*~~	~~*200*~~	~~*310*~~	~~*365*~~	~~*1.55*~~	~~*12.4*~~	~~*0.17*~~	~~*0.4697*~~	~~*0.0061*~~	~~*0.1913*~~	~~*0.0016*~~
Y032A_19	170300	96	106	151	1.10	15.34	0.24	0.5581	0.0065	0.1995	0.0019
Y032A_20	100450	53	54	83	1.02	16.67	0.34	0.585	0.012	0.206	0.0025
K037A, tonalite gneiss											
UTM 607104 7161794											
~~*K037A - 21*~~	~~*1821000*~~	~~*1545*~~	~~*325*~~	~~*254*~~	~~*0.21*~~	~~*12.4*~~	~~*1*~~	~~*0.265*~~	~~*0.02*~~	~~*0.1726*~~	~~*0.0017*~~
~~*K037A - 22*~~	~~*1156000*~~	~~*992*~~	~~*111*~~	~~*97*~~	~~*0.11*~~	~~*14.28*~~	~~*0.53*~~	~~*0.5371*~~	~~*0.0096*~~	~~*0.1768*~~	~~*0.0035*~~
~~*K037A - 7*~~	~~*650000*~~	~~*532*~~	~~*29*~~	~~*31*~~	~~*0.04*~~	~~*4.59*~~	~~*0.079*~~	~~*0.3114*~~	~~*0.0029*~~	~~*0.10977*~~	~~*0.00077*~~

denotes analytical spots with Paleoproterozoic 207/206Pb ages that plot on Archean concordia space

			age (Ma)										
$^{206*}Pb$ / $^{208*}Pb$	% ±	Disc. %	$^{206*}Pb$ / ^{238}U	±	$^{207*}Pb$ / $^{206*}Pb$	±	^{176}Lu / ^{177}Hf	^{176}Hf / ^{177}Hf	εHf(t)[1]	±2s	T_{DM}[2] (Ga)	location
Y032A, bt hbl opx granodiorite (charnockite)												
UTM 597219 7161320												
~~5.63~~	~~0.33~~	~~3.03~~	~~2244~~	~~33~~	~~2314~~	~~16~~	~~0.000730~~	~~0.281033~~	~~-10.7~~	~~2.4~~	~~3059~~	~~core~~
~~5.69~~	~~0.24~~	~~-0.04~~	~~2360~~	~~140~~	~~2359~~	~~21~~	~~0.002100~~	~~0.281130~~	~~-8.4~~	~~2.8~~	~~3036~~	~~rim~~
~~4.92~~	~~0.47~~	~~-15.09~~	~~2784~~	~~77~~	~~2419~~	~~13~~	~~0.003040~~	~~0.281212~~	~~-5.7~~	~~2.6~~	~~2996~~	~~rim~~
~~2.249~~	~~0.049~~	~~3.09~~	~~2356~~	~~27~~	~~2431~~	~~18~~	~~0.000790~~	~~0.280953~~	~~-11.0~~	~~1.6~~	~~3172~~	~~rim~~
5.327	0.094	7.86	2322	39	2520	13	0.000910	0.281045	-5.9	2.4	3057	rim
2.638	0.064	6.81	2381	42	2555	23	0.000527	0.280739	-15.3	2.8	3438	rim
3.4	0.11	6.02	2419	26	2574	33	0.000187	0.280869	-9.7	1.7	3235	core
3.062	0.057	6.42	2449	36	2617	16	0.001160	0.281009	-5.4	2.0	3126	core
5.85	0.1	-0.99	2649	42	2623	17	0.000779	0.281028	-3.9	1.5	3069	rim
6.016	0.06	-0.11	2673	30	2670	11	0.000496	0.280989	-3.7	1.3	3100	core
7.2	0.25	-0.01	2675	29	2675	9	0.000464	0.280951	-4.9	1.7	3148	core
6.1	0.21	-2.62	2754	19	2684	8	0.000852	0.280982	-4.3	1.7	3138	core
1.884	0.032	0.96	2687	27	2713	11	0.001424	0.281034	-2.8	2.4	3114	core
2.797	0.029	2.06	2666	23	2722	14	0.000844	0.281014	-2.3	1.6	3094	core
2.7	0.017	-1.55	2766	16	2724	8	0.001148	0.280994	-3.5	2.4	3146	core
4.728	0.079	-3.19	2815	24	2728	13	0.000849	0.280923	-5.4	2.1	3218	core
2.841	0.023	0.51	2714	16	2728	10	0.000596	0.281090	1.0	2.1	2971	core
6.81	0.2	6.85	2544	51	2731	12	0.000409	0.281024	-0.9	2.2	3045	core
6.56	0.11	-4.90	2871	35	2737	10	0.000420	0.280898	-5.3	1.8	3216	core
9.84	0.38	-4.33	2866	33	2747	10	0.000294	0.280991	-1.5	1.7	3081	core
~~3.215~~	~~0.056~~	~~-10.63~~	~~3038~~	~~40~~	~~2746~~	~~16~~	~~0.000349~~	~~0.280932~~	~~-3.7~~	~~1.6~~	~~3164~~	~~core~~
~~2.723~~	~~0.038~~	~~9.81~~	~~2482~~	~~27~~	~~2752~~	~~14~~	~~0.000729~~	~~0.281078~~	~~0.9~~	~~1.8~~	~~2998~~	~~core~~
3.455	0.065	-1.35	2858	27	**2820**	15	0.000181	0.280823	-5.5	1.4	3296	rim
3.864	0.048	-3.24	2966	47	**2873**	20	0.000175	0.280724	-7.8	1.7	3427	core
K037A, tonalite gneiss												
UTM 607104 7161794												
~~24.5~~	~~1.4~~	~~-23.72~~	~~1977~~	~~80~~	~~1598~~	~~14~~	~~0.000012~~	~~0.281098~~	~~-23.8~~	~~1.7~~	~~2915~~	~~single grain~~
~~5.55~~	~~0.21~~	~~-4.09~~	~~1755~~	~~47~~	~~1686~~	~~18~~	~~0.000027~~	~~0.281113~~	~~-21.2~~	~~1.1~~	~~2896~~	~~single grain~~
~~31.12~~	~~0.64~~	~~16.44~~	~~1489~~	~~54~~	~~1782~~	~~12~~	~~0.000024~~	~~0.281153~~	~~-17.6~~	~~1.5~~	~~2842~~	~~single grain~~

denotes analytical spots with Paleoproterozoic 207/206Pb ages that plot on Archean concordia space

zonation	notes

Y032A, bt hbl opx granodiorite (charnockite)
UTM 597219 7161320

~~unzoned~~	***~~incidental overlap of domains~~***
~~unzoned~~	
~~unzoned~~	
~~unzoned~~	
unzoned	
unzoned	
unzoned	
faint osc	
unzoned	
unzoned	
faint osc	
unzoned	
faint osc	
unzoned	
osc	
osc	
unzoned	
unzoned	
osc	
faint osc	
~~osc~~	***~~discordant~~***
~~faint osc~~	***~~discordant~~***
OSC	
OSC	

K037A, tonalite gneiss
UTM 607104 7161794

~~unzoned~~	***~~discordant~~***
~~unzoned~~	***~~discordant~~***
~~unzoned~~	***~~discordant~~***

denotes analytical spots with Paleoproterozoic 207/206Pb ages that plot on Archean concordia space

Appendix 5B - LASS-ICPMS U-Pb isotopic data from north transect samples

Spot name	Pb 206 (counts)	U (ppm)	Th (ppm)	Pb (ppm)	Th / U	$^{207*}Pb/^{235}U$	% ±	$^{206*}Pb/^{238}U$	% ±	$^{207*}Pb/^{206*}Pb$	% ±
K037A - 11	***702000***	***575***	***74***	***60***	***0.10***	***5.02***	***0.14***	***0.3265***	***0.0043***	***0.11204***	***0.00078***
K037A - 16	***652000***	***610***	***62***	***52***	***0.10***	***11.13***	***0.23***	***0.497***	***0.0064***	***0.1634***	***0.0013***
K037A - 9	***566000***	***393***	***32***	***29***	***0.08***	***4.77***	***0.1***	***0.3148***	***0.0047***	***0.11113***	***0.00085***
K037A - 8	***443600***	***305***	***35***	***30***	***0.11***	***4.88***	***0.16***	***0.3236***	***0.0066***	***0.1104***	***0.00077***
K037A - 19	***366000***	***310***	***22***	***20***	***0.07***	***10.14***	***0.3***	***0.4304***	***0.0085***	***0.17***	***0.0021***
K037A - 20	***364800***	***301***	***15***	***15***	***0.05***	***11.89***	***0.26***	***0.5039***	***0.0044***	***0.17159***	***0.00082***
K037A - 10	***452000***	***317***	***25***	***22***	***0.07***	***4.87***	***0.12***	***0.3176***	***0.0035***	***0.11143***	***0.00066***
K037A - 24	***337000***	***344***	***12***	***11***	***0.03***	***11.43***	***0.45***	***0.498***	***0.019***	***0.1808***	***0.0042***
K037A - 18	***233000***	***169***	***11***	***11***	***0.06***	***10.15***	***0.25***	***0.467***	***0.0097***	***0.1701***	***0.0034***
K037A - 12	***632000***	***466***	***54***	***49***	***0.11***	***4.791***	***0.096***	***0.3012***	***0.0035***	***0.11346***	***0.00093***
K037A - 25	***284000***	***260***	***19***	***18***	***0.07***	***12.54***	***0.54***	***0.524***	***0.017***	***0.1841***	***0.002***
~~K037A - 2~~	~~180500~~	~~74~~	~~42~~	~~50~~	~~0.54~~	~~4.5~~	~~0.12~~	~~0.3149~~	~~0.0073~~	~~0.1041~~	~~0.001~~
~~K037A - 4~~	~~283200~~	~~122~~	~~70~~	~~86~~	~~0.56~~	~~4.1~~	~~0.21~~	~~0.261~~	~~0.01~~	~~0.10846~~	~~0.00071~~
K037A - 6	141000	68	55	64	0.76	4.08	0.17	0.288	0.0095	0.10932	0.00072
~~K037A - 14~~	~~128400~~	~~67~~	~~39~~	~~49~~	~~0.57~~	~~8.22~~	~~0.14~~	~~0.2523~~	~~0.0028~~	~~0.1135~~	~~0.0015~~
~~K037A - 1~~	~~632900~~	~~254~~	~~205~~	~~245~~	~~0.77~~	~~4.15~~	~~0.18~~	~~0.331~~	~~0.015~~	~~0.09913~~	~~0.00073~~
~~K037A - 26~~	~~682000~~	~~700~~	~~67~~	~~84~~	~~0.10~~	~~11.79~~	~~0.24~~	~~0.4585~~	~~0.0053~~	~~0.1841~~	~~0.0015~~
K037A - 17	357000	230	265	268	1.12	10.94	0.2	0.4802	0.0044	0.1643	0.0011
~~K037A - 23~~	~~112100~~	~~62~~	~~43~~	~~63~~	~~0.68~~	~~11.93~~	~~0.86~~	~~0.409~~	~~0.024~~	~~0.178~~	~~0.0029~~
K037A - 5	98900	44	40	48	0.86	4.75	0.13	0.311	0.003	0.10918	0.00077
K037A - 15	167300	93	55	67	0.58	9.46	0.42	0.43	0.011	0.1476	0.0038
K037A - 3	161000	66	69	86	1.00	4.32	0.31	0.304	0.017	0.1076	0.0011
F157A, bt mt ep monzogranite											
UTM 622813 7160311											
F157A_14_2	384000	325	104	89	0.32	5.3	0.12	0.3263	0.0057	0.11203	0.00093
F157A_20	107400	97	28	24	0.29	4.894	0.087	0.316	0.0042	0.1147	0.0014
~~F157A_14~~	~~618000~~	~~445~~	~~119~~	~~138~~	~~0.26~~	~~8.43~~	~~0.4~~	~~0.418~~	~~0.019~~	~~0.1617~~	~~0.0031~~
~~F157A_13~~	***~~929000~~***	***~~561~~***	***~~212~~***	***~~248~~***	***~~0.33~~***	***~~11.47~~***	***~~0.38~~***	***~~0.4901~~***	***~~0.0088~~***	***~~0.1755~~***	***~~0.0013~~***
~~F157A_7~~	***~~735000~~***	***~~453~~***	***~~266~~***	***~~166~~***	***~~0.45~~***	***~~11.21~~***	***~~0.36~~***	***~~0.4589~~***	***~~0.0094~~***	***~~0.1783~~***	***~~0.0013~~***
~~F157A_16~~	***~~956000~~***	***~~604~~***	***~~74~~***	***~~79~~***	***~~0.11~~***	***~~10.64~~***	***~~0.34~~***	***~~0.4619~~***	***~~0.0085~~***	***~~0.1783~~***	***~~0.0016~~***
F157A_4	***325000***	***184***	***170***	***197***	***0.93***	***11.68***	***0.29***	***0.505***	***0.011***	***0.1788***	***0.0021***

			age (Ma)									
$^{206*}Pb$ / $^{208*}Pb$	% ±	Disc. %	$^{206*}Pb$ / ^{238}U	±	$^{207*}Pb$ / $^{206*}Pb$	±	^{176}Lu / ^{177}Hf	^{176}Hf / ^{177}Hf	εHf(t)[1]	±2s	T_{DM}[2] (Ga)	location
64.4	***2.5***	***-0.11***	***1776***	***59***	***1774***	***21***	***0.000005***	***0.281092***	***-19.9***	***1.9***	***2923***	***rim***
7.37	***0.19***	***4.49***	***1703***	***17***	***1783***	***12***	***0.000054***	***0.281133***	***-18.3***	***2.0***	***2871***	***single grain***
45.5	***2.1***	***2.28***	***1754***	***11***	***1795***	***13***	***0.000001***	***0.281116***	***-18.6***	***1.3***	***2890***	***single grain***
97.9	***6.4***	***1.99***	***1769***	***18***	***1805***	***13***	***0.000001***	***0.281067***	***-20.1***	***1.5***	***2956***	***single grain***
5.97	***0.12***	***1.89***	***1779.7***	***8.9***	***1814***	***11***	***0.000011***	***0.281163***	***-16.5***	***1.4***	***2828***	***rim***
5.24	***0.13***	***0.44***	***1815***	***11***	***1823***	***13***	***0.000005***	***0.281120***	***-17.8***	***1.2***	***2885***	***single grain***
46.6	***0.84***	***1.86***	***1794***	***18***	***1828***	***14***	***0.000004***	***0.281142***	***-16.9***	***1.4***	***2856***	***single grain***
4.46	***0.24***	***-0.05***	***1833***	***15***	***1832***	***13***	***0.000017***	***0.281156***	***-16.3***	***1.6***	***2838***	***core***
4.76	***0.16***	***-0.27***	***1853***	***21***	***1848***	***23***	***0.000054***	***0.281142***	***-16.5***	***2.2***	***2859***	***core***
29.65	***0.97***	***8.04***	***1715***	***15***	***1865***	***15***	***0.000182***	***0.281116***	***-17.2***	***1.4***	***2904***	***single grain***
3.882	***0.097***	***-1.87***	***1905***	***16***	***1870***	***18***	***0.000034***	***0.281135***	***-16.2***	***1.6***	***2867***	***core***
~~30.89~~	~~0.42~~	~~-3.57~~	~~2581~~	~~22~~	~~2492~~	~~13~~	~~0.000359~~	~~0.280824~~	~~-13.4~~	~~2.1~~	~~3309~~	~~core fragment~~
~~53~~	~~5.9~~	~~-0.96~~	~~2527~~	~~17~~	~~**2503**~~	~~11~~	~~0.000398~~	~~0.280842~~	~~-12.6~~	~~1.3~~	~~3288~~	~~core~~
31.7	1.6	-1.99	2614	40	**2563**	33	0.000666	0.280894	-9.8	2.4	3241	core
~~54.2~~	~~3.3~~	~~9.47~~	~~2322~~	~~44~~	~~**2565**~~	~~21~~	~~0.000469~~	~~0.280874~~	~~-10.2~~	~~1.9~~	~~3251~~	~~core~~
~~18.6~~	~~0.31~~	~~-1.60~~	~~2615~~	~~11~~	~~**2574**~~	~~8~~	~~0.000957~~	~~0.281009~~	~~-6.0~~	~~2.0~~	~~3109~~	~~core~~
~~6.223~~	~~0.09~~	~~28.35~~	~~1870~~	~~130~~	~~2610~~	~~16~~	~~0.000496~~	~~0.281202~~	~~2.5~~	~~3.1~~	~~2811~~	~~core~~
6.8	0.14	6.24	2463	69	**2627**	27	0.000990	0.281003	-5.1	2.9	3120	core
~~3.37~~	~~0.12~~	~~*-4.31*~~	~~2758~~	~~52~~	~~**2644**~~	~~32~~	~~0.000399~~	~~0.280845~~	~~-9.2~~	~~3.3~~	~~3284~~	~~core~~
41.68	0.86	*-5.67*	2814	51	**2663**	38	0.001027	0.280899	-8.0	1.9	3265	core
23.2	3.9	*9.08*	2442	22	**2686**	13	0.000570	0.280970	-4.1	1.6	3130	core
32.4	3.5	*-4.61*	2816	34	**2692**	18	0.000669	0.280809	-9.9	2.7	3356	core
F157A, bt mt ep monzogranite												
UTM 622813 7160311												
11.83	0.29	2.03	1782	28	**1819**	15	0.000642	0.281194	-16.1	1.7	2832	rim
12.37	0.35	5.11	1781	26	**1877**	24	0.000200	0.281099	-17.6	1.7	2928	rim
~~12.8~~	~~1.3~~	~~-0.20~~	~~2464~~	~~31~~	~~**2459**~~	~~33~~	~~0.000394~~	~~0.281148~~	~~-2.7~~	~~1.8~~	~~2876~~	~~core~~
~~***11.9***~~	~~***1.1***~~	~~***0.96***~~	~~***2572***~~	~~***22***~~	~~***2597***~~	~~***12***~~	~~***0.000566***~~	~~***0.281139***~~	~~***-0.2***~~	~~***1.6***~~	~~***2901***~~	~~***mid***~~
~~***13.46***~~	~~***0.94***~~	~~***6.86***~~	~~***2443***~~	~~***45***~~	~~***2623***~~	~~***12***~~	~~***0.000215***~~	~~***0.281079***~~	~~***-1.1***~~	~~***1.5***~~	~~***2956***~~	~~***core***~~
~~***33***~~	~~***1.6***~~	~~***3.80***~~	~~***2529***~~	~~***18***~~	~~***2629***~~	~~***15***~~	~~***0.000277***~~	~~***0.281081***~~	~~***-1.0***~~	~~***1.5***~~	~~***2958***~~	~~***mid***~~
4.46	***0.24***	***-3.73***	***2728***	***37***	***2630***	***19***	***0.000363***	***0.281154***	***1.5***	***1.8***	***2866***	***mid***

zonation	notes
unzoned	
unzoned	
unzoned	
unzoned	
sector	
sector	
faint core	
faint osc	
osc	
faint osc	
faint osc	
~~faint osc~~	~~incidental overlap of cracks~~
~~faint osc~~	~~incidental overlap of domains~~
faint osc	
~~osc~~	~~discordant~~
~~light~~	~~discordant~~
~~faint osc~~	~~incidental overlap of cracks~~
faint osc	
~~faint osc~~	~~discordant~~
faint osc	
osc	
faint osc	

F157A, bt mt ep monzogranite
UTM 622813 7160311

faint osc	
~~irr~~	~~incidental overlap of domains~~
~~***faint osc***~~	~~incidental overlap of domains~~
~~***osc***~~	~~incidental overlap of domains~~
~~***faint osc***~~	~~incidental overlap of domains~~
osc	

Appendix 5B - LASS-ICPMS U-Pb isotopic data from north transect samples

Spot name	Pb 206 (counts)	U (ppm)	Th (ppm)	Pb (ppm)	Th / U	$^{207*}Pb/^{235}U$	% ±	$^{206*}Pb/^{238}U$	% ±	$^{207*}Pb/^{206*}Pb$	% ±
~~F157A_6~~	~~528000~~	~~326~~	~~95~~	~~126~~	~~0.31~~	~~11.47~~	~~0.33~~	~~0.4624~~	~~0.0061~~	~~0.181~~	~~0.0013~~
~~F157A_11~~	~~925000~~	~~623~~	~~225~~	~~267~~	~~0.24~~	~~10.65~~	~~0.54~~	~~0.461~~	~~0.018~~	~~0.1813~~	~~0.0016~~
~~F157A_12~~	~~584000~~	~~339~~	~~98~~	~~128~~	~~0.24~~	~~12.33~~	~~0.32~~	~~0.5029~~	~~0.0063~~	~~0.1813~~	~~0.001~~
~~F157A_8~~	~~608000~~	~~331~~	~~94~~	~~118~~	~~0.15~~	~~13.53~~	~~0.53~~	~~0.537~~	~~0.013~~	~~0.182~~	~~0.0012~~
~~F157A_5~~	~~700000~~	~~428~~	~~458~~	~~304~~	~~0.75~~	~~11.76~~	~~0.47~~	~~0.469~~	~~0.012~~	~~0.18174~~	~~0.00099~~
~~F157A_1~~	~~737000~~	~~416~~	~~139~~	~~192~~	~~0.23~~	~~12.35~~	~~0.36~~	~~0.495~~	~~0.011~~	~~0.1821~~	~~0.0011~~
~~F157A_9~~	~~616000~~	~~358~~	~~216~~	~~164~~	~~0.49~~	~~13.15~~	~~0.57~~	~~0.517~~	~~0.012~~	~~0.1835~~	~~0.0016~~
~~F157A_22~~	~~442000~~	~~297~~	~~305~~	~~343~~	~~1.01~~	~~11.63~~	~~0.37~~	~~0.486~~	~~0.011~~	~~0.1801~~	~~0.0013~~
~~F157A_2~~	~~584000~~	~~328~~	~~132~~	~~152~~	~~0.25~~	~~12.71~~	~~0.37~~	~~0.503~~	~~0.01~~	~~0.1846~~	~~0.001~~
~~F157A_19~~	~~410000~~	~~234~~	~~228~~	~~274~~	~~0.96~~	~~12.8~~	~~0.36~~	~~0.516~~	~~0.0082~~	~~0.18353~~	~~0.00093~~
~~F157A_10~~	~~1035000~~	~~928~~	~~484~~	~~594~~	~~0.53~~	~~7.76~~	~~0.26~~	~~0.332~~	~~0.011~~	~~0.1859~~	~~0.0016~~
~~F157A_23~~	~~202700~~	~~124~~	~~185~~	~~242~~	~~1.42~~	~~13.29~~	~~0.28~~	~~0.5233~~	~~0.0065~~	~~0.1844~~	~~0.0012~~
~~F157A_15~~	~~523000~~	~~297~~	~~59~~	~~76~~	~~0.18~~	~~12.82~~	~~0.41~~	~~0.5192~~	~~0.0092~~	~~0.1856~~	~~0.0017~~
~~F157A_3~~	~~175000~~	~~101~~	~~66~~	~~84~~	~~0.61~~	~~12.01~~	~~0.22~~	~~0.482~~	~~0.011~~	~~0.1878~~	~~0.0021~~
~~F157A_21_2~~	~~507000~~	~~273~~	~~67~~	~~90~~	~~0.15~~	~~13.75~~	~~0.52~~	~~0.573~~	~~0.017~~	~~0.1888~~	~~0.0027~~
F157A_18	293000	171	85	101	0.50	12.82	0.22	0.4991	0.0041	0.1959	0.0013
F157A_17	232700	119	59	80	0.46	15.51	0.31	0.5561	0.0062	0.2015	0.0014
F157A_21	438000	257	95	116	0.37	14.3	0.78	0.528	0.024	0.2123	0.0024
H055A, bt mt hbl monzogranite											
UTM 630315 7089316											
~~H055A_13~~	~~822000~~	~~519~~	~~147~~	~~174~~	~~0.28~~	~~11.4~~	~~0.1~~	~~0.4723~~	0.0049	~~0.1748~~	~~0.0013~~
~~H055A_19~~	~~812000~~	~~561~~	~~132~~	~~172~~	~~0.23~~	~~10.62~~	~~0.12~~	~~0.434~~	0.0052	~~0.1782~~	~~0.0014~~
H055A_2	340000	183	81	100	0.43	12.23	0.2	0.4881	0.0078	0.1807	0.0011
~~H055A_12~~	~~894000~~	~~473~~	~~119~~	~~202~~	~~0.25~~	~~14.06~~	~~0.24~~	~~0.5569~~	~~0.0073~~	~~0.1826~~	~~0.0013~~
~~H055A_3~~	~~607000~~	~~312~~	~~196~~	~~259~~	~~0.52~~	~~12.29~~	~~0.23~~	~~0.4852~~	~~0.0086~~	~~0.184~~	~~0.0012~~
~~H055A_18~~	~~476000~~	~~287~~	~~170~~	~~246~~	~~0.55~~	~~13.62~~	~~0.17~~	~~0.5313~~	~~0.007~~	~~0.1858~~	~~0.0012~~
~~H055A_1~~	~~225300~~	~~104~~	~~98~~	~~125~~	~~0.89~~	~~14.64~~	~~0.2~~	~~0.5594~~	~~0.0074~~	~~0.1881~~	~~0.0018~~
H055A_21	381000	226	69	99	0.28	13.6	0.2	0.5279	0.0059	0.1876	0.0014
H055A_16	916000	584	181	239	0.11	14.51	0.49	0.552	0.019	0.1891	0.0021
H055A_4	179100	82	82	109	0.99	14.39	0.17	0.5558	0.0072	0.188	0.0017
~~H055A_15~~	~~654000~~	~~364~~	~~125~~	~~185~~	~~0.28~~	~~13.57~~	~~0.5~~	~~0.536~~	~~0.011~~	~~0.1818~~	~~0.0026~~

			age (Ma)									
$^{206*}Pb$ / $^{208*}Pb$	% ±	Disc. %	$^{206*}Pb$ / ^{238}U	±	$^{207*}Pb$ / $^{206*}Pb$	±	^{176}Lu / ^{177}Hf	^{176}Hf / ^{177}Hf	εHf(t)[1]	±2s	T_{DM}[2] (Ga)	location
11.04	0.57	6.99	2463	15	2648	12	0.000451	0.281288	6.5	2.2	2691	rim
11.7	1.9	4.45	2532	44	2650	15	0.000584	0.281172	2.2	3.2	2858	core
14.6	1.6	1.61	2608	18	2651	10	0.000274	0.281084	-0.4	1.4	2954	mid
23.2	4.5	-2.98	2734	43	2655	11	0.000401	0.281081	-0.6	1.5	2967	core
7.08	0.56	6.46	2485	35	2657	9	0.000652	0.281365	9.1	3.1	2600	core
13.4	1.6	2.33	2599	40	2661	10	0.000449	0.281087	-0.3	1.9	2963	core
10.95	0.59	-0.07	2670	37	2668	14	0.000400	0.281150	2.2	2.0	2874	mid
~~3.97~~	~~0.075~~	~~2.88~~	~~2597~~	~~19~~	~~2674~~	~~12~~	~~0.000277~~	~~0.281081~~	~~0.1~~	~~1.7~~	~~2958~~	~~core~~
14.6	2	1.60	2641	35	2684	9	0.000424	0.281085	0.2	1.5	2964	core
4.074	0.093	-0.03	2685	23	2684	8	0.000313	0.281113	1.4	1.3	2918	core
~~4.715~~	~~0.095~~	~~27.05~~	~~1963~~	~~79~~	~~2691~~	~~14~~	~~0.000754~~	~~0.281290~~	~~7.0~~	~~2.0~~	~~2710~~	~~mid~~
2.67	0.17	-0.74	2712	28	2692	11	0.000283	0.281088	0.7	1.9	2949	core
21	1.3	-1.04	2723	17	2695	15	0.000302	0.281096	1.1	1.4	2940	core
5.59	0.16	4.83	2580	63	2711	18	0.000270	0.281069	0.5	1.9	2973	rim
~~20.6~~	~~5.7~~	~~-14.57~~	~~3130~~	~~74~~	~~2732~~	~~23~~	~~0.000348~~	~~0.281059~~	~~0.5~~	~~2.4~~	~~2993~~	~~core~~
7.92	0.15	4.99	2649	30	2788	11	0.000174	0.280971	-1.0	1.5	3097	rim
8.33	0.38	~~0.07~~	2831	21	2833	11	0.000308	0.281017	1.4	1.4	3046	core
10.3	0.26	1.30	2886	51	2924	18	0.001440	0.281162	6.5	5.1	2937	core
H055A, bt mt hbl monzogranite												
UTM 630315 7089316												
~~13.66~~	~~0.41~~	~~4.26~~	~~2493~~	~~21~~	~~2604~~	~~12~~	~~0.000361~~	~~0.281126~~	~~-0.1~~	~~2.0~~	~~2904~~	~~core~~
~~15.51~~	~~0.44~~	~~11.84~~	~~2323~~	~~24~~	~~2635~~	~~13~~	~~0.000570~~	~~0.281141~~	~~0.8~~	~~1.8~~	~~2900~~	~~mid~~
8.84	0.37	3.69	2561	33	2659	10	0.000569	0.281133	1.0	2.0	2911	rim
~~12.64~~	~~0.2~~	~~-6.61~~	~~2853~~	~~30~~	~~2676~~	~~12~~	~~0.000491~~	~~0.281180~~	~~3.0~~	~~1.7~~	~~2841~~	~~core~~
~~7.99~~	~~0.61~~	~~3.29~~	~~2593~~	~~37~~	~~2681~~	~~9~~	~~0.000804~~	~~0.281182~~	~~2.7~~	~~1.9~~	~~2862~~	~~core~~
~~6.6~~	~~0.33~~	~~-1.52~~	~~2746~~	~~29~~	~~2705~~	~~11~~	~~0.000916~~	~~0.281181~~	~~2.8~~	~~2.0~~	~~2871~~	~~core~~
~~4.58~~	~~0.22~~	~~-4.94~~	~~2848~~	~~31~~	~~2714~~	~~14~~	~~0.000683~~	~~0.281148~~	~~2.4~~	~~1.8~~	~~2899~~	~~core~~
12.68	0.46	-0.44	2732	25	2720	12	0.000566	0.281112	1.7	1.8	2939	rim
11.8	2.1	-1.21	2754	79	2721	12	0.000287	0.281095	1.7	1.4	2941	rim
4.28	0.18	-4.59	2848	30	2723	15	0.000285	0.281093	1.6	1.4	2943	rim
~~91~~	~~33~~	~~-6.76~~	~~2907~~	~~47~~	~~2723~~	~~14~~	~~0.000807~~	~~0.281130~~	~~2.2~~	~~1.8~~	~~2933~~	~~core~~

zonation	notes
unzoned	
osc	
osc	
osc	
osc	
faint osc	
osc	
~~***irr osc***~~	~~incidental overlap of domains~~
irr	
unzoned	
~~***osc***~~	~~***discordant***~~
irr	
irr	
unzoned	
~~***osc***~~	~~***discordant***~~
irr to unzoned	
irr osc	
osc	

H055A, bt mt hbl monzogranite
UTM 630315 7089316

~~osc~~	~~incidental overlap of domains~~
~~isc~~	~~discordant~~
unzoned	
~~***osc***~~	~~***discordant***~~
~~***osc***~~	~~***discordant***~~
~~***osc***~~	~~***discordant***~~
~~***osc***~~	~~***discordant***~~
unzoned	
unzoned	
unzoned	
~~***osc***~~	~~***discordant***~~

Appendix 5B - LASS-ICPMS U-Pb isotopic data from north transect samples

Spot name	Pb 206 (counts)	U (ppm)	Th (ppm)	Pb (ppm)	Th / U	$^{207*}Pb/^{235}U$	% ±	$^{206*}Pb/^{238}U$	% ±	$^{207*}Pb/^{206*}Pb$	% ±
H055A_14	*480000*	*278*	*91*	*138*	*0.32*	*13.48*	*0.15*	*0.5155*	*0.0067*	*0.189*	*0.0012*
H055A_7	*530000*	*293*	*113*	*137*	*0.19*	*13.63*	*0.24*	*0.5212*	*0.0075*	*0.1905*	*0.0014*
H055A_6	*278500*	*133*	*42*	*57*	*0.29*	*14.34*	*0.13*	*0.5485*	*0.0053*	*0.1906*	*0.0012*
H055A_9	*359000*	*182*	*82*	*101*	*0.37*	*13.93*	*0.25*	*0.5325*	*0.0091*	*0.1906*	*0.0014*
H055A_23	*545000*	*328*	*148*	*191*	*0.43*	*14.17*	*0.35*	*0.537*	*0.013*	*0.191*	*0.0013*
H055A_11	*380000*	*201*	*65*	*98*	*0.30*	*14.65*	*0.22*	*0.5547*	*0.0086*	*0.1915*	*0.0015*
H055A_8	*350000*	*178*	*84*	*95*	*0.42*	*14.25*	*0.2*	*0.5406*	*0.0075*	*0.192*	*0.0012*
H055A_17	*316000*	*191*	*81*	*113*	*0.40*	*14.46*	*0.15*	*0.5411*	*0.0065*	*0.1925*	*0.0013*
~~*H055A_22*~~	~~*215800*~~	~~*134*~~	~~*129*~~	~~*158*~~	~~*0.94*~~	~~*15.2*~~	~~*0.43*~~	~~*0.5324*~~	~~*0.0058*~~	~~*0.2066*~~	~~*0.0044*~~
~~*H055A_10*~~	~~*432000*~~	~~*211*~~	~~*78*~~	~~*123*~~	~~*0.33*~~	~~*15.34*~~	~~*0.22*~~	~~*0.5685*~~	~~*0.007*~~	~~*0.1964*~~	~~*0.0014*~~
~~*H055A_5*~~	~~*327000*~~	~~*154*~~	~~*58*~~	~~*89*~~	~~*0.29*~~	~~*15.79*~~	~~*0.26*~~	~~*0.584*~~	*0.012*	~~*0.1965*~~	~~*0.0021*~~
~~*H055A_20*~~	~~*300000*~~	~~*167*~~	~~*79*~~	~~*146*~~	~~*0.44*~~	~~*17.04*~~	~~*0.67*~~	~~*0.636*~~	*0.021*	~~*0.1967*~~	~~*0.0024*~~
Z108A, bt mt monzogranite											
UTM 662246 7122133											
~~Z108A_21~~	~~1180000~~	~~709~~	~~37~~	~~37~~	~~0.05~~	~~9.7~~	~~0.16~~	~~0.425~~	~~0.006~~	~~0.1647~~	~~0.0015~~
~~Z108A_13~~	~~1443000~~	~~1151~~	~~426~~	~~330~~	~~0.36~~	~~7.46~~	~~0.41~~	~~0.326~~	~~0.017~~	~~0.1659~~	~~0.0019~~
Z108A_22	1640000	762	30	43	0.04	12.05	0.34	0.524	0.012	0.1665	0.0017
Z108A_8	1577000	780	55	99	0.06	11.42	0.14	0.4928	0.0078	0.1689	0.0012
Z108A_14	1260000	639	50	43	0.08	10.95	0.19	0.471	0.0085	0.1689	0.001
Z108A_6	1428000	742	50	98	0.06	11.69	0.23	0.4926	0.0085	0.1722	0.0017
Z108A_5	2100000	1104	558	507	0.47	12.16	0.37	0.504	0.019	0.1759	0.0028
Z108A_7	*649000*	*292*	*67*	*97*	*0.16*	*13.85*	*0.4*	*0.531*	*0.012*	*0.1885*	*0.0019*
Z108A_12	*1170000*	*572*	*196*	*226*	*0.33*	*13.76*	*0.33*	*0.524*	*0.011*	*0.1903*	*0.0025*
Z108A_11	*527100*	*243*	*82*	*109*	*0.33*	*14.47*	*0.39*	*0.542*	*0.012*	*0.1933*	*0.0018*
Z108A_10	*748000*	*346*	*147*	*182*	*0.41*	*14.67*	*0.3*	*0.5488*	*0.0098*	*0.1934*	*0.002*
~~*Z108A_19*~~	~~*563000*~~	~~*285*~~	~~*166*~~	~~*183*~~	~~*0.52*~~	~~*12.26*~~	~~*0.55*~~	~~*0.463*~~	~~*0.02*~~	~~*0.1936*~~	~~*0.002*~~
Z108A_20	*728000*	*333*	*81*	*124*	*0.22*	*14.9*	*0.27*	*0.554*	*0.012*	*0.1941*	*0.0022*
Z108A_16	*751000*	*340*	*156*	*198*	*0.43*	*14.73*	*0.16*	*0.5464*	*0.0075*	*0.1957*	*0.0013*
Z108A_4	*338000*	*160*	*54*	*72*	*0.31*	*14.53*	*0.29*	*0.536*	*0.011*	*0.1964*	*0.0018*
Z108A_18	*519000*	*238*	*15*	*25*	*0.06*	*14.44*	*0.22*	*0.5312*	*0.009*	*0.197*	*0.0019*
~~*Z108A_2*~~	~~*338000*~~	~~*160*~~	~~*65*~~	~~*93*~~	~~*0.41*~~	~~*16.38*~~	~~*0.94*~~	~~*0.596*~~	~~*0.032*~~	~~*0.1997*~~	~~*0.0024*~~

			age (Ma)									
$^{206*}Pb$ / $^{208*}Pb$	% ±	Disc. %	$^{206*}Pb$ / ^{238}U	±	$^{207*}Pb$ / $^{206*}Pb$	±	^{176}Lu / ^{177}Hf	^{176}Hf / ^{177}Hf	εHf(t)[1]	±2s	T_{DM}[2] (Ga)	location
10.16	*0.26*	*1.98*	*2679*	*28*	*2733*	*11*	*0.000623*	*0.281142*	*3.0*	*1.6*	*2902*	*core*
16.9	*1.9*	*1.53*	*2703*	*32*	*2745*	*12*	*0.000433*	*0.281123*	*2.9*	*1.4*	*2914*	*mid*
13.43	*0.58*	*-2.62*	*2818*	*22*	*2746*	*10*	*0.000507*	*0.281131*	*3.1*	*2.1*	*2909*	*core*
10.85	*0.53*	*0.11*	*2744*	*38*	*2747*	*11*	*0.000636*	*0.281136*	*3.1*	*1.7*	*2912*	*core*
9.12	*0.44*	*-0.69*	*2769*	*53*	*2750*	*11*	*0.000480*	*0.281086*	*1.6*	*1.9*	*2967*	*core*
12.02	*0.79*	*-3.23*	*2843*	*36*	*2754*	*13*	*0.000669*	*0.281141*	*3.4*	*1.8*	*2907*	*core*
10.42	*0.53*	*-0.94*	*2785*	*32*	*2759*	*10*	*0.000699*	*0.281130*	*3.1*	*1.6*	*2925*	*core*
9.69	*0.48*	*-0.87*	*2787*	*27*	*2763*	*11*	*0.000508*	*0.281083*	*2.5*	*2.0*	*2974*	*core*
~~*3.73*~~	~~*0.22*~~	~~*3.59*~~	~~*2685*~~	~~*25*~~	~~*2785*~~	~~*18*~~	~~*0.000267*~~	~~*0.281053*~~	~~*1.9*~~	~~*2.1*~~	~~*2995*~~	~~*core*~~
~~*10.33*~~	~~*0.8*~~	~~*-3.76*~~	~~*2900*~~	~~*29*~~	~~*2795*~~	~~*12*~~	~~*0.000277*~~	~~*0.281079*~~	~~*2.8*~~	~~*1.3*~~	~~*2961*~~	~~*core*~~
~~*10.54*~~	~~*0.6*~~	~~*-10.54*~~	~~*3042*~~	~~*50*~~	~~*2752*~~	~~*17*~~	~~*0.000585*~~	~~*0.281134*~~	~~*3.2*~~	~~*2.1*~~	~~*2910*~~	~~*core*~~
~~*9.05*~~	~~*0.88*~~	~~*5.49*~~	~~*2686*~~	~~*88*~~	~~*2842*~~	~~*22*~~	~~*0.000343*~~	~~*0.281080*~~	~~*4.5*~~	~~*1.7*~~	~~*2965*~~	~~*rim*~~
Z108A, bt mt monzogranite												
UTM 662246 7122133												
~~76~~	~~3.3~~	~~8.87~~	~~2282~~	~~27~~	~~**2504**~~	~~16~~	~~0.000695~~	~~0.281037~~	~~-6.2~~	~~1.8~~	~~3051~~	~~rim~~
~~9.96~~	~~0.37~~	~~27.86~~	~~1815~~	~~83~~	~~**2516**~~	~~19~~	~~0.001321~~	~~0.281255~~	~~0.8~~	~~4.0~~	~~2800~~	~~core~~
88.8	5.2	-7.58	2712	50	**2521**	18	0.000772	0.281069	-4.8	2.0	3013	rim
43.3	3.1	-1.41	2582	33	**2546**	12	0.000772	0.281080	-3.8	1.7	2998	rim
64.6	2	2.32	2487	37	**2546**	10	0.000736	0.281066	-4.2	1.3	3014	rim
38.8	4.2	-0.12	2581	37	**2578**	16	0.000707	0.281089	-2.6	2.4	2981	rim
9.86	0.39	-0.61	2628	79	**2612**	26	0.001170	0.281185	1.6	3.6	2885	rim
20.4	*3.6*	*-0.88*	*2751*	*54*	*2727*	*17*	*0.000745*	*0.281067*	*-0.1*	*2.3*	*3014*	*core*
12.25	*0.72*	*0.98*	*2716*	*45*	*2743*	*22*	*0.000689*	*0.281084*	*1.0*	*3.0*	*2986*	*core*
11.11	*0.42*	*-0.83*	*2792*	*52*	*2769*	*16*	*0.000820*	*0.281116*	*2.5*	*2.0*	*2953*	*core*
9.53	*0.41*	*-1.77*	*2820*	*41*	*2771*	*17*	*0.001430*	*0.281120*	*1.5*	*3.3*	*2995*	*core*
~~*7.9*~~	~~*0.48*~~	~~*11.80*~~	~~*2445*~~	~~*91*~~	~~*2772*~~	~~*17*~~	~~*0.000870*~~	~~*0.281109*~~	~~*2.2*~~	~~*3.0*~~	~~*2966*~~	~~*core*~~
14.1	*1.1*	*-2.34*	*2842*	*51*	*2777*	*18*	*0.000756*	*0.281049*	*0.4*	*1.7*	*3039*	*core*
9.1	*0.66*	*-0.72*	*2810*	*31*	*2790*	*11*	*0.000743*	*0.281105*	*2.7*	*2.3*	*2962*	*core*
11.87	*0.89*	*0.64*	*2777*	*50*	*2795*	*15*	*0.000559*	*0.281103*	*3.1*	*2.4*	*2950*	*core*
51	*5.5*	*2.00*	*2745*	*38*	*2801*	*16*	*0.000373*	*0.281066*	*2.3*	*2.5*	*2986*	*outer core*
~~*9.02*~~	~~*0.28*~~	~~*-6.62*~~	~~*3010*~~	~~*130*~~	~~*2823*~~	~~*19*~~	~~*0.000579*~~	~~*0.281133*~~	~~*4.9*~~	~~*2.8*~~	~~*2911*~~	~~*core*~~

zonation	notes
osc	
osc	
osc	
osc	
osc	
osc	
osc	
osc	
~~***osc***~~	~~***discordant***~~
~~***osc***~~	~~***discordant***~~
~~***osc***~~	~~***discordant***~~
~~***unzoned***~~	~~***discordant***~~

Z108A, bt mt monzogranite
UTM 662246 7122133

~~mixed~~	~~incidental overlap of domains~~
~~osc~~	~~discordant~~
unzoned	
unzoned	
unzoned	
unzoned	
faint osc	
osc	
osc	
osc	
osc	
~~***osc***~~	~~discordant~~
osc	
osc	
osc	
osc	
~~***osc***~~	

Appendix 5B - LASS-ICPMS U-Pb isotopic data from north transect samples

Spot name	Pb 206 (counts)	U (ppm)	Th (ppm)	Pb (ppm)	Th / U	$^{207*}Pb/^{235}U$	% ±	$^{206*}Pb/^{238}U$	% ±	$^{207*}Pb/^{206*}Pb$	% ±
Z108A_15	***367000***	***140***	***48***	***86***	***0.33***	***17.17***	***0.24***	***0.6134***	***0.0084***	***0.2037***	***0.0012***
Z108A_9	***276000***	***122***	***56***	***80***	***0.47***	***15.83***	***0.52***	***0.56***	***0.018***	***0.204***	***0.0024***
Z108A_3	217000	101	38	55	0.35	17.38	0.7	0.618	0.02	0.2045	0.0033
Z108A_1	189000	80	36	55	0.46	17.19	0.15	0.6024	0.0057	0.2079	0.0016
Z108A_17	299000	135	120	160	0.87	16.45	0.46	0.562	0.013	0.2127	0.0021

table notes:
normal black font denotes metamorphic zircons, ***bold italics denotes magmatic zircons***, light grey denotes inherited zircons
denotes magmatic zircon ages interpreted to best represent the crystallization age

			age (Ma)									
$^{206*}Pb$ / $^{208*}Pb$	% ±	Disc. %	$^{206*}Pb$ / ^{238}U	±	**$^{207*}Pb$ / $^{206*}Pb$**	±	^{176}Lu / ^{177}Hf	^{176}Hf / ^{177}Hf	εHf(t)[1]	±2s	T_{DM}[2] (Ga)	location
~~10.06~~	***~~0.39~~***	***~~-7.92~~***	***~~3082~~***	***~~33~~***	***~~2856~~***	***~~10~~***	***~~0.000395~~***	***~~0.281042~~***	***~~2.7~~***	***~~1.6~~***	***~~3020~~***	***~~core~~***
~~7.81~~	***~~0.38~~***	***~~-0.18~~***	***~~2862~~***	***~~72~~***	***~~2857~~***	***~~19~~***	***~~0.000974~~***	***~~0.281121~~***	***~~4.4~~***	***~~2.6~~***	***~~2958~~***	***~~core~~***
10.32	0.74	-8.39	3101	80	2861	26	0.000292	0.281006	1.7	1.6	3060	core
8.47	0.12	-5.23	3039	23	2888	13	0.000387	0.280957	0.4	1.8	3134	core
4.268	0.079	1.74	2874	55	2925	16	0.001150	0.281051	3.1	2.5	3068	core

table notes:
normal black font denotes metamorphic zircons, ***bold italics denotes magmatic zircons***, light grey denotes inherited zircons
denotes magmatic zircon ages interpreted to best represent the crystallization age

zonation	notes

~~osc~~
~~osc~~
irregular
irregular
osc

table notes:
normal black font denotes metamorphic zircons, ***bold italics denotes magmatic zircons***, light grey denotes inherited zircons
denotes magmatic zircon ages interpreted to best represent the crystallization age

Appendix 5C - LASS-ICPMS Lu-Hf isotopic data from south transect samples

Spot name	$^{176}Yb/^{177}Hf$	±2s	$^{176}Lu/^{177}Hf$	±2s	$^{178}Hf/^{177}Hf$	$^{180}Hf/^{177}Hf$	$^{176}Hf/^{177}Hf$	±2s	$^{176}Hf_{(t)}/^{177}Hf$	εHf(t)[1]	±2s	age (Ma) T_{DM}[2] (Ga)	age (Ma) $^{207}Pb/^{206}Pb$
B007A, massive pegmatitic granite													
662715 6985512													
B007A - 25	0.00835	0.00061	0.000252	0.000016	1.467910	1.888340	0.280964	0.000043	0.280952	-9.8	1.7	3114	2426
B007A - 27	0.00629	0.00054	0.000190	0.000013	1.467650	1.887610	0.281007	0.000029	0.280998	-6.9	1.2	3051	2480
B007A - 16	0.02380	0.00130	0.000686	0.000033	1.467700	1.887700	0.281092	0.000034	0.281059	-4.3	1.4	2975	2497
B007A - 17	0.01161	0.00028	0.000352	0.000010	1.467770	1.887950	0.280998	0.000041	0.280981	-5.9	1.6	3076	2551
B007A - 26.2	0.00930	0.00230	0.000290	0.000069	1.467720	1.887690	0.281006	0.000100	0.280991	-4.4	3.6	3060	2596
B007A - 8	0.02590	0.00130	0.000809	0.000025	1.467520	1.887070	0.281033	0.000091	0.280992	-4.2	3.3	3065	2607
B007A - 10	0.00603	0.00031	0.000182	0.000006	1.467650	1.887680	0.281048	0.000039	0.281039	-1.9	1.6	2996	2635
B007A - 6	0.01358	0.00058	0.000387	0.000011	1.467460	1.887330	0.281092	0.000055	0.281072	-0.3	2.1	2952	2650
B007A - 2	0.00467	0.00013	0.000145	0.000006	1.467530	1.887310	0.281027	0.000049	0.281019	-2.1	1.9	3021	2655
B007A - 3	0.02157	0.00093	0.000635	0.000032	1.467450	1.887140	0.281062	0.000045	0.281029	-1.2	1.8	3012	2675
B007A - 13.2	0.00540	0.00069	0.000166	0.000021	1.467860	1.888280	0.281025	0.000045	0.281016	-0.9	1.8	3025	2708
B007A - 24	0.00665	0.00032	0.000206	0.000004	1.467560	1.887610	0.281030	0.000055	0.281019	-0.8	2.1	3022	2708
B007A - 1	0.01266	0.00014	0.000370	0.000002	1.467520	1.887250	0.281026	0.000038	0.281007	-1.3	1.5	3040	2709
B007A - 12	0.00541	0.00025	0.000170	0.000006	1.467640	1.887650	0.281020	0.000024	0.281011	-1.0	1.1	3032	2714
B007A - 9	0.01076	0.00014	0.000326	0.000005	1.467510	1.887350	0.281074	0.000034	0.281057	0.6	1.4	2972	2714
B007A - 15	0.00641	0.00017	0.000189	0.000010	1.467920	1.888280	0.281006	0.000069	0.280996	-1.5	2.6	3052	2715
B007A - 7	0.01523	0.00038	0.000456	0.000010	1.467890	1.887610	0.281003	0.000061	0.280979	-2.0	2.3	3077	2718
B007A - 26	0.02310	0.00470	0.000640	0.000110	1.467530	1.887680	0.280976	0.000120	0.280942	-3.3	4.3	3129	2719
B007A - 19	0.00861	0.00091	0.000266	0.000024	1.467530	1.887380	0.281039	0.000043	0.281025	-0.1	1.7	3014	2732
B007A - 23	0.00988	0.00060	0.000299	0.000021	1.467630	1.887600	0.281032	0.000058	0.281016	-0.4	2.2	3026	2733
B007A - 14	0.00637	0.00017	0.000186	0.000004	1.467880	1.888200	0.280993	0.000035	0.280983	-1.5	1.4	3069	2735
B007A - 21	0.00781	0.00026	0.000235	0.000005	1.467680	1.887980	0.280980	0.000045	0.280967	-1.9	1.8	3091	2741
B007A - 5	0.01049	0.00015	0.000318	0.000003	1.467470	1.887200	0.281050	0.000034	0.281033	0.5	1.4	3003	2743
B007A - 22	0.01570	0.00120	0.000459	0.000026	1.467850	1.888130	0.280965	0.000051	0.280940	-2.6	2.0	3129	2752
B007A - 4	0.03730	0.00620	0.001060	0.000180	1.467550	1.887310	0.281139	0.000082	0.281082	3.7	3.0	2940	2804
B007A - 11	0.01507	0.00043	0.000483	0.000011	1.467730	1.887880	0.281013	0.000054	0.280987	0.6	2.1	3066	2819
B007A - 13	0.09000	0.00200	0.002454	0.000097	1.468050	1.888390	0.281137	0.000093	0.281004	1.3	3.4	3055	2821
B007A - 4.2	0.04000	0.00220	0.001133	0.000061	1.467510	1.887230	0.281032	0.000084	0.280970	0.3	3.1	3093	2830
B007A - 20	0.02840	0.00800	0.000820	0.000200	1.467620	1.887620	0.280943	0.000048	0.280897	-0.9	1.9	3188	2891
B007A - 18	0.05650	0.00120	0.001543	0.000045	1.467620	1.887640	0.281118	0.000054	0.281032	4.3	2.1	3007	2905

Appendix 5C - LASS-ICPMS Lu-Hf isotopic data from south transect samples

Spot name	$^{176}Yb/^{177}Hf$	±2s	$^{176}Lu/^{177}Hf$	±2s	$^{178}Hf/^{177}Hf$	$^{180}Hf/^{177}Hf$	$^{176}Hf/^{177}Hf$	±2s	$^{176}Hf_{(t)}/^{177}Hf$	εHf(t)[1]	±2s	age (Ma) T_{DM}[2] (Ga)	age (Ma) $^{207}Pb/^{206}Pb$
T027A, mt bt syenogranite										-1.0		3044	
689036 7009198													
T027A - 1	0.01270	0.00160	0.000354	0.000049	1.467610	1.886670	0.281074	0.000087	0.281058	-7.6	3.2	2974	2359
T027A - 19	0.03370	0.00410	0.000906	0.000099	1.467310	1.886780	0.281072	0.000058	0.281028	-4.5	2.2	3020	2539
T027A - 14	0.03290	0.00480	0.000880	0.000100	1.467330	1.886720	0.281160	0.000069	0.281117	-1.3	2.6	2897	2540
T027A - 12	0.04310	0.00450	0.001120	0.000100	1.467360	1.886920	0.281162	0.000039	0.281107	-1.6	1.6	2913	2541
T027A - 16	0.01768	0.00040	0.000489	0.000007	1.467400	1.886670	0.281058	0.000049	0.281034	-3.5	1.9	3006	2571
T027A - 5	0.02247	0.00099	0.000533	0.000036	1.467340	1.886830	0.281076	0.000059	0.281049	-2.7	2.2	2985	2581
T027A - 15.2	0.02680	0.00240	0.000768	0.000077	1.467290	1.886660	0.281079	0.000069	0.281041	-2.8	2.6	2999	2593
T027A - 8	0.01159	0.00060	0.000357	0.000021	1.467360	1.886690	0.281068	0.000047	0.281050	-2.2	1.8	2982	2603
~~T027A - 3~~	~~0.02910~~	~~0.00290~~	~~0.000774~~	~~0.000081~~	~~1.467350~~	~~1.886550~~	~~0.281168~~	~~0.000064~~	~~0.281129~~	~~0.8~~	~~2.4~~	~~2879~~	~~2609~~
T027A - 21	0.01455	0.00053	0.000394	0.000014	1.467310	1.886740	0.281023	0.000054	0.281003	-3.7	2.0	3046	2612
T027A - 15	0.04160	0.00230	0.001038	0.000066	1.467310	1.886740	0.281094	0.000058	0.281042	-2.2	2.2	3000	2614
T027A - 11				0.000013				0.000052	0.281064	-1.1	2.0	2963	2628
T027A - 2				0.000130				0.000067	0.281117	1.5	2.5	2893	2660
T027A - 18	0.01320	0.00110	0.000333	0.000019	1.467240	1.886710	0.280979	0.000043	0.280962	-3.9	1.7	3100	2666
T027A - 17	0.03610	0.00690	0.000840	0.000140	1.467220	1.886820	0.281195	0.000150	0.281152	3.1	5.4	2847	2675
T027A - 6	0.01300	0.00130	0.000368	0.000035	1.467340	1.886730	0.281019	0.000048	0.281000	-2.1	1.9	3049	2682
T027A - 20	0.02885	0.00064	0.000753	0.000007	1.467290	1.886730	0.281116	0.000079	0.281077	0.7	2.9	2948	2684
T027A - 13	0.01670	0.00280	0.000416	0.000055	1.467280	1.886800	0.281079	0.000073	0.281057	0.3	2.7	2972	2698
T027A - 9	0.01541	0.00041	0.000391	0.000006	1.467360	1.886740	0.281067	0.000073	0.281046	0.0	2.7	2986	2703
T027A - 7	0.01971	0.00071	0.000496	0.000015	1.467310	1.886770	0.281100	0.000043	0.281074	1.7	1.7	2950	2732
T027A - 4	0.02653	0.00040	0.000700	0.000016	1.467400	1.886590	0.281072	0.000038	0.281035	0.4	1.5	3004	2738
T027A - 10	0.01610	0.00140	0.000383	0.000029	1.467250	1.886910	0.281101	0.000150	0.281080	2.5	5.4	2940	2756
										-2.4		2998	
S154A, bt mt monzogranite													
688784 7017312													
S154A - 2	0.01250	0.00140	0.000386	0.000045	1.467600	1.886600	0.281253	0.000058	0.281240	-14.9	2.1	2735	1766
S154A - 4	0.01069	0.00023	0.000342	0.000012	1.467550	1.886600	0.281036	0.000048	0.281019	-5.1	1.8	3024	2524
S154A - 10	0.01338	0.00033	0.000436	0.000006	1.467450	1.886580	0.281054	0.000028	0.281032	-3.6	1.2	3007	2570
S154A - 3	0.01260	0.00100	0.000377	0.000025	1.467450	1.886610	0.281012	0.000047	0.280992	-3.1	1.8	3059	2651
S154A - 16	0.00598	0.00039	0.000191	0.000011	1.467540	1.886610	0.280985	0.000032	0.280975	-2.1	1.4	3081	2722

Appendix 5C - LASS-ICPMS Lu-Hf isotopic data from south transect samples

Spot name	$^{176}Yb/^{177}Hf$	±2s	$^{176}Lu/^{177}Hf$	±2s	$^{178}Hf/^{177}Hf$	$^{180}Hf/^{177}Hf$	$^{176}Hf/^{177}Hf$	±2s	$^{176}Hf_{(t)}/^{177}Hf$	εHf(t)[1]	±2s	age (Ma) T_{DM}[2] (Ga)	age (Ma) $^{207}Pb/^{206}Pb$
S154A - 1	0.02430	0.00390	0.000684	0.000090	1.467410	1.886670	0.281182	0.000054	0.281146	4.3	2.1	2853	2734
S154A - 6	0.01580	0.00430	0.000450	0.000110	1.467420	1.886610	0.281078	0.000057	0.281053	2.8	2.2	2976	2810
S154A - 12	0.04960	0.00460	0.001450	0.000120	1.467400	1.886600	0.281217	0.000076	0.281138	5.9	2.8	2862	2813
S154A - 14	0.01980	0.00170	0.000594	0.000038	1.467430	1.886780	0.281039	0.000044	0.281007	1.3	1.7	3040	2816
S154A - 13	0.04460	0.00650	0.001230	0.000160	1.467390	1.886680	0.281261	0.000100	0.281194	8.1	3.6	2785	2822
S154A - 11	0.01448	0.00077	0.000449	0.000019	1.467450	1.886610	0.281039	0.000042	0.281014	2.3	1.7	3029	2847
S154A - 9	0.02720	0.00360	0.000796	0.000099	1.467410	1.886670	0.281127	0.000083	0.281083	4.9	3.1	2936	2854
S154A - 7				0.000022				0.000053	0.281123	6.3	2.0	2881	2856
S154A - 17				0.000067				0.000039	0.281035	3.7	1.6	3001	2879
S154A - 18	0.02043	0.00054	0.000626	0.000009	1.467350	1.886630	0.281030	0.000043	0.280995	2.7	1.7	3055	2893
S154A - 19	0.03100	0.00540	0.000900	0.000160	1.467410	1.886850	0.281099	0.000073	0.281049	4.7	2.7	2982	2898
S154A - 15	0.02140	0.00120	0.000663	0.000037	1.467430	1.886630	0.281098	0.000048	0.281061	5.4	1.9	2965	2909
S154A - 8	0.02200	0.00220	0.000659	0.000054	1.467430	1.886720	0.281090	0.000044	0.281053	5.2	1.7	2976	2912
										4.3		2996	
K015A, mafic tonalite													
693209 7030513													
K015A - 3	0.00794	0.00060	0.000287	0.000022	1.467390	1.886650	0.281172	0.000055	0.281162	-18.0	2.0	2837	1750
K015A - 11	0.00779	0.00037	0.000274	0.000008	1.467430	1.886880	0.281179	0.000066	0.281169	-17.6	2.4	2827	1755
K015A - 16	0.00276	0.00018	0.000086	0.000008	1.467340	1.886520	0.281182	0.000074	0.281178	-4.8	2.7	2809	2295
K015A - 9				0.000005				0.000200	0.280969	-9.1	7.1	3091	2430
K015A - 4				0.000180				0.000078	0.281010	-6.4	2.9	3042	2486
K015A - 2	0.02510	0.00860	0.000640	0.000190	1.467470	1.886630	0.281081	0.000150	0.281050	-4.2	5.4	2987	2517
K015A - 6	0.04310	0.00600	0.001120	0.000150	1.467420	1.886510	0.281202	0.000076	0.281147	-0.3	2.8	2858	2536
K015A - 8	0.02600	0.00820	0.000690	0.000210	1.467370	1.886860	0.281059	0.000090	0.281025	-3.8	3.3	3020	2573
K015A - 15	0.07090	0.00260	0.001729	0.000057	1.467340	1.886710	0.281237	0.000047	0.281151	1.1	1.8	2856	2590
K015A - 14	0.01330	0.00170	0.000389	0.000037	1.467390	1.886820	0.280961	0.000037	0.280941	-6.0	1.5	3129	2608
K015A - 7	0.01294	0.00047	0.000381	0.000012	1.467480	1.886750	0.280982	0.000046	0.280962	-4.9	1.8	3100	2620
K015A - 10	0.03740	0.00290	0.000960	0.000110	1.467460	1.886780	0.281195	0.000078	0.281146	1.6	2.9	2856	2620
K015A - 12	0.00902	0.00032	0.000280	0.000005	1.467430	1.886830	0.280973	0.000067	0.280959	-5.0	2.5	3104	2623
K015A - 17	0.02160	0.00210	0.000612	0.000049	1.467410	1.886640	0.281053	0.000063	0.281022	-2.7	2.3	3022	2623
K015A - 1	0.01032	0.00079	0.000311	0.000018	1.467500	1.886640	0.281034	0.000050	0.281018	-2.7	1.9	3024	2631
K015A - 5	0.01046	0.00058	0.000326	0.000017	1.467480	1.886610	0.280984	0.000051	0.280967	-3.7	2.0	3093	2665

Appendix 5C - LASS-ICPMS Lu-Hf isotopic data from south transect samples

Spot name	$^{176}Yb/^{177}Hf$	±2s	$^{176}Lu/^{177}Hf$	±2s	$^{178}Hf/^{177}Hf$	$^{180}Hf/^{177}Hf$	$^{176}Hf/^{177}Hf$	±2s	$^{176}Hf_{(t)}/^{177}Hf$	εHf(t)[1]	±2s	age (Ma) T_{DM}[2] (Ga)	age (Ma) $^{207}Pb/^{206}Pb$
K015A - 18	0.06300	0.01400	0.001480	0.000310	1.467330	1.886790	0.281231	0.000150	0.281154	3.5	5.4	2845	2688
K015A - 13	0.01190	0.00280	0.000333	0.000059	1.467430	1.886910	0.280992	0.000070	0.280974	-2.4	2.6	3083	2709
										-4.6		3089	
K015B, massive syenogranite													
693209 7030513													
K015B - 9	0.02070	0.00110	0.000514	0.000021	1.467420	1.886880	0.281049	0.000053	0.281025	-6.8	2.0	3020	2445
K015B - 13	0.04820	0.00150	0.001218	0.000042	1.467430	1.886750	0.281160	0.000070	0.281102	-3.2	2.6	2923	2481
K015B - 5	0.01990	0.00079	0.000515	0.000023	1.467400	1.886730	0.281134	0.000047	0.281109	-2.8	1.8	2905	2488
K015B - 7	0.03850	0.00680	0.000980	0.000170	1.467300	1.886640	0.281131	0.000080	0.281084	-3.7	2.9	2945	2489
K015B - 16	0.02250	0.00250	0.000567	0.000050	1.467250	1.886750	0.281106	0.000098	0.281079	-3.8	3.6	2947	2493
K015B - 19	0.02014	0.00081	0.000557	0.000014	1.467420	1.886810	0.281088	0.000053	0.281061	-3.8	2.0	2971	2518
K015B - 20	0.02840	0.00120	0.000775	0.000035	1.467380	1.886800	0.281158	0.000079	0.281120	-1.4	2.9	2892	2531
K015B - 11	0.02840	0.00290	0.000743	0.000059	1.467330	1.886670	0.281131	0.000110	0.281094	-1.7	4.0	2927	2555
K015B - 10	0.03010	0.00440	0.000768	0.000090	1.467340	1.886730	0.281167	0.000090	0.281129	-0.3	3.3	2880	2563
K015B - 8	0.03410	0.00880	0.000800	0.000150	1.466970	1.886810	0.281281	0.000300	0.281241	4.8	10.7	2726	2613
K015B - 4	0.04470	0.00180	0.001167	0.000044	1.467350	1.886720	0.281253	0.000062	0.281194	3.2	2.3	2791	2615
K015B - 2	0.03340	0.00150	0.000846	0.000036	1.467340	1.886890	0.281133	0.000086	0.281090	-0.3	3.1	2932	2625
K015B - 12	0.02110	0.00430	0.000577	0.000085	1.467350	1.886840	0.281100	0.000077	0.281071	-0.9	2.8	2956	2625
K015B - 14	0.02690	0.00390	0.000710	0.000110	1.467270	1.886680	0.281201	0.000100	0.281165	2.5	3.6	2829	2631
K015B - 18	0.02050	0.00210	0.000563	0.000060	1.467270	1.886780	0.281148	0.000045	0.281119	1.1	1.8	2890	2638
K015B - 6	0.03580	0.00350	0.000871	0.000056	1.467430	1.886850	0.281119	0.000085	0.281074	0.5	3.1	2953	2682
K015B - 15	0.03320	0.00660	0.000810	0.000120	1.467200	1.886710	0.281151	0.000130	0.281109	1.8	4.7	2905	2684
K015B - 17	0.02168	0.00046	0.000543	0.000022	1.467310	1.886750	0.281191	0.000110	0.281163	3.7	4.0	2830	2685
K015B - 3	0.01220	0.00150	0.000323	0.000048	1.467470	1.887030	0.281039	0.000057	0.281022	-0.7	2.2	3019	2709
K015B - 1	0.02907	0.00061	0.000709	0.000015	1.467380	1.886950	0.280925	0.000087	0.280888	-5.4	3.2	3204	2712
										2.9		2809	

Appendix 5C - LASS-ICPMS Lu-Hf isotopic data from south transect samples

Spot name	$\frac{^{176}Yb}{^{177}Hf}$	±2s	$\frac{^{176}Lu}{^{177}Hf}$	±2s	$\frac{^{178}Hf}{^{177}Hf}$	$\frac{^{180}Hf}{^{177}Hf}$	$\frac{^{176}Hf}{^{177}Hf}$	±2s	$\frac{^{176}Hf_{(t)}}{^{177}Hf}$	εHf(t)[1]	±2s	age (Ma) T_{DM}[2] (Ga)	age (Ma) $\frac{^{207}Pb}{^{206}Pb}$

Footnotes:

(1) Initial $^{176}Hf/^{177}Hf$ and εHf calculated using the 206/207Pb age determined by SHRIMP dating (see column f), and the CHUR parameters: $^{176}Lu/^{177}Hf$ = 0.0336, and $^{176}Hf/^{177}Hf$ = 0.282785 (Bouvier *et al*., 2008).

(2) depleted mantle model ages were calculated using the measured $^{176}Lu/^{177}Hf$ of each spot and a depleted mantle (DM) $^{176}Lu/^{177}Hf$ and $^{176}Hf/^{177}Hf$ of 0.038 and 0.283223, respectively (Vervoort and Blichert-Toft, 1999).

- data in grey are from magmatic zircon used to calculated the crystallization age of the unit
- strikethrough data did not meet minimum requirements and was not used in further calculations, plots or discussed in the text

Appendix 5D - LASS-ICPMS Lu-Hf isotopic data from north transect samples

Spot name	$^{176}Yb/^{177}Hf$	±2s	$^{176}Lu/^{177}Hf$	±2s	$^{178}Hf/^{177}Hf$	$^{180}Hf/^{177}Hf$	$^{176}Hf/^{177}Hf$	±2s	$^{176}Hf_{(t)}/^{177}Hf$	εHf(t)[1]	±2s	age (Ma) T_{DM}[2] (Ga)	age (Ma) $^{207}Pb/^{206}Pb$
Y032A, bt hbl opx granodiorite (charnockite)													
UTM 597219 7161320													
Y032A - 23	0.02220	0.00500	0.000730	0.000150	1.467260	1.886790	0.281033	0.000065	0.281000	-10.7	2.4	3059	2314
Y032A - 9	0.06660	0.00560	0.002100	0.000140	1.467270	1.886870	0.281130	0.000076	0.281035	-8.4	2.8	3036	2359
Y032A - 5	0.09900	0.01100	0.003040	0.000310	1.467270	1.886650	0.281212	0.000070	0.281071	-5.7	2.6	2996	2419
Y032A - 14	0.02840	0.00160	0.000790	0.000047	1.467340	1.886970	0.280953	0.000040	0.280916	-11.0	1.6	3172	2431
Y032A - 8	0.02820	0.00180	0.000910	0.000057	1.467320	1.886760	0.281045	0.000066	0.281001	-5.9	2.4	3057	2520
Y032A - 21	0.01810	0.00200	0.000527	0.000058	1.467400	1.886960	0.280739	0.000077	0.280713	-15.3	2.8	3438	2555
Y032A - 16	0.00632	0.00008	0.000187	0.000001	1.467430	1.887080	0.280869	0.000043	0.280859	-9.7	1.7	3235	2574
Y032A - 24	0.04210	0.00640	0.001160	0.000170	1.467330	1.886690	0.281009	0.000051	0.280951	-5.4	2.0	3126	2617
Y032A - 2	0.02520	0.00120	0.000779	0.000029	1.467380	1.886840	0.281028	0.000036	0.280989	-3.9	1.5	3069	2623
Y032A - 3	0.01580	0.00130	0.000496	0.000035	1.467320	1.886940	0.280989	0.000031	0.280963	-3.7	1.3	3100	2670
Y032A - 13	0.01440	0.00110	0.000464	0.000036	1.467360	1.886890	0.280951	0.000042	0.280927	-4.9	1.7	3148	2675
Y032A - 12	0.02670	0.00180	0.000852	0.000051	1.467320	1.886930	0.280982	0.000044	0.280938	-4.3	1.7	3138	2684
Y032A - 4	*0.05200*	*0.00350*	*0.001424*	*0.000094*	*1.467290*	*1.886800*	*0.281034*	*0.000064*	*0.280960*	*-2.8*	*2.4*	*3114*	*2713*
Y032A - 7	0.02943	0.00044	0.000844	0.000011	1.467380	1.886860	0.281014	0.000041	0.280970	-2.3	1.6	3094	2722
Y032A - 11	0.04061	0.00096	0.001148	0.000033	1.467350	1.886950	0.280994	0.000064	0.280934	-3.5	2.4	3146	2724
Y032A - 1	0.02950	0.00160	0.000849	0.000042	1.467340	1.886900	0.280923	0.000054	0.280923	-5.4	2.1	3218	2728
Y032A - 17	0.02096	0.00065	0.000596	0.000015	1.467310	1.886900	0.281090	0.000055	0.281059	1.0	2.1	2971	2728
Y032A - 22	0.01260	0.00250	0.000409	0.000073	1.467240	1.886820	0.281024	0.000058	0.281002	-0.9	2.2	3045	2731
Y032A - 18	0.01371	0.00070	0.000420	0.000021	1.467370	1.886780	0.280898	0.000047	0.280876	-5.3	1.8	3216	2737
Y032A - 10	0.00890	0.00180	0.000294	0.000053	1.467320	1.886870	0.280991	0.000043	0.280975	-1.5	1.7	3081	2747
Y032A - 15	0.01220	0.00150	0.000349	0.000036	1.467340	1.886860	0.280932	0.000040	0.280913	-3.7	1.6	3164	2746
Y032A - 6	0.02588	0.00044	0.000729	0.000014	1.467360	1.886690	0.281078	0.000045	0.281039	0.9	1.8	2998	2752
Y032A - 19	0.00571	0.00024	0.000181	0.000004	1.467320	1.886920	0.280823	0.000033	0.280813	-5.5	1.4	3296	2820
Y032A - 20	0.00572	0.00026	0.000175	0.000008	1.467300	1.886840	0.280724	0.000042	0.280714	-7.8	1.7	3427	2873
										-2.5		3110	
K037A, tonalite gneiss													
UTM 607104 7161794													
~~K037A - 21~~	~~0.00066~~	~~0.00018~~	~~0.000012~~	~~0.000003~~	~~1.467380~~	~~1.886870~~	~~0.281098~~	~~0.000045~~	~~0.281098~~	~~-23.8~~	~~1.7~~	~~2915~~	~~1598~~
~~K037A - 22~~	~~0.00142~~	~~0.00073~~	~~0.000027~~	~~0.000014~~	~~1.467330~~	~~1.886800~~	~~0.281113~~	~~0.000028~~	~~0.281112~~	~~-21.2~~	~~1.1~~	~~2896~~	~~1686~~
K037A - 11	0.00029	0.00003	0.000005	0.000001	1.467360	1.886860	0.281092	0.000052	0.281092	-19.9	1.9	2923	1774

Appendix 5D - LASS-ICPMS Lu-Hf isotopic data from north transect samples

Spot name	$^{176}Yb/^{177}Hf$	±2s	$^{176}Lu/^{177}Hf$	±2s	$^{178}Hf/^{177}Hf$	$^{180}Hf/^{177}Hf$	$^{176}Hf/^{177}Hf$	±2s	$^{176}Hf_{(t)}/^{177}Hf$	εHf(t)[1]	±2s	age (Ma) T_{DM}[2] (Ga)	age (Ma) $^{207}Pb/^{206}Pb$
~~K037A - 7~~	~~0.00116~~	~~0.00026~~	~~0.000024~~	~~0.000005~~	~~1.467300~~	~~1.886760~~	~~0.281153~~	~~0.000039~~	~~0.281152~~	~~-17.6~~	~~1.5~~	~~2842~~	~~1782~~
K037A - 16	0.00200	0.00160	0.000054	0.000046	1.467300	1.886930	0.281133	0.000054	0.281131	-18.3	2.0	2871	1783
K037A - 9	0.00010	0.00003	0.000001	0.000000	1.467360	1.886830	0.281116	0.000033	0.281116	-18.6	1.3	2890	1795
K037A - 8	0.00007	0.00004	0.000001	0.000000	1.467330	1.886920	0.281067	0.000040	0.281067	-20.1	1.5	2956	1805
K037A - 19	0.00060	0.00003	0.000011	0.000000	1.467300	1.886760	0.281163	0.000037	0.281163	-16.5	1.4	2828	1814
K037A - 20	0.00033	0.00004	0.000005	0.000000	1.467290	1.886830	0.281120	0.000029	0.281120	-17.8	1.2	2885	1823
K037A - 10	0.00017	0.00006	0.000004	0.000002	1.467320	1.886940	0.281142	0.000037	0.281142	-16.9	1.4	2856	1828
K037A - 24	0.00063	0.00017	0.000017	0.000005	1.467280	1.886870	0.281156	0.000042	0.281156	-16.3	1.6	2838	1832
K037A - 18	0.00210	0.00140	0.000054	0.000041	1.467330	1.886760	0.281142	0.000060	0.281140	-16.5	2.2	2859	1848
K037A - 12	0.00650	0.00240	0.000182	0.000070	1.467230	1.886760	0.281116	0.000036	0.281110	-17.2	1.4	2904	1865
K037A - 25	0.00126	0.00053	0.000034	0.000015	1.467390	1.886910	0.281135	0.000043	0.281134	-16.2	1.6	2867	1870
~~K037A - 11.2~~	~~0.01210~~	~~0.00210~~	~~0.000347~~	~~0.000056~~	~~1.467280~~	~~1.886810~~	~~0.281110~~	~~0.000099~~	~~0.281095~~	~~-7.2~~	~~3.6~~	~~2924~~	~~2322~~
~~K037A - 2~~	~~0.01325~~	~~0.00025~~	~~0.000359~~	~~0.000006~~	~~1.467340~~	~~1.886780~~	~~0.280824~~	~~0.000057~~	~~0.280807~~	~~-13.4~~	~~2.1~~	~~3309~~	~~2492~~
K037A - 4	0.01486	0.00068	0.000398	0.000020	1.467310	1.886820	0.280842	0.000031	0.280823	-12.6	1.3	3288	2503
K037A - 6	0.02630	0.00240	0.000666	0.000047	1.467280	1.886780	0.280894	0.000064	0.280862	-9.8	2.4	3241	2563
K037A - 14	0.01761	0.00035	0.000469	0.000009	1.467350	1.886880	0.280874	0.000050	0.280851	-10.2	1.9	3251	2565
K037A - 1	0.03820	0.00059	0.000957	0.000022	1.467310	1.886830	0.281009	0.000052	0.280962	-6.0	2.0	3109	2574
~~K037A - 26~~	~~0.01760~~	~~0.00210~~	~~0.000496~~	~~0.000044~~	~~1.467340~~	~~1.886870~~	~~0.281202~~	~~0.000085~~	~~0.281177~~	~~2.5~~	~~3.1~~	~~2811~~	~~2610~~
K037A - 17	0.03990	0.00500	0.000990	0.000130	1.467260	1.886810	0.281003	0.000080	0.280953	-5.1	2.9	3120	2627
K037A - 23	0.01430	0.00110	0.000399	0.000031	1.467320	1.886690	0.280845	0.000090	0.280825	-9.2	3.3	3284	*2644*
K037A - 5	0.04140	0.00220	0.001027	0.000032	1.467330	1.886930	0.280899	0.000049	0.280847	-8.0	1.9	3265	*2663*
K037A - 15	0.02151	0.00053	0.000570	0.000012	1.467260	1.886860	0.280970	0.000041	0.280941	-4.1	1.6	3130	*2686*
K037A - 3	0.02590	0.00260	0.000669	0.000065	1.467390	1.886970	0.280809	0.000072	0.280775	-9.9	2.7	3356	*2692*
										-7.4		3222	
F157A, bt mt ep monzogranite													
UTM 622813 7160311													
F157A - 14.2	0.02070	0.00230	0.000642	0.000068	1.467260	1.886820	0.281194	0.000046	0.281172	-16.1	1.7	2832	1819
F157A - 20	0.00635	0.00061	0.000200	0.000020	1.467340	1.886790	0.281099	0.000044	0.281092	-17.6	1.7	2928	1877
~~F157A - 14~~	~~0.01327~~	~~0.00049~~	~~0.000394~~	~~0.000018~~	~~1.467300~~	~~1.886960~~	~~0.281148~~	~~0.000047~~	~~0.281130~~	~~-2.7~~	~~1.8~~	~~2876~~	~~2459~~
F157A - 13	0.01950	0.00290	0.000566	0.000076	1.467310	1.886810	0.281139	0.000039	0.281111	-0.2	1.6	2901	2597
F157A - 6	0.00735	0.00017	0.000215	0.000004	1.467290	1.886830	0.281079	0.000037	0.281068	-1.1	1.5	2956	2623
~~F157A - 16~~	~~0.00945~~	~~0.00045~~	~~0.000277~~	~~0.000007~~	~~1.467340~~	~~1.886790~~	~~0.281081~~	~~0.000037~~	~~0.281067~~	~~-1.0~~	~~1.5~~	~~2958~~	~~2629~~

Appendix 5D - LASS-ICPMS Lu-Hf isotopic data from north transect samples

Spot name	$^{176}Yb/^{177}Hf$	±2s	$^{176}Lu/^{177}Hf$	±2s	$^{178}Hf/^{177}Hf$	$^{180}Hf/^{177}Hf$	$^{176}Hf/^{177}Hf$	±2s	$^{176}Hf_{(t)}/^{177}Hf$	εHf(t)[1]	±2s	age (Ma) T_{DM}[2] (Ga)	age (Ma) $^{207}Pb/^{206}Pb$
F157A - 4	0.01260	0.00110	0.000363	0.000026	1.467290	1.887010	0.281154	0.000048	0.281136	1.5	1.8	2866	2630
~~F157A -7~~	~~0.01620~~	~~0.00200~~	~~0.000451~~	~~0.000050~~	~~1.467280~~	~~1.886580~~	~~0.281288~~	~~0.000059~~	~~0.281265~~	~~6.5~~	~~2.2~~	~~2691~~	~~2648~~
F157A - 11	0.02080	0.00330	0.000584	0.000072	1.467320	1.886810	0.281172	0.000089	0.281143	2.2	3.2	2858	2650
F157A - 12	0.00926	0.00044	0.000274	0.000016	1.467280	1.886760	0.281084	0.000033	0.281070	-0.4	1.4	2954	2651
F157A - 8	0.01312	0.00091	0.000401	0.000021	1.467310	1.886770	0.281081	0.000036	0.281061	-0.6	1.5	2967	2655
F157A -5	0.02450	0.00150	0.000652	0.000026	1.467320	1.886840	0.281365	0.000084	0.281332	9.1	3.1	2600	2657
F157A - 1	0.01500	0.00180	0.000449	0.000050	1.467260	1.886720	0.281087	0.000048	0.281064	-0.3	1.9	2963	2661
F157A - 9	0.01337	0.00054	0.000400	0.000006	1.467280	1.886810	0.281150	0.000052	0.281130	2.2	2.0	2874	2668
~~F157A - 22~~	~~0.00975~~	~~0.00008~~	~~0.000277~~	~~0.000005~~	~~1.467330~~	~~1.886930~~	~~0.281081~~	~~0.000042~~	~~0.281067~~	~~0.1~~	~~1.7~~	~~2958~~	~~2674~~
F157A - 2	0.01400	0.00170	0.000424	0.000045	1.467320	1.886680	0.281085	0.000038	0.281063	0.2	1.5	2964	2684
F157A - 19	0.01100	0.00100	0.000313	0.000025	1.467340	1.886790	0.281113	0.000032	0.281097	1.4	1.3	2918	2684
~~F157A - 10~~	~~0.02690~~	~~0.00140~~	~~0.000754~~	~~0.000041~~	~~1.467300~~	~~1.886880~~	~~0.281290~~	~~0.000053~~	~~0.281251~~	~~7.0~~	~~2.0~~	~~2710~~	~~2691~~
F157A - 23	0.00936	0.00081	0.000283	0.000028	1.467350	1.887020	0.281088	0.000050	0.281074	0.7	1.9	2949	2692
F157A - 15	0.01034	0.00032	0.000302	0.000011	1.467290	1.886780	0.281096	0.000035	0.281081	1.1	1.4	2940	2695
F157A - 3	0.00891	0.00022	0.000270	0.000007	1.467340	1.886800	0.281069	0.000049	0.281055	0.5	1.9	2973	2711
~~F157A - 21.2~~	~~0.01080~~	~~0.00180~~	~~0.000348~~	~~0.000054~~	~~1.467380~~	~~1.886890~~	~~0.281059~~	~~0.000063~~	~~0.281041~~	~~0.5~~	~~2.4~~	~~2993~~	~~2732~~
F157A - 18	0.00494	0.00027	0.000174	0.000016	1.467400	1.886730	0.280971	0.000035	0.280962	-1.0	1.5	3097	2788
F157A - 17	0.01000	0.00096	0.000308	0.000029	1.467310	1.886810	0.281017	0.000033	0.281001	1.4	1.4	3046	2833
F157A - 21	0.05100	0.01400	0.001440	0.000350	1.467240	1.887110	0.281162	0.000140	0.281081	6.5 0.8	5.1	2937 2949	2924
H055A, bt mt hbl monzogranite													
UTM 630315 7089316													
H055A - 13	0.01370	0.00160	0.000361	0.000033	1.467300	1.886800	0.281126	0.000052	0.281108	-0.1	2.0	2904	2604
H055A - 19	0.01879	0.00031	0.000570	0.000012	1.467330	1.886770	0.281141	0.000048	0.281112	0.8	1.8	2900	2635
H055A - 2	0.01960	0.00160	0.000569	0.000042	1.467310	1.886840	0.281133	0.000053	0.281104	1.0	2.0	2911	2659
H055A - 15	0.01740	0.00100	0.000491	0.000023	1.467350	1.886830	0.281180	0.000044	0.281155	3.0	1.7	2841	2666
H055A - 12	0.02800	0.00190	0.000804	0.000042	1.467360	1.886830	0.281182	0.000051	0.281140	2.7	1.9	2862	2676
H055A - 3	0.03300	0.00270	0.000916	0.000071	1.467320	1.886760	0.281181	0.000053	0.281134	2.8	2.0	2871	2689
H055A - 18	0.02380	0.00120	0.000683	0.000033	1.467330	1.886740	0.281148	0.000045	0.281112	2.4	1.8	2899	2705
H055A - 21	0.01885	0.00080	0.000566	0.000021	1.467350	1.886740	0.281112	0.000045	0.281082	1.7	1.8	2939	2720
H055A - 4	0.01022	0.00038	0.000287	0.000008	1.467360	1.886850	0.281095	0.000032	0.281080	1.7	1.4	2941	2723
H055A - 1	0.00994	0.00050	0.000285	0.000011	1.467240	1.886850	0.281093	0.000034	0.281078	1.6	1.4	2943	2724

Appendix 5D - LASS-ICPMS Lu-Hf isotopic data from north transect samples

Spot name	$^{176}Yb/^{177}Hf$	±2s	$^{176}Lu/^{177}Hf$	±2s	$^{178}Hf/^{177}Hf$	$^{180}Hf/^{177}Hf$	$^{176}Hf/^{177}Hf$	±2s	$^{176}Hf_{(t)}/^{177}Hf$	εHf(t)[1]	±2s	age (Ma) T_{DM}[2] (Ga)	age (Ma) $^{207}Pb/^{206}Pb$
H055A - 16	0.02230	0.00260	0.000623	0.000065	1.467450	1.887010	0.281142	0.000039	0.281109	3.0	1.6	2902	2733
H055A - 14	0.02870	0.00170	0.000807	0.000049	1.467300	1.886810	0.281130	0.000045	0.281087	2.2	1.8	2933	2733
H055A - 7	0.01360	0.00190	0.000433	0.000033	1.467370	1.886800	0.281123	0.000035	0.281100	2.9	1.4	2914	2745
H055A - 6	0.01662	0.00097	0.000507	0.000024	1.467310	1.886710	0.281131	0.000054	0.281104	3.1	2.1	2909	2746
H055A - 9	0.02230	0.00240	0.000636	0.000059	1.467360	1.886830	0.281136	0.000044	0.281102	3.1	1.7	2912	2749
H055A - 23	0.01650	0.00150	0.000480	0.000032	1.467350	1.886960	0.281086	0.000048	0.281060	1.6	1.9	2967	2750
H055A - 11	0.02100	0.00190	0.000585	0.000045	1.467360	1.886870	0.281134	0.000055	0.281103	3.2	2.1	2910	2754
H055A - 8	0.02430	0.00120	0.000669	0.000029	1.467350	1.886770	0.281141	0.000045	0.281105	3.4	1.8	2907	2759
H055A - 17	0.02354	0.00058	0.000699	0.000017	1.467330	1.886960	0.281130	0.000040	0.281093	3.1	1.6	2925	2763
H055A - 10	0.01699	0.00090	0.000508	0.000026	1.467360	1.886900	0.281083	0.000051	0.281055	2.5	2.0	2974	2795
H055A - 5	0.00860	0.00240	0.000267	0.000062	1.467320	1.886860	0.281053	0.000056	0.281038	1.9	2.1	2995	2796
H055A - 20	0.01023	0.00023	0.000277	0.000003	1.467350	1.886730	0.281079	0.000030	0.281064	2.8	1.3	2961	2797
H055A - 22	0.01223	0.00062	0.000343	0.000012	1.467290	1.886900	0.281080	0.000043	0.281061	4.5	1.7	2965	2871
										2.8		2922	
Z108A, bt mt monzogranite													
UTM 662246 7122133													
~~Z108A - 21~~	~~0.02237~~	~~0.00085~~	~~0.000695~~	~~0.000030~~	~~1.467340~~	~~1.886820~~	~~0.281037~~	~~0.000046~~	~~0.280998~~	~~-6.2~~	~~1.8~~	~~3051~~	~~2504~~
~~Z108A - 13~~	~~0.05330~~	~~0.00140~~	~~0.001321~~	~~0.000048~~	~~1.467290~~	~~1.886650~~	~~0.281255~~	~~0.000110~~	~~0.281185~~	~~0.8~~	~~4.0~~	~~2800~~	~~2516~~
Z108A - 22	0.02550	0.00220	0.000772	0.000062	1.467330	1.886780	0.281069	0.000053	0.281025	-4.8	2.0	3013	2521
Z108A - 8	0.02652	0.00045	0.000772	0.000018	1.467350	1.886770	0.281080	0.000044	0.281041	-3.8	1.7	2998	2546
Z108A - 14	0.02480	0.00160	0.000736	0.000034	1.467310	1.886680	0.281066	0.000030	0.281027	-4.2	1.3	3014	2546
~~Z108A - 13 - 2~~	~~0.02650~~	~~0.00120~~	~~0.000791~~	~~0.000017~~	~~1.467210~~	~~1.886510~~	~~0.281095~~	~~0.000130~~	~~0.281053~~	~~-2.7~~	~~4.7~~	~~2979~~	~~2572~~
Z108A - 6	0.02468	0.00095	0.000707	0.000037	1.467350	1.886680	0.281089	0.000066	0.281054	-2.6	2.4	2981	2578
Z108A - 5	0.04580	0.00640	0.001170	0.000140	1.467330	1.886580	0.281185	0.000100	0.281128	1.6	3.6	2885	2650
Z108A - 19.2	0.02560	0.00420	0.000730	0.000120	1.467260	1.886710	0.281131	0.000094	0.281091	1.9	3.4	2926	2712
Z108A - 7	0.02770	0.00250	0.000745	0.000067	1.467300	1.886750	0.281067	0.000061	0.281030	-0.1	2.3	3014	2727
Z108A - 12	0.02590	0.00160	0.000689	0.000028	1.467290	1.886600	0.281084	0.000083	0.281047	1.0	3.0	2986	2743
Z108A - 11	0.02950	0.00430	0.000820	0.000130	1.467240	1.886690	0.281116	0.000053	0.281072	2.5	2.0	2953	2769
Z108A - 10	0.05380	0.00740	0.001430	0.000210	1.467390	1.886680	0.281120	0.000090	0.281045	1.5	3.3	2995	2771
~~Z108A - 19~~	~~0.03420~~	~~0.00550~~	~~0.000870~~	~~0.000120~~	~~1.467260~~	~~1.886660~~	~~0.281109~~	~~0.000082~~	~~0.281061~~	~~2.2~~	~~3.0~~	~~2966~~	~~2772~~
Z108A - 20	0.02740	0.00200	0.000756	0.000039	1.467380	1.886880	0.281049	0.000044	0.281007	0.4	1.7	3039	2777
Z108A - 16	0.02700	0.00230	0.000743	0.000076	1.467310	1.886800	0.281105	0.000061	0.281065	2.7	2.3	2962	2790

Appendix 5D - LASS-ICPMS Lu-Hf isotopic data from north transect samples

Spot name	$^{176}Yb/^{177}Hf$	±2s	$^{176}Lu/^{177}Hf$	±2s	$^{178}Hf/^{177}Hf$	$^{180}Hf/^{177}Hf$	$^{176}Hf/^{177}Hf$	±2s	$^{176}Hf_{(t)}/^{177}Hf$	εHf(t)[1]	±2s	age (Ma) T_{DM}[2] (Ga)	age (Ma) $^{207}Pb/^{206}Pb$
Z108A - 4	0.02090	0.00330	0.000559	0.000084	1.467360	1.886650	0.281103	0.000064	0.281076	3.1	2.4	2950	2795
Z108A - 18	0.01350	0.00120	0.000373	0.000030	1.467260	1.886540	0.281066	0.000068	0.281045	2.3	2.5	2986	2801
Z108A - 2	0.02250	0.00210	0.000579	0.000049	1.467230	1.886650	0.281133	0.000075	0.281105	4.9	2.8	2911	2827
Z108A - 15	0.01360	0.00240	0.000395	0.000064	1.467310	1.886630	0.281042	0.000040	0.281021	2.7	1.6	3020	2856
Z108A - 9	0.03640	0.00210	0.000974	0.000052	1.467230	1.886730	0.281121	0.000071	0.281070	4.4	2.6	2958	2857
Z108A - 3	0.01170	0.00250	0.000292	0.000044	1.467230	1.886660	0.281006	0.000041	0.280992	1.7	1.6	3060	2860
Z108A - 1	0.01185	0.00048	0.000387	0.000018	1.467390	1.886900	0.280957	0.000047	0.280938	0.4	1.8	3134	2888
Z108A - 17	0.04020	0.00470	0.001150	0.000110	1.467260	1.886780	0.281051	0.000066	0.280989	3.1	2.5	3068	2925
										1.7		2986	

Footnotes:

(1) Initial $^{176}Hf/^{177}Hf$ and εHf calculated using the 206/207Pb age determined by SHRIMP dating (see column f), and the CHUR parameters: $^{176}Lu/^{177}Hf$ = 0.0336, and $^{176}Hf/^{177}Hf$ = 0.282785 (Bouvier *et al*., 2008).

(2) depleted mantle model ages were calculated using the measured $^{176}Lu/^{177}Hf$ of each spot and a depleted mantle (DM) $^{176}Lu/^{177}Hf$ and $^{176}Hf/^{177}Hf$ of 0.038 and 0.283223, respectively (Vervoort and Blichert-Toft, 1999).

- data in grey are from magmatic zircon used to calculated the crystallization age of the unit
- strikethrough data did not meet minimum requirements and was not used in further calculations, plots or discussed in the text

Appendix 5E – Whole Rock Sm-Nd isotopic data from south and north transect samples

Sample	location	lithology	$^{143}Nd/^{144}Nd$	± 2 s.e.	$^{147}Sm/^{144}Nd$	$\varepsilon Nd_{(0)}$ using 0.512638	$\varepsilon Nd_{(0)}$ using 0.511847	T_{DM} (y)
B007A	South	massive granite	0.510508	0.000003	0.1142	-41.6	-26.2	4008623866
T027A	South	mt syenogranite	0.510440	0.000003	0.0691	-42.9	-27.5	2838542518
S154A	South	mt mozgranite	0.510971	0.000002	0.0971	-32.5	-17.1	2831870248
K015A	South	mafic tonalite	0.510916	0.000002	0.1028	-33.6	-18.2	3048854762
K015B	South	syenogranite	0.511029	0.000002	0.0671	-31.4	-16.0	2196177496
Y032A	North	charnockite	0.510701	0.000001	0.0996	-37.8	-22.4	3248236276
K037A	North	tonalite	0.510929	0.000002	0.1032	-33.3	-17.9	3043587602
F157A	North	mzgranite	0.510688	0.000002	0.0836	-38.0	-22.6	2866711813
H055A	North	bt-mt-hbl mzgran	0.510769	0.000002	0.0862	-36.5	-21.1	2829024619
Z108A	North	bt-mt mzgran	0.511111	0.000002	0.1014	-29.8	-14.4	2752306307

calclation values:

	εNd
143/144 Nd CHUR =	0.512638
147Sm/144Nd CHUR =	0.1967

	TDM (y)
DM 143Nd/144Nd	0.51315
DM 147Sm/144Nd	0.2137 (per year)

$\lambda = 6.54 \times 10^{-12}$

half life = 106 Ga

DePaolo and Caltech:

CHUR 143Nd/144Nd = 0.511847

CHUR 147Sm/144Nd = 0.1967

Appendix 5E – Whole Rock Sm-Nd isotopic data from south and north transect samples

Sample	T_{DM} (Ga)	$^{207}Pb/^{206}Pb$ age (Ma)	± 2 s.e.	$^{143}Nd/^{144}Nd_{(t)}$	$^{143}Nd/^{144}Nd_{CHUR(t)}$	$\varepsilon Nd_{(t)}$	± 2 s.e.
B007A	4.01	2.73E+09	9	0.50845	0.50910	-12.7	0.6
T027A	2.84	2.61E+09	15	0.50925	0.50925	1.1	0.8
S154A	2.83	2.90E+09	17	0.50911	0.50887	3.5	0.7
K015A	3.05	2.66E+09	39	0.50911	0.50918	-1.8	0.6
K015B	2.2	2.63E+09	12	0.50987	0.50923	13.6	0.8
Y032A	3.25	2.73E+09	9	0.50891	0.50910	-3.7	0.6
K037A	3.04	2.69E+09	26	0.50910	0.50915	-1.1	0.6
F157A	2.87	2.68E+09	10	0.50921	0.50916	0.9	0.7
H055A	2.83	2.75E+09	8	0.50920	0.50907	2.5	0.7
Z108A	2.75	2.78E+09	20	0.50925	0.50903	4.3	0.7

APPENDIX 5F - Lithogeochemical data from south and north transect samples.

Southern Transect

SampleID	UTM coordinates		Field Lithology	Q	Ab	Or	SiO2	Al2O3	Fe2O3(T)	MnO	MgO	CaO	Na2O	K2O	TiO2	P2O5	LOI
B007A	662715	6985512	granodiorite	46.0	44.2	9.9	71.34	15.42	2.96	0.026	0.97	3.84	3.91	1.25	0.321	0.09	0.67
T027A	689036	7009198	syenogranite	35.1	32.6	32.3	72.28	14.46	2.77	0.03	0.53	1.85	3.34	4.73	0.232	0.13	0.44
S154A	688784	7017312	monzogranite	38.6	49.8	11.6	68.49	15.83	4	0.057	1.36	4.01	4.27	1.42	0.438	0.12	0.44
K015A	693209	7030513	tonalite	12.9	54.5	32.6	57.6	15.5	8.23	0.142	3.17	5.7	3.76	3.22	1.448	0.37	0.56
K015B	693209	7030513	syenogranite	31.8	32.3	35.9	71.19	14.54	2.72	0.032	0.54	1.4	3.34	5.32	0.329	0.09	0.48

Northern Transect

Sample ID	UTM coordinates		Field Lithology	Q	Ab	Or	SiO2	Al2O3	Fe2O3(T)	MnO	MgO	CaO	Na2O	K2O	TiO2	P2O5	LOI
Y032A	597219	7161320	granodiorite	16.8	52.4	30.8	58.74	16.28	7.4	0.087	3.03	5.43	3.69	3.11	0.624	0.28	0.31
K037A	607104	7161794	tonalite	43.5	39.3	17.2	73.58	14.36	2.37	0.053	0.56	2.28	3.87	2.43	0.199	0.07	0.07
F157A	622813	7160311	monzogranite	37.1	52.2	10.6	69.94	15.91	3.53	0.04	1.12	3.44	4.73	1.38	0.38	0.11	0.31
H055A	630315	7089316	monzogranite	76.2	20.3	3.5	70.6	16.36	2.72	0.022	0.77	3.08	5.05	1.44	0.354	0.09	0.09
Z108A	662246	7122133	monzogranite	38.7	48.3	13.0	70.96	15.37	2.26	0.036	0.6	3.05	4.54	1.75	0.23	0.11	0.37

APPENDIX 5F - Lithogeochemical data from south and north transect samples.

Southern Transect

SampleID	Total	Sc	Be	V	Cr	Co	Ni	Cu	Zn	Ga	Ge	As	Rb	Sr	Y	Zr	Nb	Mo	Ag
B007A	100.8	2	1	41	30	6	< 20	10	50	19	0.7	< 5	36	482	1.4	174	1.4	< 2	0.9
T027A	100.8	1	1	41	30	4	< 20	10	50	19	1.3	< 5	146	342	6.4	332	2.8	< 2	1.7
S154A	100.4	6	2	52	40	9	< 20	< 10	70	20	1.3	< 5	63	400	6.9	137	3.8	2	0.7
K015A	99.71	15	3	105	50	19	50	< 10	140	24	1.6	< 5	106	320	28.8	263	22.6	< 2	1.4
K015B	99.97	3	1	28	30	3	< 20	10	40	22	1.4	< 5	178	212	11.7	266	9	< 2	1.6

Northern Transect

Sample ID	Total	Sc	Be	V	Cr	Co	Ni	Cu	Zn	Ga	Ge	As	Rb	Sr	Y	Zr	Nb	Mo	Ag
Y032A	98.97	19	2	133	50	19	30	30	110	26	1.6	9	59	442	24.1	212	4.8	< 2	1.6
K037A	99.85	3	2	17	< 20	3	< 20	< 10	40	16	1.3	< 5	108	146	8.1	129	6.4	< 2	0.6
F157A	100.9	5	1	47	< 20	6	< 20	< 10	50	20	0.9	< 5	46	550	3.5	131	1.9	< 2	0.6
H055A	100.6	2	1	35	< 20	5	< 20	< 10	50	22	0.9	< 5	41	504	2.7	86	< 0.2	< 2	< 0.5
Z108A	99.28	2	< 1	19	< 20	3	< 20	< 10	40	18	1	< 5	67	347	5.9	126	3.4	< 2	0.6

APPENDIX 5F - Lithogeochemical data from south and north transect samples.

Southern Transect

SampleID	In	Sn	Sb	Cs	Ba	La	Ce	Pr	Nd	Sm	Eu	Gd	Tb	Dy	Ho	Er	Tm	Yb	Lu
B007A	< 0.1	< 1	< 0.2	0.1	540	21	31.3	2.9	8.54	1.11	0.755	0.5	0.06	0.25	0.04	0.12	0.019	0.13	0.019
T027A	< 0.1	< 1	< 0.2	0.9	1225	91.7	175	17.9	54.4	6.43	0.888	3.06	0.33	1.37	0.22	0.62	0.084	0.47	0.07
S154A	< 0.1	< 1	< 0.2	1	338	18.8	35.9	4.39	16	2.5	0.794	1.79	0.24	1.26	0.23	0.65	0.088	0.61	0.08
K015A	< 0.1	3	< 0.2	0.7	866	53.8	116	14.9	56.3	9.51	2.09	6.85	0.98	5.01	0.96	2.56	0.375	2.53	0.356
K015B	< 0.1	< 1	< 0.2	0.3	1356	140	228	24.8	76.5	8.95	1.01	4.87	0.57	2.43	0.4	0.99	0.114	0.59	0.086

Northern Transect

Sample ID	In	Sn	Sb	Cs	Ba	La	Ce	Pr	Nd	Sm	Eu	Gd	Tb	Dy	Ho	Er	Tm	Yb	Lu
Y032A	< 0.1	< 1	< 0.2	0.1	1194	80	153	17.8	64.4	10.8	1.42	6.57	0.93	4.73	0.9	2.34	0.317	1.93	0.246
K037A	< 0.1	< 1	< 0.2	2.4	580	20.2	34.4	3.46	11.8	1.96	0.468	1.56	0.23	1.32	0.25	0.77	0.107	0.74	0.115
F157A	< 0.1	< 1	< 0.2	0.6	415	24.9	46.9	5.1	17.3	2.36	0.701	1.45	0.16	0.7	0.12	0.33	0.04	0.24	0.038
H055A	< 0.1	< 1	< 0.2	0.3	564	14.8	26.1	2.9	10.2	1.47	0.538	0.84	0.11	0.55	0.09	0.24	0.03	0.2	0.028
Z108A	< 0.1	< 1	< 0.2	6.2	536	23.1	26.8	4.45	16.3	2.79	0.539	2.15	0.25	1.15	0.2	0.54	0.066	0.36	0.047

APPENDIX 5F - Lithogeochemical data from south and north transect samples.

Southern Transect								
SampleID	Hf	Ta	W	Tl	Pb	Bi	Th	U
B007A	3.8	0.04	< 0.5	0.16	5	< 0.1	0.47	0.12
T027A	8.2	0.12	< 0.5	0.66	20	< 0.1	26.7	0.82
S154A	3.3	0.26	< 0.5	0.33	7	< 0.1	2.34	0.2
K015A	5.7	1.17	< 0.5	0.48	13	< 0.1	2.79	1.25
K015B	6.4	0.41	< 0.5	0.69	15	< 0.1	24.1	0.97

Northern Transect								
Sample ID	Hf	Ta	W	Tl	Pb	Bi	Th	U
Y032A	4.8	0.13	< 0.5	0.32	9	< 0.1	1.81	0.25
K037A	3.4	0.68	< 0.5	0.53	12	< 0.1	8.15	1.63
F157A	2.9	0.05	14.7	0.23	6	< 0.1	4.56	0.11
H055A	2.1	0.04	< 0.5	0.31	< 5	< 0.1	0.43	0.1
Z108A	3.1	0.16	< 0.5	0.34	7	< 0.1	2.81	0.25

6. Chapter 6. Summary, significance and future work

6.1. Summary and significance of the thesis

In the formation of supercontinents, such as Laurentia, the crustal processes governing terrane amalgamation have long been considered complex and important to study given the interconnection with the evolution of the Earth's biosphere (e.g. Worsley et al., 1986; Hoffman et al., 1998; Murphy et al., 2009). Although, the ways that Archean cratons and intervening Paleoproterozoic orogenic belts interact is quite varied, the governing processes have adhered to fairly consistent principles of crustal growth and recycling throughout geologic time. The Trans-Hudson orogen (THO) of Laurentia has been shown to be analogous in size, scope and duration to the Himalaya orogen (e.g. St-Onge et al., 2006), with the THO providing an excellent opportunity to examine deeper crustal sections of a large, hot orogen. The well exposed Archean and Paleoproterozoic rocks of the THO have been a venue of field-based geological investigation with increasingly detailed studies over the last 30 years (e.g. Hoffman, 1988; Ansdell, 2005; Henrique-Pinto et al., 2017) and regional compilation publications in the last 10 years (e.g. St-Onge et al., 2009; Corrigan et al., 2009). Since then, more detailed fieldwork and technological advances in the sensitivity, precision and speed of micro analytical techniques has led to increasingly innovative and complex data being obtained throughout different geologic terranes in the THO. This thesis builds upon existing investigations, and the growing dataset for the THO, which will continue to be used by international researchers to elucidate more detailed geologic histories, link larger regions that have overlapping geologic histories and propose more detailed and realistic geologic tectonic correlation models.

This thesis presents detailed geological mapping (Chapter 2) and analytical results using several isotopic systems (U-Pb, Lu-Hf and Sm-Nd; Chapters 3, 4 and 5) in order to characterize

the complex Archean geologic history of eastern Hall Peninsula. Firstly, SHRIMP U-Pb analyses (Geological Survey of Canada) on zircons from Archean orthogneisses within the snow bowl area yielded crystallization ages of ca. 2.98 to 2.75 Ga, expanding the known age range of rocks in the region (Chapter 3). In addition, Archean metamorphism between ca. 2.74 and 2.70 Ga was identified for the first time (Chapter 3). The snow bowl area was found to be lithologically heterogeneous and due to its location and size not representative of the entire region. Therefore, the emerging field of LASS-ICPMS analyses was employed on samples regionally representative of the Archean orthogneiss complex (University of Alberta, Arctic Resources Laboratory). In this technique, U-Pb and Lu-Hf isotopes were measured simultaneously at the same analytical spot and yielded information about the crystallization age of the zircon as well as the time of melt extraction from the mantle, effectively tracing the history of the parental magma. Another benefit of coupled U-Pb and Lu-Hf isotopic data on zircon was the additional support for the interpretation of inherited vs. magmatic vs. metamorphic zircon domains, especially in complexly zoned zircons that experienced a poly-deformational history. Assessing variations in Lu-Hf data during ablation of the zircon crystal reinforced initial interpretations of zircon domains through BSE image analysis. In processing the isotopic analysis on zircon cores, the signals were cleaned up to exclude contributions from zircon overgrowths. The U-Pb crystallization ages for the regional (LASS-ICPMS) and snow bowl area (SHRIMP) overlap (range ca. 2.98 to 2.70 Ga). As mentioned above, Lu-Hf isotopic data yield information on the crustal residence time and mixing history of each rock unit. In general, orthogneisses older than ca. 2.74 Ga yielded positive εHf(t) signatures (between 0 to 7 ±2) and mean depleted mantle model ages from ca. 3.1 to 3.0 Ga indicating the time that protolith melt was extracted from the mantle. Initial crust formation at ca. 2976 Ma was then reworked periodically at ca. 2.93, 2.84-

2.81 and 2.77-2.69 Ma. Two orthogneiss samples younger than ca. 2740 Ma, yielded negative εHf(t) values ranging from -4 to -12 and mean depleted mantle model ages of ca. 3.4 and 3.3 Ga respectively, indicating derivation from the recycling of older, Paleoarchean crust yet to be identified in outcrop on Hall Peninsula. (Chapter 4).

As Lu-Hf data are non-existent in surrounding Archean domains, granitic samples from two transects across eastern Hall Peninsula were analyzed for Sm-Nd to compare with existing Sm-Nd isotopic data on the Meta Incognita microcontinent to the west. In addition, any regional patterns and mantle extraction/protolith histories derived from the Sm-Nd isotopic data were compared to the Lu-Hf isotopic data for eastern Hall Peninsula. One transect covered the northern portion of the Archean orthogneiss complex, while the second transect covered the southern region. The Sm-Nd and Lu-Hf isotopic results showed similar results, outlining a general trend of negative $\varepsilon Nd_{(t)}$ and $\varepsilon Hf_{(t)}$ in the west along the boundary between Paleoproterozoic and Archean rocks to positive $\varepsilon Nd_{(t)}$ and $\varepsilon Hf_{(t)}$ towards the east within the Archean orthogneiss complex (Chapter 5). This data indicates the presence of significant crustal reworking and recycling in the west with more juvenile crust, derived from the mantle at ca. 3,1 Ga towards the east. While both Sm-Nd and Lu-Hf isotopic data provided similar data trends across the transects, the whole-rock sampling method for Sm-Nd analyses does not allow the isolation of minerals with specific ages and cannot be directly linked to a U-Pb crystallization age. Therefore, the LASS-ICPMS Lu-Hf data is recommended when working in complex metamorphic terranes in order to extract information both on the crystallization age and also the magmatic mixing history of the rock.

6.2. Going Further: A revised regional tectonic model

Archean rocks from eastern Hall Peninsula share an abundance of geological characteristics with rocks from adjacent crustal domains: Meta Incognita microcontinent to the west (Baffin Island), Cumberland Peninsula to the north (Baffin Island), the Aasiaat domain and the Nagssugtoqidian orogen to the east (west Greenland), and some regions of the Torngat orogen to the south (northern Labrador). These regions share some broad commonalities in rock type, presence of migmatites, and magmatic and metamorphic ages. Differences between these crustal domains, include fabric orientation and fold vergence (Table 6.1). U-Pb age data is present from all of these Archean blocks and is summarized in Figure 6.1, providing a first order comparison of magmatic crystallization ages and metamorphic dates. The following sections then examine this U-Pb data, other existing data from each of the crustal domains and explain the rationale for a newly proposed regional tectonic model (Figure 6.2).

North Atlantic Craton: Torngat orogen and Nagssugtoqidian orogen

Similarities in orthogneiss U-Pb ages of emplacement/crystallization give an indication into whether Archean blocks shared a common Archean history. The Torngat orogen of northern Labrador and the Nagssugtoqidian orogen of southern west Greenland contain Archean orthogneiss with abundant U-Pb crystallization ages older than ca. 2.99 Ga (along with ages between ca. 2.87-2.75 Ga) and paragneiss interpreted to have Archean ages of deposition (Figure 6.1; Table 6.1; Rayner, 2012). Eastern Hall Peninsula has a slightly different geological history with Archean orthogneiss U-Pb crystallization ages of ca. 2.98 Ga or younger and no documented Archean paragneiss (Table 6.1; Rayner 2014; 2015). There are metasedimentary rocks in eastern Hall Peninsula with exclusively Archean zircons, but have been interpreted to

Table 6.1. Summary of Archean terranes with their lithological, structural, metamorphic and isotopic characteristics

crustal terrane	crustal interpretation	rock types	structural characteristics	Archean U-Pb ages (Ga)		
				orthogneiss	paragneiss	metamorphism
eastern Hall Peninsula	microcontinent (Grocott and Davies, 1999); part of NAC* (Wardle, 2002)	tonalite to syenogranite, migmatitic	SSE gneissosity, E verging folds, (Steenkamp and St-Onge, 2014)	2.98-2.72, 2.62	none documented; Archean detritus 3.80-2.60	2.77, 2.74-2.70
Cumberland Peninsula	Rae craton (St-Onge et al., 2009)	tonalitie to dioritie, migmatitic	WSW gneissosity, E verging folds (Hamilton et al., 2014)	2.99, 2.94, 2.77, 2.76, 2.70	yes, >2.78, inferred by cross-cutting relationship	2.79, 2.70
Aasiaat domain (southern block)	microcontinent (Kolb, 2014)	tonalite to granodiorite, migmatitic	SW gneissosity, NW directed thrusting (Connelly et al., 2006)	2.87-2.75	none documented	2.93-2.77, 2.72
Meta Incognita	microcontinent (St-Onge et al., 2000)	tonalite to monzogranite, migmatitic	NW gneissosity; SW verging folds (St-Onge et al., 2007)	3.02-2.78, 2.68, 2.63-2.60, 2.40, 2.34-2.31	none documented	-
Torngat orogen (northern Labrador)	NAC* (Scott, 1995)	tonalite to granite, migmatitic	NNW gneissosity (Connelly et al., 2000)	> 2.96, 2.83-2.75	>3.9, 3.86-3.73, 3.10-2.82	2.76, 2.73
Nagssugtoqidian orogen (SW Greenland)	NAC* (Bridgewater et al., 1973)	tonalite to dioritie, migmatitic	ENE gneissosity, WNW directed thrusts and shallow L2 lineations (Hollis et al., 2006)	3.20-2.97, 2.87-2.80	3.8-3.5, 3.0; detritus 3.5-3.2; 3.0-2.7, 2.1-1.9	2.80-2.73; 2.74-2.70

NAC* - North Atlantic craton

Table 6.1. cont'd Summary of Archean terranes with their lithological, structural, metamorphic and isotopic characteristics

crustal terrane	Paleoproterozoic U-Pb ages (Ga)		Lu-Hf model ages	Sm-Nd model ages
	intrusives	metamorphism		
eastern Hall Peninsula	1.89, 1.87-1.83	granulite with amphibolite overprint , initially at 1.85 with regional 1.83-1.82, then 1.80 (Skipton et al., 2016)	3.36-2.73 (this study)	4.01, 3.25-2.75, 2.20 orthogneisses (this study)
Cumberland Peninsula	1.89-1.87	granulite with amphibolite overprint ,initially at 1.90-1.88 (contact with Qikiqtarjuaq plutonic suite), 1.86, 1.84, then 1.81 (Berman et al., 2013)	-	3.40-2.88 metasediments (Whalen et al., 2010)
Aasiaat domain (southern block)	1.92-1.87	1.86-1.84 (Conelly et al., 2006)	-	-
Meta Incognita	1.95, 1.87-1.84	granulite facies at 1.84, retrograde amphibolite at 1.81 (St-Ong et al., 2007)	-	3.08-2.35 (metasediments; Thériault et al., 2001); 3.25-2.90 (metasediments; Whalen et al., 2010)
Torngat orogen	2.59-2.56; 1.92-1.86	1.92-1.86 magmatic arc rocks, 1.87-1.85 (van Kranendonk, 1996)	-	-
Nagssugtoqidian orogen (SW Greenland)	2.5, 1.92-1.78	1.85, 1.84-1.80 (Connelly et al., 2006)	-	-

Figure 6.1. Summary of existing Archean U-Pb age data from eastern Hall Peninsula and the surrounding Archean blocks. Crustal affinity is shown on the left side with dashed lines indicating an interpreted suture seperating crust with similar Archean geologic histories.

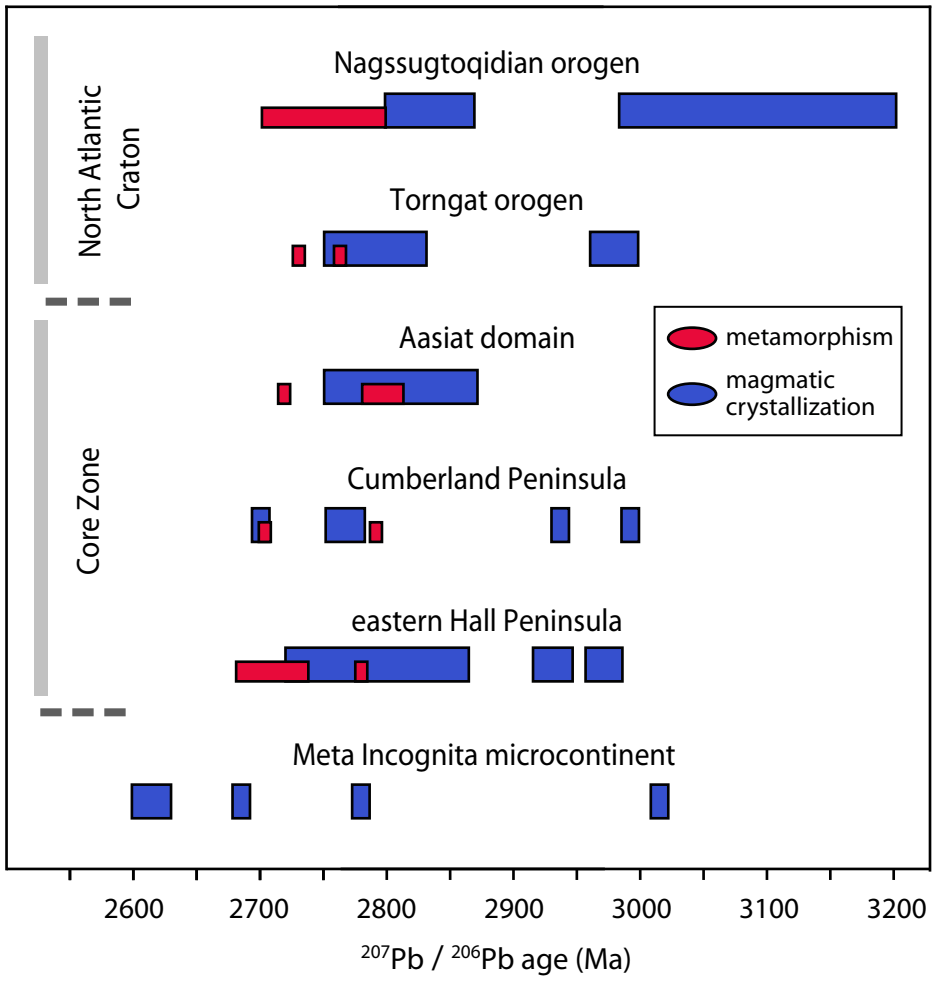

Figure 6.2. Regional crustal correlation model highlighting cratonic affinity and locations of interpreted crustal sutures (shown in red). Dates are in Ga and indicate timing of terrane accretion. CP, Cumberland Peninsula; CZ, Core zone; HP, Hall Peninsula; NAC, North Atlantic craton; MI, Meta Incognita microcontinent; RC, Rae craton. Modified after the full-fit plate reconstruction model of North America - Greenland margins (120 Ma) by Hosseinpour et al., (2013).

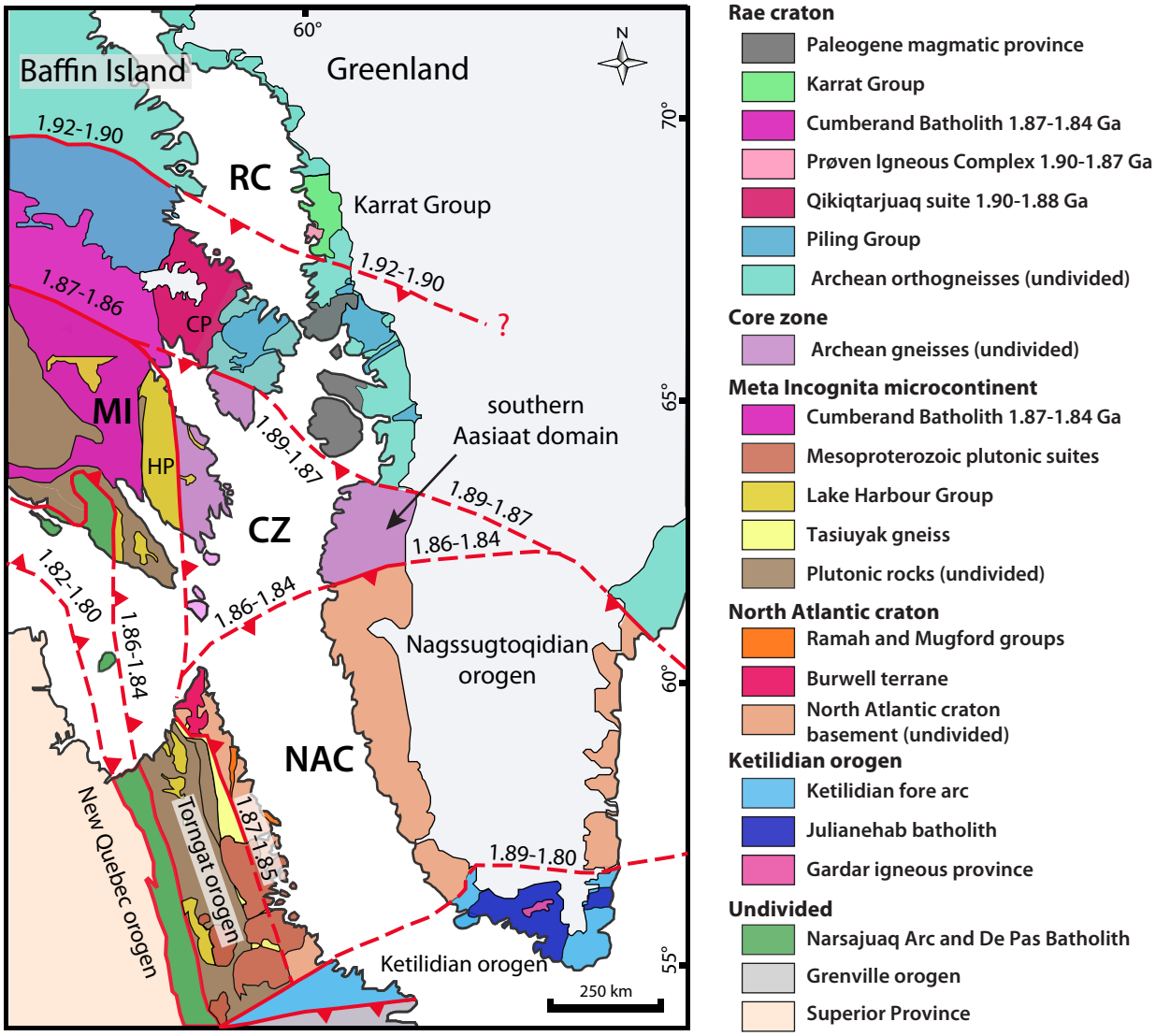

represent Proterozoic basal quartzites deposited in a basinal setting with a very restricted detrital source (Rayner, 2014; 2015). Overall, the substantial differences listed above between the eastern Hall Peninsula and North Atlantic craton of northern Labrador and west Greenland indicate that these blocks were not juxtaposed prior to Archean tectonic amalgamation at ca. 2.80-2.70 Ga (Table 6.1), however, they could have been juxtaposed at some point in the earlier Archean.

Meta Incognita microcontinent

Comparing eastern Hall Peninsula with Meta Incognita microcontinent, orthogneisses of Meta Incognita microcontinent have slightly younger crystallization ages and Paleoproterozoic intrusive ages (Figure 6.1; Table 6.1). In spite of these differences, eastern Hall Peninsula has been correlated with Meta Incognita microcontinent on the basis of an interpreted depositional contact between Paleoproterozoic supracrustal rocks (correlated with Lake Harbour Group metasediments of Meta Incognita microcontinent) and Archean basement (Steenkamp and St-Onge, 2014; Skipton et al., 2017). Nevertheless, this correlation only signifies that these two cratons were together in the Paleoproterozoic, prior to the deposition of the Lake Harbour sequence (ca. ≤1.93 to 1.88 Ga). However, as outlined in Chapter 5, the source of Neoarchean and Paleoproterozoic zircon detritus documented in Hall Peninsula supracrustal sequences is still an unresolved question but a nearby source could be the composite Rae craton to the north (which includes Cumberland Peninsula). Finally, U-Pb, Lu-Hf and Sm-Nd isotopic data from this study, along with aeromagnetic lineaments indicate that along central Hall Peninsula a Paleoproterozoic crustal suture separates the Archean orthogneiss complex from the largely Paleoproterozoic Meta Incognita microcontinent (Chapter 4, 5). Subsequent stitching plutons (ca.

1.87-1.83 Ga) have obscured any field evidence of this boundary (Chapter 5). These two Archean crustal domains share a common Paleoproterozoic tectonothermal history reaching similar peak metamorphic temperatures and maximum crustal thickening between ca. 1.87 Ga and 1.83 Ga, followed by late- to post-orogenic tectonothermal activity from ca. 1.80 to 1.75 Ga (Skipton et al., 2017).

Various pieces of evidence suggest that Meta Incognita microcontinent and the Torngat orogen are part of a laterally continuous crustal domain, these are:

(i) Similar lithological, structural and metamorphic characteristics (Corrigan et al., 2009)

(ii) Continuous trace of aeromagnetic lineaments from northern Labrador northward to Baffin Island (Bourlon et al., 2002; St-Onge et al., 2002)

(iii) Detritus from Paleoproterozoic supracrustal rocks with similar age peaks between ca. 2.10 and 1.94 Ga (Scott and Gautier, 1996; Scott et al., 2002).

(iv) Distinct Rare Earth Element and Nd isotopic signatures of metasedimentary gneisses indicating that there may have been a single depositional system along the northeastern side of what is now northern Labrador and Baffin Island (Thériault et al., 2001).

This correlation between Meta Incognita microcontinent and Torngat orogen does not change with the newly proposed regional tectonic assembly (Figure 6.2). Consequently, the Archean orthogneiss complex of eastern Hall Peninsula should no longer be considered synonymous with the pre-Paleoproterozoic history preserved on Meta Incognita microcontinent.

Cumberland Peninsula

The best geological match for eastern Hall Peninsula is southern Cumberland Peninsula and the southern block of the Aasiaat domain (Chapter 4, 5). Historically, Cumberland Peninsula has been ascribed to the Rae craton but recent geological mapping has shown the dominance of Archean rocks in the southern portion of the Peninsula, different from the rocks towards the northwest largely dominated by Paleoproterozoic plutonic rocks (Berman et al., 2013).

Orthogneiss crystallization ages in southern Cumberland Peninsula (ca. 2.99 to 2.70 Ga) overlap with orthogneiss crystallization ages in the southern block of the Aasiaat domain from ca. 2.87 to 2.75 Ga and eastern Hall Peninsula (ca. 2.98 to 2.62 Ga; Figure 6.1). Lithologic and metamorphic characteristics (e.g. rock types, timing and grade of metamorphism) of the rock units from all three domains are virtually the same with minor differences in the present orientation of structures; eastern Hall Peninsula (dominantly north-northeast), and Aasiaat domain (east-west) (Table 6.1).

In addition, metamorphic ages of ca. 1.90-1.89 Ga in the cores of zircon and monazite grains from southern Cumberland Peninsula and eastern Hall Peninsula (Rayner, 2012, Berman et al., 2013; Rayner 2014; 2015; Skipton et al., 2016) are similar to the range of metamorphic ages (ca. 1.92-1.88) for the Aasiaat domain (Connelly et al., 2006) indicates that these three blocks must have been juxtaposed prior to accretion of Meta Incognita microcontinent with the Rae Craton at ca. 1.88 to 1.87 Ga (St-Onge et al., 2007). This means that southern Cumberland Peninsula, the southern block of the Aasiaat domain and eastern Hall Peninsula could have been independent microcontinent fragments coincidently caught up together in the progressive multi-directional tectonic amalgamation during the THO. Alternatively, these three crustal blocks could have been

a single crustal entity since the Archean. Regardless of whether these three crustal fragments shared a common Archean geologic history they accreted to the composite Rae craton at ca. 1.90 Ga, subsequently drifting apart during continued tectonic activity since the THO. In the regional tectonic model presented herein, these three terranes are grouped into one "core zone" crustal domain (Figure 6.2).

The wedge shaped geometry of the "core zone" actually compares well with the Himalayan orogen, resembling the Songpan Ganze block or even the Songpan Ganze block and the Quidam terrane together that could be considered as microcontinent fragments (Figure 6.3). The wedge shape geometry is a result of being caught between the South China block, the Mongolia-North China craton and the Qiangtang block prior to terminal collision of the Indian craton (Figure 6.3a). In a very similar situation in the THO, the "core zone" is sandwiched in between the North Atlantic craton, the Rae craton and Meta-Incognita microcontinent prior to terminal collision with the Superior province (Figure 6.3b). With many characteristics being nearly identical between the THO and the Himalayan orogen (e.g. timing, duration and grade of metamorphism, deformation processes; St-Onge et al., 2006, 2009) the suture proposed by St-Onge et al. (2009) that completely separates the Cumberland Peninsula from Hall Peninsula and continues into west Greenland was one major difference because it created an Y-shaped microcontinent fragment as opposed to linear, arcuate belts observed in the rest of the THO and also in the Himalayan orogen (Figure 6.3). Understandably, the regional interpretation of St-Onge et al., (2009) was proposed prior to the re-mapping of Cumberland Peninsula and Hall Peninsula and a question mark was implicit in his reconstruction (Figure 6.3c).

Typically, in crustal suture interpretations a correlation between Cumberland Batholith and the Prøven Igneous Complex was implied across Davis Strait (Figure 6.3c). However, in a recent

Figure 6.3. Simplified regional geologic maps of a) southeast Asia showing a similar size, shape and extent of crustal constituents and intervening sutures to b) northeast Laurentia with revised crustal suture locations presented in this thesis and c) northeast Laurentia from St-Onge et al. (2009). HP, Hall Peninsula; CP, Cumberland Peninsula.

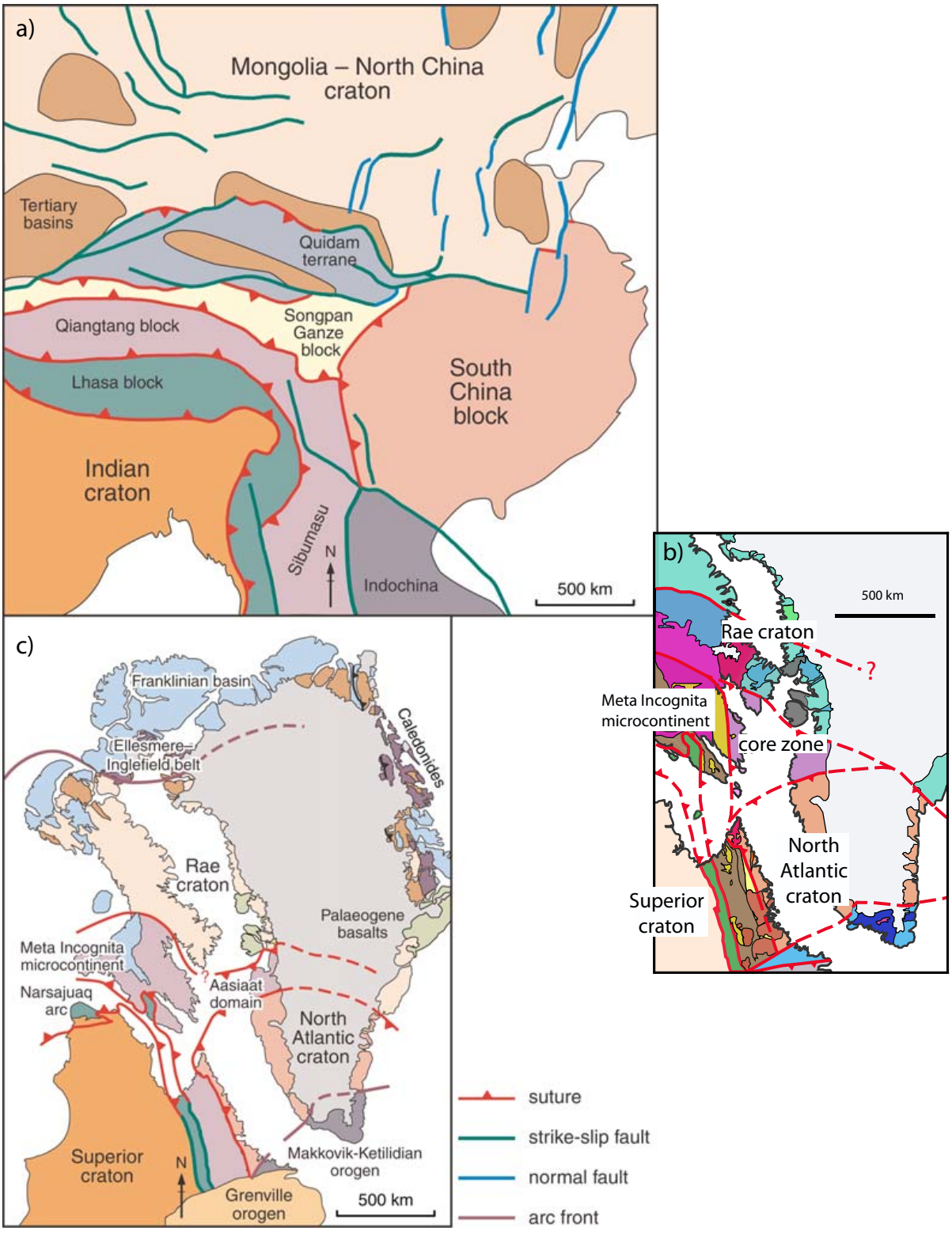

study of the Karrat Group metasedimentary package of west Greenland (Figure 6.2), U-Pb ages of igneous and detrital zircon conclude that this region experienced collisional events between ca. 1.95-1.90 Ga and refutes a link between the Prøven Igneous Complex and Cumberland Batholith (exposed on Meta Incognita microcontinent and portions of Cumberland batholith; Whalen et al., 2010; Sanborn-Barrie et al., 2017). Consequently, this thesis proposes the suture documented just north of Cumberland Peninsula across Baffin Island continue laterally more to the south, avoiding a correlation to the between rocks of the Karrat Group and Cumberland Batholith. This new orientation matches the geometry of the subsequent ca. 1.89-1.87 Ga suture and maintains geometry analogous to the Himalayan orogen (Figure 6.3), however, a question mark denotes the uncertainty to where such a suture continues underneath the ice sheet of Greenland (Figure 6.2).

Tectonic reconstructions still have unresolved issues. For example, the suture separating the Tasiuyak gneiss from the Torngat orogen could extend northward to bisect Hall Peninsula (e.g. Wardle et al., 2002) or it could curve to the east towards southern west Greenland (e.g. St-Onge et al., 2009) to maintain the long-standing interpretation of northern Labrador having a crustal affinity with North Atlantic craton (Figure 6.2; Bridgewater et al., 1973). This thesis postulates that both could be true and the wedge shaped "core zone" of eastern Hall Peninsula, southern Cumberland Peninsula and Aasiaat domain accommodates both of these interpreted sutures (Figure 6.2).

Sequence of events

(i) ca. 1.87-1.86 Ga east directed collision of Meta Incognita microcontinent against eastern Hall Peninsula (creating the N-S fabric),

(ii) ca. 1.86 to 1.82 Ga shared tectonometamorphic history between Meta Incognita microcontinent and eastern Hall Peninsula (Skipton et al., 2016).

(iii) north-northwest directed collision of the North Atlantic craton (ca. 1.86-1.84 Ga) against the southern margin of the wedge-shaped core zone (Figure 6.1) creating generally E-W fabric in the Aasiaat domain and overprinting small areas on the furthest eastern portions of Hall Peninsula.

This new regional paleotectonic reconstruction (Figure 6.2) builds from previously proposed models, incorporates new U-Pb, Sm-Nd and Lu-Hf from this thesis and satisfies important constraints from Whalen et al. (2010), who used Nd-isotopes to delineate different crustal domains within Baffin Island, Kolb (2014), who identified the Aasiaat domain as an independent microcontinent fragment with no correlatives on eastern Greenland, and Sanborn-Barrie et al., (2017) who refutes a link between Paleoproterozoic plutonic units from Cumberland Peninsula to the Karrat Group of west Greenland. Without definitive evidence that eastern Hall Peninsula, southern Cumberland Peninsula and Aasiaat domain all shared the same Archean geologic history, for now they should be considered as separate Archean microcontinent fragments that were sandwiched together during multi-directional THO tectonic amalgamation. Further work with Lu-Hf isotopes in zircon from all of these Archean domains investigating Archean magmatic signatures and model ages of extraction from the mantle could prove otherwise.

6.3. Future work

Several geological questions remain unanswered on Hall Peninsula, Baffin Island such as:

1) *What is the exact location, extent and characteristics of the cryptic crustal suture interpreted herein to separate Meta Incognita microcontinent and eastern Hall Peninsula block?*

This could be resolved by geochemical (Lu-Hf and Sm-Nd) comparison between ca. 1865–1848 Ma Cumberland Batholith and ca. 1870–1850 Ma intrusions on western Hall Peninsula. Moreover, through an assessment of the magmatic source material of these Paleoproterozoic intrusions on western Hall Peninsula, any inherited signatures of the basement material underlying western Hall Peninsula could be compared with existing Sm-Nd isotopic data from the Cumberland Batholith and Meta Incognita microcontinent. This comparison may provide information on the continuity of the Meta Incognita microcontinent towards Hall Peninsula to the east and could potentially delineate the actual location, extent and characteristics of an intervening, cryptic crustal boundary. An in-depth examination of the stratigraphic relationships of Paleoproterozoic supracrustal sequences to these intrusives should also be undertaken and could also contribute to this goal. Future work of this nature is in progress by HPIGP collaborators at the Geological Survey of Canada.

2) *What is the enigmatic source of detritus for supracrustal sequences that are tectonically interleaved with Archean basement rocks across eastern Hall Peninsula?*

A hypothesis is put forward in Chapter 5 and while some geologic work has been done on these sequences to calibrate the legend for the updated Hall Peninsula geological map (e.g. Rayner 2014, 2015; Steenkamp and St-Onge, 2014), the sampling density required to better understand such a large and complex area is much greater than the available data. Regional lithostratigraphic correlations of Paleoproterozoic supracrustal sequences between adjacent cratons is relevant here again and could yield insight into verifying the paleo-plate configuration of the Meta Incognita microcontinent, the core zone of northern Labrador, the Aasiaat domain,

West Greenland and Hall Peninsula, Baffin Island. This question could also be examined through a regional river sampling study, a technique for assessing zircon detritus in large, remote areas that has seen success elsewhere in Canada, as well as in Africa and Russia (Cawood and Nemchin, 2001; Safonova et al., 2010; Lizuka et al., 2013).

3) *Do Lu-Hf isotopes in zircon from Hall Peninsula block correlate to those of Cumberland Peninsula, Northern Labrador and/or West Greenland?*

The new U-Pb and Lu-Hf in zircon dataset presented in this study should be compared to zircon Lu-Hf signatures from adjacent cratons. This would allow examination as to whether Hall Peninsula block was once linked to another larger composite Archean craton such as Aasiaat domain, West Greenland or whether Hall Peninsula block had a unique Geologic history unto itself. In particular, the "core zone" of eastern Hall Peninsula, southern Cumberland Peninsula and the southern block of the Aasiaat domain should be further investigated. An effort was made to analyze zircon separates with existing U-Pb ages from Aasiaat domain for Lu-Hf isotopes, but this collaborative investigation is still pending. Regardless, it is hoped upon publication of this new dataset for eastern Hall Peninsula, renewed interest will be given to this area and future collaborative work can be undertaken.

6.4. References

Ansdell, K.M. 2005. Tectonic evolution of the Manitoba-Saskatchewan segment of the Paleoproterozoic Trans-Hudson orogen, Canada. Canadian Journal of Earth Sciences, v. 42, p. 741-759.

Berman, R G; Sanborn-Barrie, M; Hamilton, B M; Rayner, N; Young, M. 2013. Preliminary in situ SHRIMP geochronological constraints on the tectonometamorphic evolution of Cumberland Peninsula, Baffin Island, Nunavut. Geological Survey of Canada, Current Research article no. 2013-7, 23 p.

Bourlon, E., Mareschal, J.C., Roest, W.R. and Telmat, H. 2002. Geophysical correlations in the Ungava Bay area. Canadian Journal of Earth Sciences, v. 39, p. 625-637.

Bridgwater, D., Watson, J. and Windley, B.F. 1973. The Archaean craton of the North Atlantic region. Philosophical Transactions for the Royal Society of London. Series A, Mathematical and Physical Sciences, p. 493-512.

Cawood, P.A. and Nemchin, A.A. 2001. Paleogeographic development of the east Laurentian margin: Constraints from U-Pb dating of detrital zircons in the Newfoundland Appalachians. Geological Society of America Bulletin, v. 113, p. 1234-1246.

Connelly, J.N., Thrane, K., Krawiec, A.W. and Garde, A.A., 2006. Linking the Palaeoproterozoic Nagssugtoqidian and Rinkian orogens through the Disko Bugt region of West Greenland. Journal of the Geological Society, v. 163, p. 319-335.

Connelly, J.N., van Gool, J.A. and Mengel, F.C. 2000. Temporal evolution of a deeply eroded orogen: the Nagssugtoqidian Orogen, West Greenland. Canadian Journal of Earth Sciences, v. 37, p. 1121-1142.

Corrigan, D., Pehrsson, S., Wodicka, N., and Kemp, E. 2009. The Palaeoproterozoic Trans-Hudson Orogen: a prototype of modern accretionary processes. Geological Society, London, Special Publication, v. 327, p. 457–479.

Grocott, J. and Davies, S.C. 1999. Deformation at the southern boundary of the late Archaean Atâ tonalite and the extent of Proterozoic reworking of the Disko terrane, West Greenland. Precambrian geology of the Disko Bugt region, West Greenland. Geology of Greenland Survey Bulletin, v. 181, p. 155-169.

Hamilton, B.M. 2014. A detailed description of the Hoare Bay group and Paleoproterozoic plutonic rocks near Mischief Glacier and Clephane Bay, Cumberland Peninsula, Baffin Island, Nunavut. Geological Survey of Canada, Current Research v. 2014-3, 20 p.

Henrique-Pinto, R., Guilmette, C., Bilodeau, C. and McNicoll, V. 2017. Evidence for transition from a continental forearc to a collisional pro-foreland basin in the eastern Trans-Hudson Orogen: Detrital zircon provenance analysis in the Labrador Trough, Canada. Precambrian Research, v. 296, p.181-194.

Hoffman, P.F. 1988. United Plates of America, the birth of a craton: Early Proterozoic assembly and growth of Laurentia. Annual Review of Earth and Planetary Sciences, v. 16, p. 543–603.

Hoffman, P.F., Kaufman, A.J., Halverson, G.P., Schrag, D.P., 1998. A Neoproterozoic snowball Earth. Science 281, 1342–1346.

Hollis, J.A., Frei, D., van Gool, J.A., Garde, A.A. and Persson, M. 2006. Using zircon geochronology to resolve the Archaean geology of southern West Greenland. Geological Survey of Denmark and Greenland Bulletin, v. 10, p. 49-52.

Iizuka, T., Campbell, I.H., Allen, C.M., Gill, J.B., Maruyama, S. and Makoka, F. 2013. Evolution of the African continental crust as recorded by U–Pb, Lu–Hf and O isotopes in detrital zircons from modern rivers. Geochimica et Cosmochimica Acta, v. 107, p. 96-120.

Kolb, J. 2014. Structure of the Palaeoproterozoic Nagssugtoqidian Orogen, South-East Greenland: model for the tectonic evolution. Precambrian Research, v. 255, p. 809-822.

Murphy, J.B., Nance, R.D. and Cawood, P.A., 2009. Contrasting modes of supercontinent formation and the conundrum of Pangea. Gondwana Research, 15(3), pp.408-420.

Rayner, N.M. 2015. New (2013–2014) U-Pb geochronological results from northern Hall Peninsula, southern Baffin Island, Nunavut; in Summary of Activities 2014, Canada-Nunavut Geoscience Office, p. 31–44.

Rayner, N.M. 2014. New U-Pb geochronological results from Hall Peninsula, Baffin Island, Nunavut; in Summary of Activities 2013, Canada-Nunavut Geoscience Office, p. 39-52.

Rayner, N.M., Sanborn-Barrie, M., Young, M.D. and Whalen, J.B. 2012. U-Pb ages of Archean basement and Paleoproterozoic plutonic rocks, southern Cumberland Peninsula, eastern Baffin Island, Nunavut; Geological Survey of Canada, Current Research, v. 2012-8, 24 p.

Safonova, I., Maruyama, S., Hirata, T., Kon, Y. and Rino, S. 2010. LA ICP MS U–Pb ages of detrital zircons from Russia largest rivers: implications for major granitoid events in Eurasia and global episodes of supercontinent formation. Journal of Geodynamics, v. 50, p. 134-153.

Sanborn-Barrie, M., Thrane, K., Wodicka, N. and Rayner, N. 2017. The Laurentia–West Greenland connection at 1.9 Ga: New insights from the Rinkian fold belt. Gondwana Research, v. 51, p. 289-309.

Scott, D.J. 1995. U–Pb geochronology of the Nain craton on the eastern margin of the Torngat Orogen, Labrador. Canadian Journal of Earth Sciences, v. 32, p. 1859-1869.

Scott, D.J., St-Onge, M.R. and Corrigan, D. 2002. Geology of the Paleoproterozoic Piling Group and underlying Archean gneiss, central Baffin Island, Nunavut. Natural Resources Canada, Geological Survey of Canada.

Scott, D.J. and Gauthier, G. 1996. Comparison of TIMS (U-Pb) and laser ablation microprobe ICP-MS (Pb) techniques for age determination of detrital zircons from Paleoproterozoic metasedimentary

rocks from northeastern Laurentia, Canada, with tectonic implications. Chemical Geology, v. 131, p. 127-142.

Skipton, D.R., Schneider, D.A., Kellett, D.A. and Joyce, N.L. 2017. Deciphering the Paleoproterozoic cooling history of the northeastern Trans-Hudson Orogen, Baffin Island (Canada), using 40 Ar/39 Ar step-heating and UV laser thermochronology. Lithos, v. 284, p. 69-90.

Skipton, D.R., Schneider, D.A., McFarlane, C.R.M., St-Onge, M.R. and Jackson, S.E. 2016. Multi-stage zircon and monazite growth revealed by depth profiling and in situ U–Pb geochronology: Resolving the Paleoproterozoic tectonics of the Trans-Hudson Orogen on southeastern Baffin Island, Canada. Precambrian Research, v. 285, p. 272-298.

St-Onge, M.R., Van Gool, J.A.M., Garde, A.A. and Scott, D.J. 2009. Correlation of Archaean and Palaeoproterozoic units between northeastern Canada and western Greenland: constraining the pre-collisional upper plate accretionary history of the Trans-Hudson Orogen. Geological Society of London Special Publication v. 318, p. 193–235.

St-Onge, M.R., Wodicka, N. and Ijewliw, O. 2007. Polymetamorphic evolution of the Trans-Hudson Orogen, Baffin Island, Canada: integration of petrological, structural and geochronological data. Journal of Petrology, 48, 271–302.

St-Onge, M.R., Searle, M.P. and Wodicka, N. 2006. Trans-Hudson Orogen of North America and Himalaya–Karakorum–Tibetan Orogen of Asia: structural and thermal characteristics of the lower and upper plates. Tectonics, v. 25, p. 1–22.

St-Onge, M.R., Scott, D.J. and Wodicka, N. 2002. Review of crustal architecture and evolution in the Ungava Peninsula–Baffin Island area: connection to the Lithoprobe ECSOOT transect; Canadian Journal of Earth Sciences, v. 39, p. 589-610.

St-Onge, M.R., Scott, D.J. and Lucas, S.B. 2000. Early partitioning of Quebec: Microcontinent formation in the Paleoproterozoic. Geology, v. 28, p. 323-326.

Steenkamp, H.M., Bros, E.R. and St-Onge, M.R. 2014. Altered ultramafic and layered mafic-ultramafic intrusions: new economic and carving stone potential on northern Hall Peninsula, Baffin Island, Nunavut. in Summary of Activities 2013, Canada-Nunavut Geoscience Office, p. 11-20.

Thériault, R.J., St-Onge, M.R. and Scott, D.J. 2001. Nd isotopic and geochemical signature of the Paleoproterozoic Trans-Hudson Orogen, southern Baffin Island, Canada: implications for the evolution of eastern Laurentia. Precambrian Research, v. 108, p. 113-138.

Van Kranendonk, M.J. 1996. Tectonic evolution of the Paleoproterozoic Torngat Orogen: Evidence from pressure‐temperature‐time‐deformation paths in the North River map area, Labrador. Tectonics, v. 15, p. 843-869.

Wardle, R.J., James D.T., Scott, D.J. and Hall, J. 2002. The southeastern Churchill Province: synthesis of a Palaeoproterozoic transpressional orogen; Canadian Journal of Earth Sciences, v. 39, p. 639-663. doi:10.1139/E02-004

Whalen, J.B., Wodicka, N., Taylor, B.E. and Jackson, G.D. 2010. Cumberland Batholith, Trans-Hudson Orogen, Canada: Petrogenesis and implications for Paleoproterozoic crustal and orogenic processes. Lithos, v. 117, p. 99-118.

Worsley, T.R., Nance, R.D., Moody, J.B., 1986. Tectonic cycles and the history of the Earth's biogeochemical and paleoceanographic record. Paleoceanography 1, 233–263.